Tae-Hwan Lim
Editor

Practical Textbook of Cardiac CT and MRI

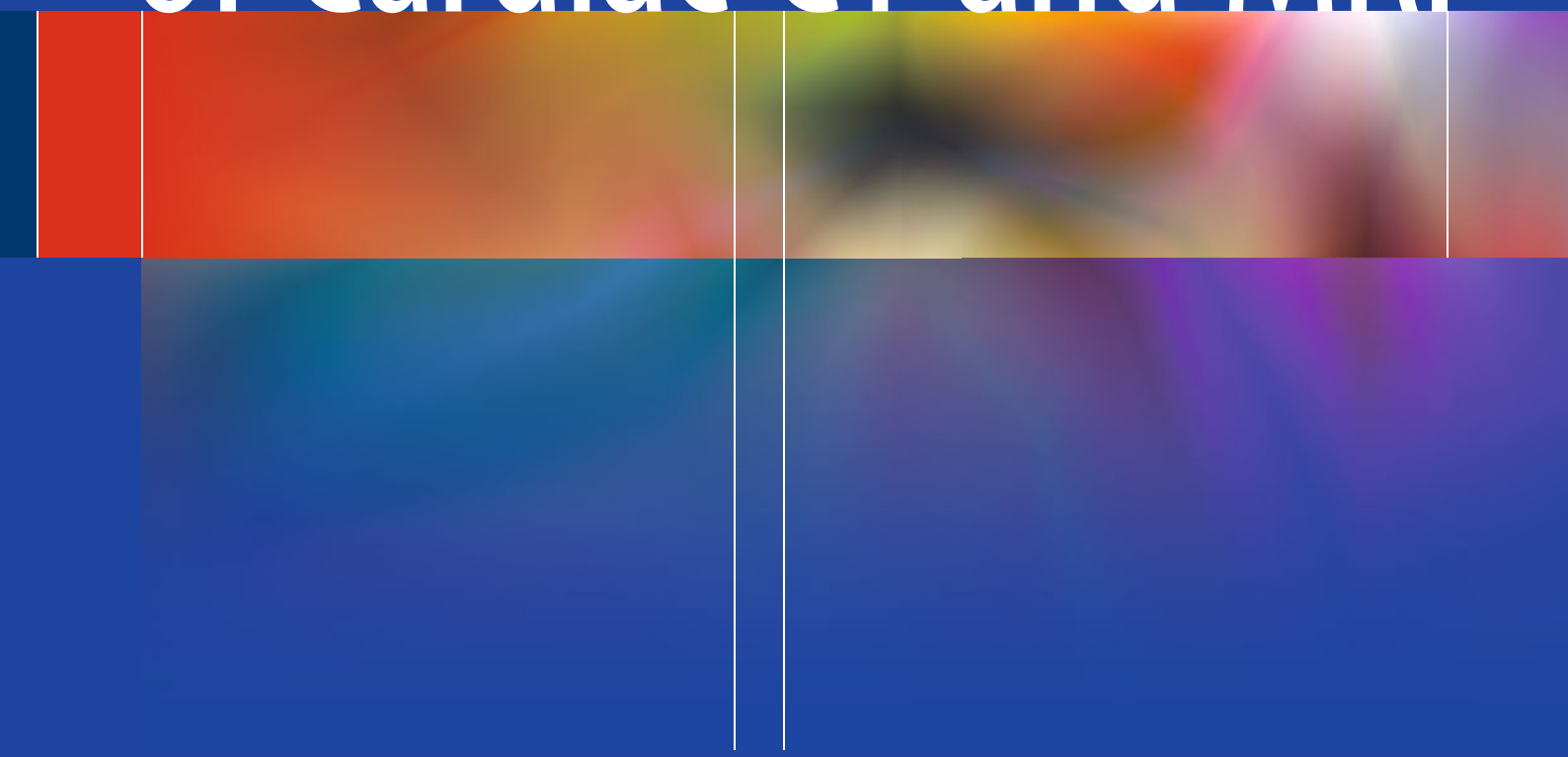

EXTRA MATERIALS
extras.springer.com

Springer

Practical Textbook of Cardiac CT and MRI

Tae-Hwan Lim
Editor

Practical Textbook of Cardiac CT and MRI

Springer

Editor
Tae-Hwan Lim
Department of Radiology
ASAN Medical Center
Seoul
Republic of Korea

Additional material to this book can be downloaded from http://extras.springer.com

ISBN 978-3-642-36396-2 ISBN 978-3-642-36397-9 (eBook)
DOI 10.1007/978-3-642-36397-9
Springer Heidelberg New York Dordrecht London

Library of Congress Control Number: 2014959420

Printed on acid-free paper

Springer is part of Springer Science+Business Media (www.springer.com)

I dedicate this book to my great teachers

My father, Jae Keun Lim, MD, PhD
My teacher and professor, Man Chung Han, MD, PhD
And my mentor, Charles B. Higgins, MD

Preface

Along with technological advancement, cardiac computed tomography (CT) and magnetic resonance imaging (CMR) have been extensively used over the past decade. Although coronary angiography has been recognized as a reference standard for the diagnosis of coronary artery disease, coronary CT angiography has replaced angiography in many clinical scenarios. Compared to conventional echocardiography, cardiac CT may provide additional anatomic information to diagnose structural heart diseases. With tissue characterization and quantitative evaluation of cardiac function, CMR has provided unique information for the diagnosis of various cardiac diseases. Newer generations of cardiac CTs with wider z-axis coverage and faster temporal resolution have facilitated the diagnosis of congenital heart disease and the evaluation of coronary stents and myocardial perfusion with an acceptable radiation dose. Recently introduced myocardial mapping techniques by CMR have helped to elucidate the pathophysiology of various myocardial diseases. With the technological advancement of hardware and software, clinical applications of cardiac CT and CMR will be dramatically expanded in the near future. Therefore, it is strongly recommended that radiologists and other imaging specialists should familiarize themselves with imaging techniques, pathophysiology, and imaging findings of various cardiac diseases.

This case-oriented textbook is written to meet the needs of residents, radiologists, and clinicians who want to learn the imaging findings of various cardiac diseases on cardiac CT and CMR. The basic anatomy of the heart, imaging findings of various cardiac diseases, and recent techniques of CT and CMR are thoroughly reviewed. This book contains many intriguing images showing the typical appearance of cardiac diseases. In particular, readers can scan QR codes for real-time online demonstration of cine imaging for the functional evaluation. CT images will also be offered online. We hope this textbook to be a companion of the reading room so the readers can find various images quickly and easily in their everyday clinical practice.

After the foundation of the Asian Society of Cardiovascular Imaging (ASCI) in 2006, many Korean radiologists have devoted themselves to establishing ASCI as a leading cardiac imaging society in Asia. The Korean Society of Cardiovascular Imaging (KOSCI) has been acknowledged as a representative cardiovascular imaging society both at home and abroad. As a founding president of ASCI and a former president of KOSCI, I am deeply honored to invite many qualified scholars from ASCI and KOSCI as co-authors for this book, including Professor Hajime Sakuma and Yeon Hyeon Choe. I would also like to appreciate Sang Il Choi, Dong Hyun Yang, Jeong A. Kim, Hyun Jung Koo, and Mi Sun Chung for their unreserved editorial assistance. Last, but not least, my very sincere appreciation and love goes to my wife Mi Ran, son Yang Kyu, and daughter Hye Yun for their lifelong endurance and support throughout my professional career.

Seoul, Republic of Korea — Tae-Hwan Lim

Contents

Contributors

Yeon Hyeon Choe Department of Radiology, Samsung Medical Center, Sungkyunkwan University School of Medicine, Seoul, Republic of Korea

Byoung Wook Choi Department of Radiology, Research Institute of Radiological Science, Severance Hospital, Yonsei University College of Medicine, Seoul, Republic of Korea

Sang Il Choi MD Department of Radiology, Seoul National University Bundang Hospital, Gyeonggido, Republic of Korea

Eui-Young Choi Division of Cardiology, Heart Center, Gangnum Severance Hospital, Yonsei University of College of Medicine, Seoul, Republic of Korea

Ki Seok Choo Department of Radiology, Pusan National University Yangsan Hospital, Pusan National University, School of Medicine, Busan, Republic of Korea

Eun Ju Chun MD Department of Radiology, Seoul National University Bundang Hospital, Gyeonggido, Republic of Korea

Jin Hur Department of Radiology, Research Institute of Radiological Science, Severance Hospital, Yonsei University College of Medicine, Seoul, Republic of Korea

Sung Ho Hwang Department of Radiology, Korea University Anam Hospital, Korea University College of Medicine, Seoul, Republic of Korea

Jung Im Jung Department of Radiology, Seoul St. Mary's Hospital, College of Medicine, The Catholic University of Korea, Seoul, Republic of Korea

Joon-Won Kang Department of Radiology and Research Institute of Radiology, Asan Medical Center, University of Ulsan College of Medicine, Seoul, Republic of Korea

Doo Kyoung Kang Department of Radiology, Ajou University School of Medicine, Suwon, Republic of Korea

Eun Young Kim Department of Radiology, Gachon University Gil Hospital, Incheon, Republic of Korea

Yun-Hyeon Kim Department of Radiology, Chonnam National University Medical School and Hospital, Gwangju, Republic of Korea

Jeong A. Kim Department of Radiology, Inje University Ilsan Paik Hospital, Ilsan, Republic of Korea

TaeHoon Kim Department of Radiology, Gangnam Severance Hospital, Yonsei University College of Medicine, Seoul, Republic of Korea

Young Jin Kim Department of Radiology, Research Institute of Radiological Science, Severance Hospital, Yonsei University College of Medicine, Seoul, Republic of Korea

Sung Min Ko MD Department of Radiology, Konkuk University Hospital, Seoul, Republic of Korea

Whal Lee Department of Radiology, Seoul National University Hospital, Seoul, Republic of Korea

Heon Lee Department of Radiology, Soonchunhyang University Hospital, Bucheon, Republic of Korea

Bae Young Lee Department of Radiology, St. Paul's Hospital, College of Medicine, The Catholic University of Korea, Seoul, Republic of Korea

Jongmin Lee Department of Radiology, Kyungpook National University and Hospital, Daegu, Republic of Korea

Tae-Hwan Lim Department of Radiology and Research Institute of Radiology, Asan Medical Center, University of Ulsan College of Medicine, Seoul, Republic of Korea

Eun-Ah Park Department of Radiology, Seoul National University Hospital, Seoul, Republic of Korea

Hajime Sakuma Department of Radiology, Mie University Hospital, Mie University Graduate School, Tsu, Japan

Hyun Ju Seon Department of Radiology, Chonnam National University Medical School and Hospital, Gwangju, Republic of Korea

Yon Mi Sung Department of Radiology, Gachon University Gil Hospital, Incheon, Republic of Korea

Dong Hyun Yang Department of Radiology and Research Institute of Radiology, Asan Medical Center, University of Ulsan College of Medicine, Seoul, Republic of Korea

Hwan Seok Yong Department of Radiology, Korea University Guro Hospital, Korea University College of Medicine, Seoul, Republic of Korea

Yeonyee E. Yoon Division of Cardiology, Department of Internal medicine, Seoul National University Bundang Hospital, Gyeonggido, Republic of Korea

Part I

Coronary Artery Imaging

Normal Cardiac Anatomy and Anatomic Pitfall/Variance

1

Jung Im Jung

Contents

J.I. Jung
Department of Radiology, Seoul St. Mary's Hospital, College of Medicine, The Catholic University of Korea, Seoul, Republic of Korea
e-mail: jijung@catholic.ac.kr

Abstract

The advent of multidetector computed tomography (CT) and magnetic resonance imaging (MRI) provides information of cardiac structures in detail with a three-dimensional data. A variety of postprocessing techniques allow noninvasive assessment of every aspect of the cardiovascular system. This capability requires a thorough understanding of essential coronary arterial and cardiac anatomy. Familiarity with normal anatomic structures is necessary to prevent misinterpretation of findings.

In this section, we review the anatomical perspective of the cardiac chambers with an emphasis on anatomic pitfall and variance that can be misinterpreted as pathologic lesion at radiologic examination. Also we introduce the imaging planes commonly used in cardiac imaging.

1.1 Right Atrium

1.1.1 Normal Anatomy

- The right atrium (RA) is composed of three components: the appendage, the venous component, and the vestibule (Fig. 1.1).
- The right atrial appendage is derived from the primitive auricle, evolving a triangular-shaped structure with trabeculation and pectinate muscles (Fig. 1.2).
- The venous component is derived from the right sinus venosus, evolving the smooth wall of the RA. It receives the superior vena cava (SVC) and inferior vena cava (IVC) on its posterior surface and the coronary sinus (CS) at its junction with the atrial septum, just above the posterior interventricular groove.
- The vestibule is also known as the supravalvular lamina and is a smooth muscle rim surrounding the tricuspid valve orifice.
- The tricuspid valve is present between the RA and right ventricle (RV).

T.-H. Lim (ed.), *Practical Textbook of Cardiac CT and MRI*,
DOI 10.1007/978-3-642-36397-9_1,

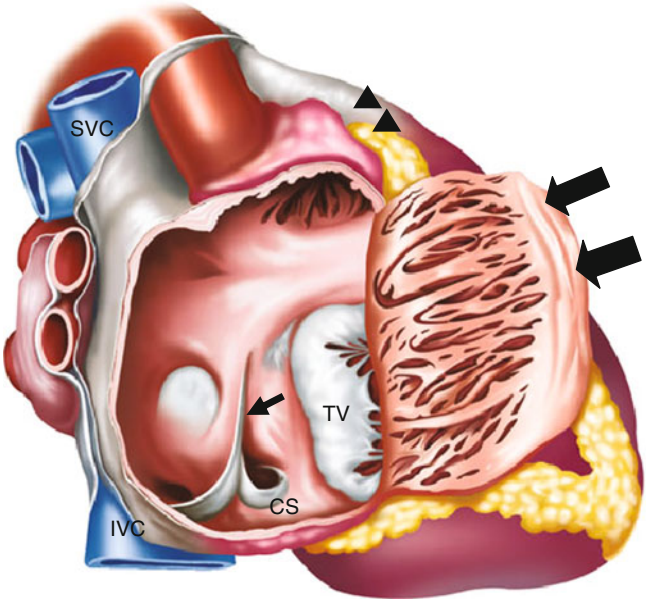

Fig. 1.1 Schematic illustration of anatomy of the right atrium. The right atrium (RA) is composed of the appendage (*arrow head*), venous component, and the vestibule. The venous component is the smooth wall of the RA and receives the SVC, IVC, and CS. The vestibule is a smooth muscle rim surrounding the tricuspid valve (*TV*) orifice. Note ridge of crista terminalis (*thick arrows*) and Eustachian valve (*thin arrow*). *RA* right atrium, *SVC* superior vena cava, *IVC* inferior vena cava, *CS* coronary sinus

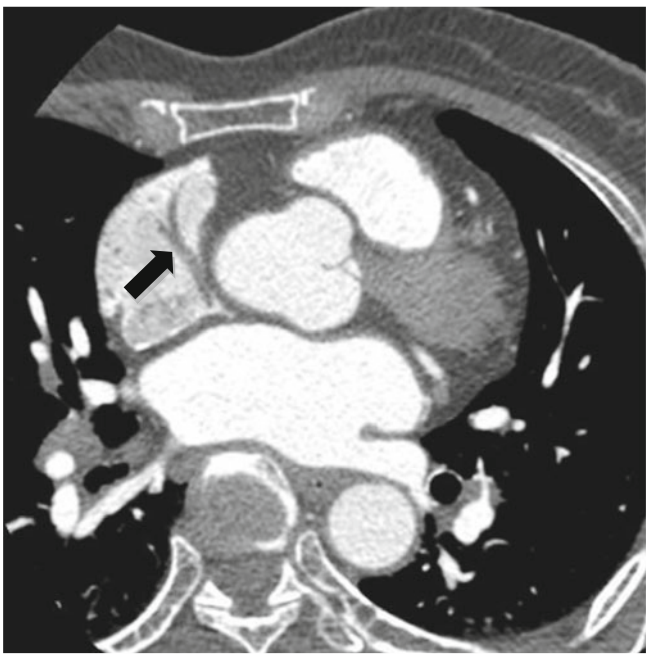

Fig. 1.2 Pectinate muscle of the right atrial appendage (*arrow*)

- The sinoatrial (SA) node is present in the subepicardial side of the superior cavoatrial junction, supplied by the SA nodal artery (Figs. 1.3 and 1.4). The atrioventricular (AV) node is present at the inferior wall of the RA (Fig. 1.5), within the boundaries of Koch's triangle near its apex (see the anatomy for electrophysiology).

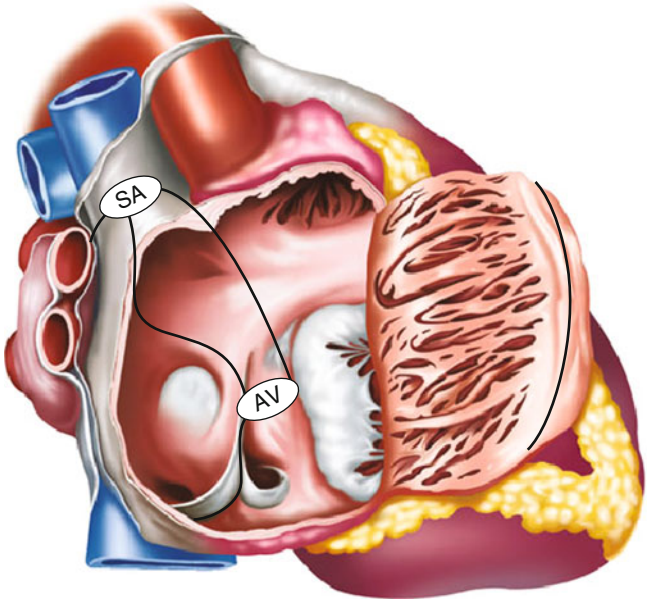

Fig. 1.3 Schematic illustration of conducting system of the right atrium. Sinoatrial node (*SA*) connects to the atrioventricular node (*AV*) through the anterior, middle, and posterior branches

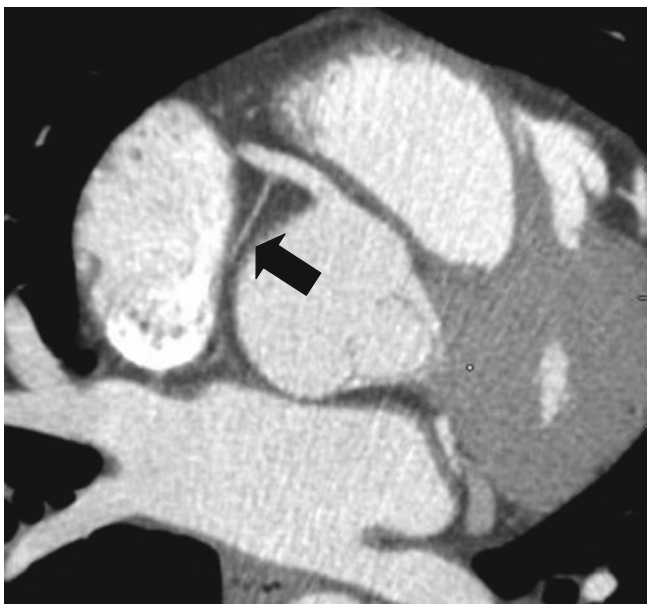

Fig. 1.4 Sinoatrial nodal branch of the RCA (*arrow*) indicates the location of SA node

1.1.2 Anatomic Pitfall and Normal Variance

1.1.2.1 Crista Terminalis

- The crista terminalis is a vertically oriented, internal muscular ridge between the RA appendage and sinus venous component, representing the line of fusion between the primitive auricle and sinus venosus. It extends from the SVC to the IVC (Fig. 1.1).
- The crista terminalis is often seen on routine contrast-enhanced chest CT and echocardiography, and is

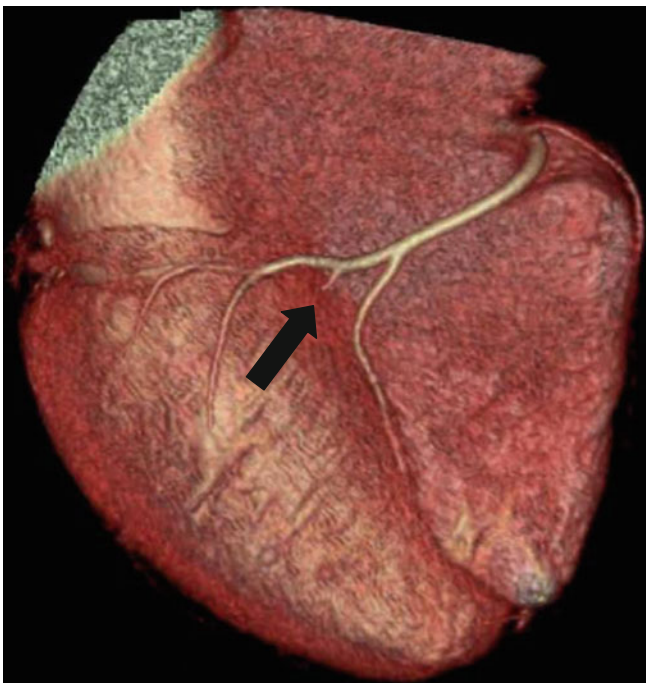

Fig. 1.5 Atrioventricular nodal branch of the RCA (*arrow*) indicates the location of AV node (floor of the right atrium)

sometimes misinterpreted as a tumor or thrombus. Cardiac CT can easily identify the location and extension of the fibromuscular prominent structure and can differentiate it from a neoplasm or a thrombus [1] (Fig. 1.6)

1.1.2.2 Eustachian Valve

- The Eustachian valve, persistent of the right sinus venosus valve, is located at the junction of the IVC and RA (Fig. 1.1).
- In a fetus, the Eustachian valve directs blood from the IVC to the foramen ovale. Normally, the Eustachian valve regresses during embryonic development. The lack of normal regression results in a prominent Eustachian valve or partial or complete septation of the RA, a condition referred to as cor triatriatum dexter [1, 2].
- The Eustachian valve is not routinely seen. Occasionally, persistent remnants of the valve may be large enough to be identified and may be mistaken for a tumor or thrombus [2]. Rarely, the Eustachian valve is complicated with endocarditis, tumor, or cyst [3].

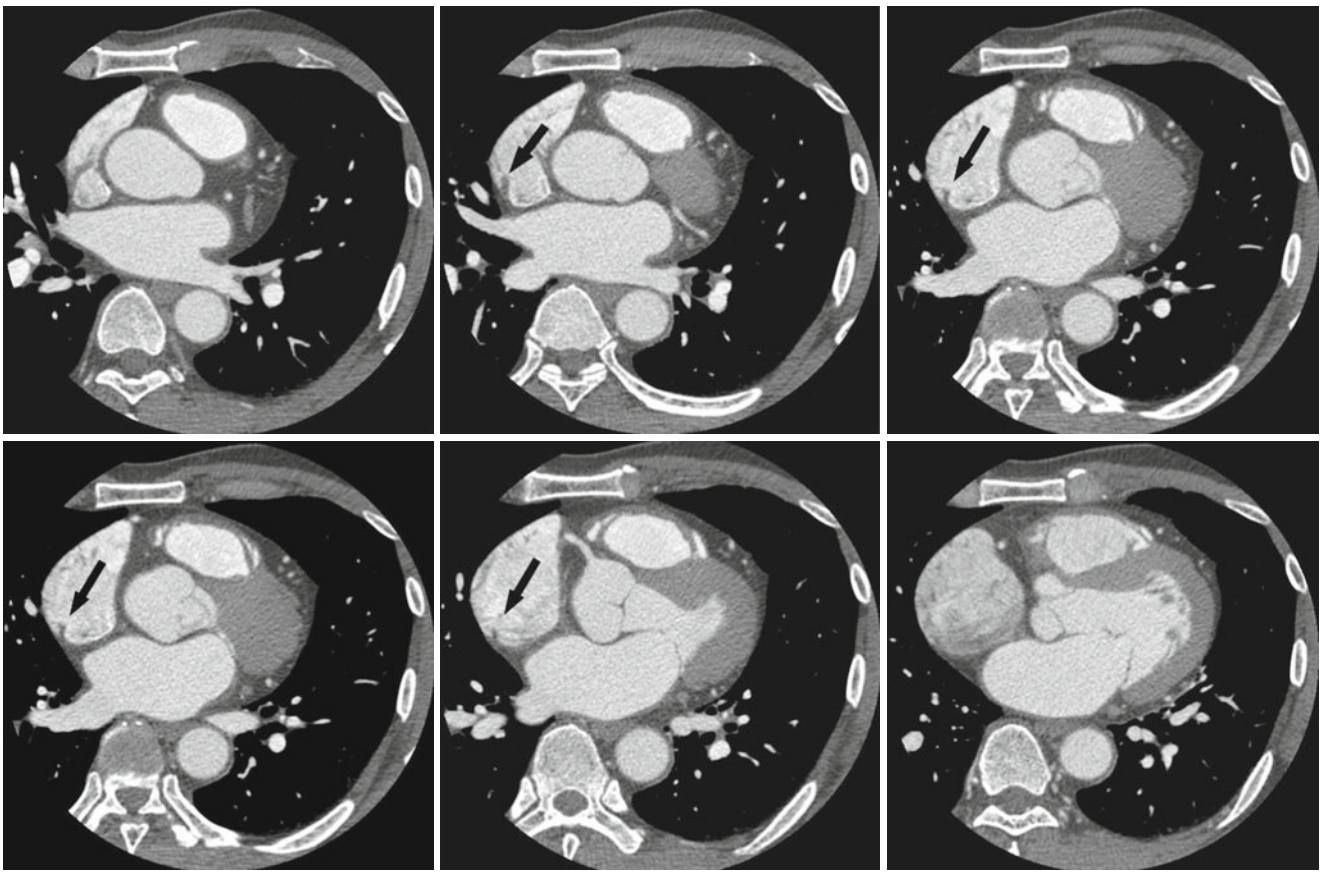

Fig. 1.6 Crista terminalis of the right atrium. Note vertically oriented internal muscular ridge (*arrows*) between the RA appendage and sinus venous components, from the SVC to the IVC

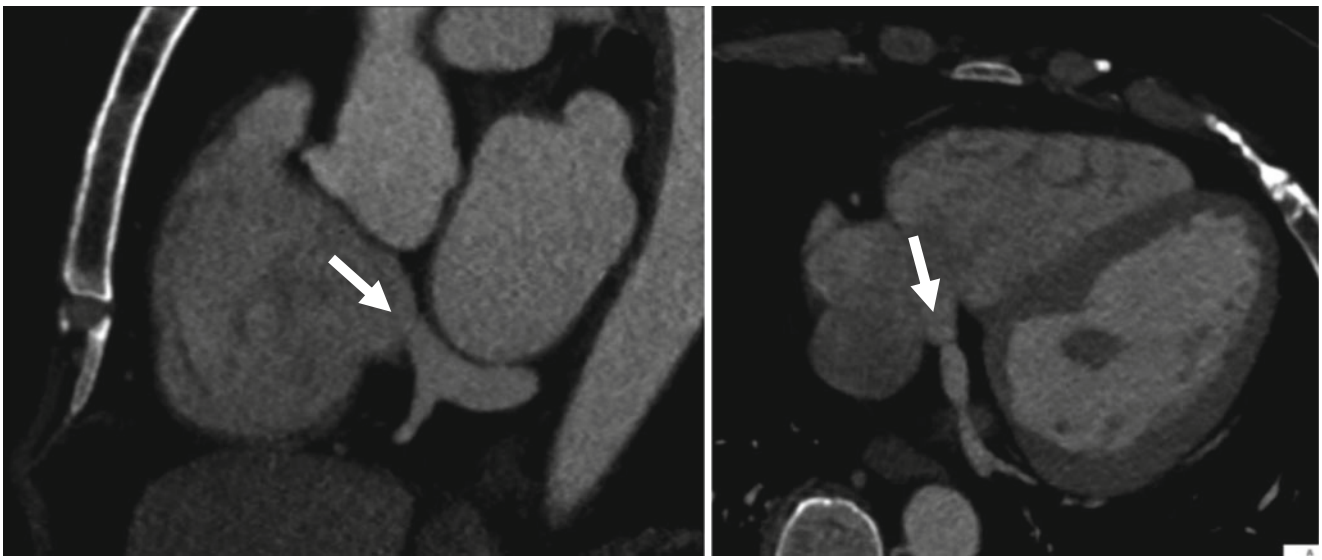

Fig. 1.7 Thebesian valve. Note the thin valve at the orifice of the coronary sinus (*arrows*)

1.1.2.3 Cor Triatriatum Dexter

- Cor triatriatum dexter has the same embryologic explanation as the Eustachian valve; however, cor triatriatum dexter is characterized by an attachment on the atrial septum giving the appearance of a divided atrium [4].

1.1.2.4 Thebesian Valve

- The Thebesian valve, also called as the valve of the CS, is a semicircular fold of the lining membrane of the RA at the orifice of the CS. It prevents reflux from the RA into the CS during contraction. The valve varies in size [5] (Fig. 1.7).
- Recently, the recognition of the Thebesian valve is more emphasized because it may cause difficulties during cardiac catheterization for cardiac resynchronization therapy [6].

1.2 Right Ventricle

1.2.1 Normal Anatomy

- The right ventricle (RV) is composed of an inlet with the tricuspid valve, an apical trabecular component, and a subpulmonic outflow tract.
- The inlet potion of the RV surrounds and supports the tricuspid valve and its tension apparatus. The tricuspid valve has three leaflets: septal (medial, conal), anterosuperior, and posterior (inferior). The septal leaflet attaches to the right ventricle septum, which makes the tricuspid valve distinguishable from the mitral valve. The valve leaflets connect to three papillary muscles through the chordae tendineae.
- The anterior papillary muscle has chordae tendineae that attach to the anterior and posterior cusps of the tricuspid valve, the posterior papillary muscle has chordae tendineae that attach to the posterior (inferior) and septal cusps, and the medial papillary muscle has chordae tendineae that attach to the anterior and septal cusps.
- The apical trabecular portion is continuous with the apparatus of the tricuspid valve. A well-known prominent trabeculation is the septomarginal trabeculation (septal band). The body of the septomarginal trabeculation runs to the apex of the ventricle, where it gives rise to the anterior papillary muscle before splitting into the general apical trabeculation. The anterior papillary muscle continues as the moderator band to the parietal wall of the RV. The moderator band contains the right bundle branch.
- Heavy trabeculation, coarse septal surface, and moderator band are the unique distinguishing features of the right ventricle (Figs. 1.8 and 1.9).
- The subpulmonic outflow tract, known as the pulmonary infundibulum (conus), is a tubular muscular structure that supports the leaflets of the pulmonary valve. The posterior wall of the infundibulum is formed by a prominent muscular ridge, known as the crista supraventricularis, that separates the tricuspid and pulmonary valves. It is also a unique feature of the RV because in the left ventricle, the aortic and mitral valves have fibrous continuity (Fig. 1.10).

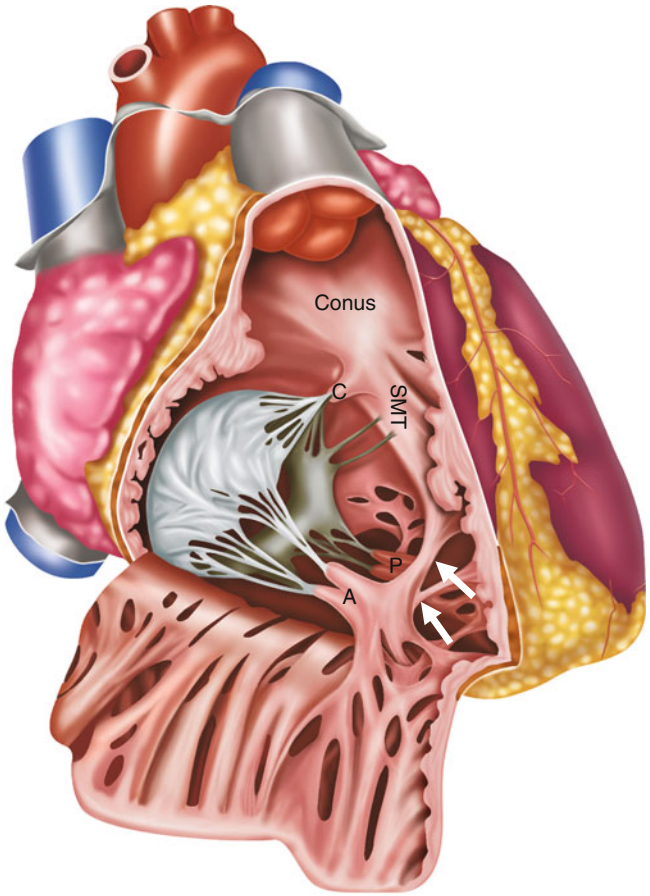

Fig. 1.8 Schematic illustration of anatomy of the right ventricle. Note the septomarginal trabeculation that gives rise to the anterior papillary muscle (*A*) and anterior papillary muscle continues as the moderator band (*arrows*). *C* conal papillary muscle, *A* anterior papillary muscle, *P* posterior papillary muscle, *SMT* septomarginal trabeculation

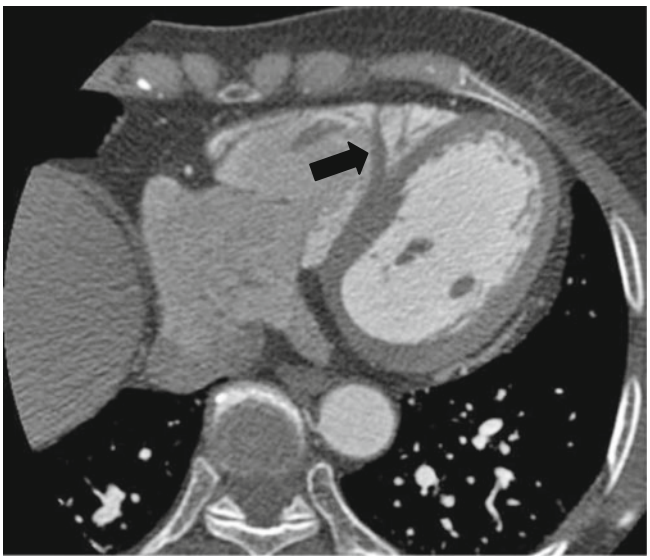

Fig. 1.9 Moderator band of the right ventricle on axial image (*arrow*)

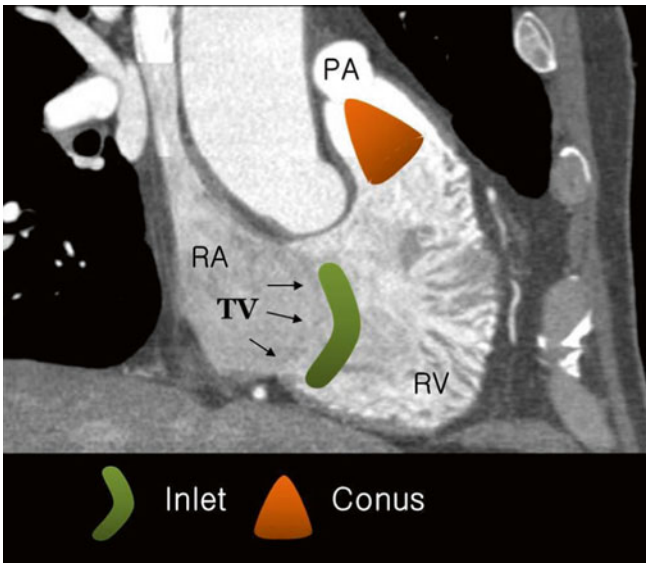

Fig. 1.10 Inlet and outlet (*conus*) of the right ventricle on oblique coronal image. Note heavy trabeculation of the right ventricular wall. *RA* right atrium, *RV* right ventricle, *TV* tricuspid valve

- The RV wall is normally very thin, approximately 3 mm in thickness.
- The pulmonary valve is composed of three leaflets: left, right, and posterior leaflets (Fig. 1.11).

1.2.2 Anatomic Pitfall and Normal Variance

1.2.2.1 Fat Deposition of the Right Ventricle

- Right ventricular fat infiltration is not rare in asymptomatic elderly patient. According to Kim et al. [7], RV fat infiltration occurs in about 17 % of asymptomatic subjects on CT. Fat infiltrations were most frequently seen in the superior wall of the base, middle segments, and the right ventricular outlow tract with normal or increased thickness (Fig. 1.12).
- The clinical significance of RV fat is not clear. Because autopsy studies indicate that the frequency and degree of RV myocardial fat increase with age, its development is considered as a part of aging process. The relationship between RV myocardial fat and other factors, such as gender and obesity, is disputed [8].
- Arrhythmogenic right ventricular dysplasia (ARVD) should be excluded when right ventricular fat infiltration is found in a symptomatic, young patient. The RV free wall of ARVD is usually almost thin because of fibrofatty replacement extending from the epicardium toward the endocardium. In contrast, with physiologic fat, the RV free wall maintains normal thickness or is sometimes thickened [8].

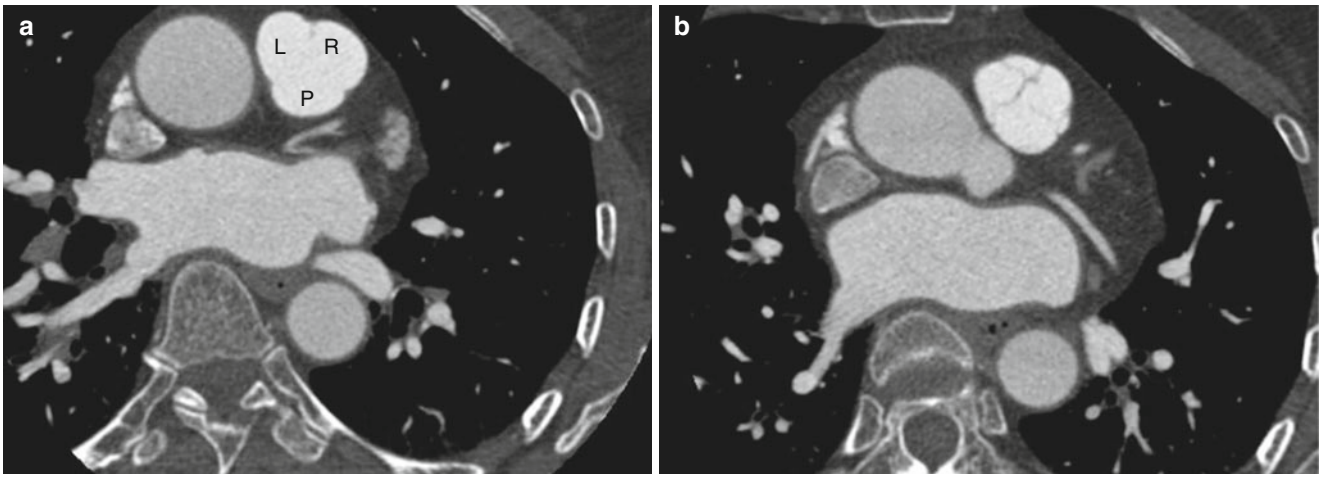

Fig. 1.11 Pulmonary valve with three leaflets (**a**, **b**): left (*L*), right (*R*), and posterior (*P*)

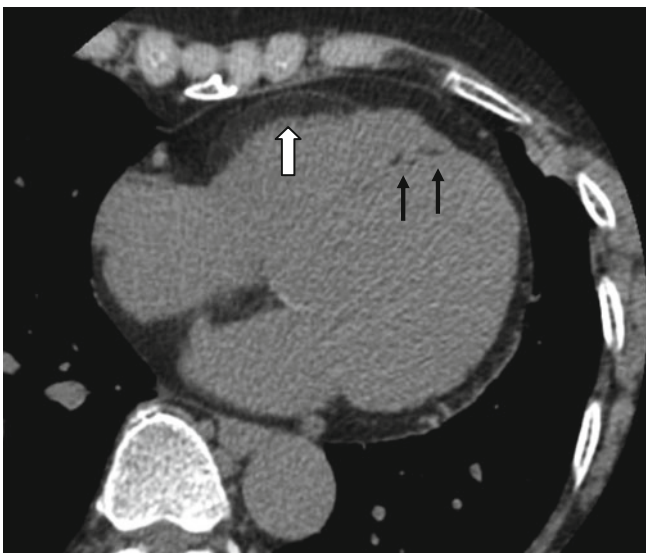

Fig. 1.12 Fat deposition of the right ventricle in a 75-year-old asymptomatic woman. Note fat deposition at right ventricular free wall (*white arrow*) and papillary muscles (*thin arrows*)

1.3 Left Atrium

1.3.1 Normal Anatomy

- The left atrium (LA) also consists of a venous component, appendage, and a supravalvular vestibule like the RA.
- The smooth-walled venous component is posteriorly located and receives blood from the four pulmonary veins.
- The LA appendage is derived from the primitive atrium and has pectinate muscle. It is a potential space for thrombus deposition because of its narrow neck with the LA. The vestibule supports the leaflets of the mitral valve.
- The mitral valve has anterior and posterior leaflets and shares the fibrous continuity with the aortic valve. The mitral valve annulus embedded in the myocardium is part of the cardiac skeleton (Fig. 1.13).

1.3.2 Anatomic Pitfall and Normal Variance

1.3.2.1 Accessory Left Atrial Appendage and Left Atrial Diverticulum

- *Accessory left atrial appendage* is an outpouching with a discernible ostium, neck, and body that display irregular contours suggestive of the pectinate muscles. Accessory appendages share a common embryonic origin from the primitive atrium with the LA appendage and have significant contractile function [9] (Fig. 1.14).
- *Left atrial diverticulum* is a saclike outpouching with a relatively broad-based ostium and a smooth contour of the body. LA diverticulum is thought to represent remnants of the cardinal venous system during embryologic development. Histologically diverticula contain normal myocardial wall structure and contract in synchrony with the rest of the atrium. However, a rare type of diverticulum that does not contain myocytes and does not exhibit contractile properties has also been found and is often classified as aneurysm [9] (Fig. 1.14).
- The prevalence and size of LA diverticula and accessory appendage are reported as 10–46 %, and 3.9–12 mm, respectively. The most common location of the LA diverticula and accessory appendage is the right anterosuperior LA wall [9].

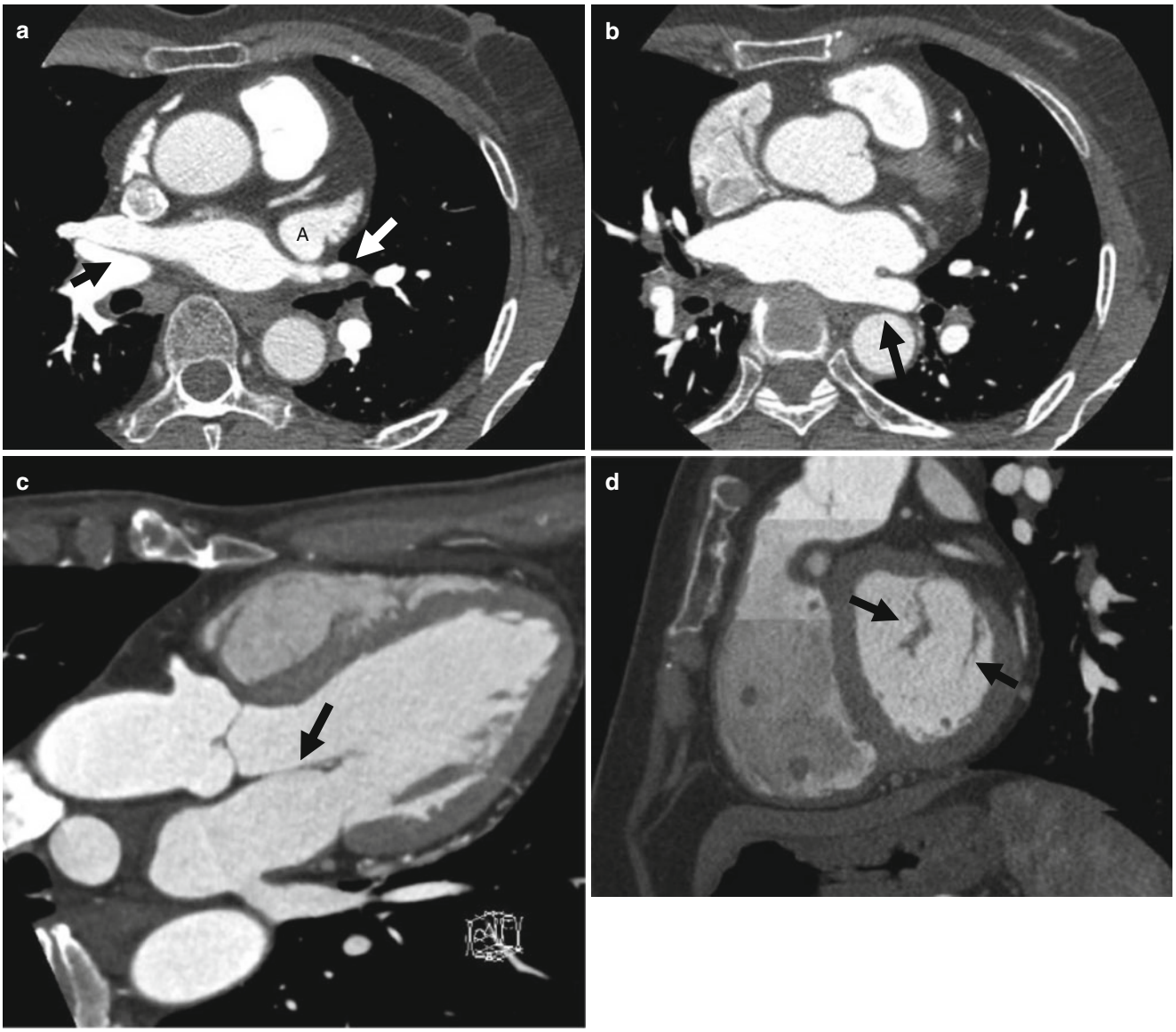

Fig. 1.13 Anatomy of the left atrium. (**a**, **b**) LA appendage (*A*) with pectinate muscle and posterior venous component draining pulmonary veins (*arrows*). (**c**) The mitral valve shares the fibrous continuity with the aortic valve (*arrows*). (**d**) Anterior and posterior leaflets of mitral valve on sagittal image (*arrows*)

- The size of accessory appendages and diverticula has been shown to correlate with the presence of ectopic electrical activity [1].
- It is important to report the presence of LA diverticula or appendage to the electrophysiologist in a patient who is planning for radiofrequency catheter ablation because their orifice may resemble the orifice of a pulmonary vein [10].

1.3.2.2 Cor Triatriatum Sinister and Remnant Common Pulmonary Vein

- Division of the left atrium by a fibromuscular diaphragm (cor triatriatum) is generally considered to be the result of an abnormal development of the junction between the pulmonary veins and the left atrium. Faulty incorporation of the common pulmonary vein, which is a temporary structure that communicates with the splanchnic plexus to establish pulmonary venous drainage to the left atrium, leaves it as a distinct structure in the left atrium. This "chamber" is separated from the anterior "fetal" left atrium (containing the left atrial appendage and communicating with the mitral valve) by a diaphragm and is known as *cor triatriatum*, one of the rarest of cardiac malformations [11] (Fig. 1.15).
- Less pronounced but still incomplete regression of this vein would result in the persistence of a portion of the common pulmonary vein appearing as a mass along the

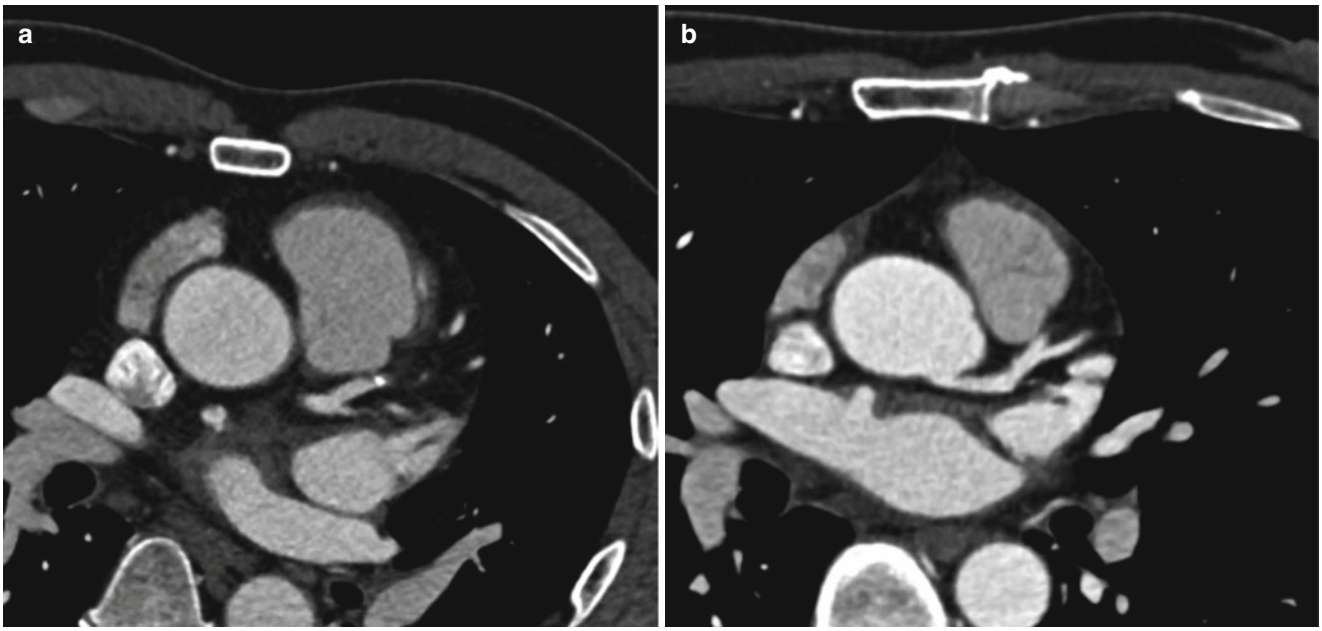

Fig. 1.14 Accessory left atrial appendage and left atrial diverticulum. (**a**) Accessory left atrial appendage. Note discernible ostium, neck, and irregular contoured body, suggesting pectinate muscle. (**b**) Saclike outpouching with broad base, suggesting left atrial diverticulum

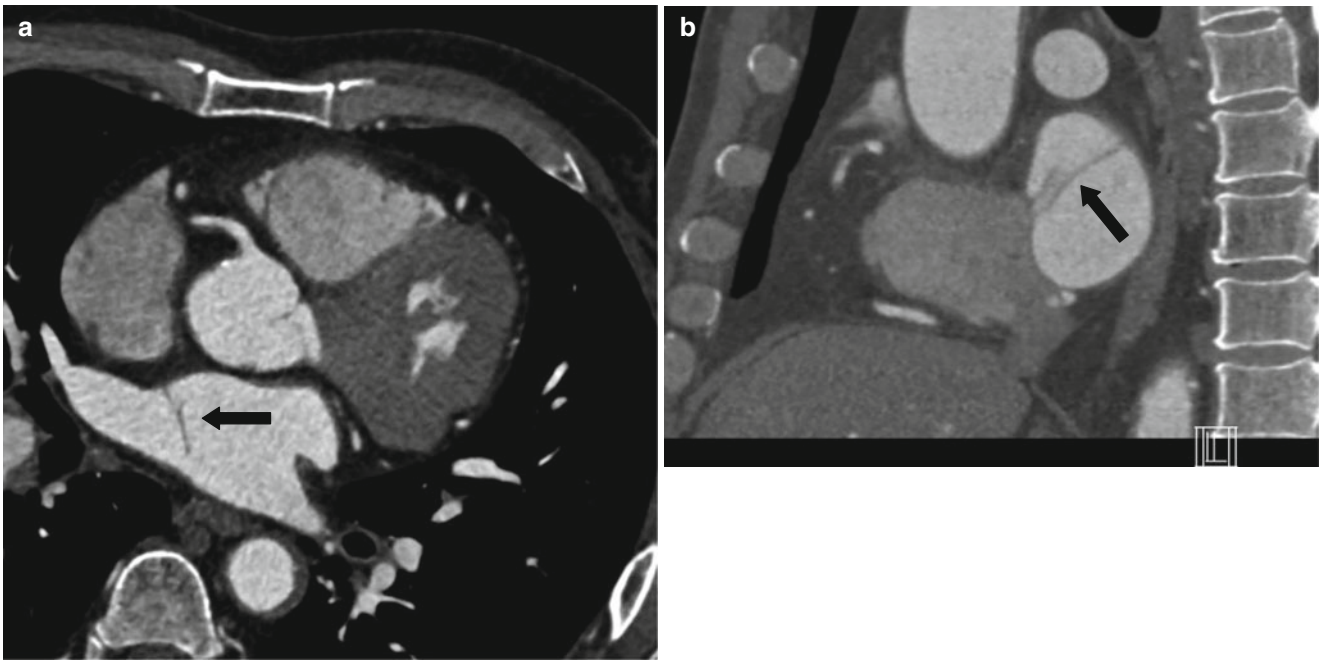

Fig. 1.15 Cor triatriatum sinister. Axial (**a**) and reformatted (**b**) images show thin diaphragm (*arrows*) separating left atrial chamber

lateral wall of the left atrium at the junction of the left atrial appendage and upper pulmonary vein [1].

1.3.2.3 Septum Primum Remnant (Atrial Septal Pouch) and Patent Foramen Ovale

- *Septum primum remnant (atrial septal pouch)*
  - In the fifth week of gestation, the cavity of the primitive atrium becomes subdivided into right and left chambers by a septum primum which grows downward into the cavity. The septum primum eventually fuses with the endocardiac cushion, while perforations appear in the superior part, forming the ostium secundum. In the meantime, to the right of the septum primum, the septum secundum starts to form as an invagination of the atrial wall. The septum secundum stops growing at the end of the seventh week of

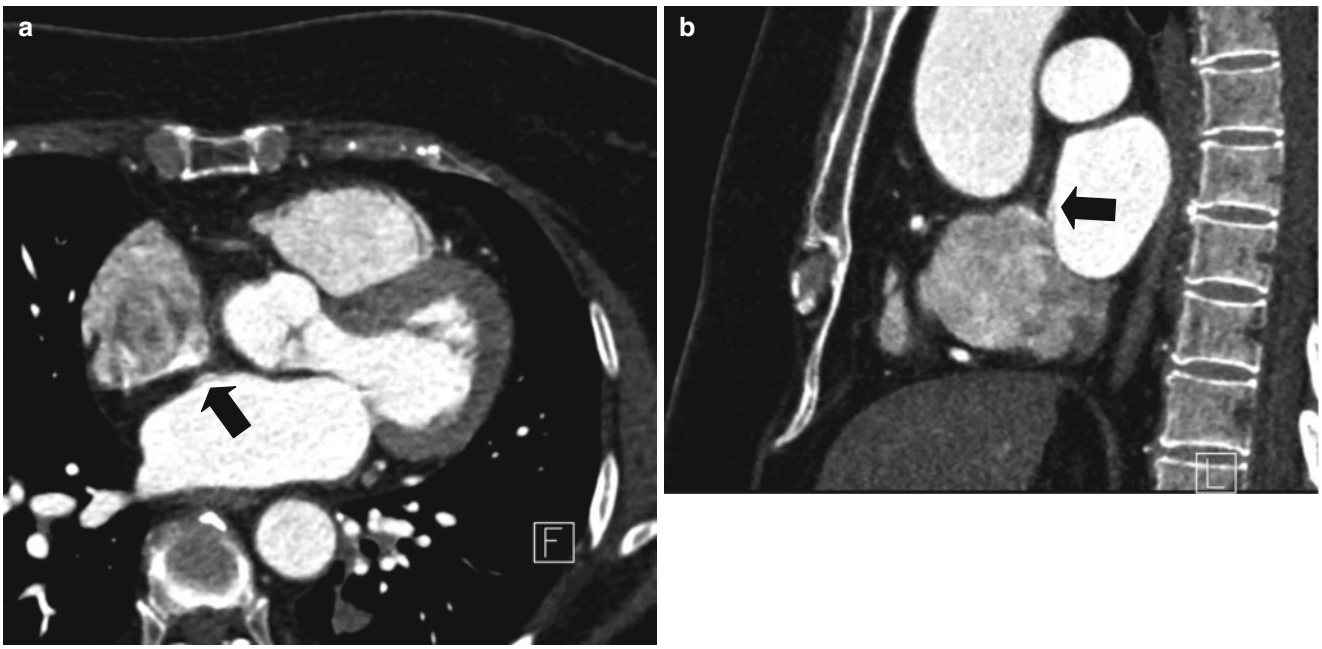

Fig. 1.16 Septum primum remnant. Axial (**a**) and reformatted (**b**) images show channel-like structure of interatrial septum (*arrows*). There is no contrast jet between atria

gestation, leaving a posterior and inferior gap known as the foramen ovale, supplying shunt blood flow from the inferior vena cava to the LA in utero. The lower part of the septum primum persists into adulthood and becomes the flap valve over the foramen ovale, which is a channel-like structure of the interatrial septum [1, 12–14] (Fig. 1.16)

- *Patent foramen ovale (PFO)*
  - After birth, right heart pressure decreases compared with the left as lung expansion, resulting in displacement of the flap valve against the septum secundum. Eventually the flap valve fuses with the septum secundum in two thirds of the population. The lack of fusion between the flap valve and septum secundum results in a probe patent foramen ovale (PFO) [15].
  - Traditionally transesophageal echocardiography (TEE) is the standard reference to diagnose the PFO. With intravenous agitated saline injection and the Valsalva maneuver, PFO is diagnosed when microbubbles are seen in the left cardiac chambers within three cardiac cycles of the maximum RA enhancement on TEE [12, 15].
  - Recently CT has become a useful diagnostic tool (sensitivity 73.1 %, specificity 98.4 %, PPV 90.5 % NPV 94.7 %). On CT, PFO is confirmed with a contrast jet from the LA to the RA toward the inferior vena cava with channel-like appearance of the interatrial septum [13] (Fig. 1.17).
  - Clinically PFO is a potential route for embolic transit from the systemic venous circulation to the brain. However, the precise role of PFO in the pathogenesis of cryptogenic stroke is not yet established [16].

Key Points

- *Septum primum remnant (atrial septal pouch)*
  - Failure of fusion between the two embryonic septa
  - Flap-like valve over the foramen ovale
  - Channel-like appearance of the interatrial septum on CT image
- *Patent foramen ovale (PFO)*
  - Incomplete closure of the interatrial septum at birth
  - Contrast jet from the LA to the RA through a channel-like interatrial septum on CT image

1.3.2.4 Interatrial Septal Aneurysm

- Interatrial septal aneurysm (IASA) indicates the saccular bulging of the interatrial septum into one or both atria (Fig. 1.18). The incidence of IASA with echocardiography is about 2–10 % of the general population [17]. Hanley's diagnostic criteria for IASA are the protrusion of the dilated portion of the septum of at least 1.5 cm beyond the plane of the atrial septum and phasic excursion of the interatrial septum during cardiac cycle of at least 1.1 cm in total amplitude with a diameter at the base of the aneurysm of at least 1.5 cm [18].

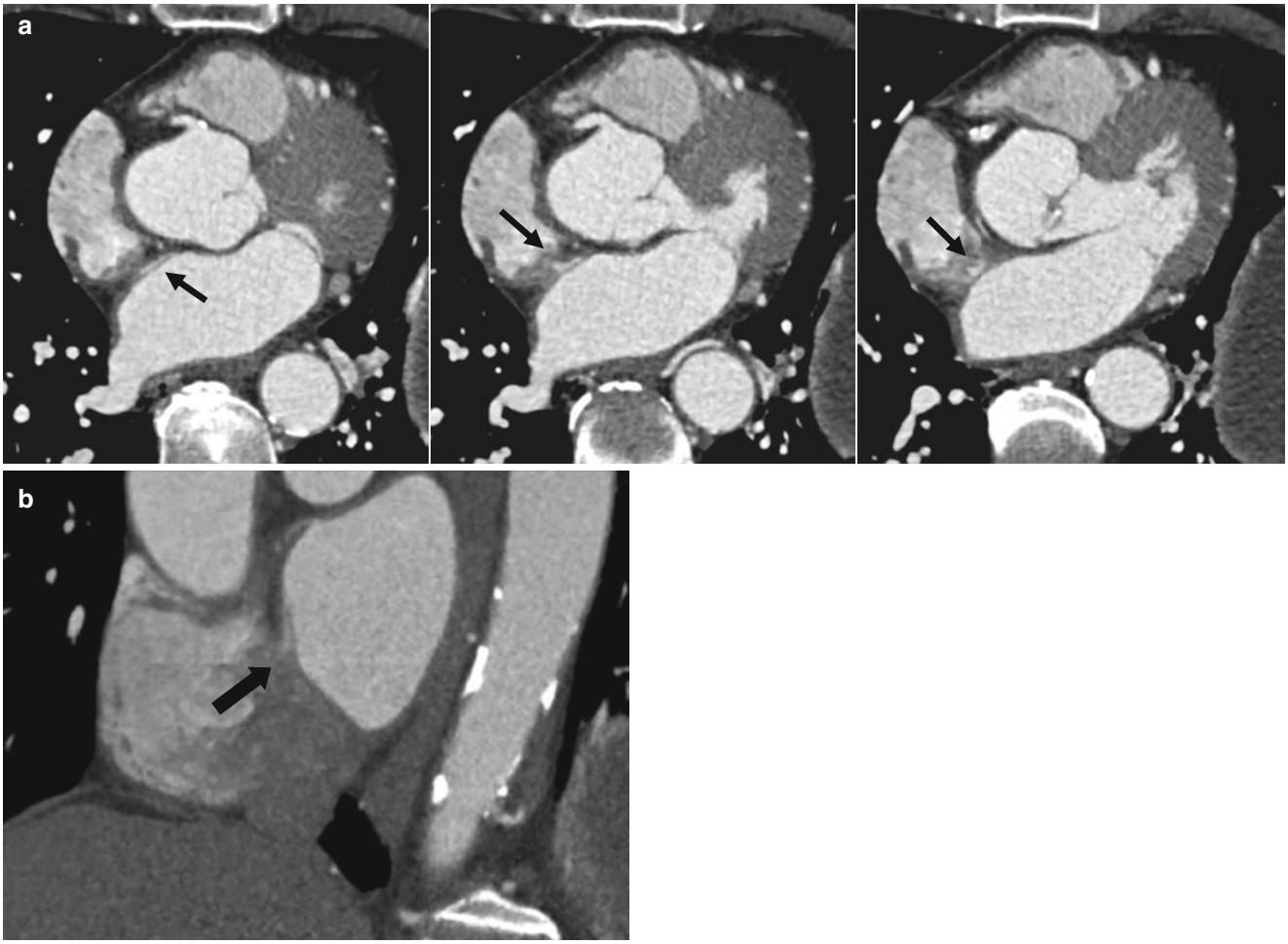

Fig. 1.17 Patent foramen ovale. Serial axial images (**a**) and reformatted image (**b**) show a contrast jet from the left atrium to right atrium toward the inferior vena cava with channel-like appearance of the interatrial septum (*arrows*), consisting of patent foramen ovale

- IASA is very commonly associated with PFO (approximately 72 %) while PFO is less commonly associated with IASA (about 22%) [17].
- IASA is known to increases the incidence of cryptogenic stroke in young patients. According to a meta-analysis on detection rates of atrial septal abnormalities in patients with cryptogenic stroke, IASA was present in about 4 to 25 % of the subjects. Redundant motion of the septum can occur in thrombi formation, and associated PFO or perforated complication could promote paradoxical embolism [19].

1.4 Left Ventricle

1.4.1 Normal Anatomy

- The left ventricle (LV) is composed of an inlet, apical trabecular component, and outlet, similar to the RV.
- The inlet portion of the LV is surrounded by the mitral valve (MV) and its tension apparatus, chordae tendineae and papillary muscles.

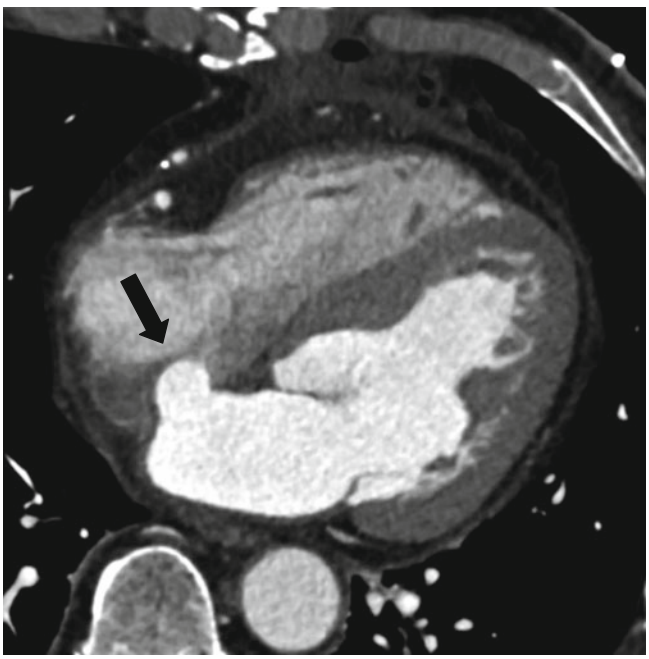

Fig. 1.18 Interatrial septal aneurysm (*arrow*)

- The MV has two cusps, anterior and posterior leaflets. The MV has fibrous continuity with the AV and no septal attachment, and these features make the MV distinguishable from the TV. The MV is supported by a rather dense collagenous annulus, known as the subvalvular membrane. Annular calcification is common and usually involves the posterior mitral ring.
- The LV contains anterior and posterior papillary muscles, which have chordae tendineae that attach to mitral leaflets (Fig. 1.19). The anterior papillary muscle is supplied by the branch of the left anterior descending artery, and the posterior papillary muscle is supplied by the branch of the dominant right coronary artery or the left circumflex artery.
- The apical trabecular component is characterized by fine trabeculations compared with those of the RV, a useful character in diagnosing morphologic LV in congenital heart disease. The LV apex is usually thin.
- The outlet of LV supports the aortic valve (AV). The AV is composed of an annulus, three cups, and commissures. Three cusps with outward bulging of aortic wall make the three sinuses of Valsalva as right coronary, left coronary, and non-coronary (posterior) sinuses (Fig. 1.20).
- The interventricular septum divides both ventricles. In the subaortic region, the septum is thin, referred to as the membranous septum. The tricuspid valve is attached to the membranous septum, dividing it into the atrioventricular and interventricular portions. The left bundle of the

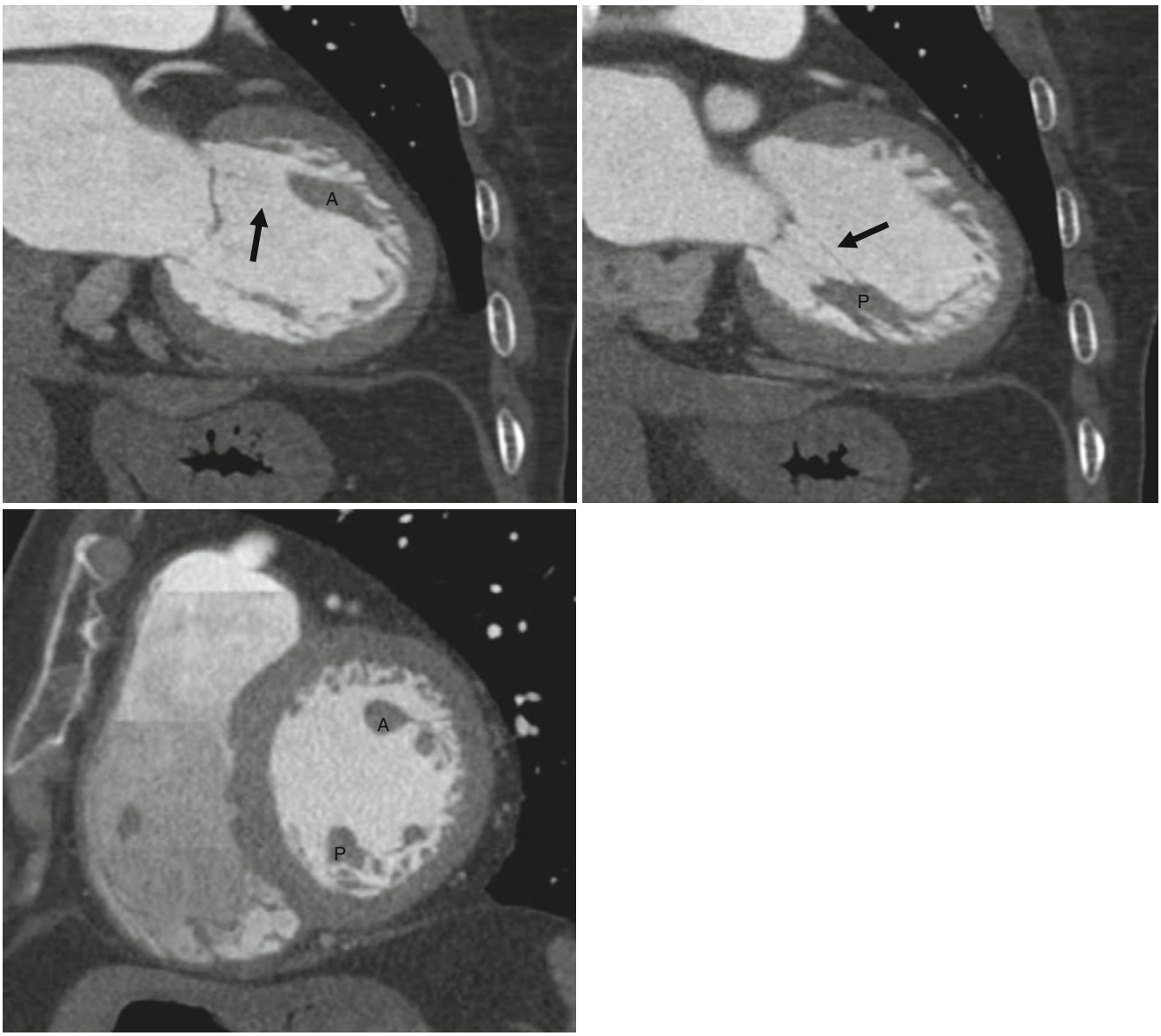

Fig. 1.19 Papillary muscle and chordae tendineae of the left ventricle. Anterior (*A*) and posterior (*P*) papillary muscles of the left ventricle have chordae tendineae (*arrows*) attaching to the mitral leaflets

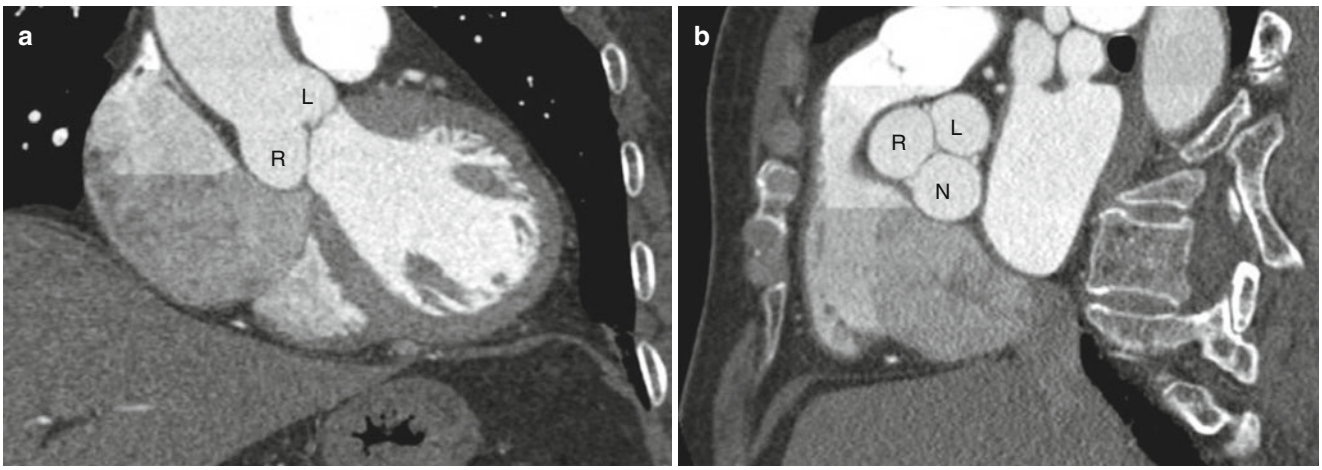

Fig. 1.20 Aortic valve. Coronal image (**a**) and reformatted image (**b**) show three cusps of the aortic valve: right (*R*), left (*L*), and non-coronary (*N*) cusp

cardiac conduction system enters the left ventricular outflow tract posterior to the membranous septum.

1.4.2 Anatomic Pitfall and Normal Variance

1.4.2.1 Left Ventricular Apical Thin Point

- Focal wall thinning at the ventricular apex can be seen in normal populations without symptoms or a previous history of a myocardial infarction. Cardiac function of the patient with left ventricular apical thin point is normal [1] (Fig. 1.21).

1.4.2.2 Interventricular Septal Aneurysm

- Ventricular septal aneurysm (VSA) appears as bulges with a distinct margin protruding into the right ventricle via the interventricular septum just under the aortic valve (Fig. 1.22).
- VSA has been known to be associated with perimembranous ventricular septal defects (VSDs). VSDs that accompany aneurysms of the membranous septum are more likely to spontaneously decrease in size or be closed than those without such aneurysms.
- VSA in adults is associated with conduction arrhythmias such as ventricular tachycardia, atrioventricular block, or bundle branch block because of its location, interfering the action of the His bundle [20].

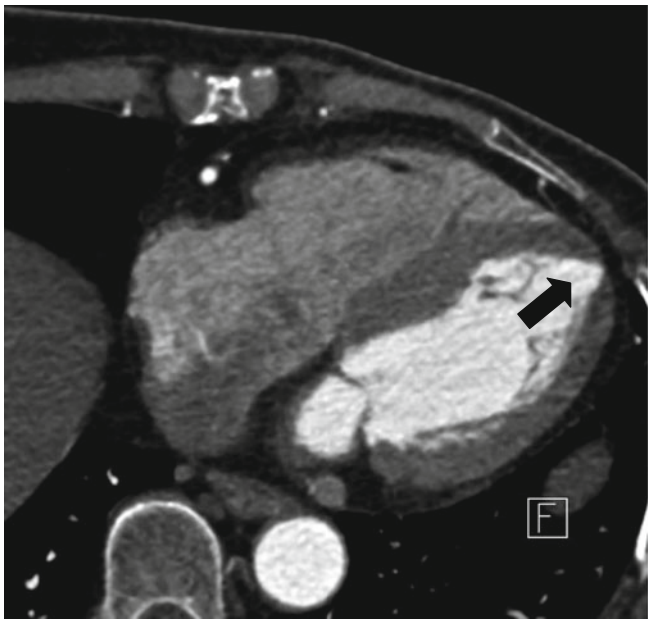

Fig. 1.21 Apical thin point of left ventricle in a 76-year-old man with normal cardiac function

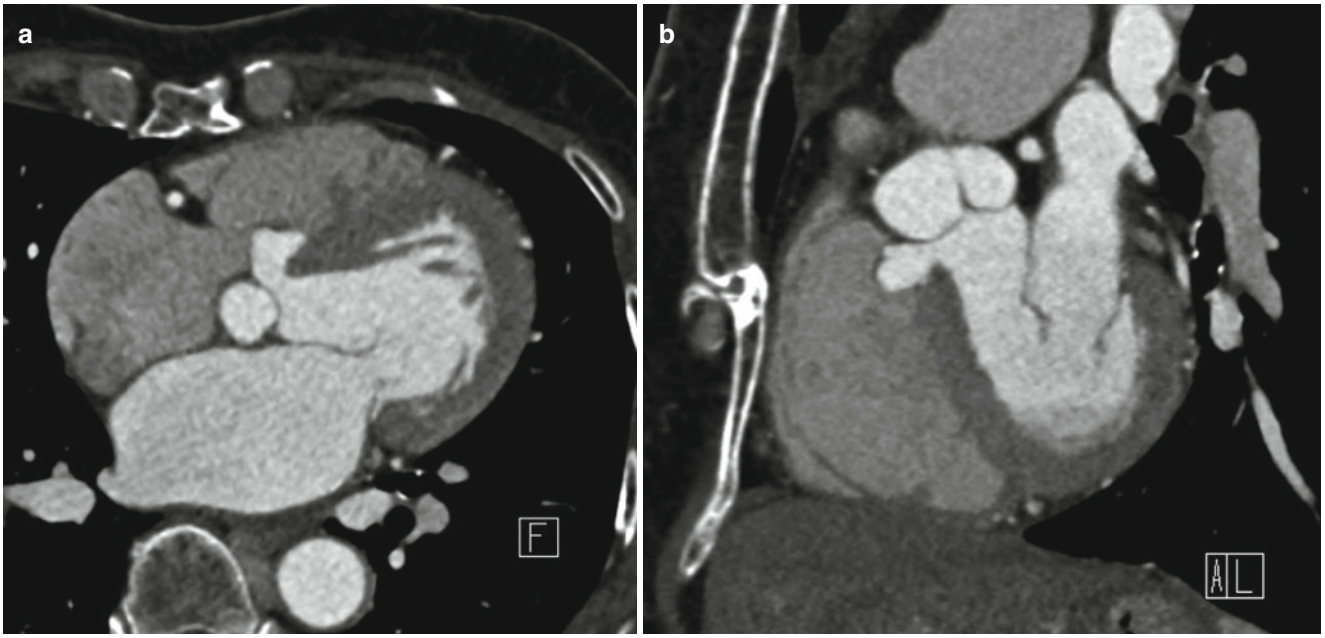

Fig. 1.22 Interventricular septal aneurysm. Axial (**a**) and reformatted (**b**) images show protrusion to the right ventricle via the interventricular septum, just under the aortic valve

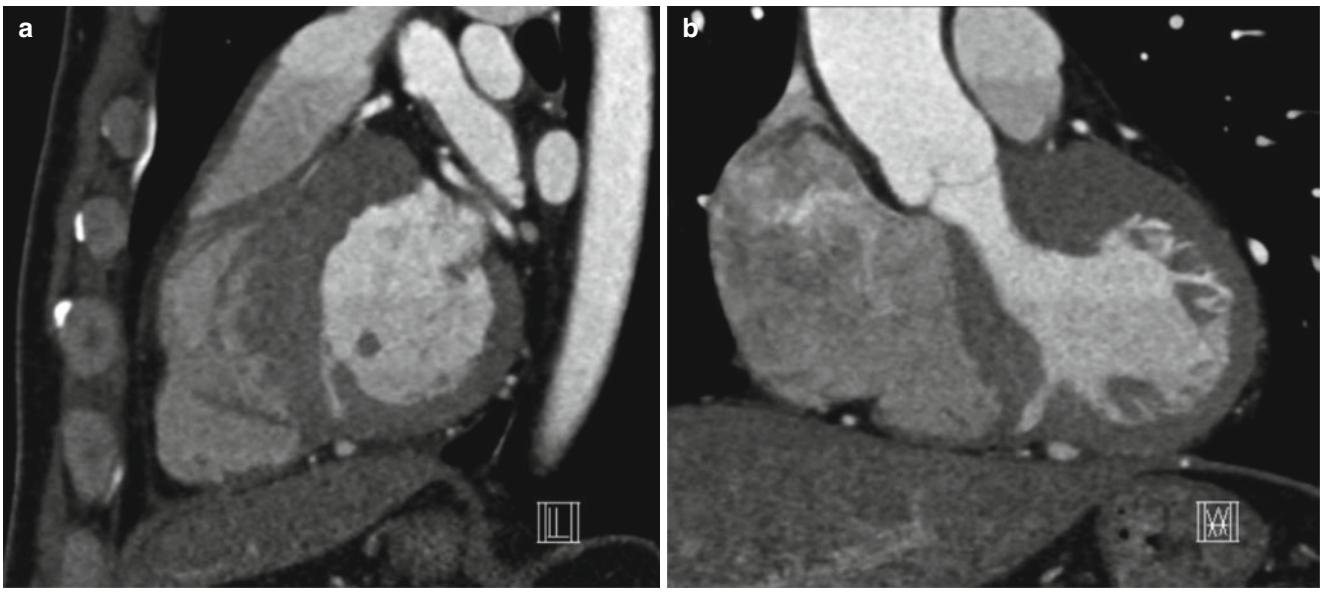

Fig. 1.23 Left ventricle crypt. Sagittal (**a**) and coronal (**b**) reformatted images show linear defect with contrast filling, confined by the myocardium at the inferoseptal wall of left ventricle

1.4.2.3 Left Ventricle Crypt

- Ventricular crypt indicates a linear defect with contrast filling or V-shaped fissure extending into but confined by the myocardium. It is located predominantly at the insertion points of the right ventricle into the left ventricle, mid- to basal inferoseptal wall of LV wall [21] (Fig. 1.23)
- Although ventricular crypt is found incidentally, ventricular crypt is known to be strongly related with hypertrophic cardiomyopathy (HCM) mutation carriers. HCM mutation carriers who had not yet developed LV hypertrophy show high occurrence of ventricular crypt (81 %) [22].

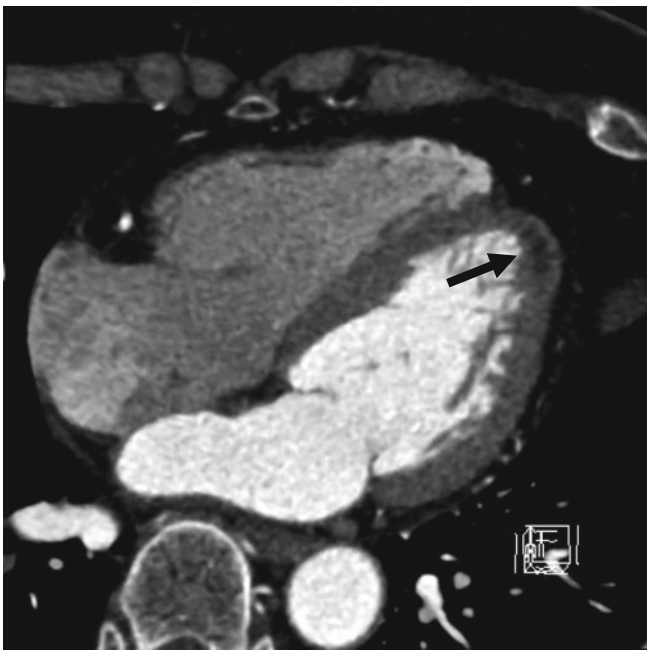

Fig. 1.24 Physiologic fat deposit in the left ventricle in a 67-year-old woman. Note fat deposit in the left ventricle apex (*arrow*). The patient has no history of myocardial infarction and no evidence of ECG or functional abnormality

- Multiple crypts in the absence of LV hypertrophy are highly specific for HCM mutation carriers and warrant clinical follow-up in recent report [23].

1.4.2.4 Left Ventricle Fat Deposit

- Small amount of fat are sometimes seen in LV, especially in the apex [8] (Fig. 1.24).

1.5 Cardiac Imaging Planes

- Functional and anatomic evaluation of the heart and the cardiac cavities requires multiple oblique planes along the axes of the heart itself. Although the exact position of these planes across the heart will vary depending on the clinical requirements and the need for visualization of different anatomic structures, commonly used image planes are present. It is essential to know how to acquire these image planes from the orthogonal planes sequentially (Fig. 1.25, illustration).

1.5.1 Vertical Long-Axis View (Two-Chamber View)

- Parasagittal plane oriented along the long axis of the LV lumen, so-called two-chamber view and used for evaluating the relationship between the left atrium and left ventricle (Fig. 1.26).
- Optimal to view the inferior and anterior walls of the LV myocardium and mitral valve as well.
- The LA appendage and coronary sinus are always seen.

1.5.2 Horizontal Long-Axis View (Four-Chamber View)

- A horizontal plane through the heart that essentially bisects all four cardiac chambers, providing assessment of chamber size and valve position (Fig. 1.27)
- Simultaneously evaluate the septal, apical, and lateral LV walls

1.5.3 Left Ventricular Outflow Tract (LVOT) View (Three-Chamber View)

- Oblique long-axis view that optimizes visualization of the LV, LA, aortic root, MV, and aortic valve (Fig. 1.28)
- Obtained from an oblique plane positioned on a coronal image along the long axis of the heart parallel to the aortic outflow tract or from an oblique plane positioned on a two chamber view along the long axis of the heart
- Very similar to the parasternal long-axis view of echocardiography and is useful for the evaluation of aortic valve anomalies

1.5.4 Short-Axis View

- An oblique coronal plane relative to the thorax, down the barrel of the LV lumen, evaluating the basal, middle, and apical portions of the LV myocardium (Fig. 1.29)
- Allowing easy assessment of LV size and myocardial contractility according to coronary artery territory

1.5.5 Right Ventricular Outflow Tract (RVOT) View

- Obtained from an oblique plane positioned on a sagittal image parallel to RVOT (Fig. 1.10)
- Optimized to assess the infundibulum and pulmonary valve

1.5.6 Aortic Valve View

- Obtained from a vertical cross-sectional view of aortic root positioned on a coronal image
- Optimized to assess the aortic valve morphology (Fig. 1.20)

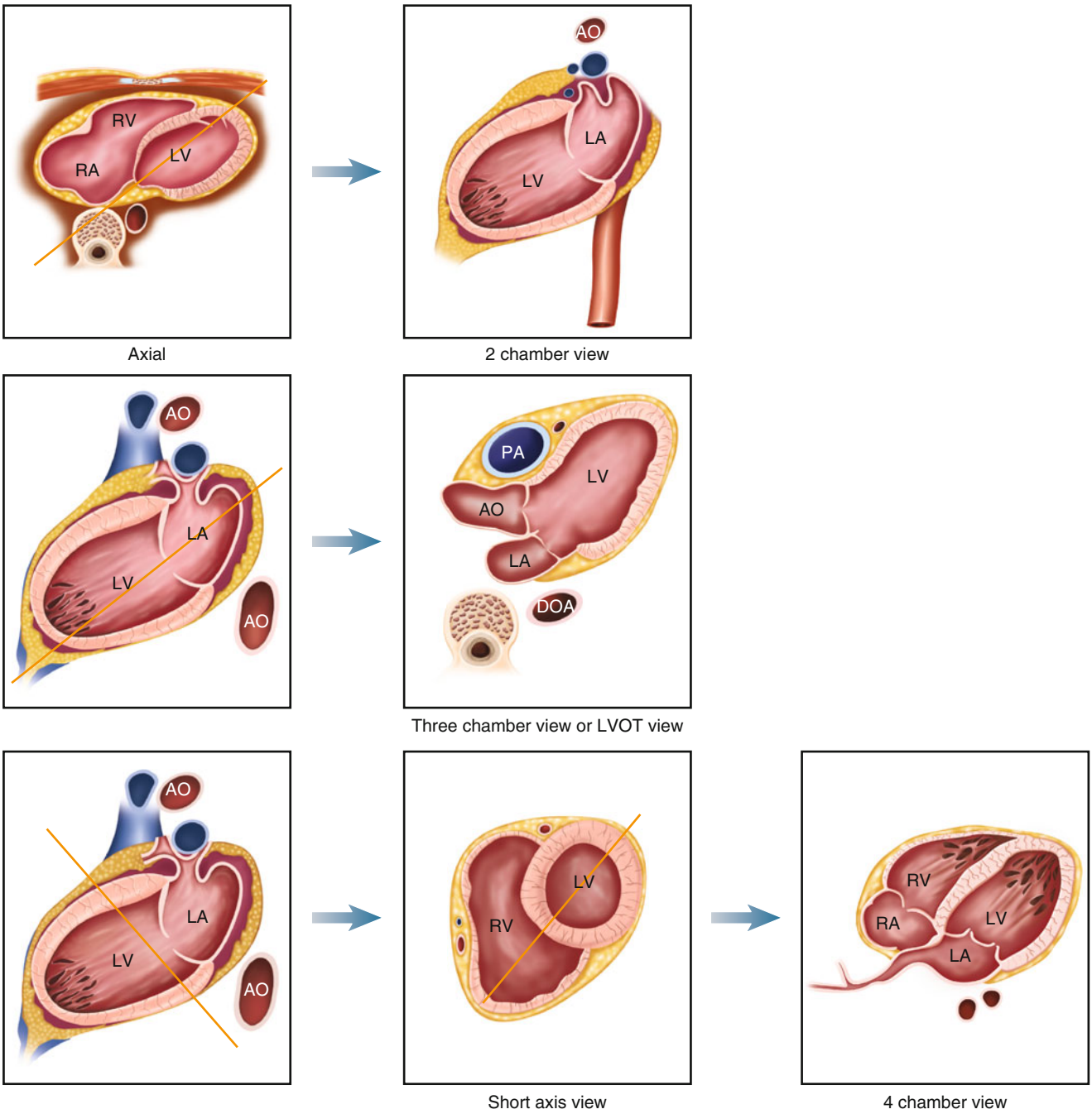

Fig. 1.25 Schematic illustration of cardiac image planes

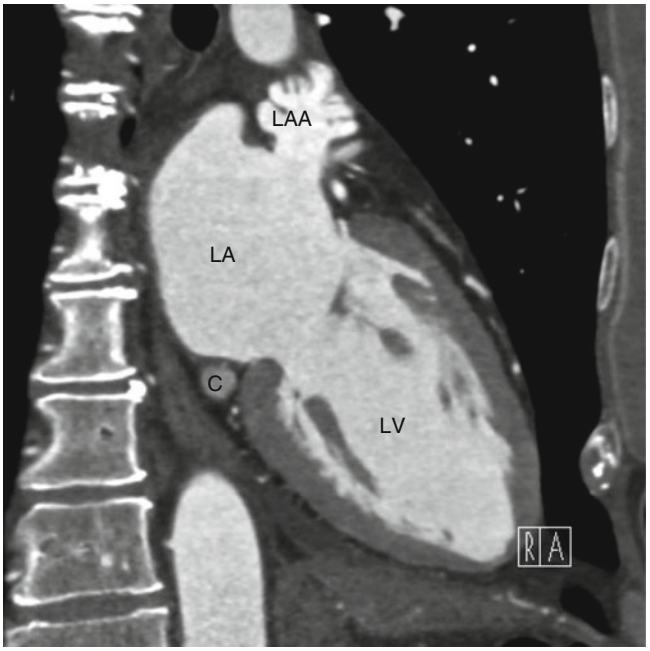

Fig. 1.26 Two-chamber view. *LA* left atrium, *LV* left ventricle, *C* coronary sinus, *LAA* LA appendage

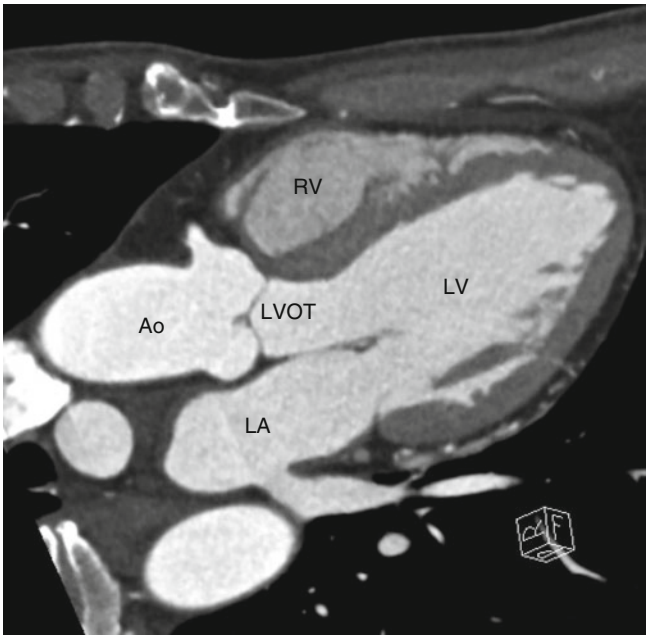

Fig. 1.28 Three-chamber view. *LVOT* left ventricular outflow tract, *Ao* aortic root

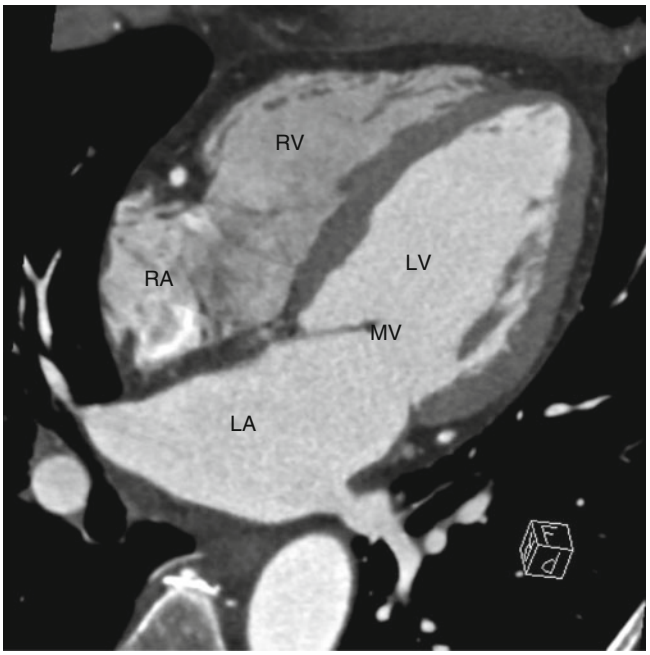

Fig. 1.27 Four-chamber view. *MV*: mitral valve

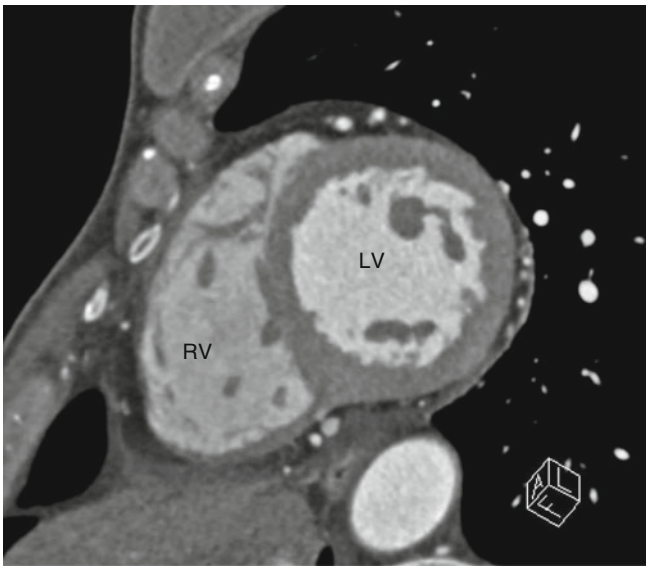

Fig. 1.29 Short-axis view

References

1. Kim EY, Park JH, Choe YH, Lee SC. Normal variations and anatomic pitfalls that may mimic diseases on coronary CT angiography. Int J Cardiovasc Imaging. 2010;26 Suppl 2: 281–94.
2. Broderick LS, Brooks GN, Kuhlman JE. Anatomic pitfalls of the heart and pericardium. Radiographics. 2005;25:441–53.
3. Cho HJ, Jung JI, Kim HW, Lee KY. Intracardiac eustachian valve cyst in an adult detected with other cardiac anomalies: usefulness of multidetector CT in diagnosis. Korean J Radiol. 2012;13: 500–4.
4. Roldán FJ, Vargas-Barrón J, Espinola-Zavaleta N, Romero-Cárdenas A, Vázquez-Antona C, Burgueño GY, Muñoz-Castellanos L, Zabalgoitia M. Three-dimensional echocardiography of the right atrial embryonic remnants. Am J Cardiol. 2002;89:99–101.
5. Hellerstein HK, Orbison JL. Anatomic variations of the orifice of the human coronary sinus. Circulation. 1951;3:514–23.
6. Katti K, Patil NP. The thebesian valve: gatekeeper to the coronary sinus. Clin Anat. 2012;25:379–85.
7. Kim E, Choe YH, Han BK, Kim SM, Kim JS, Park SW, Sung J. Right ventricular fat infiltration in asymptomatic subjects: observations from ECG-gated 16-slice multidetector CT. J Comput Assist Tomogr. 2007;31:22–8.
8. Kimura F, Matsuo Y, Nakajima T, Nishikawa T, Kawamura S, Sannohe S, Hagiwara N, Sakai F. Myocardial fat at cardiac imaging: how can we differentiate pathologic from physiologic fatty infiltration? Radiographics. 2010;30:1587–602.
9. Abbara S, Mundo-Sagardia JA, Hoffmann U, Cury RC. Cardiac CT assessment of left atrial accessory appendages and diverticula. Am J Roentgenol. 2009;193:807–12.
10. Lazoura O, Reddy T, Shriharan M, Lindsay A, Nicol E, Rubens M, Padley S. Prevalence of left atrial anatomical abnormalities in patients with recurrent atrial fibrillation compared with patients in sinus rhythm using multi-slice CT. J Cardiovasc Comput Tomogr. 2012;6:268–73.
11. Mortensson W. Radiologic diagnosis of cor triatriatum in infants. Pediatr Radiol. 1973;1:92–5.
12. Kerut EK, Norfleet WT, Plotnick GD, Giles TD. Patent foramen ovale: a review of associated conditions and the impact of physiological size. J Am Coll Cardiol. 2001;38:613–23.
13. Kim YJ, Hur J, Shim CY, Lee HJ, Ha JW, Choe KO, Heo JH, Choi EY, Choi BW. Patent foramen ovale: diagnosis with multidetector CT-comparison with transesophageal echocardiography. Radiology. 2009;250:61–7.
14. Rojas CA, El-Sherief A, Medina HM, Chung JH, Choy G, Ghoshhajra BB, Abbara S. Embryology and developmental defects of the interatrial septum. Am J Roentgenol. 2010;195:1100–4.
15. Hara H, Virmani R, Ladich E, Mackey-Bojack S, Titus J, Reisman M, Gray W, Nakamura M, Mooney M, Poulose A, Schwartz RS. Patent foramen ovale: current pathology, pathophysiology, and clinical status. J Am Coll Cardiol. 2005;46:1767–76.
16. Kutty S, Sengupta PP, Khandheria BK. Patent foramen ovale: the known and the to be known. J Am Coll Cardiol. 2012;59:1665–71.
17. Agmon Y, Khandheria BK, Meissner I, Gentile F, Whisnant JP, Sicks JD, O'Fallon WM, Covalt JL, Wiebers DO, Seward JB. Frequency of atrial septal aneurysms in patients with cerebral ischemic events. Circulation. 1999;99:1942–4.
18. Hanley PC, Tajik AJ, Hynes JK, Edwards WD, Reeder GS, Hagler DJ, Seward JB. Diagnosis and classification of atrial septal aneurysm by two-dimensional echocardiography: report of 80 consecutive cases. J Am Coll Cardiol. 1985;6:1370–88.
19. Overell JR, Bone I, Lees KR. Interatrial septal abnormalities and stroke: a meta-analysis of case-control studies. Neurology. 2000;55:1172–9.
20. Choi M, Jung JI, Lee BY, Kim HR. Ventricular septal aneurysms in adults: findings of cardiac CT images and correlation with clinical features. Acta Radiol. 2011;52:619–23.
21. Srichai MB, Hecht EM, Kim DC, Jacobs JE. Ventricular diverticula on cardiac CT: more common than previously thought. Am J Roentgenol. 2007;189:204–8.
22. Germans T, Wilde AA, Dijkmans PA, Chai W, Kamp O, Pinto YM, van Rossum AC. Structural abnormalities of the inferoseptal left ventricular wall detected by cardiac magnetic resonance imaging in carriers of hypertrophic cardiomyopathy mutations. J Am Coll Cardiol. 2006;48:2518–23.
23. Brouwer WP, Germans T, Head MC, van der Velden J, Heymans MW, Christiaans I, Houweling AC, Wilde AA, van Rossum AC. Multiple myocardial crypts on modified long-axis view are a specific finding in pre-hypertrophic HCM mutation carriers. Eur Heart J Cardiovasc Imaging. 2012;13:292–7.

Coronary Anatomy and Anomalies

2

Bae Young Lee

Contents

Abstract

The evaluation of the precise course coronary arteries at angiography is limited because of its complex 3-dimensional geometry displayed in 2-dimensional fluoroscopy. Development of multidetector computed tomography (CT) allows the acquisition of isotropic voxels. With these scanners, image acquisition of the heart and coronary arteries with volume of data is possible. Variable postprocessing techniques including multiplanar reformation (MPR), maximum intensity projection (MIP), volume rendering (VR), curved reformation, and cine imaging allow noninvasive assessment of every aspect of the cardiovascular system. Multidetector row CT is superior to conventional angiography in defining the ostial origin and proximal path of anomalous coronary arteries.

In this section, we review and illustrate the anatomy of the coronary arteries and anomalies [1, 2].

2.1 General Concept of Coronary Arteries, Main Coronary Arteries

- Usually located in epicardial fat, sometimes located in the myocardium (myocardial bridge).
- The left main coronary artery (LM) arises from the left coronary sinus.
- The right coronary artery (RCA) arises from the right coronary sinus.
- The ostia of coronary arteries: usually located in the upper third of the sinuses, superior and posterior in the LM compared to the RCA.

Electronic supplementary material Supplementary material is available in the online version of this chapter at 10.1007/978-3-642-36397-9_2.

B.Y. Lee
Department of Radiology, St. Paul's Hospital, College of Medicine, The Catholic University of Korea, Seoul, Republic of Korea
e-mail: leebae@catholic.ac.kr

T.-H. Lim (ed.), *Practical Textbook of Cardiac CT and MRI*,
DOI 10.1007/978-3-642-36397-9_2, © Springer-Verlag Berlin Heidelberg 2015

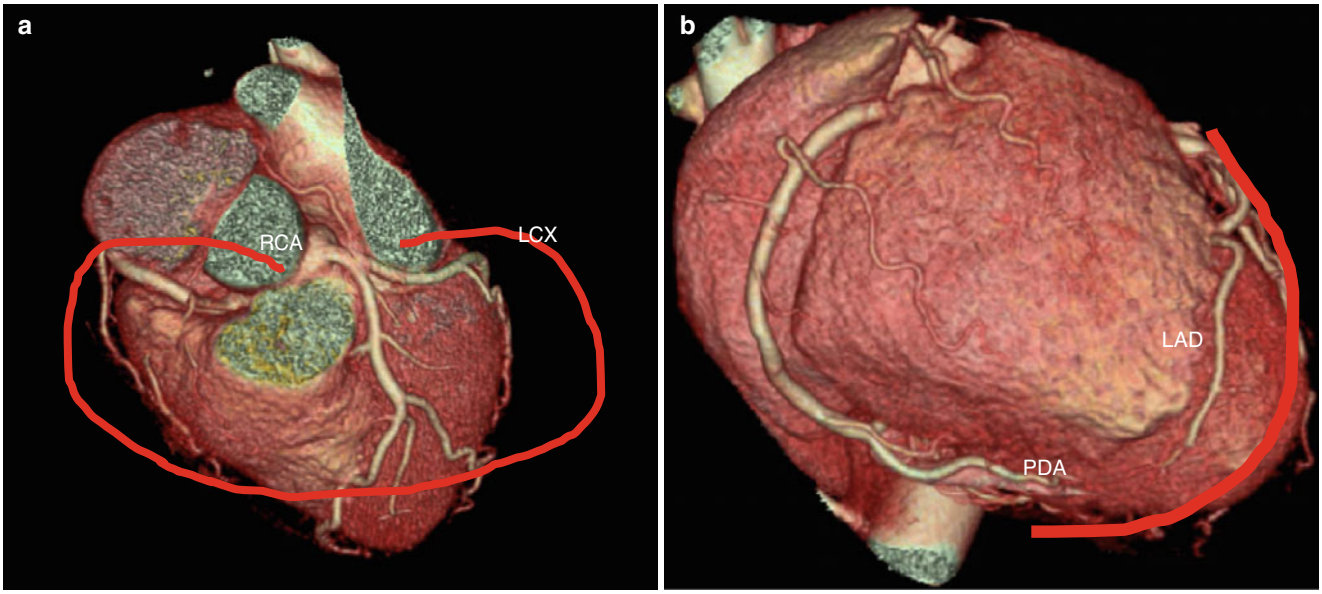

Fig. 2.1 (**a**) Circle. The RCA and LCX make a circle along the both atrioventricular grooves. (**b**) Loop. The LAD and PDA make a loop along the anterior and posterior interventricular grooves

- The LM bifurcates into the left anterior descending artery (LAD) and the left circumflex artery (LCX).
- The LAD courses anterolaterally in the anterior interventricular groove toward the apex. Major branches are the septal and diagonal (D).
- The LCX runs in the left atrioventricular groove. The major branch is the obtuse marginal (OM).
- The RCA runs in the right atrioventricular groove. Major branches are the posterior descending (PDA) and posterolateral (PL).
- Circle and loop: the RCA and LCX make a circle along both the atrioventricular grooves and LAD and PDA make a loop along the anterior and posterior interventricular grooves. These circle and loop have the potential of collateral supply (Fig. 2.1a, b) [3–5].

2.2 Dominance

- PDA and PL branches supplying inferior wall of left ventricle determine dominance.
- Right dominance (85 %): PDA and PL from RCA (Fig. 2.2a).
- Left dominance (8 %): PDA and PL from LCX (Fig. 2.2b).
- Codominance (7 %): PDA from RCA and PL from LCX or parallel branch from the right and left coronary arteries (Fig. 2.2c).

2.3 Coronary Arteries

2.3.1 Left Main Coronary Artery

Left main coronary artery usually bifurcates into left anterior descending artery (LAD) and left circumflex artery (LCX) with 5 - 10 mm length and 4 - 5 mm in diameter. Sometimes, it trifurcates into LAD, LCX, and ramus intermedius.

2.3.2 Left Anterior Descending Artery (LAD) (Fig. 2.3a, b)

- Diagonal branches supply the anterolateral wall of the left ventricle. The first branch is usually the largest. These branches are numbered as they arise from the LAD territory such as first diagonal (D1), second diagonal (D2), etc.
- Septal branches: perpendicular into the interventricular septum. The first branch is the largest and supplies the His bundle and proximal left bundle branch. It usually originates just beyond the orifice of the first diagonal branch.
- Ramus intermedius: originated from LM between LAD and LCX; its course is similar to that of D1.
- Proximal LAD: from the orifice to the origin of the first septal branch.
- Middle LAD: from the origin of the first septal branch halfway to the apex.
- Distal LAD: remained halfway to the apex.

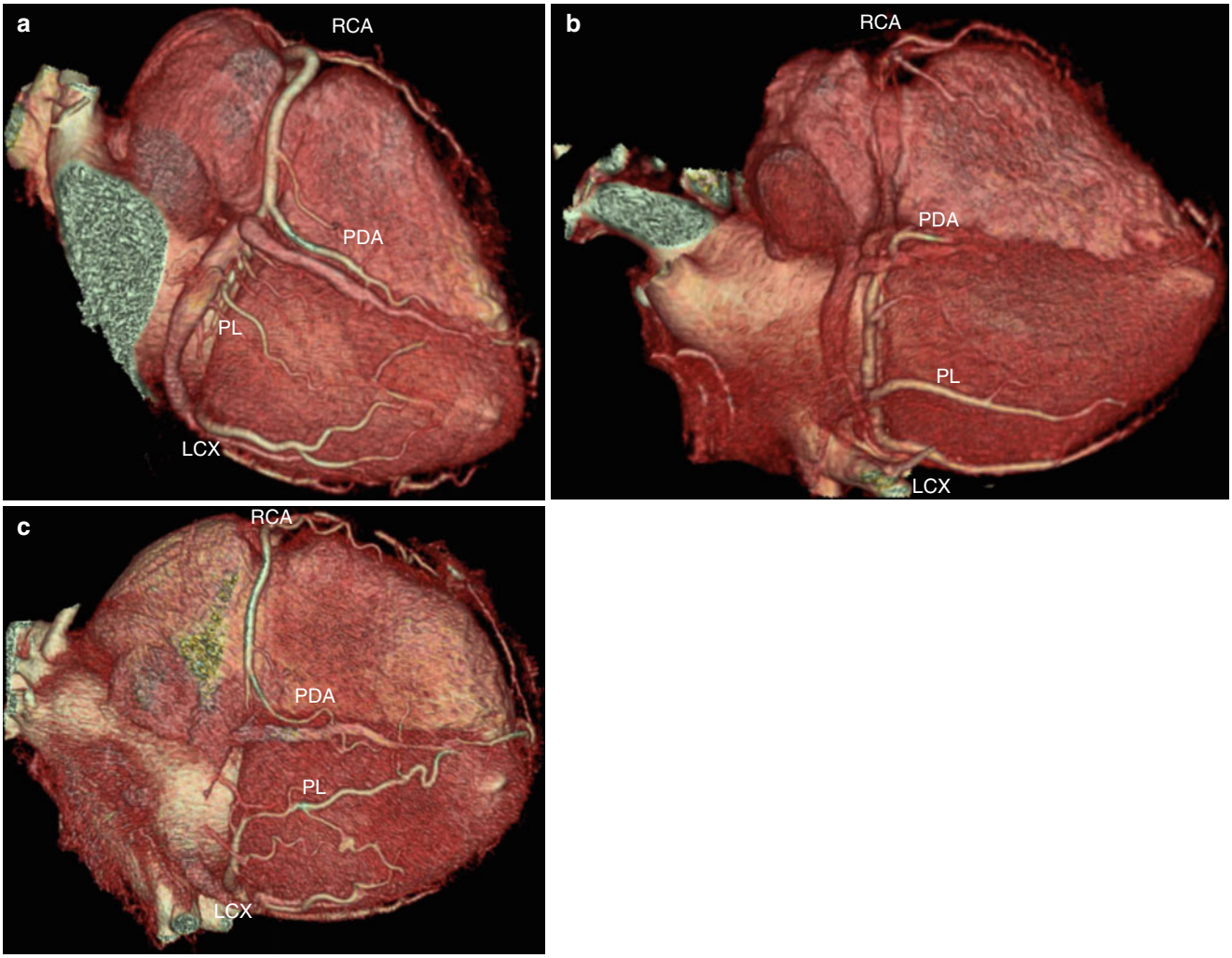

Fig. 2.2 (**a**) Right dominant supply. The PDA and PL branches arise from the RCA. (**b**) Left dominant supply. The PDA and PL branches arise from LCX. (**c**) Codominant supply. PDA arises from the RCA and PL arise from the LCX

2.3.3 Left Circumflex Artery (LCX) (Fig. 2.3c)

- The obtuse marginal branches supply the lateral portion of the left ventricle, numbered as they arise from the LCX such as the first obtuse marginal (OM1), second obtuse marginal (OM2), etc.
- Proximal LCX: from the orifice to the large first OM.
- Distal LCX: distal to the first OM.

2.3.4 Right Coronary Artery (RCA) (Fig. 2.3d, e)

- Conus branch: first branch, very proximally located, supplies the pulmonary conus of the right ventricle (RV). Separate takeoff from aorta is common.
- Sinus node artery: 60 % in RCA and 40 % in LCX.
- Acute marginal branch: anterior free wall of the RV.
- The PDA and PL branches supply the inferior wall of the left ventricle and AV node.
- Proximal LAD: from the orifice halfway to acute margin.
- Middle LAD: remained halfway to acute margin.
- Distal LAD: from acute margin to base of the heart.

2.4 Angiography Versus CT

2.4.1 Basic Angiographic View of the Left Coronary Artery

- Right anterior oblique (RAO) caudal: right side of the heart, good view of LCX, OM, and proximal LAD (Fig. 2.4a)
- Left anterior oblique (LAO) cranial: left side of the heart, good view of LM, septal, and diagonal br. (Fig. 2.4b) [6]

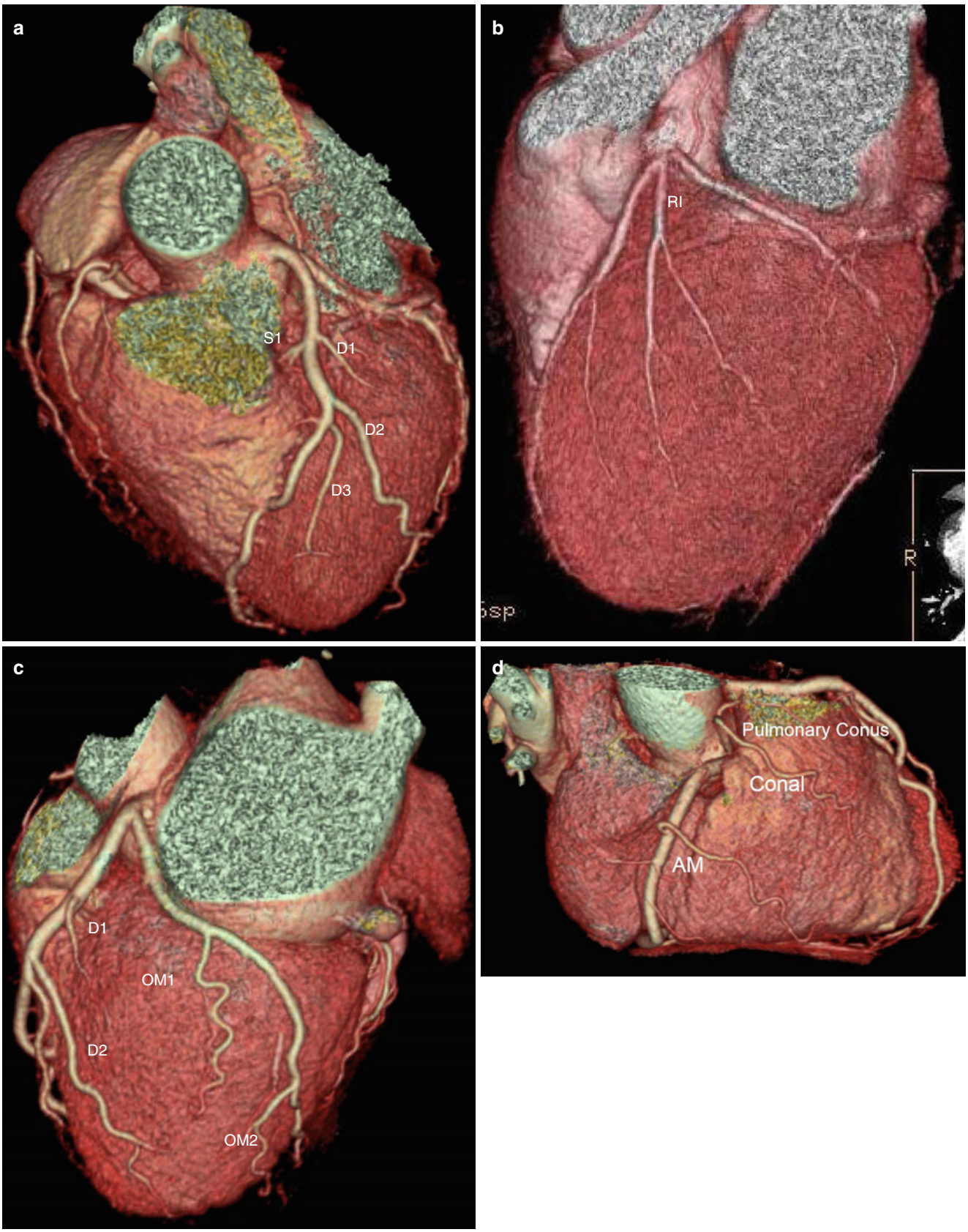

Fig. 2.3 (**a**) LAD and branches. The first diagonal branch (*D1*) is close to the first septal branch (*S1*), and the following second and third diagonal branches (*D2* and *D3*) are well delineated along the free wall of the left ventricle. (**b**) Ramus intermedius (*RI*) arises between LAD and LCX orifice. (**c**) LCX and branches. First and second obtuse marginal branches (*OM1*, *OM2*) of LCX supply the lateral portion of LV (obtuse margin). (**d**) RCA and branches. Conal branch arises from the RCA near the aorta and runs anteriorly to the pulmonary conus. Acute marginal branch (*AM*) runs along the anterior wall of the right ventricle toward the acute margin. (**e, f**) Origin of sinonodal artery (*SA*). SA is originated from the RCA (60 %) or LCX (40 %) and runs to the SVC

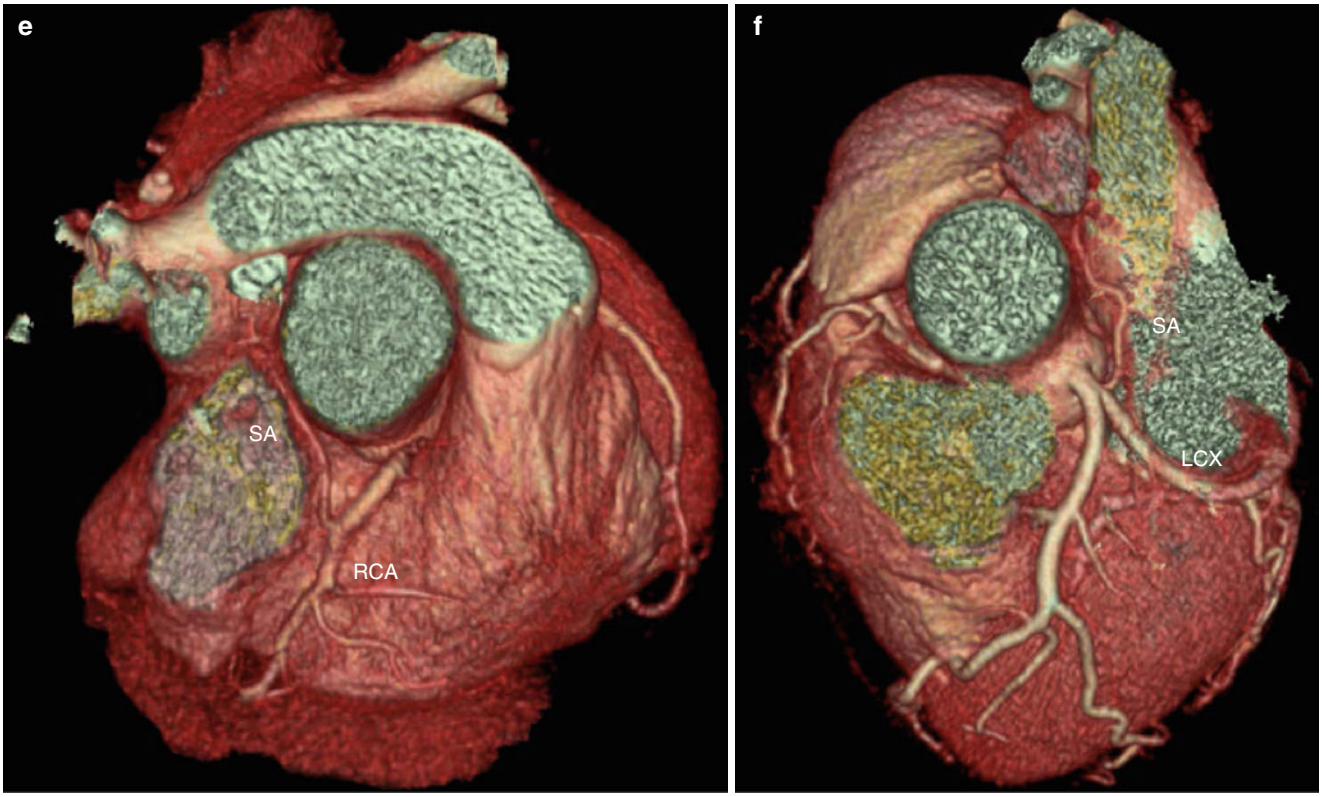

Fig. 2.3 (continued)

2.4.2 Basic Angiographic View of the Right Coronary Artery

- Left anterior oblique (LAO) cranial: good view of the ostial and proximal RCA (Fig. 2.4c)
- Right anterior oblique (RAO) straight: good view of the middle RCA (Fig. 2.4d) [6]

2.5 Coronary Artery Variation and Anomalies

2.5.1 Incidence

- Most anomalies are incidentally detected.
- Approximately 1 % of patients undergo cardiac catheterization.
- 0.29 % among autopsy specimens [7–9].

2.5.2 Clinical Significance

- Most anomalies do not create clinical problems.
- 19–33 % of sudden cardiac deaths in the young population are related to coronary artery anomalies.
- Benign (80 %) and potentially serious anomalies (20 %).
- Potentially serious anomalies: ectopic origin from the pulmonary artery, ectopic origin from the opposite aortic sinus, single coronary artery, multiple or large coronary fistulas [7–9].

2.6 Anomalies of Origin and Course

2.6.1 Anomalous Origin of the Left Coronary Artery from the Pulmonary Artery (ALCAPA) Syndrome (Fig. 2.5)

- Bland-White-Garland syndrome.
- Prevalence of one in 300,000 live births.
- Usually isolated defect, but in 5 % of cases associated with other cardiac anomalies such as atrial septal defect, ventricular septal defect, and aortic coarctation.
- "Coronary steal" phenomenon; left-to-right shunt leads to myocardial ischemia or infarction.
- Approximately 90 % of untreated infants die in the 1st year, and only a few patients survive to adulthood.
- The extent of acquired collateral circulation between the RCA and LCA during the critical period, when pulmonary arterial pressure gradually decreases, determines the extent of myocardial ischemia.

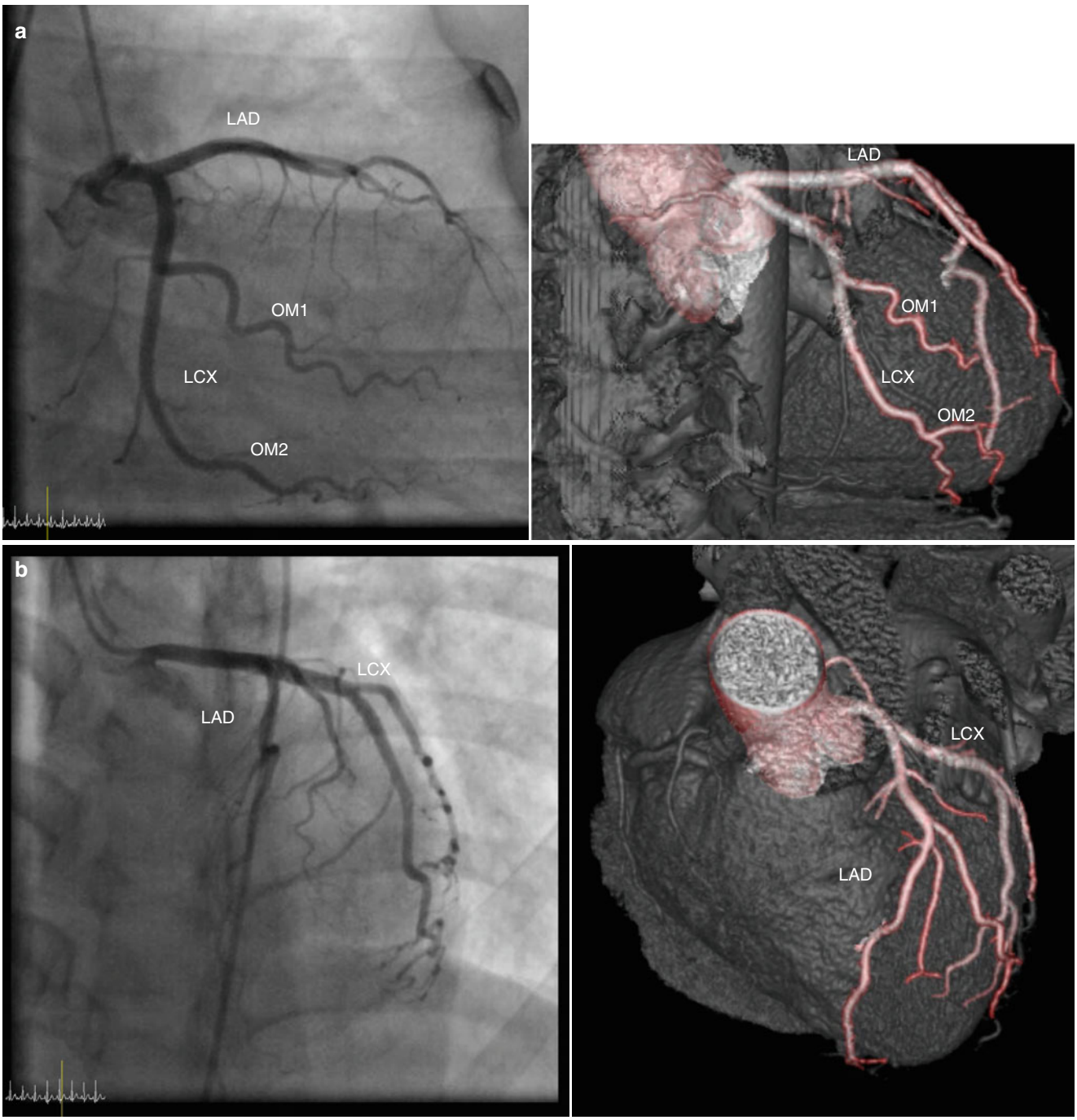

Fig. 2.4 (**a**) RAO caudal view of the left coronary artery. Angiography and transparent volume rendering image show good view of LCX with obtuse marginal branches (*OM1* and *OM2*) and proximal LAD. (**b**) LAO caudal view of the left coronary artery. Angiography and transparent volume rendering image show good view of the left main coronary artery, and this view has good delineation of diagonal and septal branches. (**c**) LAO cranial view of right coronary artery. Angiography and transparent volume rendering image show good view of ostial and proximal RCA. (**d**) RAO straight view of right coronary artery. Angiography and transparent volume rendering image show good view of middle RCA PDA, posterior descending artery, PL, posterolateral branch, AM, acute marginal branch

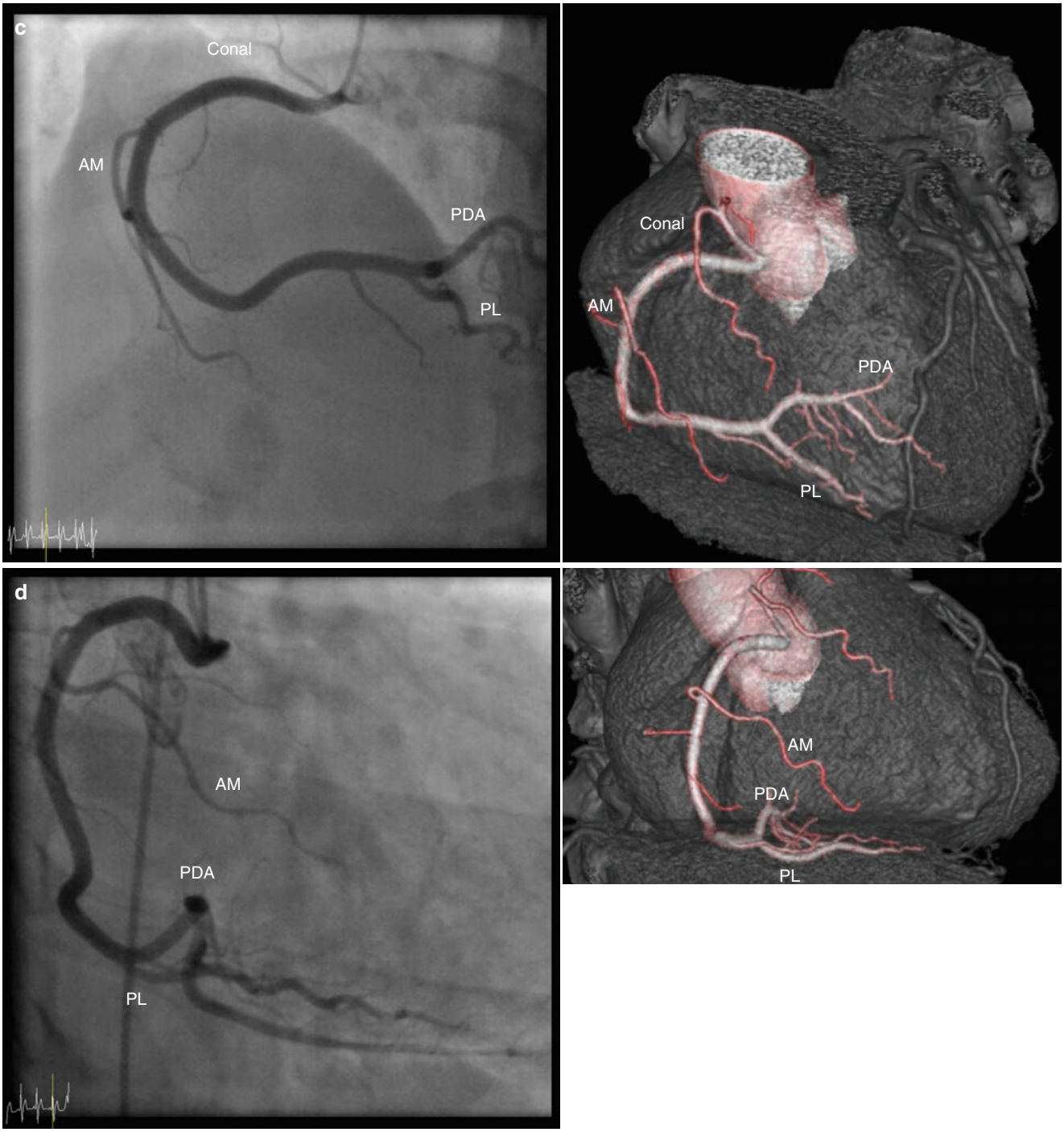

Fig. 2.4 (continued)

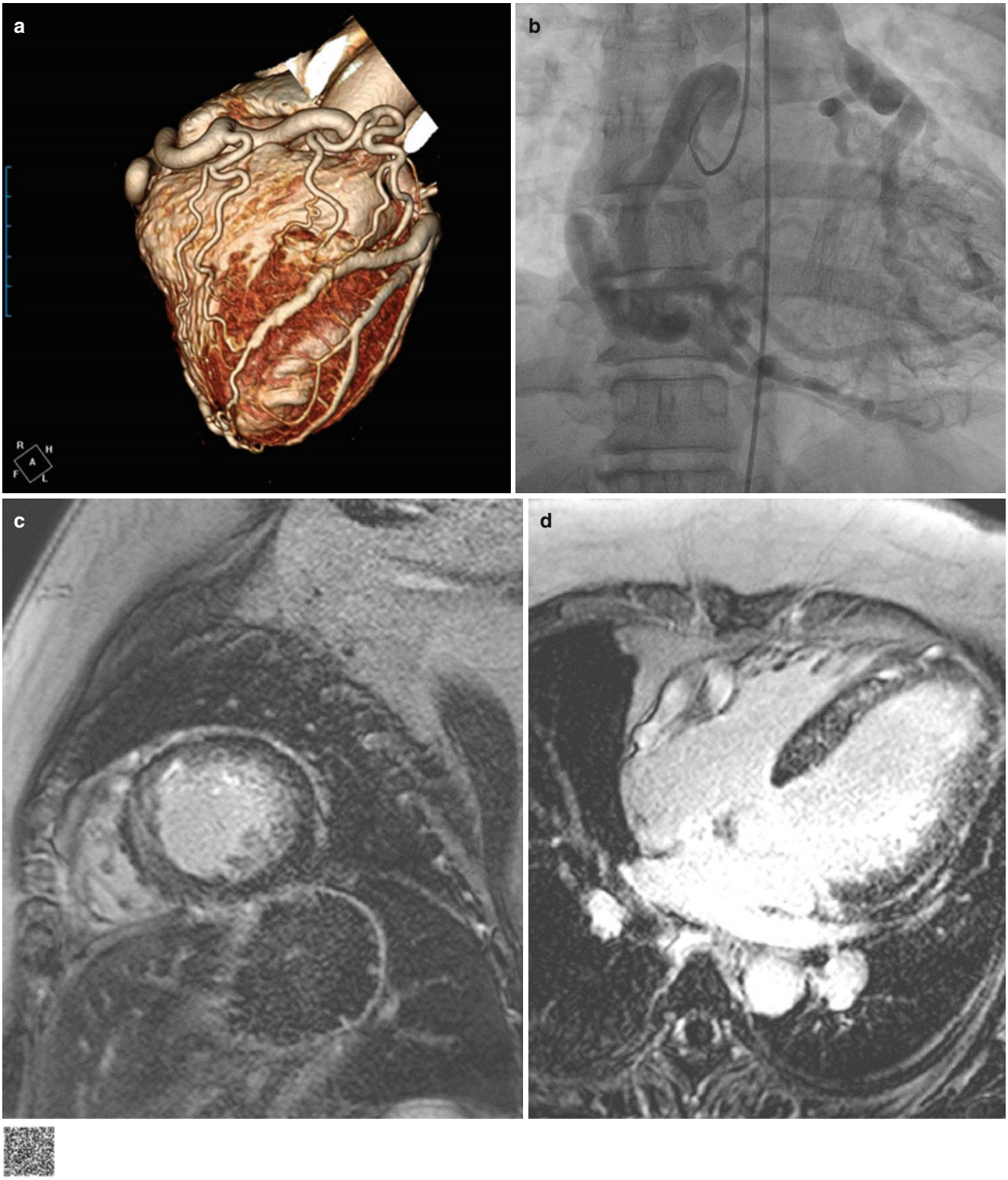

Fig. 2.5 ALCAPA. Right coronary angiography (**a**) and coronary CTA (**b**) image show well-developed collaterals from the markedly dilated right coronary artery (RCA) to the dilated and tortuous left coronary artery (LCA) originated from the main pulmonary artery (PA). Delayed enhancement MR (**c**, **d**) shows diffuse subendocardial enhancement of the left ventricle, representing diffuse ischemia (http://extras.springer.com/2015/978-3-642-36396-2)

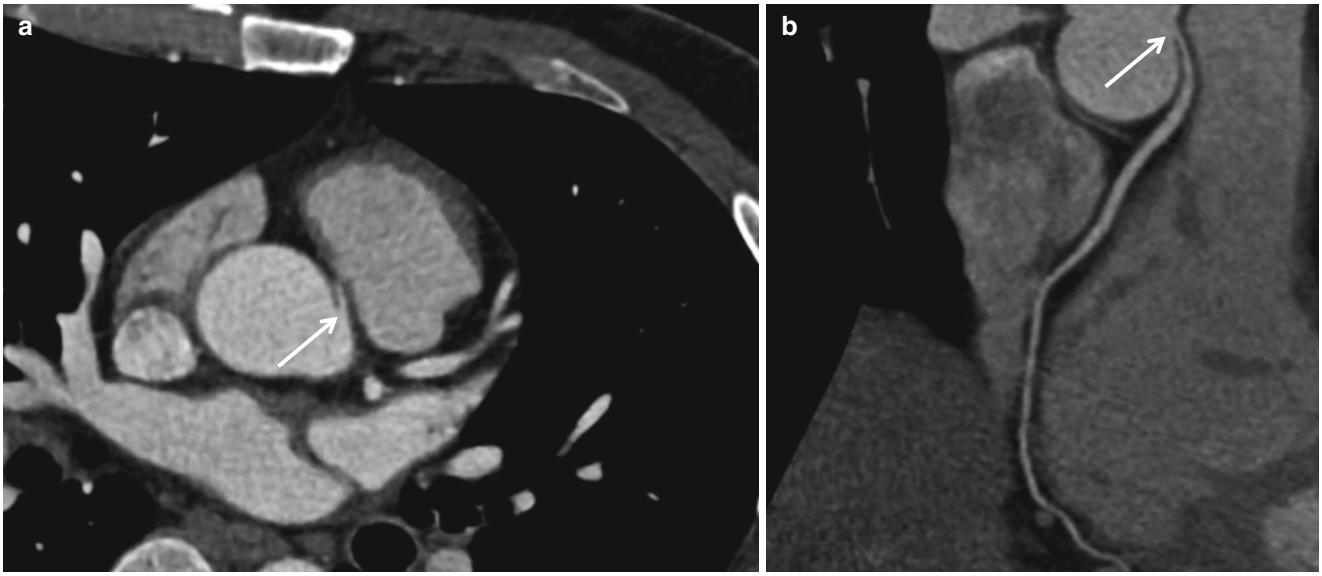

Fig. 2.6 Anomalous origin of the right coronary artery (RCA) from the left coronary sinus with interarterial course. Axial image (**a**) shows anomalous origin of RCA from the left coronary sinus with slit-like orifice (*arrow*). Curved MPR image (**b**) shows interarterial course between the aorta and pulmonary artery and marked narrowing of the RCA at the orifice, so this patient has the potential of significant narrowing with young age

- Patients with well-established collateral vessels have the *adult type* of the disease, and those without collateral vessels have the *infant type*. Both types of the disease have different manifestations and outcomes.
- Imaging features of ALCAPA syndrome on cardiac CT and MRI:
  - Direct visualization of the LCA arising from the main pulmonary artery
  - Retrograde flow from the LCA into the main pulmonary artery; steal phenomenon
  - RCA dilated and tortuous; chronic left-to-right shunt
  - Dilated intercoronary collateral vessels; collateral pathways between the RCA and the LCA
  - Left ventricular hypertrophy and dilatation; chronic myocardial ischemia
  - Left ventricular wall motion abnormalities; global hypokinesis
  - Dilated bronchial arteries; systemic supply to the LCA territory and increased perfusion pressures
  - Delayed subendocardial enhancement [8, 10]

2.6.2 Origin of Coronary Artery or Branch from Opposite Sinus (Figs. 2.6, 2.7, 2.8, and 2.9)

- Four common courses: (a) interarterial, (b) retroaortic, (c) prepulmonic, or (d) septal (subpulmonic).
- Interarterial course between the aorta and pulmonary artery: most common course, potentially dangerous (especially young).
- Possible mechanism of ischemia: acute takeoff angle, slit-like orifice, compression of the intramural segment, and compression between the aorta and pulmonary artery.
- RCA from left sinus: 0.03–0.17 % of patients in angiography.
- LCA from right sinus: 0.09–0.11 % of patients in angiography, more dangerous than RCA form left sinus due to large dependent myocardial volume.
- Young, anomaly of LCA, and longer intramural course are more dangerous [11, 12].

2.7 Anomalies of Only the Origin

2.7.1 High Takeoff (Fig. 2.10)

- Origin of either the RCA or the LCA above the sinotubular junction.
- Usually no major clinical problems.
- Difficulty in cannulating the vessels during conventional angiography.
- Transection or clamping of the high takeoff artery is possible at cardiopulmonary bypass [7, 8].

2.7.2 Single Coronary Artery (Fig. 2.11)

- Only one coronary artery arises from a single ostium.
- Extremely rare congenital anomaly: 0.0024–0.044 %.
- Usually benign, but has the potential of sudden death [7, 8].

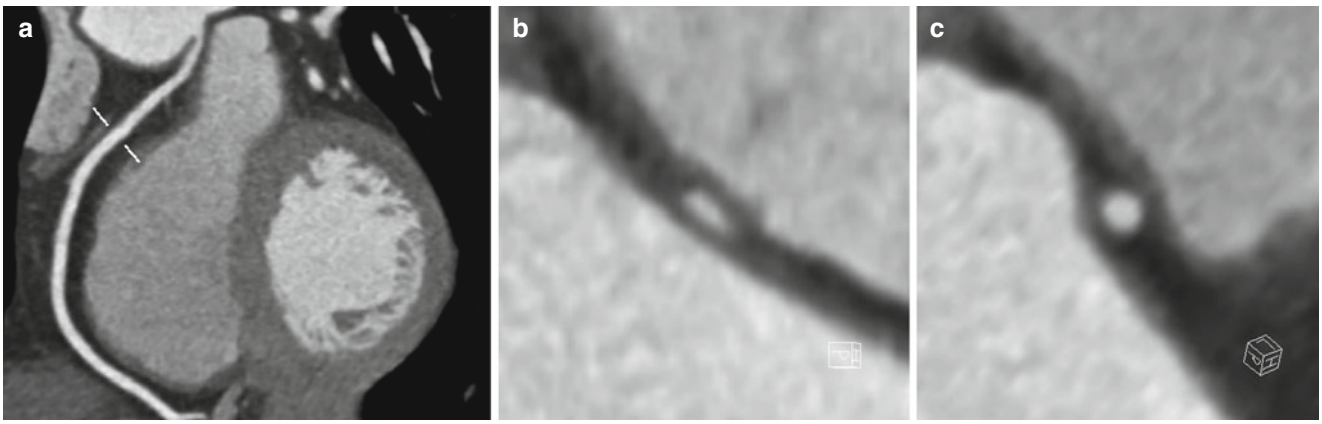

Fig. 2.7 Anomalous origin of the right coronary artery (RCA) from the left coronary sinus with interarterial course in a 59-year-old female. Curved MPR image (**a**) shows anomalous origin of RCA from the left coronary sinus with interarterial course. Short-axis images in interarterial course (**b**) show compression of the RCA between the aorta and pulmonary artery compared to normal RCA (**c**)

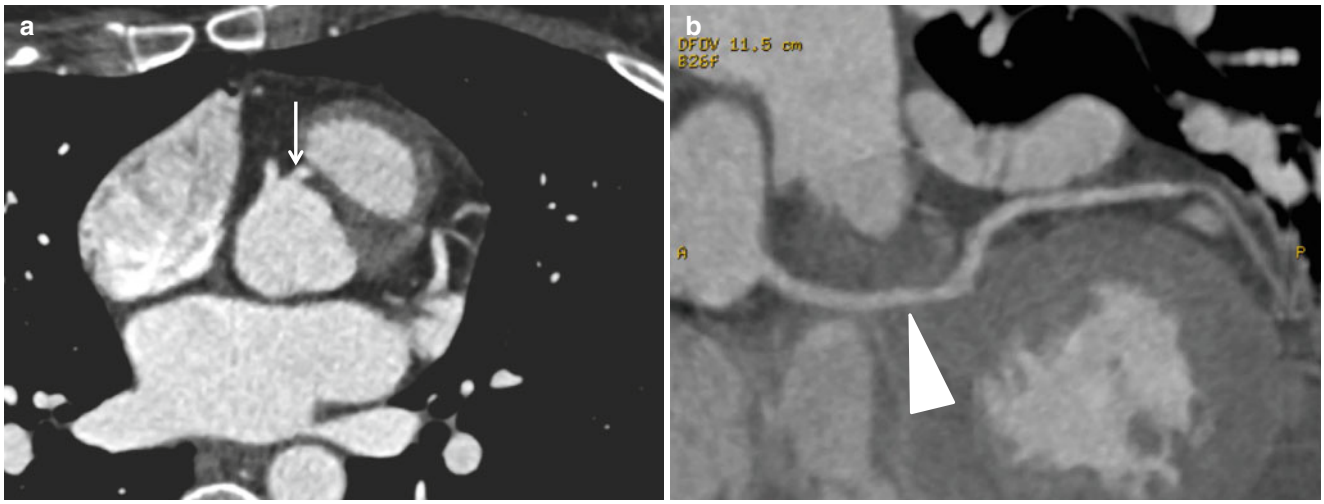

Fig. 2.8 Anomalous origin of the left coronary artery (LCA) from the right coronary sinus with interarterial course in a 29-year-old female. Axial image (**a**) shows anomalous origin of LCA from the right coronary sinus (*arrow*), and curved MPR image (**b**) shows interarterial course with long intramural course (*arrow head*), which is correlated with dangerous anomaly

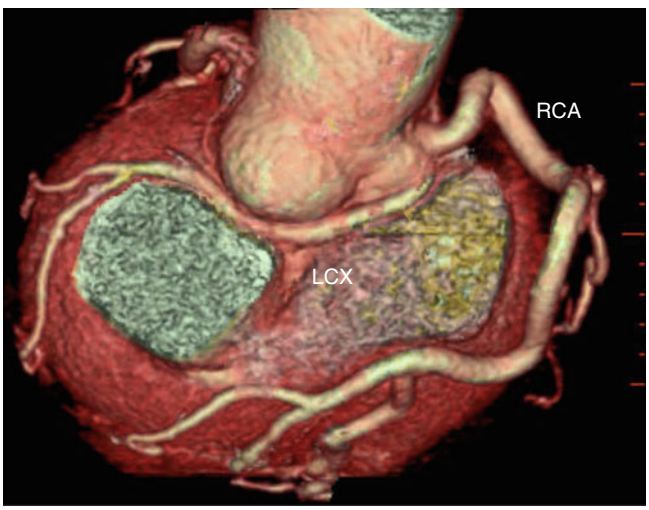

Fig. 2.9 Anomalous origin of the left circumflex artery (*LCX*) from the right coronary sinus with retroaortic course in a 64-year-old female. Volume rendering image shows anomalous origin of LCX from the right coronary sinus with retroaortic course

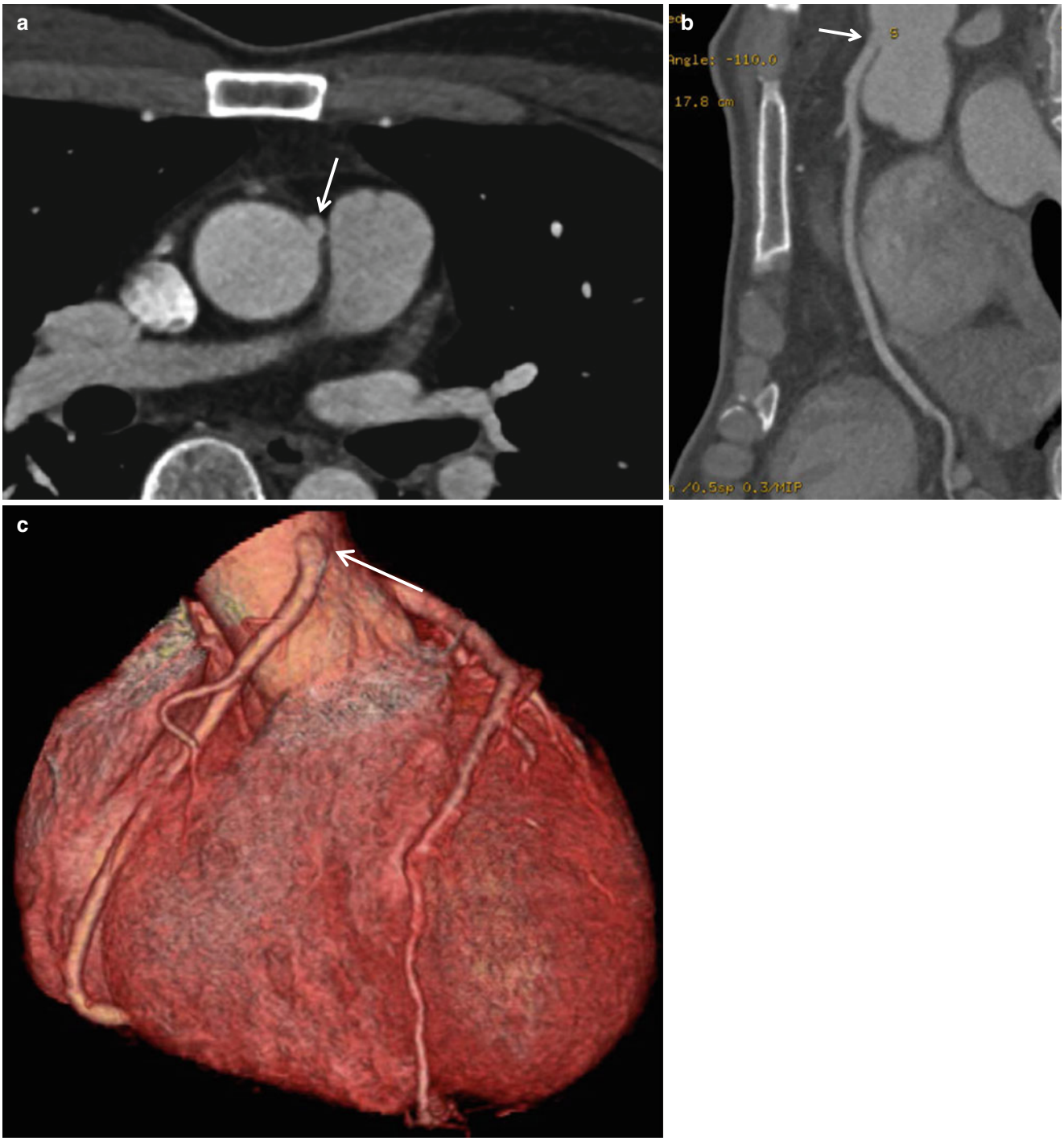

Fig. 2.10 High takeoff of right coronary artery (*RCA*) in a 39-year-old male. Axial image (**a**) shows takeoff of RCA from the aorta (*arrow*), not the coronary sinus. There is no coronary sinus contour. Curved MPR and volume rendering image (**b**, **c**) show high takeoff of RCA

2.7.3 Separate Origins of the LAD and LCX (Fig. 2.12)

- Incidence: 0.41 %
- Benign anomaly [7, 8]

2.8 Anomalies of Only the Course

2.8.1 Myocardial Bridging (Fig. 2.13)

- Benign anomaly
- Myocardial muscle overlying a segment of a coronary artery

- Most common in middle LAD
- Prevalence: variable. 0.5–12 % in angiography, 5–86 % in autopsy, 15 % in surgeons report [13]

2.8.2 Duplication: RCA, LAD Duplication (Fig. 2.14)

- 0.13–1 % of the general population
- Helpful in surgeons prior to operation [7, 8]

2.9 Anomalies of Termination

2.9.1 Coronary Artery Fistula (Figs. 2.15 and 2.16)

- Anomalous termination of coronary arteries.
- Direct connection between the coronary artery to cardiac chamber, coronary sinus, superior vena cava, or a pulmonary artery or pulmonary vein close to the heart.
- 0.002 % in the general population, 0.05–0.25 % in coronary angiography.

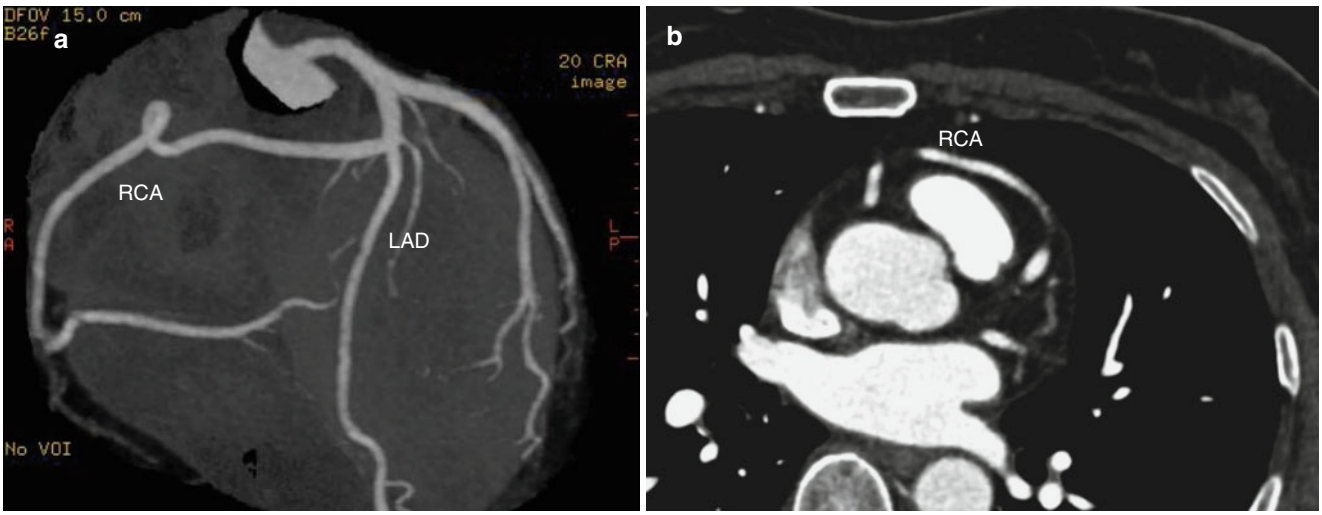

Fig. 2.11 Single coronary artery with left coronary sinus origin in a 50-year-old female. Maximal intensity projection image (**a**) shows single coronary artery, and *RCA* is originated from *LAD*. Axial image (**b**) shows RCA arc anterior to PA. There is no significant narrowing

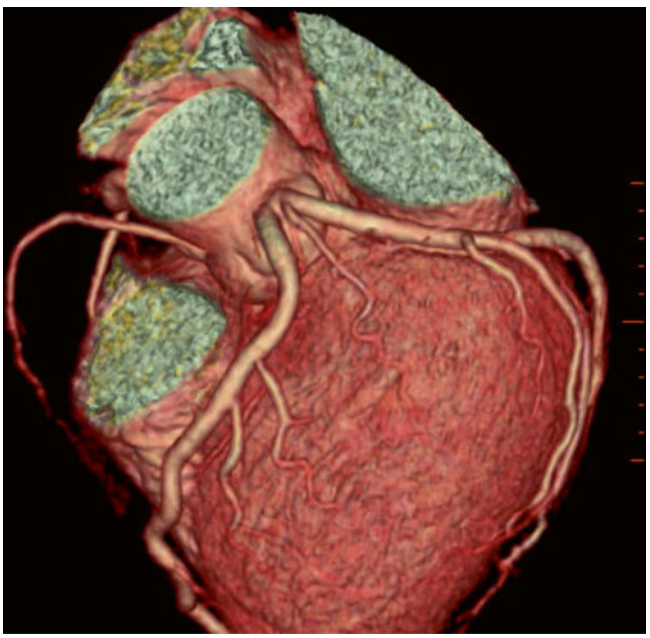

Fig. 2.12 Separate origins of the LAD and LCX in a 66-year-old female. Volume rendering image shows separate origins of the LAD and LCX from the left coronary sinus

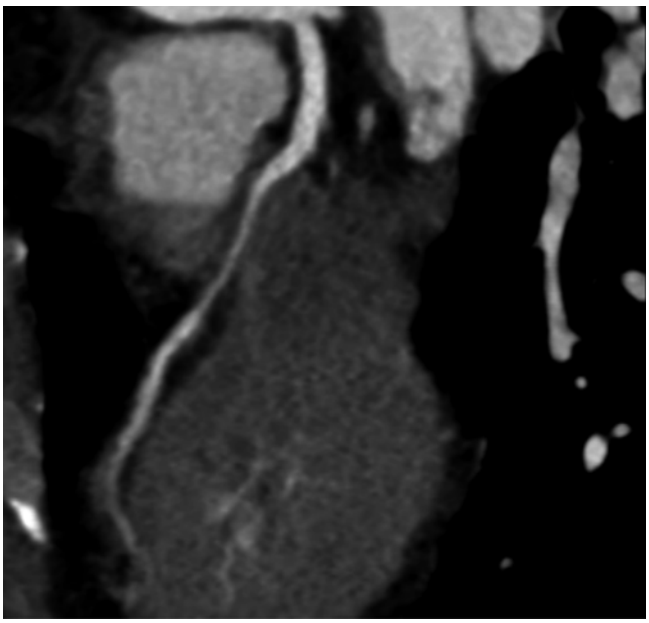

Fig. 2.13 Myocardial bridging of the LAD in a 46-year-old male. Curved MPR images show narrowing of middle LAD surrounded by the myocardium

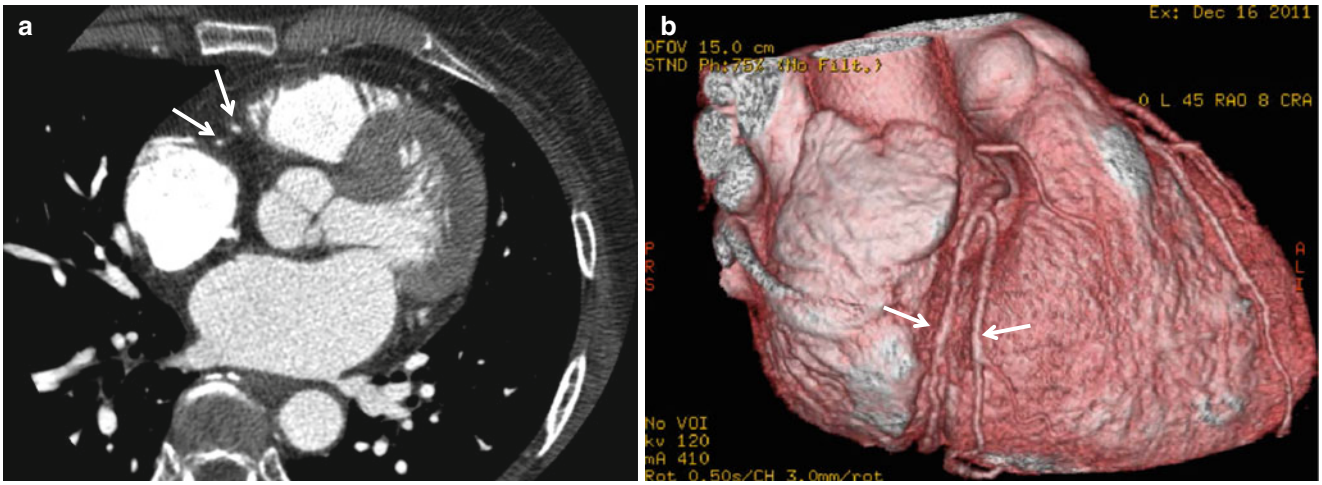

Fig. 2.14 Duplication RCA in a 59-year-old female. Axial image (**a**) shows two RCA (*arrows*) on middle portion of RCA course, and volume rendering images (**b**) show duplication of RCA with single takeoff

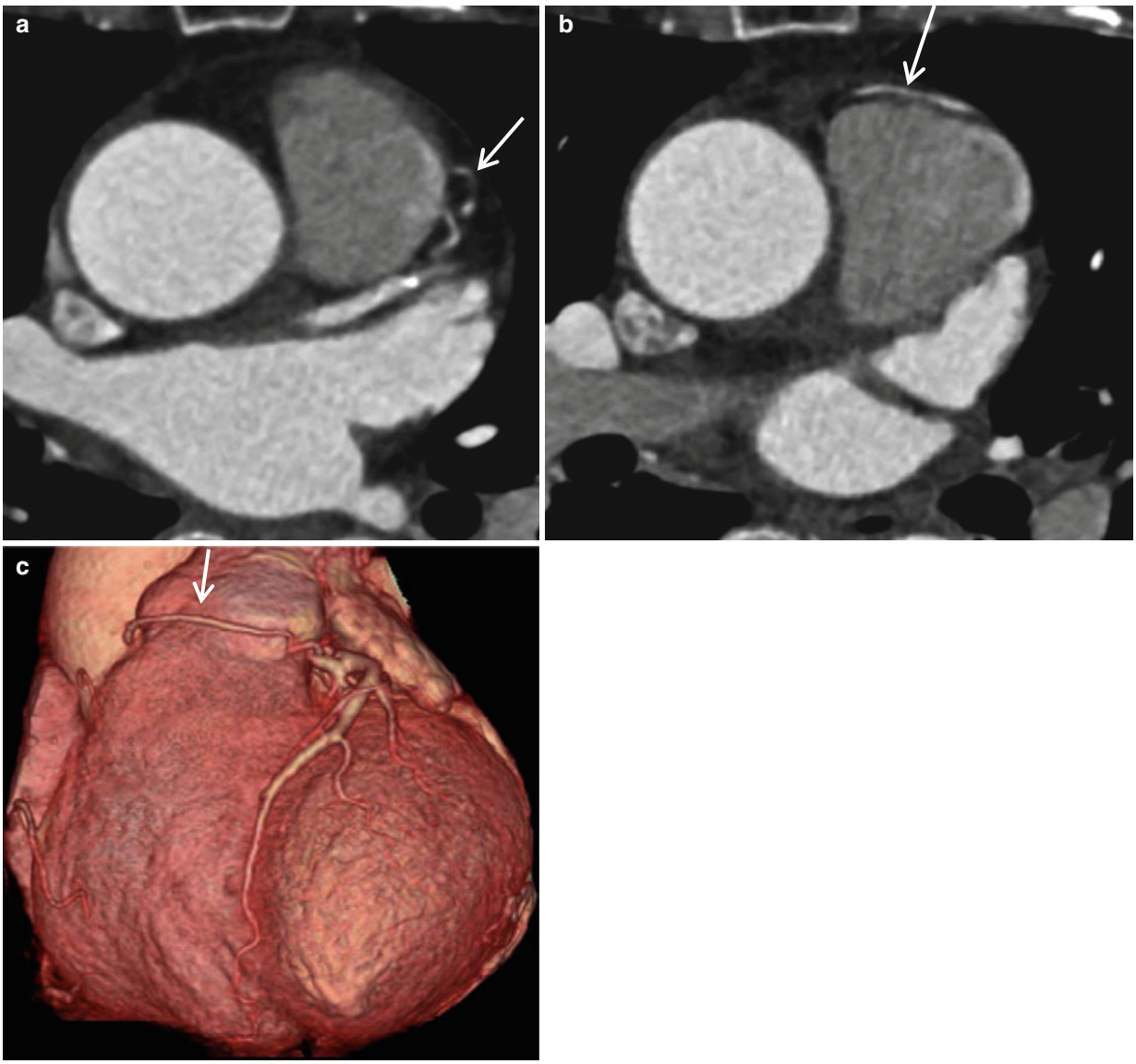

Fig. 2.15 Coronary artery fistula (*arrows*) from LAD to PA in a 52-year-old female. Axial image (**a**, **b**) shows small coronary artery fistula originated from LAD anterior to PA. Volume rendering images (**c**) well delineate this fistula anterior to PA

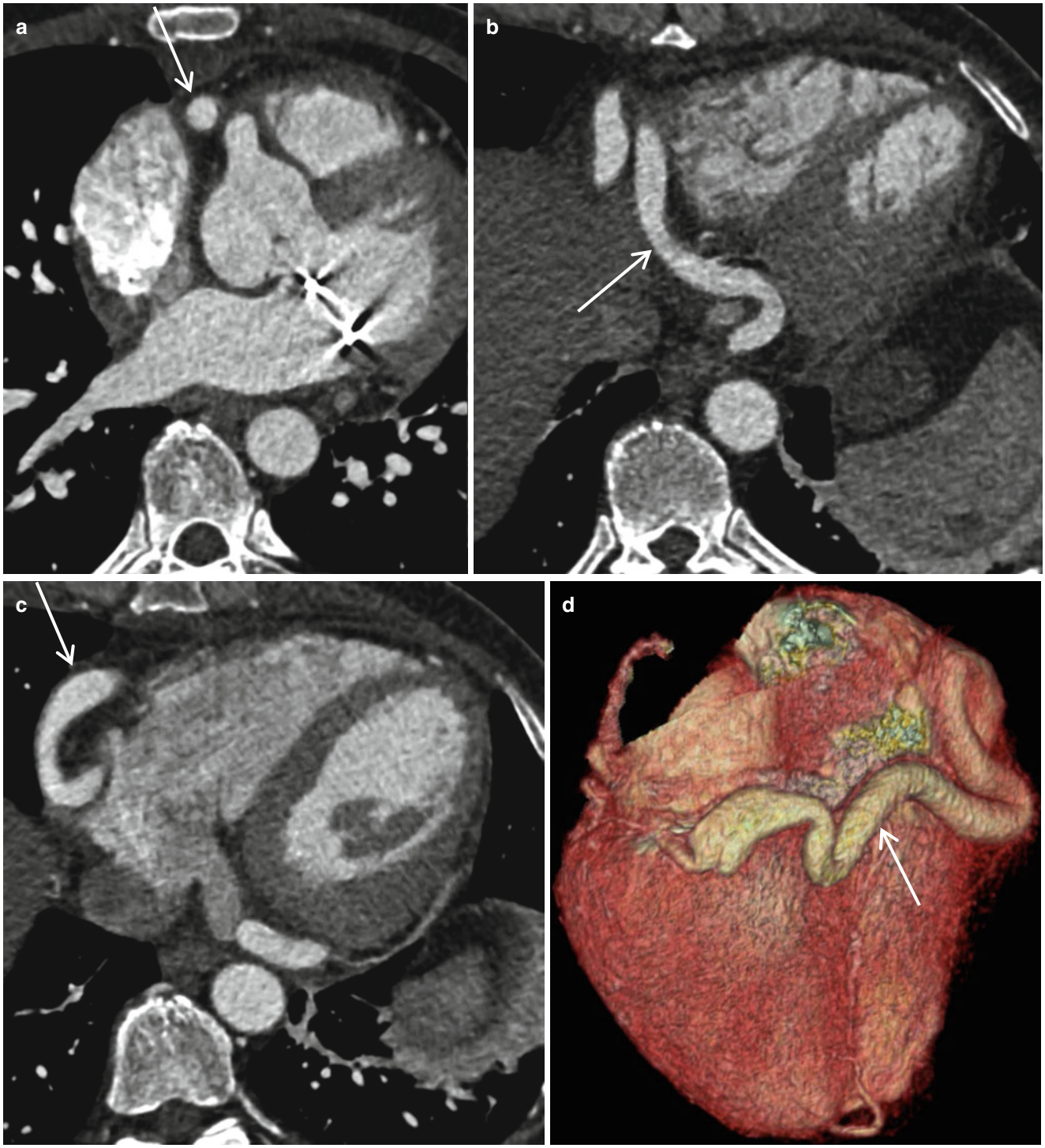

Fig. 2.16 Large coronary artery fistula (*arrows*) from RCA to coronary sinus in a 51-year-old male. Axial image (**a**–**c**) shows large RCA connecting to the coronary sinus and great cardiac vein. Volume rendering images (**d**) well demonstrate this large fistula on the inferior border

- RCA in approximately 50 %, LCA in approximately 42 % in LCA, and both the RCA and LCA in approximately 5 %.
- The clinical presentation is mainly dependent on the severity of the left-to-right shunt.
- Usually benign; most fistulas are single communication.
- May be dangerous in large or multiple communications.
- The most common drainage sites are the right ventricle (41 %), right atrium, pulmonary artery (17 %), coronary sinus (7 %), left atrium (5 %), left ventricle (3 %), and superior vena cava (1 %) [14].

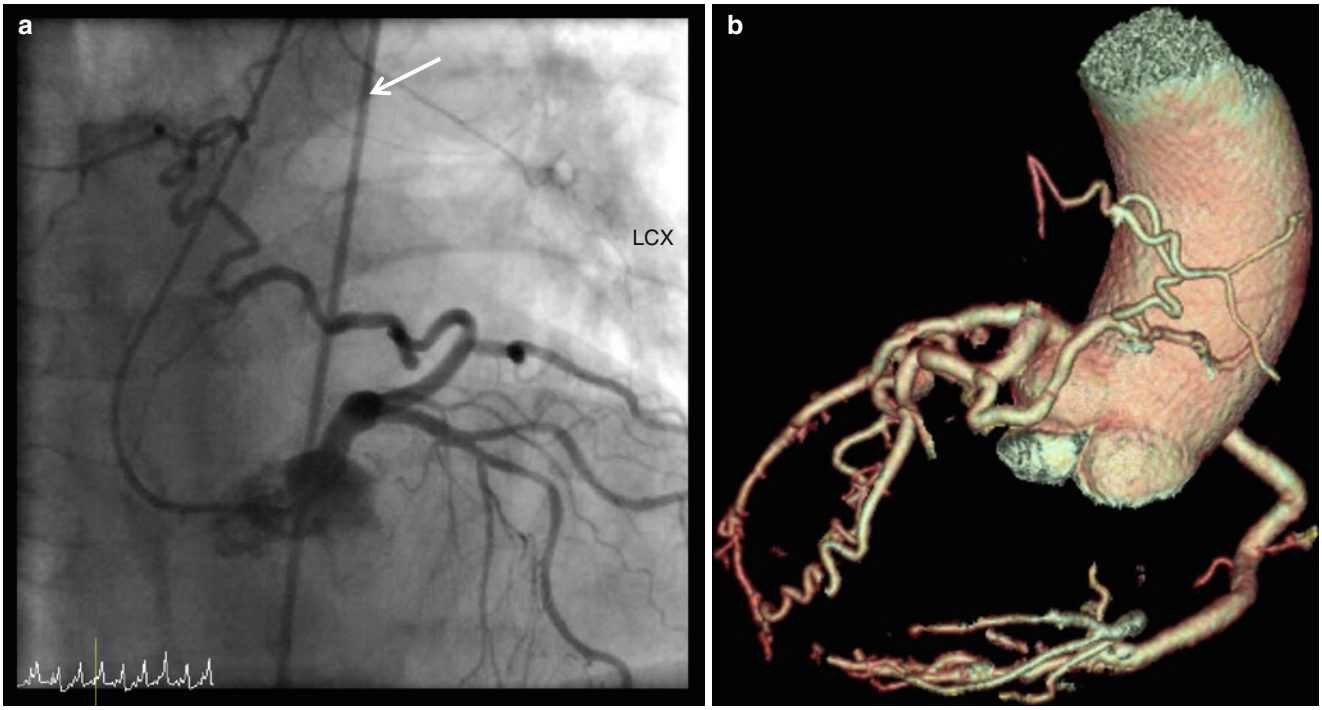

Fig. 2.17 Coronary bronchial fistula. Angiography (**a**) shows bronchial artery (*arrow*) originated from the left circumflex artery (LCX). Volume rending image (**b**) well demonstrates the bronchial artery posterior to the ascending aorta originated from the left circumflex artery (LCX)

2.9.2 Coronary Arcade

Communication that is large enough to be identified angiographically between the RCA and the LCA in the absence of coronary artery stenosis

2.9.3 Extracardiac Termination (Fig. 2.17)

Connections between the coronary arteries and extracardiac vessels [15]

References

1. O'Brien JP, Srichai MB, Hecht EM, Kim DC, Jacobs JE. Anatomy of the heart at multidetector CT: what the radiologist needs to know. Radiographics. 2007;27:1569–82.
2. Pannu HK, Flohr TG, Corl FM, Rishman EK. Current concepts in multi-detector row CT evaluation of the coronary arteries: principles, techniques, and anatomy. Radiographics. 2003;23:S111–25.
3. Alderman EL, Stadius M. The angiographic definitions of the Bypass Angioplasty Revascularization Investigation study (BARI). Coron Artery Dis. 1992;3:1189–207.
4. Scanlon PJ, Faxon DP, Audet AM, Carabello B, Dehmer GJ, Eagle KA, Legako RD, Leon DF, Murray JA, Nissen SE, Pepine CJ, Watson RM, Ritchie JL, Gibbons RJ, Cheitlin MD, Gardner TJ, Garson Jr A, Russell Jr RO, Ryan TJ, Smith Jr SC. ACC/AHA guidelines for coronary angiography. A report of the American College of Cardiology/American Heart Association Task Force on practice guidelines (Committee on Coronary Angiography). Developed in collaboration with the Society for Cardiac Angiography and Interventions. J Am Coll Cardiol. 1999;33:1756–824.
5. Faletra FF, Pandian NG, Siew Yen Ho. Coronary artery anatomy, Anatomy of the Heart by Multislice Computed Tomography 2008 John Wiley & Sons Ltd. 88–107.
6. Aquilina O, Grech V, Felice H et al. Normal adult coronary angiography. Images Paediatr Cardiol 2006;8:1–16.
7. Yamanaka O, Hobbs RE. Coronary artery anomalies in 126,595 patients undergoing coronary arteriography. Cathet Cardiovasc Diagn 1990;21:28–40.
8. Kim SY, Seo JB, Do KH et al. Coronary artery anomalies: classification and ECG-gated multi-detector row CT findings with angiographic correlation. Radiographics 2006;26:317–333.
9. Goo HW, Seo DM, Yun TJ et al. Coronary artery anomalies and clinically important anatomy in patients with congenital heart disease: multislice CT findings. Pediatr Radiol 2009;39:265–273.
10. Pena E, Nguyen ET, Merchant N, Dennie C, ALCAPA Syndrome: Not Just a Pediatric Disease. RadioGraphics 2009;29:553–565.
11. Lee BY, Song KS, Jung SE et al. Anomalous right coronary artery originated from left coronary sinus with interarterial course: evaluation of the proximal segment on multidetector row computed tomography with clinical correlation. J Comput Assist Tomogr 2009;33:755–762.
12. Lee BY. Anomalous right coronary artery from the left coronary sinus with an interarterial course: Is it really dangerous? Korean Circulation Journal 2009;39;175–179.
13. Lee BY, Song KS, Seo EJ et al. Myocardial infarction in a young female with reninoma induced hypertension and myocardial bridging. Int J Cadiovasc Imaging 2007:23:639–643.
14. Zenooz NA, Habibi R, Mammen L et al. Coronary Artery Fistulas: CT Findings RadioGraphics 2009;29:781–789.
15. Lee ST, Kim SY, Hur G, et al. Coronary-to-bronchial artery fistula: demonstration by 64 multidetector computed tomography with retrospective electrocardiogram-gated reconstructions. J Comput Assist Tomogr. 2008;32:444–7.

Cardiac Imaging to Guide Electrophysiologic Intervention

3

Sung Ho Hwang and Dong Hyun Yang

Contents

S.H. Hwang (✉)
Department of Radiology, Korea University Anam Hospital, Korea University College of Medicine, Seoul, Republic of Korea
e-mail: sungho.hwng@gmail.com

D.H. Yang
Department of Radiology and Research Institute of Radiology, Asan Medical Center, University of Ulsan College of Medicine, Seoul, Republic of Korea
e-mail: donghyun.yang@gmail.com

Abstract

With remarkable advances of catheter-based technique, the treatment of patients with cardiac arrhythmia has included catheter ablation for a precise destruction of cardiac arrhythmogenic tissue and cardiac resynchronization therapy for a pacing of different cardiac parts. In practice, the intracardiac electrophysiologic intervention is effectively performed under the knowledge of cardiac anatomy. Faster and more accurate placement of the intracardiac ablation catheters and the pacemaker leads relative to the cardiac target of interest can affect the success rate and the risk of complication. Recently, the cardiac imaging by using multidetector computed tomography (CT) or the magnetic resonance (MR) systems has been underwent positively to accurately delineate the cardiac structures and tissue characteristics for the electrophysiologic interventions.

3.1 Introduction

- Advanced understanding of pathophysiology about cardiac arrhythmia has permitted the percutaneous intracardiac approach for the ablation of arrhythmogenic foci and the cardiac resynchronization therapy.
- Generally, the mechanism of cardiac arrhythmia is determined by the major arrhythmogenic components as the trigger and the sustainer.
- Of various cardiac arrhythmias, atrial fibrillation (AF) is a common and severe rhythmic disturbance from multiple reentrant wavelets and a rapidly firing focus in the left atrium.
- In the symptomatic AF, the catheter-based ablation for isolation of arrhythmogenic myocardial tissue has become the standard therapy.
- The chronic heart failure may be combined with an intraventricular conduction delay at the onset of right or left ventricular systole.
- In the chronic heart failure, the cardiac resynchronization therapy (CRT) with biventricular pacing can improve the synchrony of contractions of the bilateral ventricles.

T.-H. Lim (ed.), *Practical Textbook of Cardiac CT and MRI*,
DOI 10.1007/978-3-642-36397-9_3,

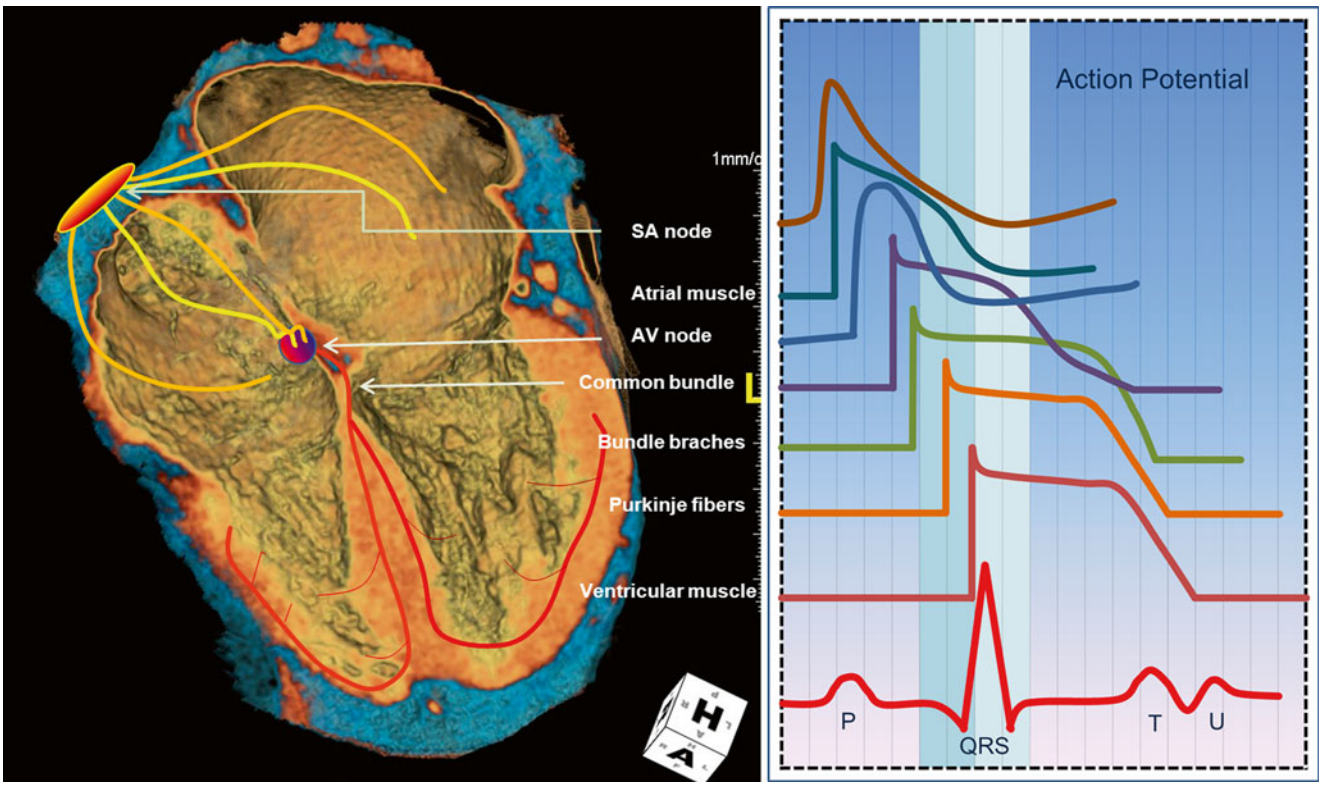

Fig. 3.1 Diagram of the cardiac conduction system and action potential. Firstly, the sinoatrial (SA) node at the junction between the superior vena cava and the right atrium initiates the electronic pulse in the cardiac conduction system. The penetrating bundle perforates the insulating tissue plane of the atrioventricular (AV) junction to be the only bridge of muscular continuity between the atrial and ventricular myocardium. *SA node* sinoatrial node, *AV node* atrioventricular node

- If a detail "roadmap" is provided, the electrophysiologist can perform the catheter ablation and the CRT pacing procedures more successfully.
- Cardiac imaging by CT or MR system has become possible to provide the detail "roadmap" of a higher level for the electrophysiologic intervention.
- In this chapter, by interpreting the cardiac imaging to guide the electrophysiologic intervention, we describe the critical information on the cardiac images in the view of the electrophysiologist.

3.2 Cardiac Conduction System

3.2.1 Anatomy of Cardiac Conduction System

- The cardiac conduction system consists of the sinoatrial node (SAN), the atrioventricular node (AVN), the His bundle, the right and left bundle branches, and peripheral ramifications of these bundle branches which make up the subendocardial and intramyocardial Purkinje network (Fig. 3.1).
- The atrial components of conduction system such as SAN and AVN are in contract with the atrial myocardium.
- The body of the SAN is in the epicardial wall of the right atrium, at the junction between the right atrium and the superior vena cava.
- From the SAN, extensions run down along the sulcus terminalis of right atrium toward the AVN.
- The AVN lies in the floor of the right atrium, with a variable distance to the coronary sinus opening.
- The upper end of AVN is in continuity with the atrial myocardium and fibers of the internodal tracts.
- The lower end of AVN forms the common bundles as His bundle, which passes through the right fibrous trigone (the central fibrous body) along the posterior edge of the membranous septum.
- Below the His bundle level, the common bundle divides into right and left bundle branches which extend subendocardially along the ventricular septal surfaces.
- The left bundle branches rapidly subdivide to form a broad sheet of fascicles sweeping over the left interventricular septal surface.
- The right bundle branches extend throughout the moderator band and other parts over the endocardial surface of the ventricle.

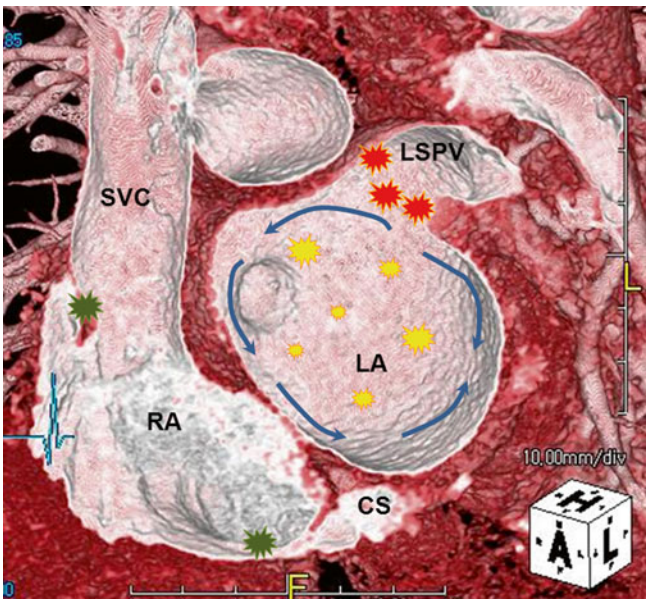

Fig. 3.2 Mechanism of atrial fibrillation. On the left atria and right atria, the four different patterns for atrial fibrillation (AF) consist of the pulmonary vein (PV) triggers, the reentrant wavelets, the non-PV triggers, and the ganglionic plexus overactivity. The posterior wall of the left atrium is considered as the common location of PV triggers (*red star*) and non-PV triggers (*yellow star*). Blue arrows demonstrate reentrant wavelets to initiate and sustain the AF. Most of the cardiac ganglionic plexuses (*green star*) are in the left atrial fat pad near the inferior and superior vena cava. *SVC* superior vena cava, *RA* right atrium, *CS* coronary sinus, *LA* left atrium, and *LSPV* left superior pulmonary vein

3.2.2 Mechanism of Cardiac Arrhythmia

- In the tissue level, the pathogenesis of cardiac arrhythmia is based on the triggers and sustainer of arrhythmia (Fig. 3.2).
- The arrhythmogenic substrate to trigger or maintain the arrhythmia can be located in the normal cardiovascular structure as well as the injured myocardium.
- Of the various cardiac arrhythmias, also atrial fibrillation (AF) can be initiated by the rapid firing of ectopic foci or the reentrant wavelets [1–3].
- Depending on the location of arrhythmogenic substrate, the mechanisms of AF are classified into four patterns: pulmonary vein (PV) trigger, reentrant wavelet in the left atrium, non-PV triggers, and ganglionic plexus overactivity.
- The common locations of PV triggers and non-PV triggers are located in the posterior wall of the left atrium.
- A number of non-PV sites (e.g., the superior vena cava [SVC], coronary sinus [CS], ligament of Marshall, crista terminalis, and posterior wall of left atrium) that share an embryologic relationship to the sinus venosus have been involved as the triggers and sustainer of AF.
- Reentrant wavelet in the left atrium can be associated with the atrial remodeling and the injured myocardium and have a potential of reentry induction of AF.
- Parasympathetic ganglionic plexuses as the vagus plexuses of the heart are located in the fat pad of superior and inferior cavoatrial junction.

3.3 Electrophysiologic Intervention and Pre-procedural Cardiac Imaging

3.3.1 Electrophysiologic Intervention

- Under fluoroscopic guidance, intracardiac catheters are passed into the right atrium or right ventricle (Fig. 3.3).
- Arteriovenous conduction is studied by positioning a separate catheter across the tricuspid annulus and obtaining a His bundle electrogram.
- To record activity from the left atrium (LA) and the left ventricle, a catheter is guided into the coronary sinus.
- Left-sided procedures in the LA and left ventricle are performed with a transseptal approach or with a retrograde approach from the femoral artery.
- In the catheter ablation of AF, the most common catheter technique includes the isolation of PVs using a circumferential extraostial ablation on the atrial side of the PVs (Fig. 3.4).
- Catheter ablation can create a linear or box-shaped ablation lesion set around the posterior wall of the left atrium, because the non-PV trigger points are commonly located in the posterior wall of the LA rather than the PV [4].
- To achieve the successful management of AF, additional stepwise approach can make multiple linear ablations focusing on the roof of LA, mitral isthmus, coronary sinus, and superior vena cava.
- The role of cardiac resynchronization therapy (CRT) has been established in medically refractory, systolic heart failure with abnormal QRS duration and morphology.
- The CRT with pacing of the left ventricle is accomplished via the coronary sinus.
- In the cardiac venous system, the left marginal vein and posterolateral vein along the lateral border of the left ventricle are considered as the target veins for pacemaker lead placement in CRT.
- Pacing in a scarred region may provide inadequate resynchronization, and a posterolateral scar is a strong predictor of nonresponse of CRT.

3.3.2 Cardiac Imaging Modality

- With introduction of multidetector computed tomography (CT), cardiac CT image can provide excellent temporal and spatial resolutions, which are sufficient for pre-procedural evaluation before the electrophysiologic intervention.

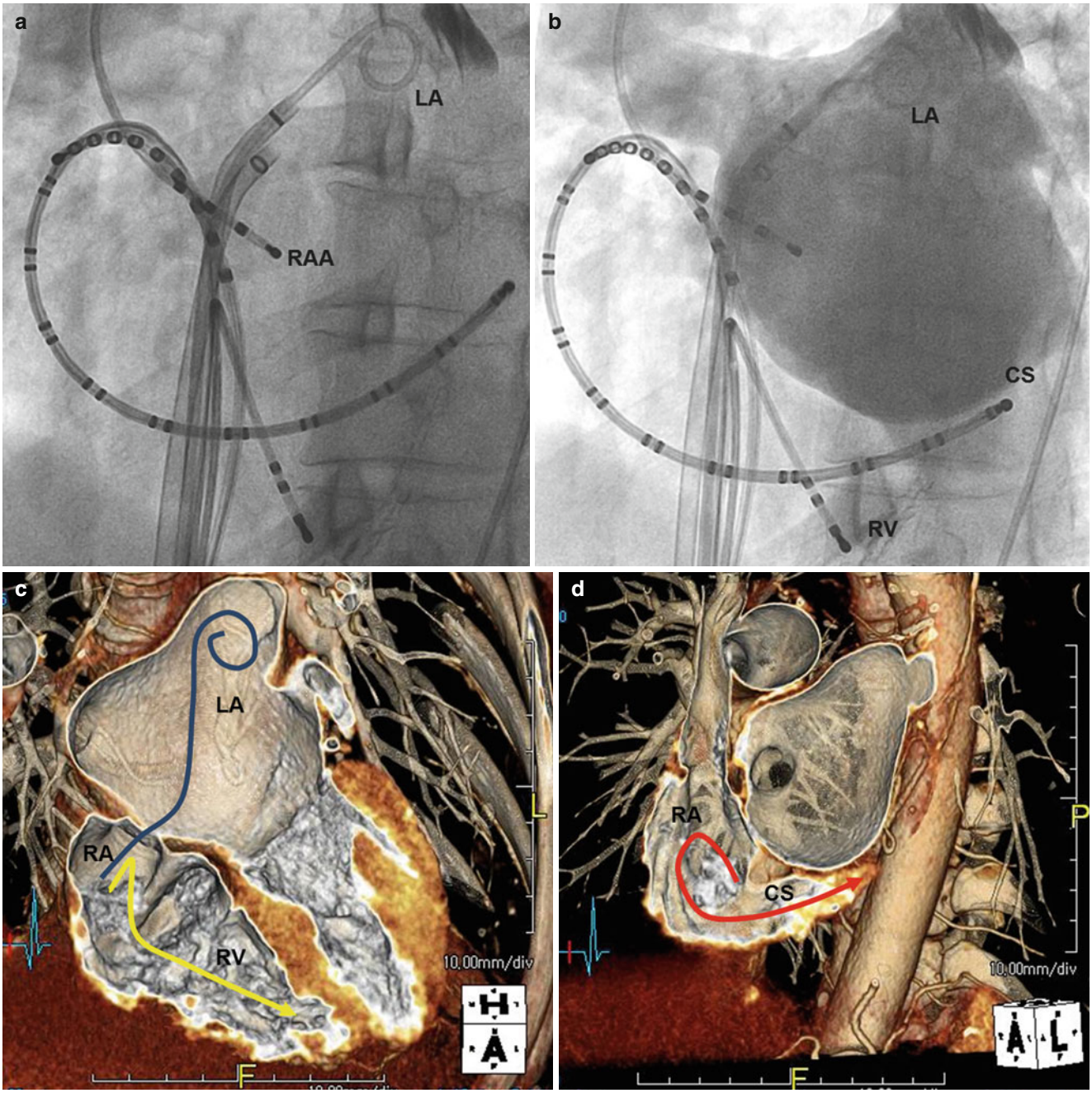

Fig. 3.3 Interventional electrophysiologic approach. For the fluoroscopy, radiographies (**a**, **b**) show three intracardiac catheters, which have been introduced via the inferior vena cava into the coronary sinus, the right ventricular apex, and the right atrial appendage. Volume-rendered CT images (**c**, **d**) show the routes of intracardiac catheters into CS (*red line*), RV apex (*yellow line*), and the transseptal puncture over the oval fossa to perform the left-sided procedure (*blue line*) in the LA. *RA* right atrium, *RAA* right atrial appendage, *LA* left atrium, *CS* coronary sinus, *RV* right ventricle

- Despite the presence of irregular heartbeat, the retrospective electrocardiography (ECG)-gated CT covering the entire cardiac cycle can provide a better image quality for advanced 3D post-processing and catheter guidance system.
- Retrospective ECG-gated cardiac CT image reconstructions can be performed at 10 % increments throughout the cardiac cycle in addition to three fixed temporal delay reconstructions in end systole at 150, 200, and 250 ms.
- For the pre-procedural cardiac CT imaging, the bolus injection of contrast media can be followed by the admixing of contrast media and saline (e.g., 30 % contrast media, 70 % saline) at the end of the injection to reduce the streak artifacts and evaluate the right heart (Fig. 3.5).
- Cardiac magnetic resonance (MR) imaging has been tried to alternate the CT image. But, one potential limitation of

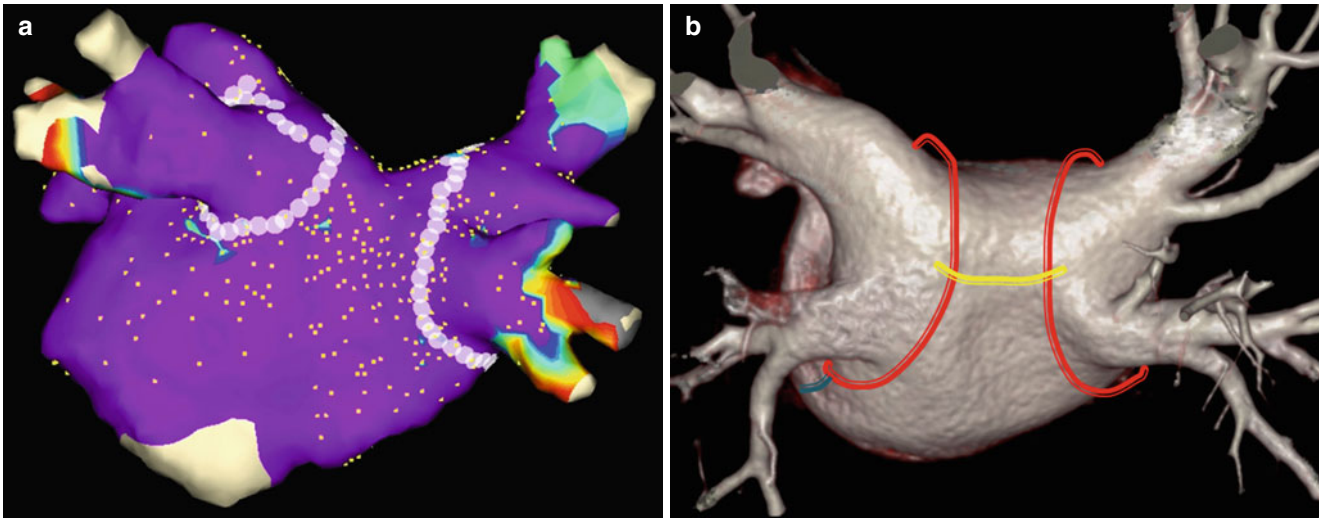

Fig. 3.4 Catheter ablation strategies for atrial fibrillation. Posterior electroanatomic map (**a**) and volume-rendered CT image (**b**) of the left atrium and pulmonary vein show the circumferential pulmonary vein ablation. In volume-rendered CT image (**b**), circumferential ablation line (*red*) around two pulmonary vein lesions is connected by a roof ablation line (*yellow*). A mitral isthmus ablation line (*blue*) is creased between the left inferior pulmonary vein and the lateral mitral annulus

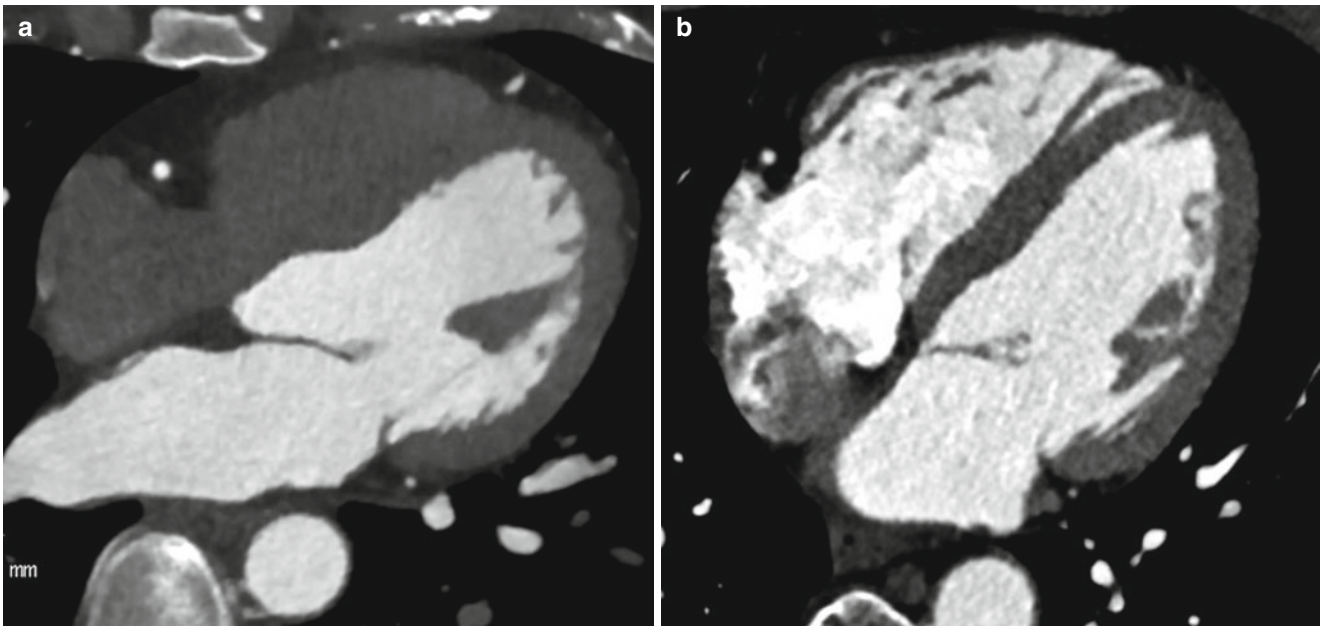

Fig. 3.5 Cardiac CT imaging to evaluate the right heart. When compared to the conventional coronary CT image (**a**), the cardiac CT image (**b**) to guide the electrophysiologic intervention was obtained by flushing of admixture with contrast media and saline and can help to delineate the right heart chamber more clearly

cardiac MR is the contraindication to imaging patients with pacemakers and defibrillator (Fig. 3.6).

- The best merit of cardiac MR imaging is to delineate the injured myocardium. When using the late-gadolinium enhancement MR sequence to evaluate the myocardial scar, the prognosis and treatment result after the electrophysiologic intervention can be predicted [5–7].
- Time-resolved contrast-enhanced MR angiography of the pulmonary vein can be used to provide a "road map" for catheter ablation of AF [8].
- In 2008, the feasibility of a live cardiac MR during the catheter ablation procedure was reported [9]. The potential advantage of such live MR setting is to ascertain the live formation of complete pulmonary vein scar by radiofrequency ablation.

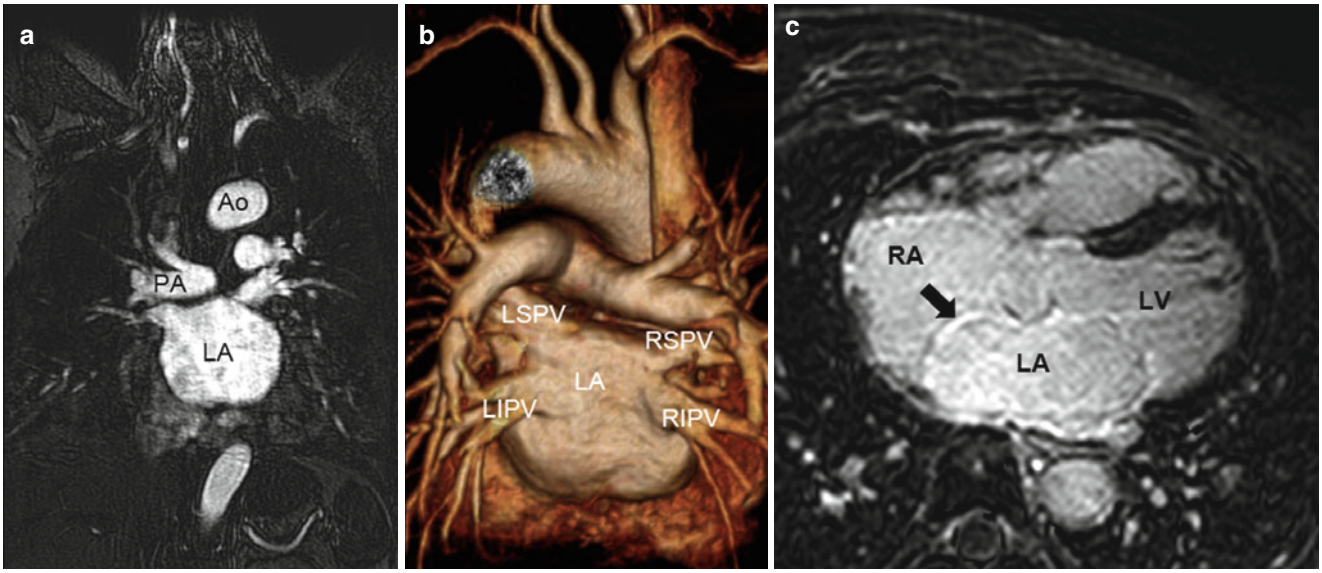

Fig. 3.6 Cardiac MR images to prepare the catheter ablation of atrial fibrillation. In the basis of three-dimensional time-resolved contrast-enhanced MR angiography (**a**), the volume-rendered MR image (**b**) provides the virtual appearance of the left atrium and pulmonary vein for the "roadmap" in the catheter ablation. Sequentially, late-gadolinium enhancement MR image (**c**) shows the myocardial injury of well enhancement (*arrow*) along the interatrial septum in patients with atrial fibrillation. *Ao* aorta, *PA* pulmonary artery, *LA* left atrium, *LSPV* left superior pulmonary vein, *LIPV* left inferior pulmonary vein, *RSPV* right superior pulmonary vein, *RIPV* right inferior pulmonary vein, *RA* right atrium, and *LV* left ventricle

3.4 Discerning Appearances of Cardiac Structures in the Electrophysiologic Intervention

3.4.1 Right Atrium

- The right atrium (RA) as the chamber of the heart that receives systemic venous blood return is located anterior to the LA.
- The RA consists of the appendage, the venous part (sinus venarum), and the vestibule.
- The anatomic characteristic of RA is the crista terminalis, "C-shaped muscular ridge" separating the smooth-walled sinus venarum from the trabeculated appendage (Fig. 3.7).
- The RA includes the important conduction components such as the SA node and AV node.
- In the terminal groove corresponding internally to crista terminalis, the SAN is located near the superior cavoatrial junction.
- The AV node is located within the boundaries of Koch's triangle, an important anatomic landmark for electrophysiologic study (Fig. 3.8).
- Koch's triangle is bordered posteriorly by the tendon of Todaro (fibrous extension from the eustachian ridge), anteriorly by the septal leaflet of the tricuspid valve, and inferiorly by the ostium of the coronary sinus.
- The central fibrous body at the apex of Koch's triangle is a landmark of penetrating His bundle in the atrioventricular (AV) junction.
- Using the cardiac CT image, Yasushi et al. reported that a large RA volume (≥99 mL) at the end systole of the left ventricle was significantly associated with AF recurrence after catheter ablation [10].
- The inferior wall of the RA between the inferior PV and the tricuspid valve is a quadrilateral region as cavotricuspid isthmus (CTI) as the ablation target for isthmus-dependent atrial flutter [11].
- In the inferior wall of the RA, obstacles such as large eustachian ridge, aneurysmal pouches, or a concave deformation of CTI may lead to more difficult ablation sessions [12].

3.4.2 Cardiac Venous System

- The cardiac veins can be grouped into the following categories, according to the region being drained: the coronary sinus (CS) and its tributaries, the anterior cardiac veins, and the Thebesian veins.
- The Thebesian veins (venae cordis minimae) are a number of small veins that drain the subendocardium and are continuous with the endothelial lining of the cardiac chambers.
- CS is the most constant structure emptying into the LA and can be used as a conduit for the catheter treatment of arrhythmias as well as the left ventricular pacing.
- The major tributaries of the CS include the anterior interventricular vein, the great cardiac vein (GCV), the left marginal vein, the posterior vein, and the middle cardiac vein.
- Congenital coronary sinus anomalies include diverticulum, stenosis, ectasia, unroofed sinus, ostial atresia, agenesis, and duplication (Fig. 3.9).

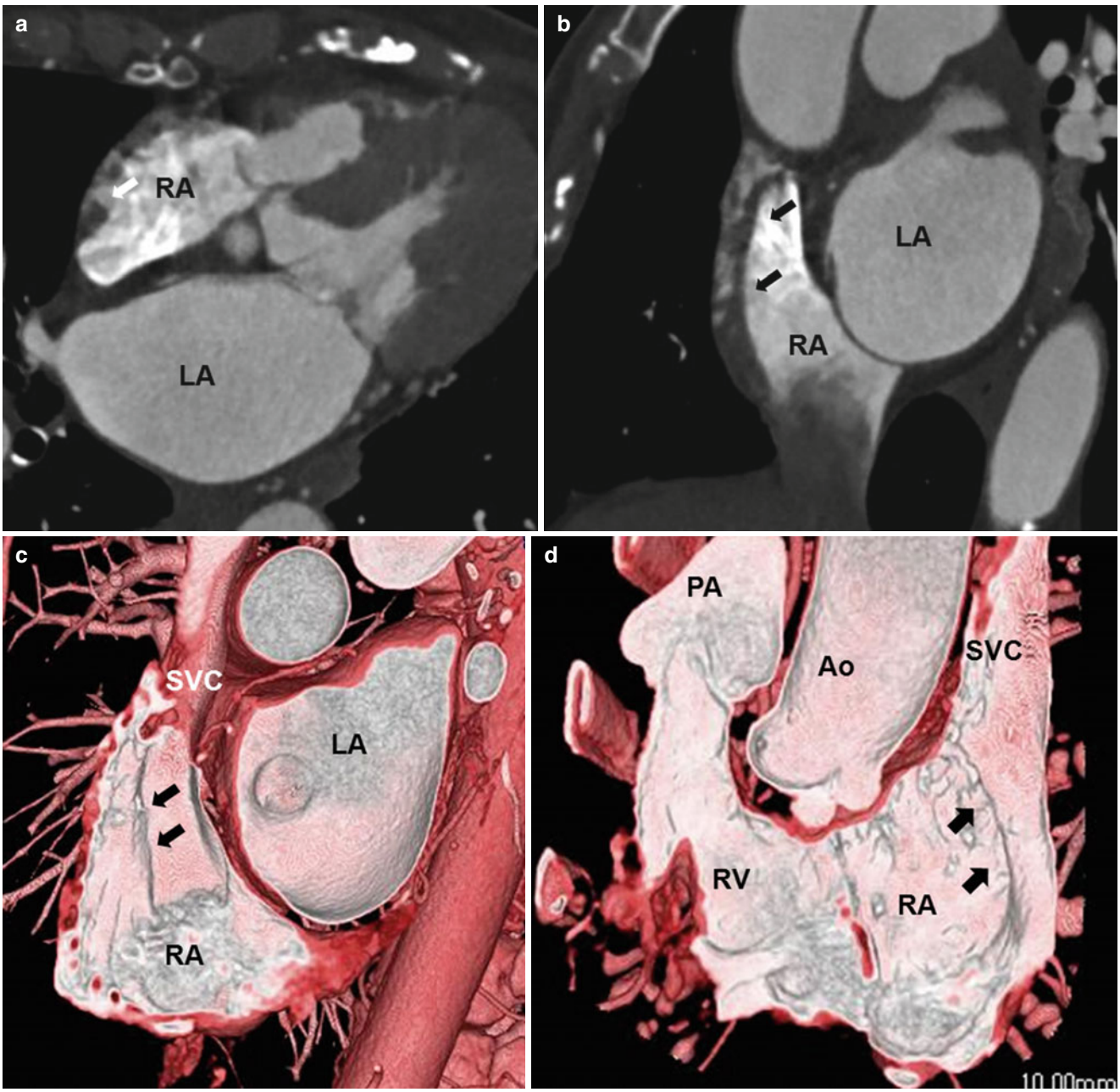

Fig. 3.7 Crista terminalis. Transverse (**a**), coronal-reformatted (**b**), and volume-rendered (**c**, **d**) CT images show the crista terminalis (*arrows*) extending from the superior vena cava to the inferior vena cava. *Ao* aorta, *PA* pulmonary artery, *LA* left atrium, *SVC* superior vena cava, *RA* right atrium, and *RV* right ventricle

- In the pathogenesis of AF, the CS enveloped by muscular fibers as the connections to the LA can be considered as the non-PV triggers.
- As the minor cardiac vein, the vein of Marshall runs inferiorly along the LA inferior wall to join the CS with muscular connections to the left PVs. So, the ligament or vein of Marshall can be another origin of non-PV trigger for AF (Fig. 3.10).
- Also the persistent LSVC draining into the CS can act as the non-PV triggers.

3.4.3 Interatrial Septum

- The interatrial septum with complex process of several tissue components comprises the foramen ovale (septum primum) which is a flap valve and typically fuses by early adulthood.
- The flap of the foramen ovale closes against the atrial septum, with fusion usually occurring within the first 2 years of life. Incomplete fusion results in probe patent defect, or patent foramen ovale (PFO).

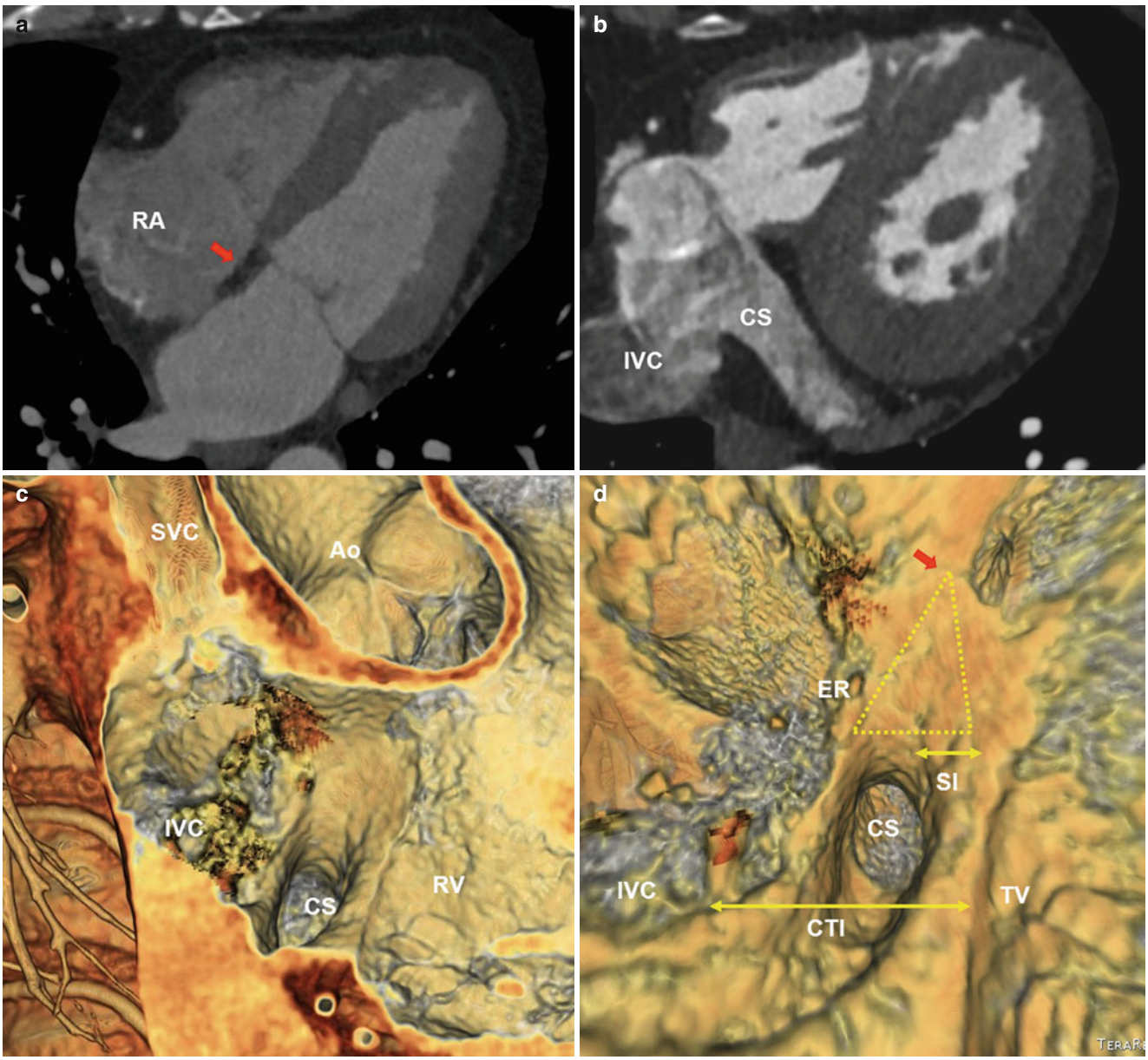

Fig. 3.8 Koch's triangle, eustachian ridge, and cavotricuspid isthmus. Transverse cardiac CT images (**a**, **b**) show the central fibrous body (CFB) (*red arrow*) and coronary sinus as the borders of the Koch's triangle. Endocardial view CT images (**c**, **d**) of the right atrioventricular (AV) junction shows Koch's triangle (*yellow triangle*) and the right atrial isthmus (*small double arrows*). Koch's triangle is demarcated by the tendon of Todaro–Eustachian ridge (*ER*) posteriorly, the septal tricuspid valve anteriorly (*yellow arrows*), coronary sinus (*CS*) inferiorly, and central fibrous body (CFB) at the apex (*red arrow*). The septal isthmus (SI), the area between the CS and septal tricuspid valve, is the target for ablation of AV node reentrant tachycardia. The CTI (*large double arrow*) is defined as the inferior wall of the right atrium between the inferior vena cava and the tricuspid valve. The CTI is the target of catheter ablation for isthmus-dependent atrial flutter. *Ao* aorta, *RA* right atrium, *SVC* superior vena cava, *IVC* inferior vena cava, *RV* right ventricle, *SI* septal isthmus, and *TV* tricuspid valve

- The foramen ovale is the only portion of the septum that can be traversed without risk of exiting the heart.
- Common anatomic variation of the interatrial septum includes PFO, atrial septal aneurysm, atrial septal defect, and lipomatous hypertrophy of the septum (LHS) (Fig. 3.11).
- The superior rim (the septum secundum) of the foramen ovale is the infolded wall between the superior vena cava and the right pulmonary veins known as the interatrial groove.
- The relative thickness of the interatrial septum is directly proportional to the amount of fat in the interatrial groove. Furthermore, thickness greater than 2 cm is defined as lipomatous hypertrophy of the septum (LHS) [13].
- In the electrophysiologic intervention, the left atrium is accessed via a PFO or using a transseptal puncture of the foramen ovale.
- Cardiac arrhythmias including AF can be associated with increase in thickness of fat in the interatrial septum [14].
- The septal components of the AV junction are important because they conduct the cardiac impulse from the atria to the ventricles.

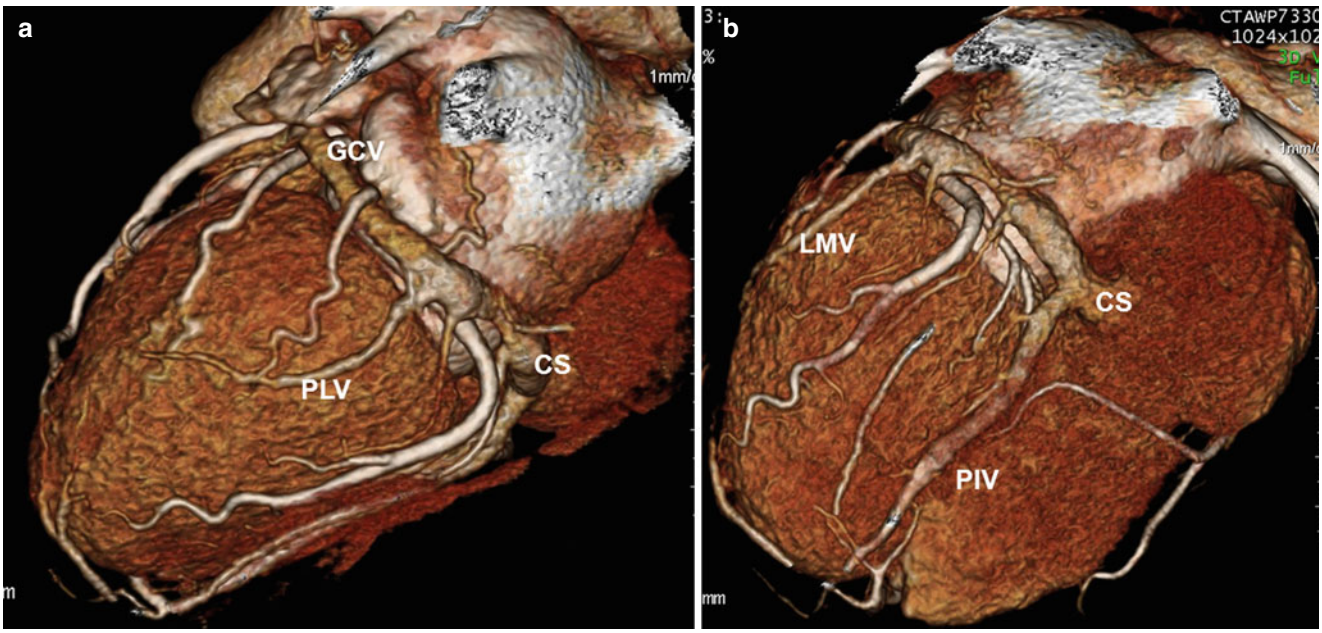

Fig. 3.9 Cardiac venous anatomy. Three-dimensional images (**a**, **b**) shows normal cardiac venous anatomy including the coronary sinus. The great cardiac vein (*GCV*) receives two main branches: the left marginal vein (*LMV*) in the lateral border of the left ventricle and the posterolateral vein (*PLV*). *CS* coronary sinus, *PIV* posterior interventricular vein

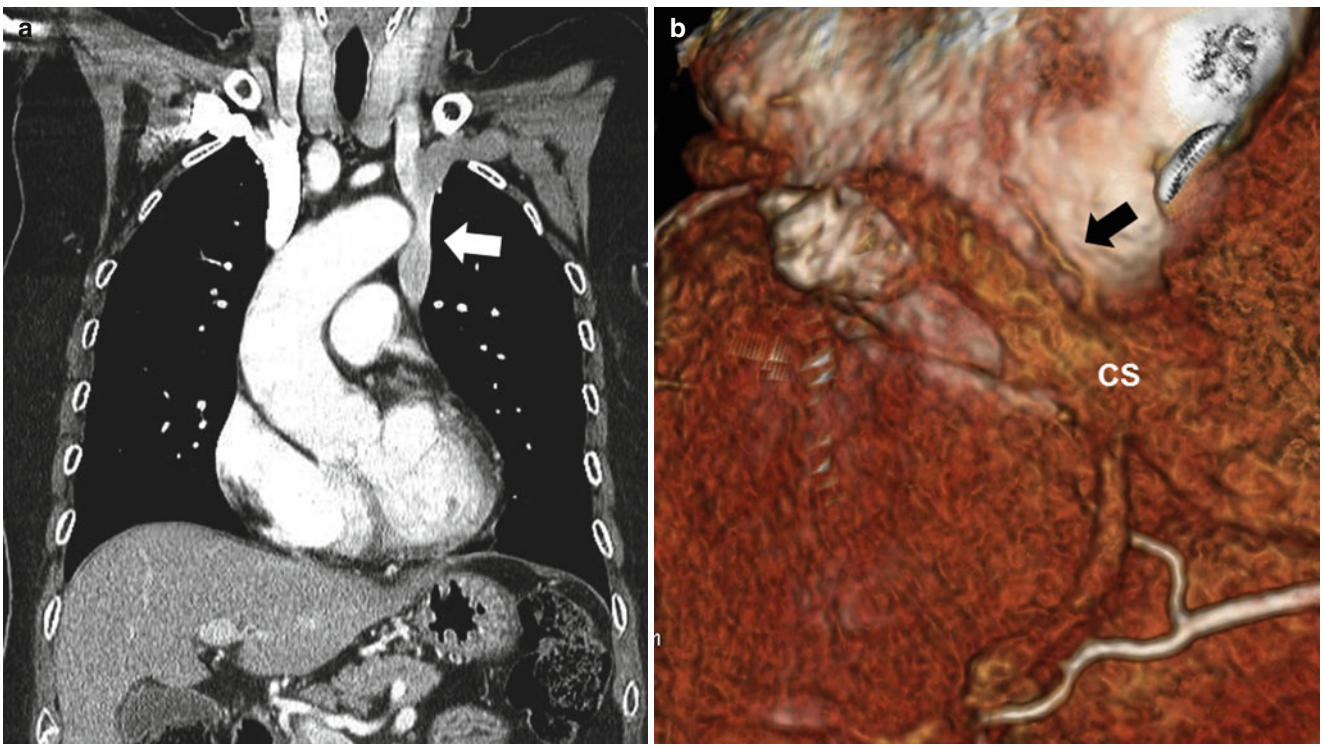

Fig. 3.10 Persistent left SVC and vein of Marshall. Coronal-reformatted CT image (**a**) shows preferential drainage of blood into the left SVC (*arrow*) from the left brachiocephalic vein. The 3D CT image of the inferior wall of the heart (**b**) shows the vein or ligament of Marshall (*arrow*) as the remnant of the left superior vena cava, which descends between the left atrial appendage and left pulmonary vein to join into the coronary sinus (*CS*)

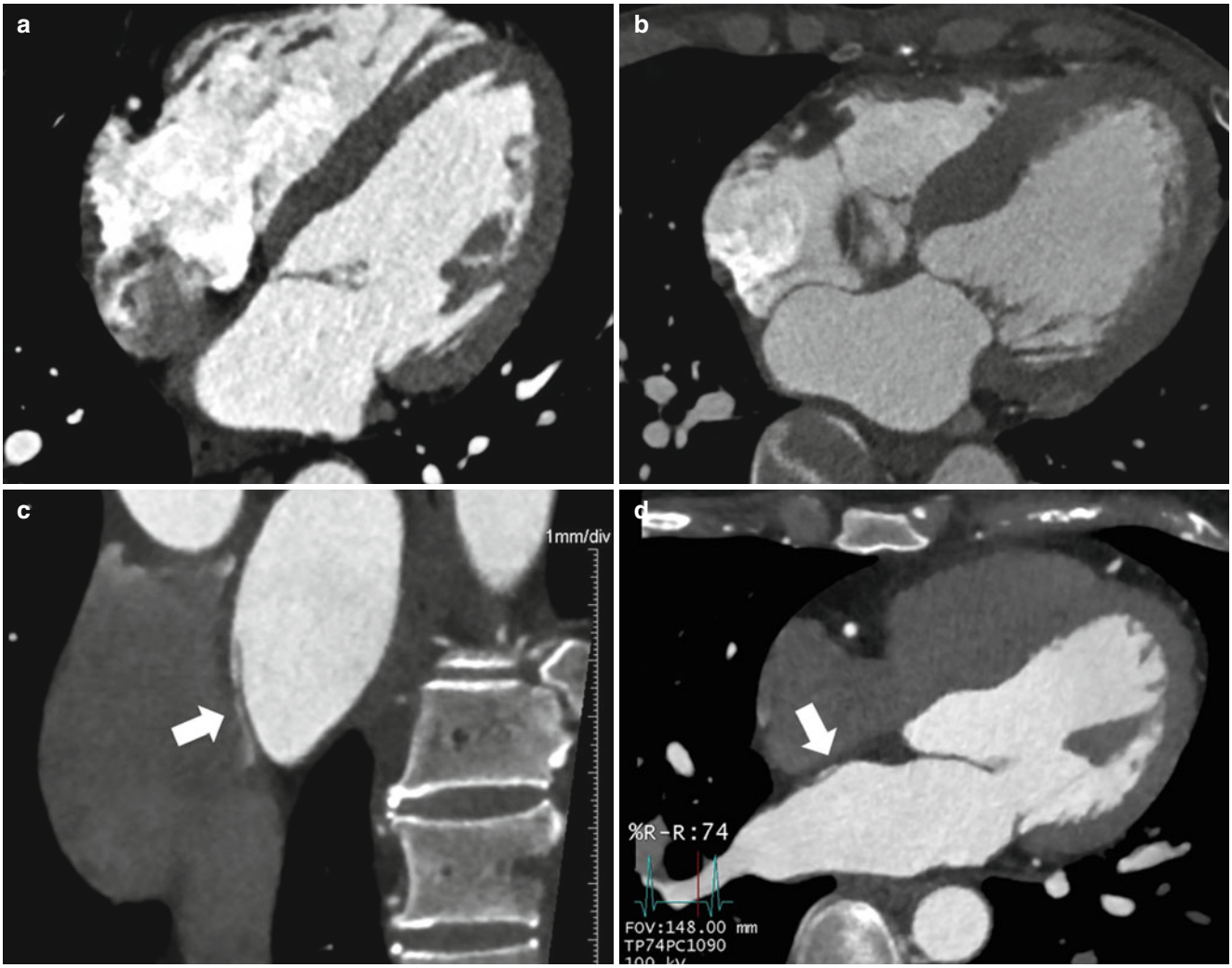

Fig. 3.11 Components of the interatrial septum. Four-chamber view CT images (**a**, **b**) show the interatrial groove (*arrow*), eustachian ridge, and muscular atrioventricular septum. The only true septum between the two atria is confined to the area of the oval fossa and a small portion of the inferior rim. The reformatted CT images (**c**, **d**) show anatomic variants of the patent foramen ovale (*arrow*). *IAG* interatrial groove and *ER* eustachian ridge

3.4.4 Left Atrium

- The left atrium (LA) is a complex structure that comprises three anatomic compartments of different embryologic origins: the venous LA, the left atrial appendage, and the anterior LA [15] (Fig. 3.12).
- Of the three anatomic LA compartments, the venous LA connected with PV can show a chamber dilatation correlated with the chronicity of AF [16].
- The vestibule area between the left inferior PV and the mitral annulus is known as mitral isthmus, which may be the source of AF recurrence after catheter ablation (Fig. 3.13).
- In patients with AF, mechanical remodeling of the LA leads to LA enlargement with decreased atrial contractility and increased atrial compliance [17].
- In the assessment of LA volume before catheter ablation, Yasushi et al. reported that a large LA volume (≥87 mL) at the end systole of the left ventricle was significantly associated with AF recurrence after ablation [10] (Fig. 3.14).
- Depending on the LA scar extent of entire LA wall by MR image, the Utah classification is defined as Utah score 1 (<5 % LA scar), 2 (5–20 %), 3 (20–35 %), and 4 (>35 %) [5]. The absence of a pre-ablation significant LA scar identifies a group of patients with a high success rate [18] (Fig. 3.15).
- In the anterior superior cardial aspect of the LA, the most muscular bridge is the Bachmann bundle (BB). Changes in the musculature of the BB can affect the interatrial conduction and result in abnormal atrial excitability and atrial dysfunction. The BB is directly invisible but can be estimated by the replaced fat pad on CT image [19].

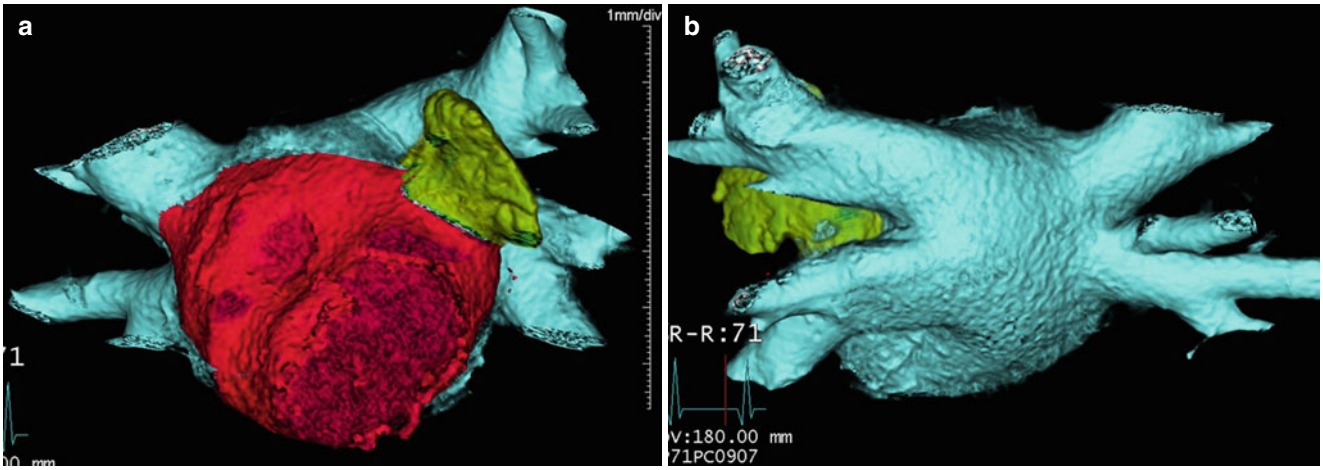

Fig. 3.12 Three anatomic compartment of the left atrium. Volume-rendered CT image on anterior (**a**) and posterior (**b**) aspects of the left atrium (LA) shows three anatomic compartment of the LA: the venous LA (*blue*), the left atrial appendage (*red*), and the anterior LA (*green*)

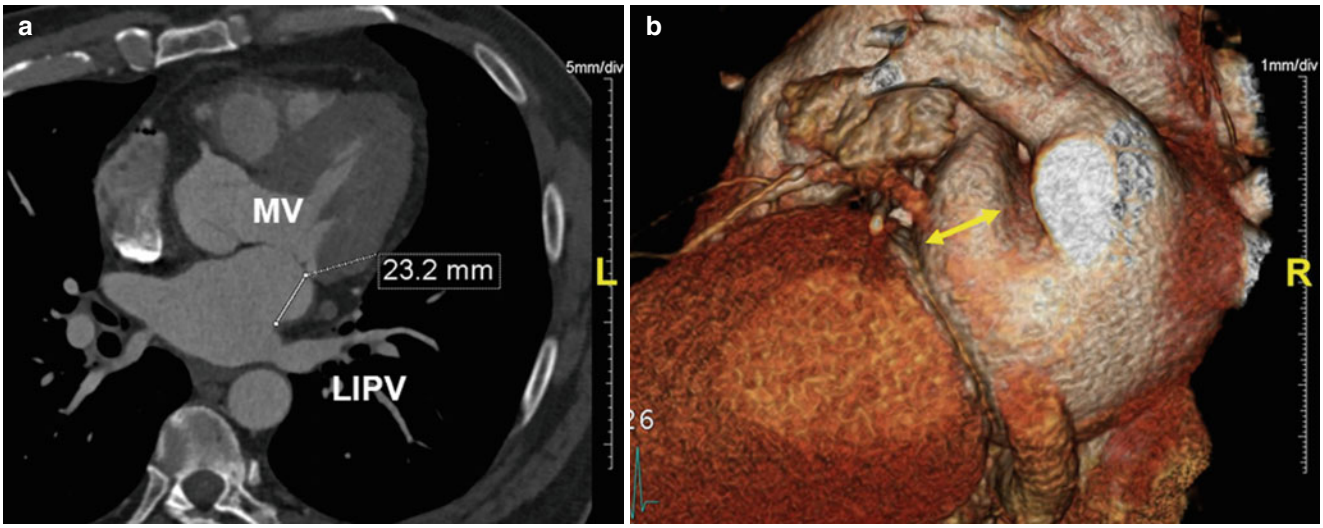

Fig. 3.13 The left atrial isthmus. Transverse CT image (**a**) and 3D volume-rendered CT image (**b**) show the left atrial isthmus between the orifice of the left inferior pulmonary vein and the posteroinferior margin of the mitral annulus (*double yellow arrow*). The left atrial isthmus may be the source of recurrence after catheter ablation. *MV* mitral valve, *LIPV* left inferior pulmonary vein

- Left atrial ablation should not be performed in the presence of known atrial thrombus.
- The left atrial appendage (LAA) is the most common location of thrombus formation, usually secondary to blood stasis from AF [20] (Fig. 3.16).
- On contrast-enhanced cardiac CT, unmixed blood and contrast material in the LAA can mimic a thrombus or mass. So, a negative CT almost invariably rules out an LAA thrombus. But, the opposite is not true with an overall diagnostic accuracy and specificity varying from 34 to 100 % and 44 to 85 %, respectively [21–23].
- Kim et al. used the ratio of LAA to ascending aorta HU (LAA/AA HU) and showed that a ratio cutoff of 0.25 improved the specificity to 96 % in diagnosis of LAA thrombi [21].
- Delayed cardiac CT imaging can also differentiate thrombus from slow flow [24].
- The accessory LAA is a common anatomic variant and can be seen in the anterior wall of the LA and the left atrial isthmus [25] (Fig. 3.17).
- A nonobstructive membrane of the left atrium should raise the possibility of cor triatriatum, the rare but surgically correctable anomaly (Fig. 3.18).

3.4.5 Pulmonary Veins

- The pulmonary vein (PV) anatomy as well as the left atrium (LA) anatomy has been of interest to the operators during the planning for catheter ablation of AF.

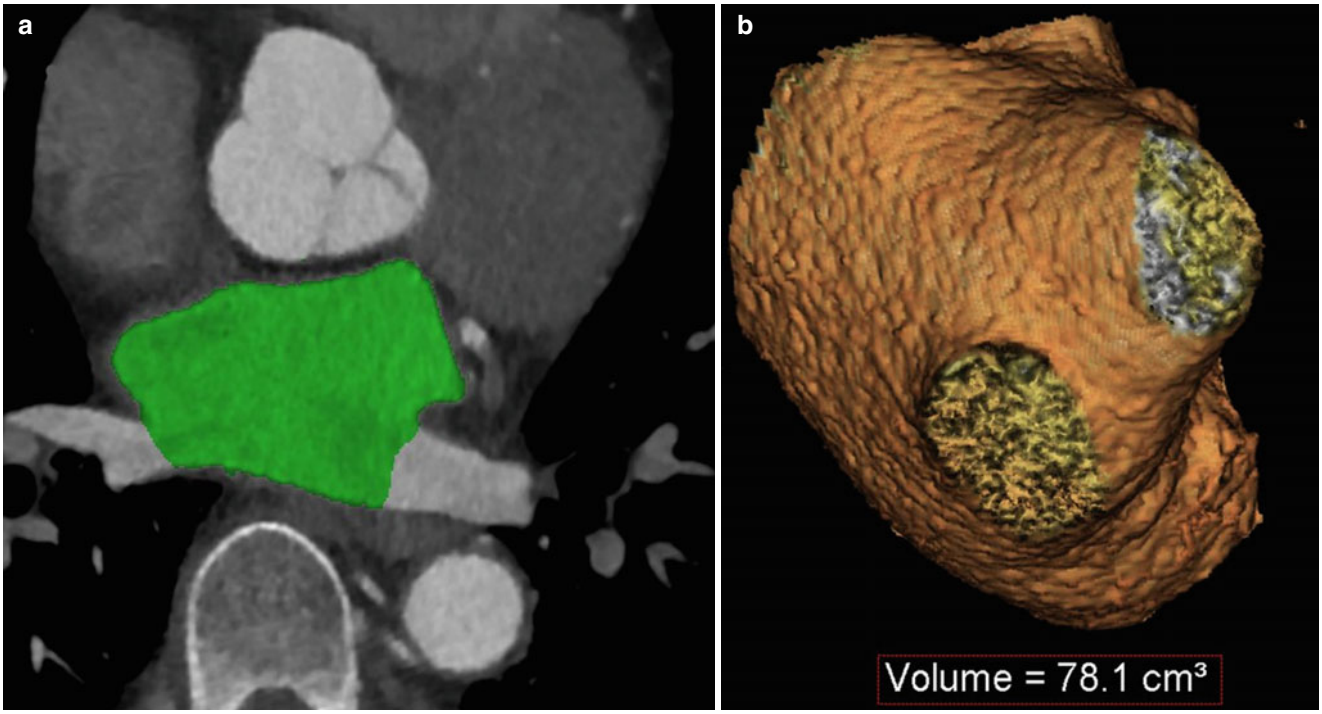

Fig. 3.14 Quantification of the left atrium by using cardiac CT. Transverse cardiac CT image (**a**) shows a segmentation of the left atrium (*green*), and 3D volume-rendered CT image (**b**) provided a quantification of left atrial volume, 78.1 cm^3

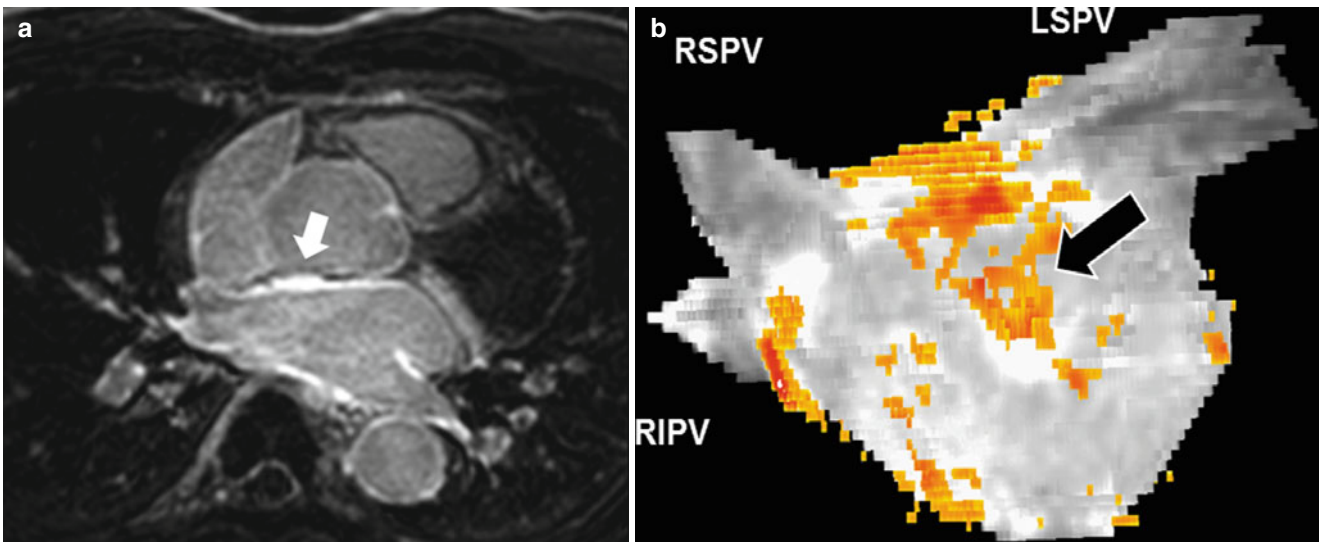

Fig. 3.15 Quantification of the left atrium by using cardiac MR. By using cardiac MR with late-gadolinium enhancement sequence, the transverse MR image (**a**) shows the left atrial wall scar (*arrow*) of bright signal intensity, and the 3D MR image (**b**) provides a reformatted 3D appearance of the color-coded left atrial wall scar. *RSPV* right superior pulmonary vein, *LSPV* left superior pulmonary vein, *RIPV* right inferior pulmonary vein

- In basis of cardiac CT or MR isotropic voxel data, three-dimensional and endoluminal views of the LA and PVs show most of the information regarding pulmonary vein location and ostia.
- Classic cardiac anatomy shows bilateral superior and inferior PVs, which drain into the LA. The normal pulmonary venous anatomy consists of two right pulmonary veins and two left pulmonary veins with separate ostia (Fig. 3.19).
- The pulmonary venous trunk is defined as the distance from the ostium to the first-order branch.
- It is important to report the trunk length and the ostial diameters of each vein, which influence the selection of catheter diameter.

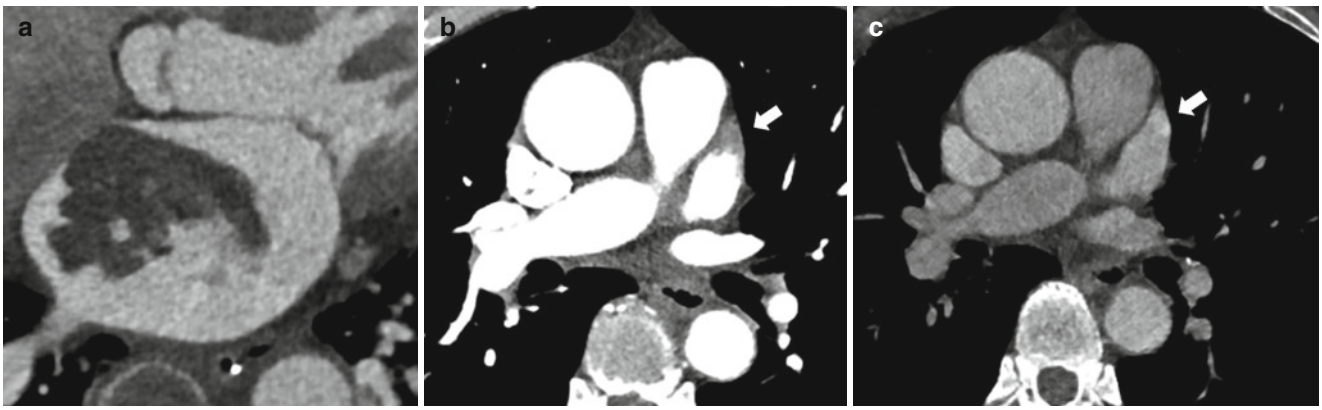

Fig. 3.16 Left atrial thrombus. Contrast material-enhanced CT image (**a**) shows filling defects in the left atrium, suggestive of thrombus. But, (**b**) the heterogeneous attenuation from unmixed blood and contrast material can mimic a thrombus in the left atrial appendage (*arrow*). (**c**) On a CT scan obtained 30 s after **b**, the blood layering has completely disappeared in left atrial appendage (*arrow*)

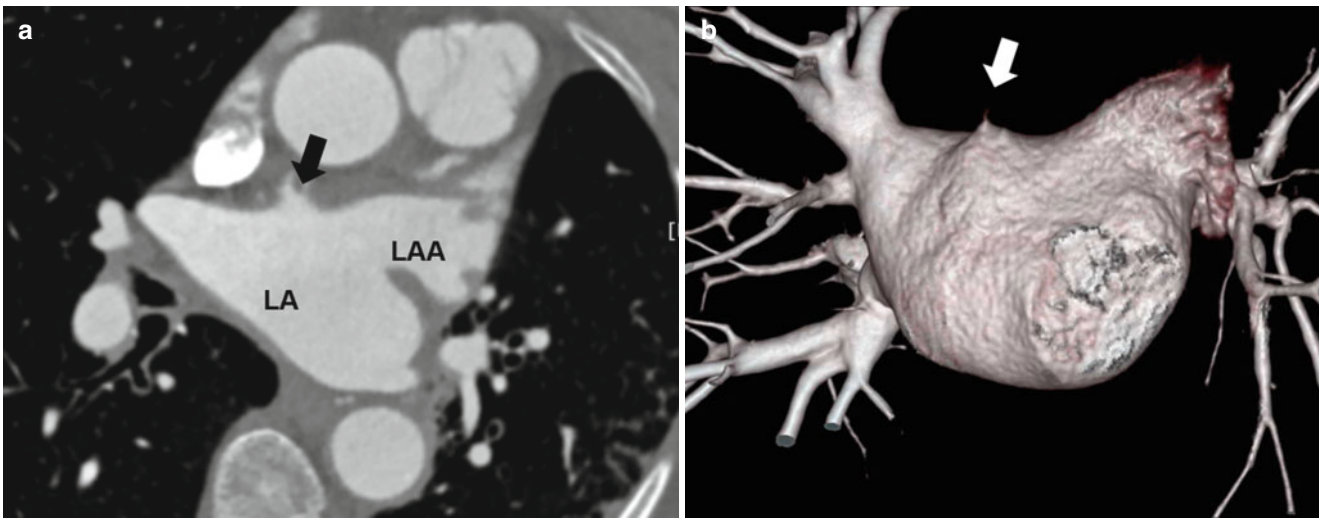

Fig. 3.17 Accessory left atrial appendage. Coronal-reformatted (**a**) and volume-rendered (**b**) CT images show a small accessory left atrial appendage (*arrow*) in the roof of the left atrium. *LA* left atrium, *LAA* left atrial appendage

- The PV trunk is defined as the distance from the ostium to the first-order branch. The superior pulmonary vein ostia are larger (19–20 mm) than the inferior pulmonary vein ostia (16–17 mm), and the superior pulmonary veins have a longer trunk (21.6 ± 7.5 mm) than the inferior pulmonary veins (14.0 ± 6.2 mm) [26, 27].
- Common anomalies include a conjoined pulmonary vein, which is more frequently seen on the left side than on the right [27].
- An accessory right middle PV is the most common variant, occurring 20–30 %, and it has typically 1 cm or less in diameter.
- The next most common accessory vein drains the superior segment of the right lower lobe independently.
- All accessory veins must be identified and reported, but these veins are frequently less than 1 cm in diameter which may increase risk of stenosis if they are unrecognized before catheter ablation.
- Partial anomalous pulmonary venous return drains to CS should be identified before the procedure. This is in the expected location for a typical PV ablation line.
- Although a larger vein diameter (>24 mm) or the presence of a separate right middle pulmonary vein has a trend toward AF recurrence after catheter ablation [28], it has been shown that the pulmonary vein anatomy assessment by cardiac CT or MR does not affect long-term efficacy of the procedure [28–30].

3.5 Ancillary CT Finding

3.5.1 Esophagus, Coronary Artery, and Phrenic Nerve

- The esophagus is a thin structure that lies close to the posterior left atrial wall and may be injured during AF ablation.

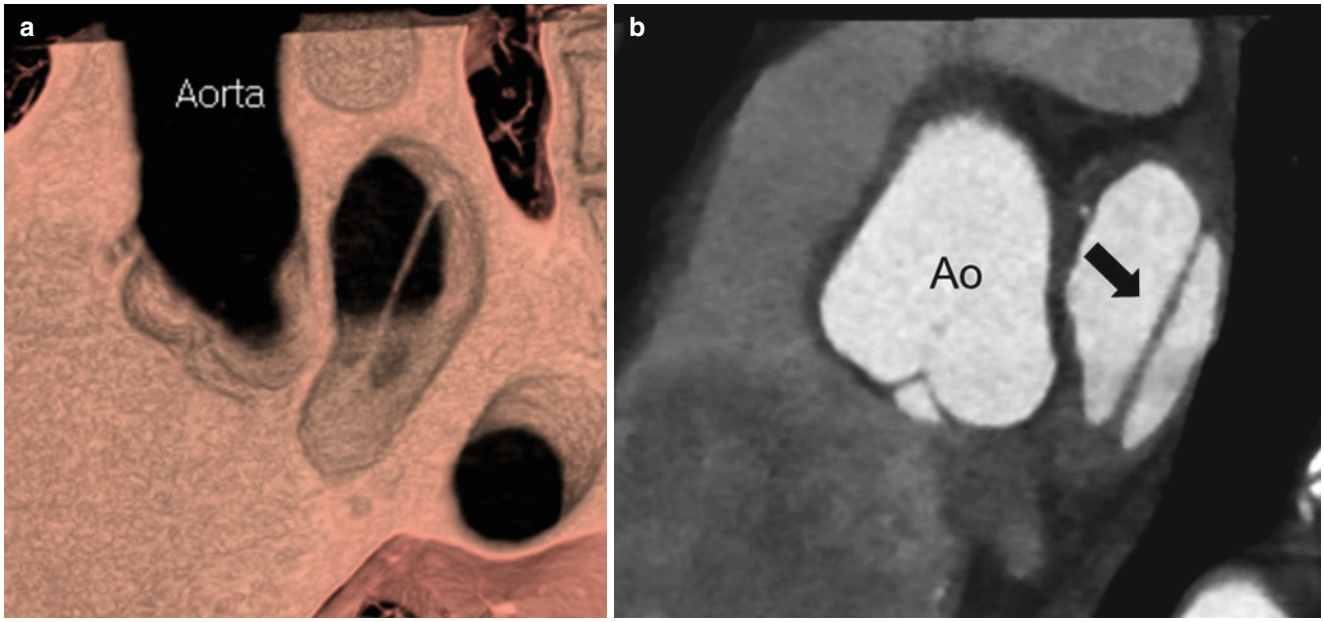

Fig. 3.18 Cor triatriatum. Three-dimensional (**a**) and two-chamber view (**b**) CT images show a nonobstructive membrane or columnar structure as the cor triatriatum within the left atrial chamber

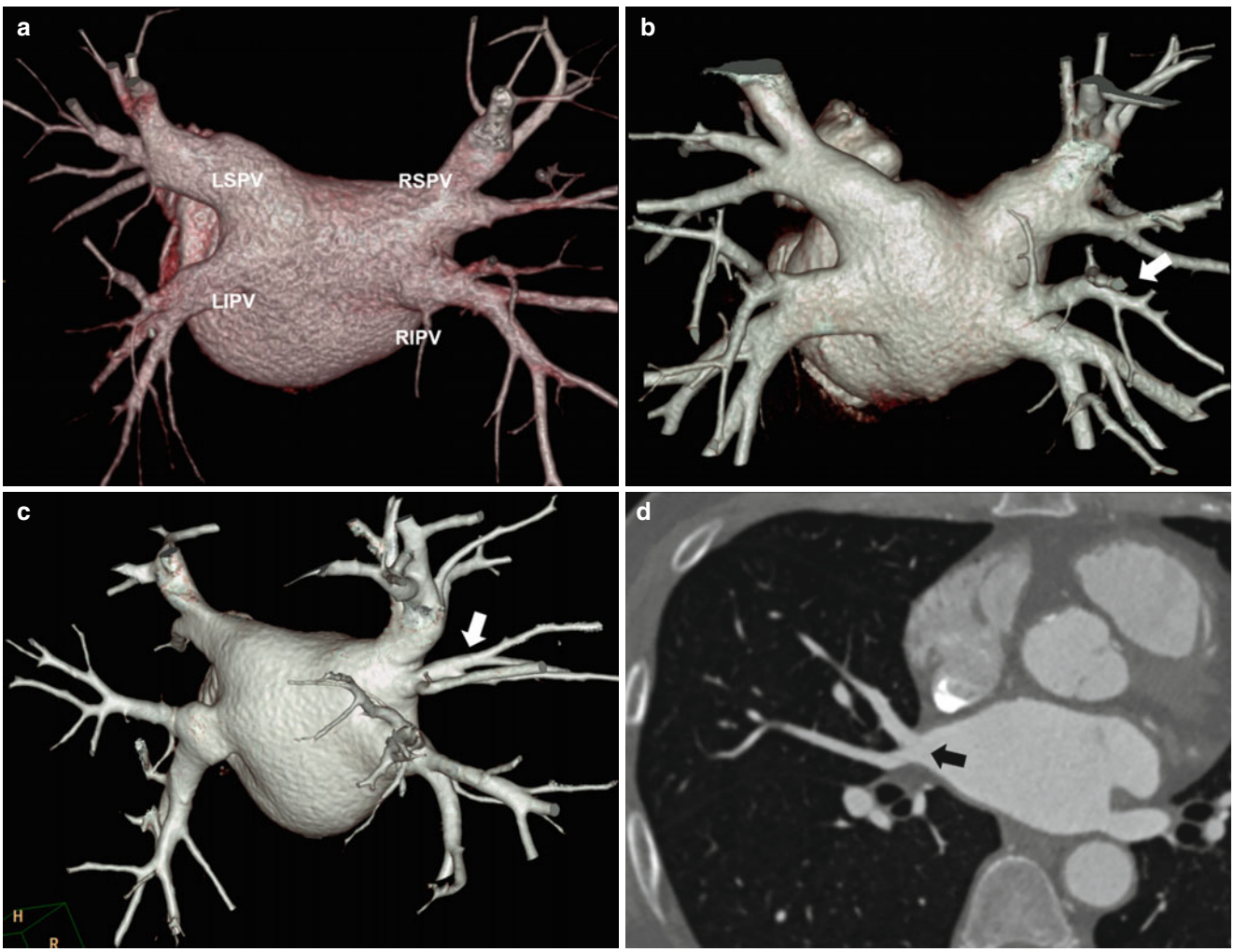

Fig. 3.19 Anatomy of the pulmonary veins. Three-dimensional CT images show normal appearance and anatomic variants of the pulmonary veins: (**a**) normal appearance, (**b**) an early branching of the pulmonary vein (ostial branch, *arrow*), and (**c**, **d**) a small right middle accessory pulmonary vein (*arrow*) draining the right middle lobe as the most common variant. *LIPV* left inferior pulmonary vein, *LSPV* left superior pulmonary vein, *RIPV* right inferior pulmonary vein, *RSPV* right superior pulmonary vein

- Catheter ablation procedures involving the posterior wall of LA may cause esophageal damage and result in formation of an atrial esophageal fistula [31].
- A more posterior mitral isthmus line may increase the risk to the esophageal injury.
- CT is a valuable tool to show the relation of the LA wall and esophagus, but peristalsis and dynamic movement of esophagus can result in discordance between the pre-procedure and intra-procedure anatomy [32].
- Acute occlusion of the left circumflex coronary (LCx) artery during catheter ablation within the CS to complete the line of block of mitral isthmus has been reported [33].
- In the association between the coronary artery disease (CAD) and AF, CAD has been found to increase the risk of AF [34]. Furthermore, the CAD and AF share a number of risk factors (e.g., increasing age, obesity, diabetes, heart failure, and hypertension) and often coexist [34–36].
- The phrenic nerves lie along the lateral mediastinum and run from the thoracic inlet to the diaphragm.
- Phrenic nerve injury results from direct thermal injury, usually to the right phrenic nerve near the right superior PV and the SVC [37].
- Less frequently, catheter ablation within the LAA can result in left phrenic nerve injury. And, left phrenic nerve stimulation after CRT is a well-recognized complication.
- Given the anatomic variability of the target coronary veins for CRT and the proximity of the left phrenic nerve to these structures, it is clinically important to identify the relationship between the left phrenic nerve and the left lateral marginal vein to avoid the diaphragmatic paralysis.

Interpretation of cardiac imaging for the electrophysiologic intervention
For the catheter ablation of atrial fibrillation
1. Right atrial volume, cavotricuspid isthmus, eustachian ridge near the coronary sinus
2. Variation/anomaly of coronary sinus
3. Variation of interatrial septum (e.g., PFO, atrial septal aneurysm, atrial septal defect, and LHS)
4. Left atrial volume, mitral isthmus, intracardiac thrombus, accessory left atrial appendage
5. Left atrial scar, when using on cardiac MR
6. Normal anatomy and anatomic variants of the pulmonary veins (e.g., ostial diameters of each vein and the distance to the first-order branch and accessory or supernumerary pulmonary veins)
7. Other vascular anomalies, such as a common ostium to the superior and inferior pulmonary veins, persistent left superior vena cava, vein of Marshall, or anomalous pulmonary venous return
8. Anatomic course of the esophagus relative to the posterior left atrial wall
For the cardiac resynchronization therapy
1. Comprehensive evaluation of the coronary venous anatomy
2. Measurement of the coronary sinus orifice and the target veins
3. Phrenic nerve, the relationship of the left phrenic neurovascular bundle to the target vein
4. Left ventricular scar, when using the cardiac MR (e.g., a posterolateral scar and total scar size)

3.6 Summary

- With advances of catheter-based electrophysiologic intervention, management of cardiac arrhythmia has become more active and aggressive in patients with AF or chronic heart failure.
- Until now, the major electrophysiologic intervention includes catheter ablation of arrhythmogenic foci associated with AF and cardiac resynchronization therapy in chronic heart failure.
- The comprehensive knowledge of cardiac anatomy can help to enhance the understanding of complex pathophysiology of cardiac arrhythmia.
- In addition, the more active and aggressive is the electrophysiologic intervention, the more essential the delineation of precise cardiac anatomy would be for the success of the procedure.
- Recently, a remarkable development of cardiac imaging by CT or MR can provide the delineation of cardiac anatomy as well as the cardiac tissue characterization related to the prognosis of electrophysiologic intervention.
- Eventually, as the need of cardiac imaging has been increased with advances of technique, the radiologist should be familiar to the clinical need and the technical consideration in the electrophysiologic intervention.

References

1. Haissaguerre M, Jais P, Shah DC, et al. Spontaneous initiation of atrial fibrillation by ectopic beats originating in the pulmonary veins. N Engl J Med. 1998;339:659–66.
2. Saksena S, Skadsberg ND, Rao HB, Filipecki A. Biatrial and three-dimensional mapping of spontaneous atrial arrhythmias in patients with refractory atrial fibrillation. J Cardiovasc Electrophysiol. 2005;16:494–504.
3. Li J, Wang L. Catheter ablation of atrial fibrillation originating from superior vena cava. Arch Med Res. 2006;37:415–8.
4. European Heart Rhythm A, European Cardiac Arrhythmia S, American College of C, et al. HRS/EHRA/ECAS expert Consensus Statement on catheter and surgical ablation of atrial fibrillation: recommendations for personnel, policy, procedures and follow-up. A report of the Heart Rhythm Society (HRS) Task Force on catheter and surgical ablation of atrial fibrillation. Heart Rhythm. 2007;4:816–61.
5. Oakes RS, Badger TJ, Kholmovski EG, et al. Detection and quantification of left atrial structural remodeling with delayed-enhancement magnetic resonance imaging in patients with atrial fibrillation. Circulation. 2009;119:1758–67.
6. White JA, Yee R, Yuan X, et al. Delayed enhancement magnetic resonance imaging predicts response to cardiac resynchronization therapy in patients with intraventricular dyssynchrony. J Am Coll Cardiol. 2006;48:1953–60.
7. Ypenburg C, Roes SD, Bleeker GB, et al. Effect of total scar burden on contrast-enhanced magnetic resonance imaging on response to cardiac resynchronization therapy. Am J Cardiol. 2007;99:657–60.
8. Faggioni L, Zampa V, Ortori S, et al. Time-resolved contrast-enhanced magnetic resonance angiography (CEMRA) of the left atrium-pulmonary veins complex with half dose of intravenous gadolinium-based contrast agent. Technical feasibility and

comparison with a conventional CEMRA, full contrast dose protocol. Eur J Radiol. 2012;81:250–6.
9. Nazarian S, Kolandaivelu A, Zviman MM, et al. Feasibility of real-time magnetic resonance imaging for catheter guidance in electrophysiology studies. Circulation. 2008;118:223–9.
10. Akutsu Y, Kaneko K, Kodama Y, et al. Association between left and right atrial remodeling with atrial fibrillation recurrence after pulmonary vein catheter ablation in patients with paroxysmal atrial fibrillation: a pilot study. Circ Cardiovasc Imaging. 2011;4:524–31.
11. Poty H, Saoudi N, Nair M, Anselme F, Letac B. Radiofrequency catheter ablation of atrial flutter. Further insights into the various types of isthmus block: application to ablation during sinus rhythm. Circulation. 1996;94:3204–13.
12. Da Costa A, Faure E, Thevenin J, et al. Effect of isthmus anatomy and ablation catheter on radiofrequency catheter ablation of the cavotricuspid isthmus. Circulation. 2004;110:1030–5.
13. Reyes CV, Jablokow VR. Lipomatous hypertrophy of the cardiac interatrial septum. A report of 38 cases and review of the literature. Am J Clin Pathol. 1979;72:785–8.
14. Heyer CM, Kagel T, Lemburg SP, Bauer TT, Nicolas V. Lipomatous hypertrophy of the interatrial septum: a prospective study of incidence, imaging findings, and clinical symptoms. Chest. 2003;124:2068–73.
15. Kerut EK. Anatomy of the left atrial appendage. Echocardiography. 2008;25:669–73.
16. Park MJ, Jung JI, Oh YS, Youn HJ. Assessment of the structural remodeling of the left atrium by 64-multislice cardiac CT: comparative studies in controls and patients with atrial fibrillation. Int J Cardiol. 2012;159:181–6.
17. Mathew ST, Patel J, Joseph S. Atrial fibrillation: mechanistic insights and treatment options. Eur J Intern Med. 2009;20:672–81.
18. Akoum N, Daccarett M, McGann C, et al. Atrial fibrosis helps select the appropriate patient and strategy in catheter ablation of atrial fibrillation: a DE-MRI guided approach. J Cardiovasc Electrophysiol. 2011;22:16–22.
19. Saremi F, Channual S, Krishnan S, Gurudevan SV, Narula J, Abolhoda A. Bachmann Bundle and its arterial supply: imaging with multidetector CT–implications for interatrial conduction abnormalities and arrhythmias. Radiology. 2008;248:447–57.
20. Yamanaka K, Sekine Y, Nonaka M, et al. Left atrial appendage contributes to left atrial booster function after the maze procedure: quantitative assessment with multidetector computed tomography. Eur J Cardiothorac Surg. 2010;38:361–5.
21. Kim YY, Klein AL, Halliburton SS, et al. Left atrial appendage filling defects identified by multidetector computed tomography in patients undergoing radiofrequency pulmonary vein antral isolation: a comparison with transesophageal echocardiography. Am Heart J. 2007;154:1199–205.
22. Feuchtner GM, Dichtl W, Bonatti JO, et al. Diagnostic accuracy of cardiac 64-slice computed tomography in detecting atrial thrombi. Comparative study with transesophageal echocardiography and cardiac surgery. Invest Radiol. 2008;43:794–801.
23. Hur J, Kim YJ, Lee HJ, et al. Cardioembolic stroke: dual-energy cardiac CT for differentiation of left atrial appendage thrombus and circulatory stasis. Radiology. 2012;263:688–95.
24. Saremi F, Channual S, Gurudevan SV, Narula J, Abolhoda A. Prevalence of left atrial appendage pseudothrombus filling defects in patients with atrial fibrillation undergoing coronary computed tomography angiography. J Cardiovasc Comput Tomogr. 2008;2:164–71.
25. Duerinckx AJ, Vanovermeire O. Accessory appendages of the left atrium as seen during 64-slice coronary CT angiography. Int J Cardiovasc Imaging. 2008;24:215–21.
26. Scharf C, Sneider M, Case I, et al. Anatomy of the pulmonary veins in patients with atrial fibrillation and effects of segmental ostial ablation analyzed by computed tomography. J Cardiovasc Electrophysiol. 2003;14:150–5.
27. Cronin P, Sneider MB, Kazerooni EA, et al. MDCT of the left atrium and pulmonary veins in planning radiofrequency ablation for atrial fibrillation: a how-to guide. AJR Am J Roentgenol. 2004;183:767–78.
28. Mulder AA, Wijffels MC, Wever EF, Boersma LV. Pulmonary vein anatomy and long-term outcome after multi-electrode pulmonary vein isolation with phased radiofrequency energy for paroxysmal atrial fibrillation. Europace. 2011;13:1557–61.
29. Hof I, Chilukuri K, Arbab-Zadeh A, et al. Does left atrial volume and pulmonary venous anatomy predict the outcome of catheter ablation of atrial fibrillation? J Cardiovasc Electrophysiol. 2009;20:1005–10.
30. Anselmino M, Scaglione M, Blandino A, et al. Pulmonary veins branching pattern, assessed by magnetic resonance, does not affect transcatheter atrial fibrillation ablation outcome. Acta Cardiol. 2010;65:665–74.
31. Sanchez-Quintana D, Cabrera JA, Climent V, Farre J, Mendonca MC, Ho SY. Anatomic relations between the esophagus and left atrium and relevance for ablation of atrial fibrillation. Circulation. 2005;112:1400–5.
32. Lemola K, Sneider M, Desjardins B, et al. Computed tomographic analysis of the anatomy of the left atrium and the esophagus: implications for left atrial catheter ablation. Circulation. 2004;110:3655–60.
33. Takahashi Y, Jais P, Hocini M, et al. Acute occlusion of the left circumflex coronary artery during mitral isthmus linear ablation. J Cardiovasc Electrophysiol. 2005;16:1104–7.
34. Goto S, Bhatt DL, Rother J, et al. Prevalence, clinical profile, and cardiovascular outcomes of atrial fibrillation patients with atherothrombosis. Am Heart J. 2008;156:855–63. 863 e852.
35. Benjamin EJ, Levy D, Vaziri SM, D'Agostino RB, Belanger AJ, Wolf PA. Independent risk factors for atrial fibrillation in a population-based cohort. The Framingham Heart Study. JAMA. 1994;271:840–4.
36. Kannel WB, Wolf PA, Benjamin EJ, Levy D. Prevalence, incidence, prognosis, and predisposing conditions for atrial fibrillation: population-based estimates. Am J Cardiol. 1998;82:2N–9.
37. Sacher F, Monahan KH, Thomas SP, et al. Phrenic nerve injury after atrial fibrillation catheter ablation: characterization and outcome in a multicenter study. J Am Coll Cardiol. 2006;47:2498–503.

Calcium Scoring

4

Jongmin Lee

Contents

Abstract

Coronary artery calcium (CAC) is calcium compound deposited within atherosclerotic plaque along its aging. The amount of the calcium is known to be proportional to the whole plaque burden in the subject. Based on this acknowledgment, the quantitative amount of CAC has been applied in clinical field as an indicator for cardiovascular event risk. Among several methods to score the CAC, Agatston score has been widely used in research and practice as a representative scoring method. To stratify cardiovascular risk, CAC score was stratified by the score or percentile within a corresponding cohort by age and gender. In spite of controversy, the CAC scoring methods were validated to be feasible in clinical routine practice. The certain facts about the CAC are that the CAC score predicts CAD risk of intermediate- and high-risk populations; zero CAC score suggests very low risk of CAD unless other risk factors are associated; faster CAC score increase suggests higher risk of CAD; ethnic and sexual differences exist; CAC score is not for diagnosing CAD but for cardiovascular risk assessment.

Abbreviations

AS	Agatston score
CAC	Coronary artery calcium
CAD	Coronary artery disease
CaHA	Calcium hydroxyapatite
CCS	Calcium coverage score
EBCT	Electron-beam CT
HU	Hounsfield units
MS	Mass score
VS	Volume score

J. Lee
Department of Radiology, Kyungpook National University and Hospital, Daegu, Republic of Korea
e-mail: jonglee@knu.ac.kr

T.-H. Lim (ed.), *Practical Textbook of Cardiac CT and MRI*,
DOI 10.1007/978-3-642-36397-9_4, © Springer-Verlag Berlin Heidelberg 2015

4.1 Concept of CAC

- Calcium compound deposited within atherosclerotic plaque.
- The calcium volume suggests atherosclerotic plaque volume in coronary artery [1].
- Quantitative calcium volume evaluation (CAC score) can predict the extent of coronary atherosclerotic disease and its clinical risks [2].

4.2 Scoring Methods

- The first quantification method for CAC was suggested by Agatston using electron-beam CT (EBCT) [3].
- Besides scoring methods, the reference standard is important for practical application.

4.2.1 Agatston Score [3]

- Scanning protocol is suggested for standardization of image quality.

Parameters	Conditions
Prospective data acquisition	At 80 % of R-R interval
Tube voltage	130 kVp
Tube current	(630 mA)
Slice thickness	(3 mm)
Acquisition time	(100 ms)
Contrast enhancement	None

The values in parentheses, original protocol for EBCT, which can be adjustable by scanners

- Coronary artery calcium should be identified by analyzers with classifying branches.
- Calcium area segmentation is semiautomatic using threshold technique, higher than 130 Hounsfield units (HU) and larger than single pixel.
- The density of calcium area is stratified as "density factor" based on peak HU in two-dimensional ROI.

Density factors	Hounsfield units
1	130–199
2	200–299
3	300–399
4	Over 400

- Agatston score (AS) is a global sum of products by calcium areas, density factors, and slice thickness.

$$\mathrm{AS} = \sum_{x=1}^{n} \left(\frac{A_x \cdot D_x \cdot \mathrm{SL}}{3} \right)$$

x, serial number of ROIs; A, area of ROIs; D, density factor; SL, slice thickness

4.2.2 Volume Score [4]

- The volume score (VS) was invented to overcome drawbacks of AS such as nonlinear measurement of HU (density factors) and complexity of measurement.
- Scanning protocol and threshold value for segmentation are same as AS.
- The VS is acquired as a global sum of ROI volumes.

$$\mathrm{VS} = \sum_{x=1}^{n} \left(A_x \cdot \mathrm{SL} \right)$$

- The reproducibility of examination is higher by VS than by AS.
- However, AS has greater reference standard criteria.

4.2.3 Mass Score [5]

- Instead of adopting indirect parameters, the mass score (MS) was designed for more direct assessment of calcium mass.
- Scanning field includes calcium hydroxyapatite [$Ca_{10}(PO_4)_6(OH)_2$, CaHA] phantoms as reference standard materials.
- Initially, the HUs of CaHA phantoms are measured in corresponding images. Based on real calcium density in the phantoms, density-HU plotting with a linear fitting equation is possible.

$$\mathrm{HU} = a \cdot [\mathrm{CaHA}] + b$$

[*CaHA*], calcium densities in CaHA phantoms

- Since the calcium mass is a product of calcium density and its volume, the MS can be acquired from the fitting equation and the volume of ROIs.

$$\mathrm{MS} = \sum_{x=1}^{n} \left[\left(\frac{\mathrm{HU}_x - b}{a} \right) \cdot A_x \cdot \mathrm{SL} \right]$$

- The strength of MS is the consistency of measured values throughout different scanning environments.
- The MS is the most accurate and reproducible technique for CAC quantification.
- Drawbacks of the MS are the complexity of assessment and lack of reference standard criteria for clinical application.

4.2.4 Other Scores

4.2.4.1 CAC Progression Rate [6]

- Based on the fact that CAC increasing speed is associated with the risk of CAD, CAC progression rate (R) is suggested.
- R reflects a percentile interval change of VS.

$$R = 100 \cdot e^{\left\{\frac{\Delta[\ln(VS)]}{T}\right\}-1}$$

T, time interval between examinations

- The R may be a useful marker for a subsequent monitoring of the coronary atherosclerotic burden in single subject.
- Drawbacks are the complexity of assessment and lack of the reference standard criteria.

4.2.4.2 Calcium Coverage Score [7]

- The calcium coverage score (CCS) is the percentage of coronary arteries affected by calcium.
- In a multiethnic large-scale cohort study, the CCS predicted cardiovascular events better than AS and MS.
- A drawback is insufficient clinical application results including reference standard criteria.

4.3 Clinical Significance of CAC

4.3.1 Cardiovascular Risk by Plaque Burden (Figs. 4.1, 4.2, 4.3, 4.4, and 4.5)

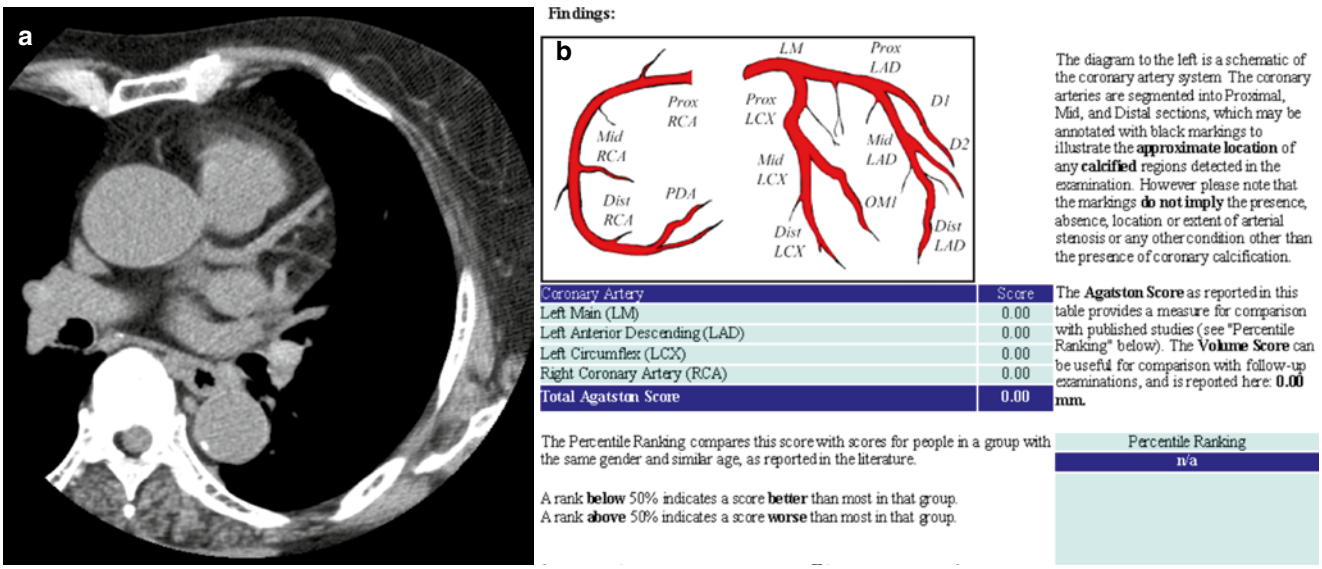

Fig. 4.1 A 72-year-old female. (**a**) Non-enhanced axial CT for calcium scoring shows no calcium in the coronary arteries. Small nodular calcification is noted in the descending aortic wall. (**b**) Total Agatston score is zero (From Hoff et al. [9])

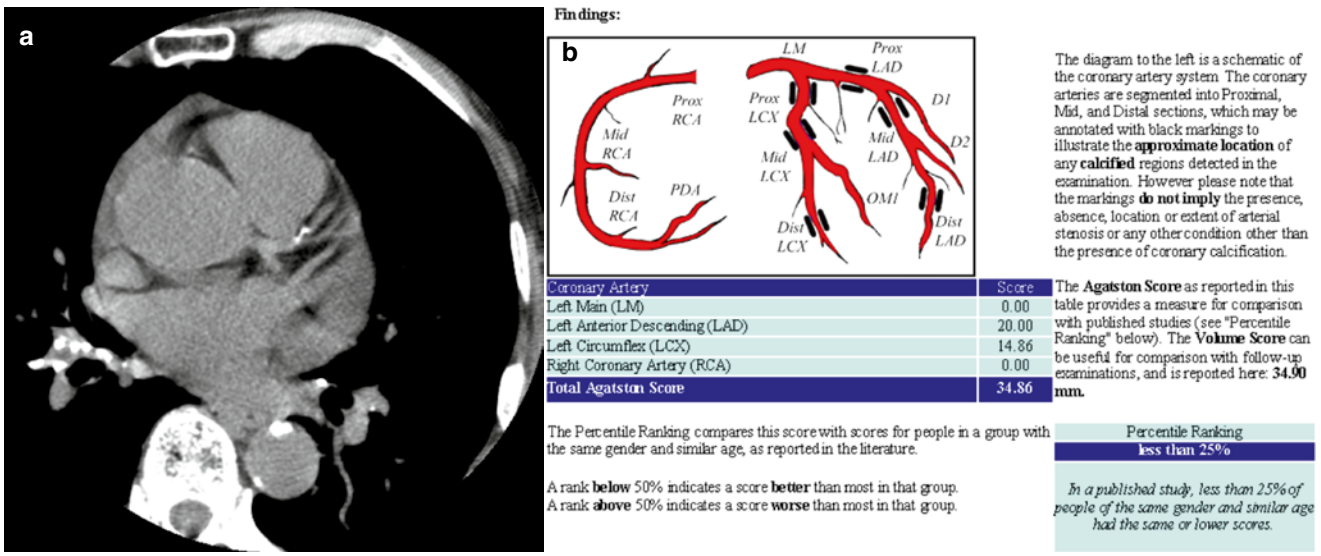

Fig. 4.2 A 77-year-old male. (**a**) Small calcific nodules are noted in the mid left anterior descending artery. Other calcific nodules are noted in the descending aortic wall and hilar lymph nodes. (**b**) Total Agatston score is 34.86, which means mild plaque burden. The subject is less than the 25th percentile in the same age and gender group (From Hoff et al. [9])

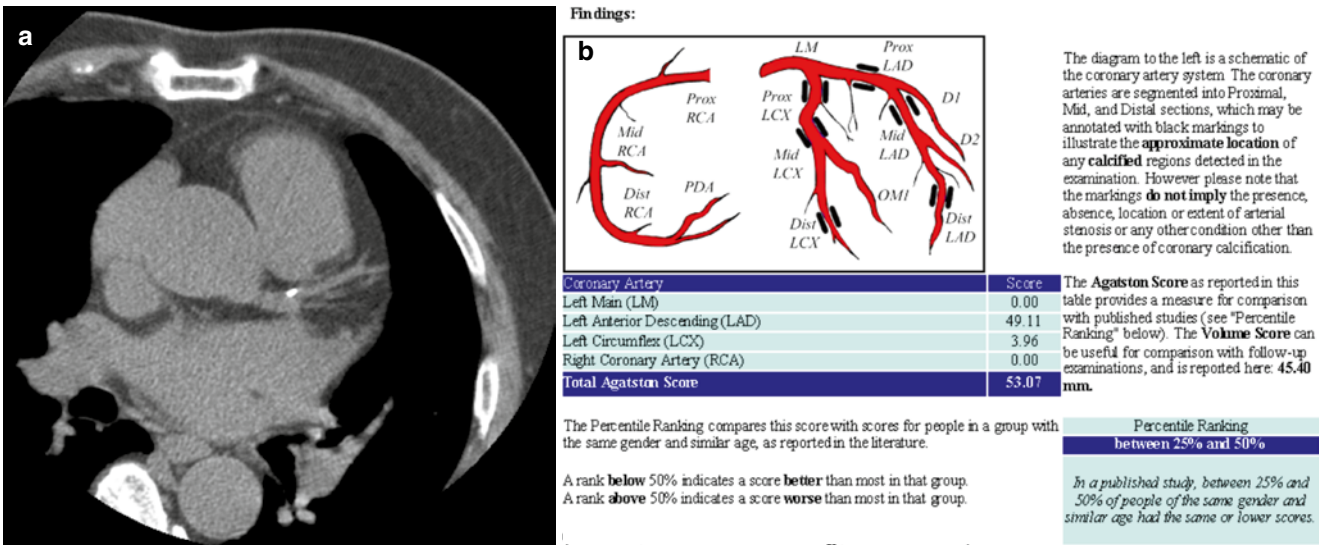

Fig. 4.3 A 69-year-old male. (**a**) Small nodular calcification is noted at the branching level of the left main coronary artery. (**b**) Total Agatston score is 53.07, which means mild plaque burden. Due to younger age than case 2, this subject is plotted between the 25th and 50th percentiles in the same age and gender group (From Hoff et al. [9])

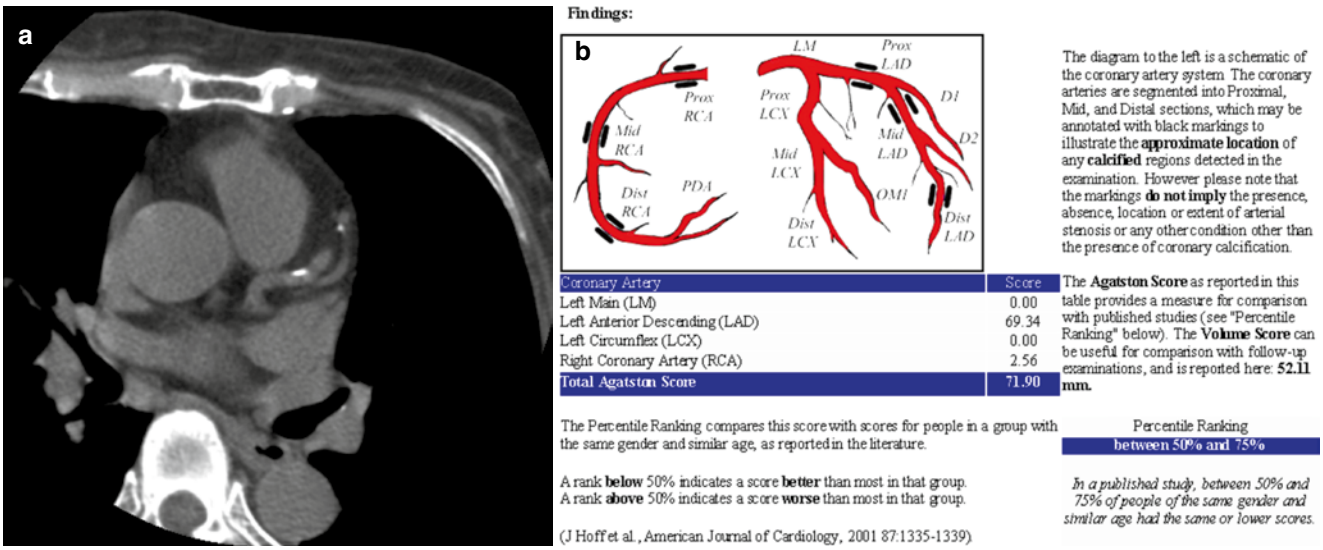

Fig. 4.4 A 71-year-old female. (**a**) Two calcific nodules are noted at the left anterior descending artery. (**b**) Total Agatston score is 71.90, which means mild plaque burden. Due to female gender, this subject is plotted between the 50th and 75th percentiles in the same age and gender group (From Hoff et al. [9])

- An initial meta-analysis-based guideline for CAC Agatston score focused on plaque burden and its clinical interpretation (Table 4.1) [8].
- Nonlinear stratification of Agatston score matched with plaque burden and its clinical interpretation.
- This guideline is simple to apply on routine practice.
- However, diversity of CAC score by sex and age was not considered.

4.3.2 Cardiovascular Risk by Percentile Stratification (Figs. 4.1, 4.2, 4.3, 4.4, and 4.5)

- Based on multicenter large cohort prospective research, Agatston score distributions by age strata and genders were suggested as an interpretation guideline (Table 4.2) [9].

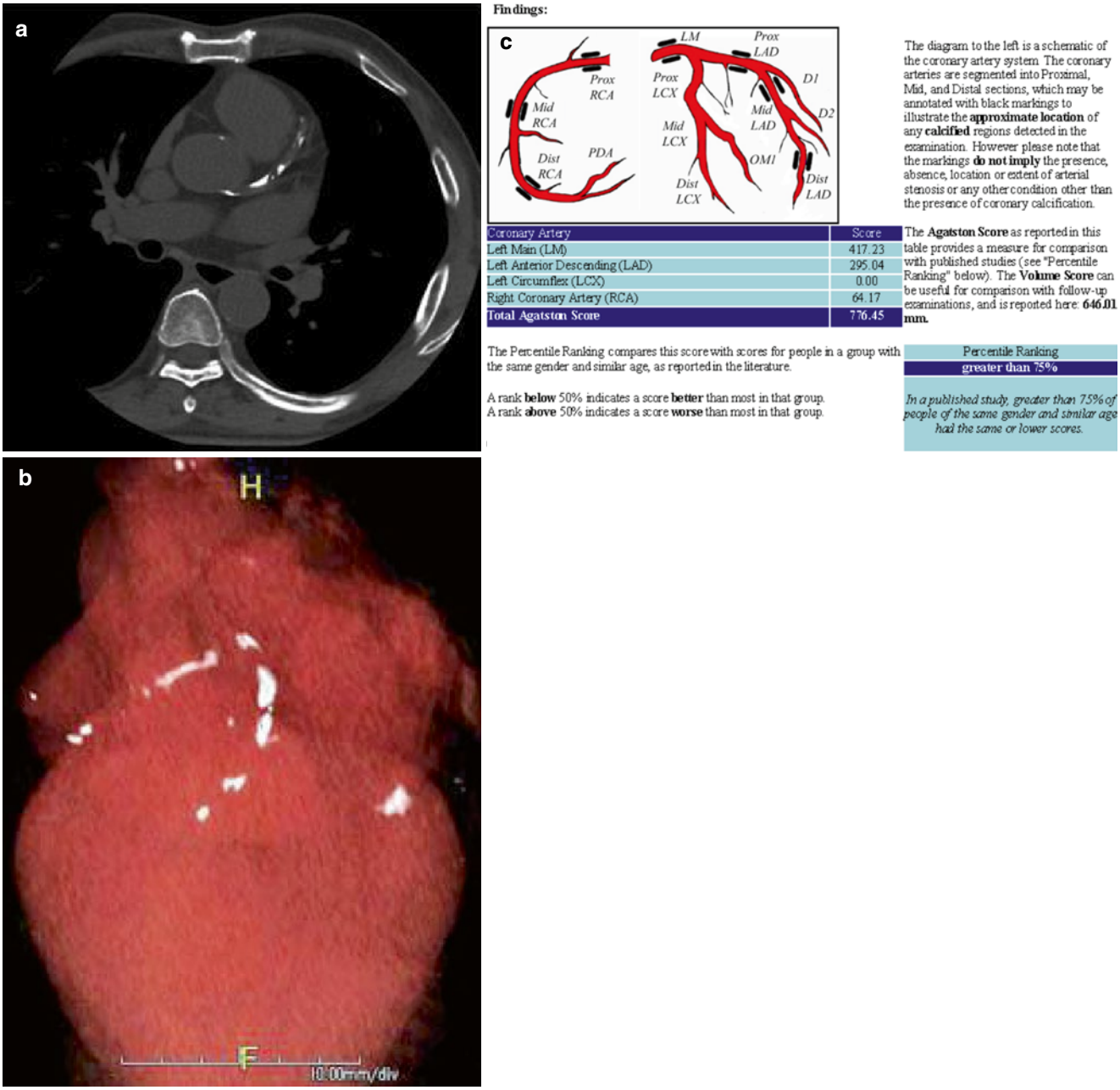

Fig. 4.5 A 61-year-old male with diabetes mellitus. (**a**) Diffuse calcification is noted from the orifice level of the left main coronary artery to the mid level of the left anterior descending artery. (**b**) Volume rendered 3-D image in 4-chamber orientation reveals heavy calcium in the left anterior descending and right coronary arteries. (**c**) Total Agatston score is 776.45, which means extensive plaque burden. This subject is stratified to higher than the 75th percentile in the same age and gender group. Stratification higher than the 75th percentile means high cardiovascular risk (From Hoff et al. [9])

Table 4.1 The interpretation guideline of Agatston score

Calcium score	Plaque burden	Clinical interpretation
0	None	Very low CVD risk
		Less than 5 % chance of presence of CAD
		A negative examination
1–10	Minimal	Significant CAD very unlikely
11–100	Mild	Likely mild or minimal coronary stenosis
101–400	Moderate	Moderate nonobstructive CAD highly likely
Over 400	Extensive	High likelihood of at least one significant coronary stenosis (>50 % diameter)

Table 4.2 Distributions of Agatston score by age strata and genders

	Age (years)								
Percentile	<40	40–44	45–49	50–54	55–59	60–64	65–69	70–74	>74
Men									
25th	0	0	0	1	4	13	32	64	166
50th	1	1	3	15	48	113	180	310	473
75th	3	9	36	103	215	410	566	892	1,071
90th	14	59	154	332	554	994	1,299	1,774	1,982
Women									
25th	0	0	0	0	0	0	1	3	9
50th	0	0	0	0	1	3	24	52	75
75th	1	1	2	5	23	57	145	210	241
90th	3	4	22	55	121	193	410	631	709

- Since the age factor is stratified as decades, interpolated data can demonstrate percentile zone graph for practical application.
- This guideline reflects the diversity of CAC by genders and ages so that more practical application on clinical field is possible.
- Since the result display is intuitive, this guideline is equipped in most CAC analyzing tools.
- CAC score higher than the 75th percentile was reported to present higher cardiovascular risk than the score below the 25th percentile [10].

4.3.3 CAD Risk Per Patient

- The CAC scoring pursues an evaluation of cardiovascular risk in a target subject based on data from communities.
- Can we use CAC score to evaluate CAD per patient?
- Based on histological comparison, intraplaque calcium amount was reported to be proportional to the total plaque volume [11]. This means the positive CAC score can estimate total plaque burden per plaque and per patient.
- Through many reports supporting the relationship between CAC score and CAD severity per patient, some papers suggest cutoff values (AS 371 or 400) of CAC score for prediction of flow-limiting CAD per patient [12, 13].
- The regional distribution and specific patterns of calcium may suggest plaque features in per patient level. Shell-like and diffuse calcifications have higher relationship with significant stenosis and noncalcified plaque than nodular calcification [14].
- Yes, we can use CAC score to predict the severity of CAD in per patient level when the CAC score is high enough. In contrast, low to zero CAC score is limited to preclude the possibility of significant CAD generally.

4.3.4 Zero Calcium Score

- According to interpretation guidelines of CAC, a zero score means very low cardiovascular risk with the lowest percentiles in both male and female (Tables 4.1 and 4.2).
- However, no calcium is detected in uncalcified soft plaque, which is more important for acute coronary syndrome.
- Theoretically, CAC cannot reflect the risk of acute coronary syndrome, which is more fatal than stable angina.
- The clinical meaning of zero CAC score reaches a consensus, although some controversy continues until now [15].
- The zero CAC score virtually exclude cardiovascular risk more likely in subjects older than 50 years of age and subjects without other significant risk factors [16, 17].
- The zero CAC score implies very low cardiovascular risk in the intermediate term (around 3.5 years) [18].

Table 4.3 Prediction of coronary age based on Agatston score by ethnicity and gender

Ethnicity	Gender	Formulae	R^2
White	Male	$y=7\cdot10^{-12}\cdot x^5-10^{-8}\cdot x^4+6\cdot10^{-6}\cdot x^3-0.001\cdot x^2+0.248\cdot x+53.65$	0.998
	Female	$y=10^{-9}\cdot x^5-5\cdot10^{-7}\cdot x^4+8\cdot10^{-5}\cdot x^3-0.006\cdot x^2+0.376\cdot x+65.89$	0.999
Black	Male	$y=3\cdot10^{-6}\cdot x^{53}-0.001\cdot x^2+0.254\cdot x+62.64$	0.995
	Female	$y=2\cdot10^{-5}\cdot x^3-0.003\cdot x^2+0.321\cdot x+69.97$	0.999
Hispanic	Male	$y=3\cdot10^{-6}\cdot x^3-0.001\cdot x^2+0.243\cdot x+59.71$	0.998
	Female	$y=3\cdot10^{-5}\cdot x^3-0.004\cdot x^2+0.384\cdot x+70.94$	0.998
Chinese	Male	$y=7\cdot10^{-6}\cdot x^3-0.002\cdot x^2+0.444\cdot x+57.75$	0.999
	Female	$y=6\cdot10^{-6}\cdot x^3-0.001\cdot x^2+0.250\cdot x+66.50$	0.997

y coronary age, *x* Agatston score

- Based on specific conditions, the zero CAC score can be used as an indicator to preclude significant CAD.

4.3.5 CAC-Concordant Clinical Parameters

- Currently, the CAC score is regarded as a feasible independent marker for cardiovascular risk stratification.
- The CAC score is used as a reference standard or a major input factor for cardiovascular risk estimation during the other clinical studies.

4.3.5.1 Coronary Age [19]

- As a cardiovascular risk predictor, the "coronary age" was suggested by a large cohort study using MESA data.
- Based on the 50th percentile CAC score by ethnicity and gender, the coronary age is calculated as a polynomial function of Agatston score (Table 4.3).
- A true biological age of the subject's coronary artery as well as the degree of the coronary arterial damage during the subject's aging process.
- The coronary age can be applied to enhance patient's compliance to treatment of CAD and modification of one's lifestyle.

4.3.5.2 DM Mortality

- The National Cholesterol Education Program (NCEP) regards diabetes mellitus as a CAD equivalent condition due to its high incidence in diabetic group [20].
- The cardiovascular risk of the diabetics, especially asymptomatic patients, can be monitored using CAC score.
- In a large cohort study based on US National Death Registry, the all-cause mortality of the asymptomatic diabetics increased in proportion to Agatston score [21].
- Relative risk ratios for all-cause mortality in asymptomatic diabetic patients are 3.76, 1.76, 1.44, and 1.06 by hypertension, current smoking, CAC score, and age, respectively ($p<0.05$) [21].
- Combining with other hazardous variables, the diabetics can be monitored in a more strict way.

4.3.5.3 Cardiac Risk of Hypertensive Disease

- Left ventricular hypertrophy of the hypertensive suggests a high cardiovascular risk.
- In a hypertensive cohort, CAC score showed a significant correlation with the severity of left ventricular hypertrophy as well as its clinical marker, QT dispersion on ECG [22].
- Since CAC score is correlated with abnormal lipid profile and ascending aortic prominence, CAC score monitoring may be a comprehensive indicator of cardiovascular risk for hypertensive patients.

4.4 Appropriateness Criteria for CAC

4.4.1 AHA Criteria [23]

- When is CAC score appropriate for detection of CAD and risk assessment?

	Without	With
Asymptomatic patients		Low pretest-probability
		Family history of premature CAD
	Known CAD	Intermediate pretest-probability

The *CAD*, coronary heart disease

- When is CAC score inappropriate for detection of CAD and risk assessment?

	Without	With
Asymptomatic patients	Known CAD	Low pretest-probability

4.4.2 European Criteria [24]

- CAC score is a good predictor of cardiovascular events in intermediate-risk Caucasian population.
- Rapid CAC progression is associated with higher risk of events.
- A zero CAC score is associated with a very low prevalence of CAD.

4.4.3 ASCI Criteria [25]

- How is CAC scored in the coronary artery disease (CAD) risk assessment for the general population?

	Framingham risk score	Criteria
Asymptomatic subjects with	Low	Inappropriate
	Moderate	Appropriate
	High	Appropriate

4.5 Summary

- CAC score predicts CAD risk of intermediate- and high-risk populations.
- A zero score suggests very low risk of CAD unless other risk factors are associated.
- Faster CAC score increase suggests higher risk of CAD.
- Ethnic and sexual differences exist.
- CAC score is not for diagnosing CAD but for cardiovascular risk assessment.

References

1. Rumberger JA, Simons DB, Fitzpatrick LA, Sheedy PF, Schwartz RS. Coronary artery calcium area by electron-beam computed tomography and coronary atherosclerotic plaque area. A histopathologic correlative study. Circulation. 1995;92:2157–62.
2. Schmermund A, Bailey KR, Rumberger JA, Reed JE, Sheedy 2nd PF, Schwartz RS. An algorithm for noninvasive identification of angiographic three-vessel and/or left main coronary artery disease in symptomatic patients on the basis of cardiac risk and electron-beam computed tomographic calcium scores. J Am Coll Cardiol. 1999;33:444–52.
3. Agatston AS, Janowitz WR, Hildner FJ, Zusmer NR, Viamonte Jr M, Detrano R. Quantification of coronary artery calcium using ultrafast computed tomography. J Am Coll Cardiol. 1990;15:827–32.
4. Callister TQ, Cooil B, Raya SP, Lippolis NJ, Russo DJ, Raggi P. Coronary artery disease: improved reproducibility of calcium scoring with an electron-beam ct volumetric method. Radiology. 1998;208:807–14.
5. Hong C, Becker CR, Schoepf UJ, Ohnesorge B, Bruening R, Reiser MF. Coronary artery calcium: absolute quantification in nonenhanced and contrast-enhanced multi-detector row ct studies. Radiology. 2002;223:474–80.
6. Yoon HC, Emerick AM, Hill JA, Gjertson DW, Goldin JG. Calcium begets calcium: progression of coronary artery calcification in asymptomatic subjects. Radiology. 2002;224:236–41.
7. Brown ER, Kronmal RA, Bluemke DA, Guerci AD, Carr JJ, Goldin J, Detrano R. Coronary calcium coverage score: determination, correlates, and predictive accuracy in the multi-ethnic study of atherosclerosis. Radiology. 2008;247:669–75.
8. Rumberger JA, Brundage BH, Rader DJ, Kondos G. Electron beam computed tomographic coronary calcium scanning: a review and guidelines for use in asymptomatic persons. Mayo Clin Proc. 1999;74:243–52.
9. Hoff JA, Chomka EV, Krainik AJ, Daviglus M, Rich S, Kondos GT. Age and gender distributions of coronary artery calcium detected by electron beam tomography in 35,246 adults. Am J Cardiol. 2001;87:1335–9.
10. Georgiou D, Budoff MJ, Kaufer E, Kennedy JM, Lu B, Brundage BH. Screening patients with chest pain in the emergency department using electron beam tomography: a follow-up study. J Am Coll Cardiol. 2001;38:105–10.
11. Rumberger JA. Coronary artery calcification: "…Empty your cup.". Am Heart J. 1999;137:774–6.
12. Rumberger JA, Sheedy PF, Breen JF, Schwartz RS. Electron beam computed tomographic coronary calcium score cutpoints and severity of associated angiographic lumen stenosis. J Am Coll Cardiol. 1997;29:1542–8.
13. Moser KW, O'Keefe Jr JH, Bateman TM, McGhie IA. Coronary calcium screening in asymptomatic patients as a guide to risk factor modification and stress myocardial perfusion imaging. J Nucl Cardiol. 2003;10:590–8.
14. Thilo C, Gebregziabher M, Mayer FB, Zwerner PL, Costello P, Schoepf UJ. Correlation of regional distribution and morphological pattern of calcification at ct coronary artery calcium scoring with noncalcified plaque formation and stenosis. Eur Radiol. 2010;20:855–61.
15. Lee J. Coronary artery calcium scoring and its impact on the clinical practice in the era of multidetector CT. Int J Cardiovasc Imaging. 2011;27 Suppl 1:9–25.
16. Knez A, Becker A, Leber A, White C, Becker CR, Reiser MF, Steinbeck G, Boekstegers P. Relation of coronary calcium scores by electron beam tomography to obstructive disease in 2,115 symptomatic patients. Am J Cardiol. 2004;93:1150–2.
17. Ergun E, Kosar P, Ozturk C, Basbay E, Koc F, Kosar U. Prevalence and extent of coronary artery disease determined by 64-slice CTA in patients with zero coronary calcium score. Int J Cardiovasc Imaging. 2011;27:451–8.
18. Church TS, Levine BD, McGuire DK, Lamonte MJ, Fitzgerald SJ, Cheng YJ, Kimball TE, Blair SN, Gibbons LW, Nichaman MZ. Coronary artery calcium score, risk factors, and incident coronary heart disease events. Atherosclerosis. 2007;190:224–31.
19. Sirineni GK, Raggi P, Shaw LJ, Stillman AE. Calculation of coronary age using calcium scores in multiple ethnicities. Int J Cardiovasc Imaging. 2008;24:107–11.
20. Grundy SM, Benjamin IJ, Burke GL, Chait A, Eckel RH, Howard BV, Mitch W, Smith Jr SC, Sowers JR. Diabetes and cardiovascular disease: a statement for healthcare professionals from the American Heart Association. Circulation. 1999;100:1134–46.
21. Raggi P, Shaw LJ, Berman DS, Callister TQ. Prognostic value of coronary artery calcium screening in subjects with and without diabetes. J Am Coll Cardiol. 2004;43:1663–9.
22. Pan NH, Yang HY, Hsieh MH, Chen YJ. Coronary calcium score from multislice computed tomography correlates with QT dispersion and left ventricular wall thickness. Heart Vessels. 2008;23:155–60.
23. Taylor AJ, Cerqueira M, Hodgson JM, Mark D, Min J, O'Gara P, Rubin GD, American College of Cardiology Foundation Appropriate Use Criteria Task Force; Society of Cardiovascular Computed Tomography; American College of Radiology; American Heart Association; American Society of Echocardiography; American Society of Nuclear Cardiology, North American Society for Cardiovascular Imaging; Society for Cardiovascular Angiography and Interventions; Society for Cardiovascular Magnetic Resonance. ACCF/SCCT/ACR/AHA/ASE/ASNC/NASCI/SCAI/SCMR 2010 appropriate use criteria for cardiac computed tomography. A report of the American College of Cardiology Foundation Appropriate Use Criteria Task Force, the Society of Cardiovascular Computed Tomography, the American College of Radiology, the American Heart Association, the American Society of Echocardiography, the American Society of Nuclear Cardiology, the North American Society for Cardiovascular Imaging, the Society for Cardiovascular Angiography and Interventions, and the Society for Cardiovascular Magnetic Resonance. Circulation. 2010;122:e525–55.

24. Oudkerk M, Stillman AE, Halliburton SS, Kalender WA, Mohlenkamp S, McCollough CH, Vliegenthart R, Shaw LJ, Stanford W, Taylor AJ, van Ooijen PM, Wexler L, Raggi P, European Society of Cardiac Radiology; North American Society for Cardiovascular Imaging. Coronary artery calcium screening: current status and recommendations from the European Society of Cardiac Radiology and North American Society for Cardiovascular Imaging. Eur Radiol. 2008;18:2785–807.

25. ASCI CCT and CMR Guideline Working Group, Tsai IC, Choi BW, Chan C, Jinzaki M, Kitagawa K, Yong HS, Yu W, Asian Society of Cardiovascular Imaging Cardiac Computer Tomography; Cardiac Magnetic Resonance Imaging Guideline Working Group. ASCI 2010 appropriateness criteria for cardiac computed tomography: a report of the Asian Society of Cardiovascular Imaging Cardiac Computed Tomography and Cardiac Magnetic Resonance Imaging Guideline Working Group. Int J Cardiovasc Imaging. 2010;26 Suppl 1:1–15.

Atherosclerotic Coronary Artery Disease

5

Hyun Ju Seon and Yun-Hyeon Kim

Contents

Abstract

Atherosclerosis is the principal cause of coronary artery diseases. In patients with acute chest pain, CT coronary angiography (CTCA) is an easily applicable and powerful imaging technique, and the precise evaluation for an atherosclerotic coronary disease is the most important role of CTCA. Without sufficient experiences, however, a reader can miss easily even significant stenosis and overestimate a moderate stenosis as a significant stenosis by many mistakes including various artifacts. The correct interpretation of CTCA is very important especially as the reported high negative predictive value of CTCA is a major strength of this imaging technique. The sophisticated evaluation of coronary atherosclerotic disease with CTCA provides useful information for proper management of patients as well as simple diagnosis.

In this chapter, we will describe how to determine the location, the degree, and the lesion specific characteristics of coronary artery stenosis, and how to determine the number of diseased vessels. We will also provide practical guide to avoid mistakes when assessing for coronary artery stenosis by demonstrating various cases in clinical practice with conventional angiographic correlation.

5.1 Important Determinants of Coronary Artery Stenosis by CT

5.1.1 Determination of Location of Coronary Artery Stenosis

- Standardized approach to coronary segmentation improves description and communication of findings of CT coronary angiography.
- The standard American Heart Association (AHA) has been adapted for coronary CTA with minimal alterations for clarity (Fig. 5.1 and Table 5.1).
- The lumen of the coronary arteries should be examined for overall caliber and smoothness.

H.J. Seon (✉) • Y.-H. Kim
Department of Radiology, Chonnam National University Medical School and Hospital, Gwangju, Republic of Korea
e-mail: sunaura@hanmail.net; yhkim001@jnu.ac.kr

T.-H. Lim (ed.), *Practical Textbook of Cardiac CT and MRI*,
DOI 10.1007/978-3-642-36397-9_5, © Springer-Verlag Berlin Heidelberg 2015

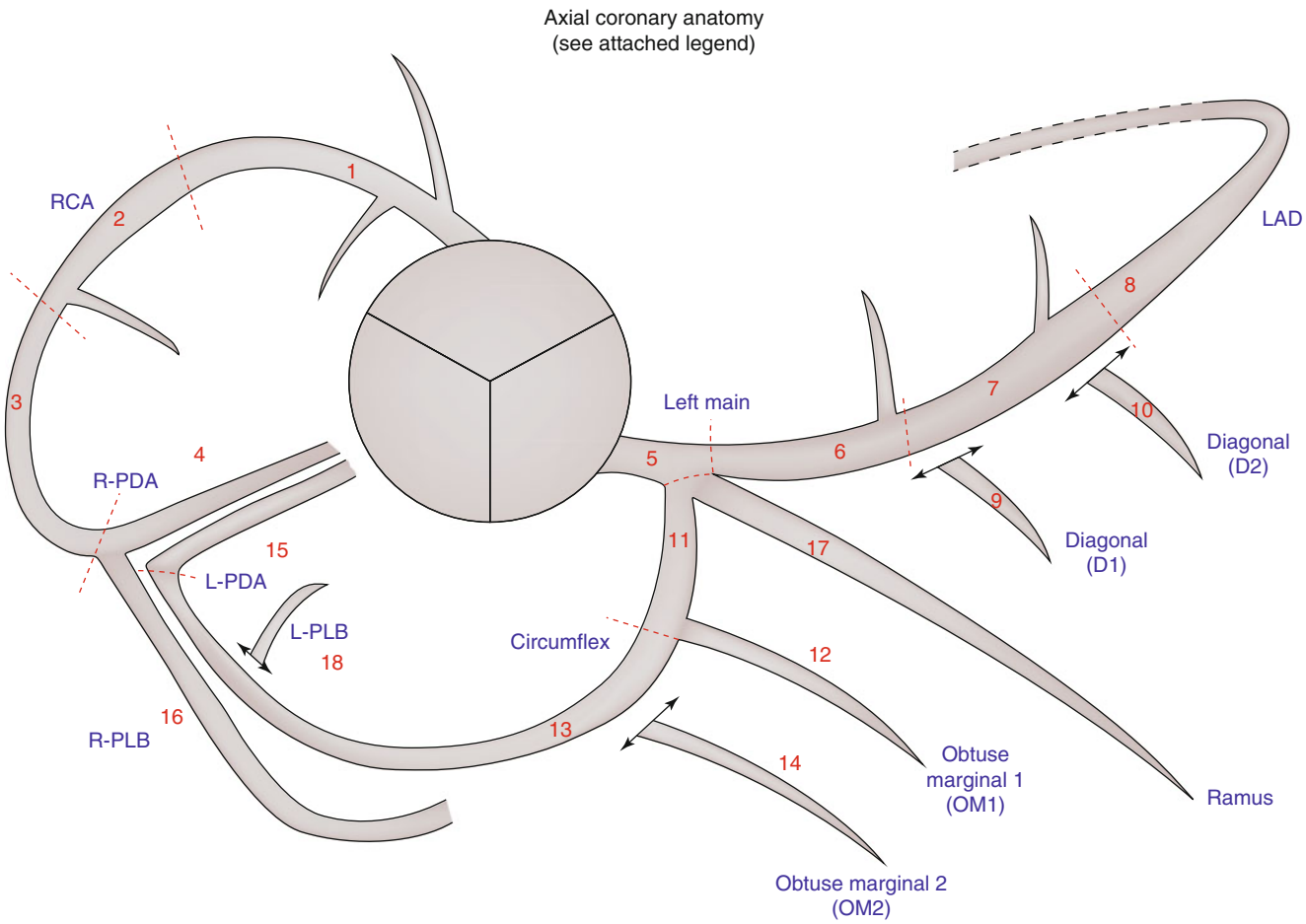

Fig. 5.1 Schematic diagram of SCCT coronary segmentation. *RCA* right coronary artery, *R-PDA* right posterior descending artery, *L-PDA* left posterior descending artery, *L-PLB* left posterolateral branch, *R-PLB* right posterolateral branch, *LAD* left anterior descending artery. *1* pRCA, *2* mRCA, *3* dRCA, *4* R-PDA, *5* LM, *6* pLAD, *7* mLAD, *8* dLAD, *9* D1, *10* D2, *11* pLCx, *12* OM1, *13* dLCx, *14* OM2, *15* L-PDA, *16* R-PLB, *17* Ramus, *18* L-PLB

Table 5.1 Explanation of abbreviation of SCCT coronary segmentation diagram

Proximal RCA	pRCA	Ostium of the RCA (right coronary artery) to one-half the distance to the acute margin of heart
Mid RCA	mRCA	End of proximal RCA to the acute margin of heart
Distal RCA	dRCA	End of mid RCA to origin of the PDA (posterior descending artery)
PDA-RCA	R-PDA	PDA from RCA
PLB-RCA	R-PLB	PLB (posterior-lateral branch) from RCA
LM	LM	Ostium of LM (left main) to bifurcation of LAD (left anterior descending artery) and LCx (left circumflex artery)
Proximal LAD	pLAD	End of LM to the first large septal or D1 (first diagonal), whichever is most proximal
Mid LAD	mLAD	End of proximal LAD to one-half the distance to the apex
Distal LAD	dLAD	End of mid LAD to end of LAD
Diagonal 1	D1	First diagonal branch D1
Diagonal 2	D2	Second diagonal branch D2
Proximal LCx	pLCx	End of LM to the origin of the OM1 (first obtuse marginal)
OM1	OM1	First OM1 traversing the lateral wall of the left ventricle
Mid and distal LCx	LCx	Traveling in the AV groove, distal to the first obtuse marginal branch to the end of the vessel or origin of the L-PDA (left PDA)
OM2	OM2	Second marginal OM2
PDA-LCx	L-PDA	PDA from LCx
Ramus intermedius	RI	Vessel originating from the left main between the LAD and LCx in case of a trifurcation
PLB-L	L-PLB	PLB from LCx
		Dashed lines represent division between RCA, LAD, and LCx and the end of the LMPLB = PLV (posterior left ventricular branch) Additional nomenclature may be added for example: D3, R-PDA2, SVG (saphenous vein graft) mLAD

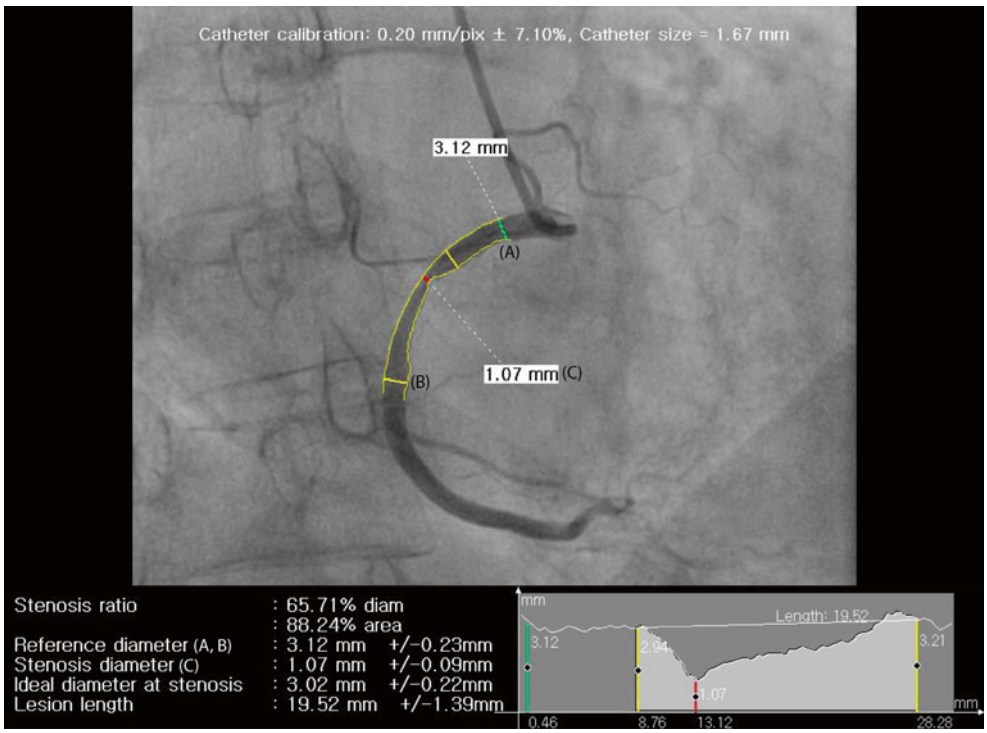

Fig. 5.2 Example of quantitative stenosis assessment by quantitative coronary angiography (QCA). Conventional coronary angiography (CCA) image of the right coronary artery (RCA) is shown demonstrating longitudinal measurements of percentage diameter stenosis, calculated by comparing minimal luminal diameter at the site of maximal stenosis (C) with normal reference diameters proximal (A) and/or distal (B). Percentage diameter stenosis = $\{1 - C/[(A + B)/2]\} \times 100$ (%)

Table 5.2 Recommended qualitative and quantitative stenosis grading by the Society of Cardiovascular Computed Tomography (SCCT)

Descriptive lumen obstruction	Qualitative stenosis grading	Quantitative stenosis grading
Normal	Absence of plaque/no luminal stenosis	Absence of plaque/no luminal stenosis
Minimal	Plaque with negligible impact on lumen	Plaque with <25 % stenosis
Mild	Plaque with no flow-limiting stenosis	25–49 % stenosis
Moderate	Plaque with possible flow-limiting stenosis	50–69 % stenosis
Severe	Plaque with probable flow-limiting	70–99 % stenosis
Occluded	Stenosis	100 % stenosis

- Variations in CT density within the mural and intraluminal portions of the coronary artery should be noted and compared with the adjacent interstitium, contrast-containing lumen, and calcific densities such as the bone or calcified plaque.
- Atherosclerotic lesions should be considered in relationship to their segmental position due to the affected extent of the myocardium.
- The worst lesion should be reported if there are more than two lesions in one segment.

5.1.2 Determination of Degree of Coronary Artery Stenosis

- Generally described as diameter stenosis rather than area stenosis.
- The critical narrowing of a lesion (*A*) may be estimated as the percentage of ratio between 1 minus actual (*B*) lumen diameter and the expected (*C*) lumen diameter.
- Because of progressively tapering coronary arteries, the expected diameter of the lumen at the level of the lesion is determined as an average of the normal arterial segment proximal to it and the distal arterial lumen equidistant from the lesion.
- Visual stenosis estimate:
  - Most commonly performed coronary lumen assessment in clinical practice, both for coronary CTA and CAG.
  - Comparing the MLD (minimum lumen diameter) to an arterial diameter at an appropriate reference site (i.e., a non-diseased arterial segment in closest proximity to the lesion, preferably with no branch vessels in between).
  - Grading of maximum diameter stenosis severity can be done using either a qualitative or semi-quantitative stenosis grading (Table 5.2).
  - Overestimation of coronary arterial stenosis severity compared with quantitative coronary angiography (QCA) by 10–20 points.
- Quantitative stenosis estimate (Fig. 5.2):
  - Manually or semiautomatically
  - Drawing of diameter using cross-sectional or longitudinal lumen display with similar accuracy compared with QCA
  - Advantage of cross-sectional displaying: assessing all lumen borders in 1 view

Table 5.3 ACC/AHA classification of coronary arterial lesions

	Type A	Type B	Type C
Lesion character			
Length	<10 mm	10–20 mm	>20 mm
Angulation	<45°	45° to <90°	90° or more
Contour	Smooth	Irregular	
Calcium	Nil or little	Moderate or heavy	
Thrombus	Present	Absent	
Total occlusion		<3 months old	>3 months old
Eccentricity	Concentric	Eccentric	
Lesion location			
Ostial or not	Non-ostial	Ostial	
Tortuosity or proximal segment	Nil or mild	Moderate	Severe
Major side branch involvement	Absent	Bifurcation lesion needing guidewire	Inability to protect major side branch
Others			
			Degenerated vein graft with friable lesion

  - One important caveat for quantitative stenosis assessment by MDCT: adjustment of window width and level settings
  - A trend to establish quantitative method by MDCT evaluation as the routine assessment also for clinical applications
- Reporting by 2° (commonly used reporting method in coronary CTA):
  - Insignificant: 0–50 % diameter stenosis
  - Significant: 51–99 % diameter stenosis

5.1.3 Determination of the Number of Diseased Vessels

- Impossible evaluation of distal portions of the coronary artery <2 mm in diameter because of the limits of spatial and temporal resolution of current coronary CTA.
- Definition: Number of vessel with >50 % diameter stenosis in five major vessels, which are more than 2 mm in diameter.
- Determination of coronary artery dominancy is essential.
- Five major vessels:
  - LAD: LAD, big diagonal, big ramus intermedius, big septal
  - LCX: LCX, big OM (obtuse marginal)
  - RCA: RCA, big AM (acute marginal), PDA, PL branch
  - LMCA
  - Graft: LIMA (left internal mammary artery), SVG (saphenous vein graft), GEA (gastroepiploic artery), RA (radial artery)
- Examples:
  - LAD + big OM: two-vessel disease
  - LAD + small RCA (vessel diameter 1 mm): one-vessel disease
  - LMCA + RCA: three-vessel disease

5.1.4 Lesion-Specific Characteristics of Coronary Artery Stenosis

- Three possible outcomes of a percutaneous coronary intervention (PCI)
  - Technical success
  - Clinical success
  - Unsuccessful uncomplicated result
- Technical success requires
  - The ability to deliver the balloon or the device to the lesion
  - The ability to adequately dilate the vessel or otherwise improve the lumen
- Characteristics of ACC/AHA Type A, B, and C lesions: reflects the difficulty of the procedure – the likelihood of success or complications (Table 5.3)
  - Type A lesions: (high success, >85 %; low risk) (Fig. 5.5)

Discrete (<10 mm length)	Little or no calcification
Concentric	Less than totally occlusive
Readily accessible	Not ostial in location
Nonangulated segment <45°	No major branch involvement
Smooth contour	Absence of thrombus

  - Type B lesions: (moderate success, 60–85 %; moderate risk) (Fig. 5.6)

Tubular (10–20 mm length)	*Ostial in location*
Eccentric	*Bifurcation lesions requiring double guidewires*
Moderate tortuosity of proximal segment	Some thrombus present
Moderately angulated, 45–90°	Total occlusion <3 months old
Irregular contour	
Moderate to heavy calcification	

– Type C lesions: (low success, <60 %; high risk)

Diffuse (>2 cm length)	*Degenerated vein grafts with friable lesions*
Excessive tortuosity of proximal segment	Total occlusion >3 months old
Extremely angulated, >95°	
Inability to protect major side branch	

- High-risk obstructive coronary artery disease (Fig. 5.6)
  - Left main stenosis >50 %
  - Two-vessel disease (>70 %) involving the proximal LAD
  - Three-vessels disease (>70 %)
  - Complex or high-risk lesion or diffuse lesion

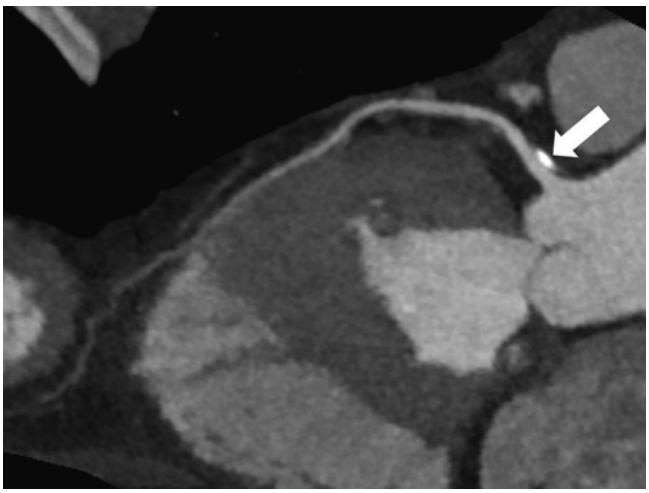

Fig. 5.3 Insignificant luminal narrowing of the coronary artery with a marginal plaque. Bidimensional MPR image (B-MPR) of LAD on coronary CTA shows marginal calcified plaque (*white arrow*) in pLAD

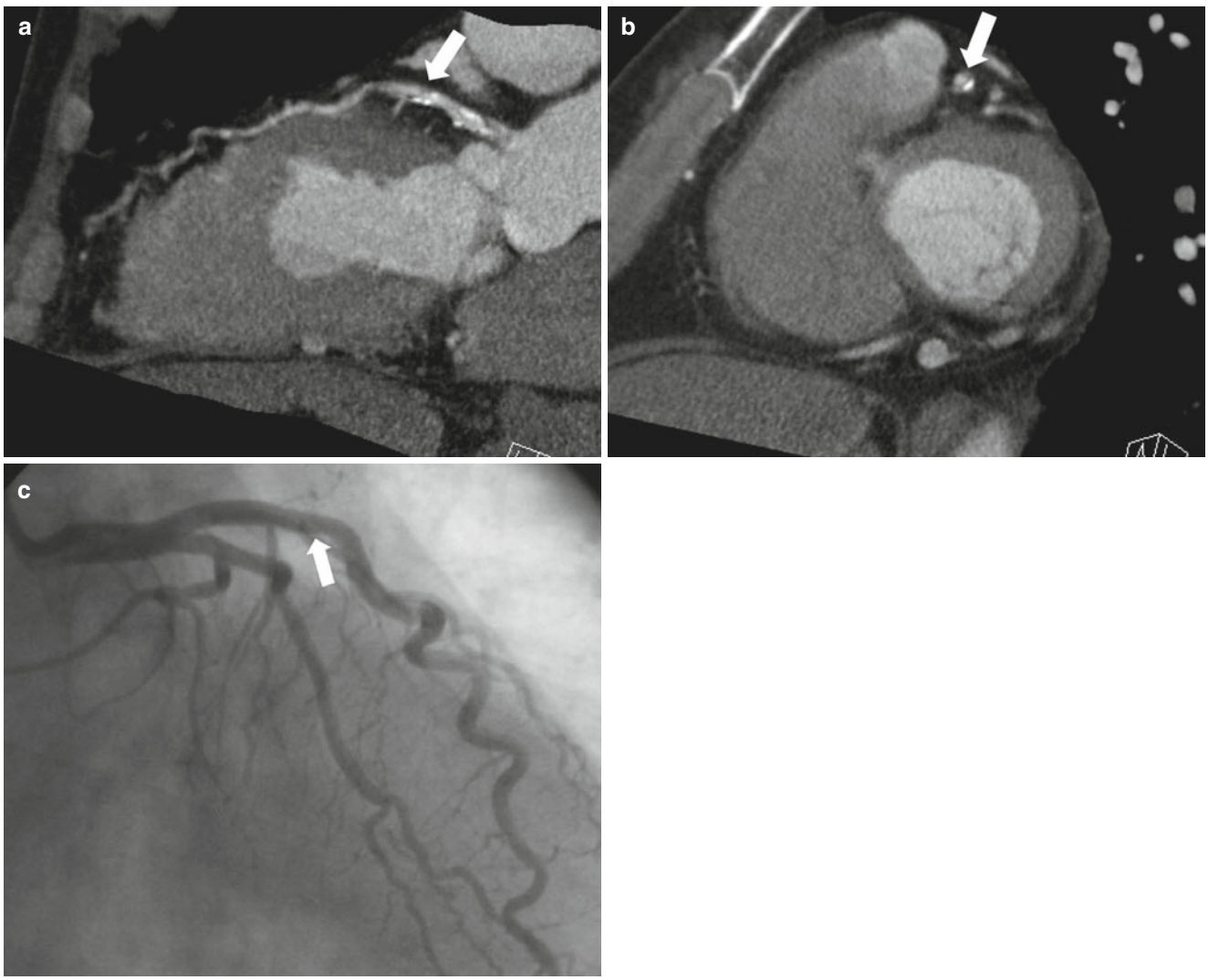

Fig. 5.4 Moderate degree of atherosclerotic stenosis in mLAD on CTA with moderate amount of plaque burden on intravascular ultrasonography (IVUS). (**a**) B-MPR image of LAD on coronary CTA shows mixed plaque (*arrow*) in mLAD. (**b**) Short-axis (SA) image on coronary CTA shows moderate degree of luminal narrowing in mLAD (*arrow*) after adjustment of window width and level to minimize the blooming artifact by calcified plaque, and this view well demonstrates the degree of stenosis of mLAD with X-sectional plane. (**c**) Conventional coronary angiogram (CAG) of LAD shows mild degree of luminal narrowing in mLAD (*arrow*). (**d**) IVUS-virtual histology (VH) shows moderate amount of fibrotic plaque (*arrows*) in mLAD with 59 % of plaque burden

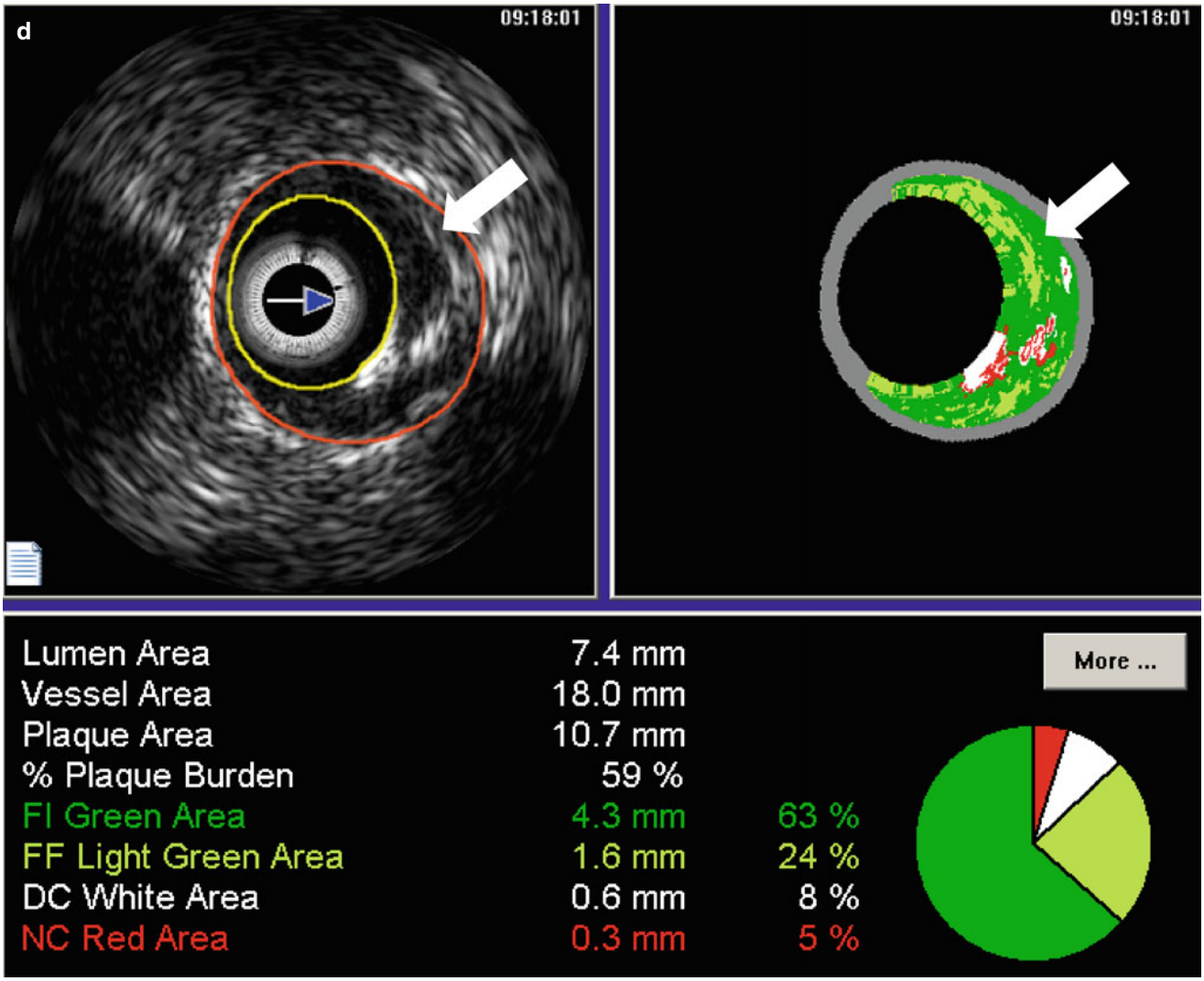

Fig. 5.4 (continued)

Learning Points

Coronary angiogram as a "luminogram" can underestimate plaque burden, especially in the case with positive remodeling. In such cases, vessel wall image of coronary CTA can show good correlation with plaque burden on IVUS

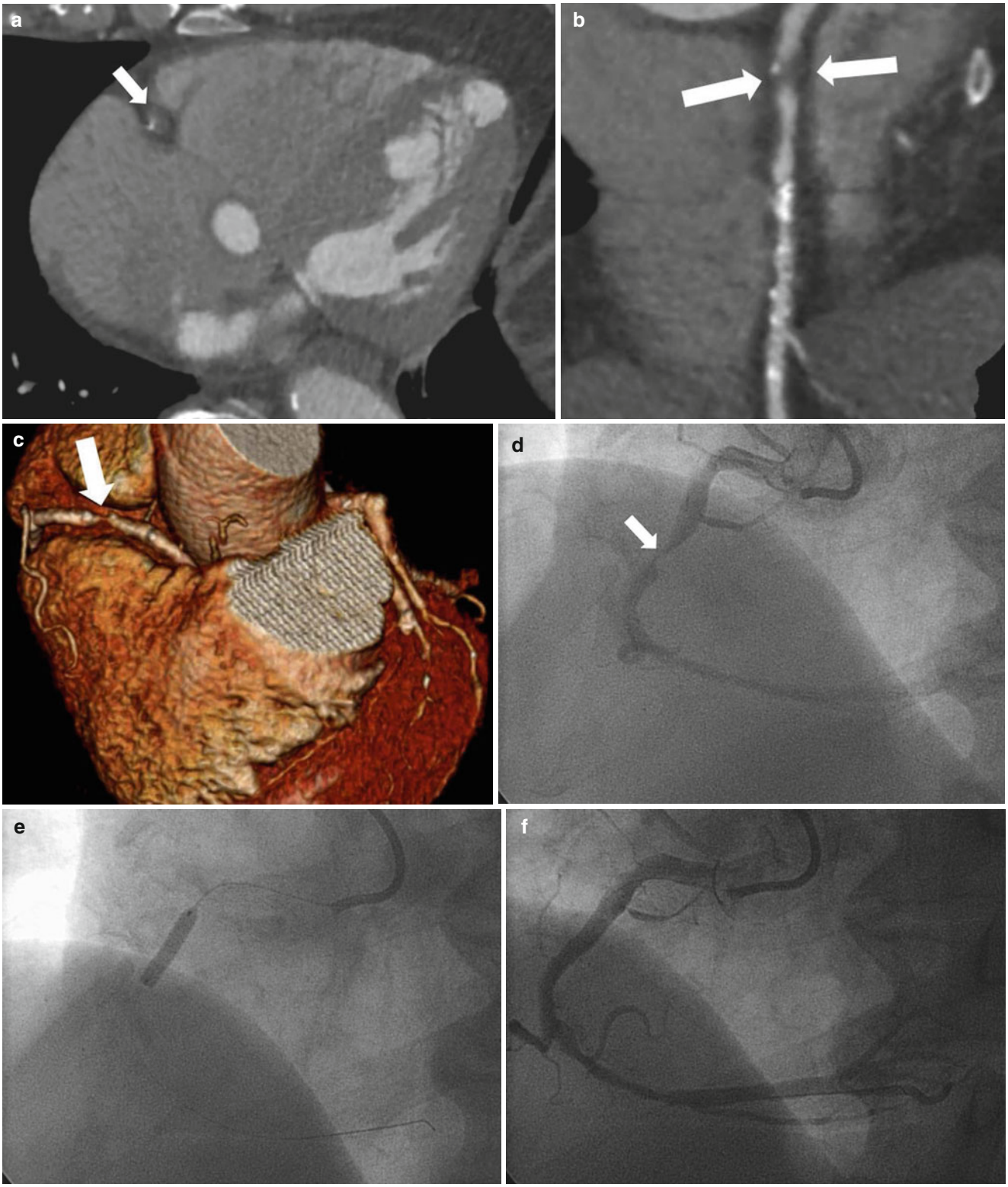

Fig. 5.5 Severe degree of atherosclerotic stenosis in mRCA on CTA with one-vessel disease and Type A lesion. (**a**) Axial image of the right coronary artery (RCA) on coronary CTA shows severe degree of luminal narrowing with soft plaque in mRCA (*arrow*, one-vessel disease), and this view well demonstrates the degree of stenosis of mRCA with X-sectional plane. (**b**, **c**) Curved MPR (**b**) image and 3D volume-rendered (VR) (**c**) image of RCA on coronary CTA shows concentric soft plaque and discrete luminal narrowing (<1 cm long, Type A lesion) in mRCA (*arrows*). (**d**) Initial CAG of RCA also shows concentric and discrete luminal narrowing with severe stenosis (95 %) in mRCA (*arrow*). (**e**) Balloon angioplasty with 2.5 mm balloon was successfully performed. (**f**) Final CAG of RCA after stent implantation shows good distal flow without residual stenosis

Learning Points

In patients who are planning to undergo percutaneous coronary intervention (PCI), classification of lesion-specific characteristics of coronary arterial stenosis is needed for the prediction of success rate of PCI according to the greater amounts of tortuosity, angulation of the segment, the length of the vessel, the presence of occlusions, issues with side branches, and potential for protection

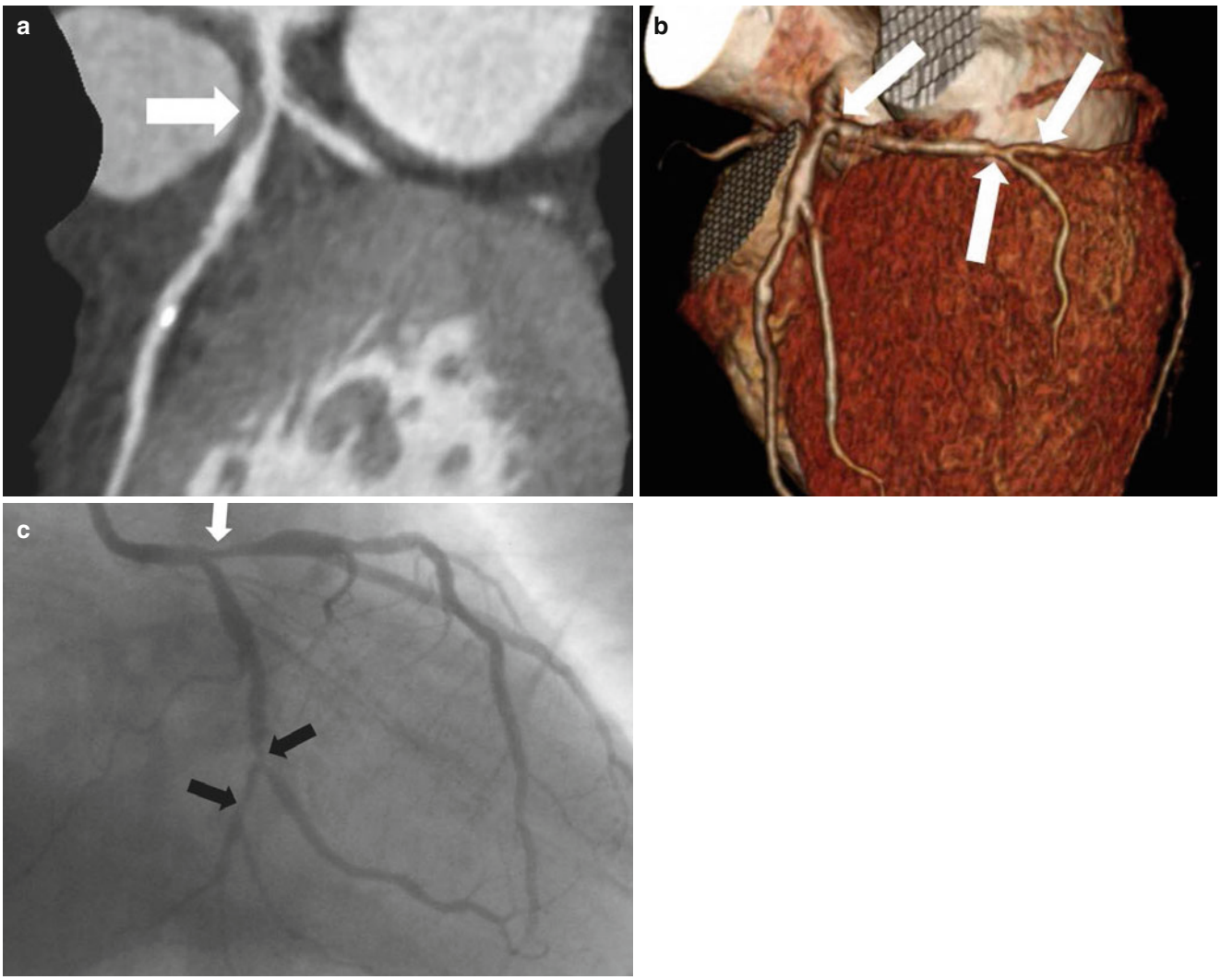

Fig. 5.6 Two-vessel disease of coronary artery with Type B lesion and high-risk obstructive disease. (**a**) Curved MRP image of LAD on coronary CTA shows eccentric soft plaque (*arrow*) with tubular (1–2 cm long) and significant luminal narrowing in left main (LM) to pLAD (high-risk obstructive disease). (**b**) 3D-VR image of left circumflex artery (LCx) provides an overview of lesions of LCx with multifocal significant stenosis in pLCx and dLCx (*arrows*). (**c**) Initial CAG shows multiple significant luminal narrowing in LM to pLAD (*white arrow*, 90 %) and dLCx (*black arrows*, 85 %). (**d**) Axial image of LCx with thin-slice thickness (0.8 mm) well demonstrates eccentric soft plaque in dLCX (*arrow*) causing significant luminal narrowing. Such a soft plaque must be differentiated from perivascular fat or accompanying vein. (**e**) Final CAG of left coronary artery after stent implantation shows good distal flow without residual stenosis to LM to pLAD (*white arrow*) and dLCx (*black arrows*)

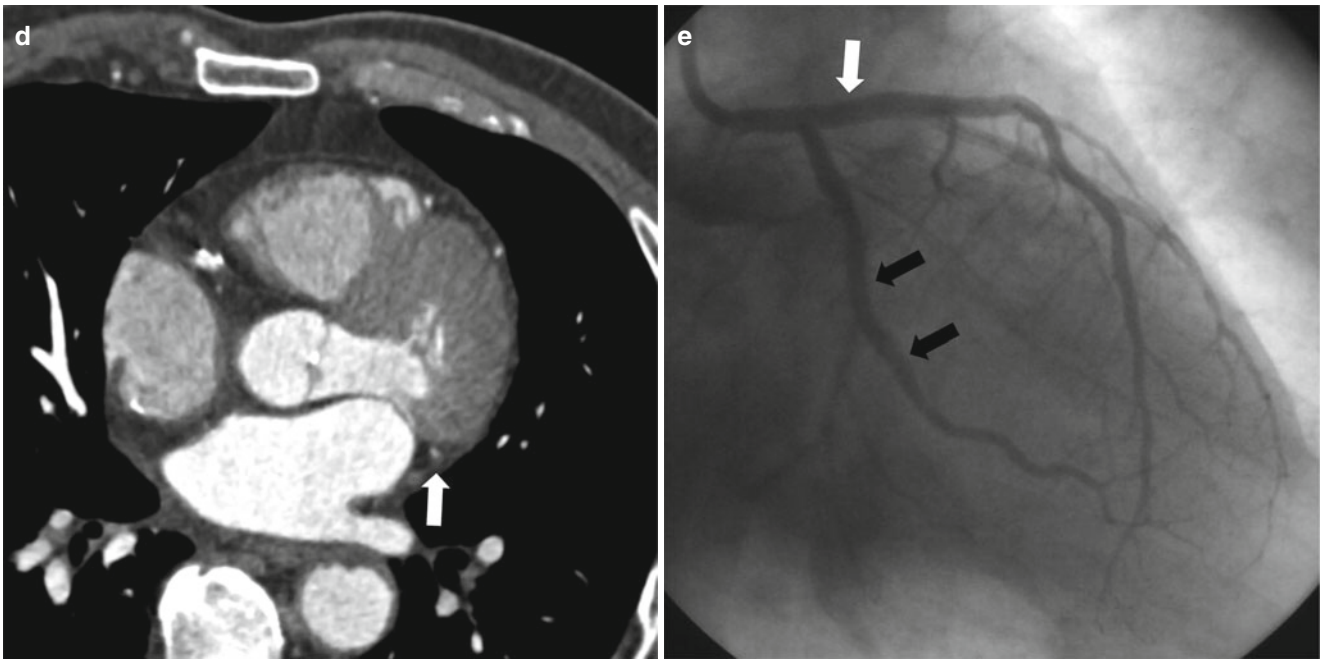

Fig. 5.6 (continued)

Learning Points

For the exact diagnosis of plaque and determination of degree of stenosis on coronary CTA, the careful evaluation of each segment of coronary arteries using curved or orthogonal bidimensional planes (so-called planimetric technique) such as multi-planar reformatting images and entire package of three-dimensional data (so-called volumetric technique) is essential. However, initial assessment must be made using the axial source images followed by the post-processed images. Especially, for the evaluation of distal or small branch, evaluation using more thin section thickness is often needed.

5.1.5 Practical Guide to Avoid Mistakes When Assessing for Coronary Stenosis

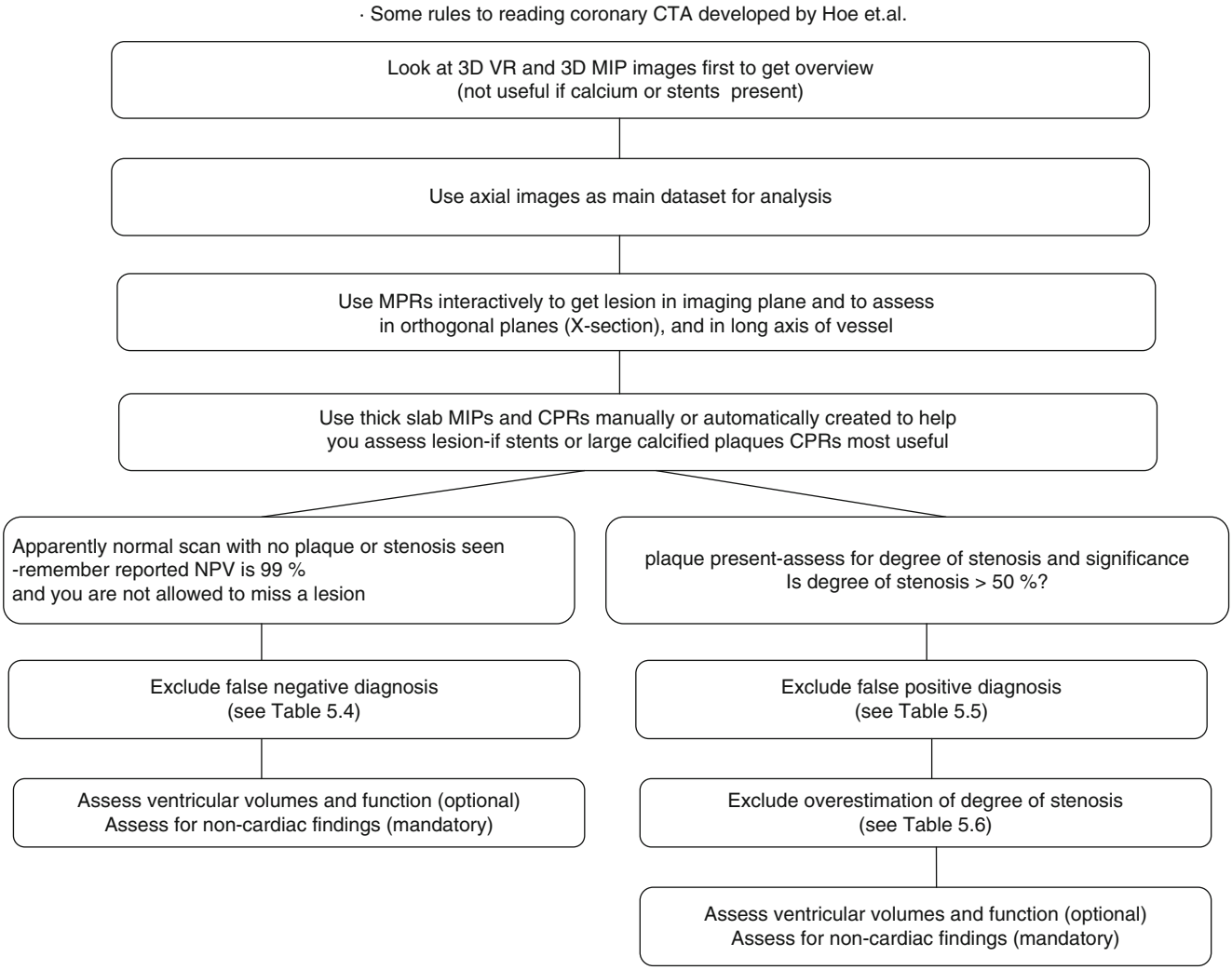

Table 5.4 How to reduce false-negative scan result (i.e., not miss plaque or significant stenosis)

Use 3D-VR or 3D-MIP images to get overview and look for segment of stenosis not obvious on axial data sets, especially if no calcium is present
Contrast-filled lumen of an artery must always be white-look for "dark lumen" sign, especially in vessels in longitudinal plane on axial images, e.g., mid LAD, distal RCA
Use MPRs and CPRs to help you if you suspect a lesion
Use the correct WW/WL to view the images
Do not use thick slab MIPs that are too thick (not >3–5 mm)
Always recheck the three review areas carefully

Table 5.5 How to reduce false-positive scan result (resulting in unnecessary conventional angiogram)

Always confirm stenosis is present on another percentage pthase of reconstruction to exclude artifact, e.g., motion artifact
A segment of stenosis should have visible plaque noncalcified or calcified associated with it
The current major challenge to the diagnosis of coronary stenosis is calcium – commonest cause of false-positive scan result. Look at segment with calcium with different WW/WL, e.g., 1,500/350 or use filtering software (as for stents) to try to help you decide

Table 5.6 How to reduce overestimation of stenosis (resulting in unnecessary conventional angiogram)

Look at the minimal luminal diameter of the vessel on orthogonal planes, especially in the X-sectional plane. Do not just view lesion in one plane, e.g., axial image of proximal LAD, to assess the degree of stenosis
Assess contrast-filled "lumen to lumen" of lesion to normal reference diameter, not "wall to wall" of artery containing plaque when deciding on degree of diameter stenosis, especially when positive remodeling is present
Use different WW/WL especially when there is poor contrast enhancement (i.e., 700/250)

Plaque Morphology Evaluation by CT

6

Jin Hur and Byoung Wook Choi

Contents

Abstract

Noninvasive imaging tools that allow reliable determination of plaque burden and plaque composition are important for risk stratification and monitoring of coronary atherosclerosis. Coronary computed tomographic angiography (CCTA) has tremendous potential to provide uniquely valuable information concerning coronary atherosclerosis. Beyond the detection of coronary artery stenosis, CCTA can demonstrate coronary atherosclerotic plaque. Certain plaque characteristics, such as positive remodeling or very low CT attenuation, are associated with plaque vulnerability. In this chapter, an overview of CT imaging with a focus on the characterization of coronary artery plaque will be highlighted. In addition, limitations and future directions of CT imaging on coronary artery plaque characterization will be discussed.

6.1 Introduction

- Progression of coronary atherosclerotic plaque contributes to the development of acute coronary syndrome (ACS).
- Noninvasive imaging tools that allow reliable determination of plaque burden and plaque composition are important for risk stratification and monitoring of coronary atherosclerosis.
- Coronary computed tomographic angiography (CCTA) has been suggested as a novel, noninvasive modality for coronary atherosclerotic plaque detection, characterization, and quantification.
- Definition of coronary artery plaque: structures larger in area than 1 mm^2 within and/or adjacent to the coronary artery lumen and which could be distinguished clearly from the vessel lumen and the surrounding pericardial tissue.
- In this chapter, we reviewed current imaging modalities for coronary artery plaque assessment as well as discussed the role of CCTA with a focus on the characterization of coronary artery plaque.

J. Hur (✉) • B.W. Choi
Department of Radiology,
Research Institute of Radiological Science,
Severance Hospital, Yonsei University College of Medicine,
Seoul, Republic of Korea
e-mail: khuhz@yuhs.ac; bchoi@yuhs.ac

T.-H. Lim (ed.), *Practical Textbook of Cardiac CT and MRI*,
DOI 10.1007/978-3-642-36397-9_6,

6.2 Modalities for Plaque Imaging

6.2.1 IVUS

- Intravascular ultrasound (IVUS) is a catheter-based imaging technique, which is considered an accurate method for visualizing the wall of the coronary artery [1].
- Visual interpretation of echogenicity on IVUS gray-scale images has been used to provide information on plaque characteristics.
- Various real-time determinations of plaque components using IVUS signals with matched histology results have shown that spectral analysis has between 80–92 % in vitro and 87–97 % in vivo accuracy when used to identify the four different types of atherosclerotic tissue: fibrous, fibrofatty, dense calcium, and necrotic core [2, 3].
- Cross-sectional analysis of IVUS images permits the measurements of atherosclerotic plaque dimensions, and IVUS is considered the "reference standard" modality for plaque quantification.
- IVUS is valuable for assessing changes in plaque volume in response to anti-atherosclerotic treatments.
- IVUS has several limitations for routine clinical applications:
  - Invasive nature of IVUS with the associated risks precludes its use in asymptomatic patients.
  - Use of IVUS is limited in patients with severe coronary stenosis or occlusion.
  - IVUS-based plaque measurements are typically limited to 1 or 2 coronary segments.
  - Difficulty in differentiating the borderline between intramural thrombus and fibrous plaque (Fig. 6.1).

6.2.2 CT

- Current multi-detector row computed tomography (MDCT) now provides technical prerequisites for coronary atherosclerotic plaque imaging [4].
- Thus, CT has enabled qualitative and quantitative assessment of coronary plaque, including assessment of plaque size, composition, and remodeling.
- CCTA is able to define plaque vulnerability by differentiating plaque composition based on density measurements [5].

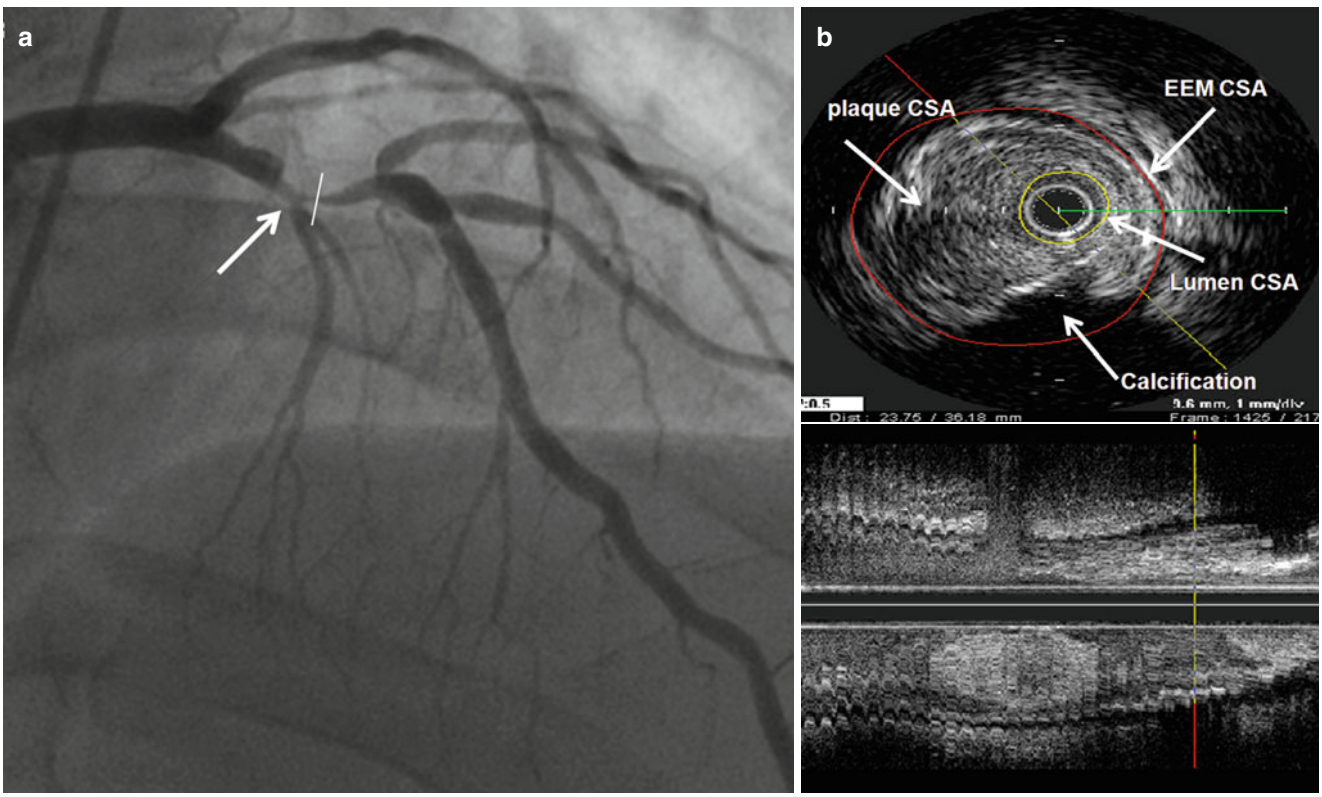

Fig. 6.1 Invasive coronary angiography and intravascular ultrasound (IVUS) of the left anterior descending artery (LAD). (**a**) Invasive angiogram shows significant coronary artery stenosis in the proximal segment of LAD (*arrow*). (**b**) Cross-sectional image of IVUS on the level of *white line* on image **a**. IVUS demonstrates significant luminal narrowing by hypoechoic plaque combined with calcification indicating mixed plaque. *Red circle* indicating *EEM CSA* external elastic membrane cross-sectional area, *yellow circle* indicating *lumen CSA* lumen cross-sectional area, *plaque CSA* plaque cross-sectional area

- Several limitations exist in the routine use of CT for coronary plaque assessment:
  - Use of iodinated contrast and radiation exposure to image coronary plaque
  - Limited by motion-related image artifacts and inadequate resolution to visualize plaque components
  - Inadequate resolution in determining plaque area, volume, and remodeling (Figs. 6.2 and 6.3)

6.2.3 MRI

- Technical improvements of coronary magnetic resonance imaging (CMR) have enabled reliable visualization of the proximal and midportion of the coronary artery tree for exclusion of significant coronary artery disease.
- Current technical developments focus on direct visualization of the diseased coronary vessel wall and imaging of coronary plaque [6].
- MRI has several limitations for routine clinical applications:
  - Limited by the small size of the target and lower spatial resolution
  - Limited by cardiac motion artifact and respiration artifact
  - Considerable length of time for imaging (Fig. 6.4, Table 6.1)

6.3 Classification of Plaque

- Based on the relative amount of calcified and non-calcified components, plaques are usually classified into one of three categories: calcified plaque, mixed plaque, or non-calcified plaque.
- Classification of coronary plaque as calcified, mixed, or non-calcified relies on the ability of CCTA to distinguish their respective attenuations.

6.3.1 Calcified Plaque

- Definition: plaques occupied by calcified tissue (any structure with a density of 130 HU or more that could be visualized separately from the contrast-enhanced coronary lumen) more than 50 % of the plaque area (Fig. 6.5)

6.3.2 Mixed Plaque

- Definition: plaques occupied by calcified tissue (any structure with a density of 130 HU or more that could be visualized separately from the contrast-enhanced coronary lumen) less than 50 % of the plaque area (Fig. 6.6)

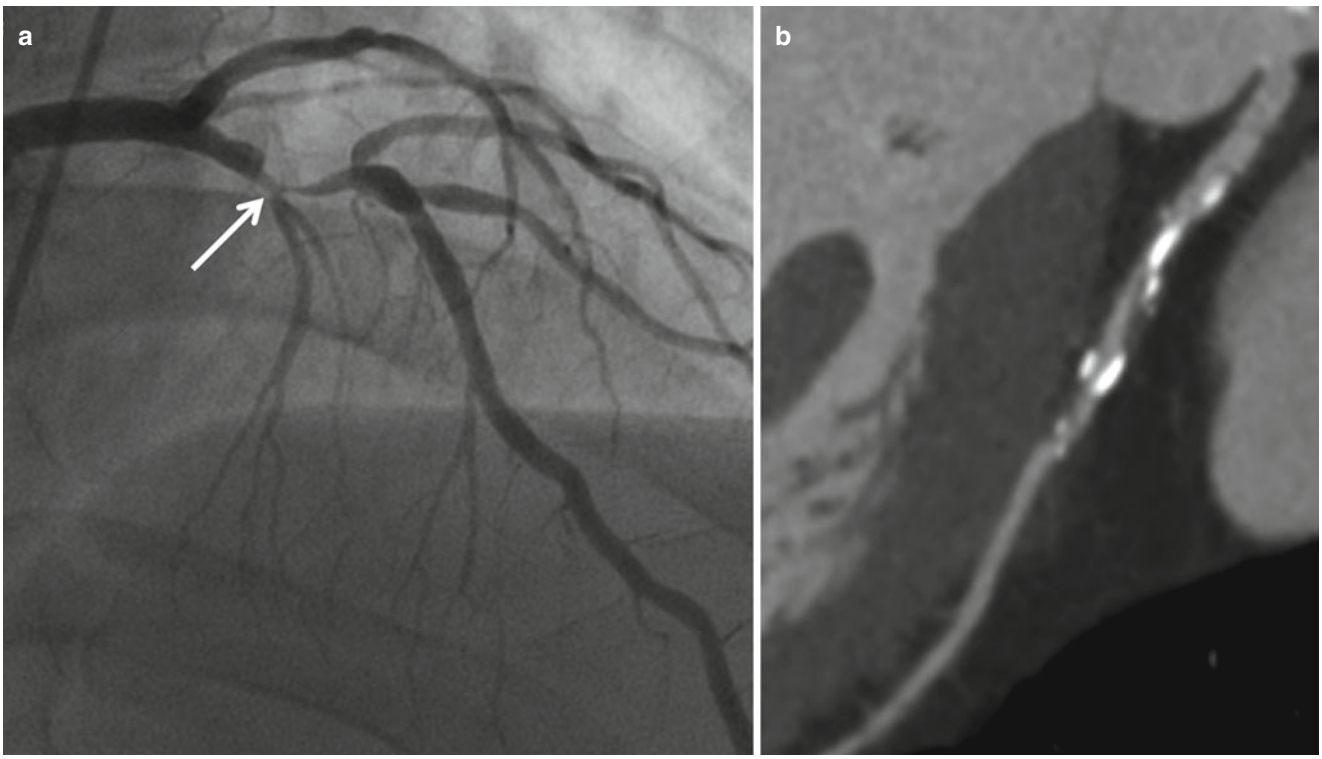

Fig. 6.2 Invasive coronary angiography and coronary computed tomographic angiography (CCTA) of the left anterior descending artery (LAD). (**a**) Invasive angiogram shows significant coronary artery stenosis in the proximal segment of LAD (*arrow*). (**b**) Curved multiplanar reformatted (MPR) image demonstrates calcified and mixed plaques in the proximal segment of LAD

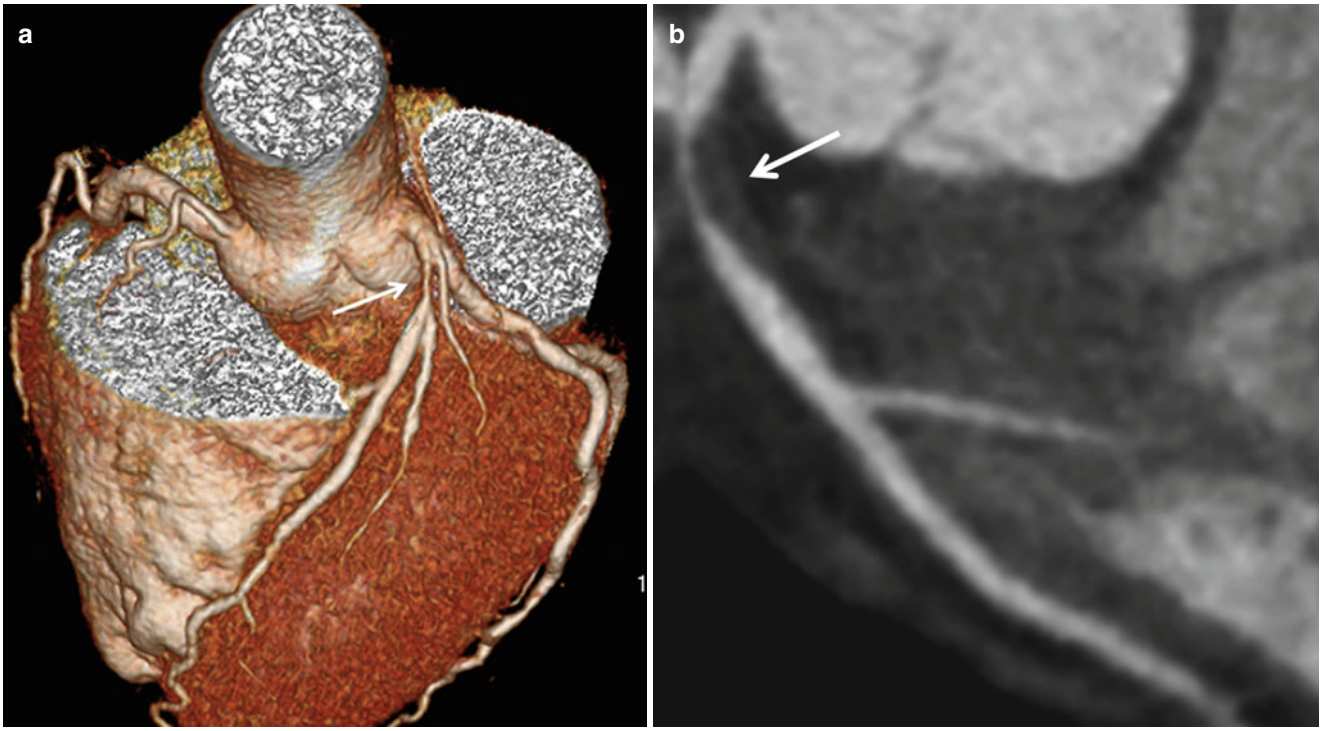

Fig. 6.3 Coronary computed tomographic angiography (CCTA) with significant coronary artery stenosis of the left anterior descending artery (LAD). (**a**) Volume rendering (VR) image demonstrates significant coronary artery stenosis in the proximal segment of LAD (*arrow*). (**b**) Curved multiplanar reformatted (MPR) image demonstrates non-calcified plaque in the proximal segment of LAD (*arrow*) with significant coronary artery stenosis

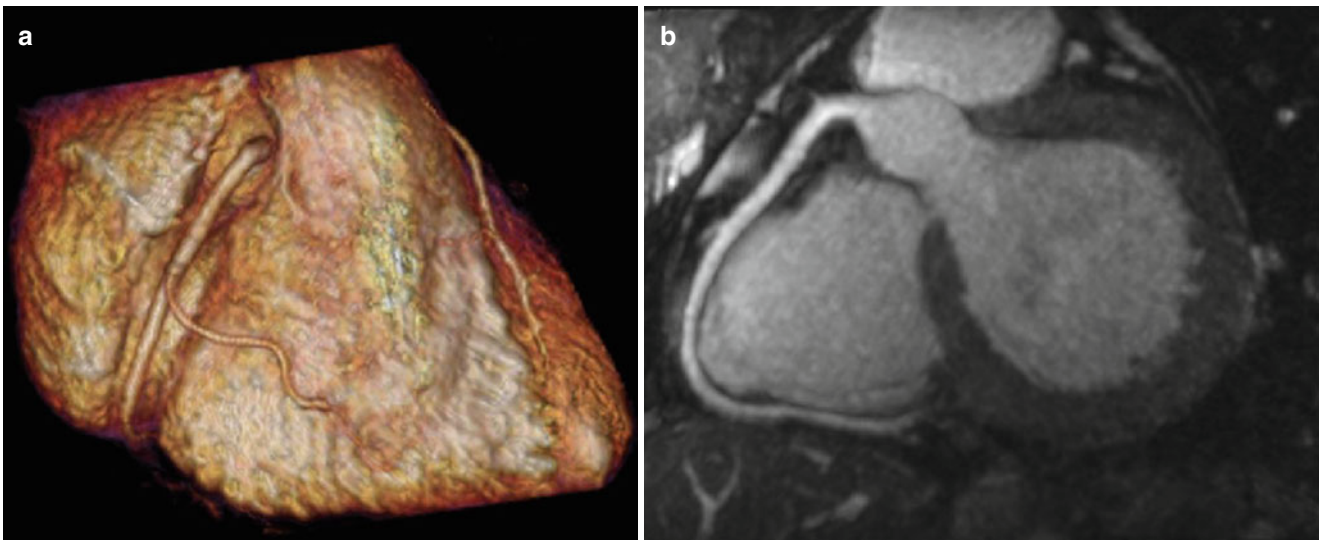

Fig. 6.4 Coronary magnetic resonance angiography (MRA) of the right coronary artery (RCA). (**a**) Volume rendering (VR) image of MRA demonstrates right coronary artery without coronary artery stenosis. (**b**) Curved multiplanar reformatted (MPR) image of MRA demonstrates right coronary artery without coronary artery stenosis

Table 6.1 Comparison of each modality for plaque imaging

Imaging modality	Determination of plaque characteristics	Advantages	Disadvantages
IVUS	Plaque echogenicity	Reference modality	Invasive modality
	Plaque volume and size	Good depth of penetration	Limited in coronary artery occlusion or severe stenosis
		Complementary modality of coronary angiography	Difficulty in differentiating the borderline between intramural thrombus and fibrous plaque
CT	Quantification of calcium	Noninvasive identification of vulnerable plaques	Use of iodinated contrast agents and radiation
	Density measurement		Limited by motion artifacts
			Inadequate resolution to visualize plaque components
MRI	Signal intensity	Noninvasive modality	Lower spatial resolution
		No use of iodinated contrast agent	Limited by cardiac motion artifact and respiration artifact
		No need to radiation exposure	Longer length of study time

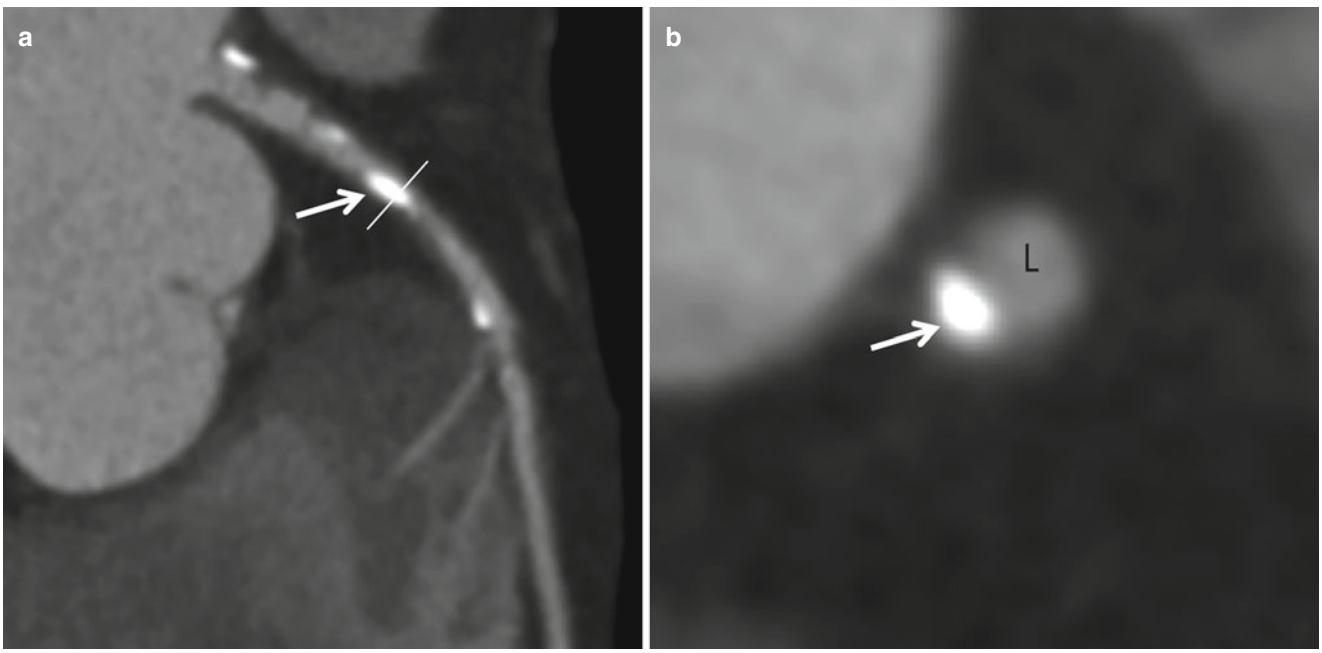

Fig. 6.5 Calcified plaque. (**a**) Curved multiplanar reformatted (MPR) image of coronary computed tomographic angiography (CCTA) demonstrates multiple calcified plaques in the left main and proximal segment of left anterior descending artery (*arrow*). (**b**). Cross-sectional image of CCTA on the level of *white line* on image **a**. Eccentric dense calcified plaque (*arrow*) is seen with mild luminal narrowing of the coronary artery. *L* Lumen

6.3.3 Non-calcified Plaque

- Definition: plaques occupied without any calcified tissue (any structure with a density of 130 HU or more that could be visualized separately from the contrast-enhanced coronary lumen) on the plaque area (Fig. 6.7)

6.3.4 Vulnerable Plaque

- Definition: all thrombosis-prone plaques and plaques with a high probability of undergoing rapid progression, thus becoming culprit plaques [7, 8].
- In an attempt to unify the understanding of what constitutes a vulnerable plaque, morphological studies suggest

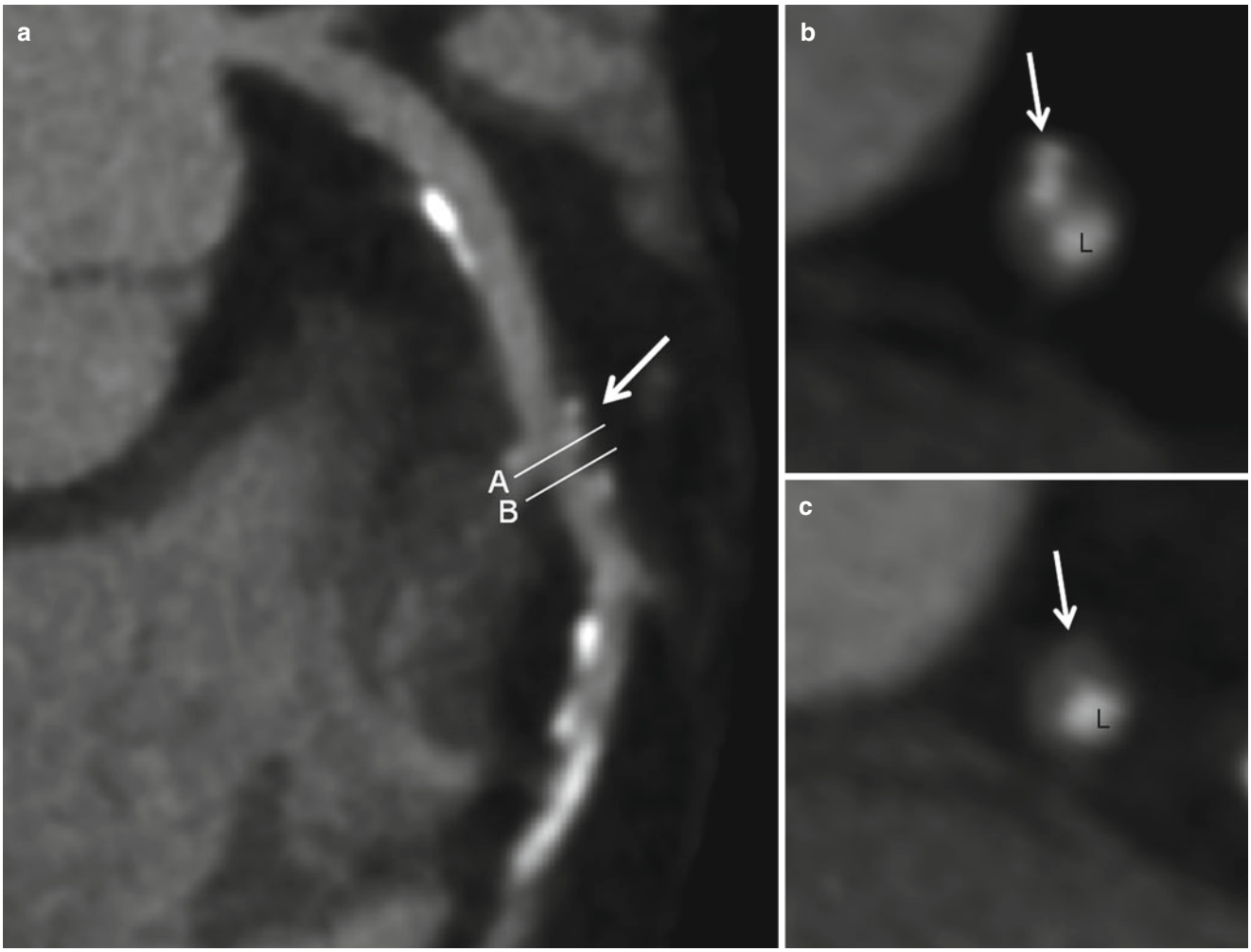

Fig. 6.6 Mixed plaque. (**a**) Curved multiplanar reformatted (MPR) image of coronary computed tomographic angiography (CCTA) demonstrates multiple calcified plaques and mixed plaque (*arrow*) in the proximal and middle segments of the left anterior descending artery with significant stenosis caused by mixed plaque. (**b**) Cross-sectional image of CCTA on the level of *white line* (*B*) on image **a**. Mixed plaque in this area is composed of soft tissue and spotty calcifications (*arrow*). (**c**) Cross-sectional image of CCTA on the level of *white line* (*C*) on image **a**. Mixed plaque in this area is composed of soft tissue (*arrow*). *L* lumen

the importance of necrotic core size, inflammation, and fibrous cap thickness.
- A large number of vulnerable plaques are relatively uncalcified and relatively non-stenotic, but different types of vulnerable plaque exist (Table 6.2, Figs. 6.8 and 6.9).

6.4 Analyzing Methods of Coronary Plaque

6.4.1 Plaque Quantification (Area and Volume)

- Establishing plaque burden requires estimation of plaque volume, and for this IVUS scanning is considered the "reference standard."
- The most widely used CT metrics for plaque size are based on area and volume measurements.
- The cross-sectional view of the vessel permits the assessment of the lumen area and outer vessel area.
- Agreement of plaque quantification varies with plaque composition, because the dimensions of non-calcified tissue are underestimated, whereas the volume of calcified plaque is usually overestimated compared with IVUS. This can be explained mainly by calcium blooming and by partial volume effects caused by the contrast-enhanced vessel lumen [9, 10].
- The main challenge for plaque quantification is the exact separation of the lumen, plaque, and vessel wall (Figs. 6.10 and 6.11).

6.4.2 Plaque Composition

- Atherosclerotic plaque composition and configuration are important predictors of plaque stability.

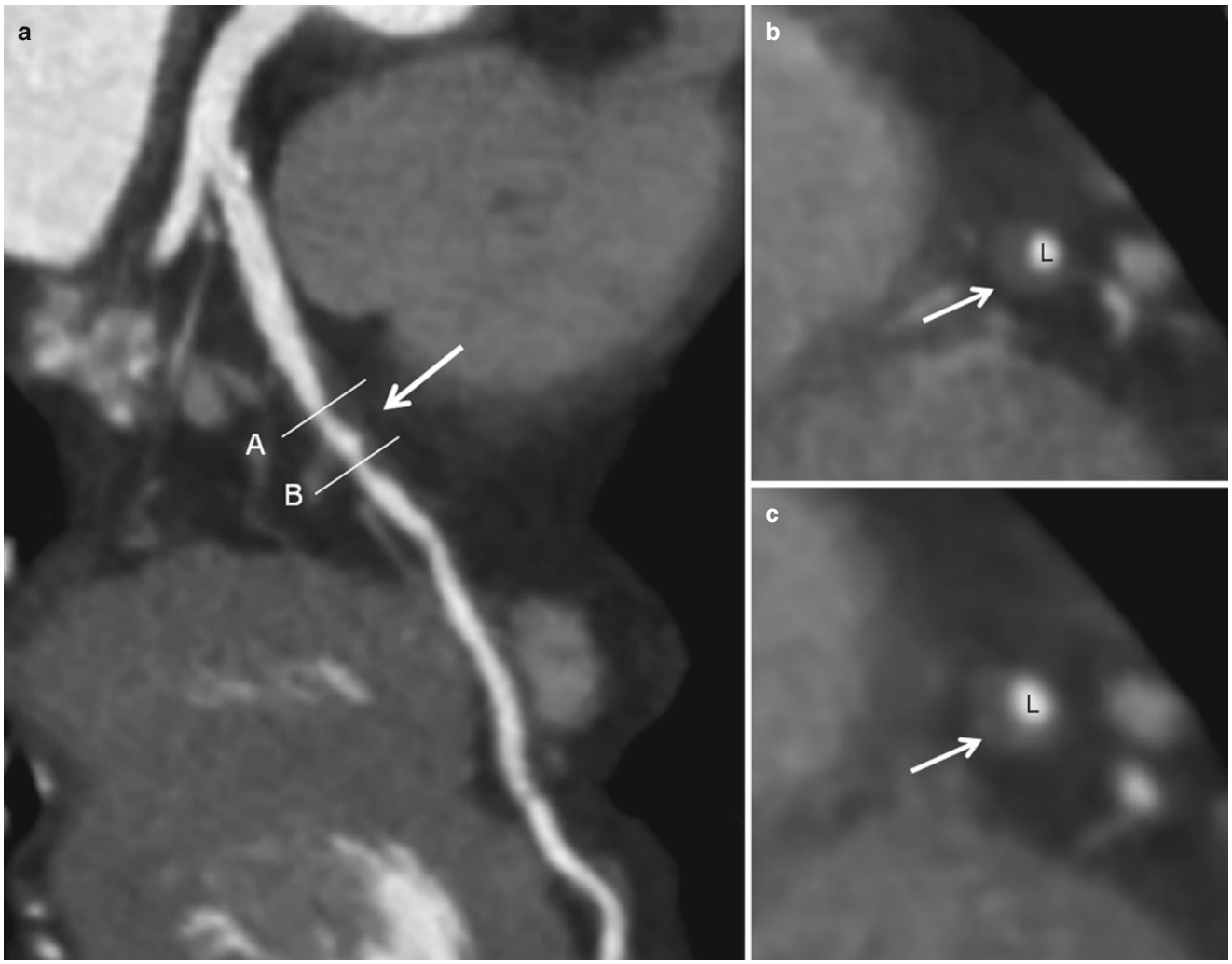

Fig. 6.7 Non-calcified plaque. (**a**) Curved multiplanar reformatted (MPR) image of coronary computed tomographic angiography (CCTA) demonstrates non-calcified plaque in the proximal segment of LAD (*arrow*). (**b**, **c**) Cross-sectional images of CCTA on the level of *white lines* (*B*) and (*C*) on image **a**. The non-calcified plaque is composed of soft tissue without any calcifications (*arrow*). *L* lumen

Table 6.2 Criteria for defining vulnerable plaque, based on the study of culprit plaques

Major criteria	Minor criteria
Active inflammation (monocyte/macrophage and sometimes T-cell infiltration)	Superficial calcified nodule
Thin cap with large lipid core	Glistening yellow
Endothelial denudation with superficial platelet aggregation	Intraplaque hemorrhage
Fissured plaque	Endothelial dysfunction
Stenosis >90 %	Positive remodeling

- CT enabled plaque characterization based on density measurements, and several studies reported that CT density measurements were significantly different among calcified, mixed, and non-calcified plaques [11–13].
- Plaque occupying calcified tissue in >50 % of the plaque area (density >130 Hounsfield units) was classified as calcified plaque, plaque with no calcified tissue was classified as non-calcified plaque, and plaque with <50 % of calcified tissue was classified as mixed plaque.
- Because of a significant overlap in CT density measurements between lipid and fibrous plaques, reliable classification of non-calcified plaques as vulnerable or stable plaques based on CT density measurements is currently limited [14, 15].
- For CT-derived measurements of lumen and plaques, the image display setting may exert a significant influence.
- Density measurements in structures as small as coronary atherosclerotic plaque are heavily influenced by image noise, contrast attenuation in the adjacent lumen, and partial volume effects (Figs. 6.12, 6.13, and 6.14).

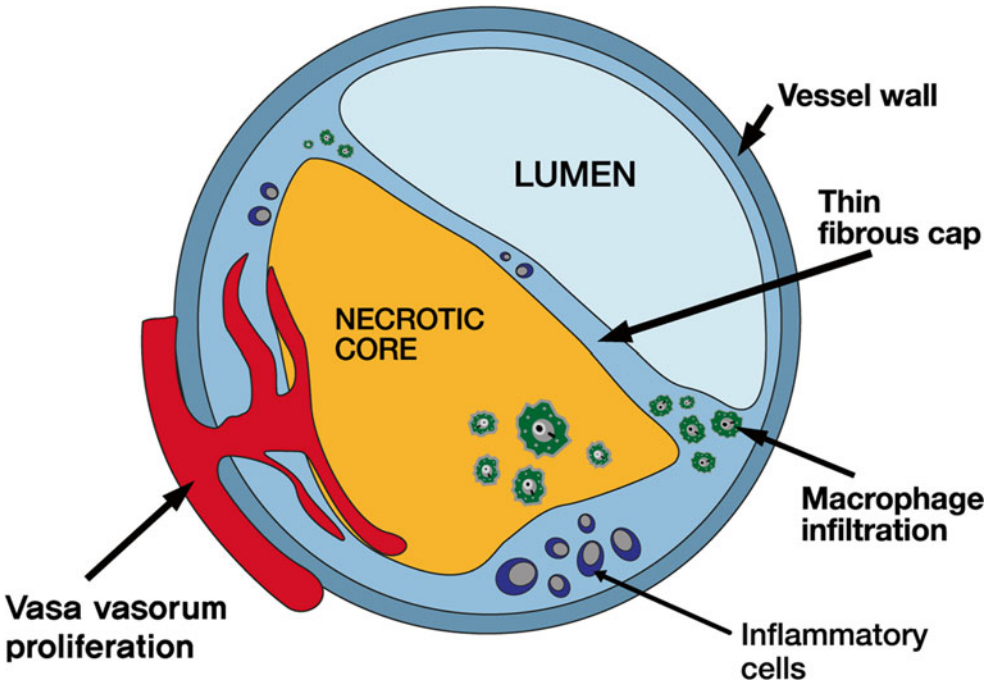

Fig. 6.8 Schematic illustration of vulnerable plaque. Schematic drawing of the morphologic features of a thin-cap fibroatheroma, which is commonly referred to as vulnerable plaque. A thin-cap fibroatheroma has histological characteristics, including a large necrotic core with an overlying thin intact fibrous cap, macrophages and inflammatory cell infiltration, and often increased number of intraplaque vasa vasorum

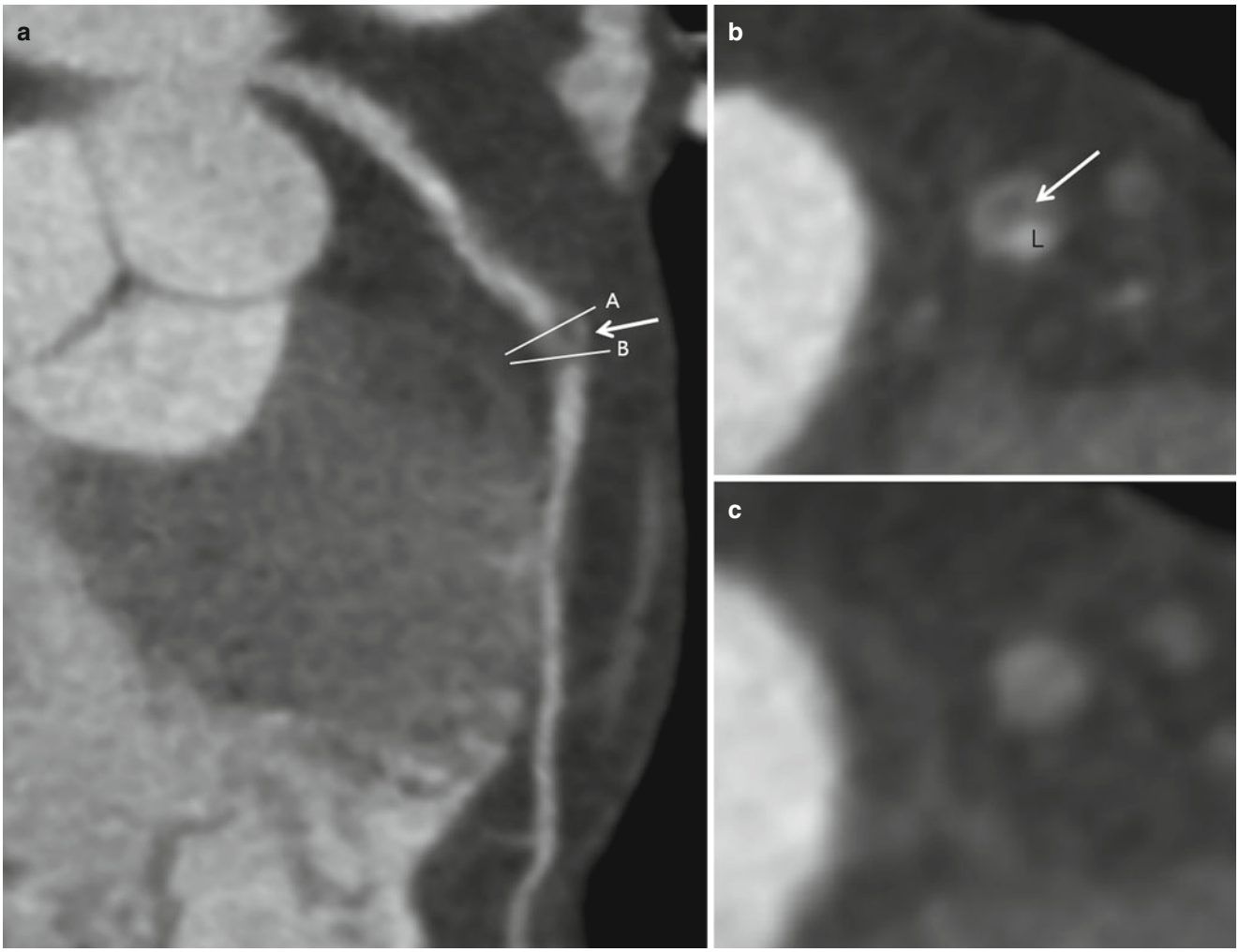

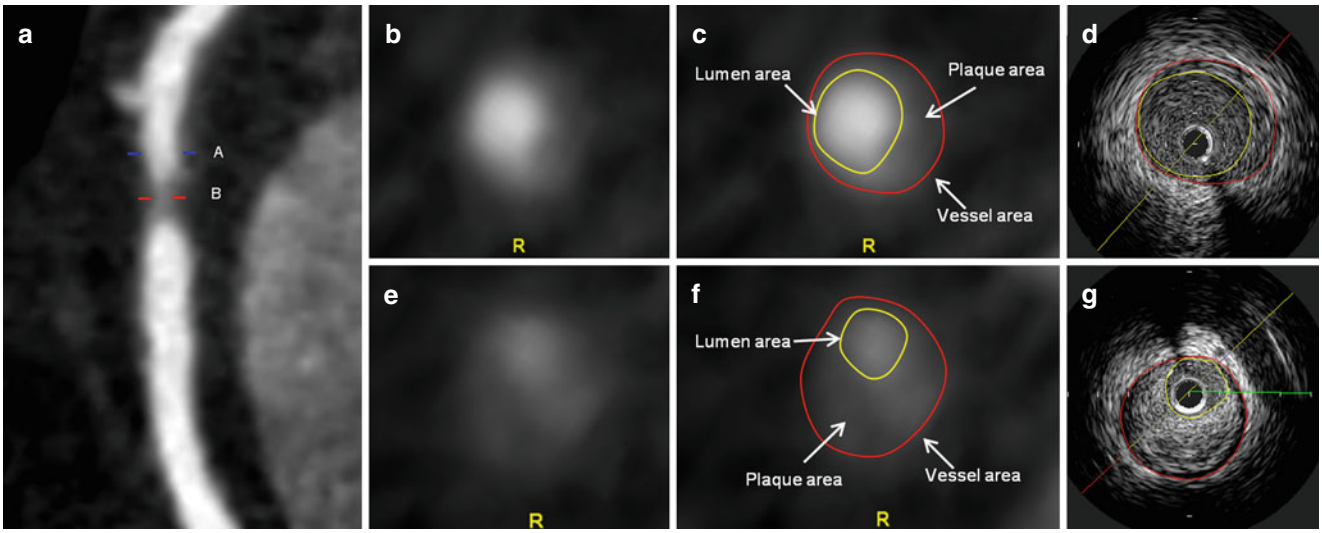

Fig. 6.10 Comparison of plaque area using coronary computed tomography (CCTA) and intravascular ultrasound (IVUS) with significant coronary artery stenosis of the right coronary artery (RCA). (**a**) Curved multiplanar reformatted (MPR) image of CCTA demonstrates significant coronary artery stenosis in the proximal segment of RCA by non-calcified plaque. (**b**, **c**) Cross-sectional images of CCTA on the level of the *Blue line* (*A*) on image **a**. Measurements of vessel area, lumen area, and plaque area were 15.9, 5.5, and 10.4 mm^2, respectively. (**d**) Corresponding intravascular ultrasound cross-sectional image of non-calcified plaque. Measurements of EEM CSA, lumen CSA, and plaque area were 16.7, 5.6, and 11.1 mm^2, respectively. *Red circle indicating EEM CSA* external elastic membrane cross-sectional area, *yellow circle indicating lumen CSA* lumen cross-sectional area, *plaque CSA* plaque cross-sectional area. (**e**, **f**) Cross-sectional images of CCTA on the level of the *red line* (*B*) on image **a**. Measurements of vessel area, lumen area, and plaque area were 16.8, 3.2, and 13.6 mm^2, respectively. (**g**) Corresponding intravascular ultrasound cross-sectional image. Measurements of EEM CSA, lumen CSA, and plaque area were 17.5, 3.6, and 13.9 mm^2, respectively. *Red circle indicating EEM CSA* external elastic membrane cross-sectional area, *yellow circle indicating lumen CSA* lumen cross-sectional area, *plaque CSA* plaque cross-sectional area

6.4.3 Positive Remodeling

- Positive remodeling: non-stenotic lesion undergoes expansive, or outward remodeling, namely, compensatory enlargement before impinging significantly on the vascular lumen (remodeling index >1.05).
- Remodeling index=CSA of the stenotic site/CSA of the reference site, CSA=cross-sectional area of outer wall of a vessel.
- Recent study has suggested that such positive remodeling is a potential surrogate marker of plaque vulnerability [16] (Figs. 6.15 and 6.16).

6.4.4 Napkin-Ring Sign

- Napkin-ring sign: specific attenuation pattern of atherosclerotic plaques on CCTA images characterized by a plaque core with low CT attenuation surrounded by a rim-like area of higher CT attenuation.
- Napkin-ring signs have been described in patients with acute coronary syndromes potentially representing a culprit coronary lesion [17, 18]. The CT attenuation of the core of these napkin-ring plaques was less than 60 HU (Fig. 6.17).

Fig. 6.9 Vulnerable plaque. (**a**) Curved multiplanar reformatted (MPR) image of coronary computed tomographic angiography (CCTA) demonstrates non-calcified plaque with lower attenuation within the central part of the plaque (*arrow*) as compared to the outer rim of the non-calcified plaque, suggestive of necrotic core. (**b**) Cross-sectional image of CCTA on the level of *white line* (*B*) on image **a**. The CT image shows a large non-calcified plaque with significant coronary artery luminal narrowing. The CT density of low attenuation within the central part of the plaque (*arrow*) was 7.9 ± 10.2 HU, indicating a necrotic core with lipid component. *L* lumen. (**c**) Cross-sectional image of CCTA on the level of *white line* (*C*) on image **a**. This cross-sectional image shows total occlusion by non-calcified plaque. The non-calcified plaque shows a higher CT attenuation compared to cross-sectional image on **b**. The mean attenuation of the non-calcified plaque was 67.9 ± 8.5 HU, indicating this area of plaque was composed of fibrous tissues

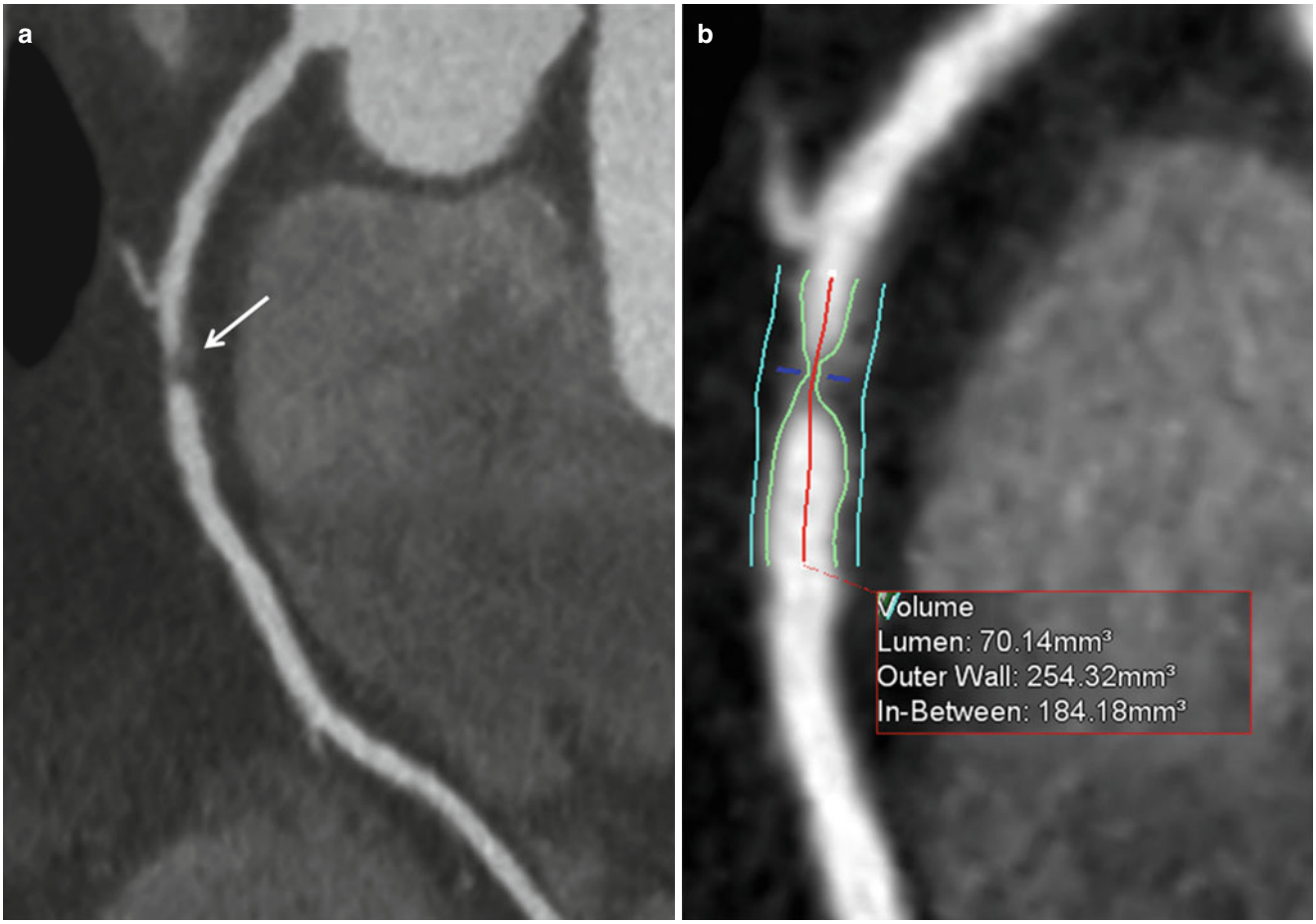

Fig. 6.11 Quantification of plaque volume using coronary computed tomography (CCTA) with significant coronary artery stenosis of the right coronary artery (RCA). (**a**) Curved multiplanar reformatted (MPR) image of CCTA demonstrates significant coronary artery stenosis in the proximal segment of RCA by non-calcified plaque (*arrow*). (**b**) Measurements of vessel volume, lumen volume, and plaque volume were 254.32, 70.14, and 184.18 mm^3, respectively

6.4.5 Plaque Analyzing Software

- Software assessment allows detailed investigation of plaques by color-coding on preset Hounsfield unit ranges.
- Using plaque analyzing software, contrast-enhanced lumen, vessel wall, and plaque composition (soft, fibrous, or calcified) can be depicted in different colors according to their corresponding CT Hounsfield unit ranges.
- Plaque analyzing software has the following technical limitations:
  - No standard recommendations for absolute density results of plaque software tools
  - Difficult to further differentiate or classify the non-calcified plaque because of the overlap of CT values of different composition in non-calcified plaque (Fig. 6.18)

6.5 Prognostic Implication of Coronary Plaque

- CCTA is increasingly used to provide the prognostic information about coronary artery disease.
- Recent studies reported that findings of cardiac CT have been closely associated with future cardiac events, with 0 or 1 % cardiac events being reported in patients with normal cardiac CT or mild coronary artery disease [19, 20].
- In a recent study, Motoyama et al. demonstrated that beyond the mere assessment of plaque burden, specific plaque parameters may be associated with a particularly high risk. They clearly showed that plaques with positive remodeling and low CT attenuation were at particularly high risk for causing future cardiovascular events [21].

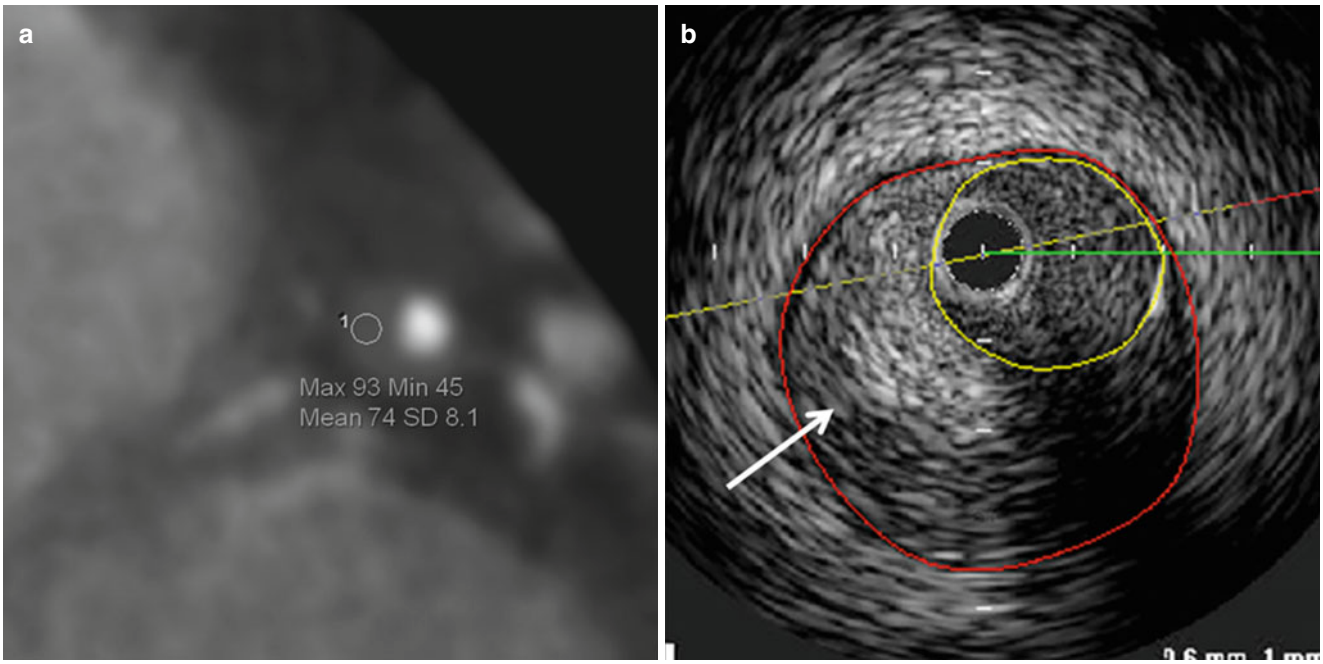

Fig. 6.12 Plaque density measurement of fibrous plaque. (**a**) Cross-sectional image of coronary CT angiography (CCTA) shows non-calcified plaque. The mean CT density value in a region of interest (ROI) of the non-calcified plaque was 74 HU ± 8.1. (**b**) Corresponding cross-sectional image of intravascular ultrasound. IVUS image shows hyperechoic plaque (*arrow*)

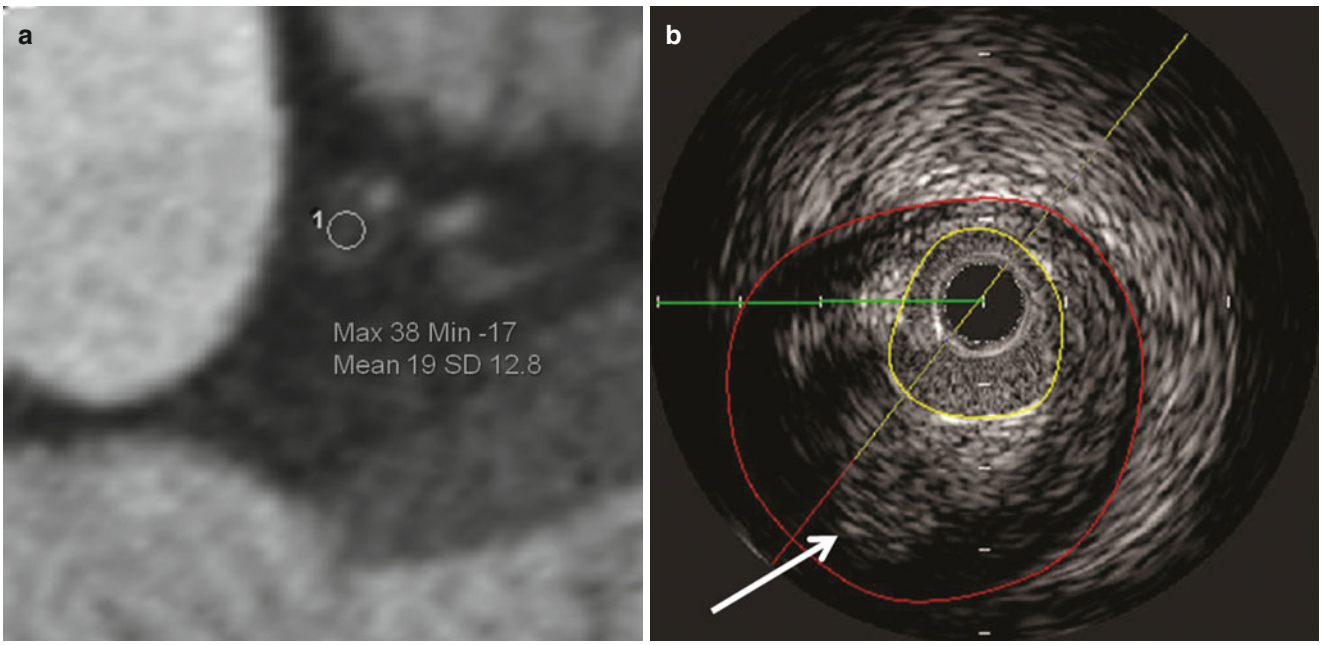

Fig. 6.13 Plaque density measurement of lipid-rich plaque. (**a**) Cross-sectional image of coronary CT angiography (CCTA) shows non-calcified plaque. The mean CT density value in a region of interest (ROI) of the non-calcified plaque was 19 HU ± 12.8. (**b**) Corresponding cross-sectional image of intravascular ultrasound. IVUS image shows hypoechoic plaque (*arrow*)

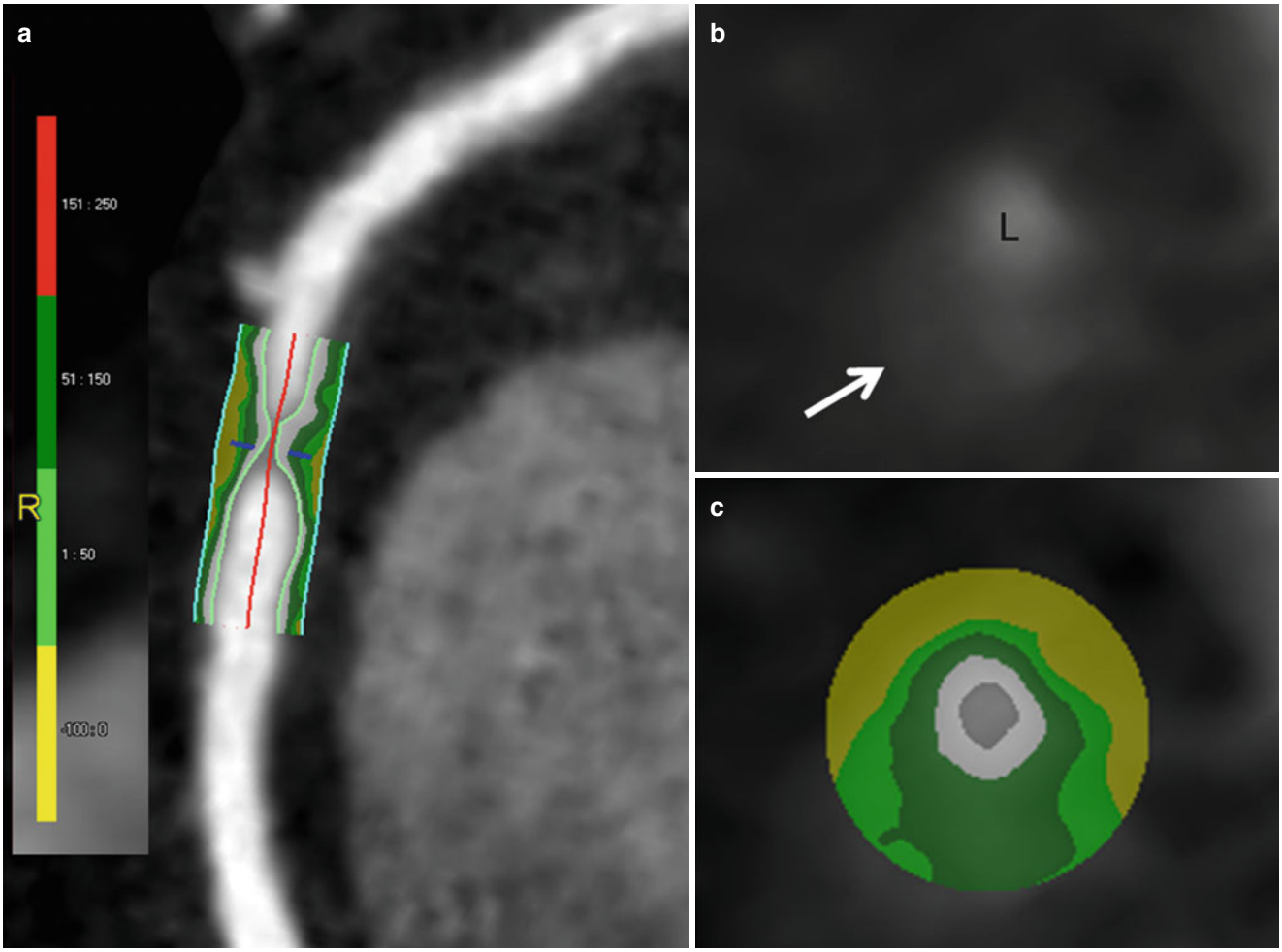

Fig. 6.14 Illustration of plaque characterization with automated software. (**a**) Color-coded map of curved multiplanar reformatted (MPR) image. The non-calcified plaque is composed of soft tissue with *green and yellow-green* in the central area and *yellow* in the outer area of plaque, indicating fibrofatty tissue. (**b**) Cross-sectional image of CCTA on the level of *blue line* on image **a**. The non-calcified plaque is composed of soft tissue without any calcifications (*arrow*). *L* Lumen. (**c**) Color map image corresponding to cross-sectional image **b**. Color map image shows *yellow-green* and *green* in the central area and *yellow* in the outer area of plaque, indicating the plaque is composed of fibrofatty tissues without calcifications

- The actual clinical utility of CCTA for risk stratification purposes is very uncertain, especially when considering extending the currently available findings to a "screening" situation. In fact, a trial of 1,000 middle-aged asymptomatic Korean was not able to identify any prognostic value of coronary CTA over a 17-month follow-up period [22].
- While of intense scientific interest, the clinical use of CCTA to detect plaque in asymptomatic individuals for purposes of risk stratification is currently not considered an "appropriate" indication.

6.6 Limitations and Future Directions

- Current CCTA is unable to distinguish a predominately lipid lesion with a thin fibrous plaque (the unstable plaque) from a predominately fibrous plaque with small lipid component (which would be more stable).
- Another limitation regarding plaque classification with CCTA is the effect of contrast concentration on plaque attenuation.
- Attempts at plaque quantification and characterization have been successful, but further refinements regarding reproducibility, accuracy, and ability to predict future events are required.
- The evolution of software algorithms for the classification and quantification of coronary plaque will improve reproducibility and accuracy of the technique.
- Refinement of semiautomated plaque quantification would broaden the clinical applicability of CCTA for atherosclerosis evaluation.
- In the future, technical developments could lead to CT becoming a surrogate marker for cardiovascular events and a tool for assessing the effects of treatment in clinical trials.

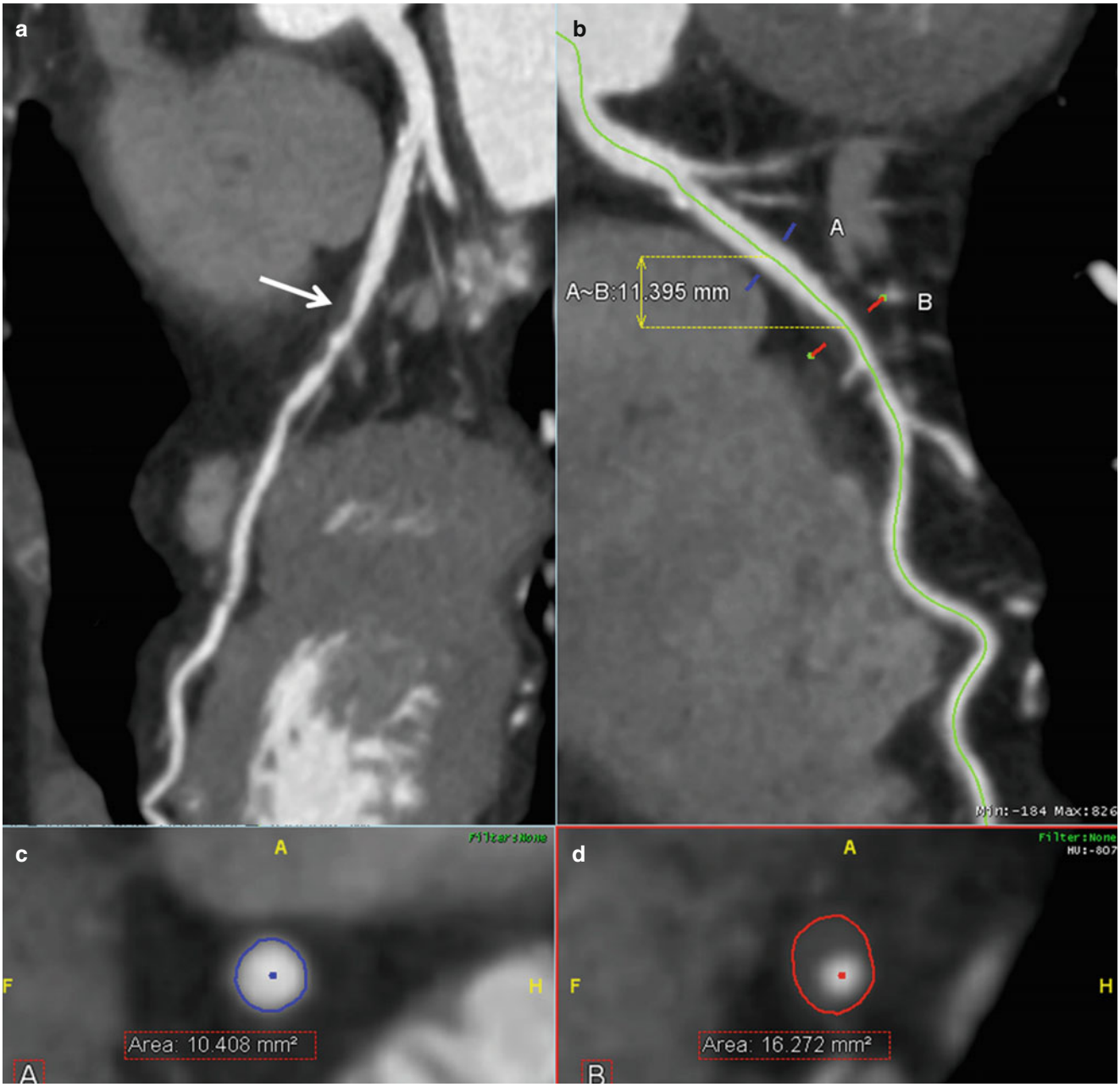

Fig. 6.15 Positive remodeling in the left anterior descending artery (LAD). (**a**) Curved multiplanar reformatted (MPR) image demonstrates non-calcified plaque in the proximal segment of LAD (*arrow*). (**b**) MPR image that was automatically traced using software. *Blue line* (**a**) indicates reference level and *red line* (**b**) indicates most significant coronary artery stenotic level due to non-calcified plaque. *Green line* = center line of the coronary artery. (**c**) Corresponding cross-sectional image of CT on the level of *blue line* on image **b**. The EEM CSA of the reference site was 10.408 mm^2. (**d**) Corresponding cross-sectional image of CT on the level of *red line* on image **b**. The EEM CSA of the lesion site was 16.272 mm^2. The remodeling index (RI) was 16.272 (EEM area lesion)/10.408 (EEM area reference) = 1.56, indicating positive remodeling. *EEM CSA* external elastic membrane cross-sectional area

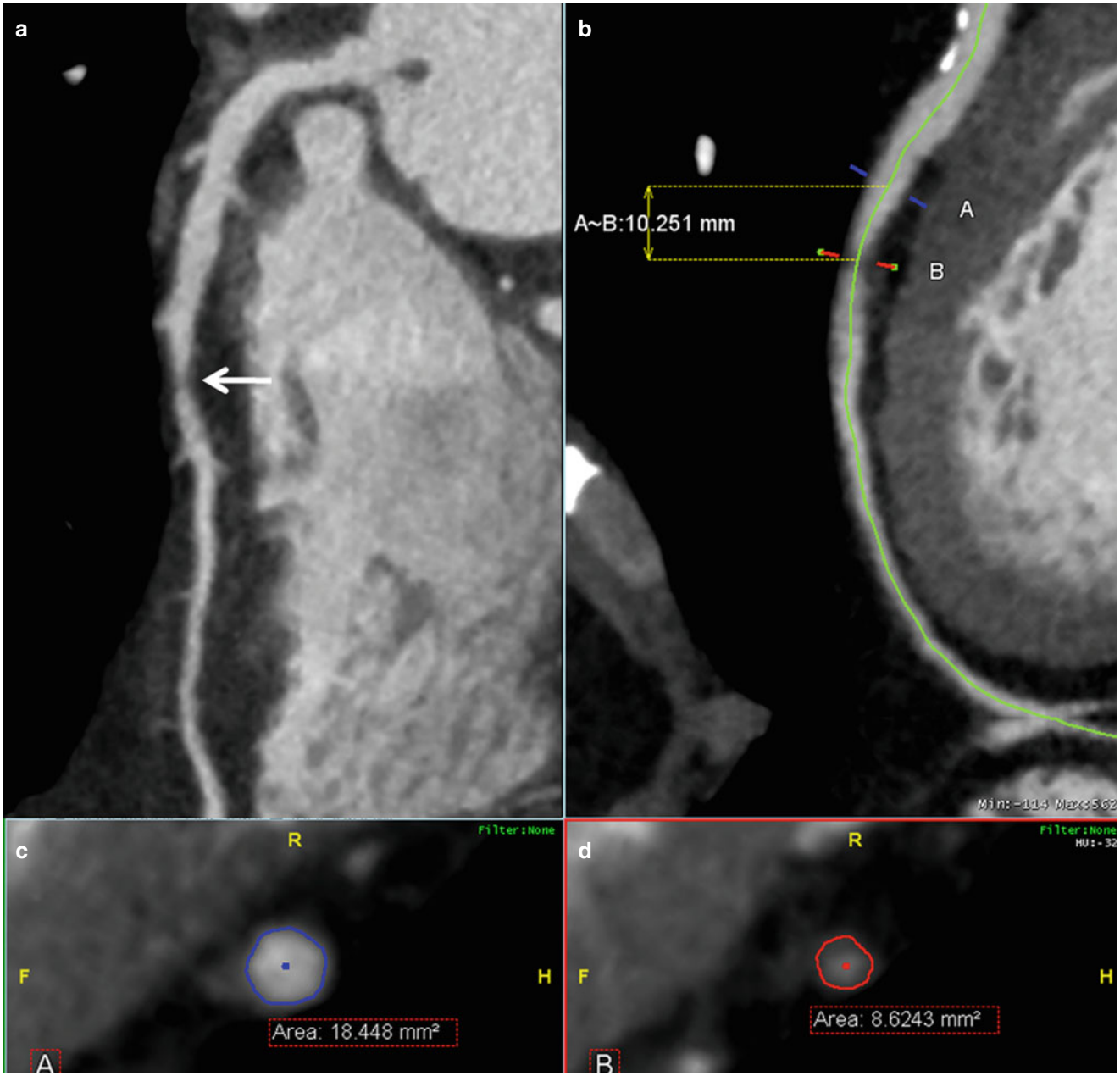

Fig. 6.16 Negative remodeling in the left anterior descending artery (LAD). (**a**) Curved multiplanar reformatted (MPR) image demonstrates non-calcified plaque in the mid-segment of LAD (*arrow*). (**b**) MPR image that was automatically traced using software. *Blue line* (*A*) indicates reference level and *red line* (*B*) indicates most significant coronary artery stenotic level due to non-calcified plaque. *Green line* = center line of the coronary artery. (**c**) Corresponding cross-sectional image of CT on the level of *blue line* on image **b**. The EEM CSA of the reference site was 18.448 mm^2. (**d**) Corresponding cross-sectional image of CT on the level of *red line* on image **b**. The EEM CSA of the lesion site was 8.642 mm^2. The remodeling index (RI) was 8.642 (EEM area lesion)/18.448 (EEM area reference) = 0.468, indicating negative remodeling. *EEM CSA* external elastic membrane cross-sectional area

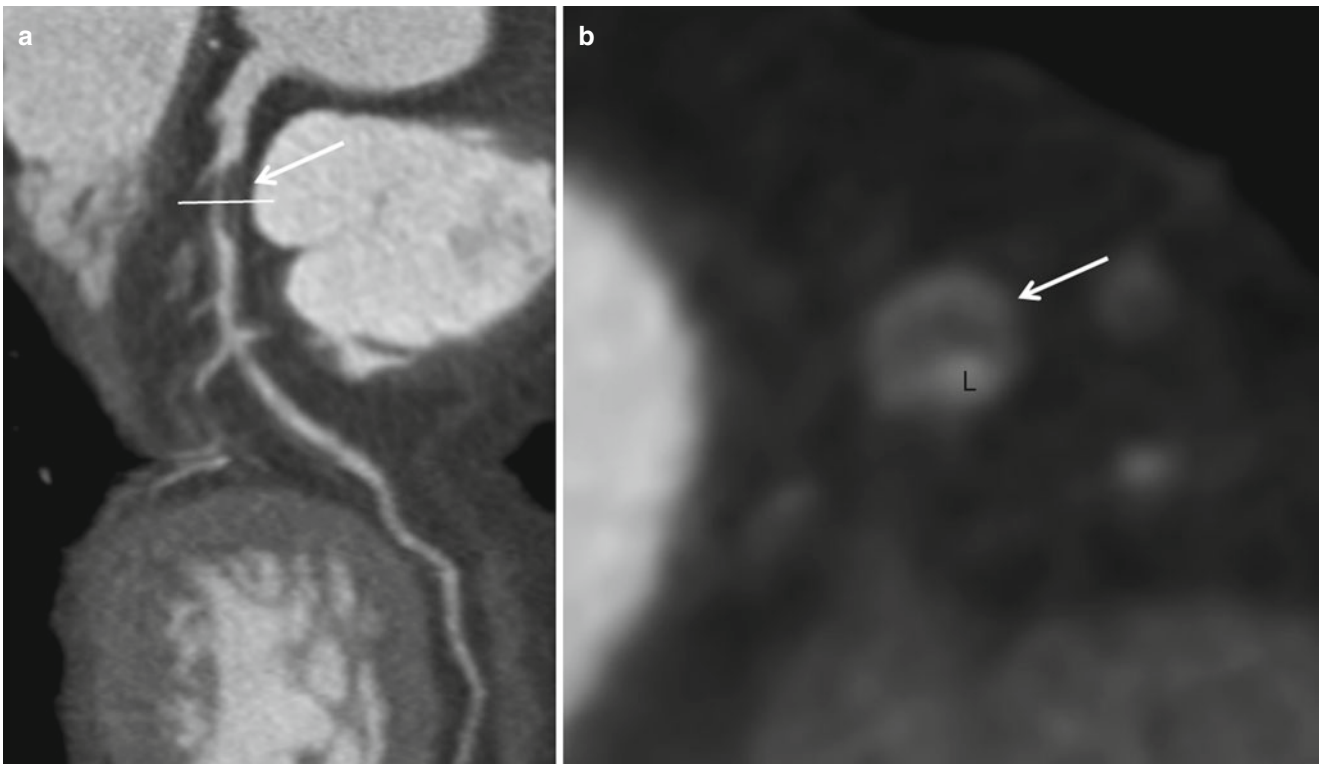

Fig. 6.17 Napkin-ring sign in a 63-year-old man with chest pain. (**a**) Curved multiplanar reformatted (MPR) image demonstrates non-calcified plaque with low attenuation (*arrow*) in the proximal segment of the left anterior descending coronary artery (LAD). (**b**) Cross-sectional image of CCTA on the level of the *white line* on image **a**. The CT image shows a large non-calcified plaque with napkin-ring-like attenuation pattern. The circumferential outer rim (*arrow*) of the plaque has a higher CT attenuation as compared to the attenuation within the central part of the plaque. *L* Lumen

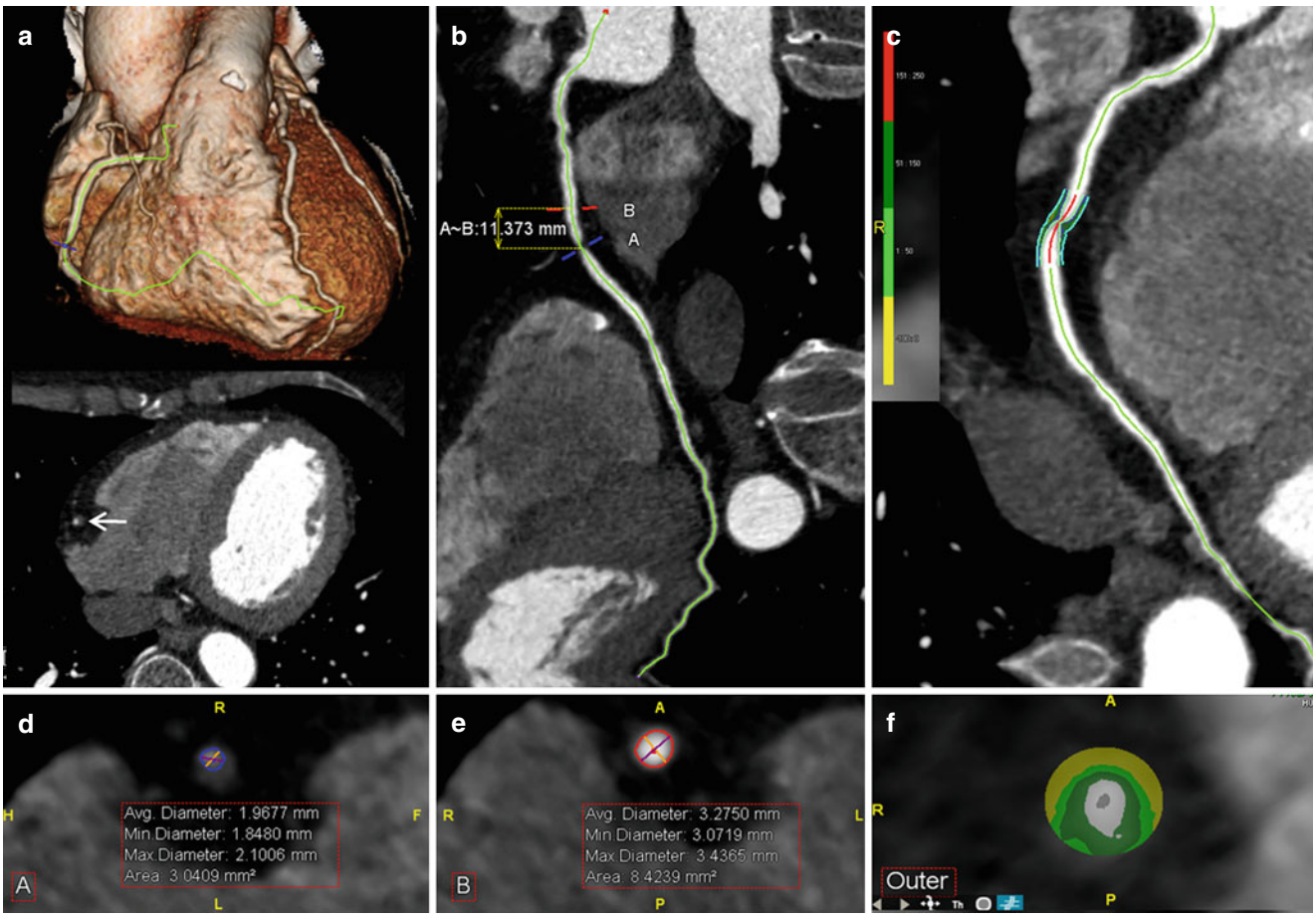

Fig. 6.18 Illustration of plaque analyzing software in a 64-year-old man with significant coronary artery stenosis of the right coronary artery (RCA). (**a**) 3D volume rendering (VR) image shows significant coronary artery stenosis (*blue line*) on the middle segment of the RCA. Corresponding axial image demonstrates non-calcified plaque (*arrow*) in the middle segment of the RCA. (**b**) Curved multiplanar reformatted (MPR) image that was automatically traced using the software. *Red line* (*B*) indicates reference level and *blue line* (*A*) indicates most significant coronary artery stenotic level due to non-calcified plaque. *Green line* = center line of the coronary artery. (**c**) Corresponding cross-sectional image of CT on the level of *blue line* on image **b**. Measurements of EEM CSA, lumen CSA, and plaque CSA were 9.8239, 3.0409, and 6.783 mm^2, respectively. *EEM CSA* external elastic membrane cross-sectional area, *blue circle indicating lumen CSA* lumen cross-sectional area, *plaque CSA* plaque cross-sectional area. (**d**) Corresponding cross-sectional image of CT on the level of *red line* on image **b**. The EEM CSA of the reference site was 8.4239 mm^2. The remodeling index (RI) was 9.8239/8.4239 = 1.166, indicating positive remodeling. (**e**, **f**) Color map images demonstrate yellow-green and green in the central area and yellow in the outer area of plaque, indicating the plaque is composed of fibrofatty tissues. HU range of color bar: *yellow* −100-0 HU, *yellow-green* 1–50 HU, *green* 51–150 HU, *red* 151–250

6.7 Summary

- CCTA has tremendous potential to provide uniquely valuable information concerning coronary atherosclerosis.
- Both for risk stratification of an individual and for obtaining new information on the disease process itself, the ability to directly visualize coronary atherosclerotic lesions is of great potential.
- As image quality of CCTA shows continuous improvement, the amount of detailed information that can be obtained from a CCTA will undoubtedly increase and even better characterization of coronary atherosclerosis will become possible.

References

1. Mintz GS, Nissen SE, Anderson WD, et al. American College of Cardiology clinical expert consensus document on standards for acquisition, measurement and reporting of intravascular ultrasound studies (IVUS): a report of the American College of Cardiology Task Force on Clinical Expert Consensus Documents. J Am Coll Cardiol. 2001;37:1478–92.
2. Nair A, Kuban BD, Tuzcu EM, Schoenhagen P, Nissen SE, Vince DG. Coronary plaque classification with intravascular ultrasound radiofrequency data analysis. Circulation. 2002;106:2200–6.
3. Nasu K, Tsuchikane E, Katoh O, et al. Accuracy of in vivo coronary plaque morphology assessment: a validation study of in vivo virtual histology compared with in vitro histopathology. J Am Coll Cardiol. 2006;47:2405–12.

4. Schoepf UJ, Zwerner PL, Savino G, Herzog C, Kerl JM, Costello P. Coronary CT angiography. Radiology. 2007;244:48–6.
5. Cordeiro MA, Lima JA. Atherosclerotic plaque characterization by multidetector row computed tomography angiography. J Am Coll Cardiol. 2006;47(8 Suppl):C40–7.
6. Spuentrup E, Botnar RM. Coronary magnetic resonance imaging: visualization of the vessel lumen and the vessel wall and molecular imaging of arteriothrombosis. Eur Radiol. 2006;16:1–14.
7. Finn AV, Nakano M, Narula J, Kolodgie FD, Virmani R. Concept of vulnerable/unstable plaque. Arterioscler Thromb Vasc Biol. 2010; 30:1282–92.
8. Naghavi M, Libby P, Falk E, et al. From vulnerable plaque to vulnerable patient: a call for new definitions and risk assessment strategies: part I. Circulation. 2003;108:1664–72.
9. Leber AW, Knez A, von Ziegler F, et al. Quantification of obstructive and nonobstructive coronary lesions by 64-slice computed tomography: a comparative study with quantitative coronary angiography and intravascular ultrasound. J Am Coll Cardiol. 2005;46:147–54.
10. Leber AW, Becker A, Knez A, et al. Accuracy of 64-slice computed tomography to classify and quantify plaque volumes in the proximal coronary system: a comparative study using intravascular ultrasound. J Am Coll Cardiol. 2006;47:672–7.
11. Achenbach S, Moselewski F, Ropers D, et al. Detection of calcified and noncalcified coronary atherosclerotic plaque by contrast-enhanced, submillimeter multidetector spiral computed tomography: a segment based comparison with intravascular ultrasound. Circulation. 2004;109:14–7.
12. Schroeder S, Kopp AF, Baumbach A, et al. Noninvasive detection and evaluation of atherosclerotic coronary plaques with multi-slice computed tomography. J Am Coll Cardiol. 2001;37:1430–5.
13. Leber AW, Knez A, Becker A, et al. Accuracy of multi-detector spiral computed tomography in identifying and differentiating the composition of coronary atherosclerotic plaques: a comparative study with intracoronary ultrasound. J Am Coll Cardiol. 2004;43:1241–7.
14. Pohle K, Achenbach S, Macneill B, et al. Characterization of non-calcified coronary atherosclerotic plaque by multi-detector row CT: comparison to IVUS. Atherosclerosis. 2007;190:174–80.
15. Hur J, Kim YJ, Lee HJ, et al. Quantification and characterization of obstructive coronary plaques using 64-slice computed tomography: a comparison with intravascular ultrasound. J Comput Assist Tomogr. 2009;33:186–92.
16. Varnava AM, Mills PG, Davies MJ. Relationship between coronary artery remodeling and plaque vulnerability. Circulation. 2002;105: 939–43.
17. Narula J, Achenbach S. Napkin-ring necrotic cores: defining circumferential extent of necrotic cores in unstable plaques. JACC Cardiovasc Imaging. 2009;2:1436–8.
18. Kashiwagi M, Tanaka A, Kitabata H, et al. Feasibility of noninvasive assessment of thin-cap fibroatheroma by multidetector computed tomography. JACC Cardiovasc Imaging. 2009;2:1412–9.
19. Carrigan TP, Nair D, Schoenhagen P, et al. Prognostic utility of 64-slice computed tomography in patients with suspected but no documented coronary artery disease. Eur Heart J. 2009;30:362–71.
20. Chow BJ, Wells GA, Chen L, et al. Prognostic value of 64-slice cardiac computed tomography severity of coronary artery disease, coronary atherosclerosis, and left ventricular ejection fraction. J Am Coll Cardiol. 2010;55:1017–28.
21. Motoyama S, Sarai M, Harigaya H, et al. Computed tomographic angiography characteristics of atherosclerotic plaques subsequently resulting in acute coronary syndrome. J Am Coll Cardiol. 2009;54:49–57.
22. Choi EK, Choi SI, Rivera JJ, et al. Coronary computed tomography angiography as a screening tool for the detection of occult coronary artery disease in asymptomatic individuals. J Am Coll Cardiol. 2008;52:357–65.

MR Coronary Angiography: Real-Word Practice of Coronary MR Angiography

7

Yeonyee E. Yoon and Hajime Sakuma

Contents

Abstract

Coronary magnetic resonance angiography (CMRA) has emerged over as a possible noninvasive alternative for coronary imaging without exposing patients to ionizing radiation. Currently, free-breathing 3-dimensional CMRA acquired with respiratory and electrocardiographic gating is the most commonly used MR approach. Whole-heart CMRA has been shown to be useful for the detection of significant coronary artery disease and for the prediction of future adverse cardiac events. Although long imaging time, low spatial resolution, and operator dependency have limited the widespread use of CMRA, technical advances, including high-field strength MR imaging and multichannel cardiac coils, may provide more accurate detection of CAD with reduced imaging time.

7.1 Coronary Magnetic Resonance Angiography

7.1.1 Introduction

- Coronary MR angiography (CMRA) allows noninvasive visualization of the coronary artery without exposing the patients to ionizing radiation (Fig. 7.1).
- Free-breathing 3-dimensional (3D) whole-heart CMRA can provide visualization of all major coronary arteries with a single axial 3D acquisition.
- At 1.5 T, excellent blood contrast can be obtained by using SSFP MR angiographic sequence without administration of gadolinium-based contrast agent.

7.1.2 Image Acquisition

- For the acquisition of free-breathing 3D coronary MR angiography, two sources of motion should be considered: cardiac contraction and respiratory motion (Fig. 7.2).

Y.E. Yoon (✉)
Division of Cardiology, Department of internal medicine, Seoul National University Bundang Hospital, Gyeonggido, Republic of Korea
e-mail: islandtea@gmail.com

H. Sakuma
Department of Radiology, Mie University Hospital, Mie University Graduate School, Tsu, Japan
e-mail: sakuma@clin.medic.mie-u.ac.jp

T.-H. Lim (ed.), *Practical Textbook of Cardiac CT and MRI*,
DOI 10.1007/978-3-642-36397-9_7,

- Electrocardiographic (ECG) gating is used to account for intrinsic cardiac motion. The patient-specific rest period of the coronary artery in the cardiac cycle is usually determined by visual inspection of cine images perpendicular to the long axis of the proximal to mid-right coronary artery (RCA).
- A navigator echo method to track a patient's diaphragmatic motion is employed for respiratory gating as well as adoptive motion correction.
- Abdominal belt can be applied to decrease breathing movement and to increase scan efficiency of navigator-gated whole-heart CMRA.
- Administration of sublingual nitrates induced coronary vasodilation and helps to improve the signal-to-noise ratio of CMRA.
- Since the temporal resolution of free-breathing CMRA can be flexibly determined by using imaging parameters, CMRA can be performed without the use of β-blockers even in patients with a high heart rate.
- Narrow acquisition window in the cardiac cycle (30–75 ms) compared with cardiac CT is important to reduce blurring of the coronary arteries by cardiac contraction.

7.1.3 Image Analysis

- CMRA can be assessed on source 3D images, multiplanar reformation (MPR) images, thin maximal intensity projection (MIP) images, or volume-rendered images.
- The presence or absence of significant coronary stenosis on CMRA is qualitatively assessed.
- The current whole-heart CMRA approach could not provide sufficient spatial resolution for quantitative analysis of luminal diameter narrowing of the coronary artery.

7.2 Coronary MR Angiography for Identification of Coronary Artery Disease

- CMRA can assess the lumen of coronary artery even in a segment with heavy calcification (Fig. 7.3).
- Non-contrast-enhanced CMRA can be useful for the evaluation of CAD in patients with renal failure.
- Whole-heart CMRA has been shown to be useful for the detection of significant coronary artery disease (CAD) (Fig. 7.4).

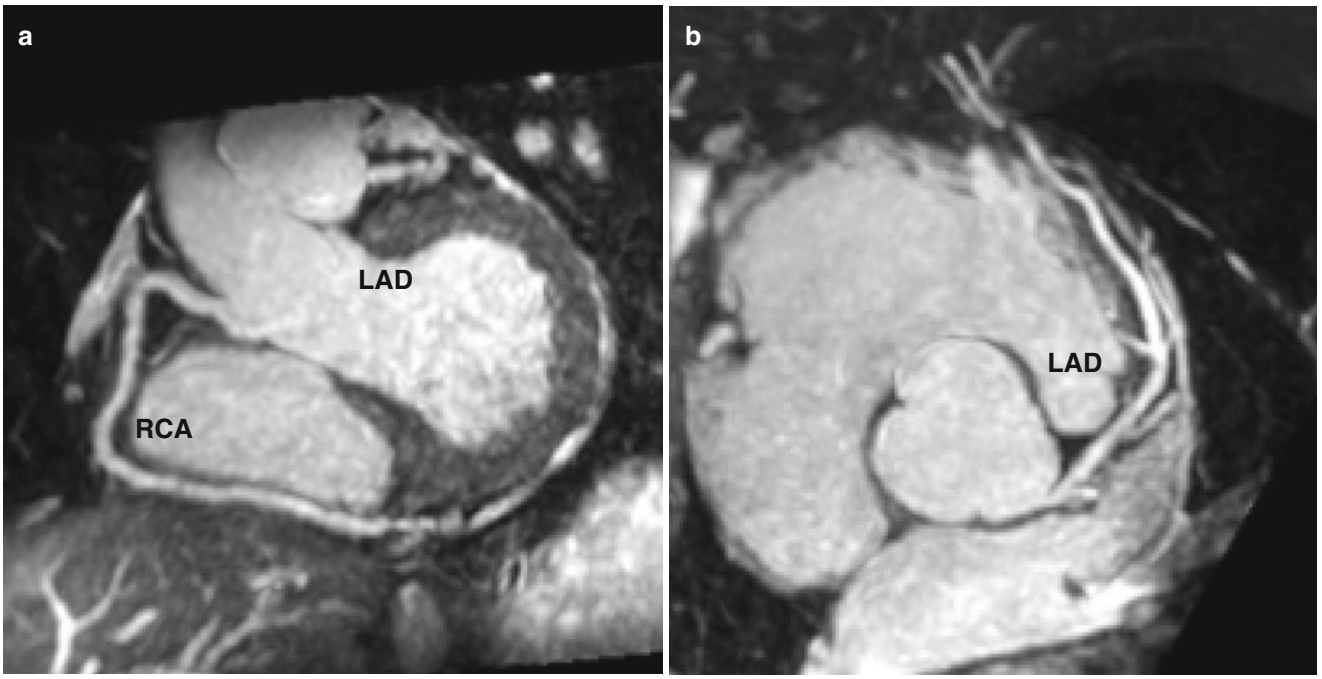

Fig. 7.1 1.5 T Free-breathing whole heart coronary MR angiography in a subject with normal coronary artery. Non-contrast-enhanced three-dimensional coronary MR angiography images were acquired with a 1.5 T MR imager by using a steady-state free precession (SSFP) sequence, navigator echo gating, T2 preparation, spectral presaturation inversion-recovery fat saturation (repetition time/echo time, 4.6/2.3 ms; flip angle, 90°; sensitivity encoding [SENSE] factor, four; field of view, 280×280×120 mm; acquisition matrices, 256×256×80; reconstruction matrices, 512×512×160). (**a**) Thin-section maximal intensity projection (MIP) images of right coronary artery (*RCA*). (**b**) Thin-section MIP images of left main and let anterior descending arteries (*LAD*). (**c**) Volume rendered images of RCA. (**d**) Volume rendered images of LAD and left circumflex coronary artery (*LCX*)

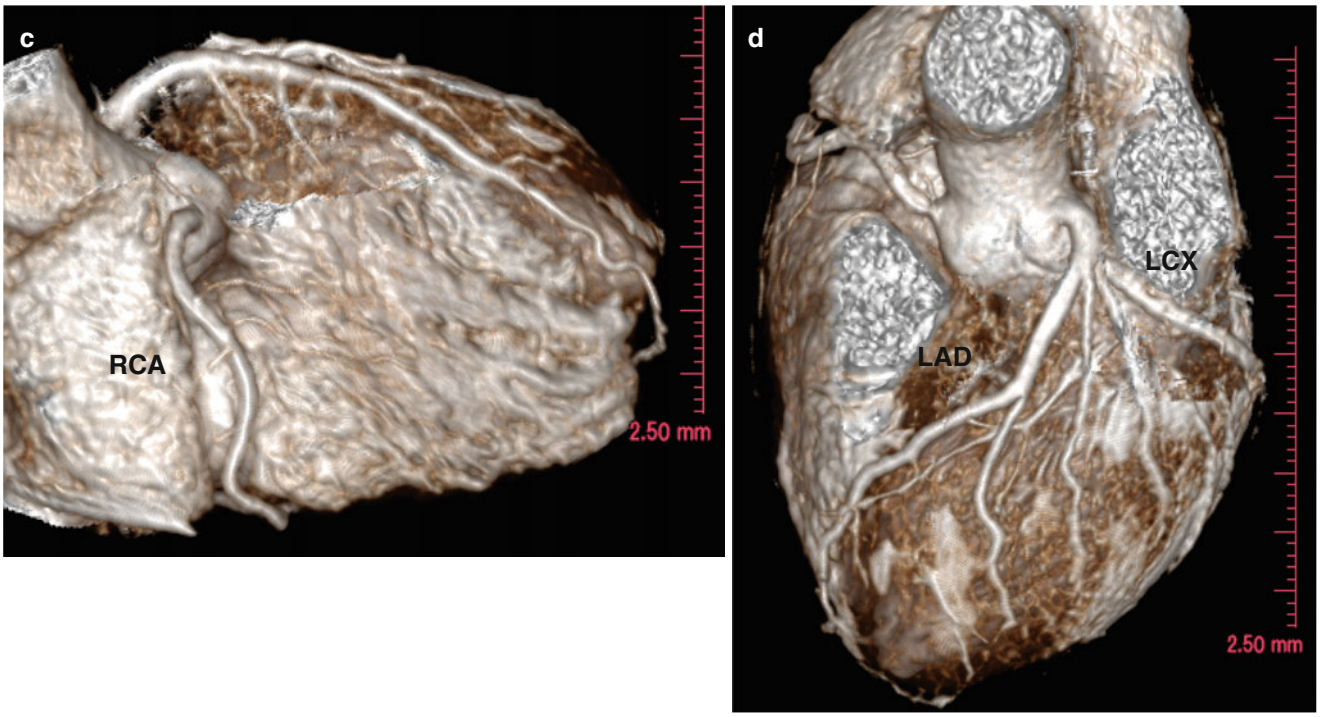

Fig. 7.1 (continued)

Learning Point
Coronary MR angiography allows noninvasive visualization of the coronary artery without exposing the patients to ionizing radiation.

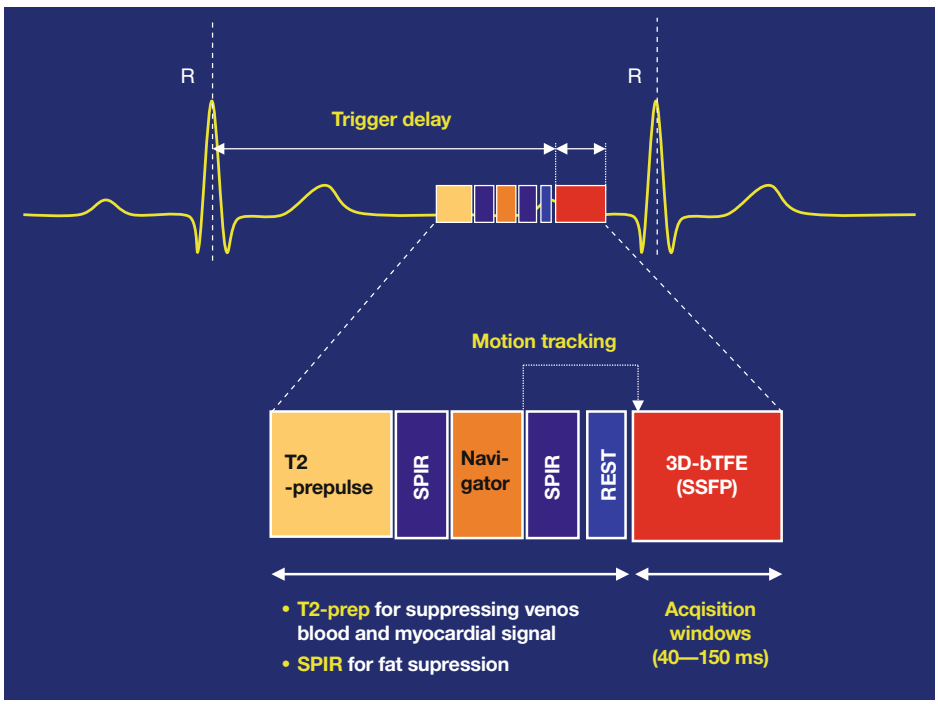

Fig. 7.2 Schematic representation of pulse sequence of free-breathing 1.5 T coronary MR angiography. Image acquisition is performed after a trigger delay from the R wave of the ECG. The imaging block is preceded by a T2 preparation, spectral presaturation inversion-recovery fat saturation, and a navigator pulse for respiratory motion compensation. These sequence blocks are repeated with every heart cycle

Learning Point
At 1.5 T, excellent blood contrast can be obtained by using SSFP MR angiographic sequence without injection of gadolinium-based contrast medium.

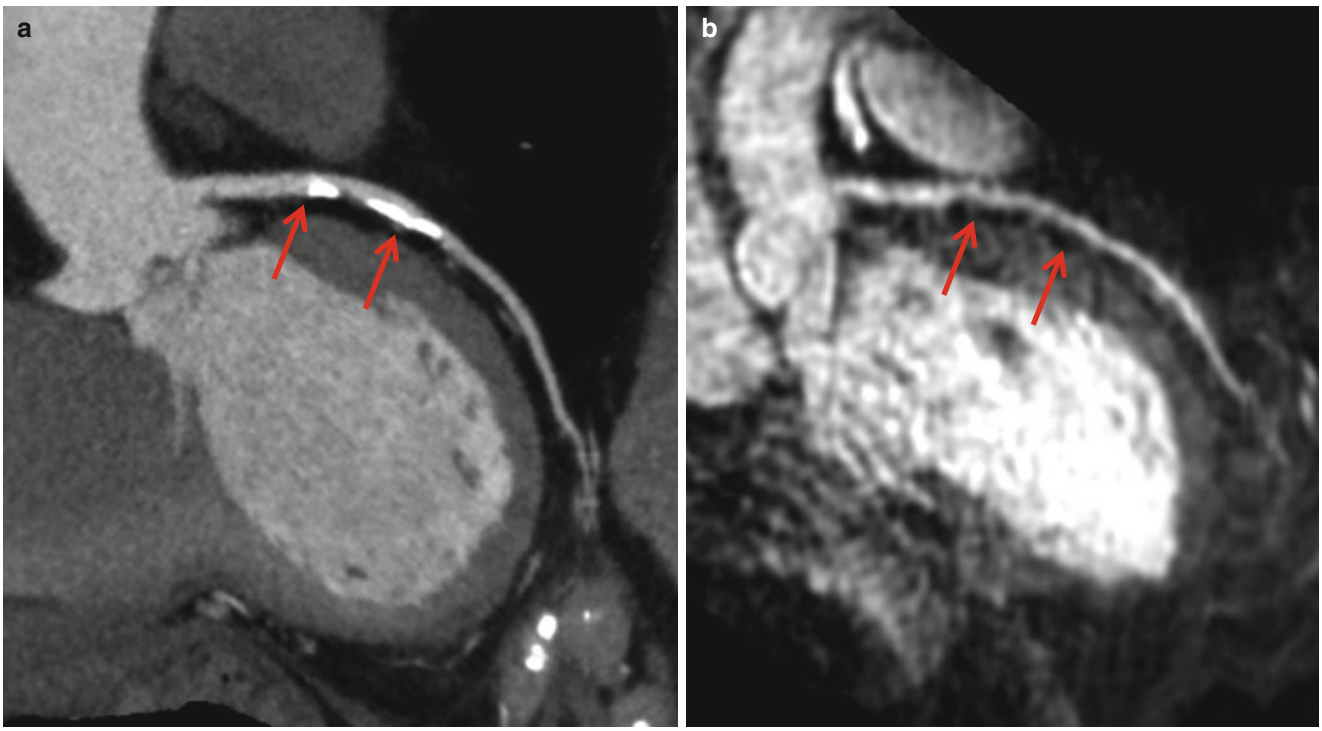

Fig. 7.3 Comparison of coronary CT angiography and MR angiography in a patient with calcified plaque at LAD. A 64-year-old female patient with chest pain. Non-contrast-enhanced three-dimensional coronary MR angiography images were acquired with a 1.5 T MR imager by using a steady-state free precession (SSFP) sequence, navigator echo gating, T2 preparation, spectral presaturation inversion-recovery fat saturation (repetition time/echo time, 4.6/2.3 ms; flip angle, 90°; sensitivity encoding [SENSE] factor, four; field of view, 280×280×120 mm; acquisition matrices, 256×256×80; reconstruction matrices, 512×512×160). (**a**) Curved multi-planar reconstruction (MPR) images of coronary computed tomography (CT) images showed diffuse calcified plaque (*arrows*) in the proximal LAD. (**b**) Thin-section MIP image of coronary MR angiography revealed patent LAD (*arrows*)

Learning Point

Coronary MR angiography may provide better diagnostic accuracy in patients with heavily calcified plaque.

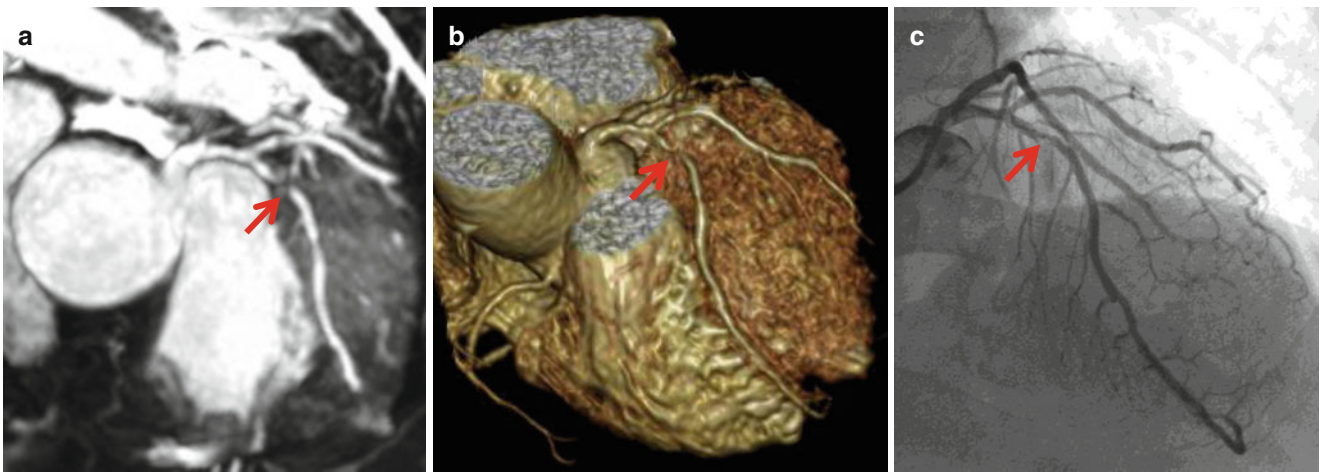

Fig. 7.4 Significant stenosis of LAD. A 65-year-old male patients with chest pain. Non-contrast-enhanced three-dimensional coronary MR angiography images were acquired with a 1.5 T MR imager by using a steady-state free precession (SSFP) sequence, navigator echo gating, T2 preparation, spectral presaturation inversion-recovery fat saturation (repetition time/echo time, 4.6/2.3 ms; flip angle, 90°; sensitivity encoding [SENSE] factor, four; field of view, 280×280×120 mm; acquisition matrices, 256×256×80; reconstruction matrices, 512×512×160). (**a**) Thin-section MIP and (**b**) volume rendered image of whole-heart coronary MR angiography showed significant stenosis of mid LAD (*arrow*). (**c**) Good agreement was observed between coronary MR angiography (*arrow*) and invasive coronary angiography (*arrow*)

- The combination of CMRA with cine MR imaging, stress perfusion MR imaging, and late gadolinium-enhanced MR imaging provides a comprehensive assessment of CAD (Fig. 7.5 and 7.6).
- Whole-heart CMRA can predict future risk for adverse cardiac events in patients with suspected CAD.

7.3 Technical Development

- Prolonged imaging time has been a major disadvantage of 3D whole-heart CMRA.
- Introduction of 32-channel cardiac coils permits the use of a higher parallel imaging acceleration factor (SENSE factor of ≥4) and substantially reduced the imaging time of CMRA (several minutes to 10 min).
- Reduced imaging time leads to low likelihood of failure in respiratory-gated acquisition.
- Higher-field, 3 T system provides better signal and contrast values relative to 1.5 T system, thus may improve the detection of coronary artery disease with coronary MR angiography (Fig. 7.7).
- Because of the increased magnetic field inhomogeneity and radiofrequency energy deposition at higher-field strength, gradient-echo sequence instead of the SSFP sequence has a better clinical performance at 3 T.
- Administration of gadolinium contrast agent is useful to improve blood contrast on 3 T gradient-echo CMRA (Fig. 7.8 and 7.9).

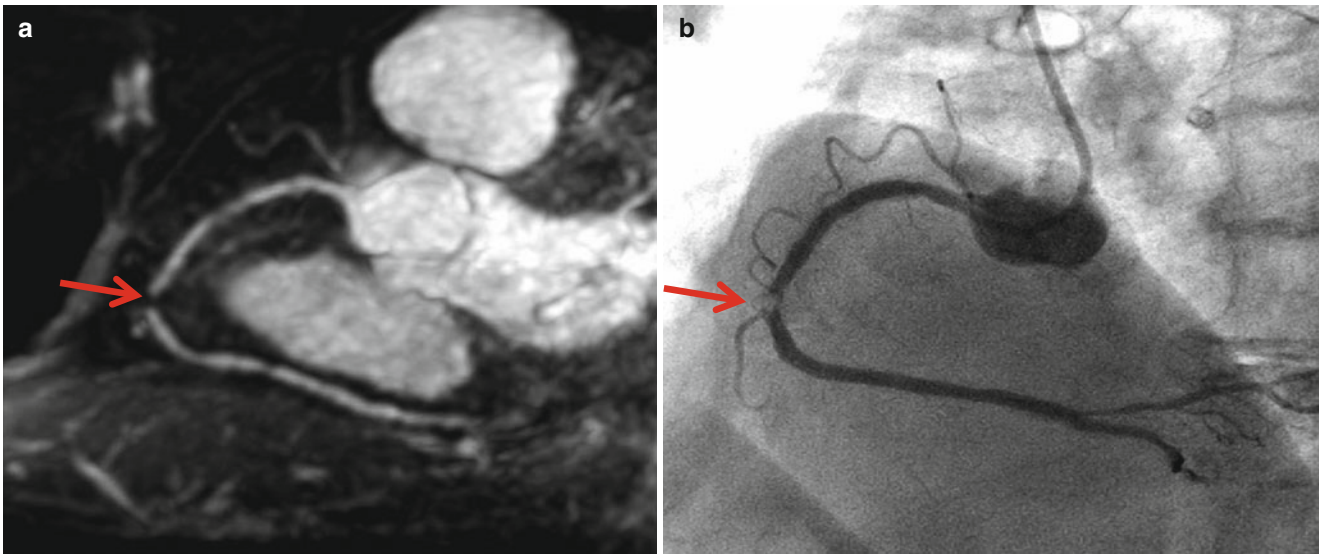

Fig. 7.5 Significant stenosis of RCA with myocardial ischemia. An 82-year-old female patient with chest pain. Non-contrast-enhanced three-dimensional coronary MR angiography images were acquired with a 1.5 T MR imager by using a steady-state free precession (SSFP) sequence, navigator echo gating, T2 preparation, spectral presaturation inversion-recovery fat saturation (repetition time/echo time, 4.6/2.3 ms; flip angle, 90°; sensitivity encoding [SENSE] factor, four; field of view, 280×280×120 mm; acquisition matrices, 256×256×80; reconstruction matrices, 512×512×160). (**a**) Thin-section MIP image of whole heart coronary MR angiography showed significant stenosis of RCA (*arrow*). (**b**) Good agreement was observed between coronary MR angiography and invasive coronary angiography (*arrow*). (**c**) Short axis cine MR images at end-diastole, and (**d**) end-systole did not show significant regional wall motion abnormality. (**e**) Stress and (**f**) rest myocardial perfusion MR images revealed severe ischemia (*arrows*) in the inferior wall, which corresponded to the RCA territory. (**g**, **h**) Late gadolinium enhanced MR images did not show myocardial scar

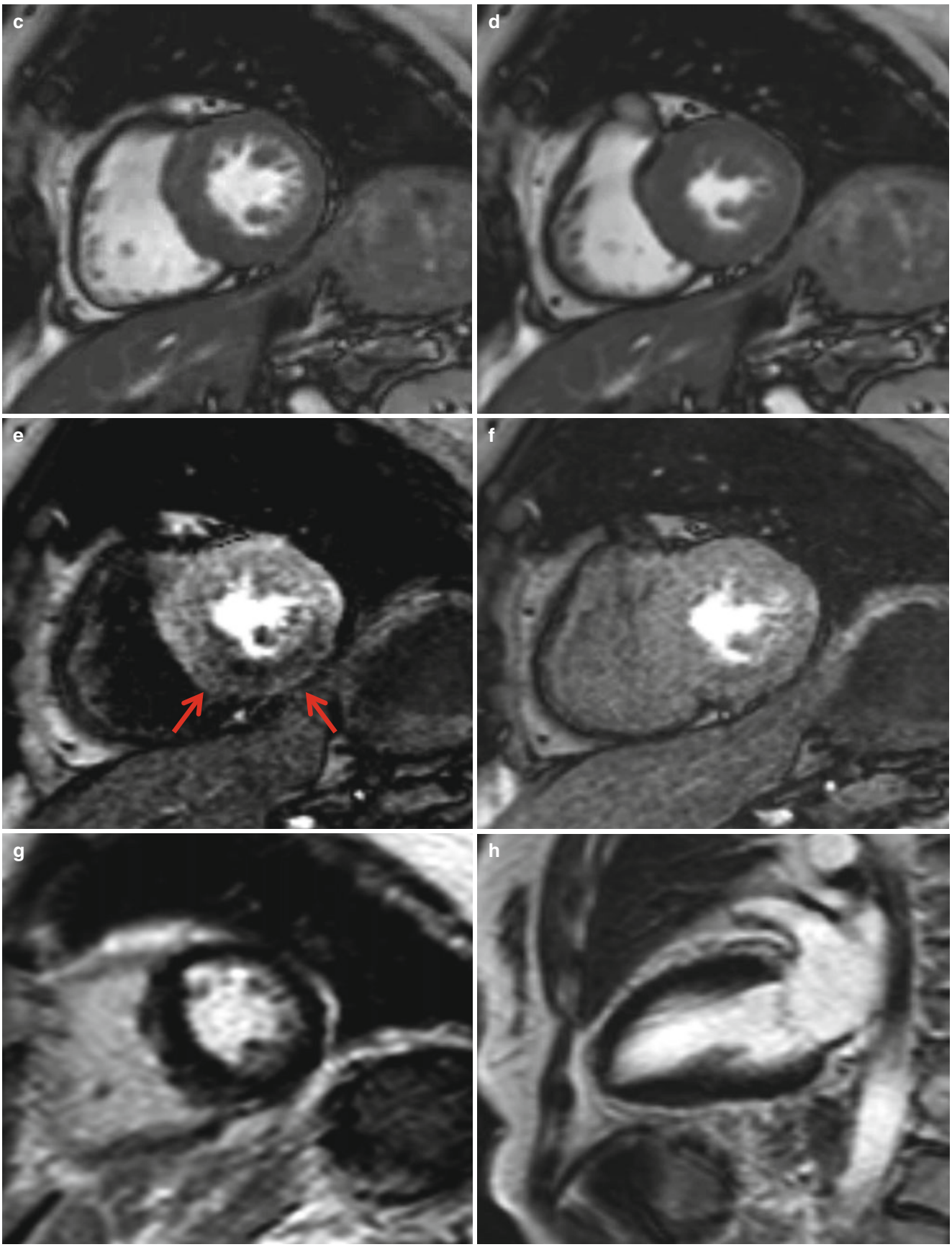

Fig. 7.5 (continued)

Learning Point
The capability to assess ventricular wall motion, myocardial ischemia, and viability is a major strength of cardiac MR imaging

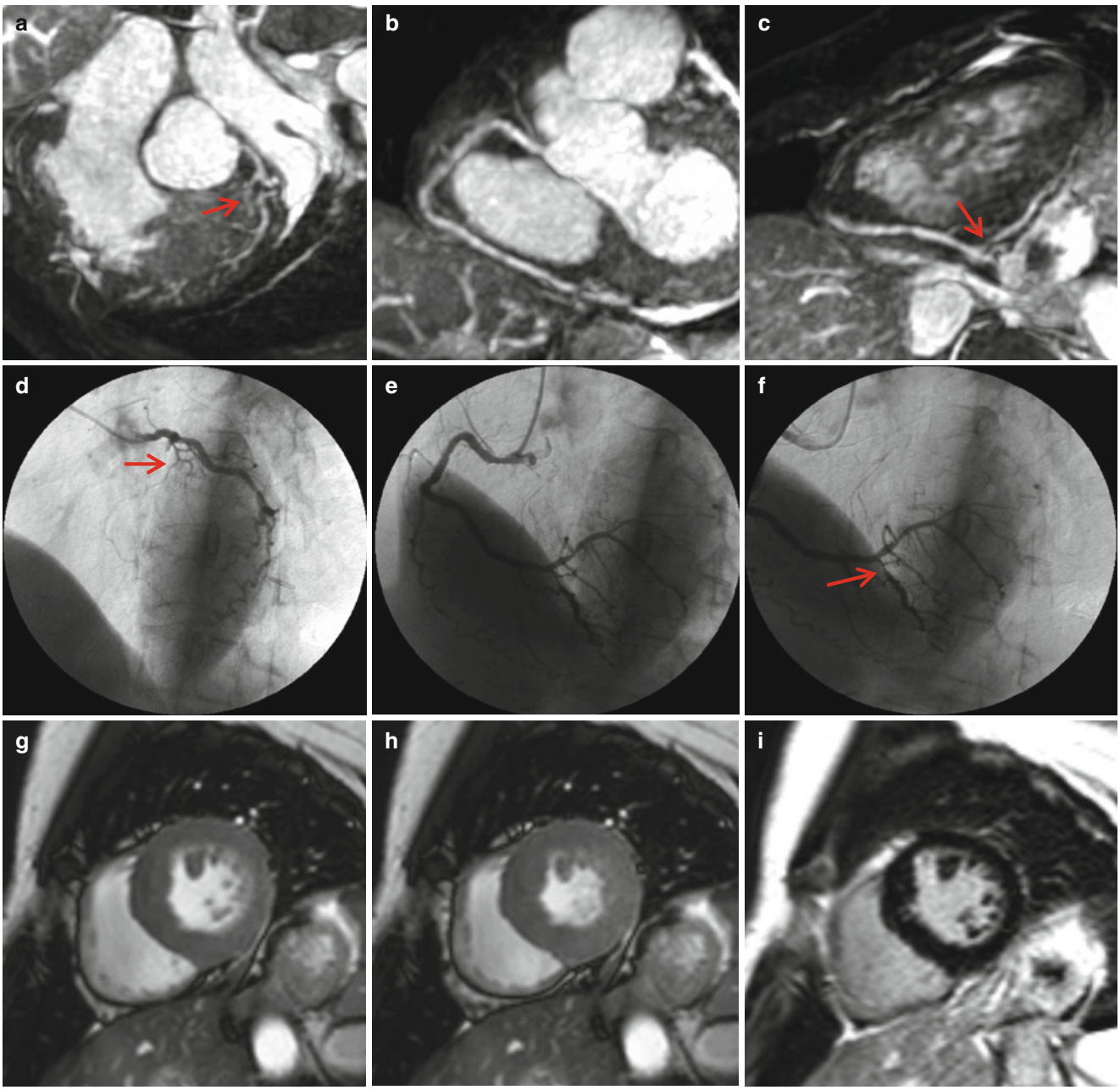

Fig. 7.6 Significant stenosis of LAD with myocardial ischemia. A 40-year-old male patient with chest pain. Non-contrast-enhanced three-dimensional coronary MR angiography images were acquired with a 1.5 T MR imager by using a steady-state free precession (SSFP) sequence, navigator echo gating, T2 preparation, spectral presaturation inversion-recovery fat saturation (repetition time/echo time, 4.6/2.3 ms; flip angle, 90°; sensitivity encoding [SENSE] factor, four; field of view, 280×280×120 mm; acquisition matrices, 256×256×80; reconstruction matrices, 512×512×160). (**a**) Thin-section MIP image of whole heart coronary MR angiography showed severe stenosis or occlusion of proximal LAD (*arrows*). (**b**, **c**) There is also significant stenosis at posterior descending artery (PDA). (**d–f**) Good agreement was observed between coronary MR angiography and invasive coronary angiography (*arrows*). (**g**) Short axis cine MR images at end-diastole, and (**h**) end-systole did not show significant regional wall motion abnormality. (**i**) Late gadolinium enhanced MR images did not show myocardial scar. (**j–l**) Stress and perfusion MR images revealed severe ischemia (*arrows*) in the anteroseptal wall, which corresponded to the LAD territory

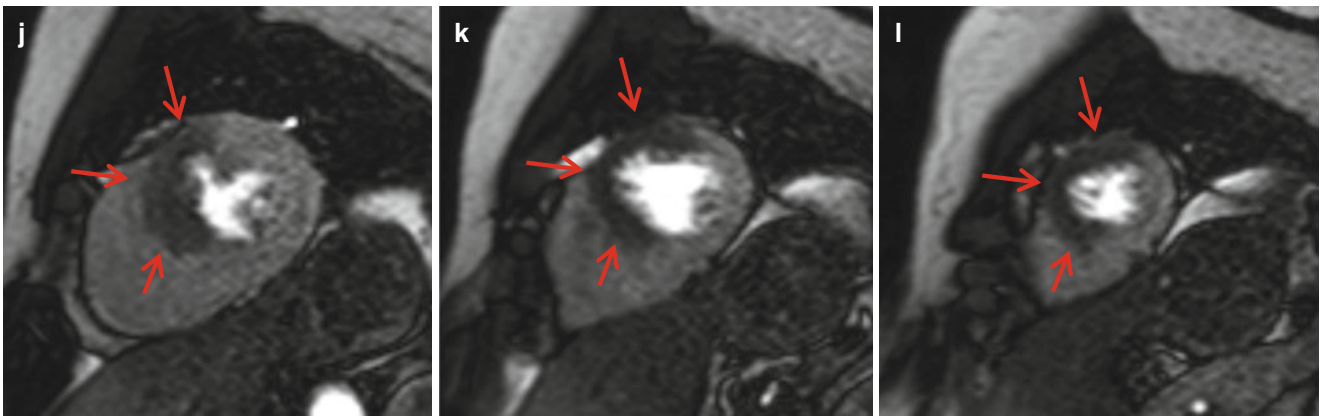

Fig. 7.6 (continued)

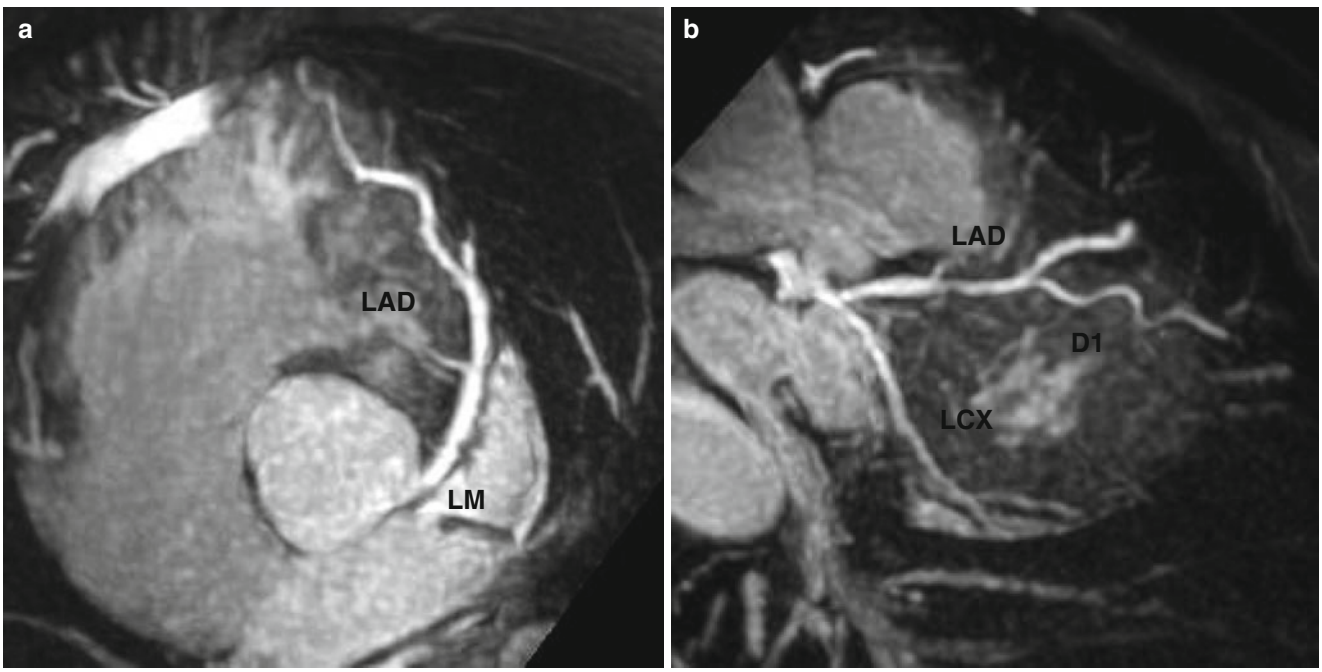

Fig. 7.7 Contrast-enhanced 3.0-T whole-heart coronary MR angiography in a subject with normal coronary artery. Gradient-echo 3D MR angiographic images were acquired by using fat saturation pulse in the equilibrium phase after administration of 0.15 mmol/kg of gadopentetate dimeglumine (Magnevist; Schering, Berlin, Germany) (repetition time/echo time, 4.2/2.1 ms; flip angle, 20°; SENSE factor, four; field of view, 280×280×120 mm; acquisition matrices, 256×256×80; reconstruction matrices, 512×512×160). (**a**) Thin-section MIP image of left main coronary artery (*LM*) and LAD. (**b**) Thin-section MIP image of LAD, first diagonal branch (*D1*). (**c**) Thin-section MIP image of RCA. (**d**) Thin-section MIP image of distal RCA and posterior descending artery (*PDA*) and posterolateral branch (*PL*)

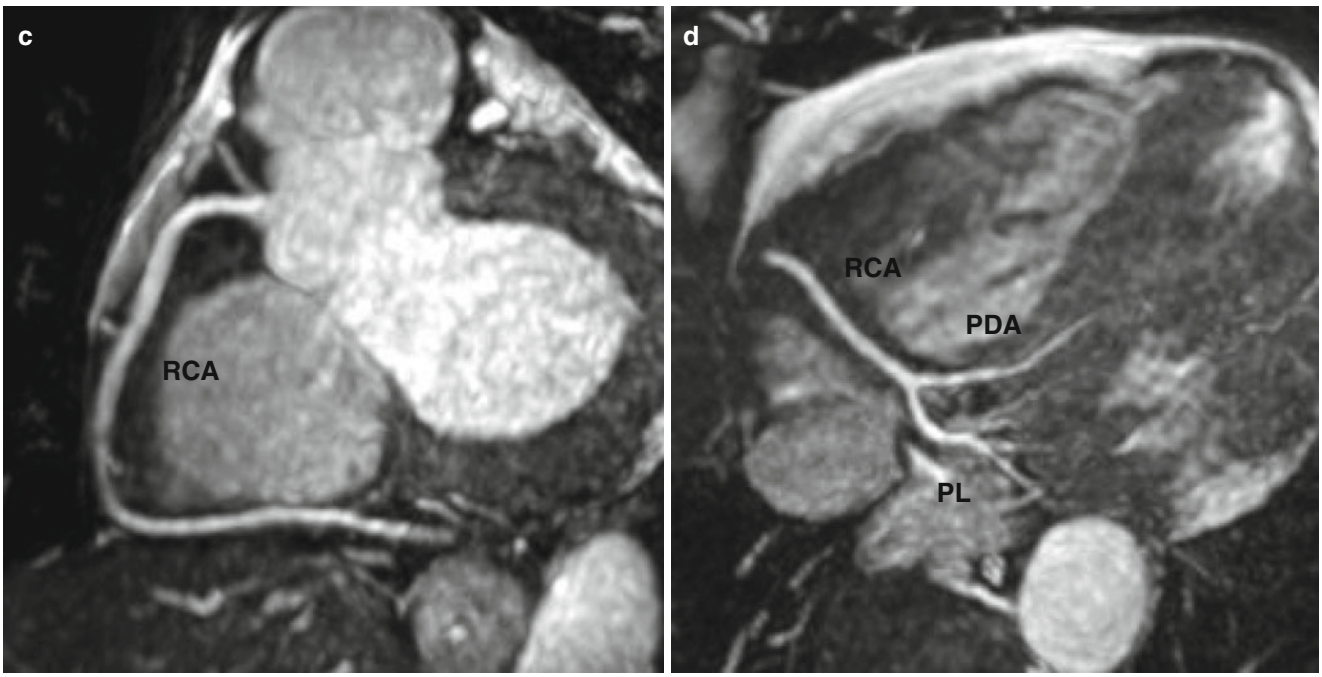

Fig. 7.7 (continued)

Learning Point
3 T system provide better signal and contrast values relative to 1.5 T system, thus may improve the detection of coronary artery disease with coronary MR angiography.

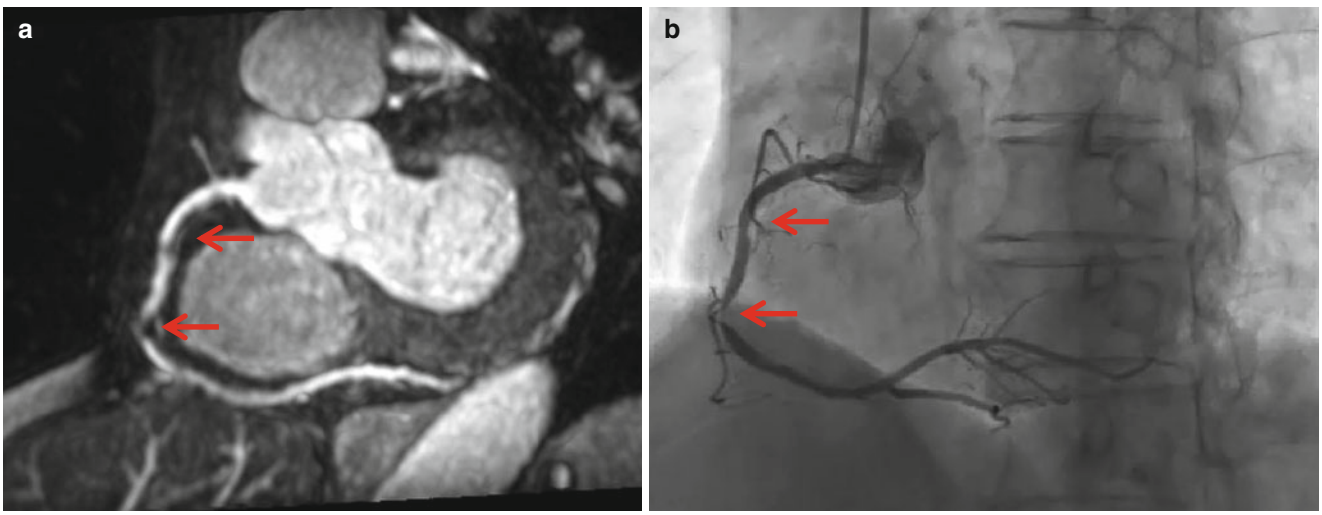

Fig. 7.8 Significant stenosis of RCA with myocardial ischemia. A 69-year-old female patient with chest pain. Gradient-echo 3D MR angiographic images were acquired by using fat saturation pulse in the equilibrium phase after administration of 0.15 mmol/kg of gadopentetate dimeglumine (Magnevist; Schering, Berlin, Germany) (repetition time/echo time, 4.2/2.1 ms; flip angle, 20°; SENSE factor, four; field of view, 280×280×120 mm; acquisition matrices, 256×256×80; reconstruction matrices, 512×512×160). (**a**) Thin-section MIP image of whole heart coronary MR angiography showed significant stenosis of RCA (*arrows*). (**b**) Good agreement was observed between coronary MR angiography and invasive coronary angiography (*arrows*). (**c**) Short axis cine MR images at end-diastole, and (**d**) end-systole did not show significant regional wall motion abnormality. (**e**) Stress myocardial perfusion MR images revealed ischemia in the inferior wall (*arrows*), which corresponded to the RCA territory. (**f**) Late gadolinium enhanced MR images did not show myocardial scar

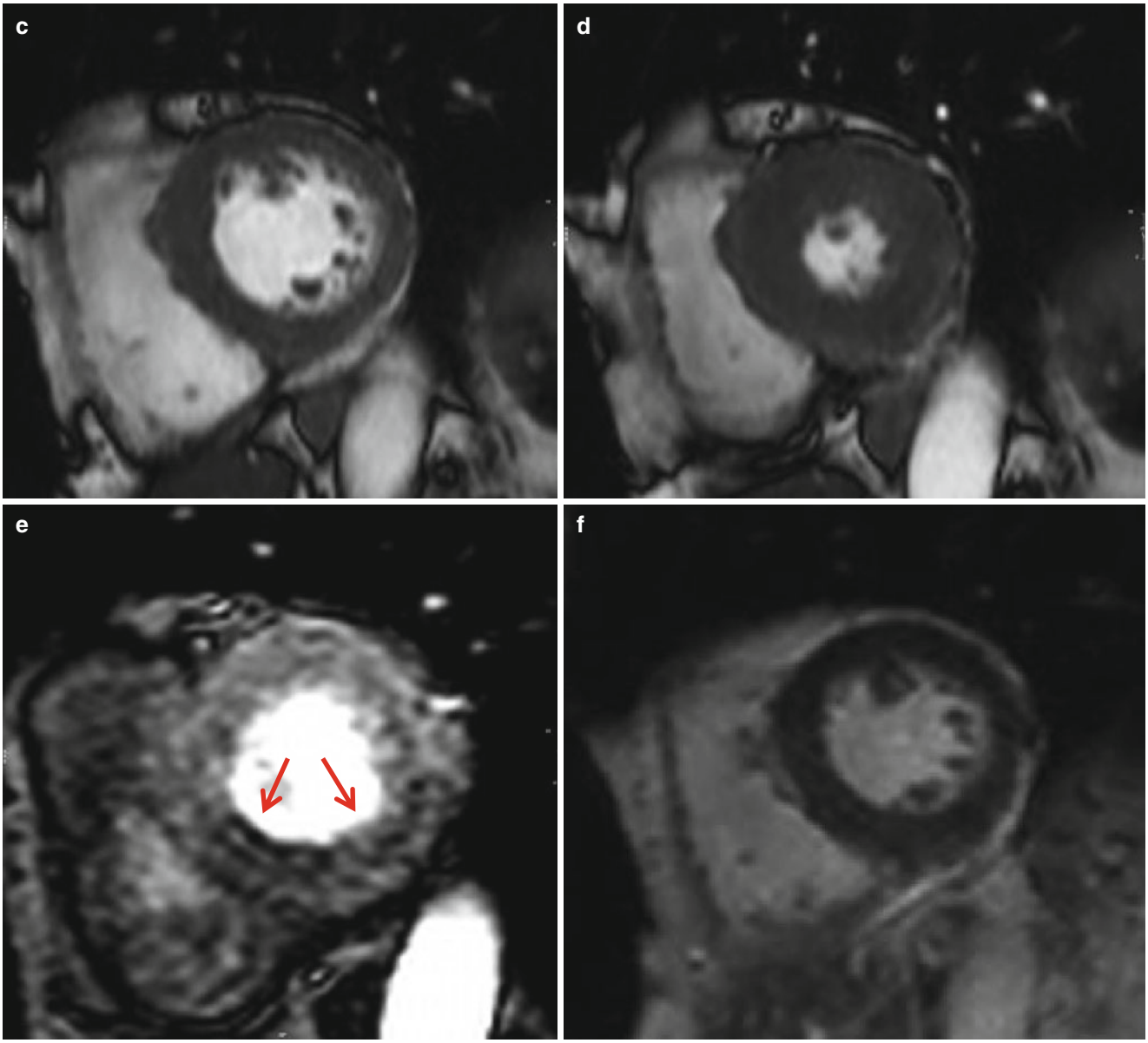

Fig. 7.8 (continued)

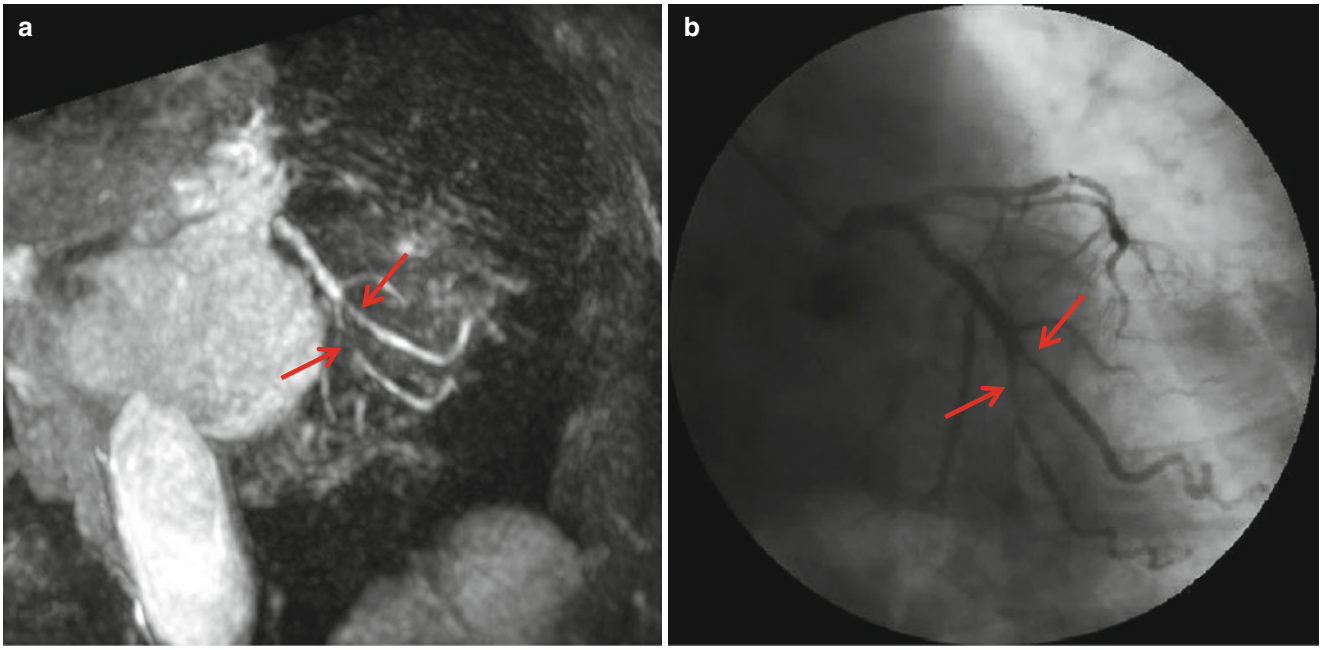

Fig. 7.9 Significant stenosis of LCX with myocardial ischemia. A 78-year-old female patient with chest pain. Gradient-echo 3D MR angiographic images were acquired by using fat saturation pulse in the equilibrium phase after administration of 0.15 mmol/kg of gadopentetate dimeglumine (Magnevist; Schering, Berlin, Germany) (repetition time/echo time, 4.2/2.1 ms; flip angle, 20°; SENSE factor, four; field of view, 280×280×120 mm; acquisition matrices, 256×256×80; reconstruction matrices, 512×512×160). (**a**) Thin-section MIP image of whole heart coronary MR angiography showed significant stenosis of LCX (*arrows*). (**b**) Good agreement was observed between coronary MR angiography and invasive coronary angiography (*arrows*)

7.4 Summary

- Free-breathing 3-dimensional (3D) whole-heart CMRA can provide visualization of all major coronary arteries with a single axial 3D acquisition.
- Whole-heart CMRA has been shown to be useful for the detection of significant coronary artery disease (CAD).
- The combination of CMRA with cine MR imaging, stress perfusion MR imaging, and late gadolinium-enhanced MR imaging provides a comprehensive assessment of CAD.

Acknowledgments We thank Tatsuro Ito, MD, for his support in writing this textbook.

Imaging of Coronary Revascularization: Stent and CABG

8

Dong Hyun Yang and Byoung Wook Choi

Contents

D.H. Yang
Department of Radiology and Research Institute of Radiology, Asan Medical Center, University of Ulsan College of Medicine, Seoul, Republic of Korea
e-mail: donghyun.yang@gmail.com

B.W. Choi (✉)
Department of Radiology, Research Institute of Radiological Science, Severance Hospital, Yonsei University College of Medicine, Seoul, Republic of Korea
e-mail: bchoi@yuhs.ac

Abstract

Percutaneous coronary intervention (PCI) using coronary stent and coronary artery bypass graft (CABG) have been established as mainstay myocardial revascularization therapy in patients with coronary artery disease. Coronary CTA allow for reliable evaluation of coronary stent and bypassed graft. In this chapter, clinical background of both procedures, technical tips to obtain good CT image of coronary stent, and CT imaging findings of in-stent restenosis and bypass graft occlusion will be highlighted. In addition, mechanical deformity of stent and postoperative complication of the bypass graft will be discussed.

8.1 Introduction

8.1.1 Indication of Myocardial Revascularization Therapy

- Myocardial revascularization therapy has been established as a mainstay treatment of coronary artery disease (CAD) for over three decades.
- For the treatment of acute myocardial infarction with ST-segment elevation, primary coronary intervention (PCI) is considered superior to fibrinolysis [1].
- In patients with stable CAD, treatment by optimal medical therapy (OMT) only or combined with revascularization using PCI or CABG could be chosen. The treatment strategy depends on patient's symptom and anatomical complexity of CAD.
- Based on the current evidences, revascularization therapy in patients with stable CAD can be appropriate in clinical situations as follows [2] (Table 8.1):
  - Patients with persistent limiting symptoms (angina or angina equivalent) despite OMT for symptomatic benefit.

T.-H. Lim (ed.), *Practical Textbook of Cardiac CT and MRI*,
DOI 10.1007/978-3-642-36397-9_8,

Table 8.1 Indications for revascularization therapy in stable CAD patients

	Subset of CAD by anatomy	Class[a]
For prognosis	Left main >50 %[b]	I
	Any proximal LAD stenosis >50 %[b]	I
	2VD or 3VD with impaired LV function[b]	I
	Proven large area of ischemia (>10 % of LV)	I
	Single remaining patent vessel >50 % stenosis[b]	I
	1VD without proximal LAD and without >10 % ischemia	III
For symptoms	Any stenosis >50 % with limiting angina or angina equivalent, unresponsive to OMT	I
	Dyspnea/CHD and >10 % LV ischemia/viability supplied by >50 % stenotic artery	IIa
	No limiting symptoms with OMT	III

Modified from the ESC/EACTS guidelines 2010 [2]
CHD chronic heart failure, *LAD* left anterior descending, *LV* left ventricle, *OMT* optimal medical therapy, *VD* vessel disease
[a]Classes of recommendations
Class I: evidence that a given treatment is beneficial, useful, and effective
Class IIa: weight of evidence is in favor of usefulness
Class IIb: usefulness of treatment is less well established by evidence
Class III: evidence that the given treatment is not useful/effective, and in some cases may be harmful
[b]With documented ischemia or FFR <0.80 for angiographic diameter stenosis 50–90 %

Table 8.2 Indications for CABG versus PCI in stable CAD patients

	Favors CABG	Favors PCI
Subset of CAD by anatomy	Class[a]	Class[a]
1VD or 2VD – non-proximal LAD	IIb	I
1VD or 2VD – proximal LAD	I	IIa
3VD simple lesions, full-functional revascularization achievable with PCI, SYNTAX score ≤22	I	IIa
3VD complex lesions, incomplete revascularization achievable with PCI, SYNTAX score >22	I	III
Left main (isolated or 1VD, ostium/shaft)	I	IIa
Left main (isolated or 1VD, distal bifurcation)	I	IIb
Left main + 2VD or 3VD, SYNTAX score ≤32	I	IIb
Left main + 2VD or 3VD, SYNTAX score >32	I	III

Modified from the ESC/EACTS guidelines 2010 [2]
VD vessel disease, *LAD* left anterior descending
[a]Same with class of recommendations in Table 8.1

– Certain anatomical patterns of disease (Table 8.1) or a proven significant ischemic territory even in asymptomatic patients for prognostic benefit. Significant LM stenosis and significant proximal LAD disease, especially in the presence of multivessel CAD, are strong indications for revascularization.

8.1.2 Indication for CABG Versus PCI in Stable CAD

- CABG appears to be better in terms of survival benefit as well as reduction of revascularization in patients with high risk of CAD; multivessel disease with complex morphology and left main disease (Table 8.2) [2].

8.2 Coronary Stent

8.2.1 Clinical Background

- Coronary stents, which was developed in the mid-1980s, have been preferred method of performing PCI and replaced plain balloon angioplasty [3].
- Drug-eluting stents (DES) are highly efficacious at reducing the risk of target-vessel revascularization without an increase in any safety outcomes, including stent thrombosis [4].
- In contemporary PCI practice, newer-generation DES with novel coating and biodegradable stents are widely used.
- Newer-generation DES have thinner stent struts for improvement of stent deliverability and more biocompatible polymers coating for reduction of in-stent restenosis (Fig. 8.1) (Table 8.3).

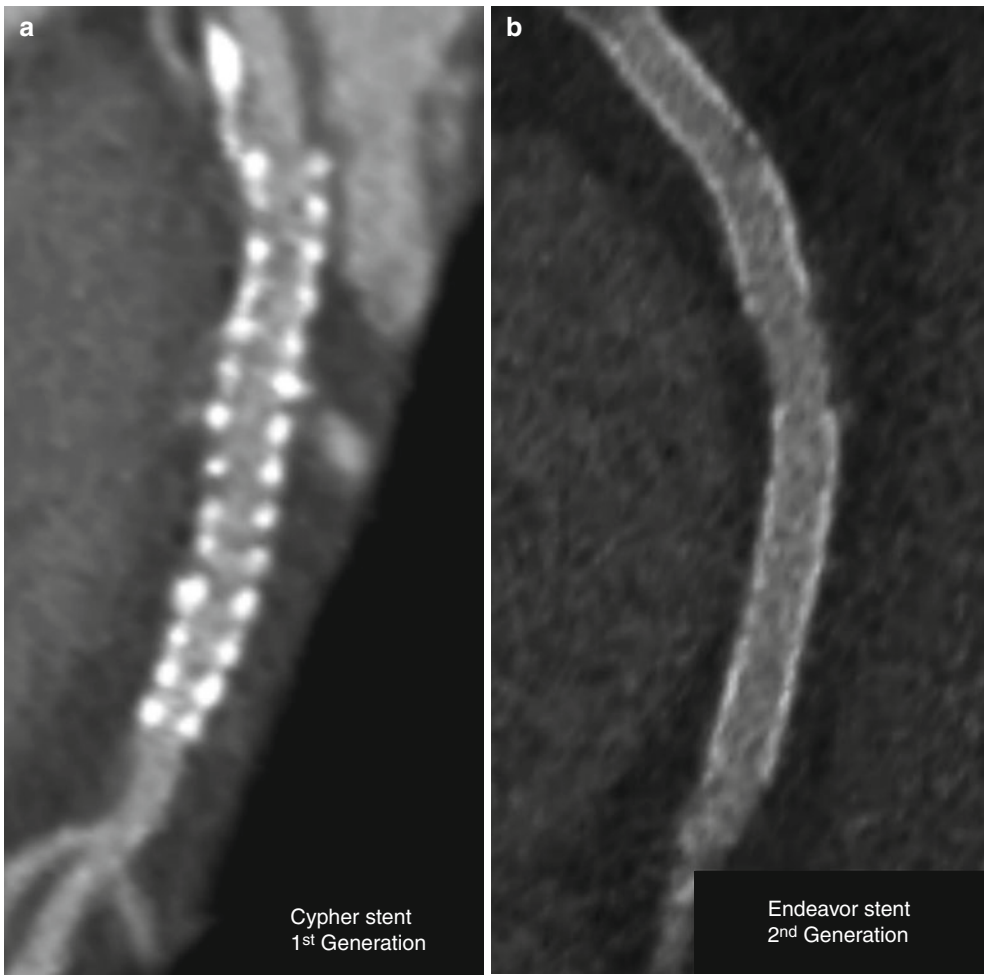

Fig. 8.1 First-generation (**a**) and second-generation DES on CT image. (**a**) Curved planar CT image of sirolimus-eluting stent (Cypher) shows relative thick strut. (**b**) Curved planar CT image of zotarolimus-eluting stent (Endeavor) shows thin strut

Table 8.3 First- and second-generation DES

Stent name	Drug	Metal	Polymer thickness (μm)	Strut thickness (μm)
Cypher	Sirolimus	Stainless steel	12.6	140
Taxus Express	Paclitaxel	Stainless steel	16.0	132
Taxus Liberte	Paclitaxel	Stainless steel	16.0	97
Endeavor	Zotarolimus	Cobalt chromium	4.1	91
Xience V	Everolimus	Cobalt chromium	7.6	81

Modified from reference [3]

8.2.2 Application of CTA for Coronary Stent Imaging

- Reduction of motion artifact and achievement of optimal contrast enhancement of CT angiography are very important for stent imaging.

- Image reconstruction and analysis tips for good quality of image.
  - Use sharp kernel reconstruction for reduction of blooming artifact (Fig. 8.2).
  - Use wide window of ≥700 HU with a center of about 200 HU for an acceptable trade-off between blooming and visibility of the stent lumen.
  - Use reconstruction mode of high spatial resolution, if available (Fig. 8.3).
  - Correct centerline of curved planar image carefully (Fig. 8.4).
  - Thick-slab maximal intensity projection (MIP) image may be helpful for delineation of a mechanical deformity (e.g., fracture) of the stent (Fig. 8.5).
  - Generate cross-sectional image of the stent to evaluate in-stent restenosis (Fig. 8.6).

- Application of CTA for coronary stent [5]
  - In-stent restenosis
  - Mechanical deformity including stent fracture, longitudinal compression, and inadequate expansion
  - Edge stenosis and peri-stent plaque
  - Jailed branches
  - Late stent thrombosis
  - Bifurcation stents
  - Aneurysm of the coronary artery

8.2.3 In-Stent Restenosis

- Meta-analysis of 18 studies showed that CTA was an acute noninvasive imaging modality for detection of in-stent restenosis (Figs. 8.6 and 8.7) [6].
  - Sensitivity (89 %), specificity (92 %), and accuracy (92 %) [6].
  - Evaluability of stent was increased in a stent with larger diameter, thinner struts, and non-overlapping stents.
- For the assessment of stent diameter and area, CTA showed good correlation with intravascular ultrasound in the left main coronary artery stent [7].
- Combined coronary CTA and myocardial CT perfusion improves diagnosis of CAD and in-stent restenosis in patients with stents compared with CTA alone [8].

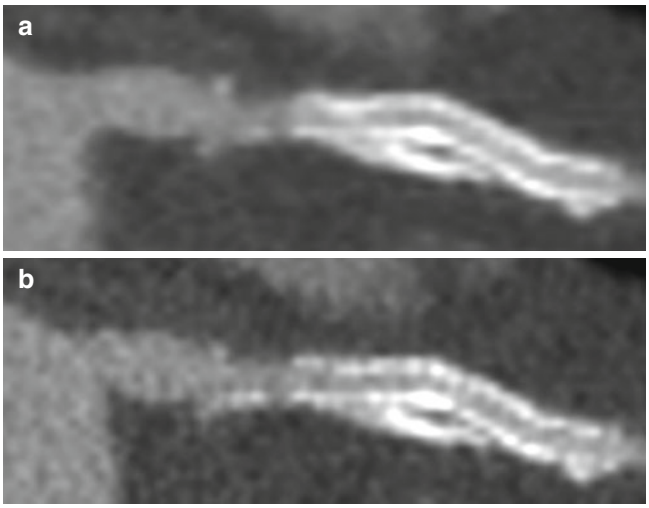

Fig. 8.3 Effect of high spatial resolution mode on image quality. Curved planar CT image of sirolimus-eluting stent (Cypher) with standard mode (GE, Discovery 750) (**a**) and high-definition mode (**b**). In the high-definition mode image, blooming artifact from stent strut and calcified plaque was markedly reduced as compared with that of standard mode

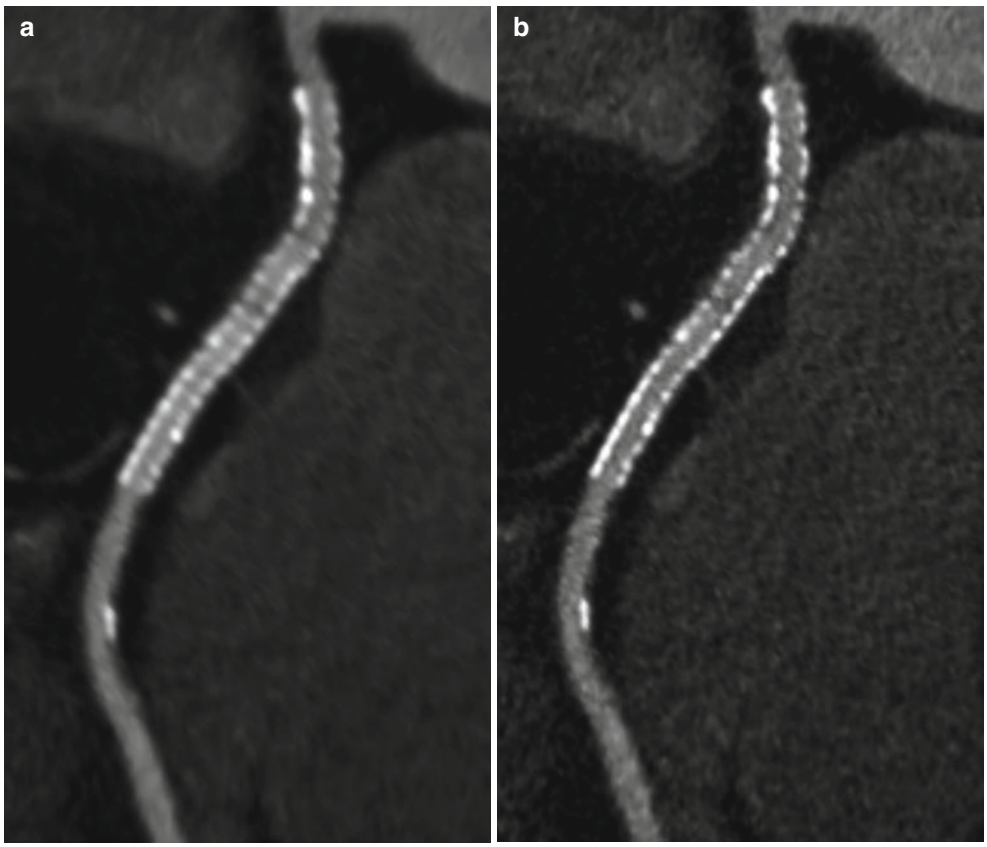

Fig. 8.2 Effect of image reconstruction kernel on image quality. Curved planar CT image of sirolimus-eluting stent (Cypher) with soft reconstruction kernel (B26; Siemens, Definition FLASH CT) (**a**) and sharp reconstruction kernel (B46) (**b**). In the sharp kernel image, blooming artifact from stent strut was markedly reduced as compared with that of soft kernel image

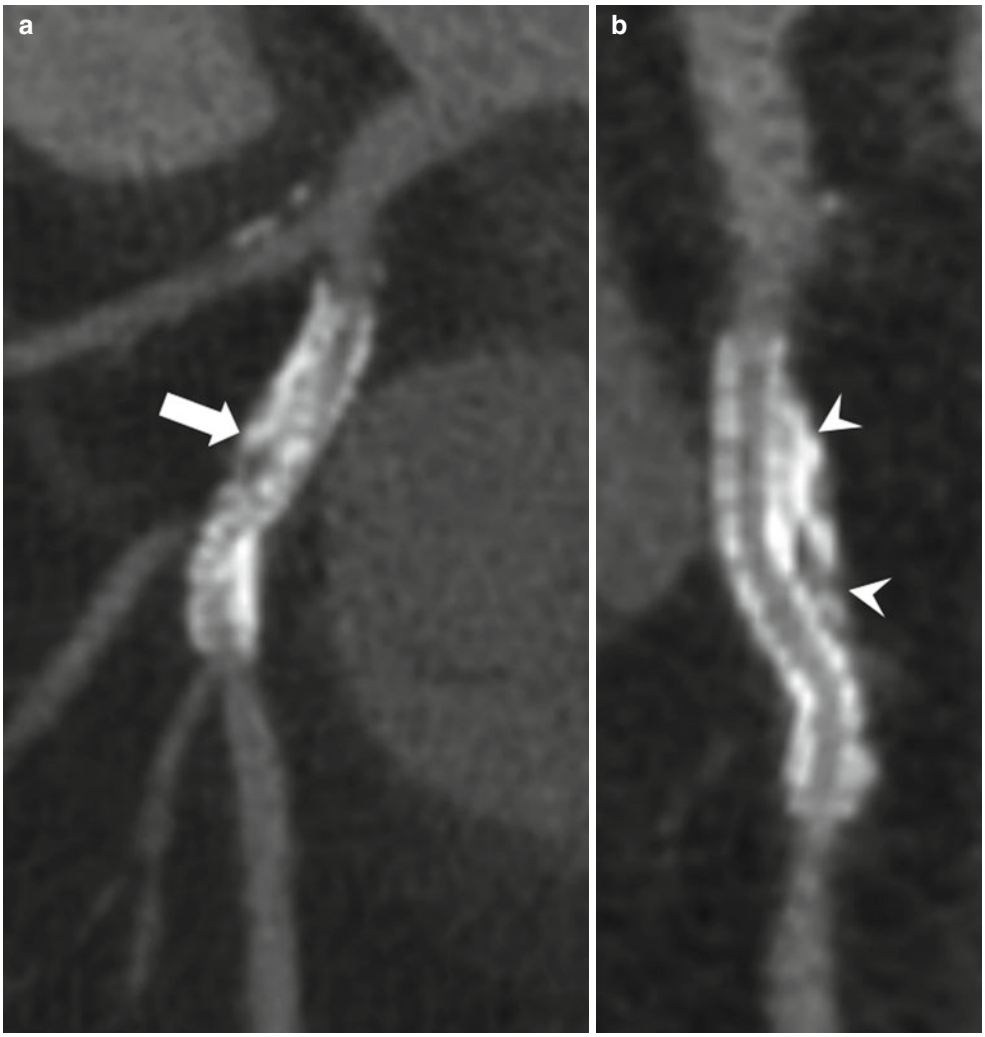

Fig. 8.4 Importance of correct centerline on curved planar image. (**a**) Curved planar CT image of sirolimus-eluting stent (Cypher) in LAD shows high-density area (*arrow*) in the lumen of the stent. Patency of the stent lumen was not delineated in this image because of incorrect centerline. (**b**) After careful correction of the centerline, the lumen of the stent was demonstrated clearly. Note massive calcified plaque burden (arrowheads) outside of the stent. This calcified plaque may cause a pseudolesion in a curved planar image (**a**) which was generated using incorrect centerline

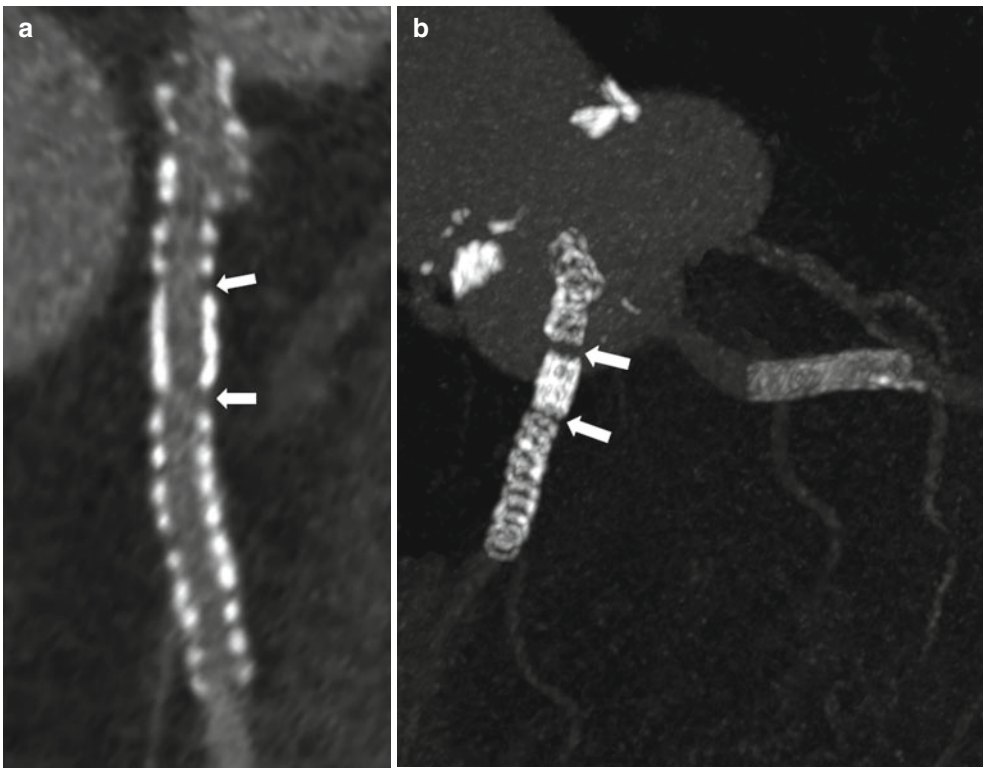

Fig. 8.5 Usefulness of thick-slab MIP image for diagnosis of mechanical deformity of stent. (**a**) Curved planar CT image of sirolimus-eluting stent (Cypher) shows fractures (*arrows*) in the midportion of the stent. Lumen of the stent was patent. (**b**) On the thick-slab MIP image, stent fracture was delineated more clearly (*arrows*)

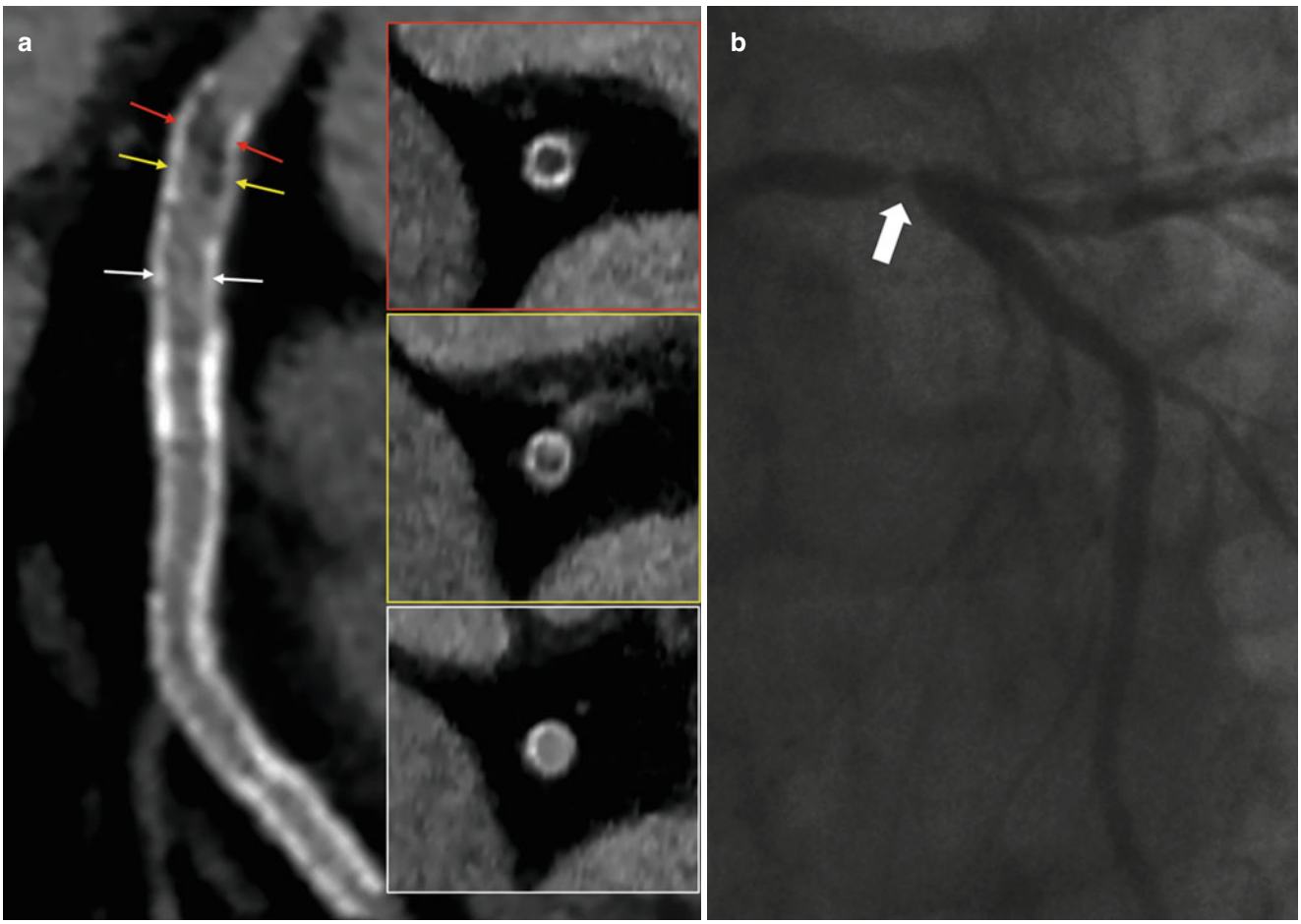

Fig. 8.6 Usefulness of cross-sectional image for diagnosis of in-stent restenosis. (**a**) Curved planar CT image and cross-sectional images (*in box*) of zotarolimus-eluting stent (Resolute Integrity) show significant in-stent restenosis in the proximal portion of the stent. On cross-sectional image, degree of in-stent stenosis was clearly delineated (approximately 50 % of stenosis in *yellow box*, near total occlusion in *red box*, no in-stent restenosis in *white box*). The red, white and yellow arrows indicate the level of the cross sectional images in each colored boxes. (**b**) Invasive coronary angiography shows tight stenosis in the proximal portion of the stent (*arrow*)

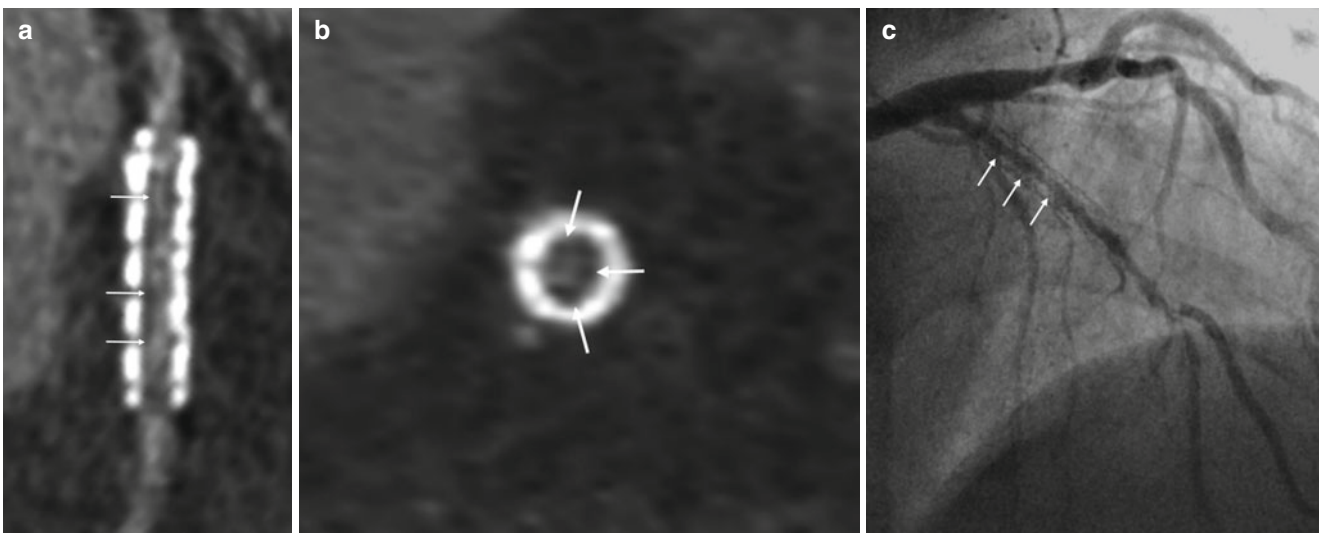

Fig. 8.7 In-stent restenosis in bare-metal stent (BMS). (**a**, **b**) Curved planar (**a**) and cross-sectional (**b**) CT image of bare-metal stent in LAD shows diffuse in-stent restenosis along stent inner wall (*arrows*). (**c**) Invasive coronary angiography confirmed diffuse in-stent restenosis (*arrows*) in proximal LAD. *LAD* left anterior descending

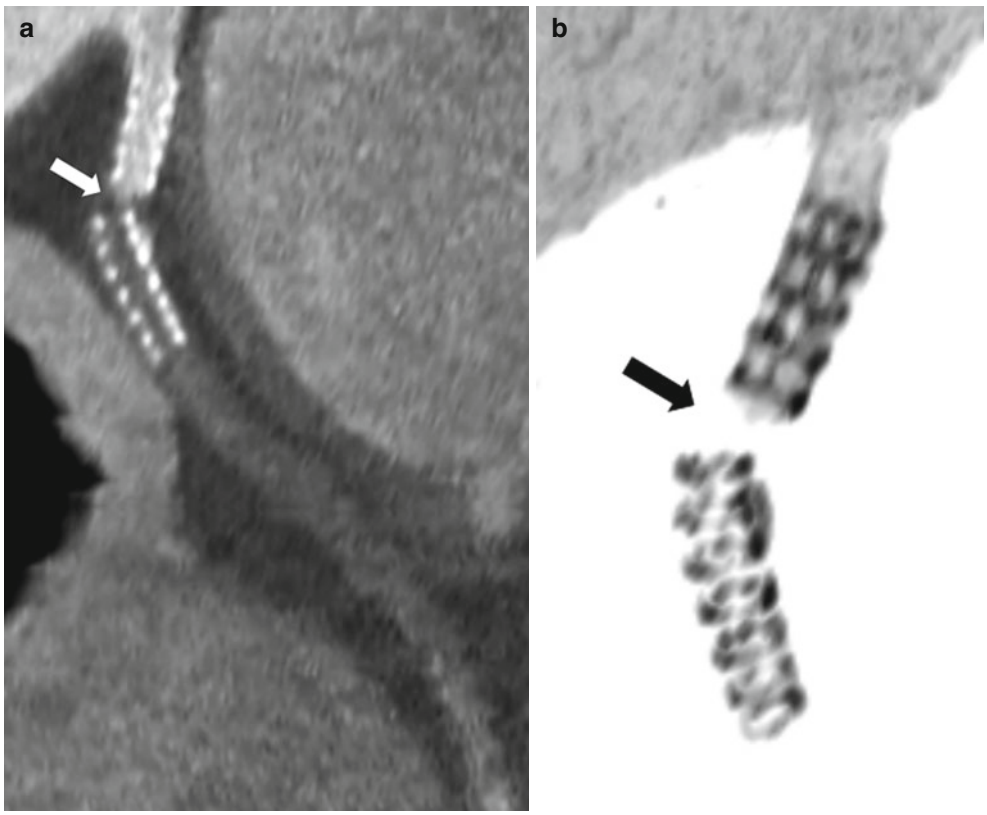

Fig. 8.8 Stent fracture with total occlusion in DES. (**a**) Curved planar CT image of DES (Cypher) in proximal LAD shows severe stent fracture with total separation of distal portion (*arrow*). From the fracture site, the coronary lumen was totally occluded. (**b**) Thin-slab MIP image demonstrates overall morphology of the stent fracture (*arrow*) and displacement of the stent distal portion. *LAD* left anterior descending

8.2.4 Mechanical Deformity of the Coronary Stent

- Coronary CTA can depict mechanical deformity of the coronary stent such as stent fractures and longitudinal compression (Fig. 8.8), even those findings that are not clearly depicted by conventional angiography [9, 10].
- In a pathology study, stent fracture was found in 29 % from 177 consecutive lesions. Predisposing factors of the stent fracture were sirolimus-eluting stent (Cypher), overlapped stents, long stent, and long duration of implantation. Severe type of stent fracture (total separation) was associated with in-stent restenosis or stent thrombosis at the fracture site [11].
- In an imaging study, stent fracture was found in 16.9 % by CTA but only 1 % by catheter angiography [10]. Stent fracture was associated with 25 % of in-stent restenosis, and in-stent restenosis was found in 46 % of stent fracture.

8.3 Coronary Artery Bypass Graft (CABG) Surgery

8.3.1 Clinical Background

- CABG has been used for myocardial revascularization since the 1960s. In CABG, bypass grafts are connected to the mid- or distal portion of the coronary artery, providing protection against the consequences of further proximal obstructive disease. In contrast, a purpose of PCI is restoring of the normal conductance of the native coronary artery.
- The superiority of CABG to medical therapy in the management of specific type of CAD was established [2], particularly in patients with left main or three-vessel CAD.
- CABG vs. PCI for patient outcome:
  - In patients with isolated proximal LAD artery disease, there was no significant difference in mortality, myocardial infarction, or cerebrovascular accident, but a threefold increase in recurrent angina and a fivefold increase in repeat target-vessel revascularization [2].
  - In patients with multivessel disease with complex morphology and left main disease, CABG appears to be better in terms of survival benefit as well as reduction of target-vessel revascularization (Table 8.2) [2].

8.3.2 Graft Vessels and Surgical Methods

- For the assessment of CTA in patients who underwent CABG, knowledge of coronary graft procedures and anatomy is required.
- Type of coronary bypass grafts
  - Arterial graft: the internal mammary artery, radial artery, and gastroepiploic artery

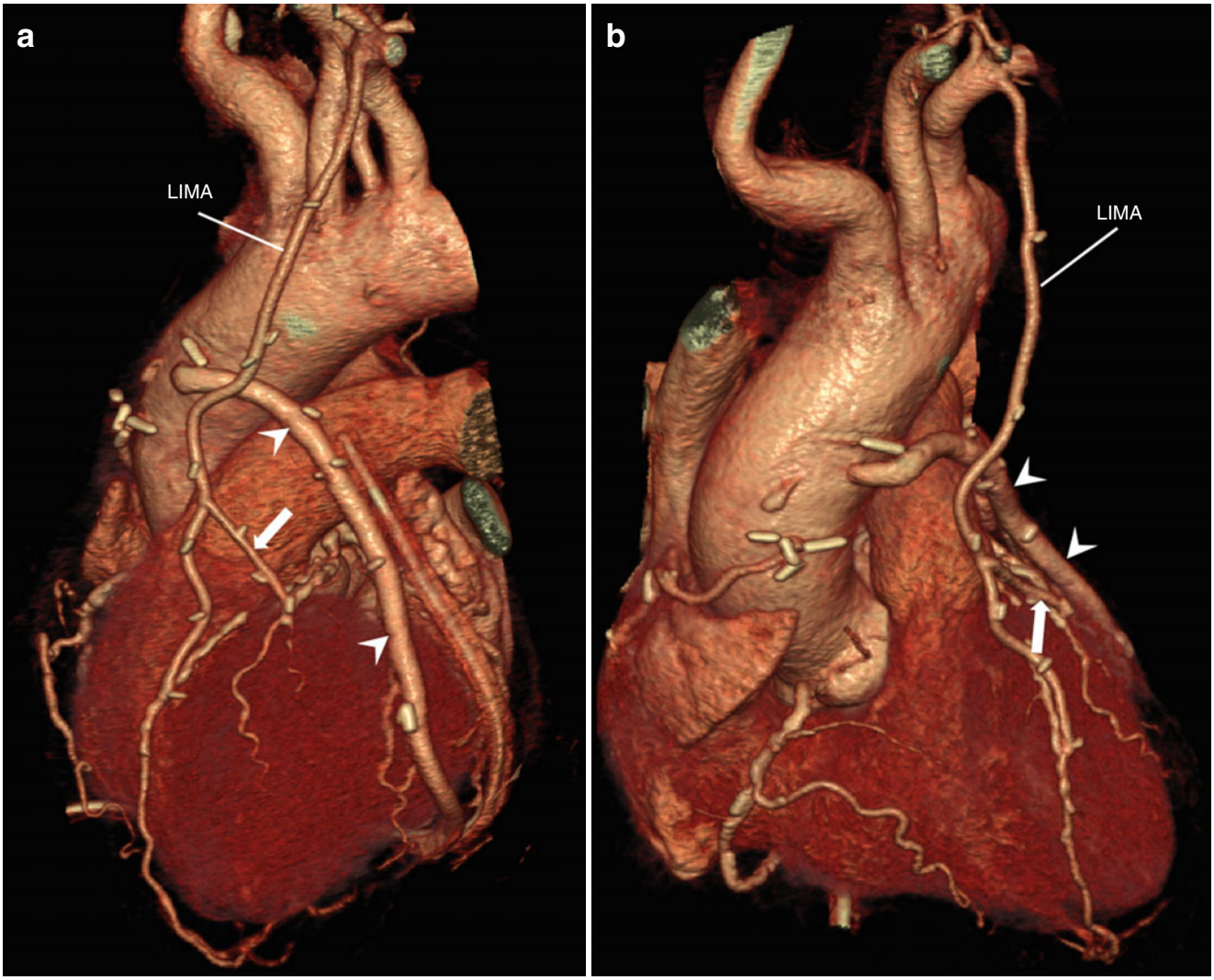

Fig. 8.9 Type of coronary bypass grafts. (**a**, **b**) Volume rendering CT images show in situ graft (left internal mammary artery, *LIMA*) to mid-portion of LAD, central arterial vessel grafting using saphenous vein (*arrowhead*) to obtuse marginal artery, and composite grafting using radial artery (*arrow*) from LIMA graft to diagonal branch. *LAD* left anterior descending

  - Non-arterial graft: the saphenous vein, cephalic vein, and prosthetic material
- Type of graft inflow (Fig. 8.9)
  - In situ grafting (anatomical flow): the internal mammary artery and gastroepiploic artery
  - Central arterial vessel grafting: graft flow from the ascending aorta, aortic arch, and supra-aortic vessel
  - Composite grafting: graft flow from the internal mammary artery or other vascular graft
- In current surgical revascularization technique, venous graft from ascending aorta is used to restore the right coronary artery circulation [12].
- Internal mammary artery graft is the most important graft for the surgical revascularization of the LAD because of its easy accessibility (Fig. 8.10), near location to the LAD, and low risk of occlusion. Ten-year patency of internal mammary graft is above 80 %.

8.3.3 Diagnosis of Graft Obstruction Using CT

- In a meta-analysis, graft assessability including distal anastomosis ranged from 78 to 100 %. CTA provided high accuracy for the evaluation of CABG obstruction in assessable conduits (Figs. 8.11, 8.12, and 8.13). Pooled sensitivity and specificity for diagnosis of conduit stenosis were 94.4 and 98.0 %, respectively [13].
- CTA provides incremental anatomical data to help determine the prognosis of patients after CABG. Coronary artery protection score calculated using CTA were predictive of clinical outcomes [14].
- Pitfall and limitation of post-CABG CT:
  - Flow competition vs. graft spasm vs. graft occlusion
  - Vascular clips around anastomosis site or graft vessel
  - Extensive calcification in the native coronary artery

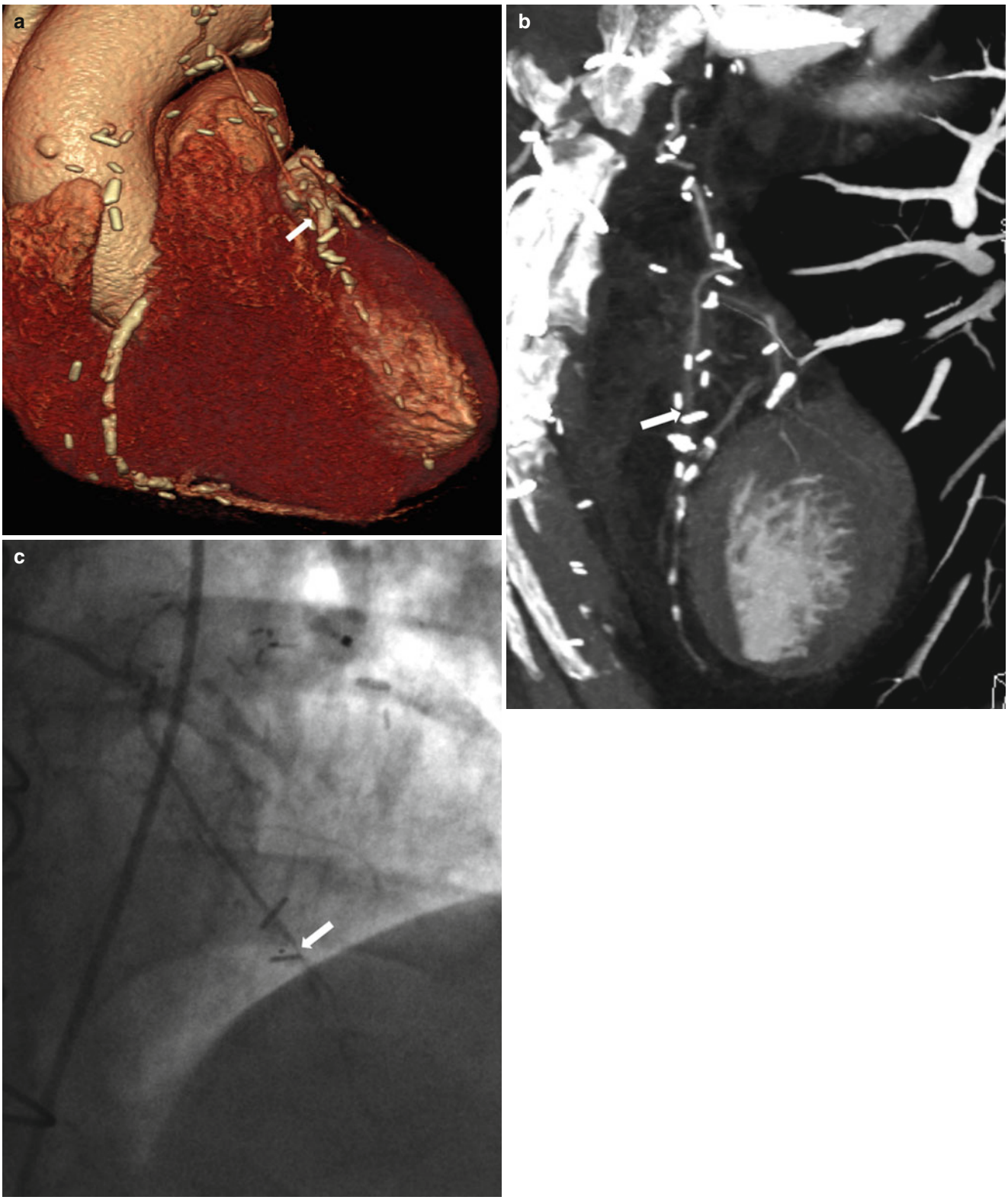

Fig. 8.10 Severe stenosis in LIMA graft. (**a**) Volume rendering and (**b**) maximal intensity projection CT images demonstrated severe stenosis (*arrows*) in the distal portion of the LIMA graft and anastomosis site. Anastomosis site between LIMA graft and LAD was poorly opacified. (**c**) Invasive angiography showed diffuse and severe stenosis (*arrow*) in the distal portion of the LIMA graft. *LAD* left anterior descending

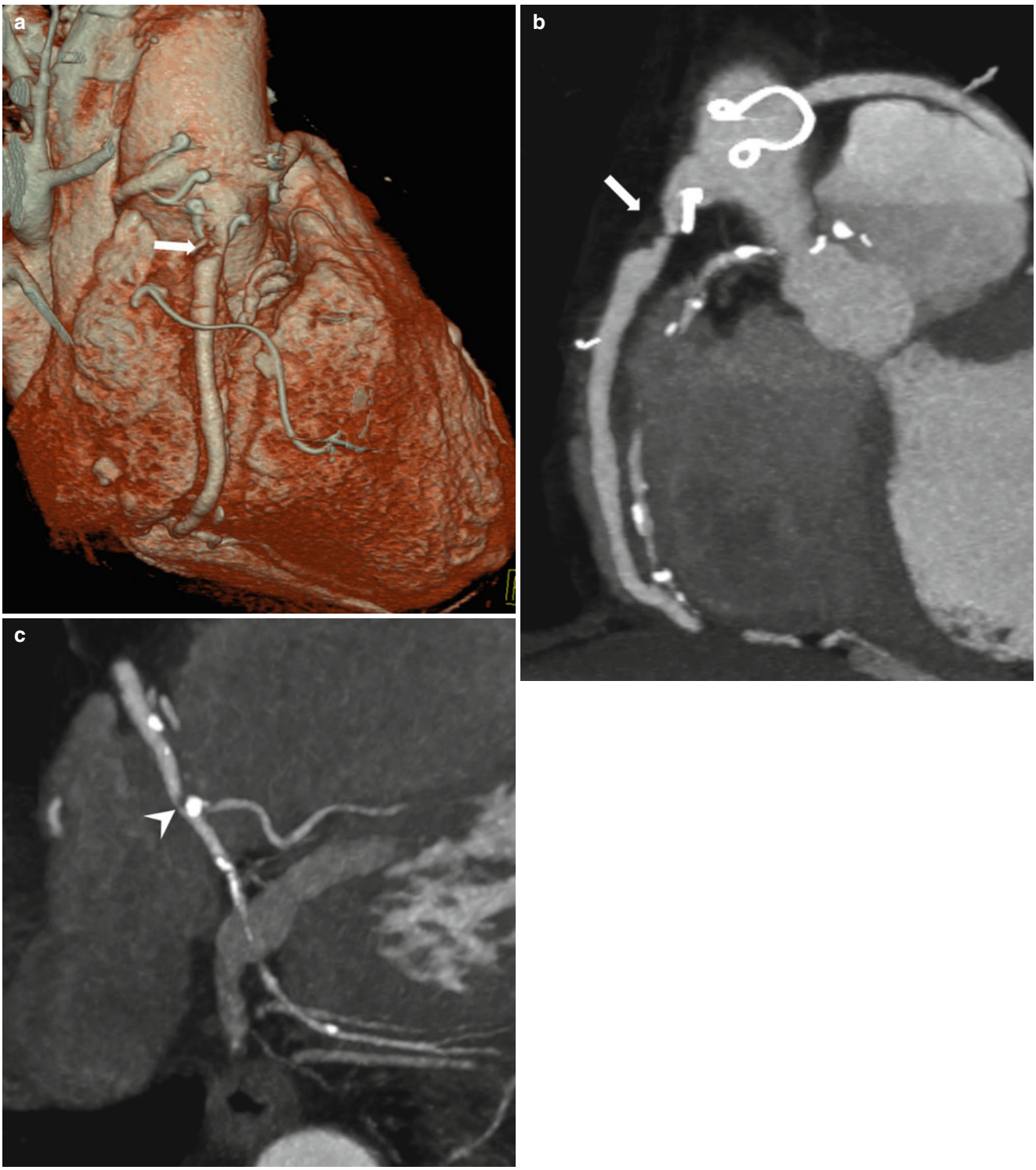

Fig. 8.11 Severe stenosis in free saphenous vein graft involving both proximal and distal portion of the graft. (**a**) Volume rendering and (**b**) oblique coronal CT images demonstrated severe stenosis (*arrows*) in the proximal portion of the saphenous vein graft from the ascending aorta to the posterior descending artery. (**c**) Oblique axial CT image shows severe stenosis in the anastomosis site (*arrowhead*) between saphenous vein graft and posterior descending artery

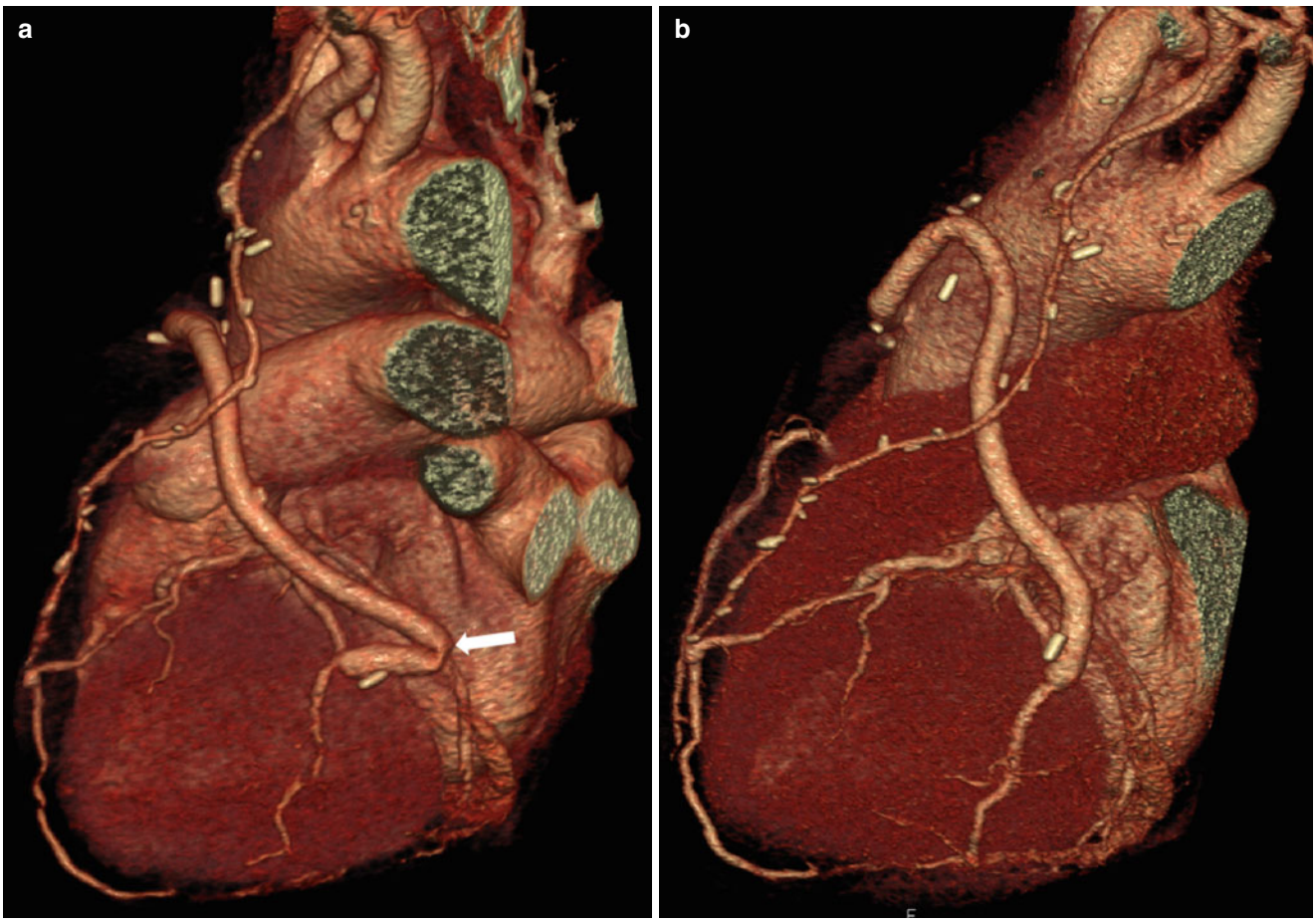

Fig. 8.12 Kinking of the saphenous vein graft. (**a**) Volume rendering CT image obtained at three days after bypass surgery showed kinking of the saphenous vein graft (*arrow*) to the obtuse marginal artery. On surgical exploration, hematoma and adhesion were observed around the saphenous vein graft. (**b**) After relieving of the graft kinking, volume rendering CT image demonstrates restoration of the graft geometry

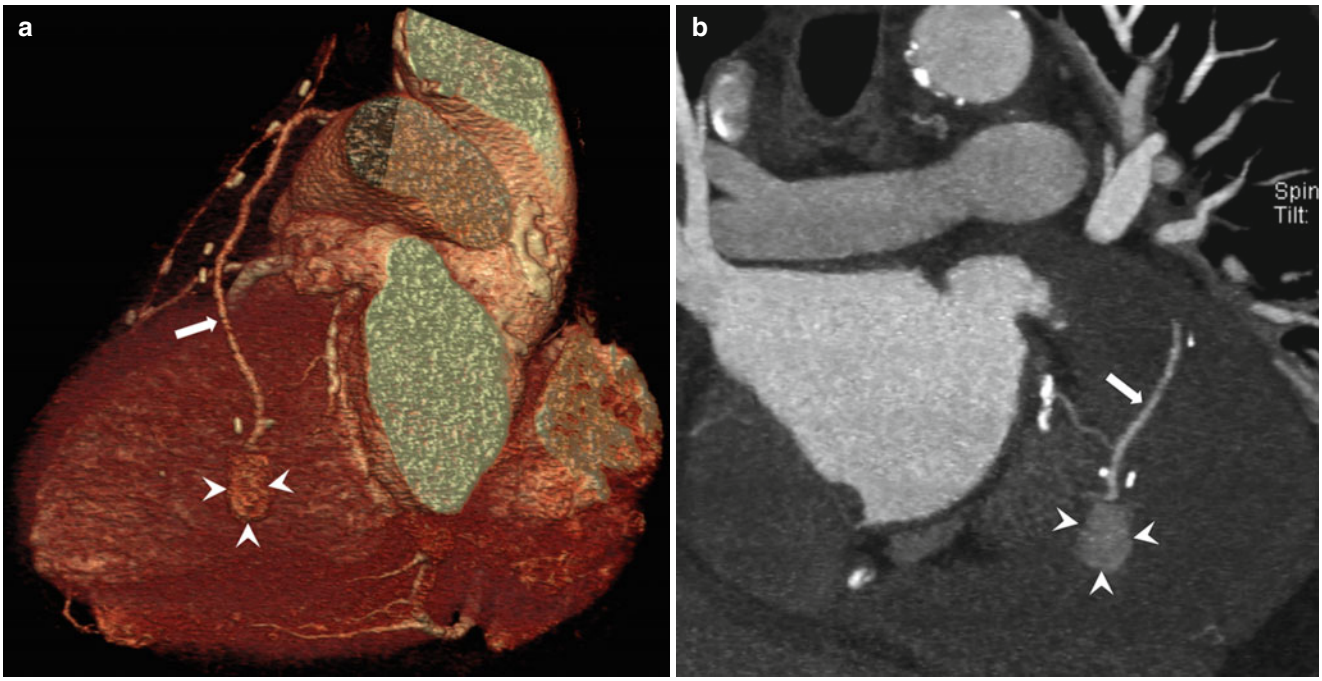

Fig. 8.13 Pseudoaneurysm formation around distal anastomosis site. (**a**) Volume rendering and (**b**) oblique coronal CT images obtained at 6 months after bypass surgery showed pseudoaneurysm formation (*arrowheads*) around distal anastomosis site between radial artery graft (*arrow*) and the obtuse marginal artery

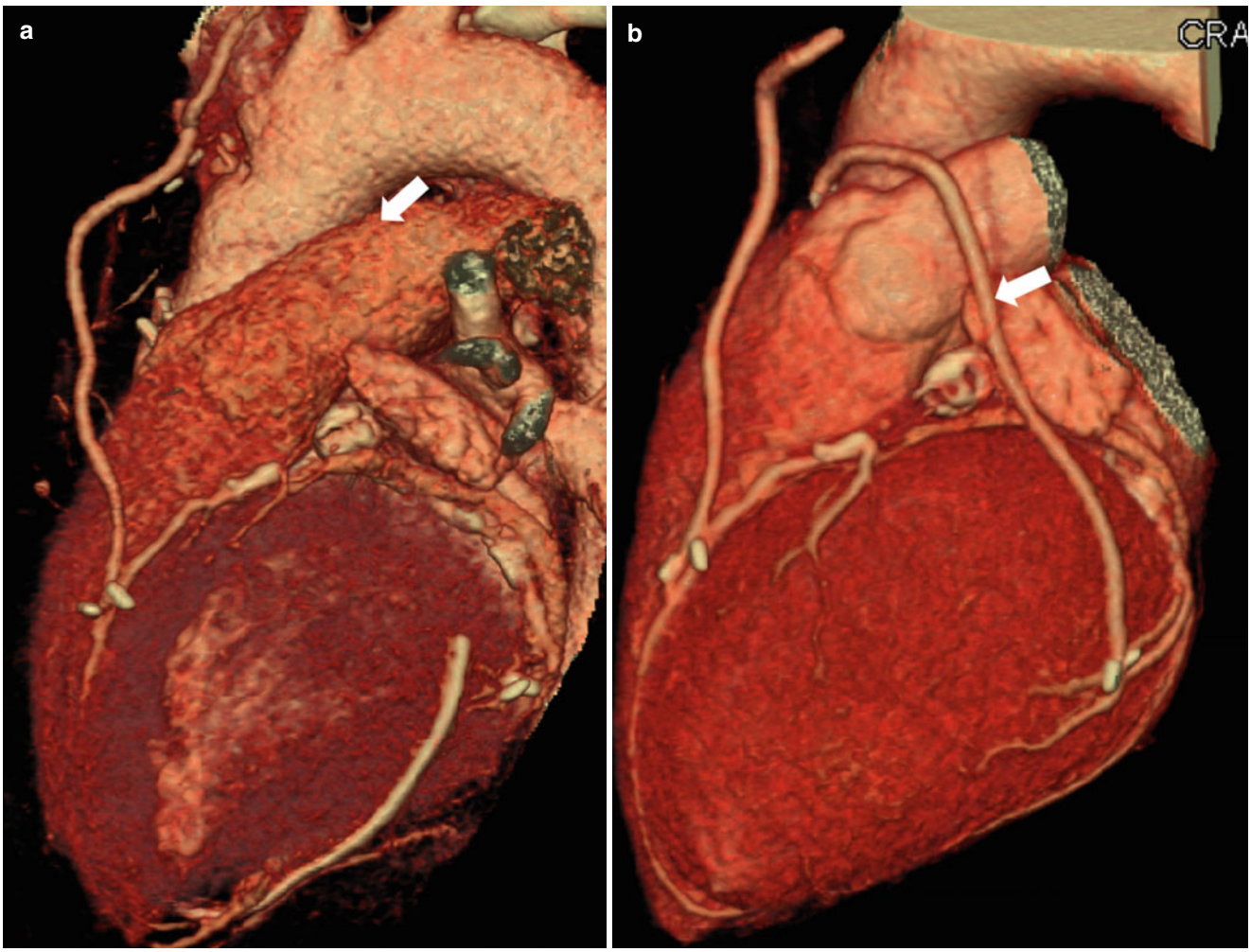

Fig. 8.14 Postoperative graft spasm and its spontaneous resolution. (**a**) On volume rendering CT image obtained at 5 days after bypass surgery, radial artery graft was barely opacified (*arrow*) due to graft spasm. (**b**) Six months after, patency of the radial artery graft was restored (*arrow*)

8.3.4 CT Imaging of Postsurgical Complication

- CTA may reveal unexpected cardiac findings with potential clinical significance as follows [15]: left ventricular thrombus, left ventricular pseudoaneurysm, pseudoaneurysm of the native coronary artery or grafted vessel, right ventricular compression by pectus excavatum, and left atrial thrombus.
- Bypass grafts initially showing poor patency after surgery have occasionally shown improvement on serial CT follow-up (Fig. 8.14). In a single-center study, an improvement in graft patency occurred in 60 %. Larger target-vessel size and target-vessel stenosis of at least 90 % were significant correlative factors [16].

References

1. Andersen HR, Nielsen TT, Rasmussen K, et al. A comparison of coronary angioplasty with fibrinolytic therapy in acute myocardial infarction. N Engl J Med. 2003;349(8):733–42.
2. Task Force on Myocardial Revascularization of the European Society of C, the European Association for Cardio-Thoracic S, European Association for Percutaneous Cardiovascular I, et al. Guidelines on myocardial revascularization. Eur Heart J. 2010;31(20):2501–55.
3. Garg S, Serruys PW. Coronary stents: current status. J Am Coll Cardiol. 2010;56(10 Suppl):S1–42.
4. Bangalore S, Kumar S, Fusaro M, et al. Short- and long-term outcomes with drug-eluting and bare-metal coronary stents: a mixed-treatment comparison analysis of 117 762 patient-years of follow-up from randomized trials. Circulation. 2012;125(23):2873–91.
5. Hecht HS, Gade C. Current and evolving stent evaluation by coronary computed tomographic angiography. Catheter Cardiovasc Interv. 2011;77(6):843–59.

6. Andreini D, Pontone G, Mushtaq S, Pepi M, Bartorelli AL. Multidetector computed tomography coronary angiography for the assessment of coronary in-stent restenosis. Am J Cardiol. 2010;105(5):645–55.
7. Van Mieghem CA, Cademartiri F, Mollet NR, et al. Multislice spiral computed tomography for the evaluation of stent patency after left main coronary artery stenting: a comparison with conventional coronary angiography and intravascular ultrasound. Circulation. 2006;114(7):645–53.
8. Rief M, Zimmermann E, Stenzel F, et al. Computed tomography angiography and myocardial computed tomography perfusion in patients with coronary stents: prospective intraindividual comparison with conventional coronary angiography. J Am Coll Cardiol. 2013;62(16):1476–85.
9. Lim HB, Hur G, Kim SY, et al. Coronary stent fracture: detection with 64-section multidetector CT angiography in patients and in vitro. Radiology. 2008;249(3):810–9.
10. Hecht HS, Polena S, Jelnin V, et al. Stent gap by 64-detector computed tomographic angiography relationship to in-stent restenosis, fracture, and overlap failure. J Am Coll Cardiol. 2009;54(21):1949–59.
11. Nakazawa G, Finn AV, Vorpahl M, et al. Incidence and predictors of drug-eluting stent fracture in human coronary artery a pathologic analysis. J Am Coll Cardiol. 2009;54(21):1924–31.
12. Gilkeson RC, Markowitz AH. Multislice CT evaluation of coronary artery bypass graft patients. J Thorac Imaging. 2007;22(1):56–62.
13. Hamon M, Lepage O, Malagutti P, et al. Diagnostic performance of 16- and 64-section spiral CT for coronary artery bypass graft assessment: meta-analysis. Radiology. 2008;247(3):679–86.
14. Small GR, Yam Y, Chen L, et al. Prognostic assessment of coronary artery bypass patients with 64-slice computed tomography angiography: anatomical information is incremental to clinical risk prediction. J Am Coll Cardiol. 2011;58(23):2389–95.
15. Mueller J, Jeudy J, Poston R, White CS. Cardiac CT angiography after coronary bypass surgery: prevalence of incidental findings. AJR Am J Roentgenol. 2007;189(2):414–9.
16. Kim JB, Kang JW, Song H, et al. Late improvement in graft patency after coronary artery bypass grafting: serial assessment with multidetector computed tomography in the early and late postoperative settings. J Thorac Cardiovasc Surg. 2011;142(4):793–9.

Nonatherosclerotic Coronary Artery Disease

9

Eun-Ah Park and Whal Lee

Contents

Abstract

This chapter deals with various CT imaging features of non-atherosclerotic, non-anomalous coronary artery diseases, including coronary artery inflammation, infection, trauma, substance use, embolism, spasm, dissection, and extrinsic compression or invasion. Non-atherosclerotic coronary artery disease can present as aneurysm, ectasia, luminal stenosis, or occlusion. Each disease entity has typical imaging features radiologists should be familiar with.

9.1 Introduction

Although atherosclerosis is the most common cause of coronary artery disease, there are many different nonatherosclerotic causes of coronary artery disease including congenital coronary anomalies, coronary artery inflammation, infection, trauma, substance use, embolism, spasm, dissection, and extrinsic compression or invasion [1].

Nonatherosclerotic coronary artery disease can present as aneurysm, ectasia, luminal stenosis, or occlusion with clinical presentation including angina, myocardial infarction, congestive heart failure, or sudden cardiac death [2].

Approximately 5 % of patients with acute myocardial infarction do not have atherosclerotic coronary artery disease but have other causes for coronary artery disease [3].

Currently, coronary CT angiography has evolved into a widely used imaging tool in clinical practice. Consequently, radiologists should be familiar with the diverse imaging findings of nonatherosclerotic coronary artery disease that can be identified with coronary CT angiography to facilitate accurate diagnosis and proper management. In this chapter, various imaging findings of nonatherosclerotic, nonanomalous coronary artery disease will be illustrated.

Electronic supplementary material Supplementary material is available in the online version of this chapter at 10.1007/978-3-642-36397-9_9.

E.-A. Park (✉) • W. Lee
Department of Radiology,
Seoul National University Hospital, Seoul, Republic of Korea
e-mail: iameuna1@gmail.com; whal.lee@gmail.com

T.-H. Lim (ed.), *Practical Textbook of Cardiac CT and MRI*,
DOI 10.1007/978-3-642-36397-9_9, © Springer-Verlag Berlin Heidelberg 2015

Table 9.1 Potential causes of coronary artery aneurysm or ectasia and their underlying pathologic mechanisms [3, 5, 6]

Cause	Age group	Comments	Pathologic mechanism
Atherosclerosis	Adults (>50 years)	Most common cause of coronary artery aneurysm or ectasia	Local mechanical stress from stenosis, atherosclerotic pathologic findings extending into tunica media
Kawasaki disease	Childhood	Most common cause of coronary artery aneurysm or ectasia in childhood and in Japan and Korea, spontaneous resolution occurs in 50 %	Autoimmune, vasculitis
Inflammatory disease	Young adults	Takayasu arteritis, systemic lupus erythematosus, rheumatoid arthritis, giant cell arteritis, ankylosing spondylitis, antiphospholipid syndrome, Wegener's granulomatosis, Buerger's disease (thromboangiitis obliterans), polyarteritis nodosa, Churg-Strauss syndrome, sarcoid, CREST syndrome, Reiter syndrome, psoriatic arthritis, microscopic polyangiitis	Inflammatory mediators: VCAM-1, ICAM-1, E selectin
Congenital			
Idiopathic		Presenting as coronary artery ectasia	
Fistula	Any age	Most are congenital, about 50 % of fistulas originate from RCA	Compensatory dilatation secondary to high-flow state
Coronary anomalies (i.e., ALCAPA)	Childhood form, adult form	In infant type, death occurs early in life due to myocardial infarction; in adult form, collateral vessels between RCA and LCA are common	Compensatory dilatation secondary to myocardial ischemia
Miscellaneous			
Connective tissue diseases	Young adults	Ehlers-Danlos syndrome, Marfan syndrome, Loeys-Dietz syndrome, Noonan syndrome	IL-6, C-reactive protein, MMP-2, MMP-9
Infectious diseases	Any age	Infection with *Staphylococcus aureus* or *Pseudomonas aeruginosa*, fungal, syphilis, *Salmonella*, Lyme disease, leprosy, typhus, tuberculosis	Microembolization to vasa vasorum, direct pathogen invasion of the arterial wall, immune complex deposition
Myxoma related	Any age		Microembolization to vasa vasorum, direct pathogen invasion of the arterial wall, immune complex deposition
Trauma/iatrogenic	Adults	Clinical history helps establish diagnosis	Trauma from oversized balloon or high inflation pressures, coronary dissection, interventions in the setting of acute myocardial infarction, inadequate healing because of antiproliferative treatment with cortisone, colchicine, and anti-inflammatory drugs
Drug related Cocaine, amphetamines, protease inhibitors	Adults	Clinical history helps establish diagnosis	Direct endothelial damage from severe episodic hypertension, vasoconstriction, and underlying atherosclerosis

Note: *CREST* calcinosis cutis, Raynaud phenomenon, esophageal dysfunction, sclerodactyly, and telangiectasia, *ICAM-1* intercellular adhesion molecule 1, *IL-6* interleukin-6, *MMP-2* matrix metalloproteinase 2, *MMP-9* matrix metalloproteinase 9, *VCAM-1* vascular cell adhesion molecule 1, *ALCAPA* Anomalous left coronary artery from the pulmonary artery, *RCA* right coronary artery, *LCA* left coronary artery

Table 9.2 Differential finding of nonatherosclerotic coronary ectasia and aneurysm [19]

Disease entity	Imaging findings	Differential finding
Kawasaki disease	Multiple focal coronary artery aneurysms	In young patients with a history of viral infection
Coronary artery fistula	Tortuous coronary artery associated with dilated epicardial veins and coronary sinus	Arteriovenous communication; only the artery leading to the fistula is dilated
Takayasu arteritis	Coronary artery aneurysms and stenoses	Involvement of the aorta and great vessels
ALCAPA syndrome (adult type)	Diffuse dilatation of the anomalous LCA and the RCA with dilated intercoronary collateral vessels	LCA arises from the main pulmonary artery

9.2 Nonatherosclerotic Nonanomalous Aneurysmal Coronary Artery Disease

Aneurysmal coronary artery disease is defined as coronary dilatation which exceeds the diameter of normal adjacent segments or the diameter of the patient's largest coronary vessel by 1.5 times [4]. The reported frequency of coronary artery aneurysms varies widely from 0.3 to 5 %, which may be related to different angiographic criteria used to define aneurysms [5]. The different etiologies which have been postulated for coronary artery aneurysms are summarized in Table 9.1 and their differential imaging findings are presented in Table 9.2. The most common etiology is

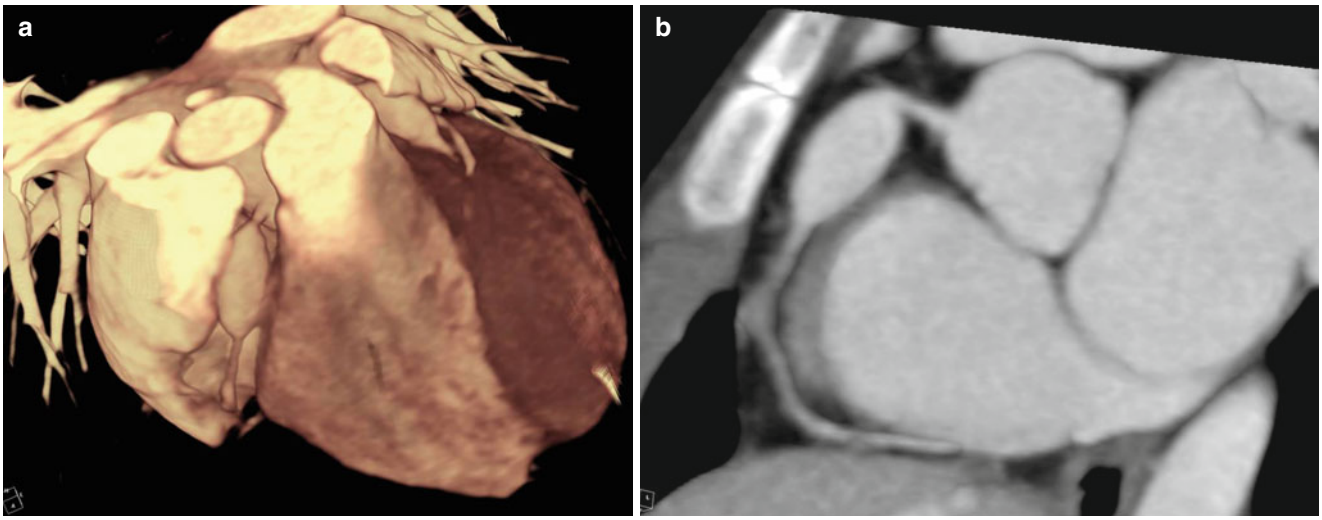

Fig. 9.1 A 6-year-old girl with Kawasaki disease presenting with non-thrombosed coronary aneurysm. (**a**) 3D volume-rendering CT image shows fusiform aneurysm at the right coronary artery and the left anterior descending artery. (**b**) Curved multiplanar reformation (cMPR) image shows non-thrombosed fusiform aneurysm at the proximal segment of the right coronary artery

atherosclerosis accounting for 50 % of coronary aneurysms diagnosed in adults. This is followed by Kawasaki disease and congenital aneurysms [4].

- *Definition of coronary artery aneurysm*
  - Coronary artery segments that have a diameter of a 50 % or greater increase compared with adjacent arterial segment and involve less than 50 % of the total length of the vessel. It can be fusiform or saccular. In saccular aneurysms, the transverse diameter is greater than the longitudinal measurement of the aneurysm, whereas in fusiform aneurysms, the longitudinal measurement is greater than the transverse diameter. True aneurysm is defined when the vessel wall is composed of three layers (adventitia, media, and intima), whereas false aneurysm or pseudoaneurysm is defined as the vessel wall composed of one or two layers [5].

- *Definition of coronary artery ectasia*
  - Coronary artery segments that have a diameter of a 50 % or greater increase compared with adjacent arterial segment and involve more than 50 % of the total length of the vessel [5].
  - Classification of coronary artery ectasia
    - Coronary artery ectasias are classified into four types according to the definition of Markis et al. as follows: (1) diffuse ectasia with aneurysmal lesions in two vessels (type I), (2) diffuse ectasia in one vessel and discrete ectasia in another (type II), (3) diffuse ectasia in one vessel (type III), and (4) discrete ectasia in one vessel (type IV) [7]. This classification may have prognostic implications, with the worst outcomes in type I and II [5].

9.2.1 Coronary Artery Vasculitis

- Kawasaki disease (mucocutaneous lymph node syndrome)
  - An acute, self-limited multisystemic panarteritis that affects young children [5]. The etiology of Kawasaki disease remains unknown, although several epidemiologic and clinical features strongly suggest that an infectious cause triggers an immunologic response in genetically predisposed individuals and autoimmunity may play a role in the pathogenesis. In the acute phase of Kawasaki disease, various anatomic regions of the heart can be involved including the pericardium, myocardium, endocardium, valves, and coronary arteries. Coronary artery aneurysms or ectasia develops in approximately 15–25 % of untreated children with the disease (Figs. 9.1 and 9.2). The thrombotic occlusion, progression to ischemic heart disease, and premature atherosclerosis may also be involved [8, 9]. In the chronic phase, aneurysms undergo regression or remodeling. One half of the patients have spontaneous regression of the aneurysms within 2 years after the onset of Kawasaki disease [5]. However, marked intimal thickening may be often found in the portion of the regressed coronary aneurysm even though the luminal diameter looks angiographically normal [9].
- Takayasu arteritis
  - An inflammatory large-vessel vasculitis that predominantly affects young women. In early systemic phase, the involved vascular wall shows the double-ring pattern: a poorly enhanced inside ring representing mucoid or gelatinous swelling of the intima and a well-enhanced outside ring representing active medial and adventitial inflammatory change on enhanced CT (Figs. 9.3 and 9.4). In late occlusive

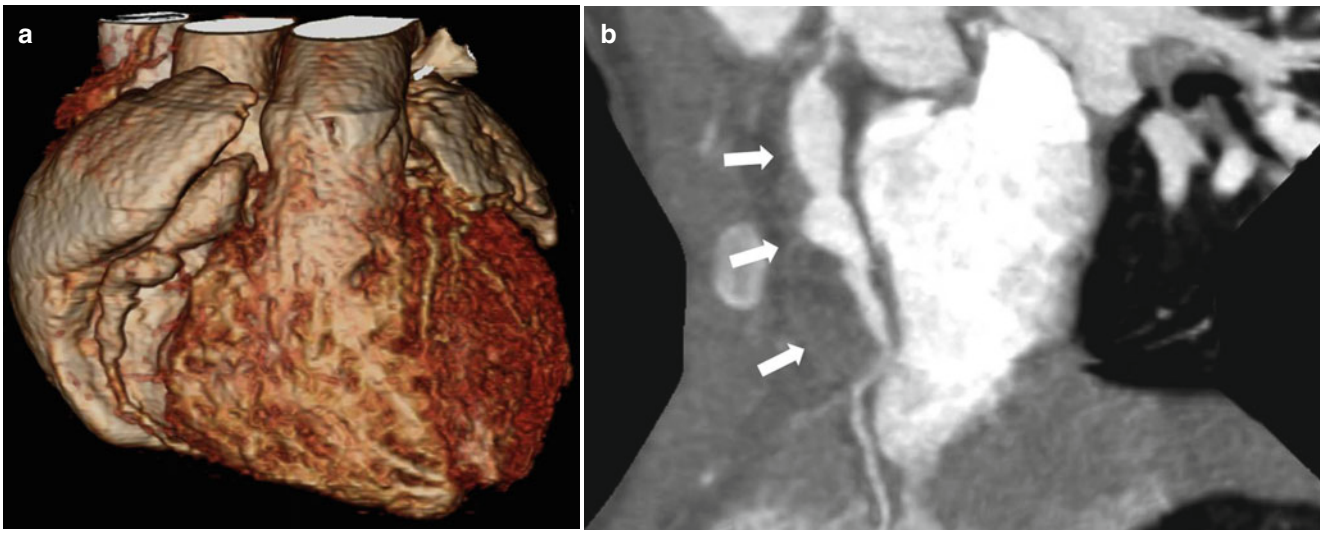

Fig. 9.2 A 3-year-old girl with Kawasaki disease presenting with thrombosed coronary aneurysm. (**a**) 3D volume-rendering CT image shows long segmental fusiform aneurysm at the right coronary artery. (**b**) On curved multiplanar reformation (cMPR) image, partial mural thrombus (*arrows*) was seen at the peripheral portion of huge fusiform aneurysm involving the proximal to midsegment of the right coronary artery. Actual diameter of aneurysm is much larger than that seen on 3D volume-rendering image

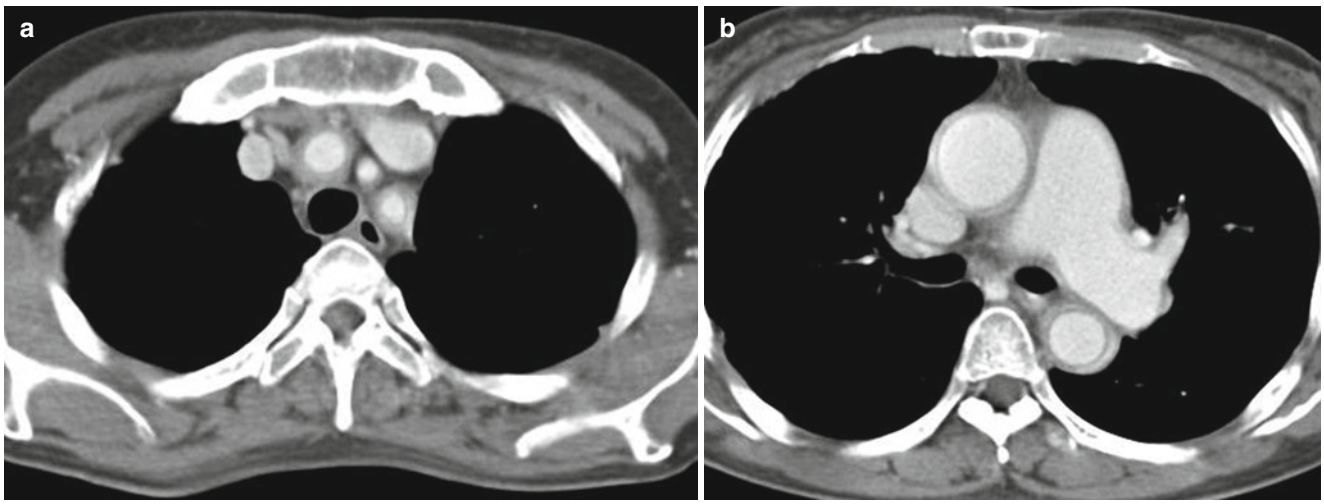

Fig. 9.3 A 49-year-old woman with active stage of Takayasu arteritis. (**a**) Transaxial contrast-enhanced CT image shows concentric wall thickening at the right brachiocephalic and the left subclavian arteries. (**b**) Transaxial contrast-enhanced CT image shows typical "double-ring" sign with poorly enhanced inner ring and well-enhanced outer ring at the ascending and descending thoracic aorta

phase, typical angiographic findings include a diffuse luminal narrowing or occlusion with/without circumferential calcification of the aorta and major branches [10, 11] (Fig. 9.5). The incidence of coronary artery involvement has been reported to be 9–10 %. Signs and symptoms result from ischemia due to arterial stenosis or occlusion. On the basis of pathological features, coronary artery lesions can be classified into the following three types: type 1 (most common), stenosis or occlusion of the coronary ostia and the proximal segments of the coronary arteries; type 2, diffuse or focal coronary arteritis, which may extend diffusely to all epicardial branches or may involve focal segments, so-called skip lesions; and type 3, coronary aneurysm [12]. Aneurysms and ectasia can also develop as a compensatory mechanism [5].

- Other reported causes of inflammatory coronary vasculitis are listed in Table 9.1. Unlike other collagen vascular diseases such as polyarteritis nodosa and rheumatoid arthritis, in which coronary arteritis has been reported in 62 and 20 %, respectively, of patients who underwent autopsy, coronary vasculitis is quite uncommonly seen in systemic lupus erythematosus (SLE) [13]. Twelve cases of SLE-associated coronary aneurysms have been reported in the literatures, involving focal or diffuse and one to three coronary arteries [14]. Myocardial infarction in SLE is caused from either coronary arteritis or premature atherosclerosis. The majority of cases are secondary to atherosclerosis,

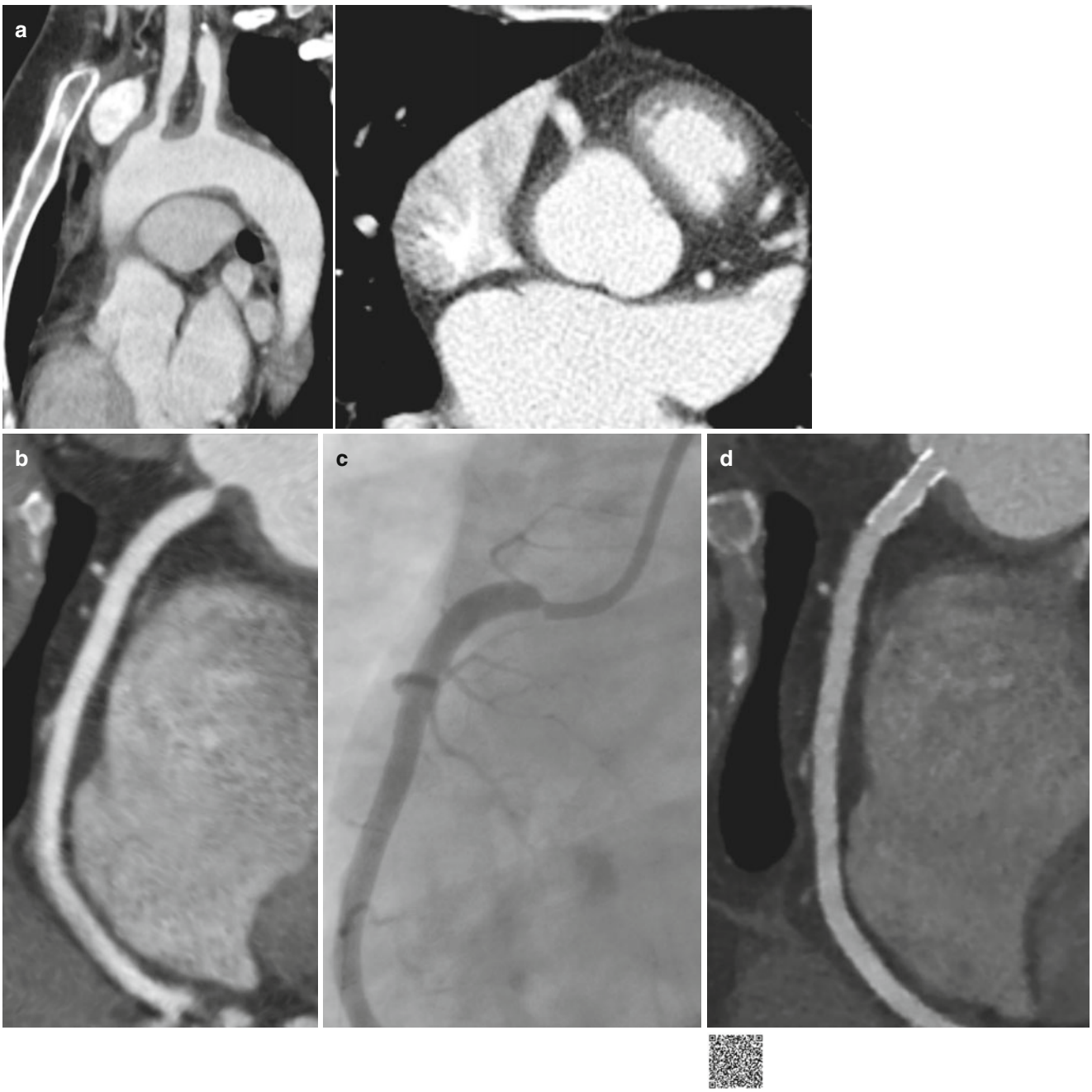

Fig. 9.4 A 29-year-old woman with Takayasu arteritis involving the right coronary artery ostium (Courtesy of Dong Hyun Yang, Asan Medical Center). (**a**) Oblique sagittal multiplanar reformation image shows diffuse wall thickening at the aortic arch and its branches. (**b**) Transaxial (**b**) and curved multiplanar reformation (**c**) images clearly demonstrate the tight luminal narrowing at the ostium of the right coronary artery by extension of inflammation presenting as wall thickening of the ascending aorta into the right coronary artery. (**c**) Invasive coronary angiogram shows same feature of luminal stenosis at the ostium of the right coronary artery. (**d**) The patient underwent subsequently stent implantation in the right coronary artery. Curved multiplanar reformation image shows excellent luminal patency of stent implanted in the right coronary artery (http://extras.springer.com/2015/978-3-642-36396-2)

which is believed to be accelerated in those treated with corticosteroids. Coronary arteritis accounts for only very few cases of myocardial infarction in patients with SLE. The representative features of coronary arteritis differentiating from atherosclerosis in SLE on the basis of changes in coronary anatomy found by angiography are reported as smooth focal lesions, aneurysmal dilatation, and an abrupt consecutive change from normal to severe obstruction of coronary arteries [13] (Fig. 9.6). The inflammation from any causes including infection may lead to in situ coronary thrombosis as well [1].

9.2.2 Connective Tissue Diseases

Ehlers-Danlos syndrome, Marfan syndrome, and Loeys-Dietz syndrome are genetic disorders that primarily affect the soft connective tissues of multisystem (Fig. 9.7).

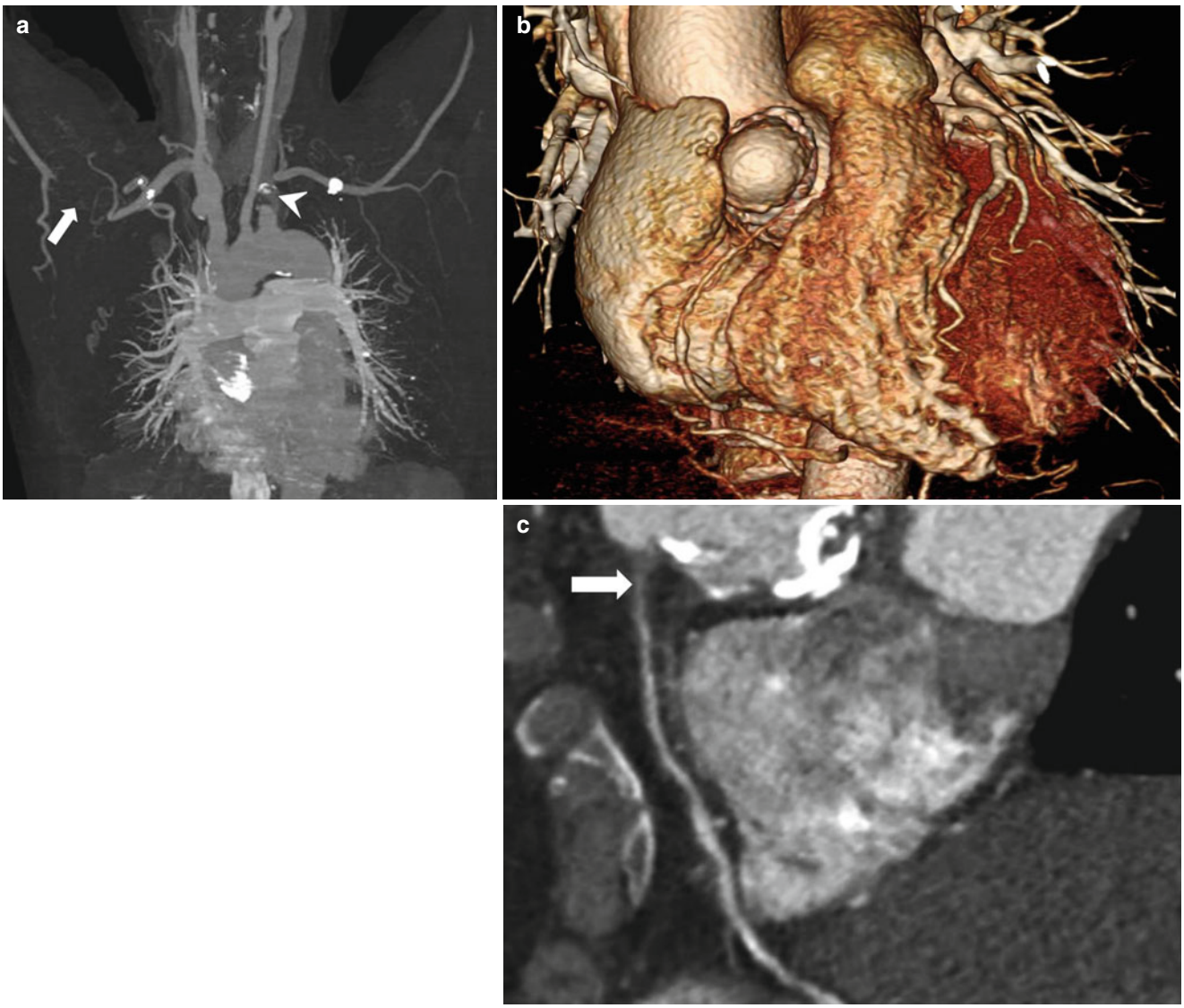

Fig. 9.5 A 55-year-old woman with Takayasu arteritis. (**a**) Maximum intensity projection (MIP) image shows segmental total occlusion involving the left subclavian artery (*arrowhead*) and the right axillary artery (*arrow*). (**b**) Three-dimensional volume-rendering image shows focal outpouching bizarre aneurysm with ring calcification at the right aortic sinus, indicating unusual manifestation of Takayasu arteritis. The right coronary artery ostium was occluded and diffuse narrowing of proximal segment was seen. (**d**) Curved multiplanar reformation (cMPR) image also shows the occluded right coronary artery proximal segment (*arrow*)

Histologically, the aortic media shows a deficiency of elastic and muscle fibers, naming cystic medial necrosis [15]. Association of coronary artery dissection from extension of a dissection from proximal aorta has been reported in patients with connective tissue diseases such as Marfan syndrome or Ehlers-Danlos syndrome [15]. Although true aneurysm of the coronary artery in Marfan syndrome is very rare, interestingly there have been predilection for the location and timing of aneurysms; there have similar reports showing dilatation of coronary origin during follow-up after total repair of annuloaortic ectasia [16, 17] (Fig. 9.8). Coronary artery aneurysms in patients with Noonan syndrome have also been reported. The association of coronary artery aneurysm with Noonan syndrome is not well understood. Several pathologic mechanisms have been proposed, including vasculitis superimposed upon a connective tissue defect, dilatation secondary to associated myocardial hypertrophy, and persistent aneurysm after the spontaneous closure of fetal coronary artery fistula [18].

9.2.3 Infectious Diseases

Various infectious diseases have been associated with coronary arteritis. Possible organisms are listed in (Table 9.1). Syphilis is reported to be one of the most common infectious

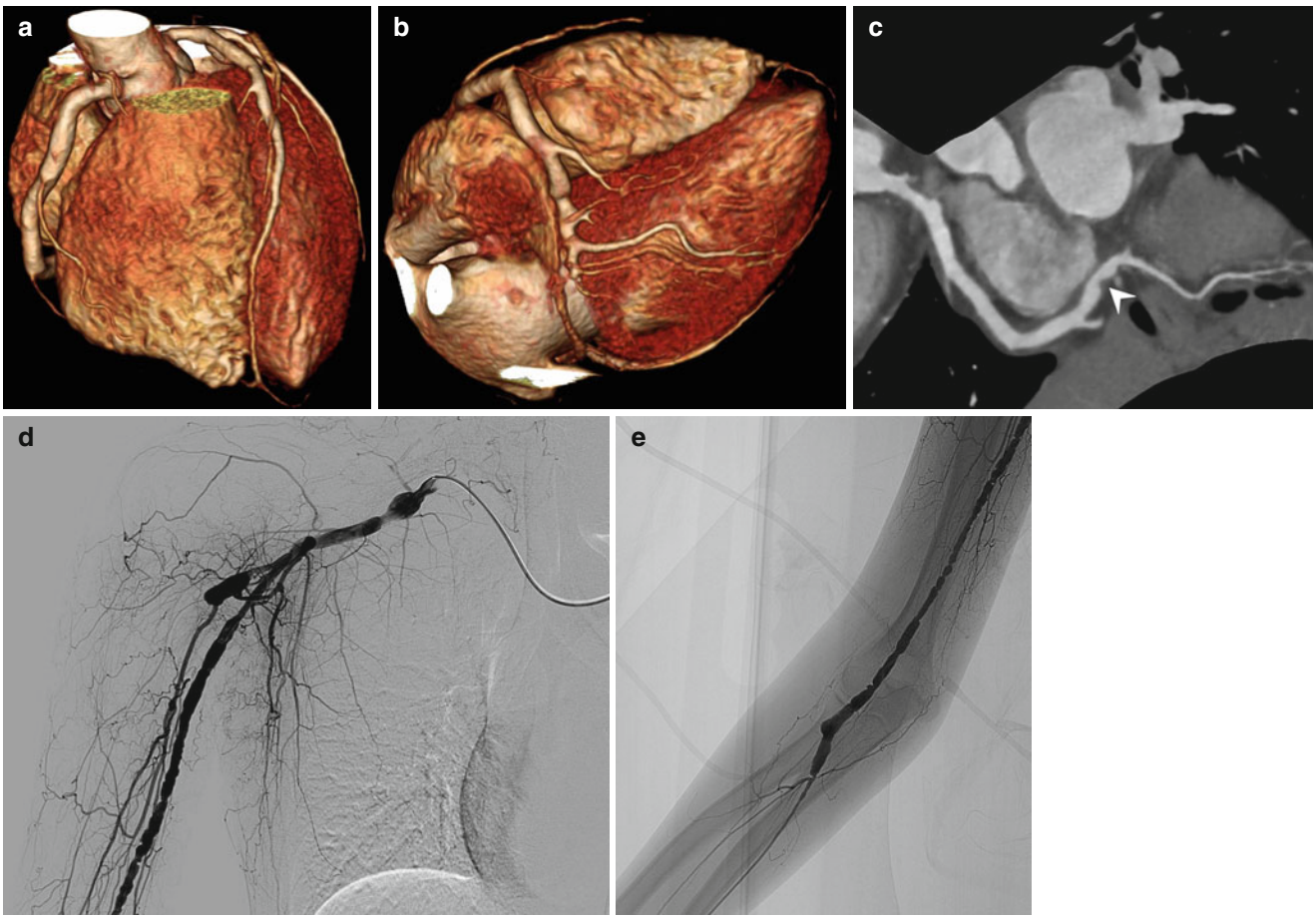

Fig. 9.6 A 22-year-old woman with systemic lupus erythematosus. (**a**, **b**) Three-dimensional volume-rendering images show diffuse dilatation (ectasia) with combined stenosis of the right coronary artery and the posterolateral branch. (**c**) Curved multiplanar reformation image shows focal wall thickening (*arrowhead*) at the site of luminal narrowing of the posterolateral branch. (**d**, **e**) Upper extremity angiograms show diffuse aneurysmal dilatation (ectasia) with multifocal combined stenosis of the brachial artery and its branches. The angiogram features look like "string of beads" appearance similar to fibromuscular dysplasia

diseases affecting the coronary arteries [3]. Up to one quarter of patients with tertiary syphilis may have ostial stenosis, presenting as obliterative arteritis [3]. In mycotic aneurysms, the injury and destruction of the tunica media may be due to microembolization to the vasa vasorum, direct pathogen invasion of the arterial wall, or immune complex deposition [5]. Infective endocarditis-related perivalvular pseudoaneurysm or abscess may compress the coronary artery externally, which is often associated with myocardial ischemia or infarction. Extension of infection into the myocardium may lead to coronary artery fistula or pseudoaneurysm [1].

9.2.4 Myxoma-Related Coronary Artery Aneurysm

Myxoma-related aneurysms are extremely rare with only approximately 40 cases having been reported in the literature. Myxoma-related aneurysms are most often confined to the cerebral arteries, mainly in the middle cerebral artery but can also involve the coronary arteries, ultimately accompanying myocardial embolic infarction (Fig. 9.9). The possible pathogenesis is suggested as follows: (a) the temporal occlusion of cerebral vessels by tumor emboli led to endothelial scarring and thus subsequent aneurysm formation, (b) embolization of tumor material from cardiac myxoma into the vasa vasorum of peripheral arteries causing weakness of subintimal tissue by proliferating into the vessel wall, and (c) the inflammatory reaction, production of interleukin-6 by myxoma cells, and high expression and activity of matrix metalloproteinases [20].

9.2.5 Trauma/Iatrogenic

Coronary artery trauma may produce myocardial ischemia or myocardial infarction. Traumatic injury may result from non-penetrating blunt chest wall injury, penetration trauma,

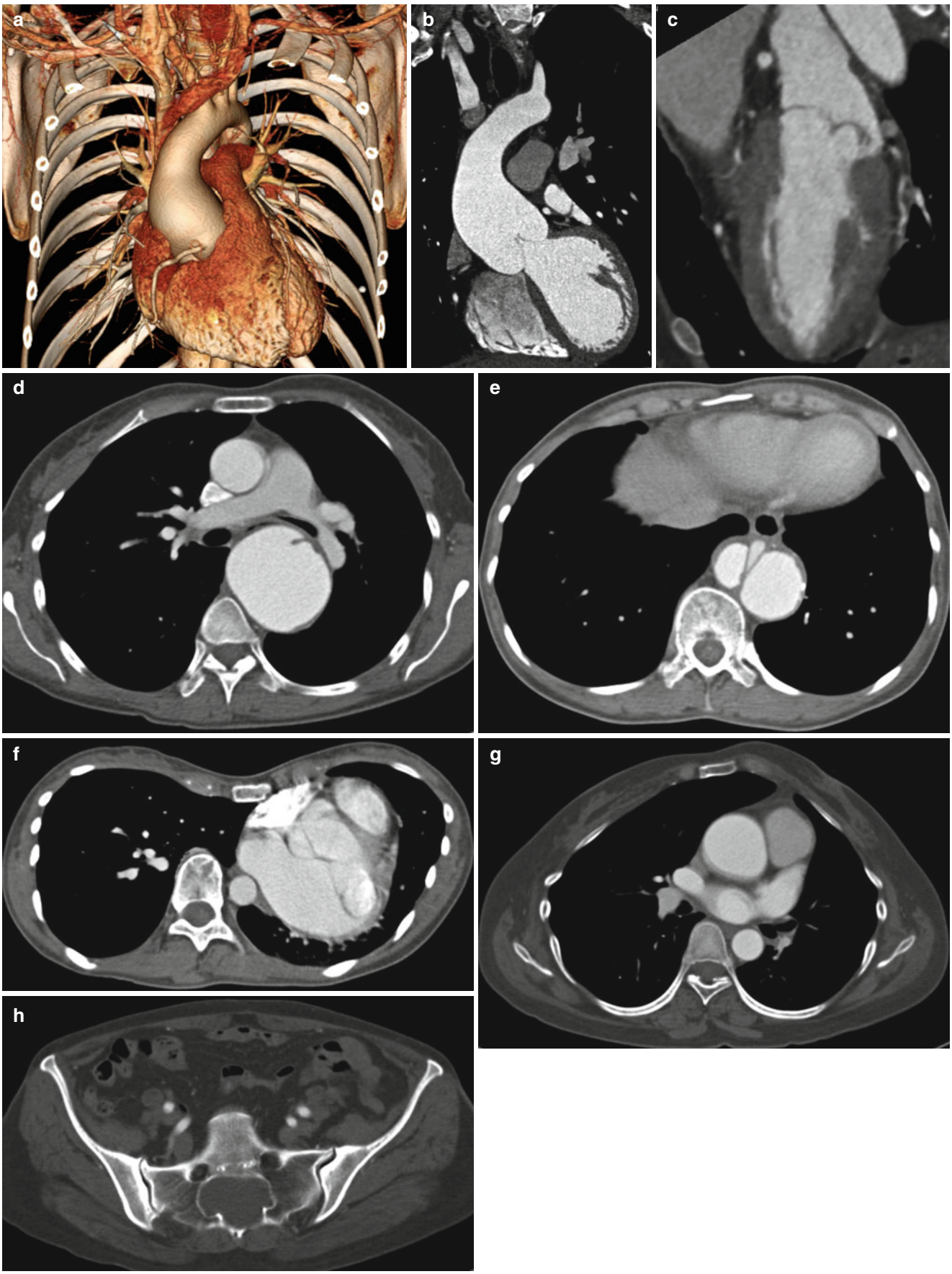
a
b
c
d
e
f
g
h

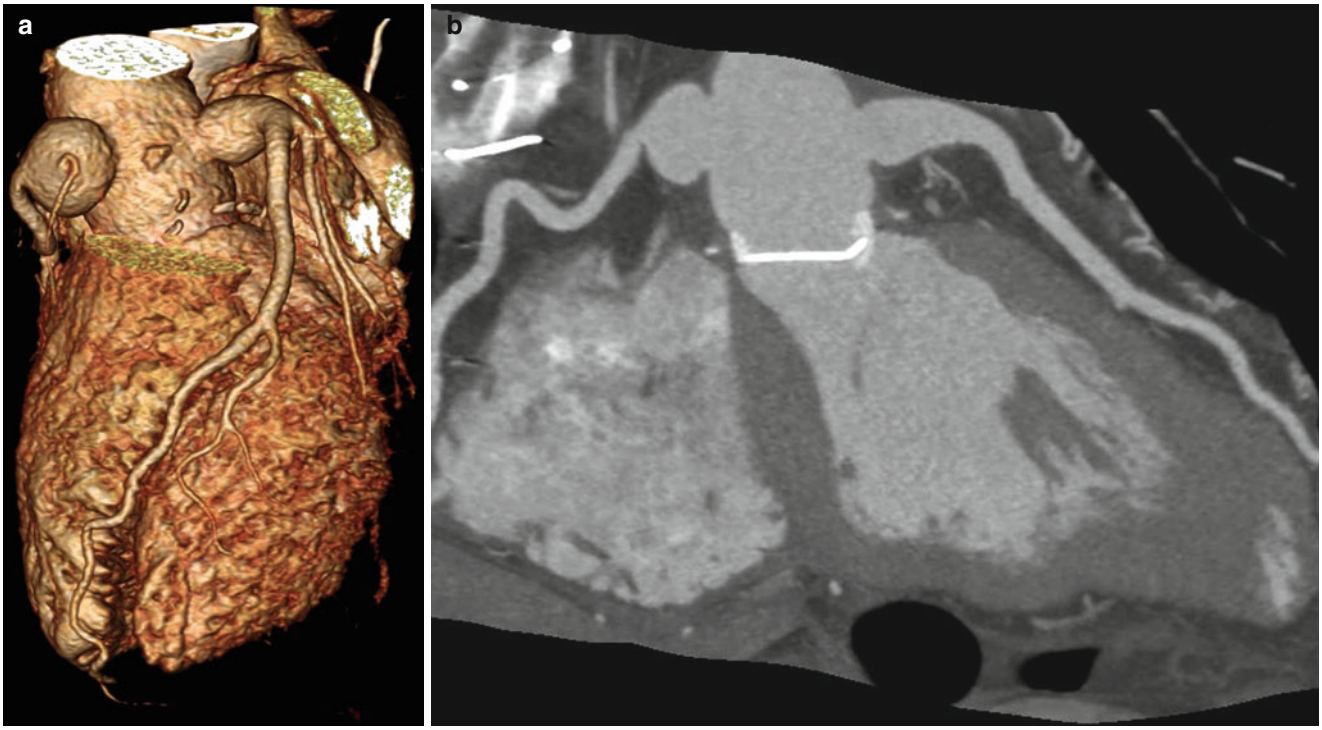

Fig. 9.8 A 25-year-old man with Marfan syndrome. The patient had a history of Bentall operation due to aortic root aneurysm. Both coronary arteries were reimplanted using button technique. (**a**, **b**) Three-dimensional volume-rendering (**a**) and curved multiplanar reformation (**b**) images show fusiform aneurysms at the ostia and the proximal segments of both coronary arteries

or during coronary angiography (laceration, dissection, embolus). Non-penetrating trauma may produce coronary injury and subsequent MI as a result of coronary dissection, contusion and thrombosis, fistula formation, or coronary artery aneurysm formation [21].

9.2.6 Cocaine Use

Patients with a history of cocaine abuse have an increased prevalence of coronary artery aneurysms (30.4 %) [5]. Cocaine use can also induce other cardiovascular abnormalities such as atherosclerosis, coronary vasospasm, aortic dissection, arterial thrombosis [2]. These patients appear to be at increased risk of acute myocardial infarction. Proposed mechanisms for the development of aneurysms related to cocaine abuse include (a) direct endothelial damage caused by severe episodic hypertension and vasoconstriction and (b) underlying atherosclerosis [5].

9.3 Coronary Embolism

Cardiac valves are the most common embolic source to coronary arteries, leading to myocardial infarction. Emboli can also arise from the left ventricle or atrium intracavitary thrombi (Fig. 9.10), left atrial myxoma (Fig. 9.9), neoplasm, and paradoxic embolism from the right side of the heart. Historically, septic emboli from infective endocarditis have been the most common cause; however, development of effective antibiotics has gradually decreased this etiology. Currently, noninfected thrombi on the prosthetic valve account for the majority of cases [22].

Fig. 9.7 Representative examples of Marfan syndrome. (**a**, **b**) Three-dimensional volume-rendering (**a**) and oblique coronal multiplanar reformation (**b**) images of patient 1 show diffuse aneurysmal dilatation from the aortic annulus to the ascending aorta indicating annuloaortic ectasia and aortic root aneurysm. (**c**) Two-chamber long-axis image of patient 2 shows mitral valve prolapse. (**d**, **e**) Transaxial images of patient 3 shows multichannel dissecting aneurysm involving the descending thoracic aorta. (**f**) Transaxial image of patient 4 shows abnormal anterior chest wall indentation (pectus excavatum). Chest wall geometry is altered due to scoliosis. (**g**, **h**) Transaxial images of patient 5 show pectus carinatum, so-called pigeon chest, and dural ectasia at the level of the sacrum

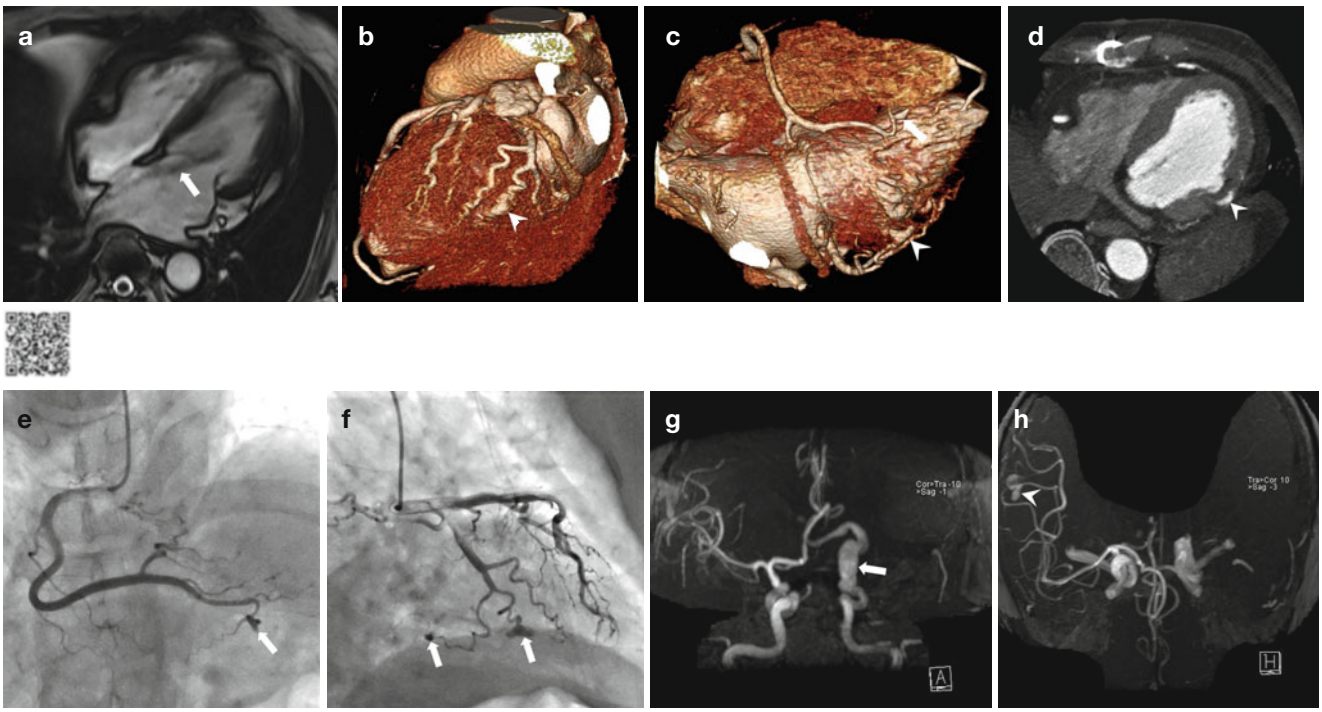

Fig. 9.9 A 58-year-old woman with cardiac myxoma-related multiple cerebral and coronary aneurysms. This patent has suffered from repetitive episodes of stroke with right-sided hemiplegia and dysarthria for 20 years. (**a**) Four-chamber MR image shows an elongated mass (*arrow*) attached to the left atrial septum. The mass was confirmed as myxoma (http://extras.springer.com/). (**b**, **c**) 3D volume-rendering images show multiple peripheral fusiform aneurysms of the posterior descending artery (*arrow*) and the obtuse marginal artery (*arrowheads*). (**d**) Transverse axial MIP image shows focal myocardial thinning suggestive of myocardial infarction in the corresponding area of obtuse marginal branch aneurysm (*arrowhead*). (**e**, **f**) Invasive coronary angiograms confirm the presence and the location of multiple coronary aneurysms (*arrows*). (**g**, **h**) Brain time-of-flight MR angiograms show a giant fusiform aneurysm (*arrow*) of the left distal internal carotid artery. Irregular aneurysms (*arrowhead*) were present in the peripheral branch of the right middle cerebral artery

9.4 Coronary Spasm

Coronary artery spasm is an abnormal contraction of an epicardial coronary artery, causing myocardial ischemia, and its incidence is relatively high in Korea and Japan as compared with Western countries. Coronary spasm affects mostly middle- and old-aged men and postmenopausal women [23]. The major risk factor for coronary spasm is cigarette smoking. Coronary spasm can be a cause of not only variant angina but also ischemic heart disease in general, including unstable angina, acute myocardial infarction, and sudden ischemic death [24]. Coronary spasm occurs most often from midnight to early morning at rest, and it is usually not induced by exercise in the daytime. The attack is transient, often lasts only a few seconds, and is unpredictable. Therefore, it is difficult to make a diagnosis by performing coronary angiography during an attack in every single patient [23]. If the initial coronary angiography examination does not reveal a significant stenosis in patients with suspected coronary spasm, increasing doses of intracoronary ergonovine or acetylcholine are administered until coronary spasm, clinical symptoms, or ECG changes are provoked. Afterward, intracoronary nitroglycerin is administered subsequently to relieve coronary artery spasm [1] (Fig. 9.11).

9.5 Coronary Artery Dissection

Coronary artery dissections may be either spontaneous or secondary. Spontaneous dissections tend to occur in young women, especially in the postpartum period, frequently presenting as ST-elevation myocardial infarction [25]. Secondary dissections may occur in patients with connective tissue diseases or may be iatrogenic (Fig. 9.12). Non-iatrogenic dissections usually require surgical revascularization, but medical therapy and percutaneous transluminal coronary angioplasty have also been used [26].

9.6 Extrinsic Compression

Any kind of mass formed around aortic root can compress the coronary artery externally, resulting in severe luminal

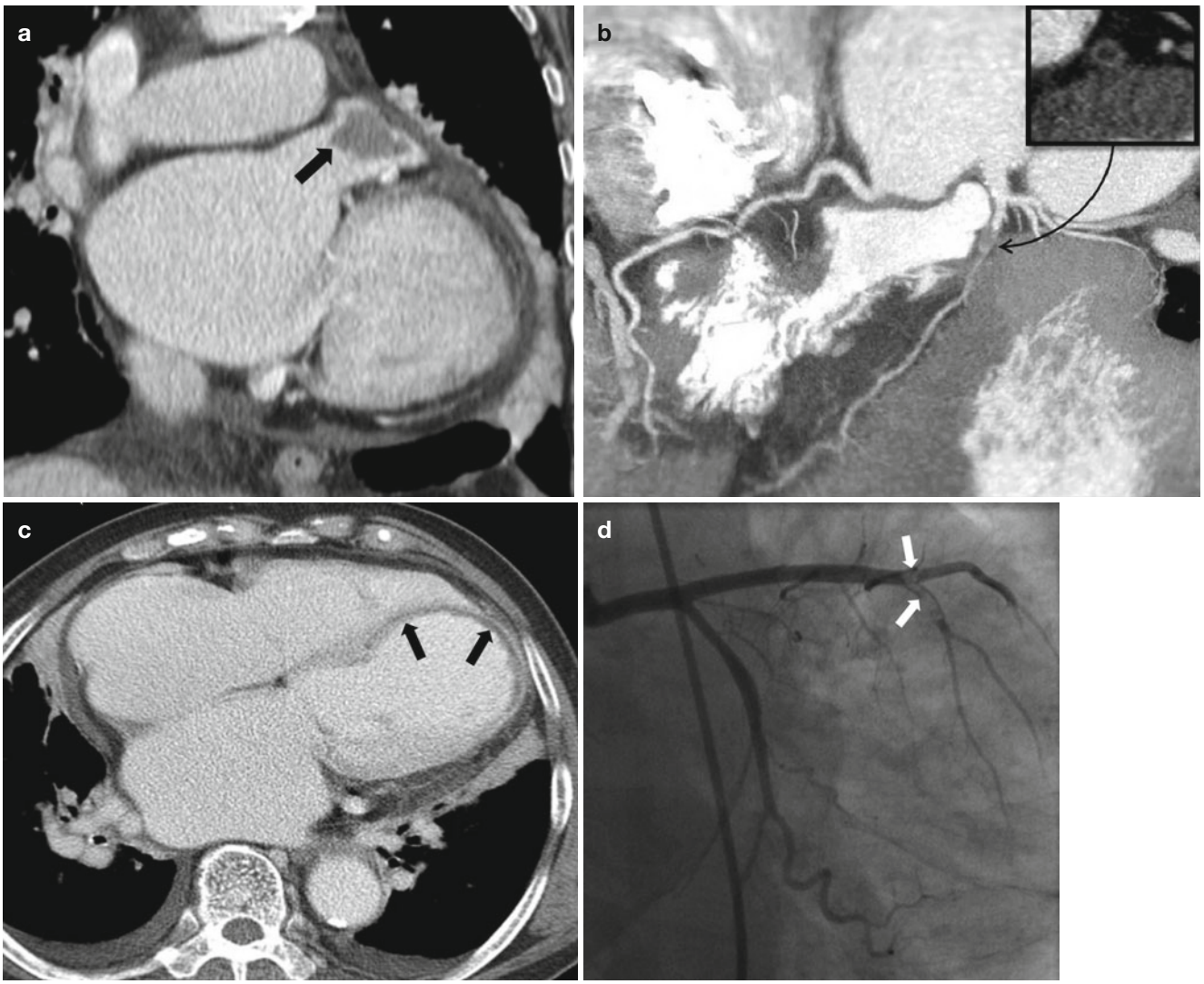

Fig. 9.10 An 83-year-old woman with atrial fibrillation and ST-elevated myocardial infarction as a result of embolic occlusion of the coronary artery by left atrial appendage thrombus (Courtesy of Jeong A Kim, Bundang Seoul National University Hospital). (**a**) Oblique coronal image shows hypoattenuating thrombus at the left atrial appendage (*arrow*). (**b**) Curved multiplanar reformation image shows total occlusion of the left anterior descending artery by hypoattenuating thrombus with enhanced wall. (**c**) Four-chamber image shows corresponding myocardial hypoenhancement (*arrows*) in the basal to mid anterior and septal wall, which is compatible with acute myocardial infarction. (**d**) Invasive coronary angiography image confirms focal filling defect (*arrows*) indicating emboli at the mid left anterior descending artery and the diagonal branch

narrowing and progressive myocardial ischemia. Acute hematoma or pseudoaneurysm due to aortic rupture (Figs. 9.13 and 9.14) or infective endocarditis-related perivalvular pseudoaneurysm or abscess can be possible causes.

9.7 Cardiac Tumor with Encasement of Coronary Arteries

Cardiac tumor is rare, with an estimated cumulative prevalence of 0.002–0.3 % at autopsy. Metastatic cardiac tumor is approximately 40 times more common than primary cardiac tumors. The majority of primary cardiac tumor is benign, and benign cardiac tumors manifest as intracavitary, mural, or epicardial focal masses, whereas malignant tumors show infiltrative growth and can invade adjacent coronary arteries [1, 27]. The mechanism of refractory angina is that an intracavitary tumor, especially myxoma, causes thrombus or tumor fragments to embolize into the coronary artery (Fig. 9.10), whereas myocardial or extracardiac tumors extrinsically compress the coronary artery (Fig. 9.15) [1, 27].

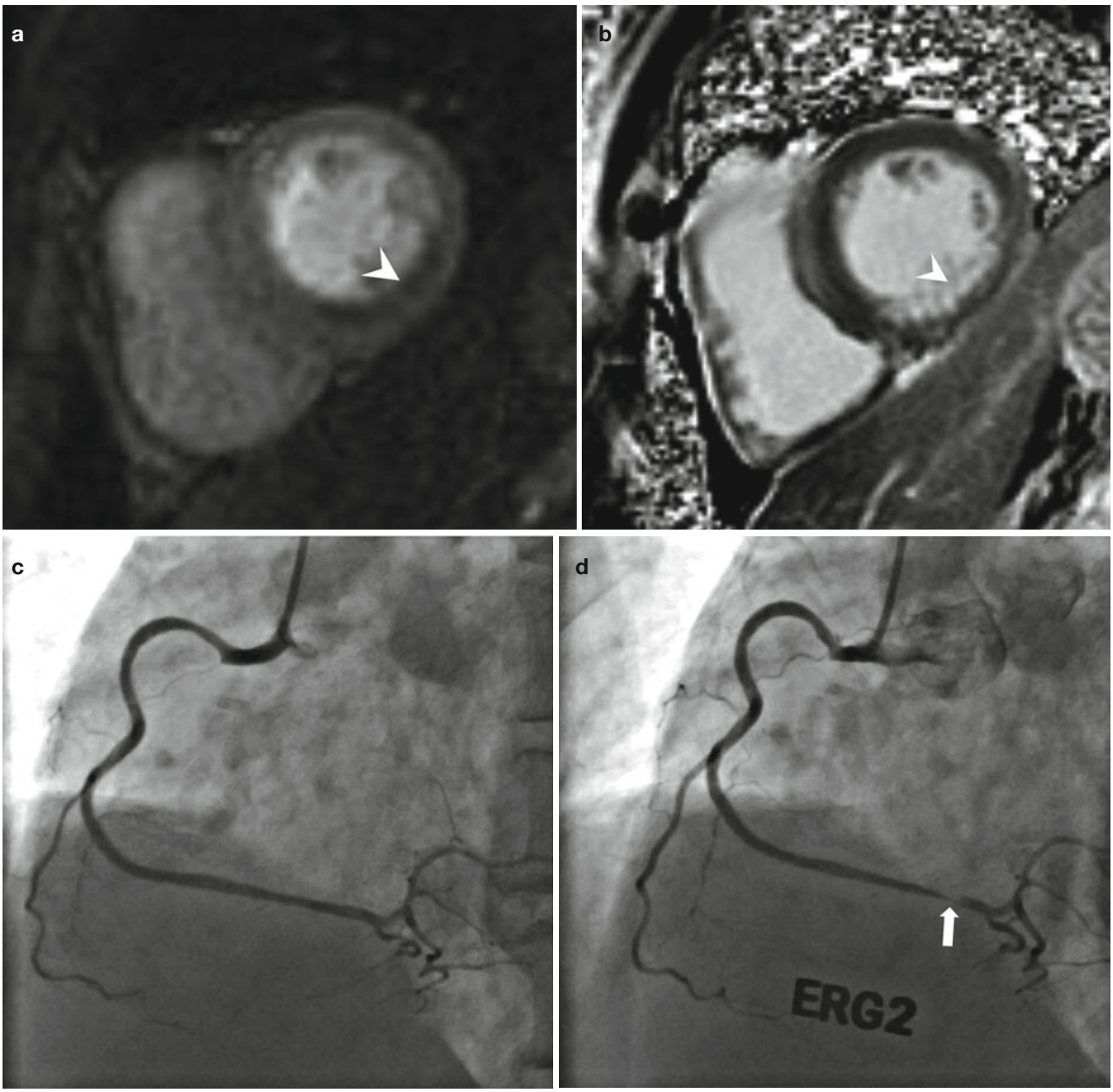

Fig. 9.11 A 61-year-old man with acute chest pain (Courtesy of Hyun Ju Seon, Chonnam National University Hospital). (**a**) *Resting* perfusion MR image shows subendocardial perfusion defect (*arrowhead*) at mid inferoseptal and inferior wall, indicating the territory of the right coronary artery. (**b**) Ten-minute delayed MR image using phase-sensitive inversion recovery sequence after administration of gadolinium contrast shows subendocardial delayed enhancement at the same area (*arrowhead*), indicating myocardial infarction. (**c**) Invasive coronary angiography image shows no stenosis at the right coronary artery. Invasive coronary angiography image obtained after intracoronary administration of ergonovine shows provoked high-grade luminal stenosis (*arrow*) at the distal right coronary artery that was completely relieved by intracoronary administration of nitroglycerin

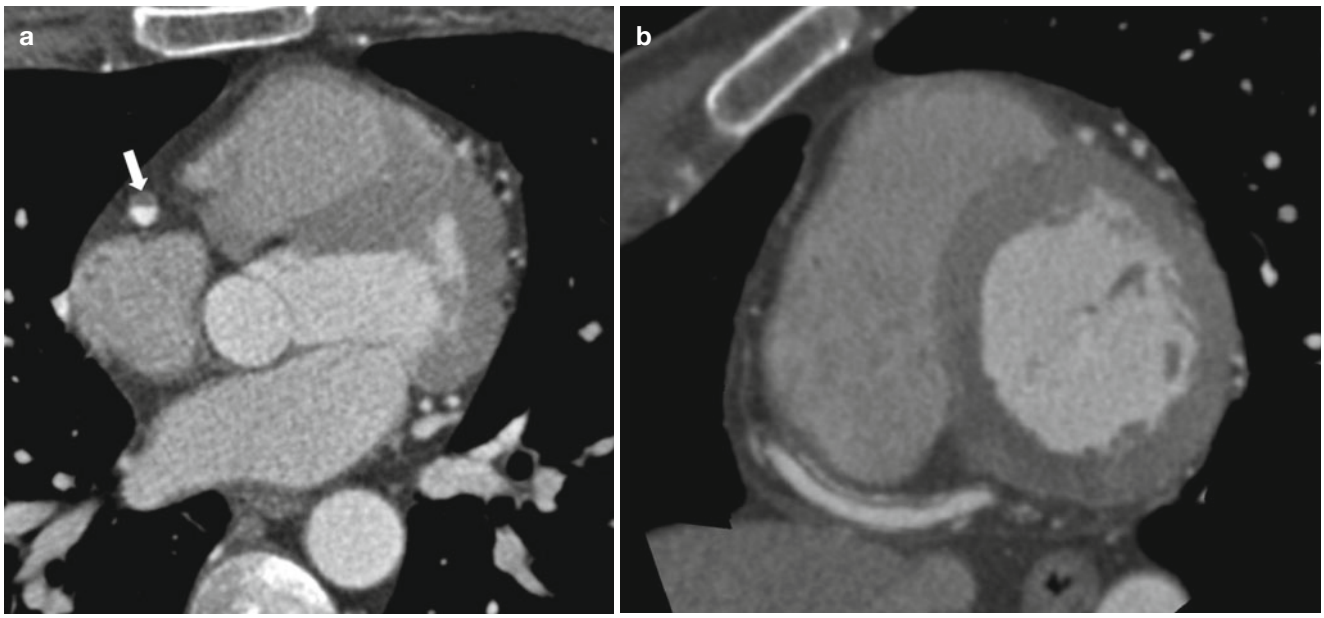

Fig. 9.12 A 46-year-old man with an iatrogenic coronary artery dissection. (**a**) The coronary CT angiography after failed percutaneous coronary artery intervention shows coronary artery dissection and an intimal flap in the right coronary artery. The false lumen (*arrow*) is partly thrombosed. (**b**) The intimal flap extends to the distal right coronary artery

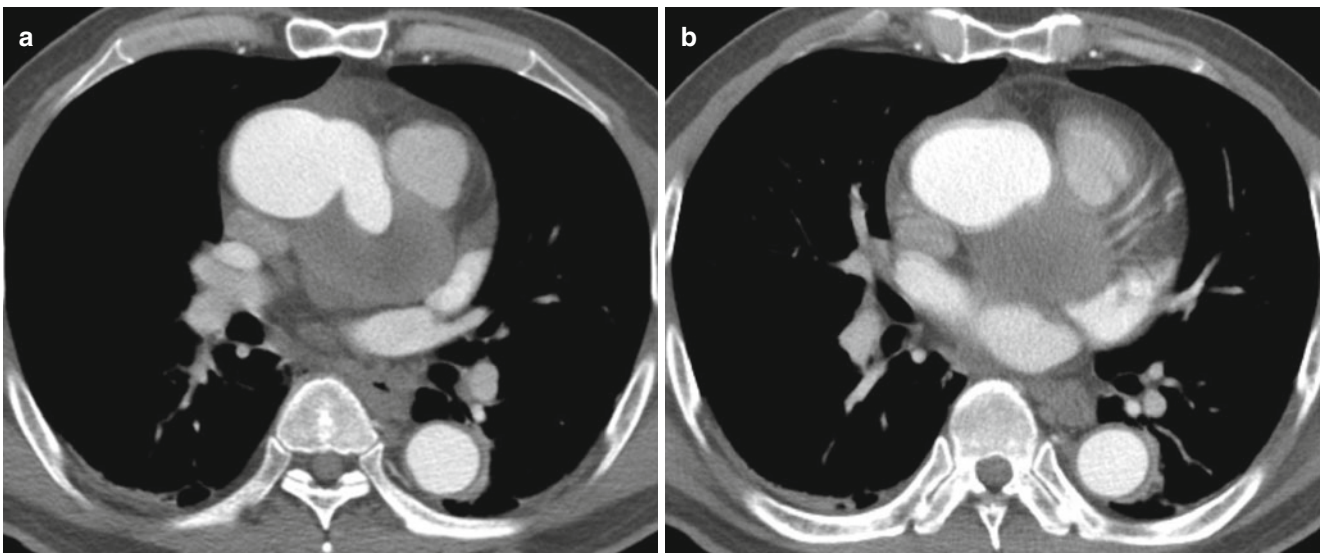

Fig. 9.13 A 66-year-old man with acute myocardial infarction due to extrinsic compression of the coronary artery by pseudoaneurysm. (**a**) Transaxial image shows a large pseudoaneurysm with surrounding hematoma at the ascending aorta. This is a contained rupture of the ascending aorta with a large defect at the lateral wall. (**b**) Transaxial image shows extrinsic compression of the left anterior descending artery and the diagonal branches by surrounding hematoma. Transaxial image shows corresponding myocardial hypoenhancement (*arrowheads*) at the apical anterior and septal wall of the left ventricle indicating acute myocardial infarction. The patient underwent emergent ascending aorta replacement. Pathologic report revealed aortic rupture caused by a penetrating atherosclerotic ulcer

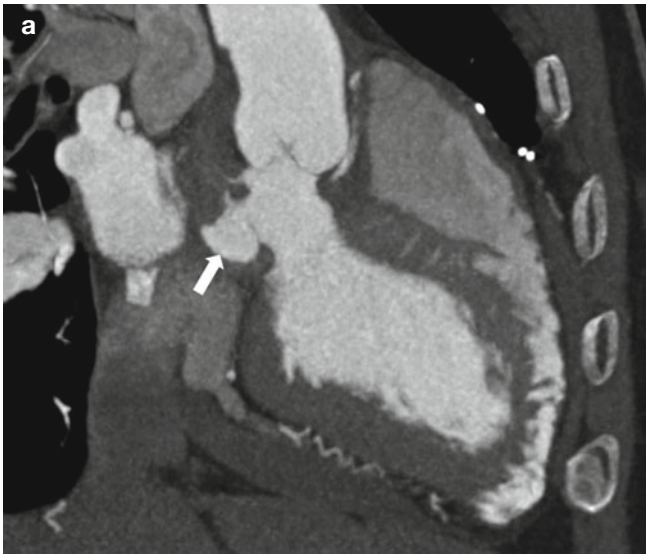

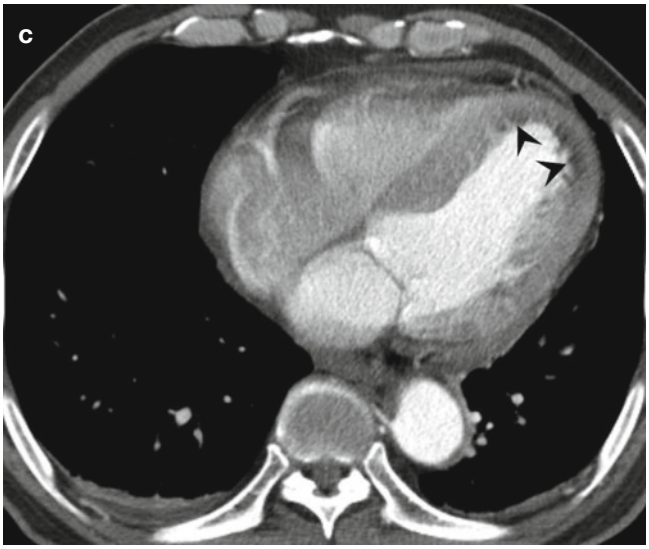

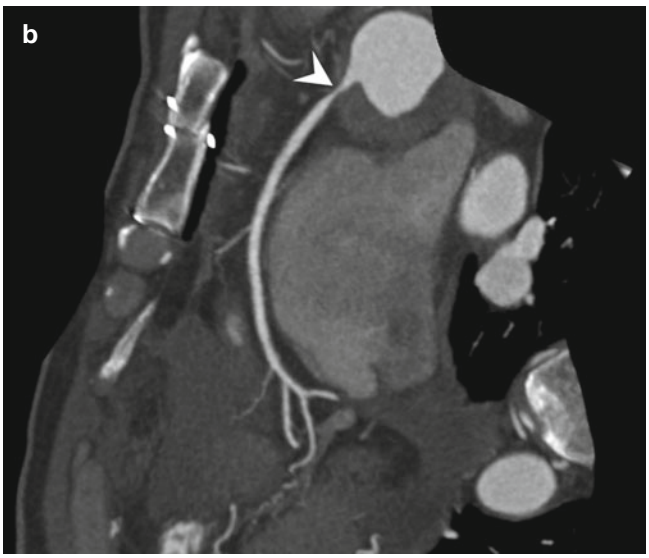

Fig. 9.14 A 54-year-old man with Behcet's disease. (**a**) Maximum intensity projection image shows pseudoaneurysm (*arrow*) involving the posterior wall of the left ventricular outflow tract. Surrounding hematoma is also seen extending to the ascending aorta. (**b**) Curved multiplanar reformation of the right coronary artery shows focal stenosis (*arrowhead*) of the proximal segment due to surrounding hematoma

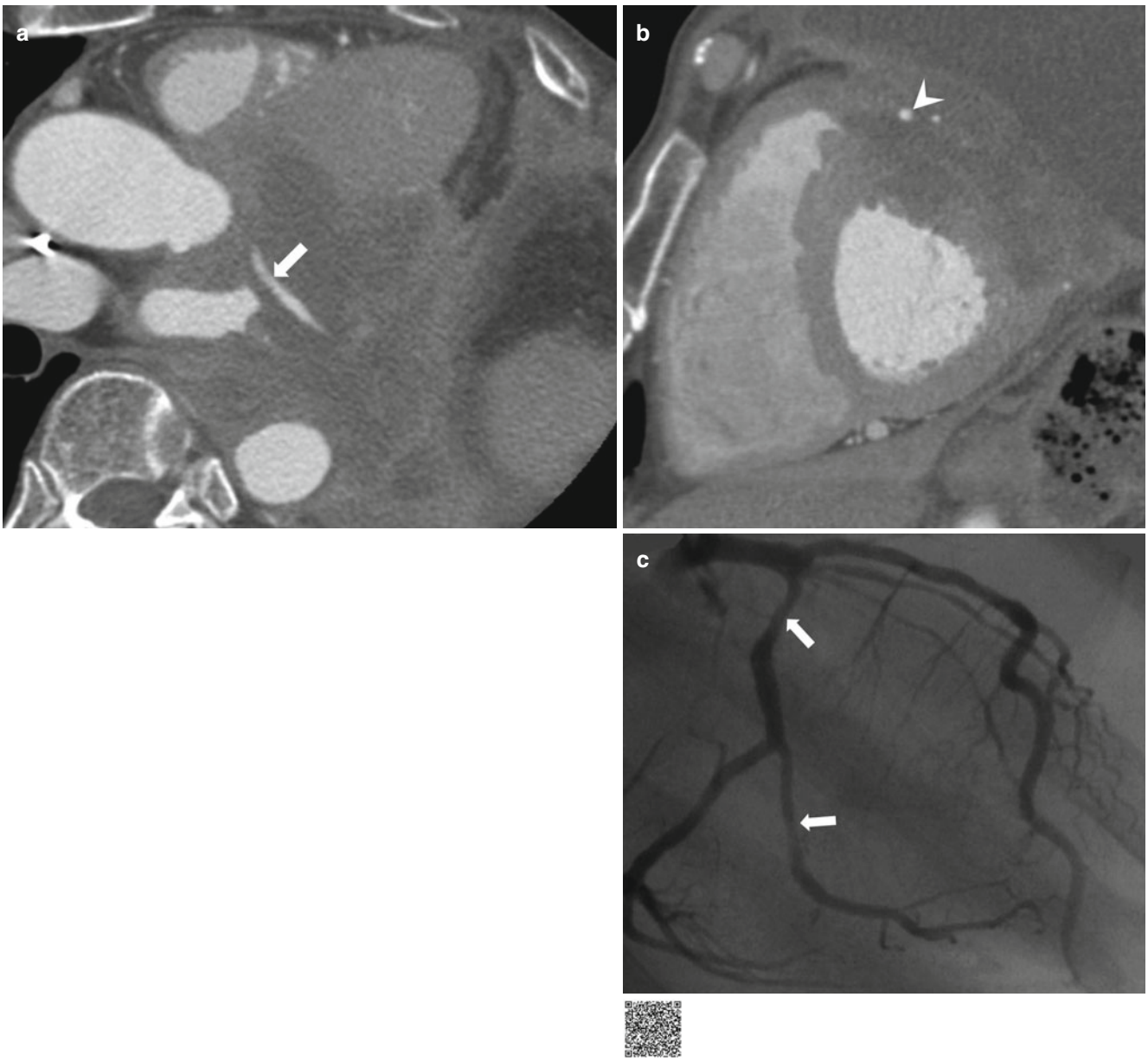

Fig. 9.15 A 62-year-old man with acute chest pain (Courtesy of Hyun Ju Seon, Chonnam National University Hospital). This patient had a history of left pneumonectomy due to squamous cell lung cancer. (**a**) Oblique transaxial image shows infiltrative and irregular hypoattenuating mass invading to the left heart, suggestive of recurred lung cancer. Note that the left circumflex (*arrow*) artery was entirely encased by the mass. (**b**) Short-axis image clearly shows a thorough encasement of the left anterior descending coronary artery (*arrowhead*) and the ramus intermedius by recurred lung cancer. (**c**) Invasive coronary angiogram shows long segmental fixed luminal narrowing and irregularity of the left circumflex artery (*arrows*) (http://extras.springer.com/2015/978-3-642-36396-2)

References

1. Kim JA, Chun EJ, Choi SI, Kang JW, Lee J, Lim TH. Less common causes of disease involving the coronary arteries: MDCT findings. AJR Am J Roentgenol. 2011;197(1):125–30.
2. Johnson PT, Fishman EK. CT angiography of coronary artery aneurysms: detection, definition, causes, and treatment. AJR Am J Roentgenol. 2010;195(4):928–34.
3. Waller BF, Fry ET, Hermiller JB, Peters T, Slack JD. Nonatherosclerotic causes of coronary artery narrowing – part III. Clin Cardiol. 1996;19(8):656–61.
4. Syed M, Lesch M. Coronary artery aneurysm: a review. Prog Cardiovasc Dis. 1997;40(1):77–84.
5. Diaz-Zamudio M, Bacilio-Perez U, Herrera-Zarza MC, Meave-Gonzalez A, Alexanderson-Rosas E, Zambrana-Balta GF, Kimura-Hayama ET. Coronary artery aneurysms and ectasia: role of coronary CT angiography. Radiographics. 2009;29(7):1939–54.

6. Cohen P, O'Gara PT. Coronary artery aneurysms: a review of the natural history, pathophysiology, and management. Cardiol Rev. 2008;16(6):301–4.
7. Markis JE, Joffe CD, Cohn PF, Feen DJ, Herman MV, Gorlin R. Clinical significance of coronary arterial ectasia. Am J Cardiol. 1976;37(2):217–22.
8. Newburger JW, Takahashi M, Gerber MA, Gewitz MH, Tani LY, Burns JC, Shulman ST, Bolger AF, Ferrieri P, Baltimore RS, et al. Diagnosis, treatment, and long-term management of Kawasaki disease: a statement for health professionals from the Committee on Rheumatic Fever, Endocarditis and Kawasaki Disease, Council on Cardiovascular Disease in the Young, American Heart Association. Circulation. 2004;110(17):2747–71.
9. Sugimura T, Kato H, Inoue O, Fukuda T, Sato N, Ishii M, Takagi J, Akagi T, Maeno Y, Kawano T, et al. Intravascular ultrasound of coronary arteries in children. Assessment of the wall morphology and the lumen after Kawasaki disease. Circulation. 1994;89(1):258–65.
10. Matsunaga N, Hayashi K, Sakamoto I, Ogawa Y, Matsumoto T. Takayasu arteritis: protean radiologic manifestations and diagnosis. Radiographics. 1997;17(3):579–94.
11. Park JH, Chung JW, Im JG, Kim SK, Park YB, Han MC. Takayasu arteritis: evaluation of mural changes in the aorta and pulmonary artery with CT angiography. Radiology. 1995;196(1):89–93.
12. Matsubara O, Kuwata T, Nemoto T, Kasuga T, Numano F. Coronary artery lesions in Takayasu arteritis: pathological considerations. Heart Vessels Suppl. 1992;7:26–31.
13. Korbet SM, Schwartz MM, Lewis EJ. Immune complex deposition and coronary vasculitis in systemic lupus erythematosus. Report of two cases. Am J Med. 1984;77(1):141–6.
14. Matayoshi AH, Dhond MR, Laslett LJ. Multiple coronary aneurysms in a case of systemic lupus erythematosus. Chest. 1999;116(4):1116–8.
15. McKeown F. Dissecting aneurysm of the coronary artery in arachnodactyly. Br Heart J. 1960;22(3):434–6.
16. Onoda K, Tanaka K, Yuasa U, Shimono T, Shimpo H, Yada I. Coronary artery aneurysm in a patient with Marfan syndrome. Ann Thorac Surg. 2001;72(4):1374–7.
17. Savunen T, Inberg M, Niinikoski J, Rantakokko V, Vanttinen E. Composite graft in annulo-aortic ectasia. Nineteen years' experience without graft inclusion. Eur J Cardiothorac Surg. 1996;10(6):428–32.
18. Gulati GS, Gupta A, Juneja R, Saxena A. Ectatic coronary arteries in Noonan syndrome. Tex Heart Inst J. 2011;38(3):318–9.
19. Pena E, Nguyen ET, Merchant N, Dennie C. ALCAPA syndrome: not just a pediatric disease. Radiographics. 2009;29:553–65.
20. Kim H, Park EA, Lee W, Chung JW, Park JH. Multiple cerebral and coronary aneurysms in a patient with left atrial myxoma. Int J Cardiovasc Imaging. 2012;28 Suppl 2:129–32.
21. Waller BF, Fry ET, Hermiller JB, Peters T, Slack JD. Nonatherosclerotic causes of coronary artery narrowing – part II. Clin Cardiol. 1996;19(7):587–91.
22. Mirza A. Myocardial infarction resulting from nonatherosclerotic coronary artery diseases. Am J Emerg Med. 2003;21(7):578–84.
23. Yasue H, Nakagawa H, Itoh T, Harada E, Mizuno Y. Coronary artery spasm – clinical features, diagnosis, pathogenesis, and treatment. J Cardiol. 2008;51(1):2–17.
24. Yasue H, Kugiyama K. Coronary spasm: clinical features and pathogenesis. Intern Med. 1997;36(11):760–5.
25. Tweet MS, Hayes SN, Pitta SR, Simari RD, Lerman A, Lennon RJ, Gersh BJ, Khambatta S, Best PJ, Rihal CS, et al. Clinical features, management, and prognosis of spontaneous coronary artery dissection. Circulation. 2012;126(5):579–88.
26. Kruskal JB, Hartnell GG. Nonatherosclerotic coronary artery disease: more than just stenosis. Radiographics. 1995;15(2):383–96.
27. Aggarwala G, Iyengar N, Horwitz P. Cardiac mass presenting as ST-elevation myocardial infarction: case report and review of the literature. J Invasive Cardiol. 2008;20(11):628–30.

Part II

Ischemic Heart Disease

Evaluation of Myocardial Ischemia Using Perfusion Study

10

Joon-Won Kang and Sung Min Ko

Contents

Abstract

Limitations of CT angiography and invasive coronary angiography are that their ability to distinguish the physiologic effects of coronary artery stenosis and to detect myocardial ischemia is quite low. Further evaluation of myocardial function such as radioisotope scan or stress function tests is often required after identifying coronary artery stenosis lesions that also requires costs and additional radiation exposure. With the advance of CT and MRI, myocardial perfusion is easily and reliably assessed. Myocardial blood flow and volume can be calculated using dynamic scan. The scan protocols, how to assess the perfusion study using CT and MR, and artifacts and limitations of CT and MR perfusion study will be described and illustrated.

10.1 Protocol and Assessment of CT Perfusion

- *Backgrounds*
  - Limitations of CT angiography and invasive coronary angiography are that their ability to distinguish the physiologic effects of coronary artery stenosis and to detect myocardial ischemia is quite low.
  - Further evaluation of myocardial function such as radioisotope scan or stress function tests is often required after identifying coronary artery stenosis lesions that also requires costs and additional radiation exposure.
  - Iodine contrast media used for CT has unique characteristics to attenuate x-rays proportional to its concentration.
  - One of the important principles in perfusion study must be performed during the early portion of first-pass circulation, as the contrast media is predominantly located intravascularly. Extravascular iodine concentration exceeds the intravascular iodine concentration approximately 1 min after injection.

Electronic supplementary material Supplementary material is available in the online version of this chapter at 10.1007/978-3-642-36397-9_10.

J.-W. Kang
Department of Radiology and Research Institute of Radiology, Asan Medical Center, University of Ulsan College of Medicine, Seoul, Republic of Korea
e-mail: joonwkang@naver.com

S.M. Ko, MD (✉)
Department of Radiology, Konkuk University Hospital, Seoul, Republic of Korea
e-mail: ksm9723@yahoo.co.kr

T.-H. Lim (ed.), *Practical Textbook of Cardiac CT and MRI*,
DOI 10.1007/978-3-642-36397-9_10, © Springer-Verlag Berlin Heidelberg 2015

- *Patient preparation and scan protocol*
  - Patients are advised to avoid caffeine, a nonselective competitive adenosine receptor antagonist, 24 h before examination.
  - Intravenous access is performed in both antecubital veins: one for adenosine or other vasodilator infusion and one for the contrast administration.
  - Using beta-blockers for CT perfusion study such as oral metoprolol are optional for heart rate control. Although using beta-blockers can mask the ischemia in vasodilator stress perfusion study, recent studies have reported no observed effect on coronary flow reserve in the study.
  - The scan protocol comprises a stress- and a rest-phase acquisition. Stress-first-and-rest-second protocol has the advantage of increased sensitivity to myocardial ischemia in stress-phase scan, and it allows administration of nitrates for subsequent rest scan, which may be contraindicated if the rest scan was performed first. Rest first and stress second protocol has the advantage that second-stress scan can be avoided and subsequently reduce radiation exposure; stress scan will be only performed when moderate to severe coronary artery stenosis is identified on the rest scan.
  - More than 10 min time interval between two acquisitions is necessary, and 20 min or more time interval is recommended. When the time interval is short, the contrast used in the first phase may still remain in the myocardium at the time of the second acquisition, which may decrease the sensitivity for detecting myocardial ischemia and infarction.

10.1.1 Snapshot or Helical CT Perfusion

- Scout images are acquired for scan positioning. Generally, scan range is from the carina to the heart base.
- ECG pulsing is used according to the heart rate of the patient. In the subject with a heart rate <65 bpm, mid-diastolic acquisition between 60 and 80 % of R-R interval is possible. In the subject with a heart rate >65 bpm, which is frequently seen during the stress scan, multi-segmental reconstruction or ECG pulsing targeting 20–80 % of R-R interval must be considered.
- For the stress perfusion imaging, intravenous adenosine infusion at the rate of 140 μg/kg/min is performed, and intravenous contrast media of 60–70 mL is delivered at the rate of 4–5 mL/s after 4–5 min from start of adenosine infusion.
- For the rest scan, intravenous contrast media of 60–70 mL is delivered at the rate of 4–5 mL/s without adenosine infusion. Nitrate can be administered before the rest scan when the stress scan is performed before the rest scan.
- Start of scan is timed to occur 2–4 s after peak contrast enhancement of the ascending aorta determined by test bolus of 10–15 mL of contrast media at the rate of 4–5 mL/s followed by a 20 mL saline flush at the same rate (test bolus method) or 8–10 s after the CT number of the ascending aorta reaches 100–150 HU (bolus tracking method).
- Image reconstruction of both stress and rest scan is performed by reconstruction of multiple phases: best systolic and diastolic phases for the "least" cardiac motion are recommended, or every 3–5 % intervals of cardiac phases are recommended. A reconstruction algorithm that can reduce beam-hardening artifact is recommended (FC03 in 320-detector CT by Toshiba, B10f by Siemens, smooth kernel by GE) (Fig. 10.1).

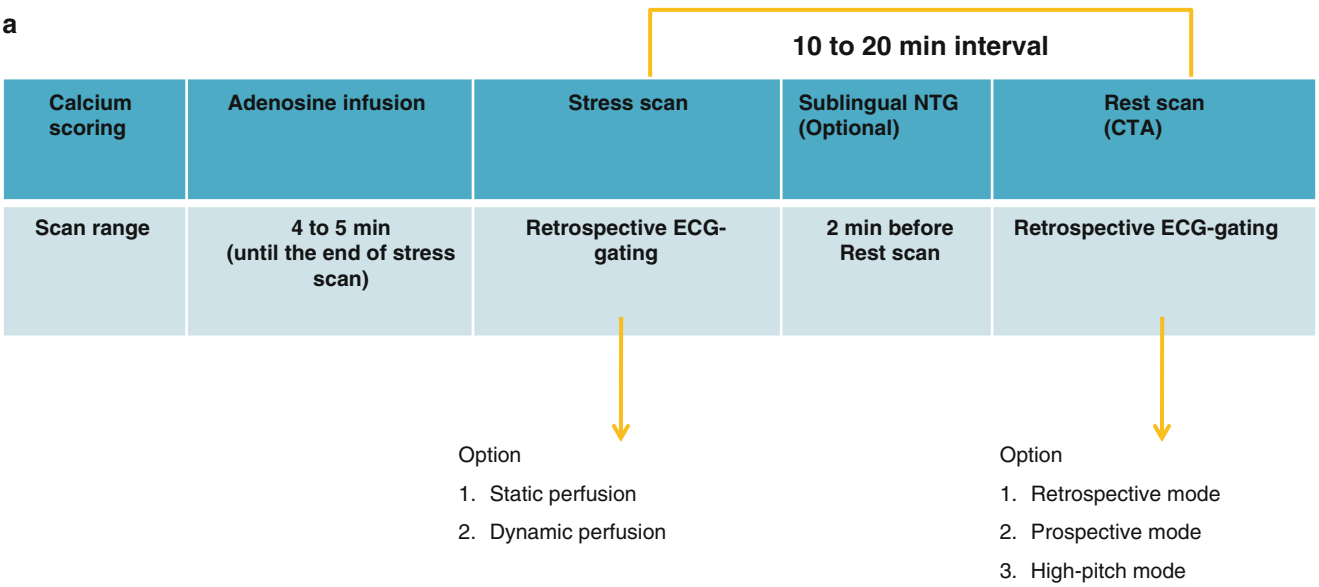

Fig. 10.1 CT imaging protocol. (**a**) "Stress-first" protocol is the stress scan that is acquired followed by the rest scan, and the nitrate can be administered before the rest scan. (**b**) "Rest-first" protocol is the rest scan that is acquired followed by the stress scan; the nitrate must not be administered before the stress scan

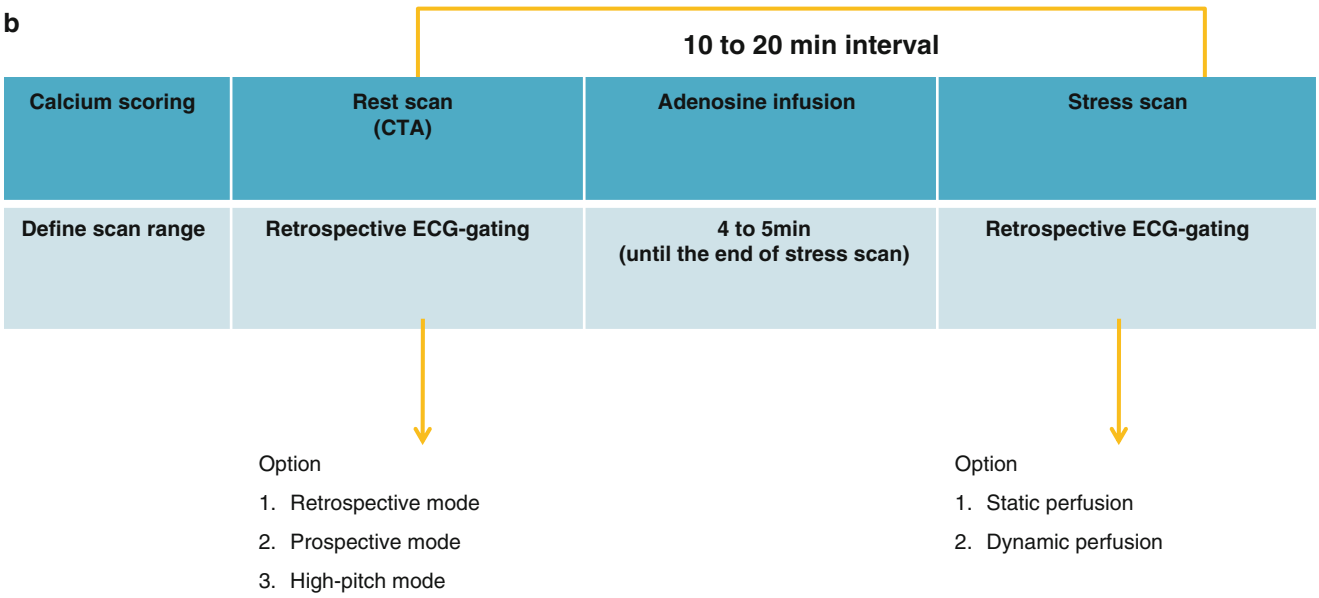

Fig. 10.1 (continued)

10.1.2 Dynamic CT Perfusion

- Dynamic perfusion scan can be performed by serially recording the kinetics of iodinated contrast media in the blood pool and myocardium for stress and/or rest scan.
- Approximately 30–40 serial scans from the injection of the iodinated contrast media are performed in every or every other heart beats.
- Until now, two different scan modes are developed. One is that the scan table is stationary during the dynamic study using 320-detector CT, and the other is that the scan table is in shuttle mode during the study using the dual-source CT.
- Time-attenuation curves (TACs) of the myocardium, the left ventricular cavity, and the aorta can be acquired. Thus, myocardial blood flow (MBF) and volume (MBV) can be derived from TACs using the mathematical model (Figs. 10.2 and 10.5).

10.1.3 Dual-Energy CT (DECT) Perfusion

- DECT is based on the principle that tissues in the body and intravascular iodinated contrast media have unique spectral characteristics to the x-rays of different energy levels.
- After processing of high-energy and low-energy data (usually 140 kVp for high-energy and 80 kVp for low-energy data), iodine content in the myocardium is detected using color-coded maps, which can provide additional information beyond the usual CT attenuation.
- The temporal resolution of DECT is increased to 165 ms (using the dual-source CT) and 250 ms (using the fast tube-power switch mode CT) until now, and thus, DECT is susceptible to motion artifact (Fig. 10.3).

10.1.4 Assessment of CT Perfusion

10.1.4.1 Qualitative Analysis

- Visual assessment of CT perfusion study has been used in most clinical studies.
- Simultaneous visualization of both rest and stress images for regions with hypo-attenuated myocardium compared with normal myocardium is necessary (see Sect. 10.3).
- Narrow setting of window width and level (window width, 200–300; window level, 100–150) and the slice thickness of 5–10-mm is recommended for the detection of subtle contrast difference of the myocardium of CT perfusion (Fig. 10.4).
- Short-axis images are widely used for the detection of the perfusion defect; additional long-axis images can provide information.
- Standard 17-segmental model of the left ventricular myocardium suggested by the American Heart Association is used for the location and scoring of the myocardial perfusion status.
- Each myocardial segment is scored for the presence or absence of the perfusion defect and graded as transmural if the perfusion defect involves ≥50 % of thickness or non-transmural. Reversibility is also graded as reversible, partially reversible, and irreversible or fixed.
- To ensure the perfusion defect is detected, images from multiple phases must be reviewed. Motion artifacts and beam-hardening artifacts can mimic perfusion defect (see Sect. 10.4.1 of this chapter).

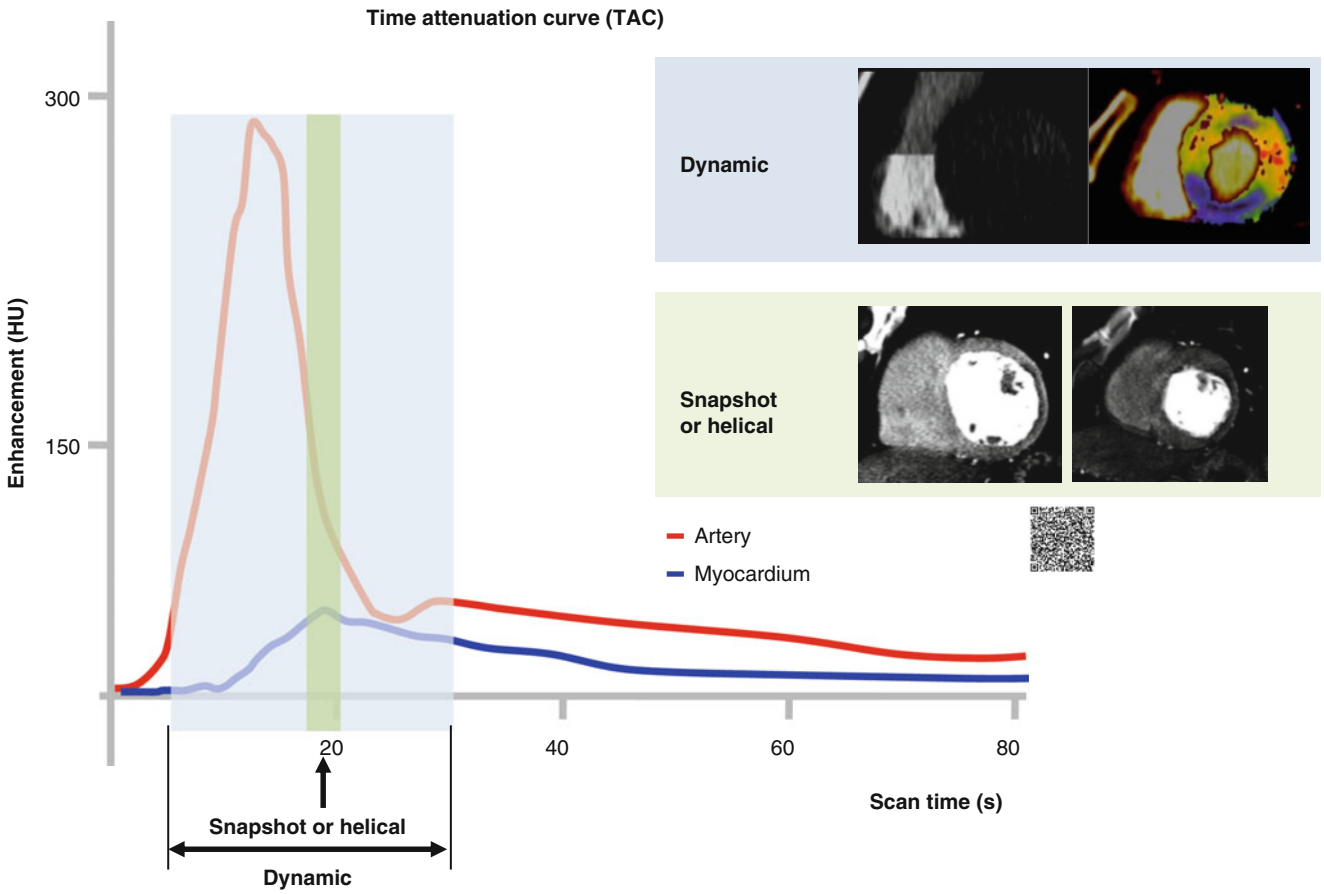

Fig. 10.2 Comparison of dynamic and snapshot or helical study. In dynamic study, serial scans are performed approximately 30 s. In the snapshot or helical study, scan was only performed during the peak enhancement of the myocardium (http://extras.springer.com/2015/978-3-642-36396-2 – cine image of the myocardium)

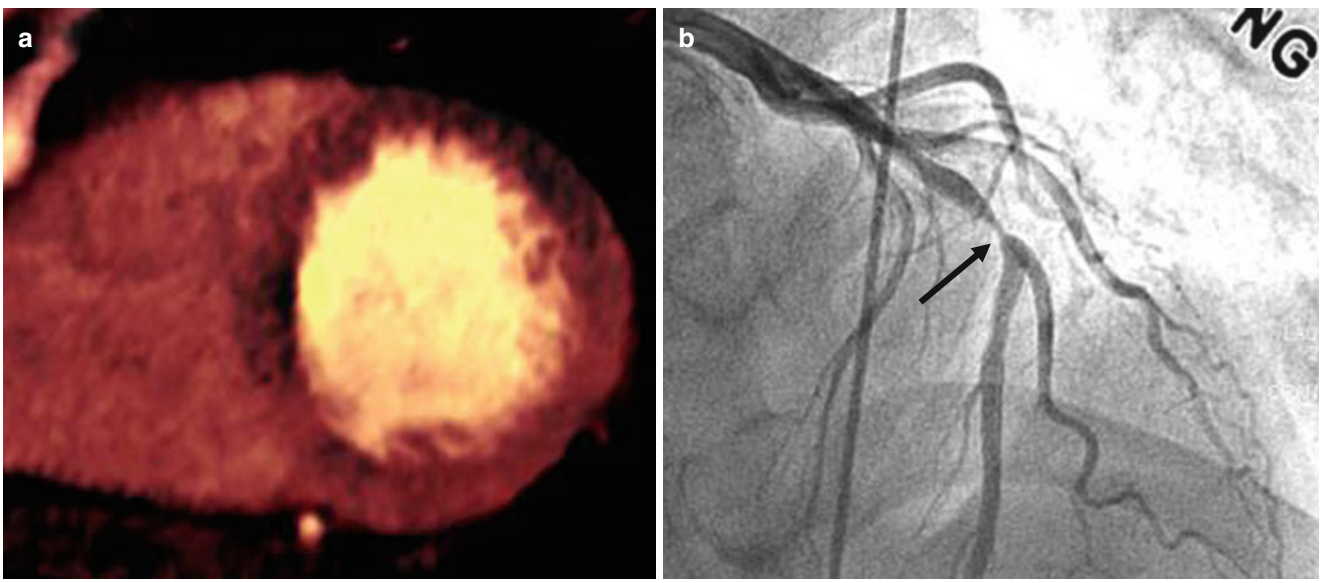

Fig. 10.3 Color-coded maps using DECT perfusion. Color-coded maps using DECT perfusion show defect of the anteroseptal, anterior wall, and anterolateral wall. (**a**) Coronary angiography shows severe stenosis of mid-LAD (**b**) (*arrow*)

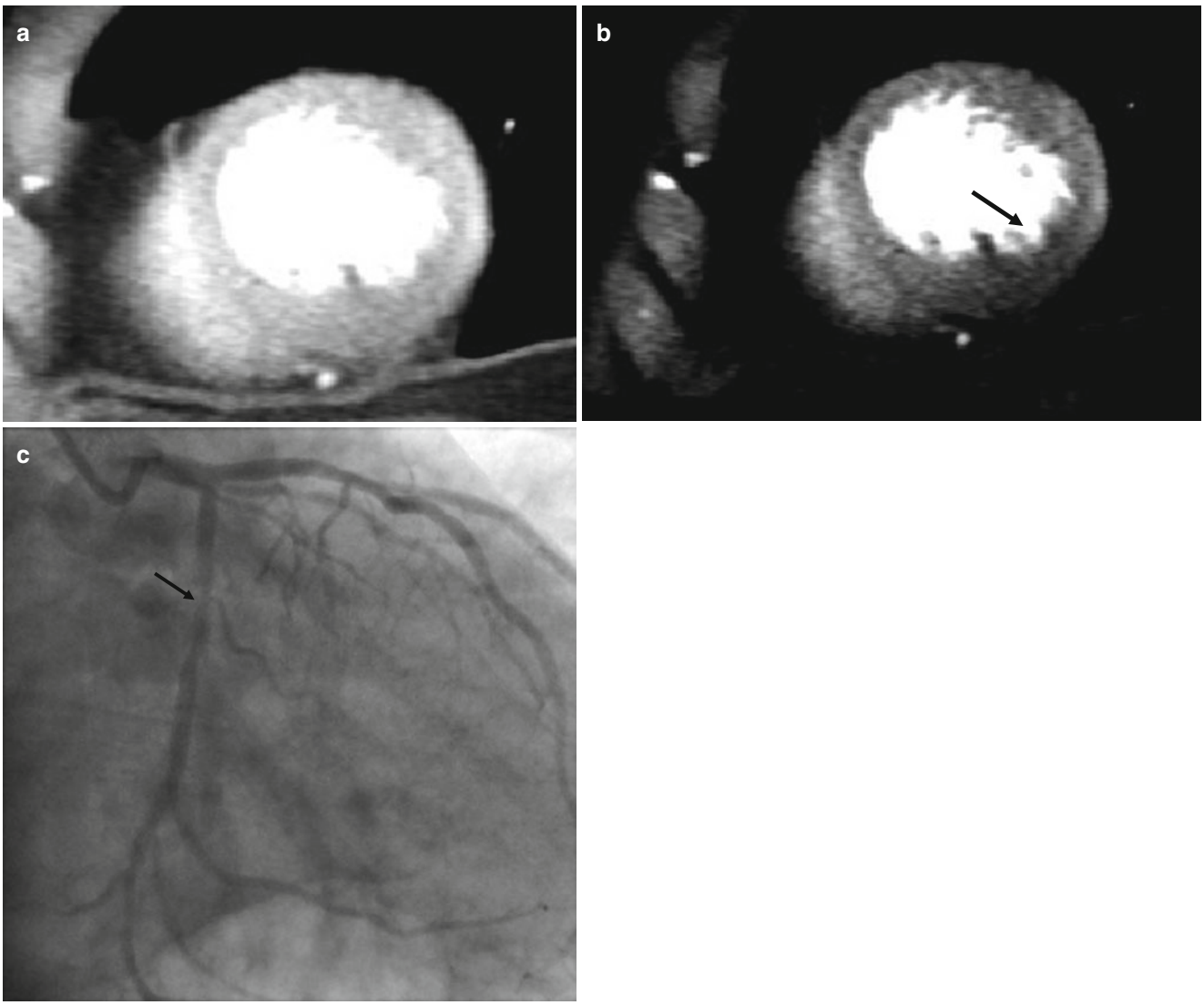

Fig. 10.4 Setting of window width/level. (**a**) Window width 350/level 35. (**b**) Window width 240/level 150. Perfusion defect on the apical inferior wall is well detected on the narrowed window and width images (*arrow*). (**c**) Severe stenosis at the proximal end of stent of left circumflex artery is seen in the patient (*arrow*)

- Finally, correlation with the coronary artery lesions on the rest scan is mandatory to match the coronary artery stenosis and the perfusion defect (Fig. 10.5).

10.1.4.2 Quantitative Analysis

- Myocardial blood flow and myocardial blood volume can be derived by the time-attenuation curves (TACs) of the myocardium, the left ventricular cavity, and the aorta using the dynamic CT perfusion study.
- Various mathematical models may be used for quantitative analysis, and more validation and clinical evidences are required (Fig. 10.6).

10.2 Protocol and Assessment of MR Perfusion

- *Backgrounds*
  - MRI has the advantage of no radiation exposure; thus, dynamic scan is possible that can be easily used for quantitative assessment.
  - One of the important principles in perfusion study must be performed during the early portion of first-pass circulation, as the contrast media is predominantly located intravascularly.

Step 1	Step 2	Step 3	Step 4	Step 5
Rest scan interpretation	**Image processing**	**Quality assess**	**Image interpretation**	**Correlation with rest scan**
• Coronary artery stenosis and plaque analysis	• Best phases of motionless myocardium • Epi-and endocardialcontour (for dynamic study)	• Motion artifact • Beam hardening • Cone-beam • Stair-step • Image noise	• Transmurality (≧50 % or <50 %) • Reversibility • Myocardial thinning • Simultaneous vision of both stress and rest scans	Match perfusion defect and coronary artery lesion

Fig. 10.5 Diagram of the flow chart of qualitative assessment of CT perfusion study

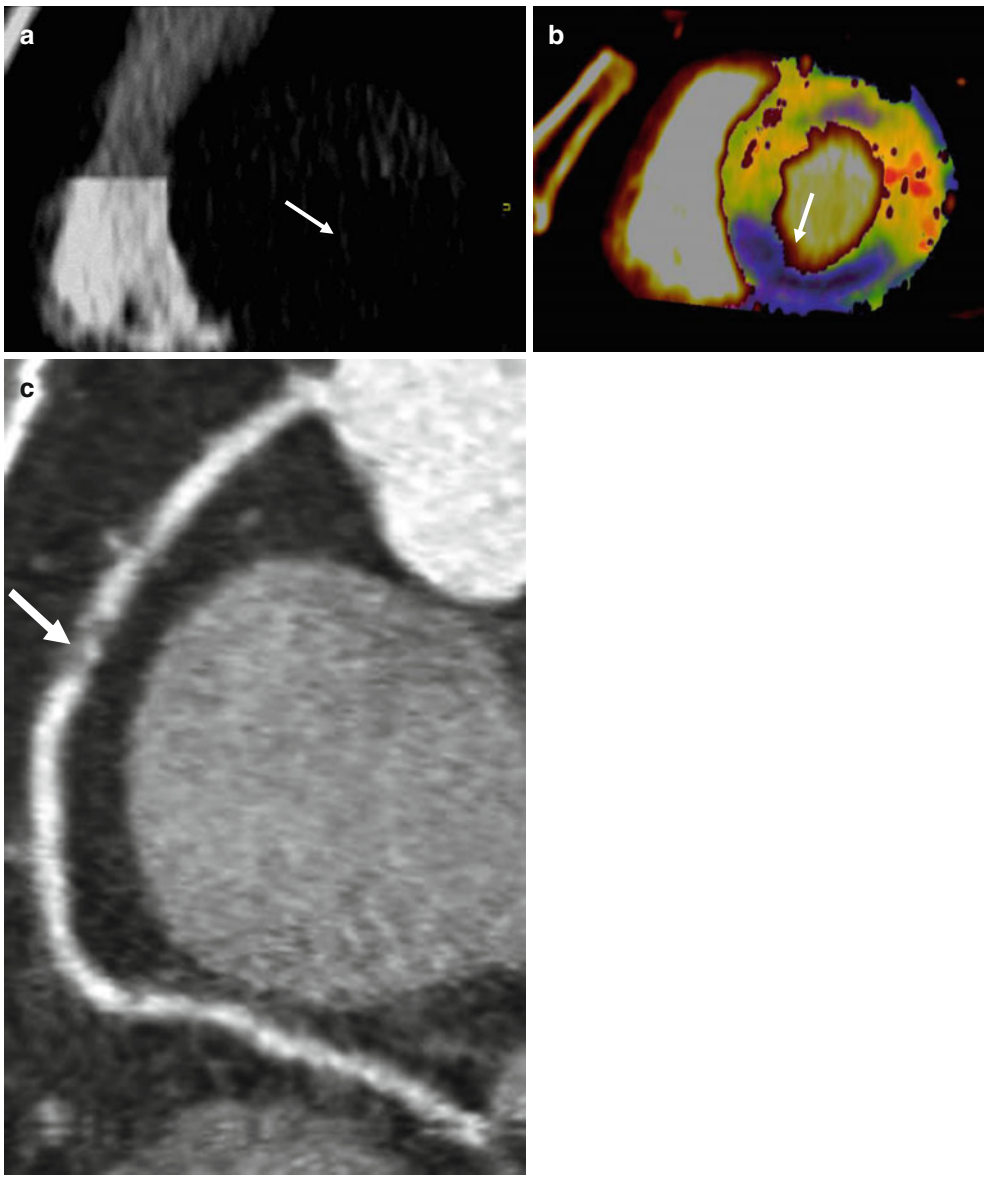

Fig. 10.6 (**a**) Dynamic perfusion scan [(**a**) and QR code at Fig. 10.2] and the derived myocardial blood flow (MBF) map show the impaired MBF of the inferior wall of the left ventricle (*arrow*) (**b**). CT coronary angiography also shows the severe stenosis of the right coronary artery (*arrow*) (**c**)

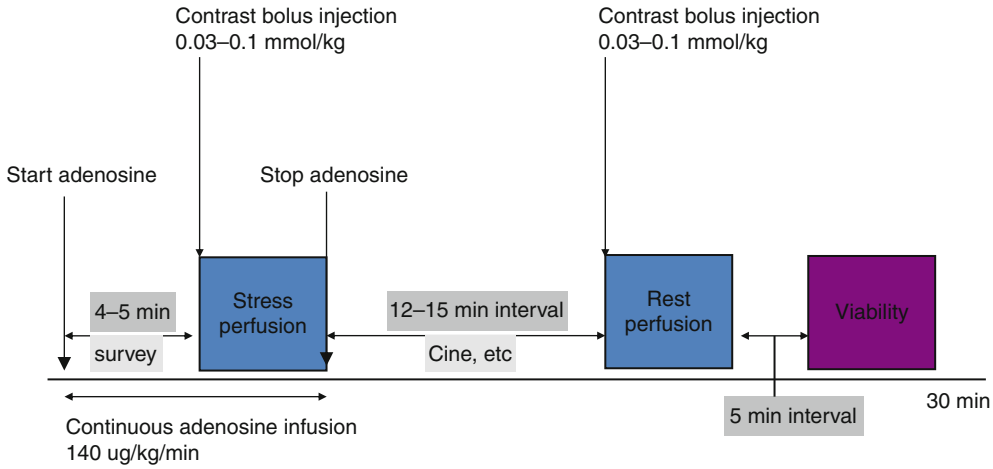

Fig. 10.7 Diagram for perfusion MR study

10.2.1 Protocols

- *Patient preparation*
  - Patients are advised to avoid caffeine, a nonselective competitive adenosine receptor antagonist, 24 h before examination.
  - Intravenous access is performed in both antecubital veins: one for adenosine or other vasodilator infusion and one for the contrast administration.
  - The scan protocol comprises a stress- and a rest-phase acquisition. Since stress-first-and-rest-second protocol has the advantage of increased sensitivity of myocardial ischemia on stress-phase scan, this "stress-first" scan is usually performed on MR stress perfusion study.
  - More than 10 min time interval between two acquisitions is necessary. When the time interval is short, the contrast used in the first phase may still remain in the myocardium at the time of the second acquisition, which may decrease the sensitivity for detecting myocardial ischemia and infarction.
- *Pulse sequences*
  - Most sequences are based on T1 contrast enhancement with magnetization preparation (inversion or saturation recovery).
  - Spoiled gradient echo (TurboFLASH, turbo fast-field echo, and GRASS) is widely used: the gradient echo image acquisition with short TR and TE and magnetization preparation. The typical parameters are TR/TE (ms) of 3/1, flip angle of 15°, 2-dimensional multisection, section thickness of 8–10 mm, bandwidth of 600–800 Hz per pixel, nonsection-selective saturation recovery, and image acquisition time of 150–200 ms per section.
  - Steady-state free precession (TrueFISP, balanced turbo field echo, turbo FIESTA) is also used for the MR perfusion study; the typical parameters are TR/TE (ms) of 2/1, flip angle of 40°, 2-dimensional multisection, section thickness of 8–10 mm, bandwidth of 1,000–12,000 Hz per pixel, nonsection-selective saturation recovery, and image acquisition time of 130–160 ms per section. It has higher contrast-to-noise ration than that of spoiled gradient echo sequence.
  - Hybrid echo planar image and gradient echo sequence are recently introduced. This sequence has the advantage of shortest image acquisition time than other sequences.
- *Acquisition of MR perfusion*
  - Cardiac localization is performed for defining imaging plane. Three or four short-axis planes are used for the perfusion study.
  - For the stress perfusion imaging, intravenous adenosine infusion at the rate of 140 μg/kg/min is performed, and intravenous gadolinium contrast media of 0.03–0.1 mmol/kg is delivered at the rate of 3–5 mL/s after 4–5 min from start of adenosine infusion. Twenty milliliters of saline chaser at the rate of 3–5 mL/s is followed.
  - For the rest scan, intravenous gadolinium contrast media of 0.03–0.1 mmol/kg is delivered at the rate of 3–5 mL/s without adenosine infusion. 20 mL of saline chaser at the rate of 3–5 mL/s is followed. Usually the time interval between the stress and the rest scan is between 12 and 15 min.
  - Dynamic scans for 3–4 short-axis planes are usually performed during both stress and rest scans. Approximately 40–60 serial scans from the injection of the gadolinium contrast media are performed in every other heartbeat. Therefore, 40–60 images of each short-axis plane are to be acquired (Fig. 10.7).

10.2.2 Assessment of MR Perfusion

10.2.2.1 Qualitative Assessment

- Simultaneous visualization of both rest and stress images for regions with hypo-intense myocardium compared with normal myocardium is necessary (see Sect. 10.3).

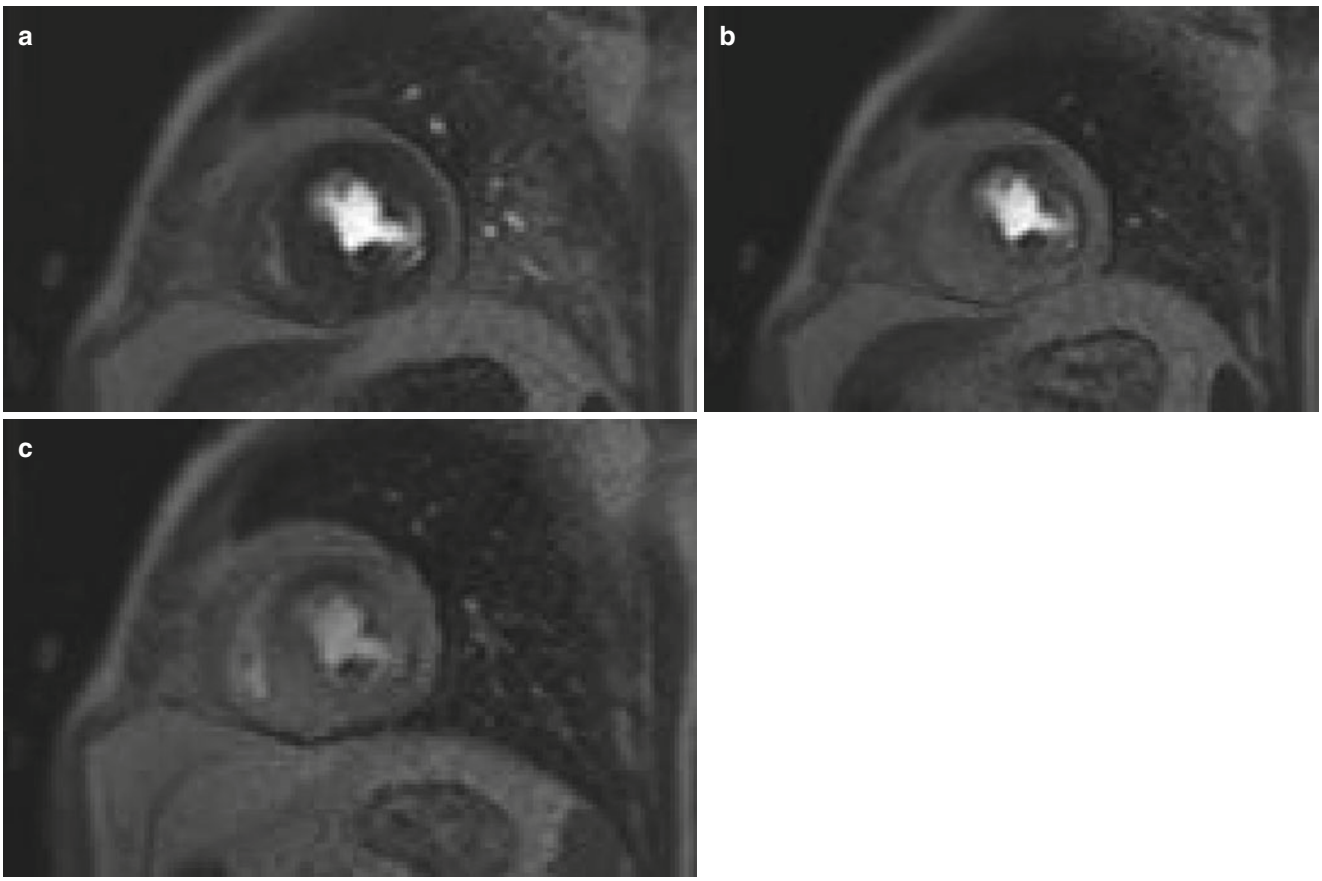

Fig. 10.8 Visual assessment of perfusion defect. Perfusion defect of the anterior wall is seen persistently from early phase (**a**), to mid phase (**b**) and late phase (**c**)

- Playing images in cine mode is essential for differentiating between image artifact such as dark-rim artifact and the true perfusion defect (see Sect. 10.4). Dark-rim artifacts typically occur in a couple of frames during peak contrast enhancement of the blood pool in the left ventricle and before peak contrast enhancement in the myocardial tissue. True perfusion defect is persistent and more prominent during the peak contrast enhancement in the myocardial tissue.
- Standard 17-segmental model of the left ventricular myocardium suggested by the American Heart Association is used for the location and scoring of the myocardial perfusion status.
- Each myocardial segment is scored for the presence or absence of the perfusion defect and graded as transmural if the perfusion defect involves ≥50 % of thickness or non-transmural. Reversibility is also graded as reversible, partially reversible, and irreversible or fixed.
- To ensure the perfusion defect is detected, images from multiple phases must be reviewed. Motion artifacts and beam-hardening artifacts can mimic perfusion defect (see Sect. 5.1 of this chapter) (Fig. 10.8).

10.2.2.2 Quantitative Assessment

- Myocardial blood flow and myocardial blood volume can be derived by the time-intensity curves (TICs) of the myocardium, the left ventricular cavity, and the aorta using the dynamic CT perfusion study.
- Drawing of endo- and epicardial border of each image in cine acquisition is required for the quantitative analysis. Blood pool in the left ventricle and epicardial fat should be excluded.
- Standard 17-segmental model of the left ventricular myocardium suggested by the American Heart Association is used for the location and scoring of the myocardial perfusion status.
- Maximal upslope, upslope, time-to-peak, maximum signal intensity, and myocardial perfusion reserve index are introduced to the semiquantitative parameter for the myocardial perfusion status (Fig. 10.9).
- Myocardial blood flow may be used for the myocardial blood flow and volume.

10.3 Representative Cases of CT Perfusion and MR Perfusion

10.3.1 One-Vessel Disease

Figure 10.10

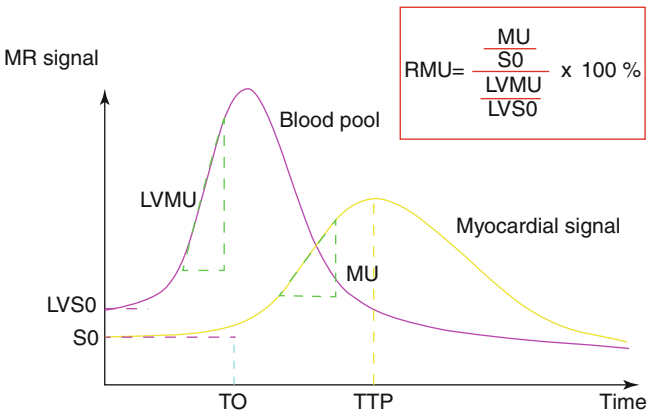

Fig. 10.9 Diagram of relative upslope (RU) for myocardial perfusion reserve index (MPRI) using the time-intensity curve

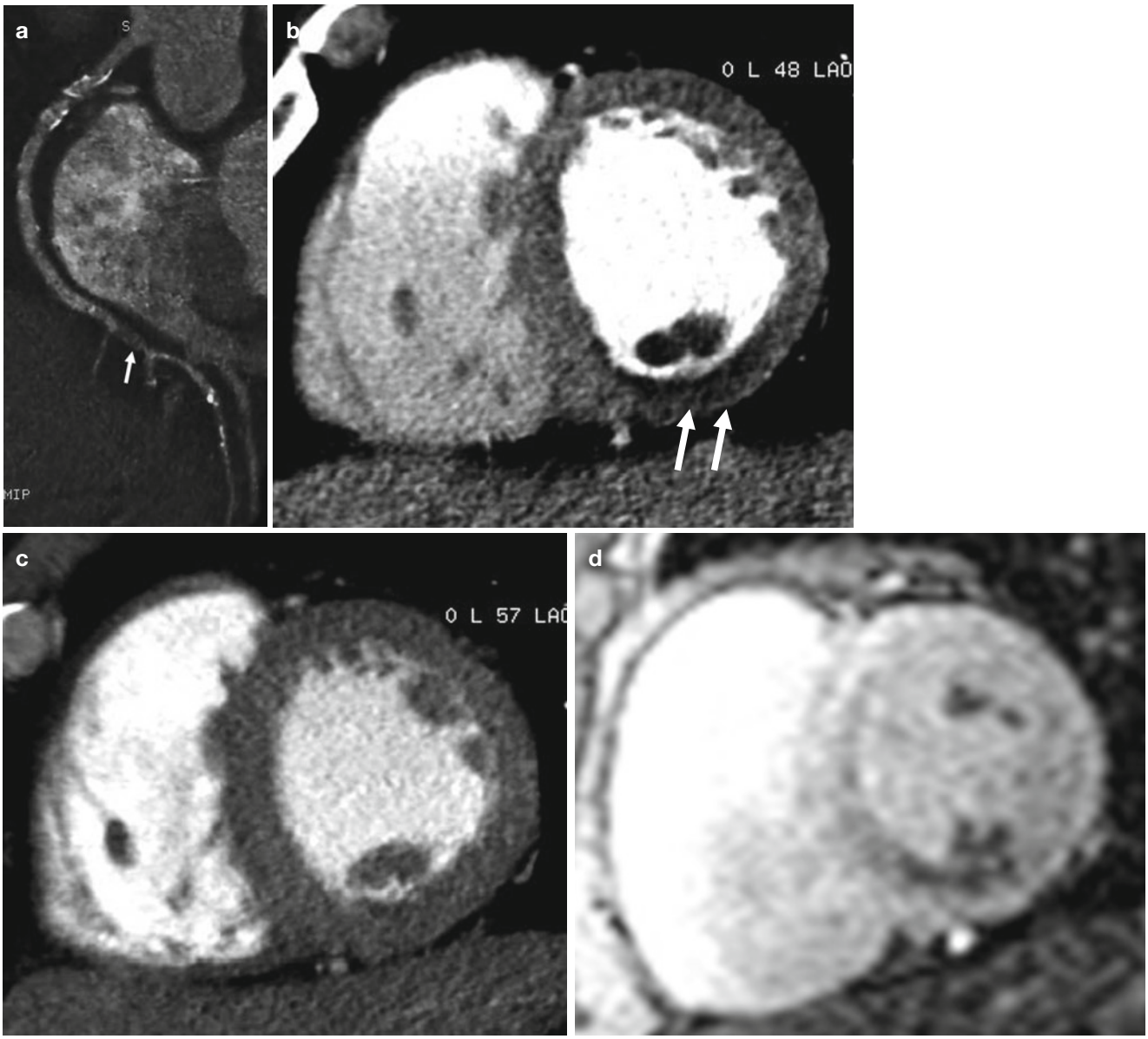

Fig. 10.10 (**a**) CT angiography of RCA in rest scan shows >70 % stenosis at the PL (*arrow*). (**b**) Stress perfusion CT study shows transmural perfusion defect at the mid-inferior wall (*arrows*). (**c**) Rest scan of CT shows reversibility of perfusion defect. MR stress (**d**) or rest (**e**) scan also shows the same perfusion defect pattern of the inferior wall. (**f**) Coronary angiography shows severe total occlusion of proximal PL (*arrows*)

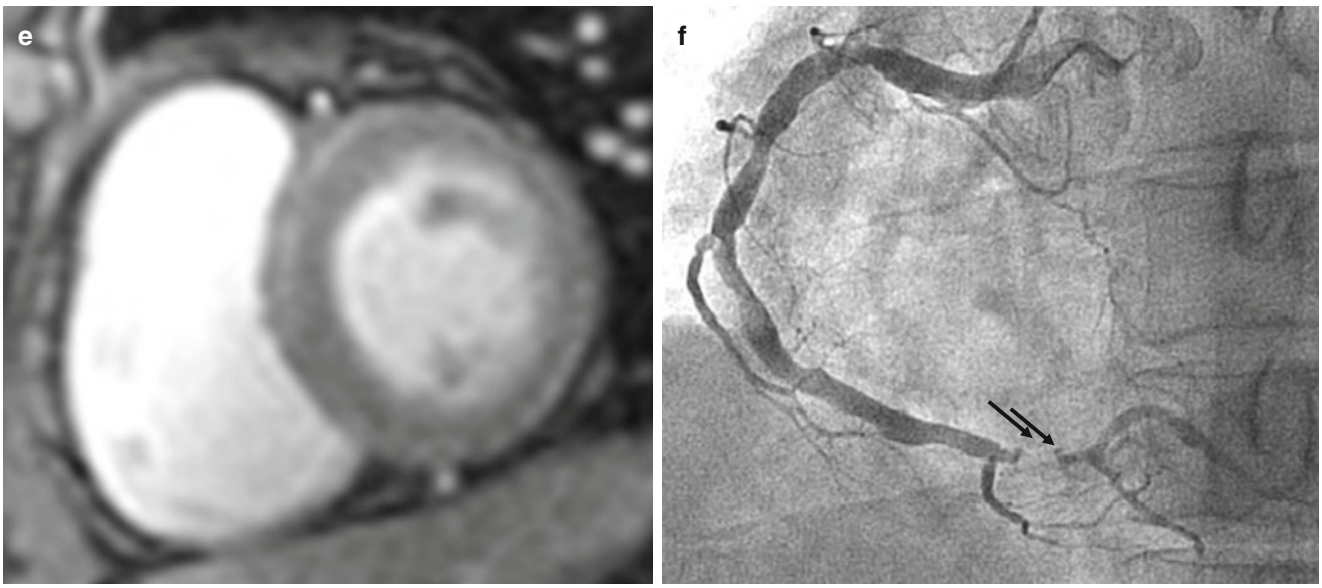

Fig. 10.10 (continued)

10.3.2 Multi-vessel Disease

Figure 10.11

10.3.3 Microvascular Angina

Figure 10.12

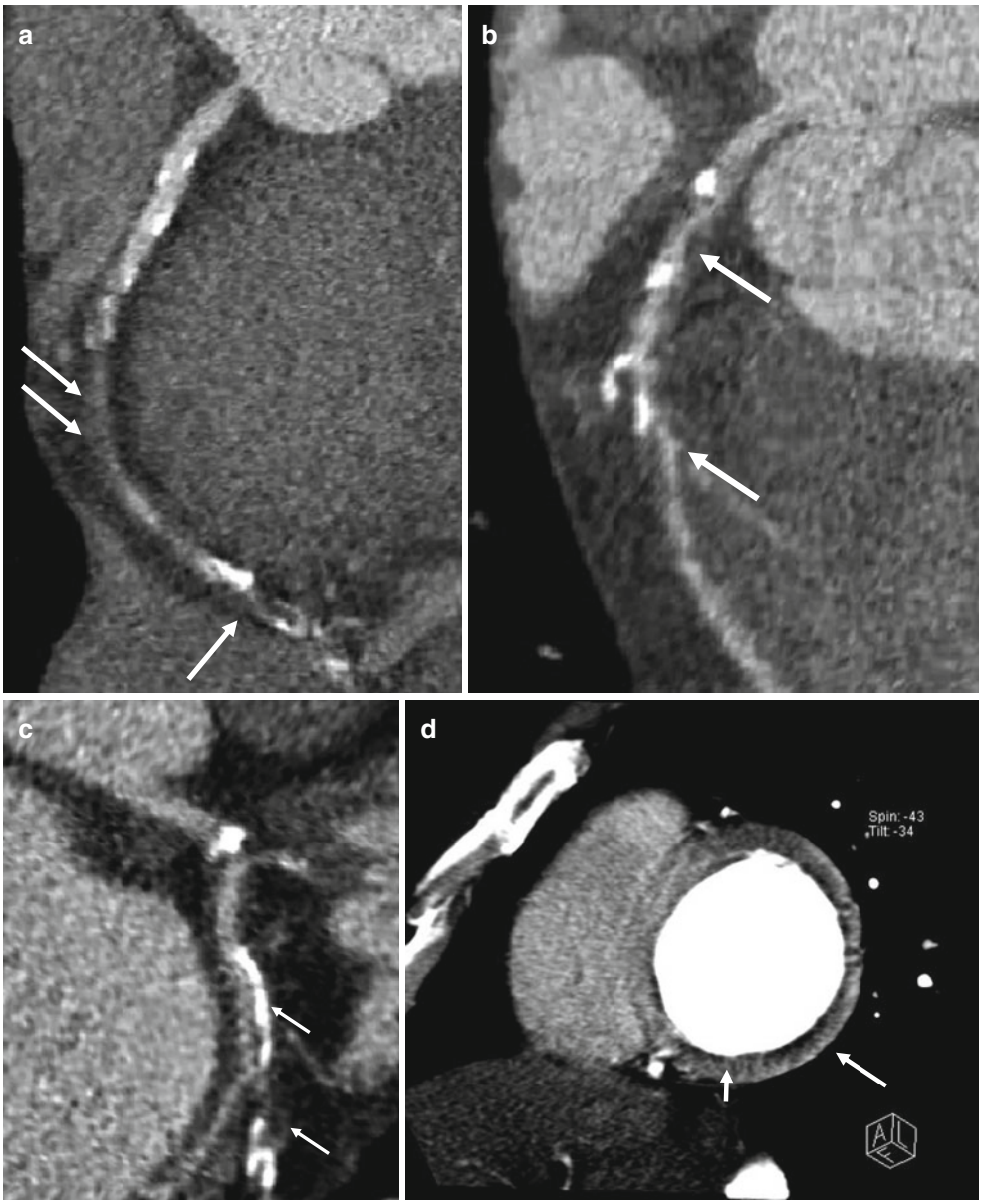

Fig. 10.11 Three-vessel disease with reversible perfusion defect. CT coronary angiography of RCA (**a**), LAD (**b**), and LCX (**c**) shows multiple severe stenosis (*arrows*). CT stress perfusion images show transmural perfusion defect on the basal inferior and inferolateral wall (**d**) and the anterior wall, septal wall, and lateral walls on the mid-ventricular level (*arrows*) (**e**). These defects are reversible on the rest scan (**f**, **g**). The perfusion defects are seen in the same segments on stress perfusion (*arrows*) (**h**, **i**) and rest perfusion (**j**, **k**) study using MRI. (Please see dynamic scans using MRI (**h**–**k**) using QR code) (http://extras.springer.com/2015/978-3-642-36396-2)

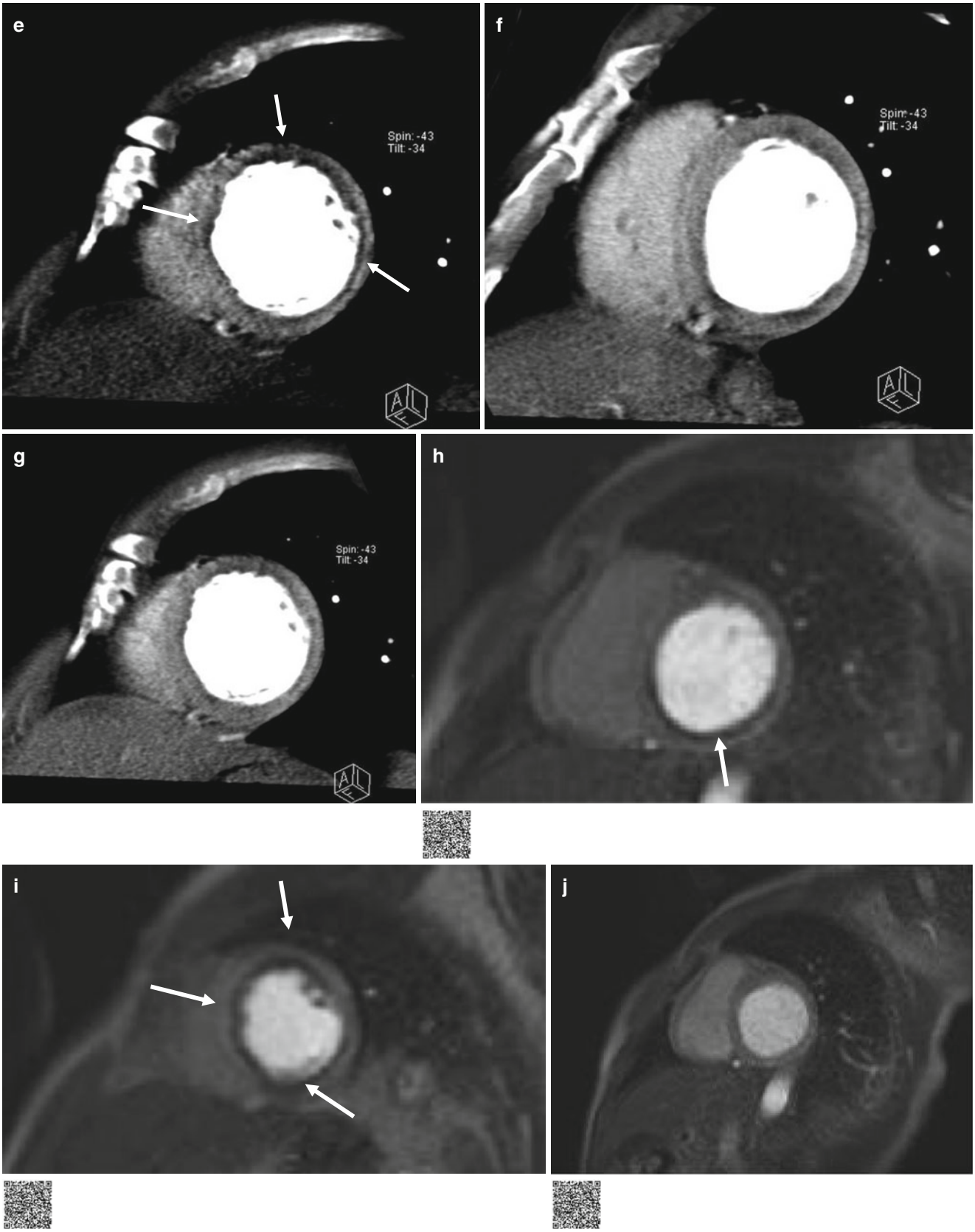

Fig. 10.11 (continued)

Fig. 10.11 (continued)

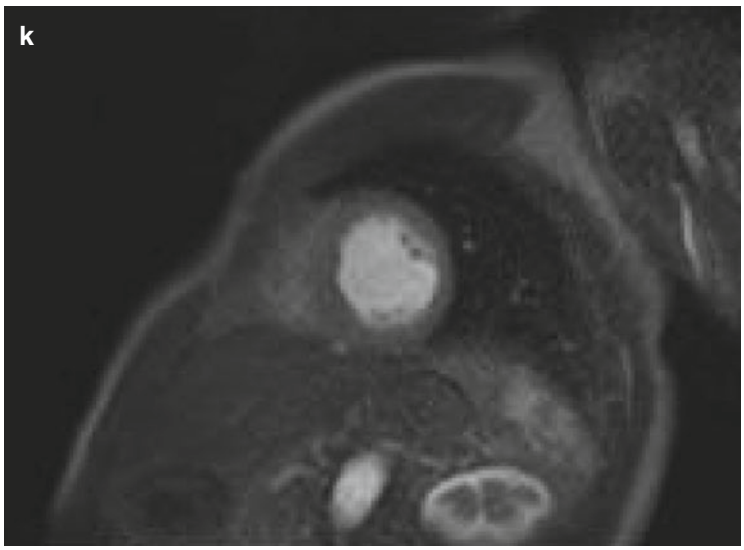

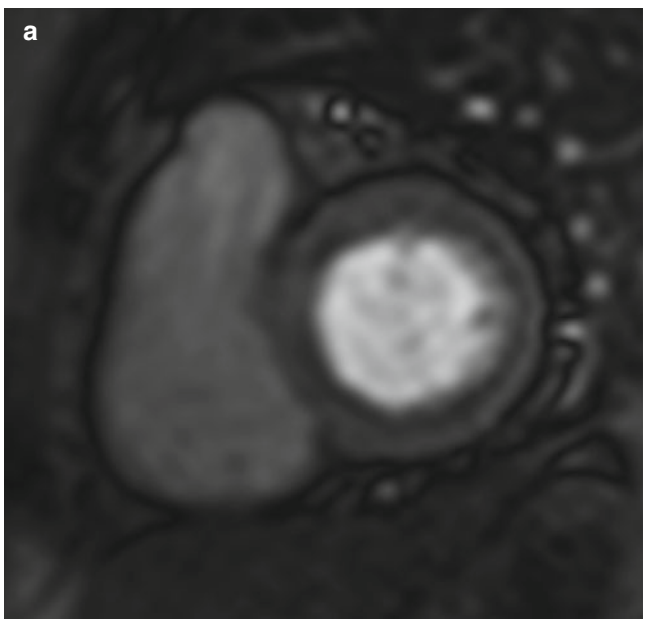

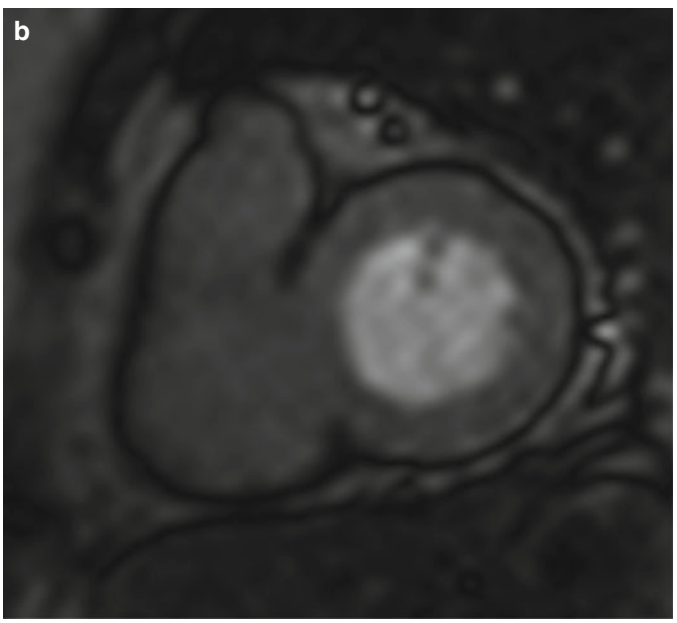

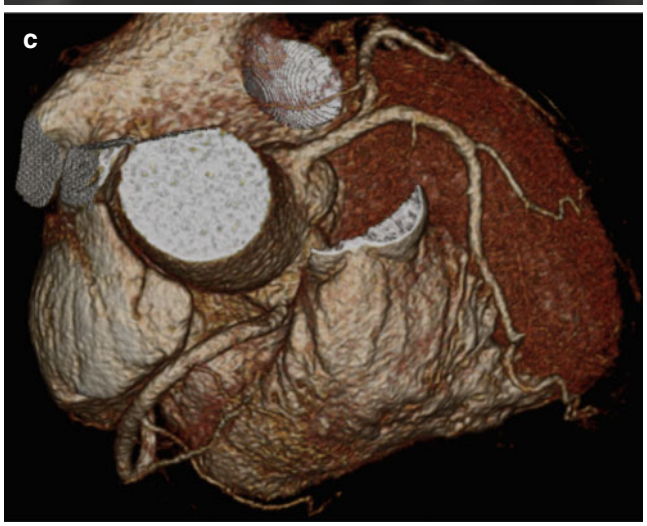

Fig. 10.12 Stress perfusion MRI shows a ring of subendocardial perfusion defect on the entire basal wall (**a, b**). However, rest perfusion MRI reveals a normal finding (**b**). CT angiography reveals normal coronary arteries (**c**)

10.3.4 Additional Value of CT Perfusion and MR Perfusion over Coronary CT Angiography (CCTA)

Figures 10.13 and 10.14

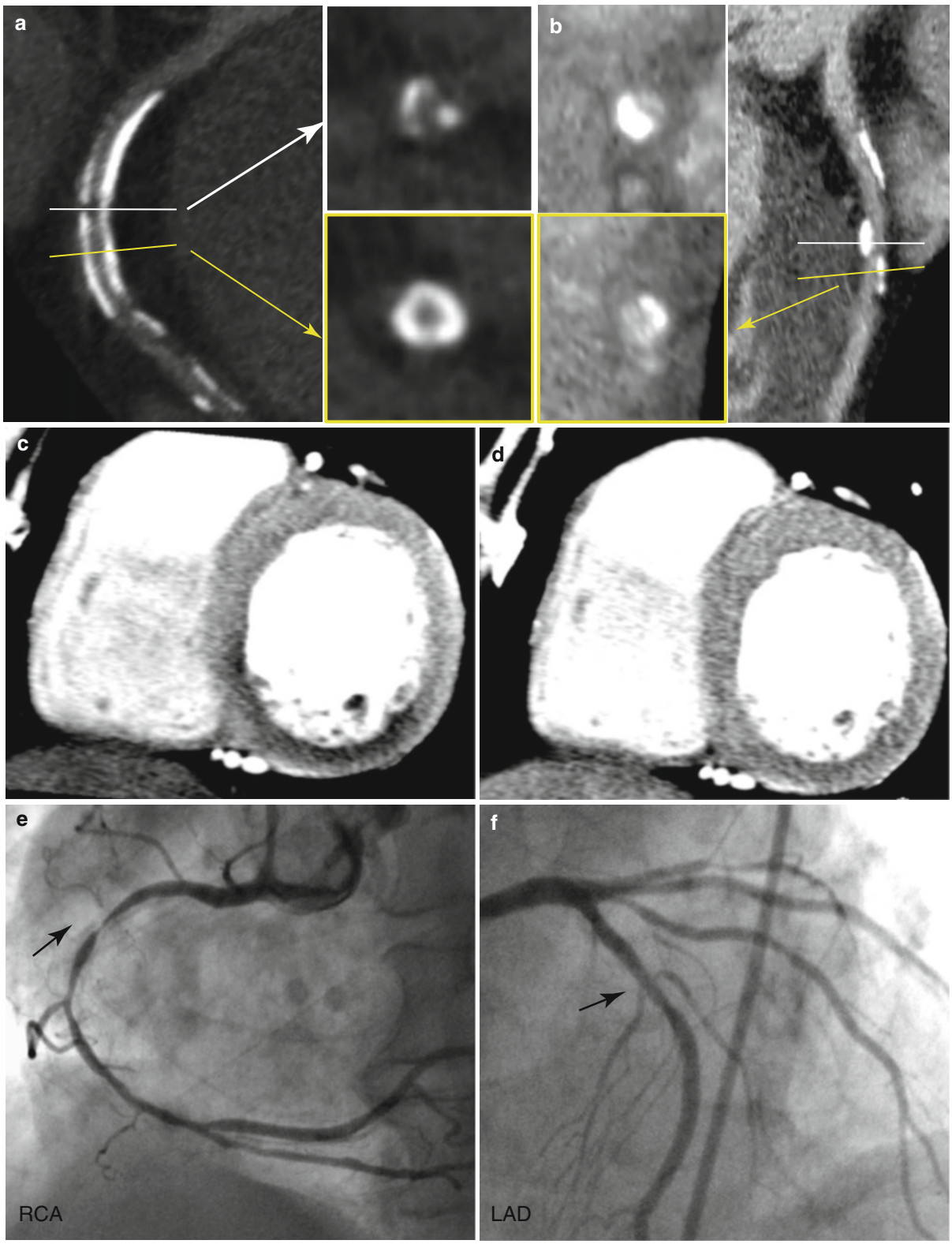

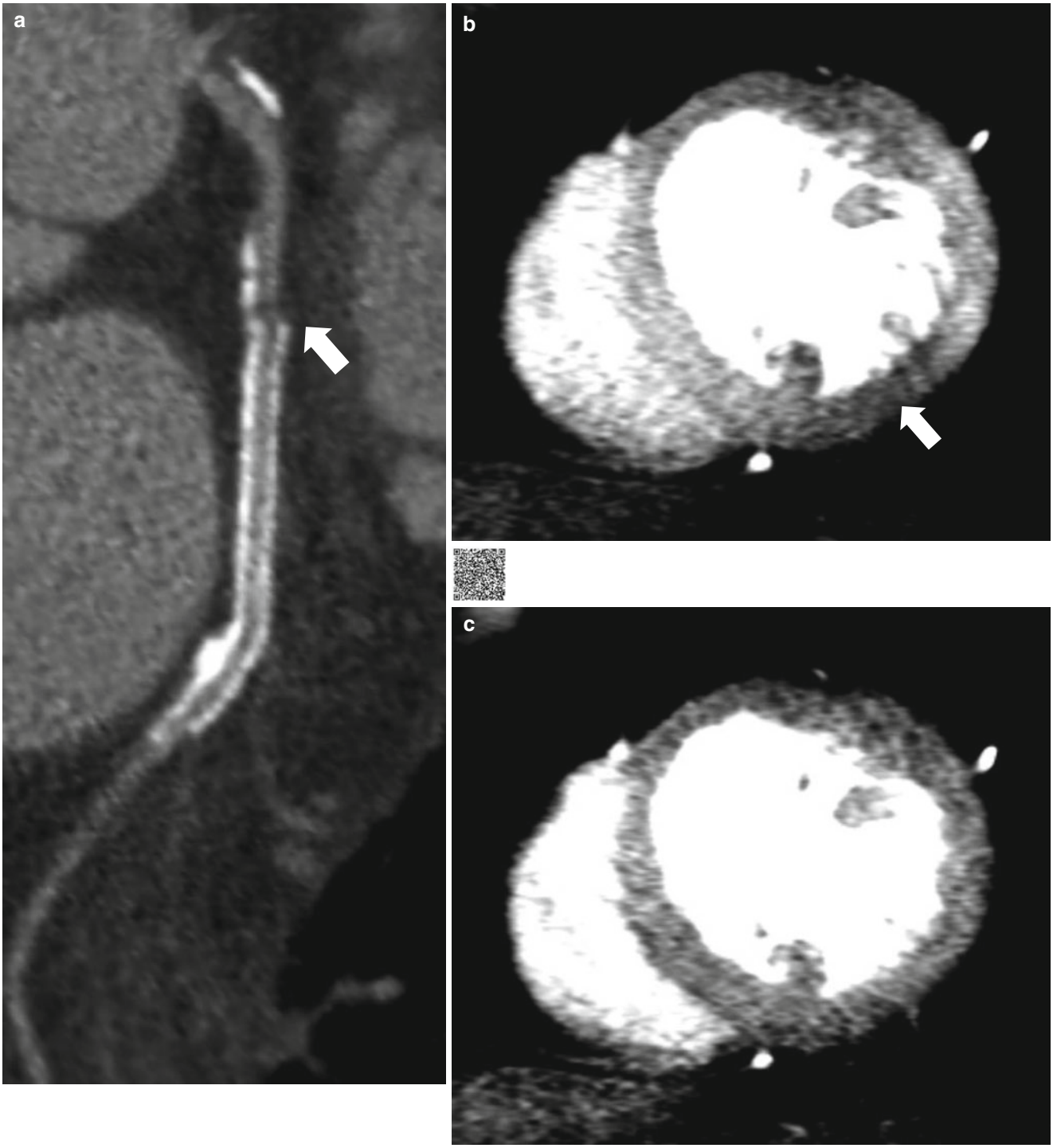

Fig. 10.14 Myocardial ischemia diagnosis and small stent in the LCX. Low-attenuated lesion at the proximal edge of the LCX stent is seen which is inconclusive for significant stenosis (*arrow*) (**a**). Stress perfusion image shows transmural perfusion defect on the mid-inferolateral wall (*arrow*) (**b**) (http://extras.springer.com/2015/978-3-642-36396-2) and reversible defect on the rest-scan image (**c**). Coronary angiography shows severe stenosis at the proximal edge of the LCX stent (*arrow*) (**d**)

Fig. 10.13 Myocardial ischemia diagnosis with severely calcified coronary arteries. CT coronary angiography of RCA (**a**) and LAD (**b**) with heavy calcified plaque failed to demonstrate the coronary artery lumen clearly due to blooming artifact that resulted from calcified plaque. Stress perfusion study (**c**) shows transmural perfusion defect only in the inferior wall (*arrows*) and reversible defect on rest study (**d**). Coronary angiography shows severe stenosis only in the RCA (*arrow*) (**e**). There was no significant stenosis at LAD (*arrow*) (**f**)

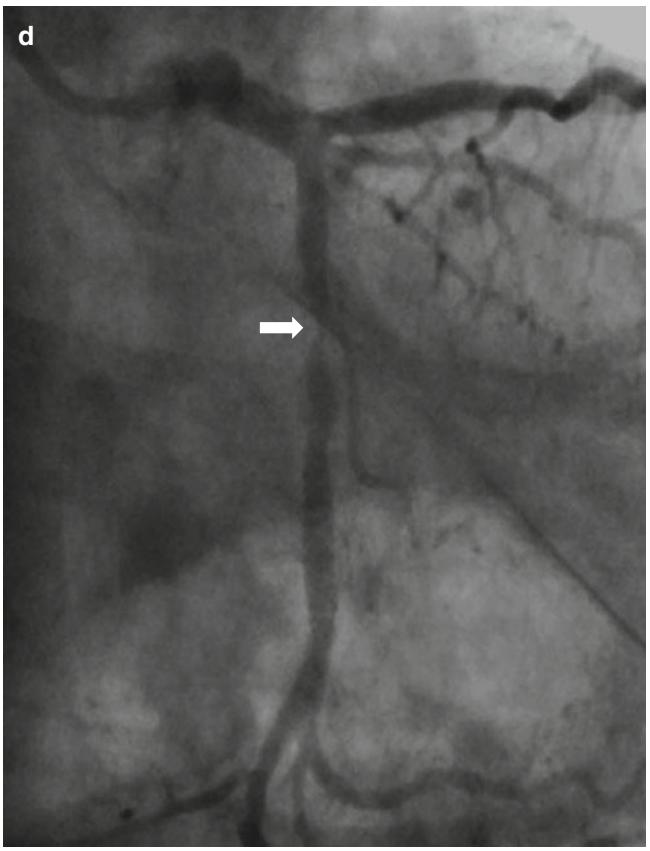

Fig. 10.14 (continued)

10.4 Limitations and Artifacts of CT Perfusion and MR Perfusion

10.4.1 CT Perfusion

- *Motion artifact* is caused by both cardiac and respiratory motion. Cardiac motion can lead to the appearance of focal low-attenuated area alternating with high-attenuated area, and thus mimicking or masking a perfusion defect. Using beta-blockers, maximizing temporal resolution, and selecting motionless images are required for minimizing the motion artifact. Also, reviewing multiphase images is important; motion artifact is not persistent in all phases (Fig. 10.15).
- *Beam-hardening artifact* occurs in the contrast-enhanced left ventricular cavity and the descending thoracic aorta and in the context of bone (ribs, spine, and sternum). The typical location is the basal inferior and inferolateral wall (the left ventricular cavity and the descending thoracic aorta) and the basal anterior wall (the left ventricular cavity and the ribs). This artifact has also a characteristic triangular shape and does not follow the distribution of the coronary artery territory. Beam-hardening effect correction algorithm helps in removing the artifact (Fig. 10.16).
- *Cone-beam artifact* occurs when the center of the patient does not lie at the isocenter of the scanner. It presents as low- and high-attenuation bands (Fig. 10.17).

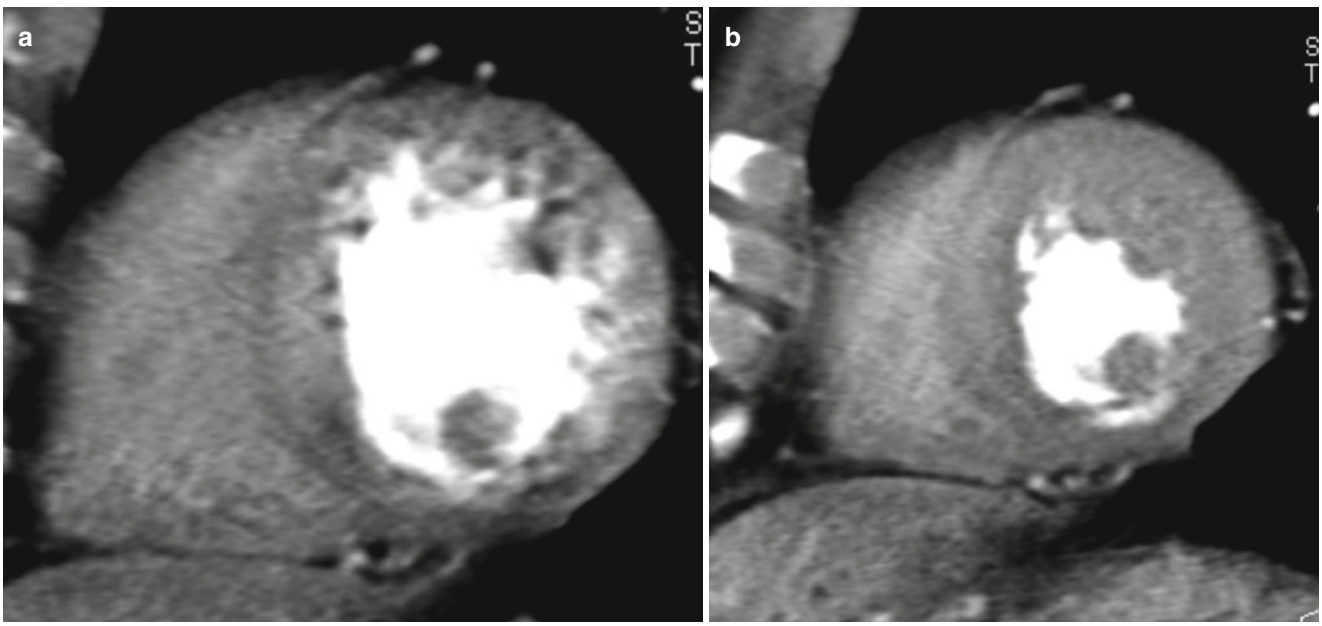

Fig. 10.15 Motion artifact in stress perfusion images. Short-axis views of 65 % (**a**) and 46 % (**b**) of R-R interval are not conclusive for the perfusion defect. Short-axis view of 87 % (**c**) provides perfusion defect of the inferior wall. Coronary angiography shows severe stenosis of the right coronary artery (**d**)

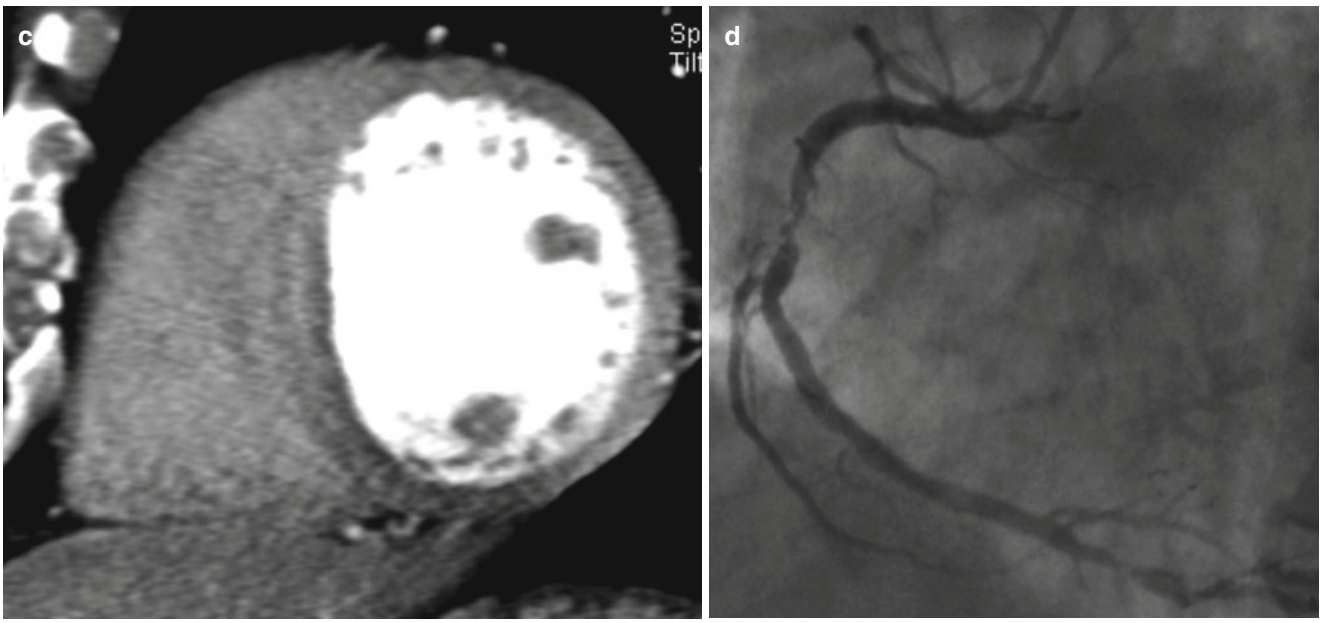

Fig. 10.15 (continued)

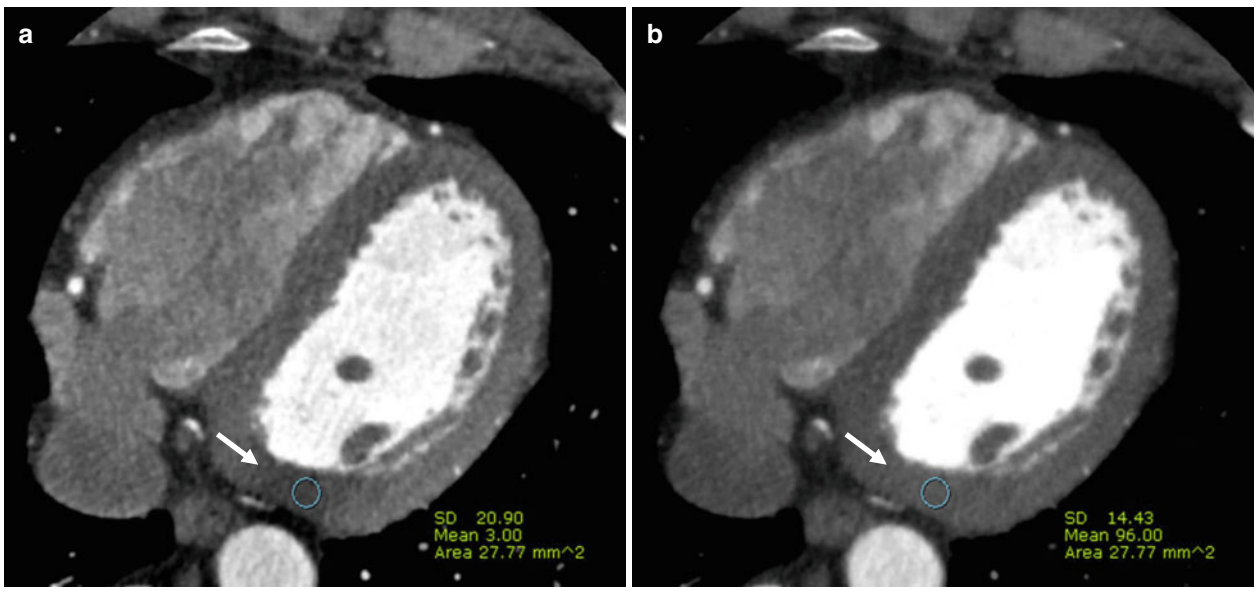

Fig. 10.16 (**a**) Beam-hardening artifact at the basal inferior wall (*arrow*). (**b**) Beam-hardening effect correction algorithm removes the artifact (*arrow*)

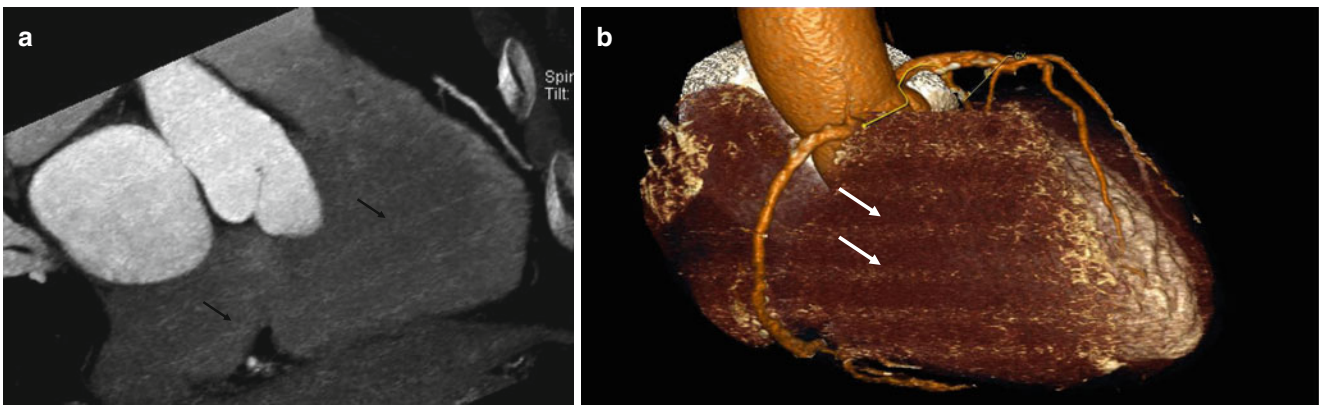

Fig. 10.17 Cone-beam artifact in the 2-chamber view (**a**) and the volume-rendered view (**b**) (*arrows*)

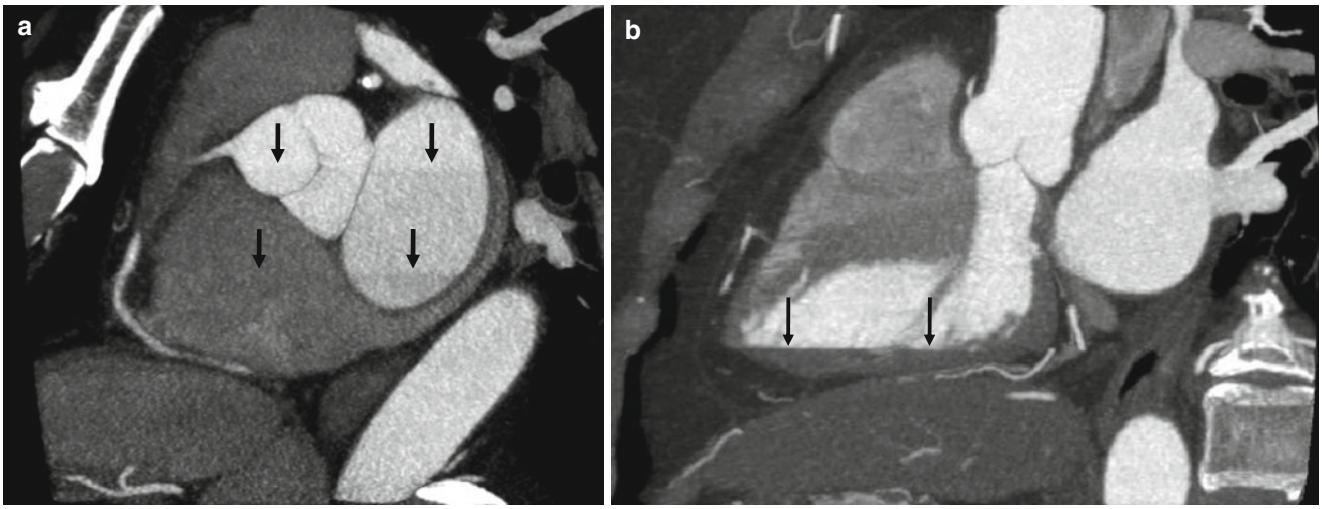

Fig. 10.18 Misalignment artifact by different contrast attenuation in the myocardium (*arrows*) (**a**) and the step-ladder artifact due to heart rate difference (*arrows*) (**b**)

- *Misalignment artifact or band artifact* is seen in 64- or 128-slice scanners that do not cover the whole heart and require helical or prospective ECG-gating acquisition. When there is beat-to-beat variation of the heart rate, the cardiac phase is different in any given heart beat. Contrast attenuation in the arterial bed and the myocardium can differ because of temporal difference. Wide detector CT or increased pitch method can diminish such artifact (Fig. 10.18).
- *Limitations*
  - Poor signal-to-noise ratio (quantum artifact) is caused by improper selection (generally lower value) of tube current and voltage and imprecise selection of image acquisition phase. It usually resulted in much image noise. It can be avoided by tube voltage and current selection by body mass index or automatic tube current and voltage selection and also by using appropriate acquisition phase selection such as test bolus or bolus tracking method.
  - Radiation exposure and iodinated contrast are inevitable limitations of CT perfusion. Notably, radiation exposure is continuously decreased as more prospective ECG-gating scans are developed including wide-detector coverage and increased pitch technique. Amount of iodinated contrast media is doubled for both stress and rest scans, and it requires caution in patients with impaired renal function.

10.4.2 MR Perfusion

- Dark-rim artifacts typically occur in a couple of frames during peak contrast enhancement of the blood pool in the left ventricle and before peak contrast enhancement in the myocardial tissue. True perfusion defect is persistent and more prominent during the peak contrast enhancement in the myocardial tissue (Fig. 10.19).
- Sequence-related artifacts
  - Spoiled gradient echo sequence has the slower image acquisition speed than steady-state free precession and echo planar imaging sequences, and it has low signal-to-noise ratio and contrast-to-noise ratio.
  - Steady-state free precession has off-resonance artifacts, and thus, it is not suitable for >1.5 T machine.
- General MR contraindications are also the limitation of MR perfusion study: claustrophobic patients, patients with pacemaker or metallic implants with non-MR-compatible materials, unstable patients, etc.

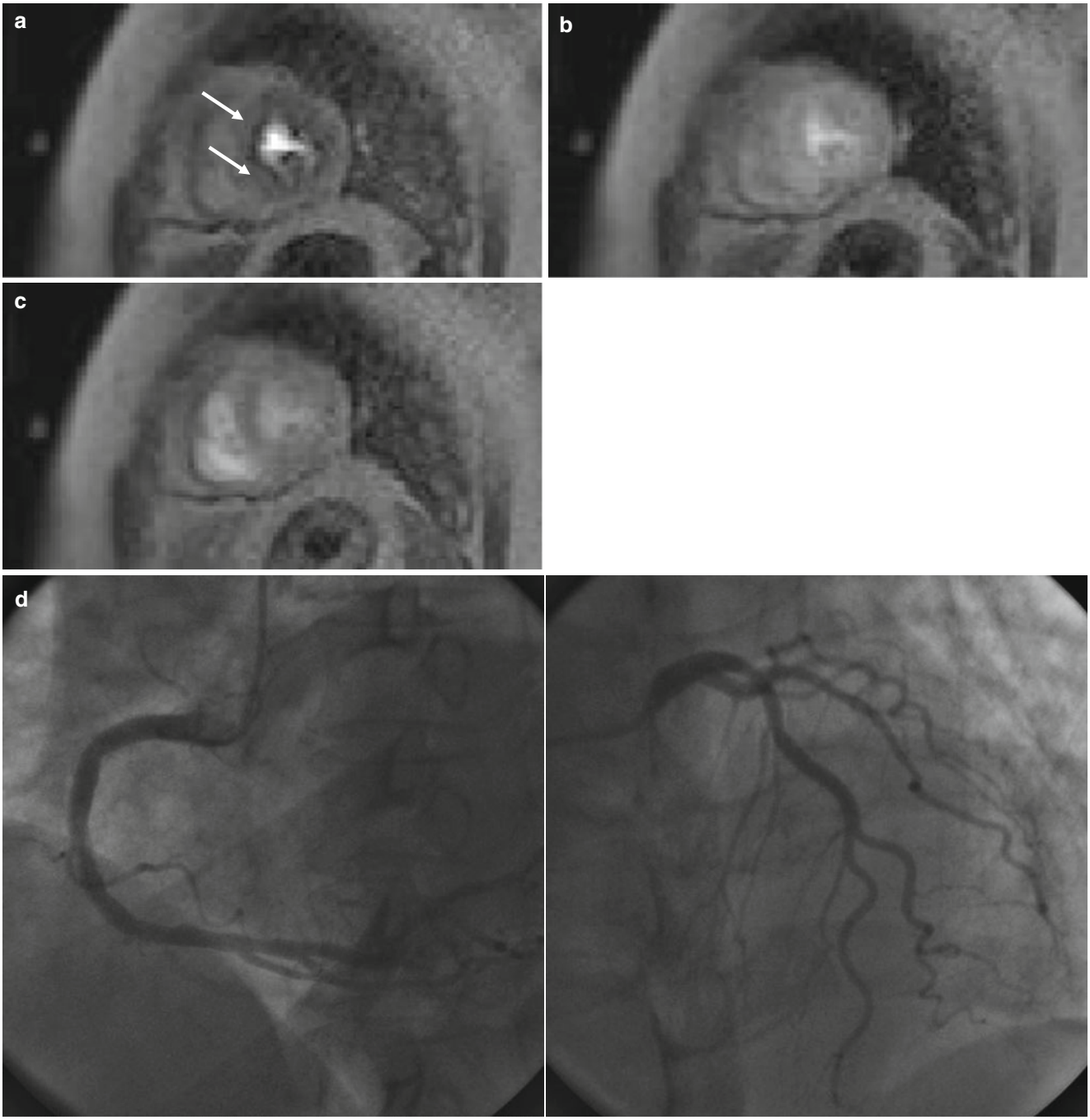

Fig. 10.19 Dark-rim artifact. Subendocardial linear low signal lines are seen in the early phase of the stress perfusion (*arrows*) (**a**). The lesions are diminished and disappear during the late phases (**b**, **c**). No coronary disease are found on coronary angiography (**d**)

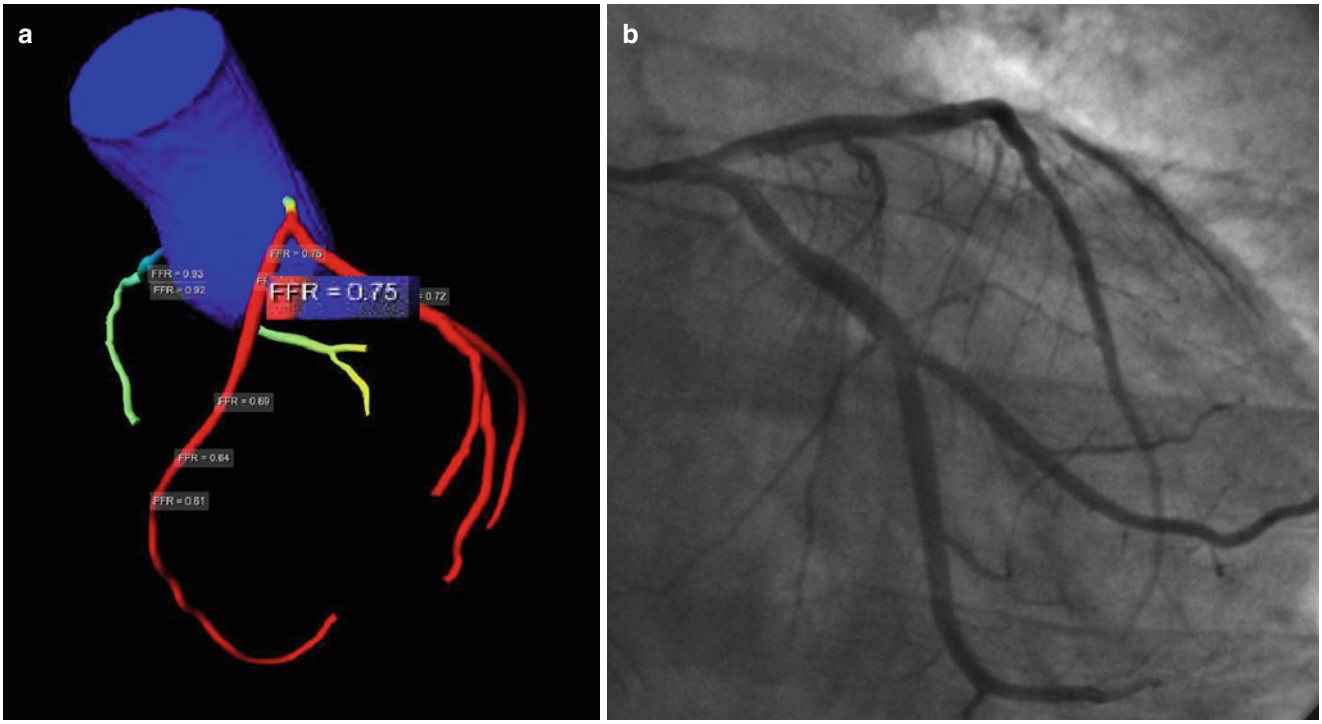

Fig. 10.20 CT-fractional flow reserve. CT-FFR of the LAD was 0.75 at the proximal LAD (**a**), real FFR was 0.70 at the proximal LAD (**b**)

Conclusions

With recent advance of CT and MRI, evaluation of myocardial ischemia using perfusion study can be performed more easily and effectively. Quantitative assessment of myocardial blood flow and volume is possible using dynamic study. Using multimodality study and computer-aided protocol such as fusion imaging, CT-fractional flow reserve, or sophisticated quantitative analysis tools, we can perform more effective evaluation of myocardial perfusion status (Fig. 10.20).

Recommended Reading

1. Arrighi JA, Dilsizian V. Multimodality imaging for assessment of myocardial viability: nuclear, echocardiography, MR, and CT. Curr Cardiol Rep. 2012;14:234–43.
2. Coelho-Filho OR, Rickers C, Kwong RY, Jerosch-Herold M. MR myocardial perfusion imaging. Radiology. 2013;266:701–15.
3. Ko BS, Cameron JD, DeFrance T, Seneviratne SK. CT stress myocardial perfusion imaging using multidetector CT—a review. J Cardiovasc Comput Tomogr. 2011;5:345–56.
4. Ko SM, Choi JW, Hwang HK, Song MG, Shin JK, Chee HK. Diagnostic performance of combined noninvasive anatomic and functional assessment with dual-source CT and adenosine-induced stress dual-energy CT for detection of significant coronary stenosis. AJR Am J Roentgenol. 2012;198:512–20.
5. Mehra VC, Valdiviezo CV, Arbab-Zadeh A, Ko BS, Seneviratne SK, Cerci R, Lima JAC, George RT. A stepwise approach to the visual interpretation of CT-based myocardial perfusion. J Cardiovasc Comput Tomogr. 2011;5:357–69.

Acute Myocardial Infarction

11

Jeong A. Kim, Sang Il Choi, and Tae-Hwan Lim

Contents

Abstract

In patients with suspected myocardial ischemia or myocardial infarction (MI), cardiac MRI (CMR) provides a comprehensive and multifaceted view of the heart.

Several CMR techniques can provide a wide range of information such as myocardial edema (myocardium at risk), location of transmural necrosis, quantification of infarct size and microvascular obstruction, the assessment of global ventricular volumes and function, and global evaluation of postinfarction remodeling.

Although several CMR techniques could be used for the diagnosis of MI, the late gadolinium enhancement (LGE) imaging is a well-validated, robust technique in detecting small or subendocardial infarcts with high accuracy and the best available imaging technique for the detection and assessment of acute MI.

The focus of this chapter will be on the impact of CMR in the characterization of acute MI pathophysiology in the current reperfusion era, concentrating also on clinical applications and future perspectives for specific therapeutic strategies.

11.1 Overview

11.1.1 Universal Definition of Acute Myocardial Infarction (AMI) [1]

- Elevated troponin value exceeding the 99th percentile of the upper reference limit
- And at least one of the following:
  1. Symptoms of ischemia
  2. Electrocardiogram (ECG) changes of new ischemia
  3. Development of pathological Q-waves on the ECG
  4. Imaging evidence of new loss of viable myocardium
  5. New regional wall motion abnormality
- Despite the use of new serological biomarkers such as troponins or imaging modalities such as echocardiography, SPECT, and coronary computed tomographic angiography (CCTA), there are still lots of uncertainty in the assessment of AMI

J.A. Kim
Department of Radiology, Inje University Ilsan Paik Hospital, Ilsan, Republic of Korea
e-mail: jakim7779@hanmail.net

S.I. Choi
Department of Radiology, Seoul National University Bundang Hospital, Gyeonggido, Republic of Korea
e-mail: drsic@daum.net

T.-H. Lim (✉)
Department of Radiology and Research Institute of Radiology, Asan Medical Center, University of Ulsan College of Medicine, Seoul, Republic of Korea
e-mail: d890079@naver.com

T.-H. Lim (ed.), *Practical Textbook of Cardiac CT and MRI*,
DOI 10.1007/978-3-642-36397-9_11,

11.1.2 Cardiac MRI in AMI

- Cardiac MRI (CMR) represents a noninvasive technique with increasing applications in AMI providing the assessment of function, perfusion, and tissue characterization during a single examination even in patients with acoustic window limitations.
- CMR can provide a wide range of information such as myocardial edema (the myocardium at risk), location of transmural necrosis, quantification of infarct size, and microvascular obstruction (MVO) leading also to intramyocardial hemorrhage.
- Moreover, CMR provides the assessment of global ventricular volumes and function and a global evaluation of postinfarction remodeling.
- Although several CMR techniques could be used for the diagnosis of MI, the most accurate and best validated is the late gadolinium enhancement (LGE) image [2–4].

11.2 Imaging Modalities for AMI

11.2.1 Cardiac MR Technique for AMI

11.2.1.1 Basic Principles of Late Gadolinium Enhancement (LGE) for Cardiac Evaluation

- LGE images are T1-weighted inversion recovery sequences acquired about 10–30 min after intravenous administration of gadolinium, and the inversion time is chosen to null myocardial signal using "inversion time scout" or "Look-Locker" sequences.
- Gadolinium is an extracellular agent, which enhances in certain conditions such as necrotic or fibrotic myocardium, assuming a bright signal (hyperenhancement), opposed to dark viable myocardium.
- The pattern of LGE is useful to differentiate postinfarction necrosis (subendocardial or transmural LGE) from fibrosis in non-ischemic-dilated cardiomyopathies (mid-wall LGE, subepicardial LGE), or myocarditis (subepicardial or focal LGE) (Fig. 11.1) [5–7].

11.2.1.2 LGE: Comparison with Other Modalities

- The high spatial resolution of LGE enables visualization of even microinfarctions, involving as little as 1 g of tissue.
- When comparing SPECT imaging, the main advantage of LGE is its spatial resolution of 1–2 mm (in plane), contrary to about 10 mm with SPECT scans. Therefore, MRI can identify subendocardial necrosis when perfusion by SPECT appears unaltered. LGE also appears to be superior to PET in clear delineation of nonviable myocardium [8].

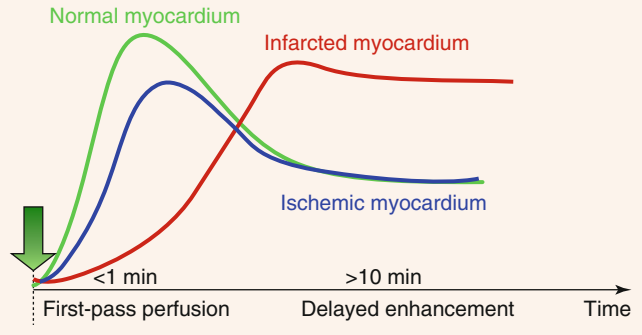

Fig. 11.1 Schematic illustration of basic principles of late gadolinium enhancement (LGE). Time-intensity curve at normal and pathologic myocardium after administration of contrast media (*arrow*)

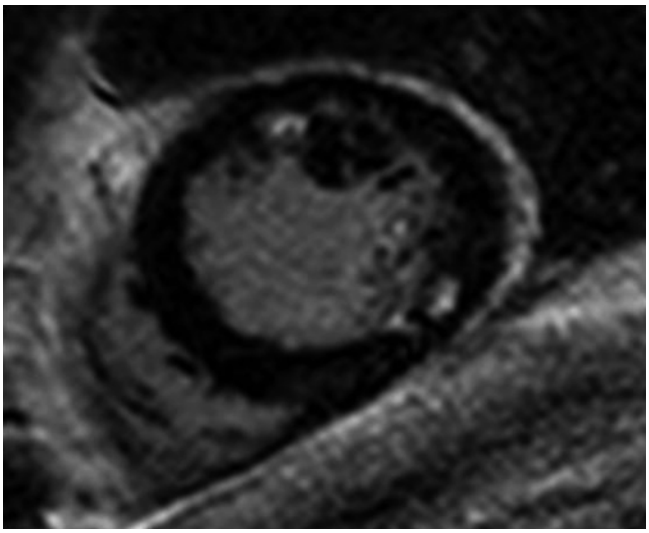

Fig. 11.2 Multifocal subendocardial infarction in anterior and inferolateral wall. High tissue contrast between blood pool and infarcted myocardium allows us to easily see the infarcted area

- LGE is in its ability to detect subendocardial LV infarction as well as RV infarction that might be missed using SPECT and PET, because it can clear delineation of nonviable myocardium at any location of the cardiac chamber (Figs. 11.2, 11.3, and 11.4).

11.3 Imaging Findings for AMI

11.3.1 Checklist of Cardiac MRI in AMI

11.3.1.1 Myocardial Edema with Area at Risk on T2-Weighted Images (T2WI)

- Myocardial edema in the acute phase of myocardial infarction can be visualized as a bright signal on T2WI, "myocardium at risk."

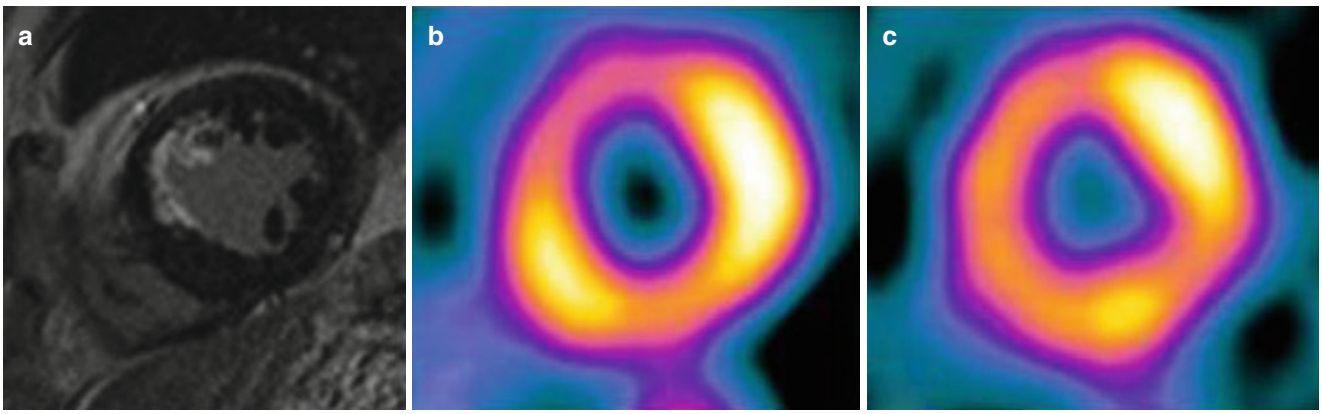

Fig. 11.3 LGE comparison with SPECT for subendocardial infarction. MRI (**a**) shows subendocardial infarction at anteroseptal wall, but SPECT (**b**, **c**) shows reversible perfusion defect

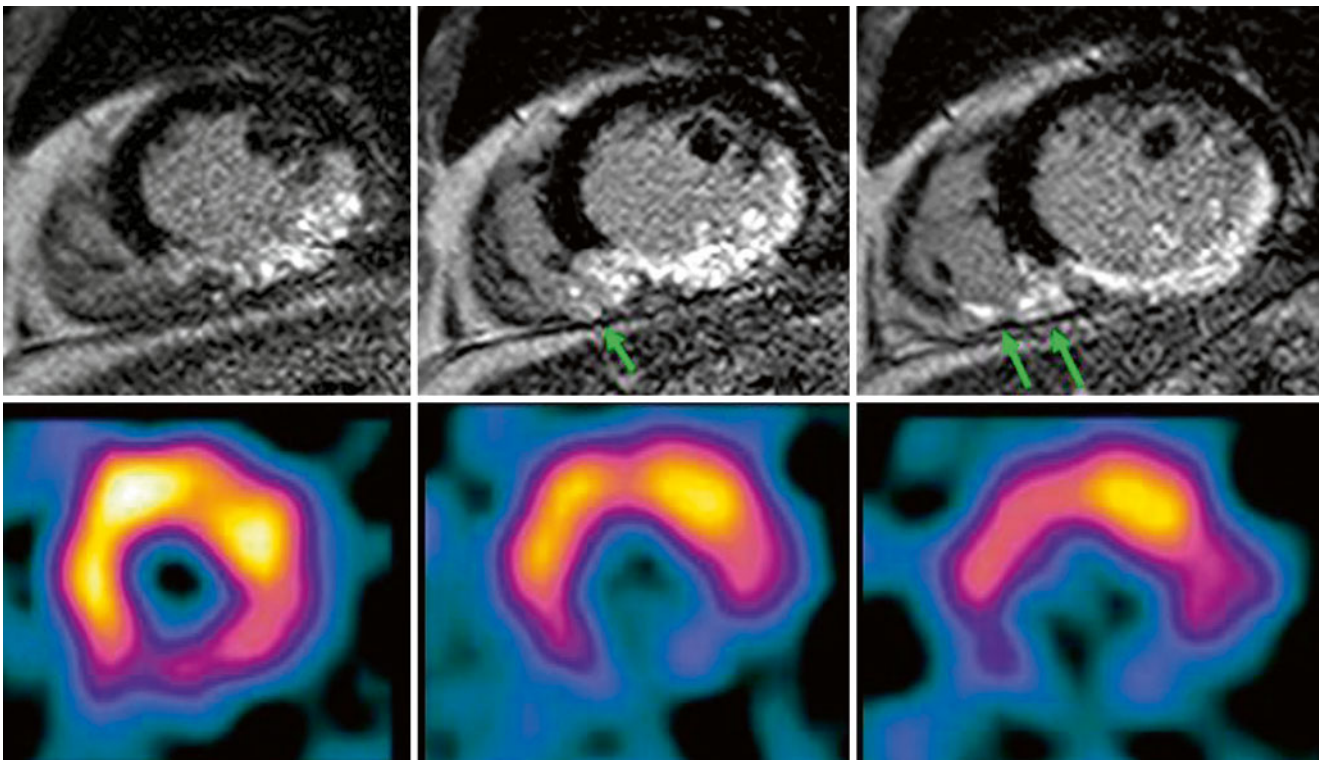

Fig. 11.4 LGE comparison with SPECT for RV infarction. LGE (*top image*) clearly shows RV infarction. (*arrows*) as well as inferior LV myocardial infarction. However, SPECT shows only perfusion defect at inferior wall of LV myocardium

- T2WI still debate to delineation of the area at risk in ischemic myocardial injury [9].
- The major advantages of T2WI:
  - To differentiate chronic from acute infarction
  - To quantify the proportion of salvage myocardium by comparing T2-weighted edematous size and late enhancement images.
  - To differentiate edema as a marker of acute myocardial injury and fibrosis as that of chronic myocardial injury [10, 11].
- During the early phase of a coronary occlusion, the subsequent discrepancy between myocardial oxygen supply and demand leads to myocardial ischemia.
- If ischemia persists, myocardial injury becomes irreversible, and the necrosis extends from the subendocardium toward the subepicardium, "wave-front phenomenon."
- The final infarct size depends on the extent of the so-called risk area, defined as the myocardial area related to an occluded coronary artery with complete absence of blood flow.

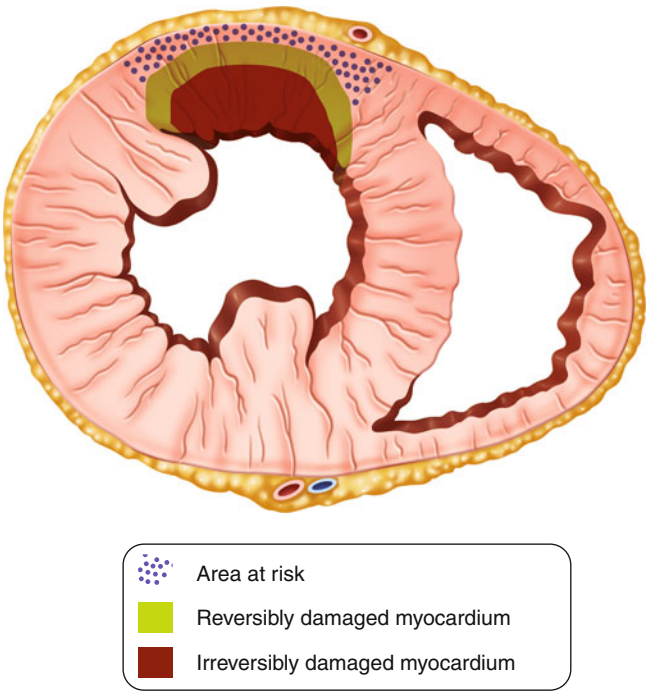

Fig. 11.5 Schematic illustration of the "wave front of myocardial necrosis" in the setting of acute myocardial infarction

- CMR is used to visualize and to quantify the "area at risk," increased myocardial signal intensity depicted by T2WI are very sensitive to water-bound protons indicating an increased water content with an active myocardial inflammation and tissue edema (Figs. 11.5, 11.6, 11.7, 11.8, and 11.9) [12, 13].

11.3.1.2 Myocardial Viability

- *Progression of necrosis*
  - According to the concept of "wave-front phenomenon of myocardial death," infarct size increases, extending from the endocardium to the epicardium with an increasing duration of coronary occlusion.
  - The major determinant of final transmural necrosis and microvascular damage is the duration of ischemia [14].
  - Infarct size measured by LGE is directly associated with clinical outcome.
  - Improvement of myocardial contractility after treatment can be predicted by the transmural extent of hyperenhancement on LGE [14, 15].
    - >75 % of transmural extent of infarction has extremely low chance of myocardial salvage (Fig. 11.10).

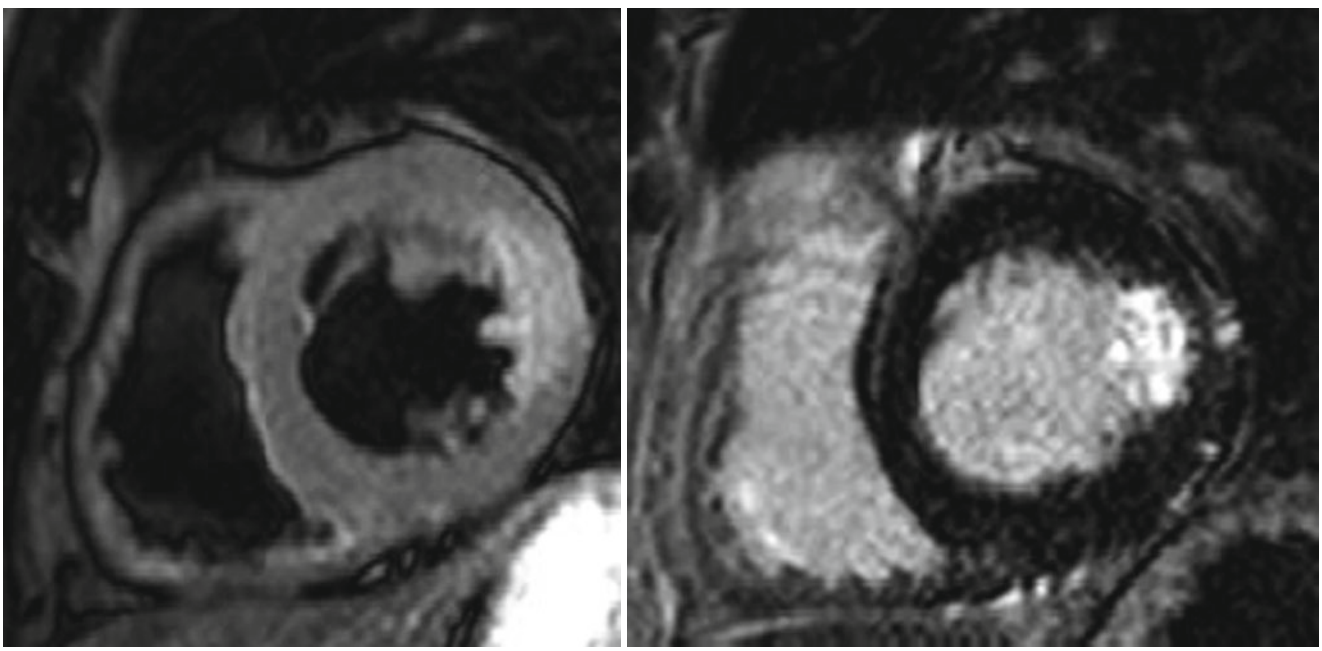

Fig. 11.6 The discrepancy between T2WI and LGE image. T2-weighted image shows transmural edema extending toward all lateral walls. Note the absence of LGE involved by edema representing reversibly damaged myocardium

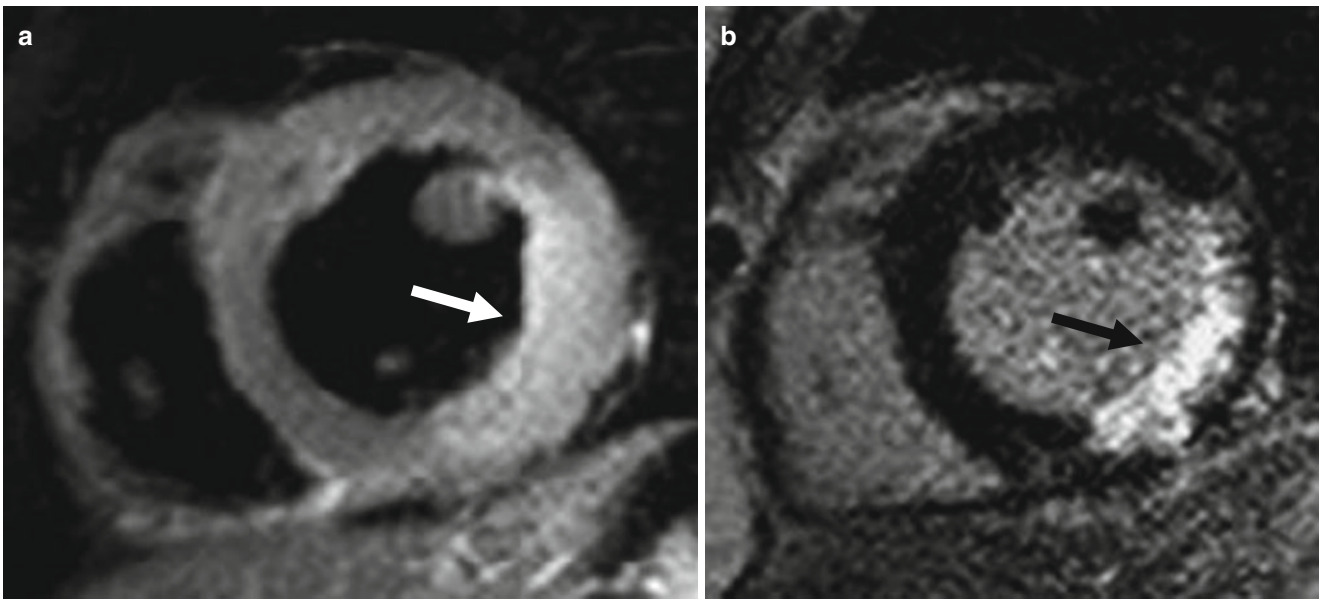

Fig. 11.7 The role of T2WI in differential diagnosis of acute and chronic MI (acute MI: 5 days ago). T2 MRI (**a**) shows high-signal area at inferior and inferolateral wall with swelling (*arrow*). LGE (**b**) also shows hyperenhancement at the same area (*arrow*)

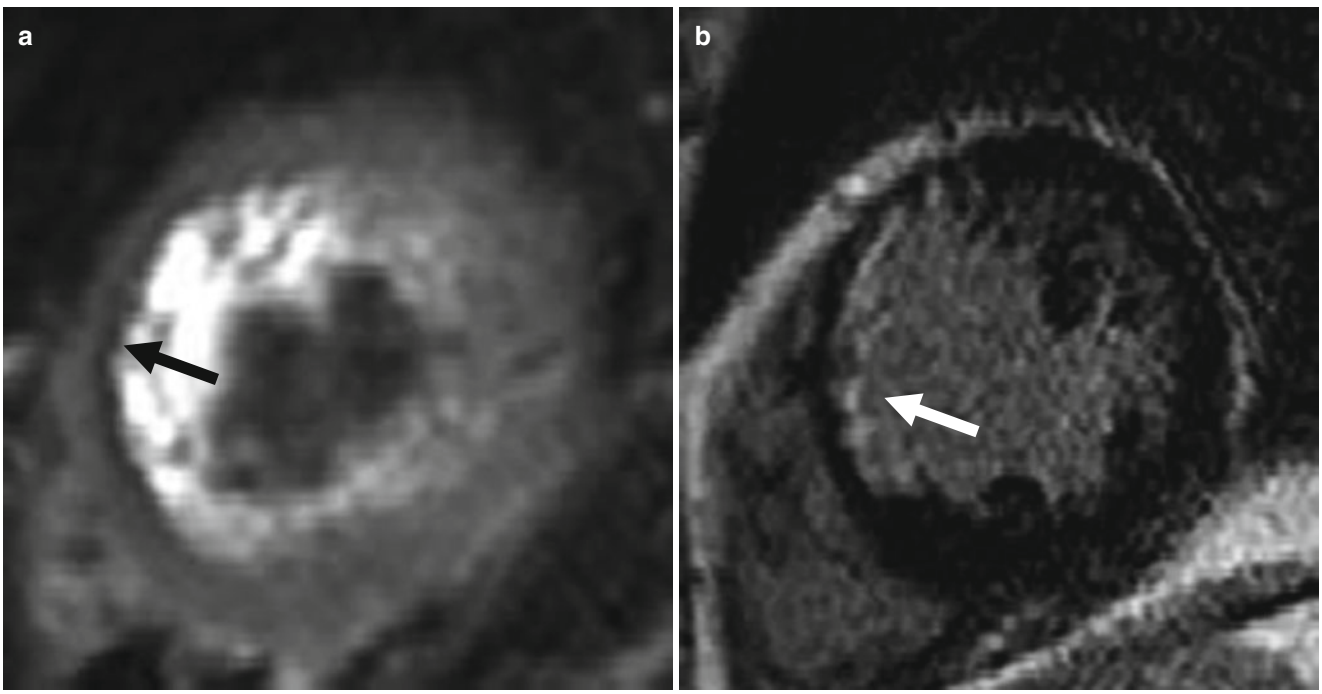

Fig. 11.8 The role of T2WI in differential diagnosis of acute and chronic MI (chronic MI: 9 years ago). T2 MRI (**a**) shows low-signal area at anterior and anteroseptal wall with thinning (*arrow*). Slow artifact is seen within LV cavity. LGE (**b**) also shows hyperenhancement at the vascular territory (LCX) (*arrow*)

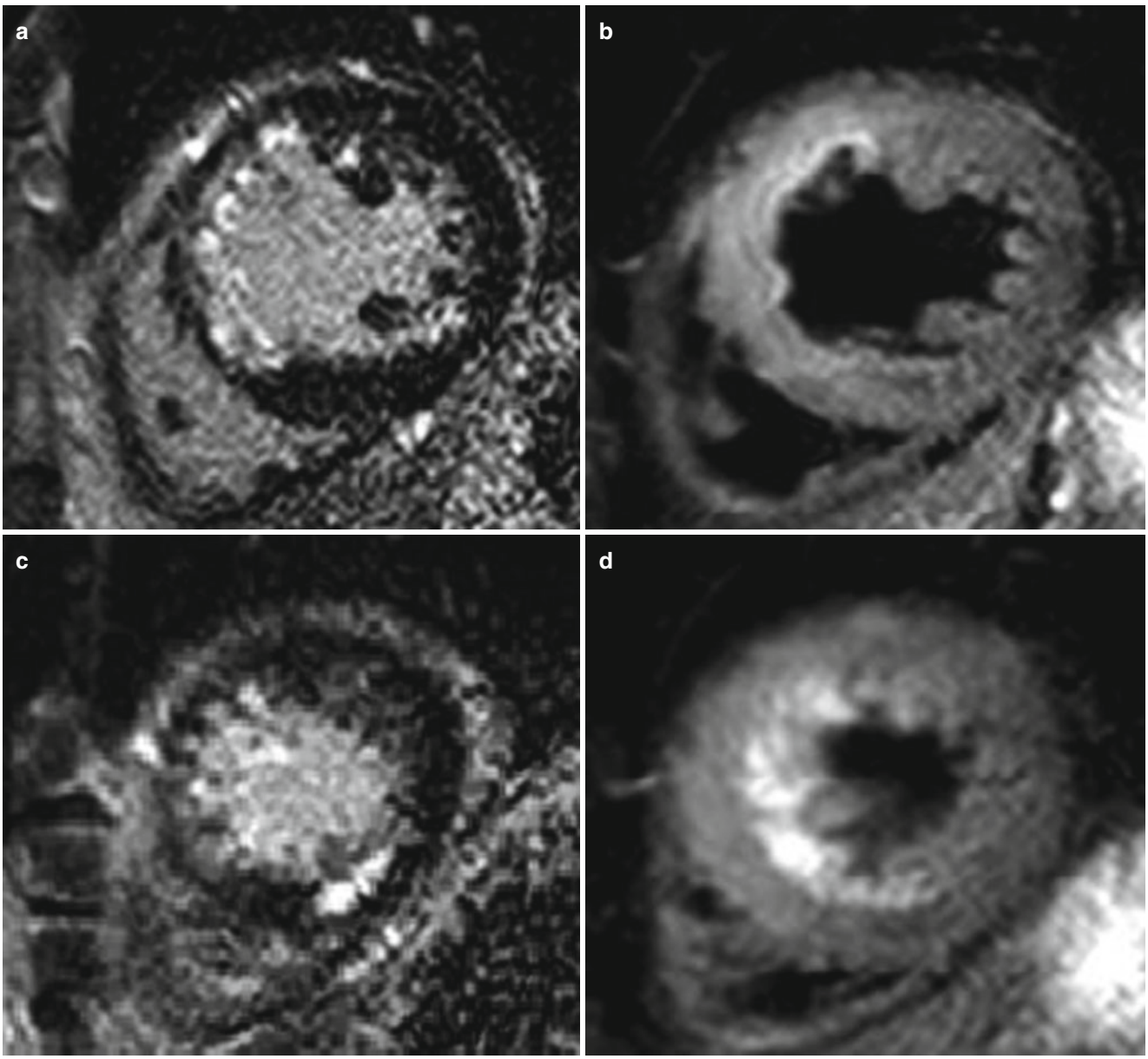

Fig. 11.9 The role of T2WI and LGE in diagnosis of coexisting acute and chronic MI. A 45-year-old male with acute chest pain examined with cardiac MRI. Hyperenhancement at the apical septal and mid-anteroseptal wall with hyperintensity on T2WI, suggestive of acute MI at LAD territory (**a**, **b**). However, another abnormal hyperenhancement at the apical inferior wall without definite T2 hyperintensity, suggestive of chronic infarction at RCA territory (**c**, **d**)

- *Aborted MI*
  - Patients treated very early in the myocardial infarction triage and intervention (MITI) trial and who had no evidence of MI after the treatment.
  - Definition: Major (≥50 %) ST-segment resolution of the initial ST-segment elevation and a lack of a subsequential enzyme ≥2 of the upper normal limit.
  - Aborted MI usually shows homogeneous high signal on T2WI with no or minimal enhancement on LGE along the vascular territory of the culprit lesion (Fig. 11.11) [15].

11.3.1.3 Reperfusion Injury

- *"No-reflow phenomenon"*
  - Absent distal myocardial reperfusion after a prolonged period of ischemia, despite the successful recanalization of the culprit coronary artery.
  - Secondary to both luminal obstruction (i.e., neutrophil plugging, platelets, atherothrombotic emboli) and external compression by edema and hemorrhage.
  - After a prolonged ischemia, the necrosis becomes transmural, and as final consequences a microvascular damage may appear inside the infarction.

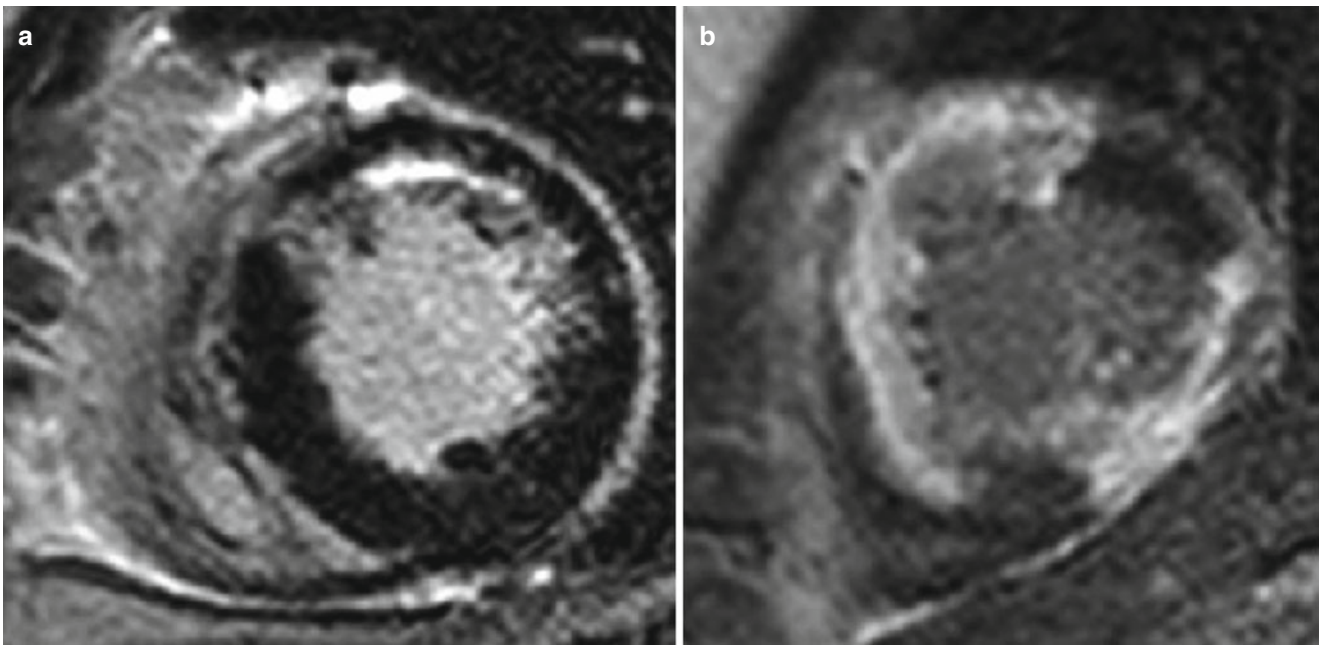

Fig. 11.10 Transmural extent of myocardial infarction. (**a**) LGE shows subendocardial infarction with 25–50 % transmural extent at the anterior wall. (**b**) LGE shows infarction with 75–100 % transmural extent at anterior, anteroseptal, and inferior wall

- *Microvascular obstruction (MVO) on LGE*
  - CMR is currently used also to evaluate persistent microvascular dysfunction/damage in the context of white LGE regions (infarcted myocardium) and may coexist dark hypoenhanced areas, traditionally referred to as MVO.
  - Defined as late hypoenhancement within a hyperenhanced region on LGE.
  - Persistent MVO is an independent predictor of LV remodeling, poor functional recovery, and higher major adverse cardiac events on follow-up.
  - In an experimental model, microvascular damage is an early event, and intramyocardial hemorrhage plays a role later in reperfusion injury. The extent of the hemorrhagic area correlates with the size of "dark zones" on LGE.
  - Hypoenhancement on T2WI, suggesting intramyocardial hemorrhage, is present in the majority of patients with dark zones on LGE and also closely related to markers of infarct size and function (Fig. 11.12).

11.3.1.4 Low-Dose Dobutamine Stress MRI

- The presence of contractile reserve can be accurately demonstrated by low-dose dobutamine stress MR (DSMR) and is a marker for myocardial viability.
- DSMR has the advantage of full visualization of the myocardium, whereas dobutamine stress echocardiography suffers from impaired image quality in patients with poor acoustic windows.
- Low-dose DSMR is superior to LGE as a predictor of functional recovery and does not depend on the transmurality of scar. Therefore, LGE and DSMR provide complementary information.

11.3.1.5 Cardiac Function

- Cine MRI is regarded as the reference standard for global systolic function and regional wall motion.
- CMR is particularly suitable for the study of large infarcts with aneurysmal dilatation [10, 16].

11.3.1.6 Infarct Complication

- Increasing experience with CMR has led to the development of new applications that may be used to diagnose adverse sequelae associated with MI, including right ventricular involvement, acute pericarditis, and LV thrombus.
  - MI-induced ventricular septal defect.
  - Dressler's syndrome (postmyocardial infarction pericarditis): A secondary form of pericarditis that occurs in the setting of injury to the heart or the pericardium.
  - Post-MI mitral value regurgitation.
  - LV thrombosis (Fig. 11.13).

11.3.1.7 Evaluation of LV Remodeling

- LV remodeling is significantly correlated with the presence of MVO, larger infarction, and higher transmural extent of infarction on LGE.
- Postinfarction remodeling has been divided into an early phase (within 72 h) and a late phase (beyond 72 h):

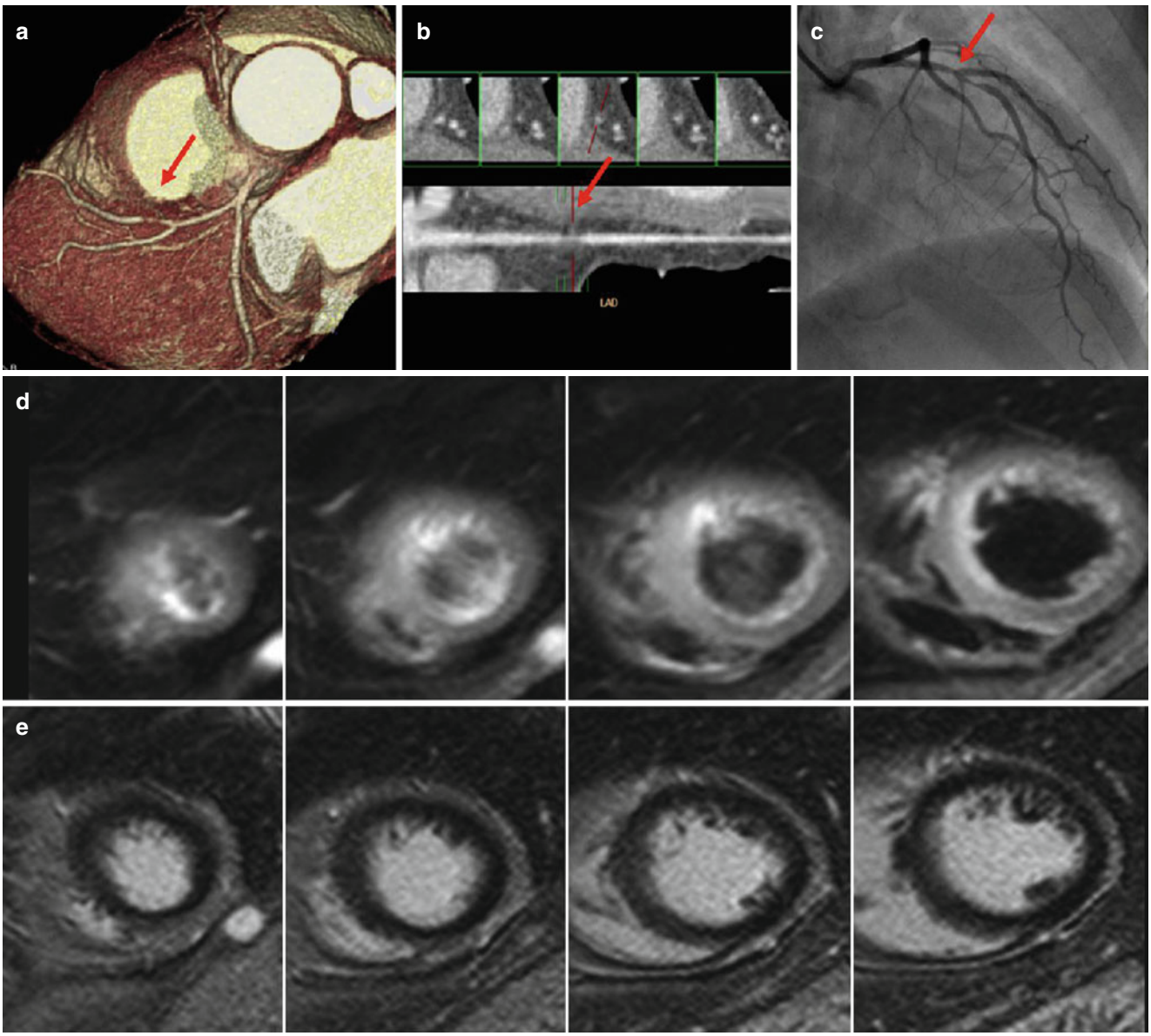

Fig. 11.11 Aborted MI. Severe discrete stenosis (*arrow*) was noted at mid-LAD on coronary CT angiography (**a**, **b**) and conventional angiography (**c**). Occluded LAD was successfully reopened after percutaneous coronary intervention (**c**). However, LGE images show no definite enhancement (**e**). Only T2-weighted images show subtle hyperintensity at the apical septal, mid-anterior, and mid-anteroseptal wall (**d**)

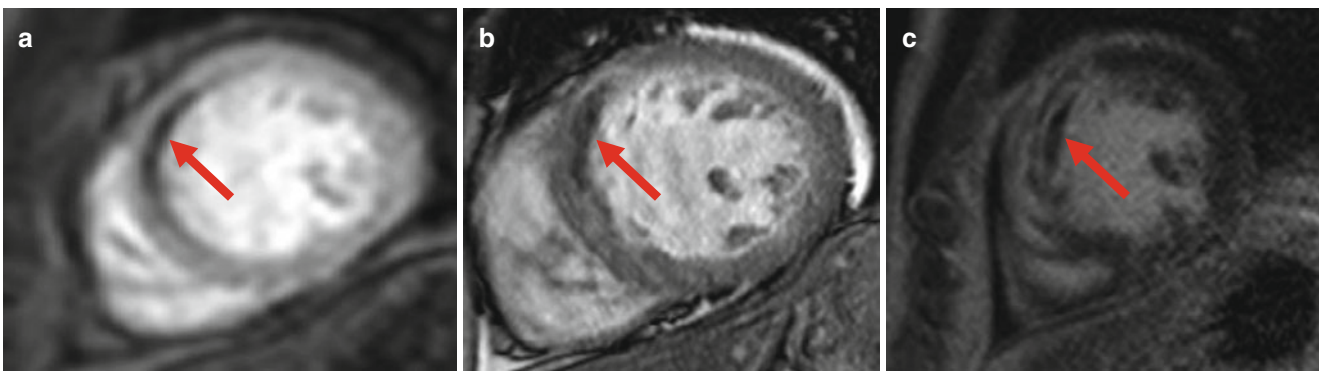

Fig. 11.12 First-pass perfusion (**a**) and cine image (**b**) 3 min after contrast injection shows low signal at the subendocardial area of the anteroseptal wall suggesting microvascular obstruction (*arrows*). DE-CMR (**c**) also shows hypoenhancement at the same area

- The early phase involves expansion of the infarct zone, which may result in early ventricular rupture or aneurysm formation.
- Late remodeling involves the left ventricle globally and is associated with time-dependent dilatation, the distortion of ventricular shape, and mural hypertrophy.

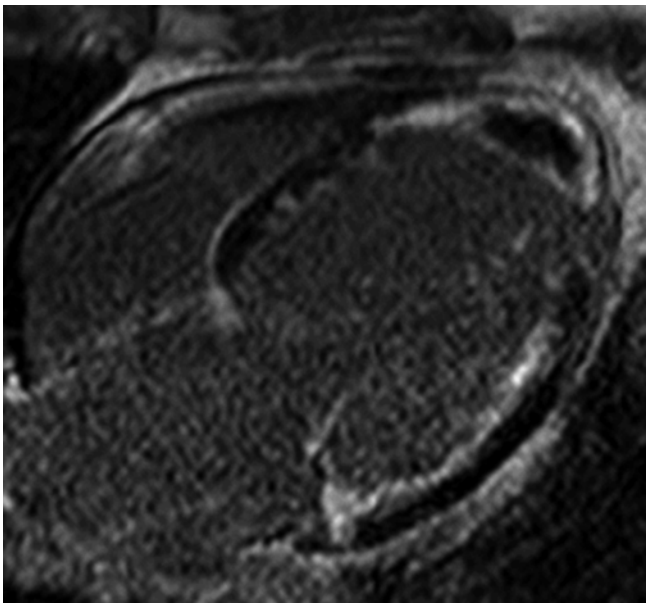

Fig. 11.13 The adverse left ventricle remodeling after myocardial infarction. Cardiac magnetic resonance shows apical thinning, aneurysmal dilatation of left ventricle, and LV thrombosis inside the aneurysmal change on LGE image

- The failure to normalize increased wall stresses results in progressive dilatation, recruitment of border zone myocardium into the scar, and deterioration in contractile function.
- Delayed reperfusion therapy may increase infarct size and lead to adverse LV remodeling due to infarct expansion, thinning of the necrotic segment associated with dilatation, as well as compensatory hypertrophy of remote myocardium.

- MRI is particularly suitable for the study of large infarcts with aneurysmal ventricular chamber dilatation since LV volume and mass evaluations are independent from geometric assumptions.
- The infarct size, transmural infarction, and persistent microvascular damage on LGE are strong predictors of adverse postinfarct remodeling over and above other clinical parameters (Fig. 11.14) [5, 17].

11.3.1.8 Post-PCI Complication

- *Microinfarctions after coronary microembolization*
  - Coronary microemboli fragmented from atherosclerotic plaque in acute coronary syndrome and after reperfusion at percutaneous coronary intervention cause microinfarctions and release of myocardial ischemic markers. It is difficult to separate the effects of reperfusion injury.
  - Coronary microembolization causes acute and subacute hypoperfusion detectable on first-pass perfusion MRI after coronary intervention. LGE-MRI has the potential to help reliably quantify subacute microinfarction [18–20].

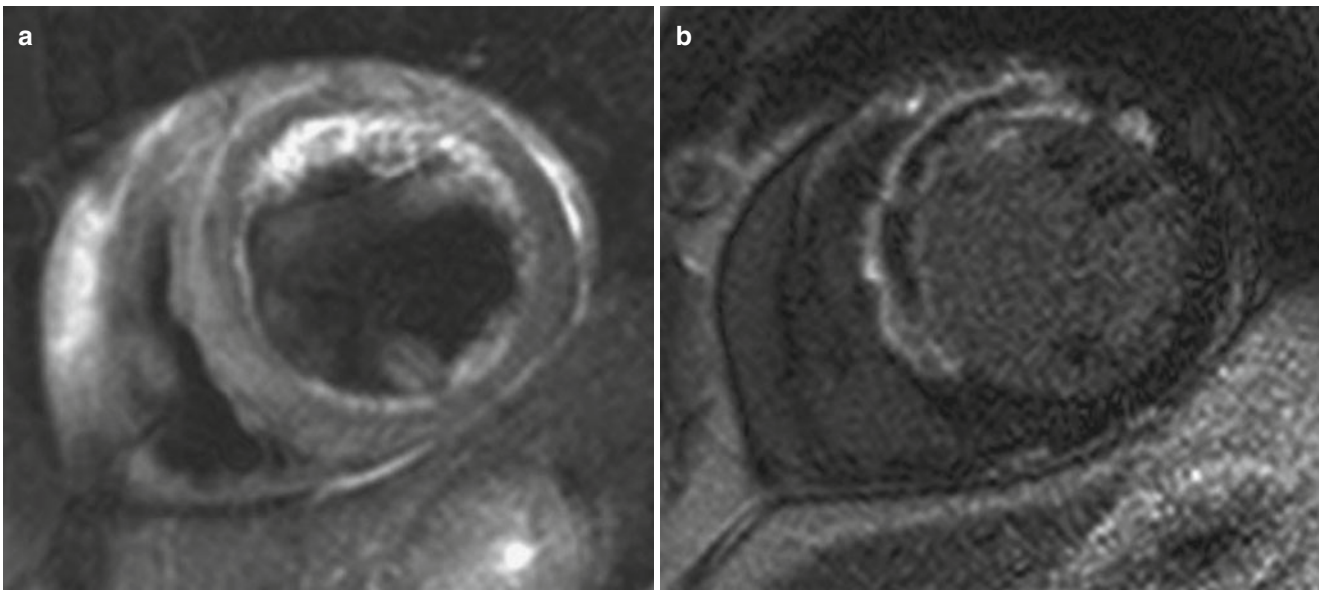

Fig. 11.14 LV remodeling and persistent microvascular damage. In this case, T2WI (**a**) shows peripheral high SI with central low SI at LAD territory. LGE (**b**) also showed peripheral delayed hyperenhancement with central PMVO at corresponding area. Initial cine MRI (**c**) demonstrated that severe hypokinesia or akinesia is noted at the anterior and anteroseptal wall. However, F/U MRI (**d**) showed myocardial thinning with akinesia at corresponding area suggesting LV remodeling

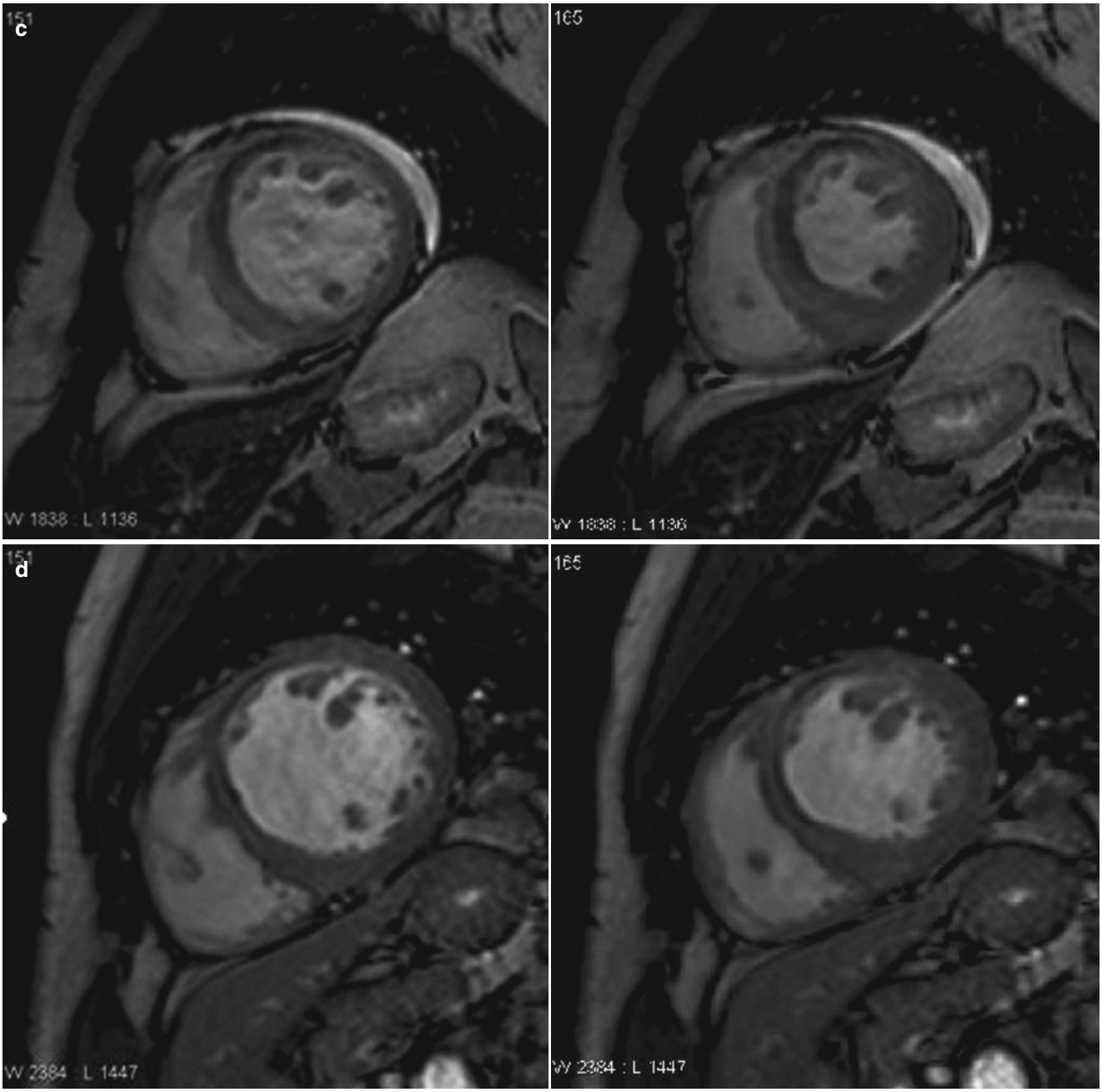

Fig. 11.14 (continued)

- Microinfarctions after coronary microembolization were patchy with a striped pattern from the endocardium to the epicardium on LGE-MRI (Fig. 11.15).

11.4 Differential Diagnosis

11.4.1 Noncoronary Disease

- Even though some patients have classic features of acute MI, sometimes their coronary angiographies do not show any culprit lesion.
- Cardiac MRI may also be useful in patients with chest pain and elevated cardiac enzyme, but normal or insignificant coronary arteries.
  - One potential advantage of LGE is that the pattern of hyperenhancement, rather than simply the presence or extent, may offer important information regarding the etiology of myocardial damage such as myocarditis on the basis of hyperenhancement patterns.
  - Cardiac MRI established that the most common diagnoses were myocarditis (31 %), Takotsubo cardiomyopathy (31 %), and STEMI with spontaneous thrombolysis (29 %) (Fig. 11.16).

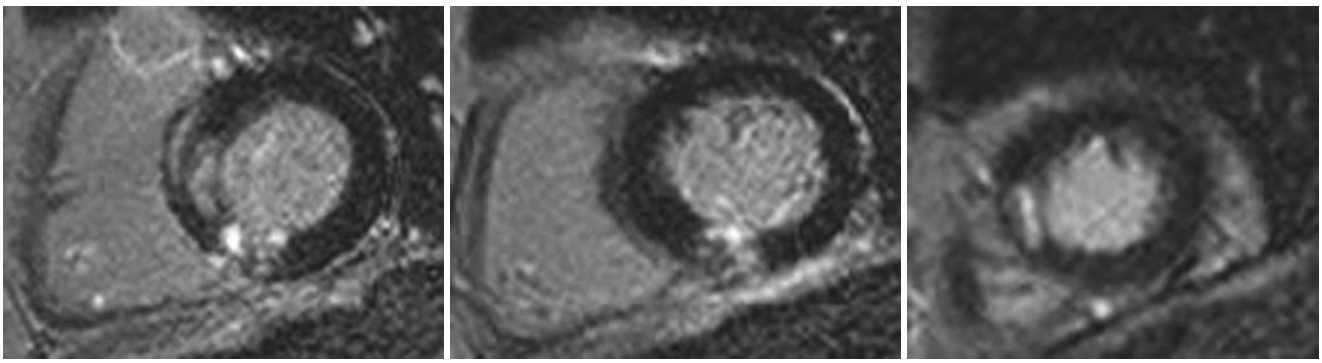

Fig. 11.15 Microinfarctions after coronary microembolization. Several discrete patchy and striped hyperenhancement was shown from the endocardium to the epicardium on LGE at the mid to basal inferior wall and apical and basal septal wall

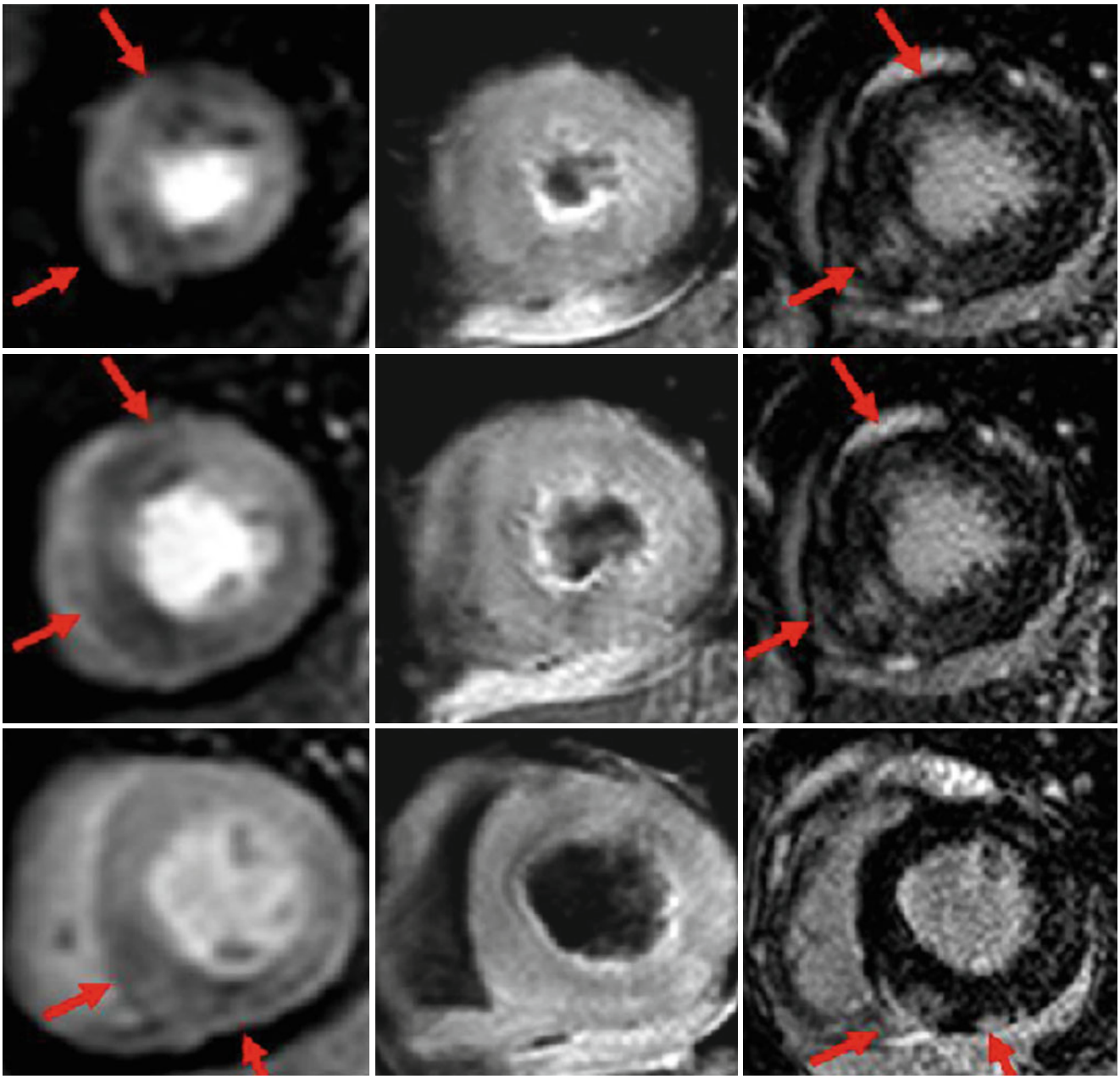

Fig. 11.16 Myocarditis. A 36-year-old female with acute chest pain and increased cardiac enzyme. She is finally diagnosed with myocarditis. Multifocal patchy perfusion defect (*left line*) and enhancement at nonvascular territory on LGE (*right line*) at the mid to epicardial layer of the apical anterior and lateral wall, midventricular anteroseptal, inferoseptal, and basal inferoseptal, and inferior wall (*arrows*)

Differential diagnosis of acute myocardial infarction in cardiac MRI
Myocarditis
Takotsubo cardiomyopathy
Dilated cardiomyopathy
Hypertrophic cardiomyopathy
Cardiac infiltrative disease (amyloidosis)
Acute pericarditis
Cardiotoxic chemotherapy
Cardiac contusion after chest wall trauma
Cardiac syndrome X
Variant angina

11.5 Summary

- Checklist of what the clinician should be informed in initial CMR:
  - Myocardial edema with area at risk on T2WI
  - Myocardial viability on LGE vs. contractile reserve on low-dose DSMR
  - Reperfusion injury
  - Cardiac function
  - Infarct complication
- Checklist on follow-up CMR:
  - Evaluation of LV remodeling
  - Evolution of infarct size on LGE
- Differential diagnosis of MI
  - Myocarditis, pericarditis, Takotsubo cardiomyopathy, DCMP, HCMP, and so on

References

1. Thygesen K, Alpert JS, White HD. Universal definition of myocardial infarction. J Am Coll Cardiol. 2007;50(22):2173.
2. Perazzolo Marra M, Lima JA, Iliceto S. MRI in acute myocardial infarction. Eur Heart J. 2011;32(3):284–93.
3. Kim HW, Farzaneh-Far A, Kim RJ. Cardiovascular magnetic resonance in patients with myocardial infarction: current and emerging applications. J Am Coll Cardiol. 2009;55(1):1–16.
4. Hundley WG, et al. ACCF/ACR/AHA/NASCI/SCMR 2010 expert consensus document on cardiovascular magnetic resonance: a report of the American College of Cardiology Foundation Task Force on Expert Consensus Documents. J Am Coll Cardiol. 2010;55(23):2614–62.
5. Wu KC, et al. Prognostic significance of microvascular obstruction by magnetic resonance imaging in patients with acute myocardial infarction. Circulation. 1998;97(8):765–72.
6. Kim RJ, et al. Relationship of MRI delayed contrast enhancement to irreversible injury, infarct age, and contractile function. Circulation. 1999;100(19):1992–2002.
7. Kim RJ, et al. Performance of delayed-enhancement magnetic resonance imaging with gadoversetamide contrast for the detection and assessment of myocardial infarction. Circulation. 2008;117(5):629–37.
8. Chung S-Y, et al. Comparison of stress perfusion MRI and SPECT for detection of myocardial ischemia in patients with angiographically proven three-vessel coronary artery disease. Am J Roentgenol. 2010;195(2):356–62.
9. Croisille P, Kim HW, Kim RJ. Controversies in cardiovascular MR imaging: T2-weighted imaging should not be used to delineate the area at risk in ischemic myocardial injury. Radiology. 2012;265(1):12–22.
10. Abdel-Aty H, et al. Delayed enhancement and T2-weighted cardiovascular magnetic resonance imaging differentiate acute from chronic myocardial infarction. Circulation. 2004;109(20):2411–6.
11. Friedrich MG, et al. The salvaged area at risk in reperfused acute myocardial infarction as visualized by cardiovascular magnetic resonance. J Am Coll Cardiol. 2008;51(16):1581–7.
12. Choi SI, et al. Application of breath-hold T2-weighted, first-pass perfusion and gadolinium-enhanced T1-weighted MR imaging for assessment of myocardial viability in a pig model. J Magn Reson Imaging. 2000;11(5):476–80.
13. Choi SH, et al. Investigation of T2-weighted signal intensity of infarcted myocardium and its correlation with delayed enhancement magnetic resonance imaging in a porcine model with reperfused acute myocardial infarction. Int J Cardiovasc Imaging. 2009;25:111–9.
14. Tarantini G, et al. Duration of ischemia is a major determinant of transmurality and severe microvascular obstruction after primary angioplasty: a study performed with contrast-enhanced magnetic resonance. J Am Coll Cardiol. 2005;46(7):1229–35.
15. Lamfers E, et al. Abortion of acute ST segment elevation myocardial infarction after reperfusion: incidence, patients' characteristics, and prognosis. Heart. 2003;89(5):496–501.
16. Shan K, et al. Role of cardiac magnetic resonance imaging in the assessment of myocardial viability. Circulation. 2004;109(11):1328–34.
17. Hombach V, et al. Sequelae of acute myocardial infarction regarding cardiac structure and function and their prognostic significance as assessed by magnetic resonance imaging. Eur Heart J. 2005;26(6):549–57.
18. Ricciardi MJ, et al. Visualization of discrete microinfarction after percutaneous coronary intervention associated with mild creatine kinase-MB elevation. Circulation. 2001;103(23):2780–3.
19. Carlsson M, et al. Heterogeneous microinfarcts caused by coronary microemboli: evaluation with multidetector CT and MR imaging in a swine model. Radiology. 2010;254(3):718–28.
20. Carlsson M, et al. Myocardial microinfarction after coronary microembolization in swine: MR imaging characterization. Radiology. 2009;250(3):703–13.

Chronic Ischemic Heart Disease

12

Ki Seok Choo and Yeon Hyeon Choe

Contents

K.S. Choo
Department of Radiology, Pusan National University Yangsan Hospital, Pusan National University, School of Medicine, Busan, Republic of Korea
e-mail: kschoo0618@naver.com

Y.H. Choe (✉)
Department of Radiology, Samsung Medical Center, Sungkyunkwan University School of Medicine, Seoul, Republic of Korea
e-mail: yhchoe@skku.edu

Abstract

Chronic ischemic cardiomyopathy (ICMP) is a major and growing problem. Coronary artery disease (CAD) is the leading cause of heart failure and left ventricular systolic dysfunction. To help differentiate between ICMP and non-ischemic cardiomyopathy (NICMP), coronary angiography (CA) has long been considered the test of choice for establishing the presence or absence of significant CAD. This chapter details the role of cardiac imaging such as coronary computed tomography and cardiac magnetic resonance imaging in the diagnosis of ICMP and in discriminating ICMP from NICMP.

12.1 Introduction

12.1.1 Chronic Myocardial Infarction

- Myocardial infarction (MI) can be defined temporally and pathologically as evolving, acute, healing, and healed. Healed MI was called as chronic MI or old MI [1].
  - Evolving MI (<6 h): minimal or no polymorphonuclear leukocytes
  - Acute MI (6 h–7 days): presence of polymorphonuclear leukocytes
  - Healing MI (7–28 days): presence of mononuclear cells and fibroblasts/absence of polymorphonuclear leukocytes
  - Healed MI (29 days and beyond): scar tissue without cellular infiltration

12.1.2 Ischemic Cardiomyopathy

- Ischemic cardiomyopathy (ICM) has been used to describe significantly impaired left ventricular function that results from coronary artery disease.

T.-H. Lim (ed.), *Practical Textbook of Cardiac CT and MRI*,
DOI 10.1007/978-3-642-36397-9_12, © Springer-Verlag Berlin Heidelberg 2015

- Two main pathogeneses of ischemic cardiomyopathy
  - Irreversible injury of the myocardium due to prior myocardial infarction with ventricular remodeling
  - Partially reversible contractile dysfunction due to at least partial reversible injury but still viable myocardium (hibernating myocardium) or transient postischemic dysfunction (stunned myocardium)
- Identification of hibernating myocardium is very important because it has been shown to be a significant survival advantage following revascularization compared with those receiving medical therapy alone.

12.2 Modalities for Chronic Ischemic Heart Disease

12.2.1 PET and SPECT

- PET and SPECT is a well-validated, noninvasive imaging for many years.
- The main disadvantages of PET and SPECT are radiation exposure and relatively low spatial resolution.

12.2.2 CT

- CT has enabled qualitative and quantitative assessment of myocardial scar, but with only a limited diagnostic value in comparison to DE-MRI.
- In a real clinical field, the main clinical application of CT is the coronary artery imaging.

12.2.3 MRI

- CMR is a comprehensive, accurate, and emerging modality to assess patients with ICM.
- CMR is regarded as the reference standard for the assessment of ventricular volume and systolic function and the visualization and quantification of myocardial scar in patients with ICM.
- DE-MRI can help determine the transmural extent of myocardial scar on the basis of higher spatial resolution, which is not possible with other imaging modalities [2].
- The likelihood of functional recovery after revascularization can be predicted based on transmurality of myocardial scar.
- Additional low-dose dobutamine stress magnetic resonance (DSMR) can be performed in intermediate degree of myocardial scar (transmurality 1–75 %). The specificity of low dose (DSMR) to detect hibernating myocardium is superior to that of radionuclide imaging.
- Stress MR perfusion at the same time can be used for the detection of inducible ischemia in patients with suspected hibernating myocardium (Fig. 12.1).

12.3 Specific Imaging Finding for Chronic Ischemic Heart Disease

12.3.1 Left Ventricular Aneurysm

- Left ventricular aneurysm is most commonly the result of myocardial infarction, usually involving LV anterior wall.
- Hypertrophic cardiomyopathy and Chagas disease can be also causes of left ventricular aneurysm. The aneurysm may be asymptomatic or present as heart failure, sustained ventricular tachyarrhythmias, or arterial embolism (Fig. 12.2) [3].

12.3.2 Left Ventricular Pseudoaneurysm

- Left ventricular pseudoaneurysm develops after an acute MI which is complicated by a ventricular free wall rupture that is contained by localized pericardial adhesions and generally occurs after inferior myocardial infarction due to occlusion of the left circumflex artery inferior wall (Table 12.1).

12.3.3 Left Ventricular Thrombus

- The detection of thrombi after a recent MI is an indication for long-term anticoagulation.
- Both MRI and CT imaging can excellently detect thrombus within LV cavity, and MRI has been shown to detect small mural thrombus within apical aneurysm better than contrast echocardiography (Fig. 12.3).

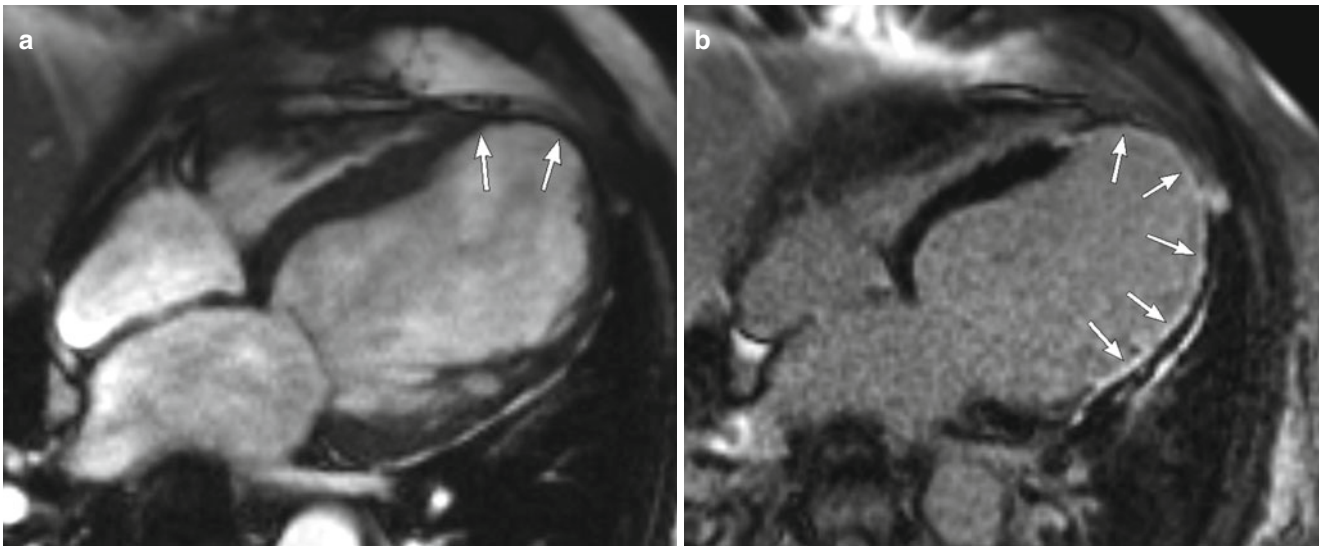

Fig. 12.1 MRI of a patient with myocardial thinning on cine and fibrosis on delayed gadolinium-enhanced imaging (DE-MRI) following MI. (**a**) Cine MRI with 4-chamber view shows myocardial thinning in apical and lateral walls with dyskinesia (*arrows*) on systole. (**b**) DE-MRI reveals hyperenhancement (*arrows*) with transmural involvement in apex and partial thickness involvement in lateral wall

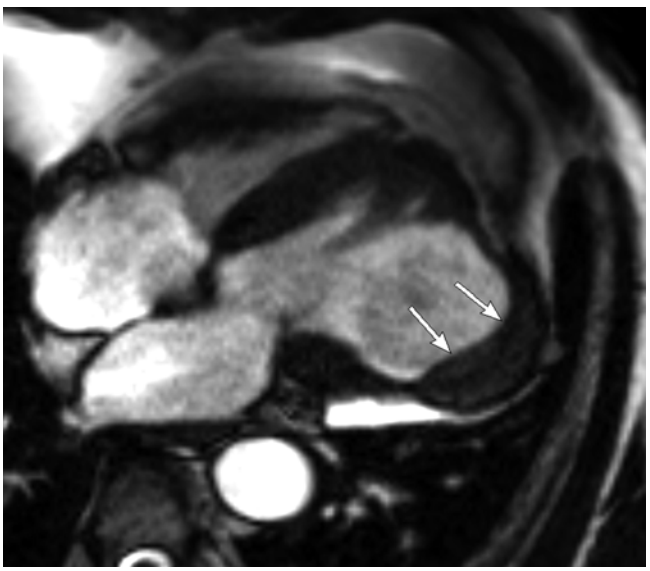

Fig. 12.2 MRI of a patient with pseudoaneurysm of LV in lateral wall. Cine MRI with 4-chamber view shows a large wide-neck aneurysm in lateral wall with thrombus (*arrows*)

Table 12.1 Differential diagnosis between true aneurysm and pseudoaneurysm [4–7]

True aneurysm	Pseudoaneurysm
Consists of an endocardium, myocardium, and epicardium ± thrombus	Consists of an epi-/pericardium ± thrombus
Wide neck/base	Narrow neck/base
Low risk of rupture	Higher risk of rupture
Commonly anterior wall	Commonly inferior wall
	Marked enhancement of the pericardium

12.3.4 Myocardial Fat Scarring

- CT imaging usually reveals that the prevalence of myocardial fat scarring at LV is 22–62 % among patients with a history of MI.

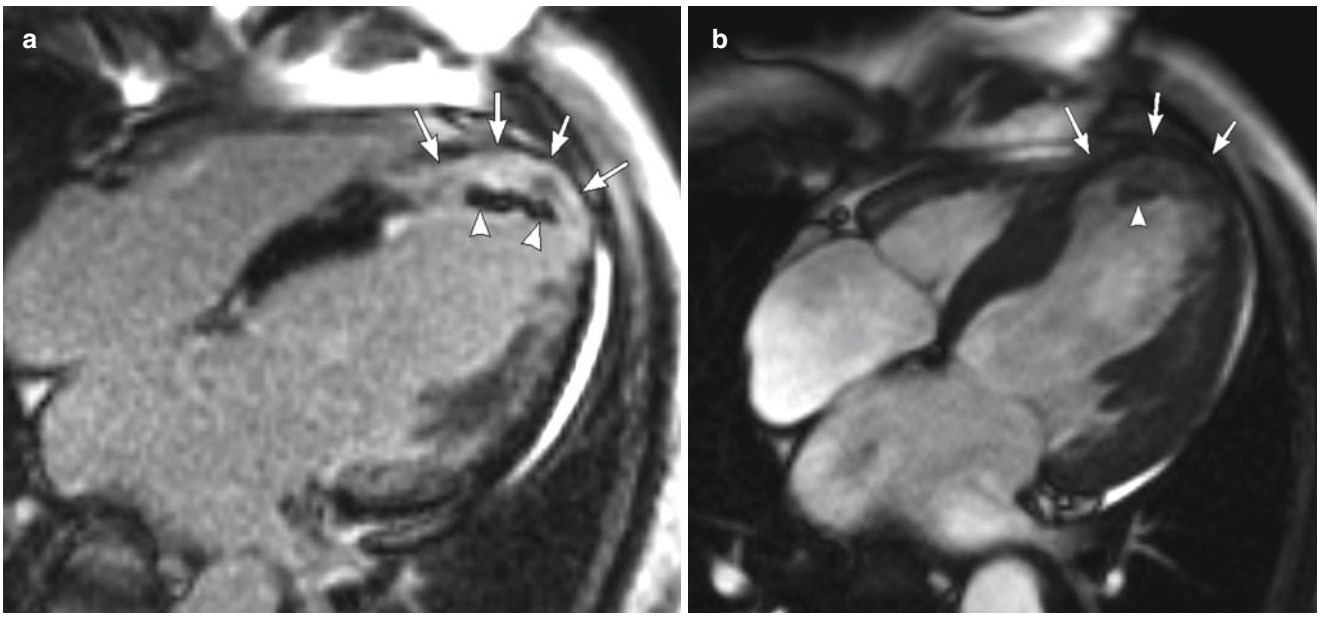

Fig. 12.3 MRI of a patient with myocardial thinning and thrombus. (**a**) DE-MRI with 4-chamber view shows wall thinning (*arrows*) with hyperenhancement (*arrows*) and mural thrombus (*arrowheads*). (**b**) Cine MRI with 4-chamber view shows wall thinning (*arrows*) and thrombus (*arrowhead*)

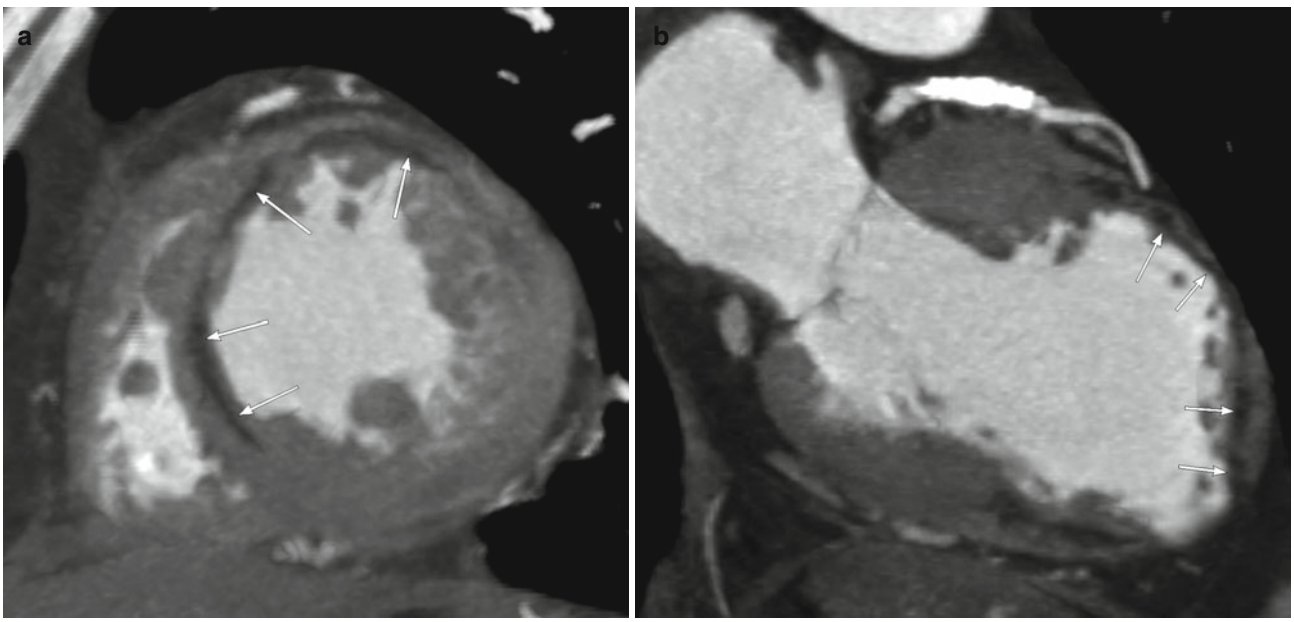

Fig. 12.4 CT of a patient with myocardial fat scarring by healed MI. Cardiac CT (short-axis and 2-chamber views) shows subendocardial myocardial fat scarring (*arrows*) at mid- to apical anteroseptal wall

- Myocardial fat scarring caused by healed MI is of thin and linear or curvilinear configuration along the vascular territory of culprit coronary artery [8].
- CT imaging studies usually shows subendocardial fat scarring of normal thickness or thin. Middle or subepicardial layer of myocardial fat scarring has rarely been observed (Fig. 12.4).

12.3.5 Myocardial Calcification

- Myocardial calcification is classified as either dystrophic or metastatic [9].
- Dystrophic myocardial calcification is usually caused by a large myocardial infarction and is reported to occur in 8 % of infarcts more than 6 years old (Fig. 12.5).

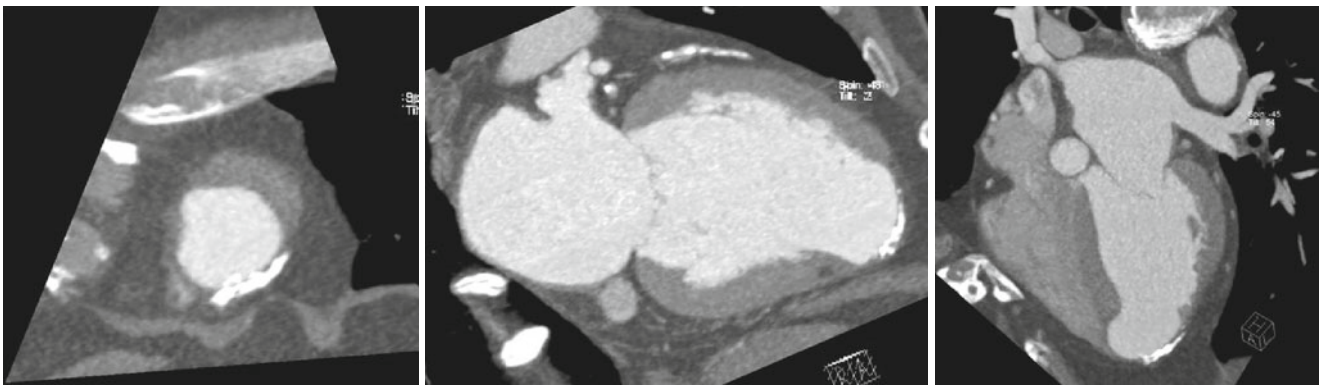

Fig. 12.5 CT of patient with linear myocardial calcification. Cardiac CT (short axis, 2-chamber, 4-chamber) shows curvilinear calcification with wall thinning at LV apex and apical inferior wall

12.4 The Role of MRI for Differentiating Between ICMP and Non-ICMP

- The main finding of differentiation between ICMP and NICMP lies in the subendocardial or transmural DE along the coronary vascular territory noted in the former compared to either no DE or a mid-wall or subepicardial DE pattern seen in the latter.
- CT and stress MR perfusion can be also used in the evaluation of significant coronary artery disease for differentiating between ICMP and non-ICMP.
- DE pattern is likely secondary to a transient thrombotic or embolic event with spontaneous recanalization sufficient to cause the myocardial injury despite no obvious disease on CCTA or stress MR perfusion as well as conventional coronary angiography.

12.5 Summary

- CCTA could be a useful tool in excluding CAD in chronic ischemic heart disease.
- CMR has become the reference of standard in the evaluation of myocardial viability in patients with ICMP.
- DE-MRI is a valuable tool for differentiating between ICMP and non-ICMP.

References

1. Thygesen K, Alpert JS, White HD. Universal definition of myocardial infarction. Circulation. 2007;116:2634–53.
2. Mahrholdt H, Wagner A, Judd RM, Sechtem U, Kim RJ. Delayed enhancement cardiovascular magnetic resonance assessment of non-ischaemic cardiomyopathies. Eur Heart J. 2005;26:1461–74, Fig. 3 Supplemental material.
3. Pretre R, Linka A, Jenni R, Turina MI. Surgical treatment of acquired left ventricular pseudoaneurysms. Ann Thorac Surg. 2000; 70:53–7.
4. Frances C, Romero A, Grady D. Left ventricular pseudoaneurysm. J Am Coll Cardiol. 1998;32:557–61.
5. Yeo TC, Malouf JF, Oh JK, Seward JB. Clinical profile and outcome in 52 patients with cardiac pseudoaneurysm. Ann Intern Med. 1998;128:299–305.
6. Yaymaci B, Bozbuga N, Balkanay M. Unruptured left ventricular pseudoaneurysm. Int J Cardiol. 2001;77:99–101.
7. Konen E, Merchant N, Gutierrez C, Provost Y, Mickleborough L, Paul NS, Butany J. True versus false left ventricular aneurysm: differentiation with MR imaging – initial experience. Radiology. 2005;236:65–70.
8. Kimura F, Matsuo Y, Nakajima T. Myocardial fat at cardiac imaging: how can we differentiate pathologic from physiologic fatty infiltration? Radiographics. 2010;30:1587–602.
9. Gowda RM, Boxt LM. Calcification of the heart. Radiol Clin North Am. 2004;42:603–17.

Part III

Non-ischemic Cardiomyopathy

Dilated Cardiomyopathy

13

Eun Young Kim and Yeon Hyeon Choe

Contents

Abstract

Dilated cardiomyopathy (DCM) is a progressive disease of heart muscle that is characterized by ventricular chamber enlargement and contractile dysfunction, and DCM is the third most common cause of heart failure and the most frequent reason for heart transplantation. Cardiac MR is useful modality for the diagnosis, and to assess the degree of cardiac dysfunction, to identify the cause, and to guide treatment.

13.1 Overview

13.1.1 Definition

- Ventricular chamber enlargement and systolic dysfunction (left ventricular ejection fraction <30–40 % or fractional shortening less than 25 %) [1, 2].

13.1.2 Prevalence

- Five to eight cases per 100,000 populations, with an estimated prevalence of 1:2,500 [3].
- The third most common cause of heart failure after ischemia and valvular disease.
- Approximately 90 % of all cardiomyopathies; approximately 50 % of all cases of dilated cardiomyopathy (DCM) are idiopathic [4].
- Idiopathic DCM is the most common cause of heart failure in the young, with an estimated prevalence of at least 36.5 per 100,000 persons in the United States.
- Due to mild clinical symptoms in the early phase of the disease, the true prevalence is probably even much higher. It has been suggested that up to 14 % of the middle-aged and elderly population have asymptomatic left ventricular systolic dysfunction [5].

Electronic supplementary material Supplementary material is available in the online version of this chapter at 10.1007/978-3-642-36397-9_13.

E.Y. Kim
Department of Radiology, Gachon University
Gil Hospital, Incheon, Republic of Korea
e-mail: oneshot0229@gmail.com

Y.H. Choe (✉)
Department of Radiology, Samsung Medical Center,
Sungkyunkwan University School of Medicine,
Seoul, Republic of Korea
e-mail: yhchoe@skku.edu

T.-H. Lim (ed.), *Practical Textbook of Cardiac CT and MRI*,
DOI 10.1007/978-3-642-36397-9_13,

Table 13.1 Causes of dilated cardiomyopathy

Ischemia	**Medications**	**Rheumatologic disease**
Infection	Chemotherapeutic agents	Systemic lupus, scleroderma
Virus	Antiretroviral drugs	**Endocrinologic disorders**
Bacteria	Phenothiazines, chloroquine	Pheochromocytoma, diabetes mellitus
Fungus	**Electrolyte abnormalities**	**Miscellaneous**
Parasite	Hypocalcemia, uremia	Radiation
Rickettsia	Hypophosphatemia	Sarcoidosis
Deposition disease	**Genetic ± neuromuscular disease**	Tachycardia
Hemochromatosis	Duchenne's muscular dystrophy	Sleep apnea
Amyloidosis	Myotonic dystrophy	Oxygen free radical
Toxins	Friedreich's ataxia	Autoimmune myocarditis
Ethanol, cocaine	Nutritional deficiencies	Familial cardiomyopathies
Lead, mercury	Thiamine, selenium, carnitine	Peripartum cardiomyopathy

13.1.3 Clinical Features

- Most commonly diagnosed in the third or fourth decade, but also in young children [3].
- Progressive heart failure and a decline in left ventricular systolic function, arrhythmias, thromboembolism, and sudden death at any stage of the disease.
- High mortality rate (median period of survival of 1.7 years for men and 3.2 years for women) [3].
- The natural history of the condition is progressive, and its cost, disability, and morbidity are among the highest of any disease.
- Histopathologic features – generally microscopic interstitial fibrosis, but some patients have grossly visible nontransmural or, rarely, transmural fibrosis [6].
- Systolic dysfunction is the most important independent predictor of outcome, and evaluation of diastolic filling allows further identification of subgroups with divergent long-term prognosis.

13.1.4 Cause (Table 13.1)

- In the World Health Organization classification, DCM is classified as its primary (e.g., idiopathic or familial) and secondary forms.
- Up to 50 % of patients diagnosed with idiopathic cardiomyopathy have a familial DCM.
- Although genetically heterogeneous, the predominant mode of inheritance for DCM is autosomal dominant, with X-linked autosomal recessive and mitochondrial inheritance less frequently.

13.2 Imaging Modalities and Findings

13.2.1 Computed Tomography

- With ECG-gated cardiac CT, coronary artery disease can be excluded because of high specificity and negative predictive value.
- Although ionizing radiation and injection of relatively large amounts of iodinated contrast agents are required, ECG-gated CT scanning enables morphological analysis of the ventricles and is an accurate means of evaluating ventricular function (Fig. 13.1).

13.2.2 Magnetic Resonance Imaging

- Detailed morphologic evaluation of ventricles.
  - In black blood images, enlarged cardiac chambers and thin myocardial walls are evident.
  - Mural thrombi can also be identified.
- Functional evaluation of ventricles.
  - Cine images usually show ventricular hypokinesia and increased volumes. Using steady-state free precession (SSFP) images, the diagnosis of left ventricle (LV) dilation is simply made when short-axis internal LV chamber diameter is larger than 5.0 cm or when the LV end diastolic volume exceeds 235 mL or 112 mL/m^2 in males and 174 or 99 mL/m^2 in females.
  - The superior quality of images obtained by SSFP technique facilitates the detection of regional wall motion abnormalities allowing an easier differentiation between ischemic and non-ischemic LV impairment [7].
  - CMR is able to overcome many of the limitations of echocardiographic assessment of ventricular function and volumes. The significantly lower inter- and intraobserver variability in CMR measurements allows better monitoring of response to medical intervention or disease progression.
- Characterization of myocardial tissue using late gadolinium enhancement (LGE) images.
  - To differentiate between DCM secondary to coronary artery disease and other causes of DCM. The differentiation between these subgroups may be fundamental in the therapeutic and prognostic approach to the patients [8].
    - In non-ischemic DCM, hyperenhancement was either absent (59–88 % of cases) or appeared as

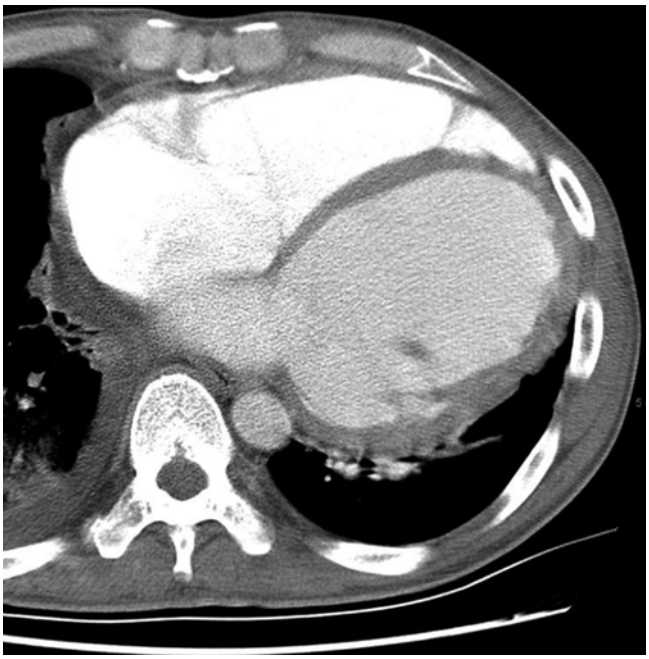

Fig. 13.1 CT of a patient with idiopathic dilated cardiomyopathy. ECG-gated cardiac CT shows a dilated left ventricle (7 cm in the internal diameter)

stripes of hyperenhancement in the mid-wall of the myocardium not related to specific coronary artery perfusion territories (9–35 % of the cases).
    - A subgroup of patients with DCM has fibrosis in a predominantly subendocardial distribution, characteristic of infarction (it has been suggested that these may represent coronary emboli-induced ischemic cardiomyopathy cases or ruptured coronary plaques that have subsequently recanalized).
- Degree of fibrosis is an important prognostic predictor.
    - In a group of patients with DCM, 35 % of these patients had mid-wall myocardial fibrosis, which is a predictor of the combined end point of all-cause mortality and cardiovascular hospitalization and also of sudden cardiac death and ventricular tachycardia [9].
    - The predictive value of mid-wall fibrosis remained significant after correction for LV volumes and ejection fraction (Figs. 13.2, 13.3, 13.4, 13.5, and 13.6).

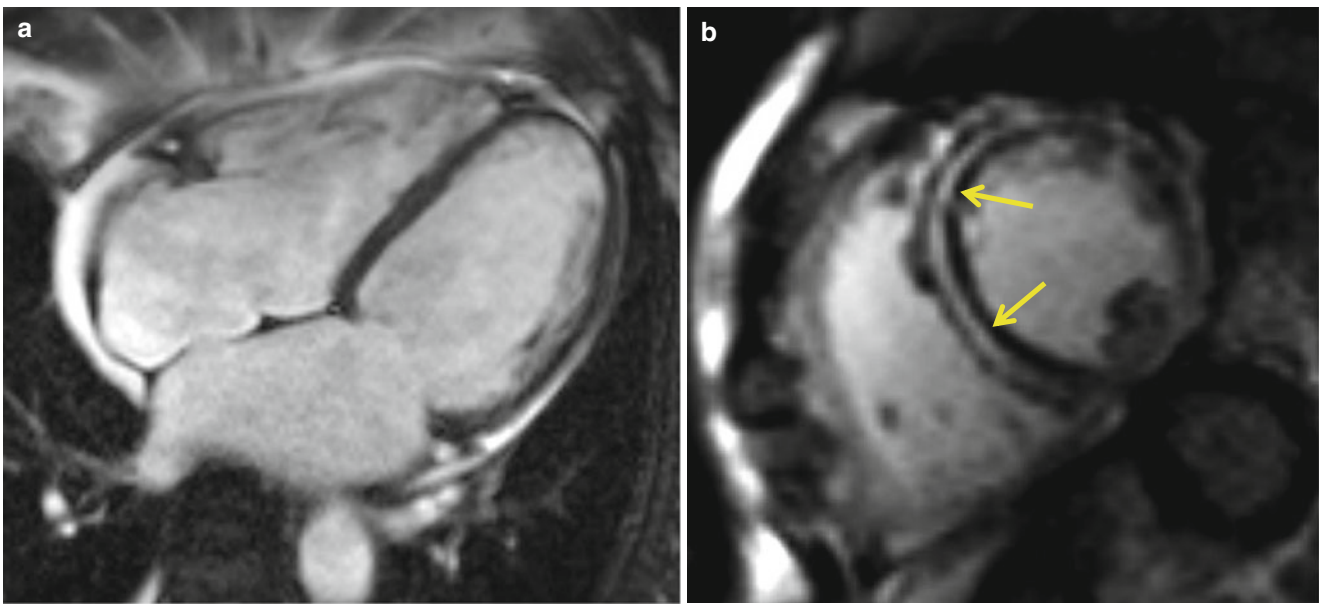

Fig. 13.2 MRI of a patient with idiopathic dilated cardiomyopathy (DCM) (http://extras.springer.com/2015/978-3-642-36396-2). (**a**) Four-chamber cine MRI shows dilated ventricles. Calculated left ventricular ejection fraction using cine MRI was 39 %. (**b**) Delayed enhancement MRI demonstrates typical non-ischemic DCM of delayed enhancement (*arrows*) in the LV, i.e., stripes of hyperenhancement in the mid-wall of the myocardium

Learning Points of DCM

Stripes of hyperenhancement in the mid-wall of the myocardium are a typical enhancement pattern in patients with non-ischemic DCM.

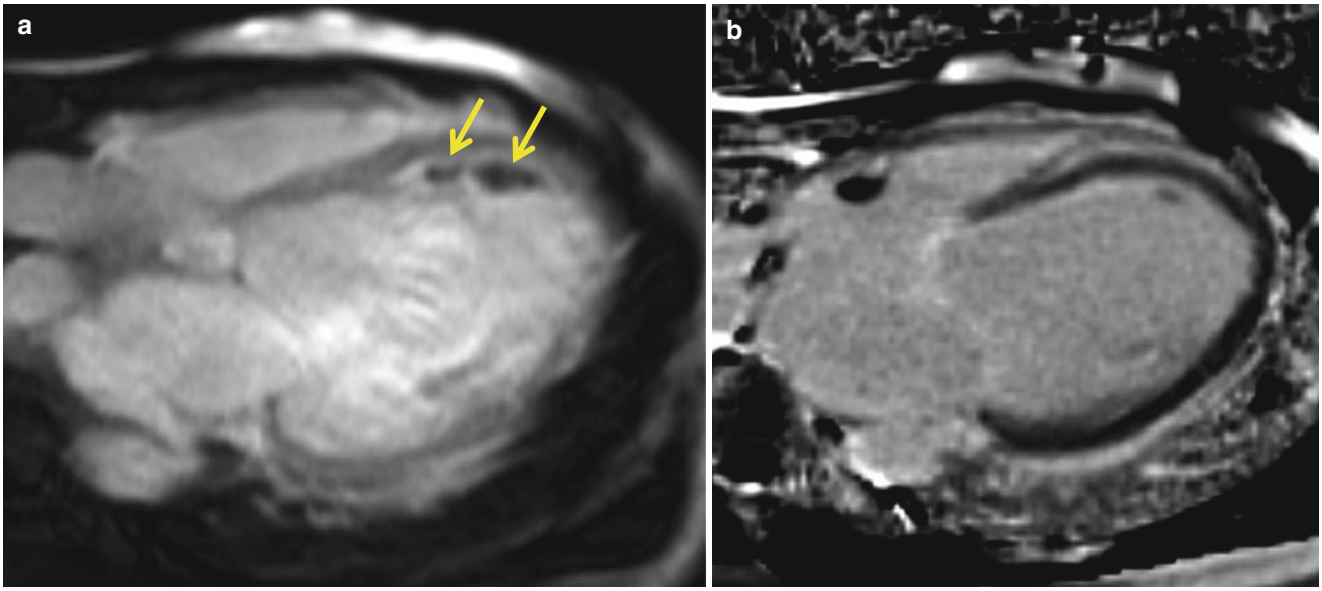

Fig. 13.3 MRI of a patient with idiopathic dilated cardiomyopathy and thrombus in the left ventricle (http://extras.springer.com/2015/978-3-642-36396-2). (**a**) Delayed enhancement MRI with long inversion time (600 ms) demonstrates non-enhancing low signal intensity area (*arrows*), indicating thrombus in the left ventricle. (**b**) Delayed enhancement MRI (phase-sensitive inversion recovery) shows no abnormal delayed myocardial enhancement

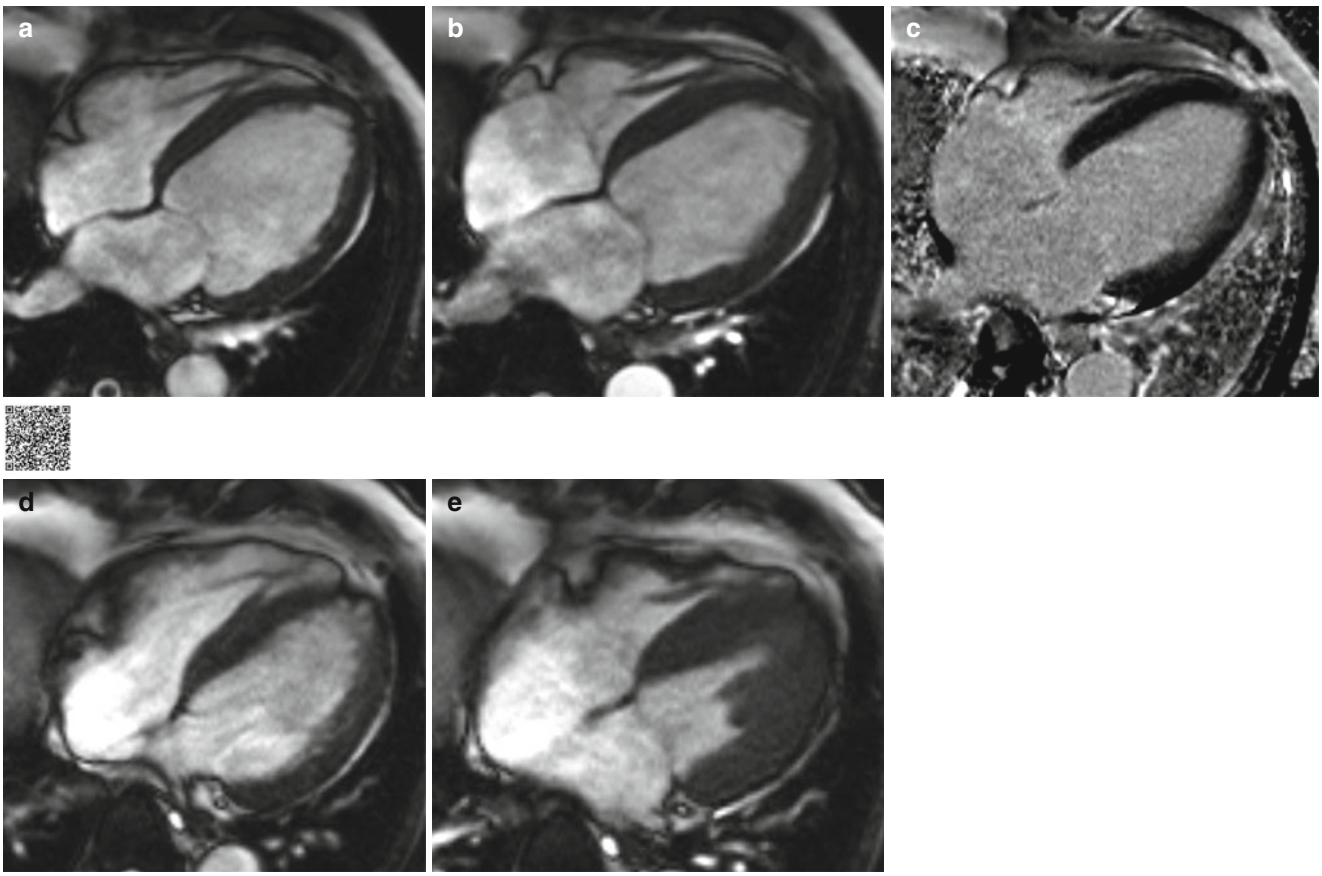

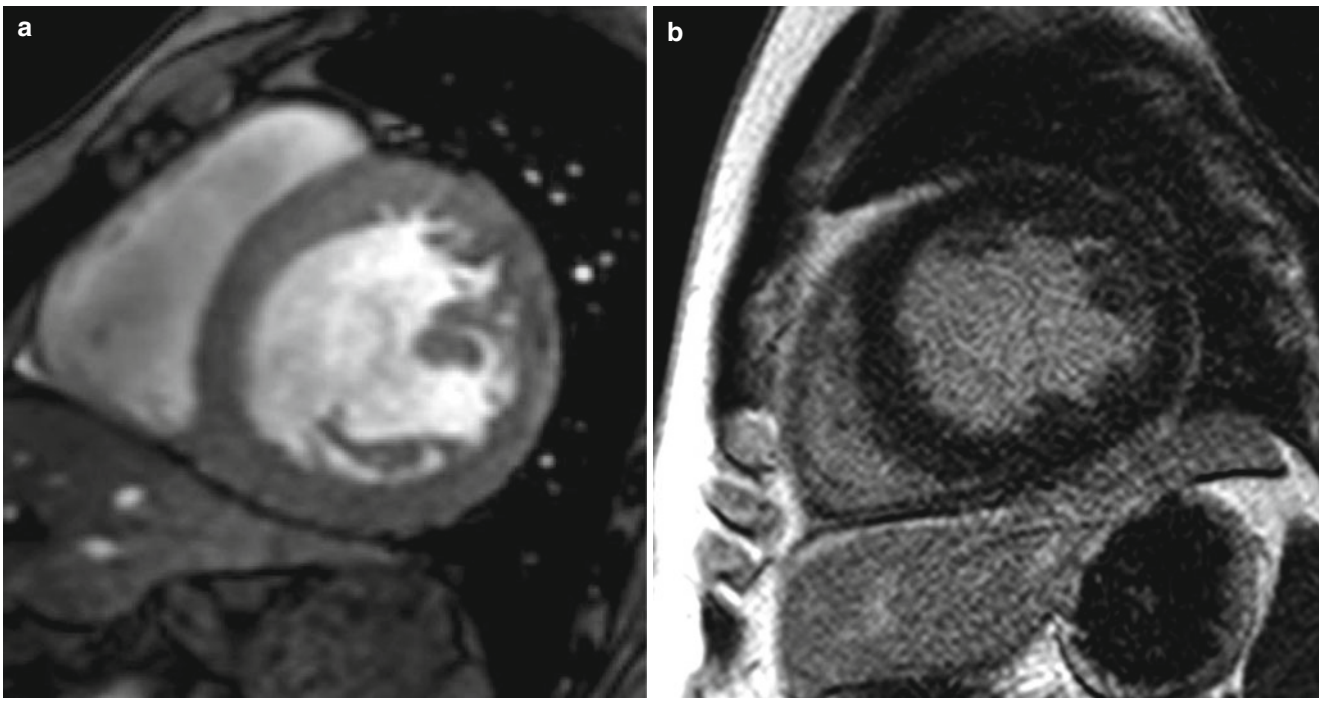

Fig. 13.5 MRI of a patient with a history of excessive alcohol consumption. Invasive coronary angiographic findings were normal (not shown here). (**a**) Short-axis cine MRI shows a dilated left ventricle. (**b**) Delayed enhancement MRI demonstrates no abnormal delayed myocardial enhancement

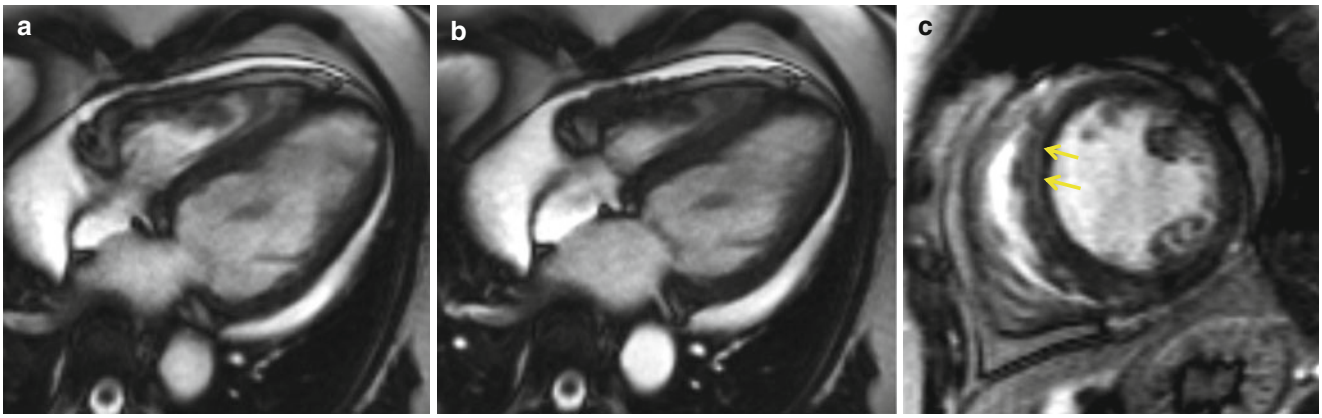

Fig. 13.6 MRI of a female patient with long-term treatment of doxorubicin for malignancy (http://extras.springer.com/2015/978-3-642-36396-2). (**a**) Four-chamber cine MRI shows a dilated left ventricle and impaired systolic contraction of the left ventricle (**b** systolic phase). Calculated left ventricular ejection fraction using cine MRI was 23 %, and the left ventricular end diastolic volume was 120 mL/m^2. (**b**) Delayed enhancement MRI demonstrates mild mid-wall enhancement in the mid-ventricular septum (*arrows*)

Fig. 13.4 MRI of a patient with idiopathic dilated cardiomyopathy. (**a**, **b**) Initial four-chamber cine MRI shows dilated ventricles and impaired systolic contraction of the left ventricle (**b** systolic phase) (http://extras.springer.com/2015/978-3-642-36396-2). (**c**) Delayed enhancement MRI demonstrates no abnormal delayed myocardial enhancement. (**d**, **e**). One-year follow-up four-chamber cine MRI reveals normal left ventricular internal dimension and improved systolic contraction (**e**) (http://extras.springer.com/2015/978-3-642-36396-2)

Learning Points of DCM

In non-ischemic DCM, hyperenhancement was either absent (59–88 % of cases) or appeared as stripes of hyperenhancement in the mid-wall of the myocardium (9–35 % of the cases). The myocardial fibrosis (enhancement area) appears to be irreversible and is regarded as a predictor of adverse outcome.

- T1 mapping
  - Postcontrast myocardial T1 time is inversely correlated with the presence of diffuse fibrosis at endomyocardial biopsy in a population with a broad spectrum of cardiomyopathies.
  - Increased gadolinium concentration in the expanded extracellular space associated with scar tissue causes T1 shortening and high signal intensity on T1-weighted images relative to areas of normal myocardium.
  - Significant myocardial fibrosis can be present at endomyocardial biopsy even when cardiac MR images do not show focal LGE. Relatively dense myocardial scar is thought to be necessary for visual identification of myocardial scar with gadolinium-enhanced cardiac MR because of the relatively low resolution of MR imaging [10].
  - In the setting of less severe or more diffuse fibrosis, the inversion-recovery cardiac MR technique is unlikely to reveal the presence of diffusely abnormal tissue given the lack of normal myocardium as a reference.
  - Direct measurement of myocardial T1 time ("T1 mapping") may improve on these problems of LGE cardiac MR in the setting of more subtle degree of diffuse fibrosis (i.e., DCM, hypertrophic cardiomyopathy, aortic valve disease, postoperative cardiac transplantation, myocarditis, restrictive cardiomyopathy, suspected arrhythmogenic right ventricle dysplasia) [10].

13.3 Summary

- DCM is associated with dilatation and dysfunction of the LV or of both ventricles.
- DCM is caused by a variety of disorders (ischemia, infections, drugs, deposition disease, toxins, electrolyte abnormalities, nutritional deficiencies, endocrine dysfunction, and genetic), although frequently no etiology can be found and the cardiomyopathy is deemed idiopathic.
- CT and MR are used to help make a diagnosis, to assess the degree of cardiac dysfunction, to identify a cause, and to guide therapy.
- Stripes of hyperenhancement in the mid-wall of the myocardium are a typical enhancement pattern, which was identified in a 9–35 % of the patients with non-ischemic DCM, which is a predictor of poor prognosis.

References

1. Maron BJ, Towbin JA, Thiene G, et al. Contemporary definitions and classification of the cardiomyopathies: an American Heart Association Scientific Statement from the Council on Clinical Cardiology, Heart Failure and Transplantation Committee; Quality of Care and Outcomes Research and Functional Genomics and Translational Biology Interdisciplinary Working Groups; and Council on Epidemiology and Prevention. Circulation. 2006;113:1807–16.
2. Richardson P, McKenna W, Bristow M, et al. Report of the 1995 World Health Organization/International Society and Federation of Cardiology Task Force on the Definition and Classification of cardiomyopathies. Circulation. 1996;93:841–2.
3. Dec GW, Fuster V. Idiopathic dilated cardiomyopathy. N Engl J Med. 1994;331:1564–75.
4. McDonagh TA, Morrison CE, Lawrence A, et al. Symptomatic and asymptomatic left-ventricular systolic dysfunction in an urban population. Lancet. 1997;350:829–33.
5. Devereux RB, Roman MJ, Paranicas M, et al. A population-based assessment of left ventricular systolic dysfunction in middle-aged and older adults: the Strong Heart Study. Am Heart J. 2001;141:439–46.
6. Giesbrandt KJ, Bolan CW, Shapiro BP, Edwards WD, Mergo PJ. Diffuse diseases of the myocardium: MRI-pathologic review of cardiomyopathies with dilatation. AJR Am J Roentgenol. 2013;200:W274–82.
7. O'Donnell DH, Abbara S, Chaithiraphan V, et al. Cardiac MR imaging of nonischemic cardiomyopathies: imaging protocols and spectra of appearances. Radiology. 2012;262:403–22.
8. Belloni E, De Cobelli F, Esposito A, et al. MRI of cardiomyopathy. AJR Am J Roentgenol. 2008;191:1702–10.
9. Assomull RG, Prasad SK, Lyne J, et al. Cardiovascular magnetic resonance, fibrosis, and prognosis in dilated cardiomyopathy. J Am Coll Cardiol. 2006;48:1977–85.
10. Sibley CT, Noureldin RA, Gai N, et al. T1 Mapping in cardiomyopathy at cardiac MR: comparison with endomyocardial biopsy. Radiology. 2012;265:724–32.

Hypertrophic Cardiomyopathy

14

Eun Ju Chun and Sang Il Choi

Contents

E.J. Chun, MD • S.I. Choi, MD (✉)
Department of Radiology, Seoul National University Bundang Hospital, Gyeonggido, Republic of Korea
e-mail: drejchun@daum.net; drsic@daum.net

Abstract

Hypertrophic cardiomyopathy (HCM) is a common inherited genetic cardiac disease with the prevalence of 0.2 %. Its early detection is important as it is the most common cause of sudden cardiac death (SCD) among young people although most of them present asymptomatic or mild symptom.

Clinical diagnosis is usually based on otherwise unexplained left ventricular hypertrophy (LVH) identified by echocardiography or cardiovascular MRI. However, currently MDCT has adopted for detecting for HCM due to its high temporal and spatial resolution. This chapter presents an overview of the definition of HCM, its various phenotypes, risk stratification of HCM, and the potential application of cardiac MRI and MDCT for the assessment of HCM.

14.1 Overview

14.1.1 Definition, Clinical Features (Sign and Symptoms)

- It is defined as a diffuse or segmental left ventricular hypertrophy (LVH) with a nondilated and hyperdynamic chamber in the absence of another cardiac or systemic disease capable of producing the magnitude of hypertrophy evident [1].
- Nomenclature: IHSS (idiopathic hypertrophic subaortic stenosis), ASH (asymmetrical septal hypertrophy), or HOCM (hypertrophic obstructive cardiomyopathy), which potentially confusing by virtue of the inference that left ventricular outflow tract (LVOT) is an invariable and obligatory component of the disease.
- Clinically, heterogeneous cardiac disease with a diverse clinical presentation from asymptomatic to premature death, although most patients are asymptomatic, but it has known to be a most common cause of sudden cardiac death (SCD) in young adult [2].

T.-H. Lim (ed.), *Practical Textbook of Cardiac CT and MRI*,
DOI 10.1007/978-3-642-36397-9_14,

- Therapy (ICD, surgical intervention, or medication) should be needed, when the disease does the result in significant complications including SCD due to ventricular tachyarrhythmias, heart failure characterized by exertional dyspnea, or atrial fibrillation [3].

14.1.2 Causes

- Familial hypertrophic cardiomyopathy (HCM) is inherited as an autosomal dominant trait which caused by more than 1,400 mutations in 11 or more genes encoding proteins of the cardiac sarcomere.
- Pathologic hallmarks of HCM are myocyte disarray and interstitial fibrosis [2].
- Abnormal dysplasia of small intramural coronary arteriole is another common histopathologic finding, caused by increased pressure from adjacent hypertrophied myocytes.

14.2 Pathophysiology of HCM

- HCM is complex and consists of multiple interrelated pathophysiological abnormalities, including LVOT obstruction, diastolic dysfunction, mitral regurgitation, and autonomic dysfunction.

14.2.1 LVOT Obstruction

- About 20–30 % of asymmetric septal HCM have an obstruction to the LVOT during rest, while 70 % of patients have dynamic obstruction, which can be provoked under certain condition (Fig. 14.1).
- Dynamic LVOT is usually due to systolic anterior motion of the anterior leaflet of the mitral valve (SAM) with mid-systolic contact with the ventricular septum.
- SAM is not pathognomonic of HCM, as it may present in patients with hypertensive heart, diabetes mellitus, acute myocardial infarction, and mitral valve repair or dysfunction.
- Anomalous insertion of the papillary muscles (heads of papillary muscles insert directly ventricular aspect of mitral leaflet) can occur in 13 % of patients with HCM and can contribute LVOT obstruction.

14.2.2 Diastolic Dysfunction

- Diastolic dysfunction arises from ventricular relaxation and chamber stiffness.
- Ventricular relaxation results from the systolic contraction load caused by LVOT obstruction and delayed inactivation caused by abnormal intracellular calcium reuptake.
- Chamber stiffness is caused by severe LVH.

14.2.3 Myocardial Ischemia

- Myocardial hypertrophy and extracellular fibrosis predispose to increased left ventricular stiffness which in concert with compromised cellular energetics and abnormal calcium handling lead to diastolic dysfunction.
- Abnormal dysplasia of small intramural coronary arteriole caused by increased pressure from adjacent hypertrophied myocytes causes myocardial ischemia.

14.2.4 Mitral Regurgitation

- Interleaflet gap (anterior leaflet motion is greater than that of the posterior leaflet) during SAM resulting in a posteriorly directed jet of mitral regurgitation
- Besides SAM, intrinsic valvular abnormalities (i.e., mitral valve prolapsed, leaflet thickening secondary to injury from repetitive septal contact, chordal rupture or elongation, etc.) were the cause of mitral regurgitation.

14.3 Role of Each Diagnostic Modalities for HCM

Because the clinical presentation is nonspecific and diverse, noninvasive imaging techniques play a pivotal role in detecting the disease and understanding its pathophysiology. The goals of noninvasive imaging for HCM are to distinctly diagnose the disease along with characterization of its phenotype, to assess the cardiac function (including presence of dynamic obstruction), to classify the disease severity and risk stratification, and to serve as a screening tool for the family and as a guide for appropriate therapy (Table 14.1) [4].

14.3.1 Cardiac Structure

- Characterization of the presence, location, and extent of LVH should be needed for all segment of the entire myocardium.
- One third of patients with HCM have RVH, thus RV wall thickness and mass also should be needed to assess.
- Intrinsic structural abnormalities of the mitral valve apparatus and papillary muscle number and location were also evaluated.

14.3.1.1 Echocardiography

- Transthoracic echocardiography (TTE) is widely used for the initial evaluation of all patients with suspected HCM (Class I, Level of Evidence B).

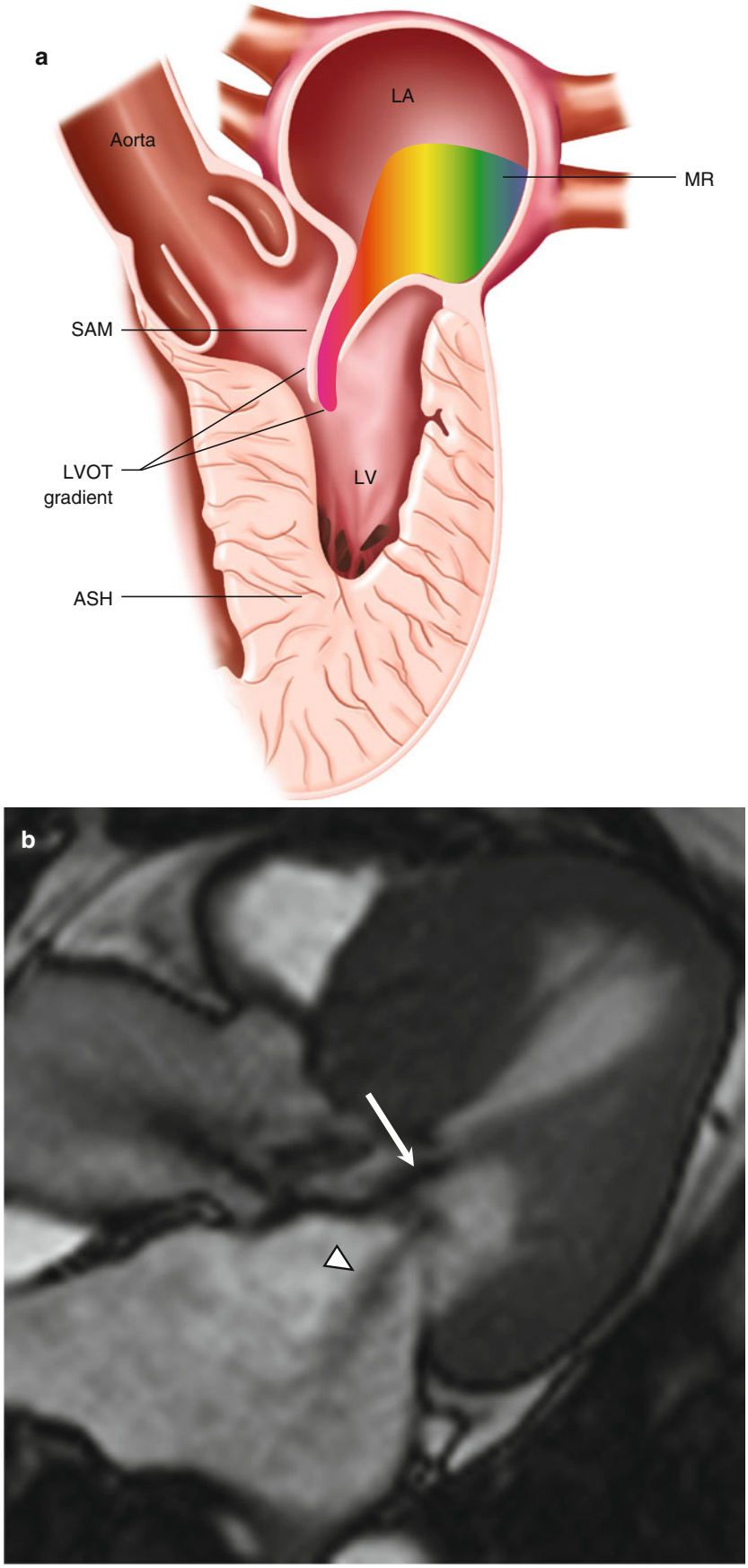

Fig. 14.1 Dynamic LVOT obstruction. Asymmetric septal HCM with systolic anterior motion (*SAM*) in a 74-year-old man who presented with chest tightness. (**a**) Schematic illustration of LVOT obstruction. (**b**) Four-chamber SSFP cine MR images show systolic anterior motion (*SAM*) of the anterior mitral valve leaflet (*arrows*) accompanied by a signal void jet flow into the LVOT. There is also a jet of mitral regurgitation (*arrowheads*) into a moderately enlarged left atrium

Table 14.1 Relative merits of each noninvasive imaging for the assessment of hypertrophic cardiomyopathy

	Echocardiography	MDCT	MRI
LV volume	+++	++	++++
LV hypertrophy	+++	++++	++++
Ejection fraction	+++	+++	++++
Regional function	+++	++	++++
LV filling pressure	+++	–	++
PA pressure	+++	–	+++
Dynamic obstruction	+++	+	+++
Mitral regurgitation	+++	–	++
Ischemia/CFR	+	–	++
Monitoring of therapy	+++	+	+++
Tissue characterization	++	+	++++
Preclinical diagnosis	++	+++	+++

This table is referred by radiographics (ref; Chun et al. [5])
LV left ventricular, *PA* pulmonary artery, *CFR* coronary flow reserve

- Echocardiography has a limitation of operator and sonic window dependency; it is sometimes unable to define the endocardial border, especially the anterolateral free wall of the left ventricle (LV) in the parasternal short-axis view and apex.
- The degree of LVH could be underestimated by echocardiography, which, in fact, can delay proper treatment, thereby failing to prevent a SCD.

14.3.1.2 MRI

- CMR has strength of 3D imaging technique with high spatial and temporal resolution useful for detection of focal LVH which may not be well visualized by 2D echocardiography.
- SSFP cine MRI sequence produces sharp contrast between the bright blood pool and the dark myocardium, including accurate wall thickness and mass measurements with high reproducibility.
- CMR is indicated in patients with suspected HCM when echocardiography is inconclusive for diagnosis (Class I, Level of Evidence B).
- CMR is reasonable in patients with HCM to define apical HCM and/or aneurysm if echocardiography is inconclusive (Class IIa, Level of Evidence B).

14.3.1.3 MDCT

- MDCT has higher spatial resolution over MRI and echocardiography; it is at least equivalent or more likely superior with respect to HCM phenotype (LV thickness, volume, EF, mass, etc.).
- MDCT provides complete tomographic coverage of the entire myocardium because of isotropic imaging; it can well assess all cardiac structures including papillary muscles.
- MDCT may be reasonable in the patient who has contraindicated CMR (i.e., pacemaker or IDC implantation, claustrophobia, etc.) or when patients cannot hold their breath for long periods.

14.3.2 Assessment of LV Systolic and Diastolic Function

14.3.2.1 Echocardiography

- Echocardiography is a validated method for a comprehensive approach of systolic and diastolic function including LA and LV filling pressure.
- TTE is useful for myocardial function (Class IIa, Level of Evidence C).

14.3.2.2 MRI

- CMR measurements of systolic function including ventricular volumes and EF are validated with high diagnostic accuracy and high reproducibility.
- CMR can measure mitral inflow, the pulmonary vein, and LV filling.

14.3.2.3 MDCT

- CT provides an accurate assessment of systolic function including LV volume and EF.
- CT is not indicated for the assessment of LV diastolic function due to limited temporal resolution than MRI or echocardiography.

14.3.3 Dynamic LVOT Obstruction and Mitral Valve Abnormalities

14.3.3.1 Echocardiography

- Echocardiography is an initial modality for LVOT obstruction or mitral regurgitation.
- Exercise TTE can be useful in the detection and quantification of dynamic LVOT obstruction (Class IIa, Level of Evidence B).

14.3.3.2 MRI

- Cine MRI can accurately identify the presence of mitral-septal contact and regurgitant signal void jet.

- Velocity encoding (VENC) sequence can measure the peak velocity through the LVOT.
- However, it has limited that CMR-derived velocities can be assessed only under basal conditions, because one third of patients with HCM have LVOT obstruction only during provocation.

14.3.3.3 MDCT

- CT is not indicated for dynamic obstruction of mitral regurgitation although it can well evaluate the papillary muscle or mitral valve apparatus.

14.3.4 Myocardial Ischemia

14.3.4.1 Echocardiography

- In general, there is a limited role for echocardiography in diagnosing myocardial ischemia, although regional wall motion abnormality is an indirect finding for ischemia.

14.3.4.2 MRI

- Stress perfusion MRI permits accurate qualitative and quantitative assessment of myocardial blood flow at rest and during pharmacologic stress, with superior spatial resolution to PET.
- The severity of perfusion impairment in HCM is correlated with the degree of LVH.

14.3.4.3 MDCT

- In patients with HCM with coexistent epicardial coronary disease, because epicardial coronary disease is one of the several etiologic mechanisms that contribute to myocardial ischemia in patients with HCM, it can be difficult to interpret whether ischemia is caused by HCM or by decreased coronary flow reserve.
- Cardiac MDCT can provide useful information for the noninvasive assessment of coexistent epicardial coronary disease in patients with HCM [5].

14.3.5 Myocardial Fibrosis

14.3.5.1 Echocardiography

- Large areas of regional fibrosis can lead to segmental dysfunction manifested by reduced strain. However, it is limited for its low specificity for fibrosis.

14.3.5.2 MRI

- *Late* delayed gadolinium-enhancement (LGE) MRI techniques can provide unique information on tissue characterization, specifically for the identification of myocardial fibrosis or scarring.
- Areas of LGE can be measured and the amount quantified and expressed as a percentage of total LV mass.
- The prevalence of LGE in HCM is approximately 50–70 % and when present occupies on average 10 % of the overall LV myocardial volume.
- The location of LGE is common at the confined area to only the LV free wall or insertion points of the RV free wall and ventricular septum. In addition, LGE tends to locate in segments with hypertrophy or with large LV mass.
- However, it still remains uncertain whether all LGE in patients with HCM with normal or hyperdynamic EF represents myocardial fibrosis.
- CMR may be considered for risk stratification with late gadolinium enhancement (LGE) and differential diagnosis from other infiltrative disease including cardiac amyloidosis or Fabry disease (Class IIb, Level of Evidence C).

14.3.5.3 MDCT

- CT has no role at the present time for the evaluation of myocardial fibrosis.

14.4 Classification of HCM by Phenotypes

- The usual diagnostic criterion for HCM is a maximal LV wall thickness greater than or equal to 15 mm on end-diastolic phase.
- Although the morphologic expression of HCM is widely variable and heterogeneous because HCM may affect any portion of the LV, the classification according to distribution of LV hypertrophy is usual as follows (Fig. 14.2) [5, 6].

14.4.1 Asymmetric (Septal) HCM

- The most common form of the HCM with prevalence rate of 60–70 %.
- Diagnosed when septal thickness is greater than or equal to 15 mm or the ratio of septal to inferior wall of LV is greater than 1.5 at mid-ventricular level (Fig. 14.3).
- The most common location of LVH is the anterior free wall and contiguous basal anterior ventricular septum.
- The presence of LVOT obstruction, which is fixed or dynamic, and the presence of associated mitral regurgitation should be checked for preventive implantation of ICD.

14.4.2 Apical HCM

- It typically shows hypertrophy of the myocardium predominantly involves the apex of the LV with diagnostic criteria as absolute apical wall thickness of >15 mm or a ratio of apical to basal left ventricular wall thicknesses of 1.3–1.5.

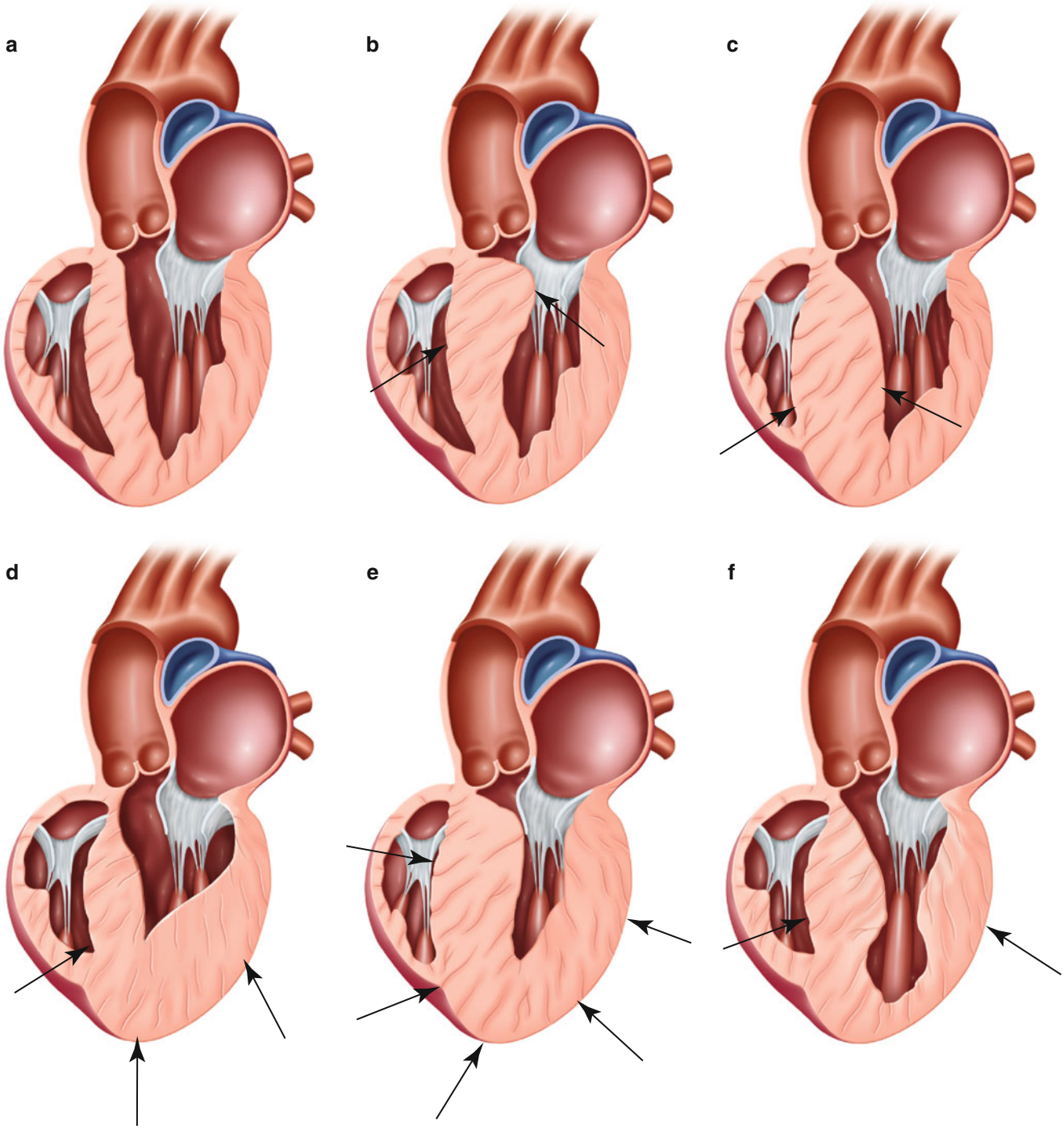

Fig. 14.2 Various phenotypes of HCM. The diagnostic criterion of HCM is that maximal LV wall thickness is greater than or equal to 15 mm on end-diastolic phase. (**a**) Normal, (**b**) asymmetric septal HCM with LVOT obstruction, (**c**) asymmetric septal HCM without LVOT obstruction, (**d**) apical HCM, (**e**) symmetric HCM (concentric HCM), (**f**) midventricular HCM, (**g**) mass-like HCM, and (**h**) noncontiguous HCM

Fig. 14.2 (continued)

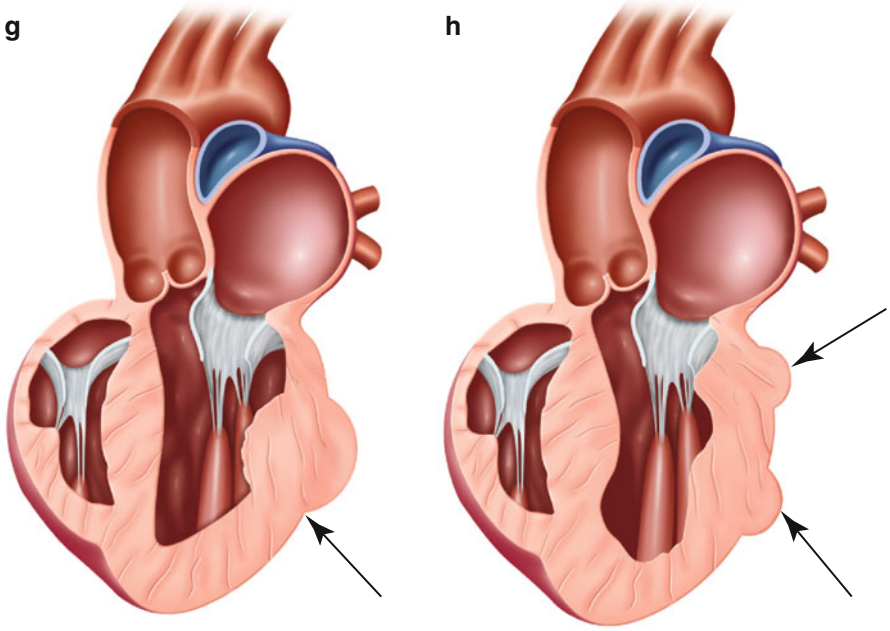

- Its prevalence is higher in Asians as 25 % of all patients with HCM in Japan than that of Western populations.
- It shows typical ECG abnormalities in the form of giant negative T waves
- Unlike typical HCM, apical HCM shows a predilection for middle-aged men, is rarely associated with SCD, is frequently complicated by hypertension, and has a relatively good prognosis.
- "Spade-like" configuration of the LV cavity at end-diastole caused by localized apical hypertrophy is a characteristic imaging finding (Fig. 14.4).
- The LV apex may not be well assessed by echocardiography, which can lead to false-negative interpretations in apical HCM. Hence, cardiac MRI is strongly recommended as the optimal imaging technique for evaluation of apical HCM [7].

14.4.3 Symmetric HCM (Concentric HCM)

- Characterized by concentric LVH with a small cavity dimension and no evidence of secondary cause, it is known to occur in up to 42 % of HCM cases (Fig. 14.5).
- It should be differentiated from other causes of symmetric increased thickness of LV wall, including athlete's heart, amyloidosis, sarcoidosis, Fabry disease, and secondary adaptive pattern of LVH due to hypertension or aortic stenosis,
- Cardiac MRI is helpful in differentiating other causes of myocardial hypertrophy from HCM due to its unique ability to characterize different enhancement patterns in diseased myocardium with DE-MRI [8].

14.4.4 Mid-ventricular HCM

- Characterized by hypertrophy occurring predominantly in the middle third of the LV wall and by systolic apposition of the mid-ventricular wall.
- It may be associated with apical aneurysm caused by increased systolic pressures in the apex from mid-ventricular obstruction, which is assumed to be a "dumb-bell" configuration (Fig. 14.6).
- It is frequently associated with ventricular arrhythmia, myocardial necrosis, and systemic embolism.

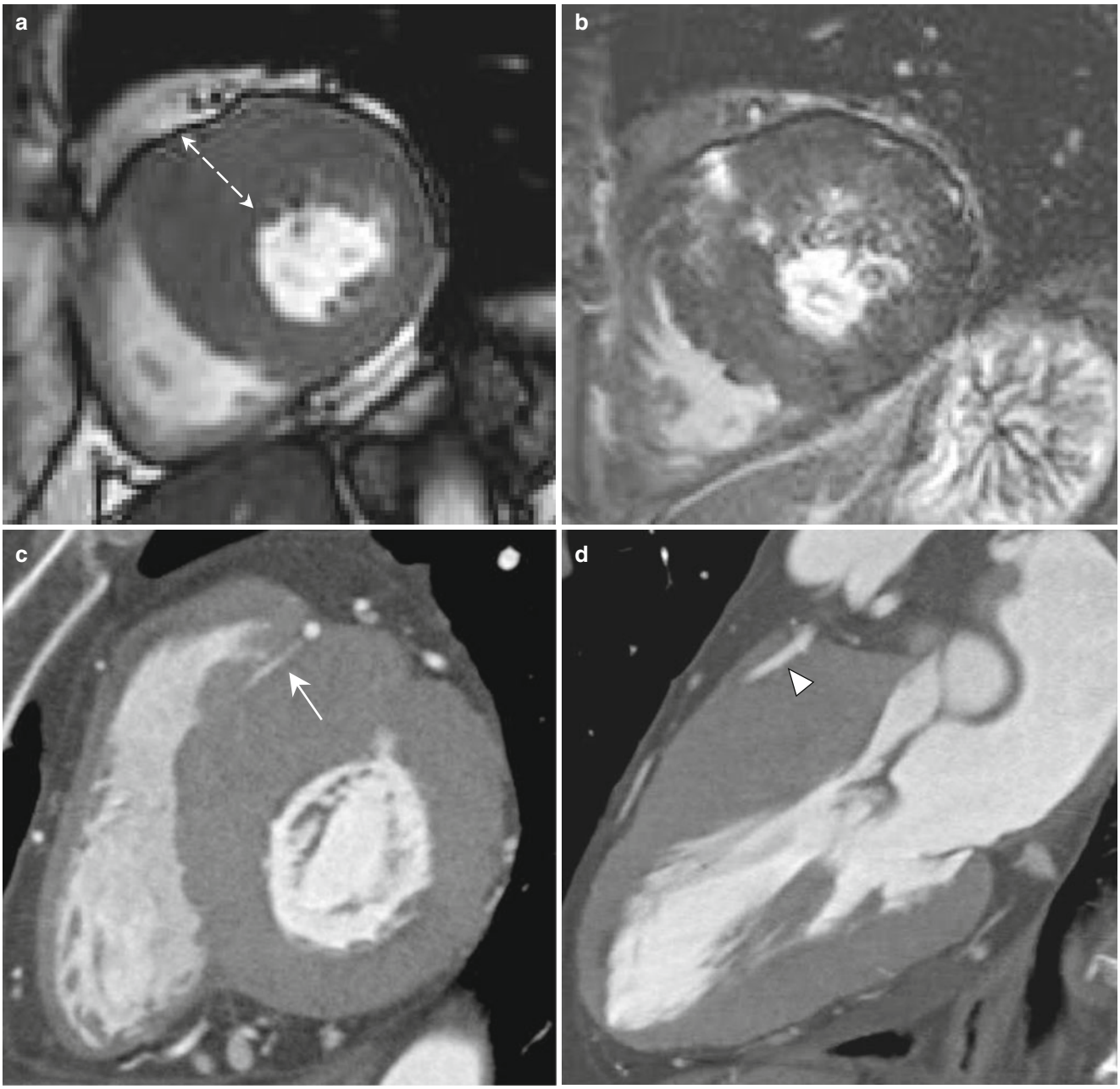

Fig. 14.3 Asymmetric septal HCM with various modalities. (**a**) Short-axis steady-state free precession (SSFP) cine MR image shows the asymmetric septal wall hypertrophy at anteroseptal wall with the measured maximal thickness as 20 mm on end-diastole (*dashed arrow*) . (**b**) Short-axis delayed-enhanced MR image shows patchy enhancement in hypertrophied segment. MDCT short-axis (**c**) and two-chamber (**d**) images in diastole clearly demonstrates asymmetric septal wall hypertrophy at the anteroseptal wall with engorged septal branch (*arrow*) and myocardial bridging of mid LAD (*arrowhead*)

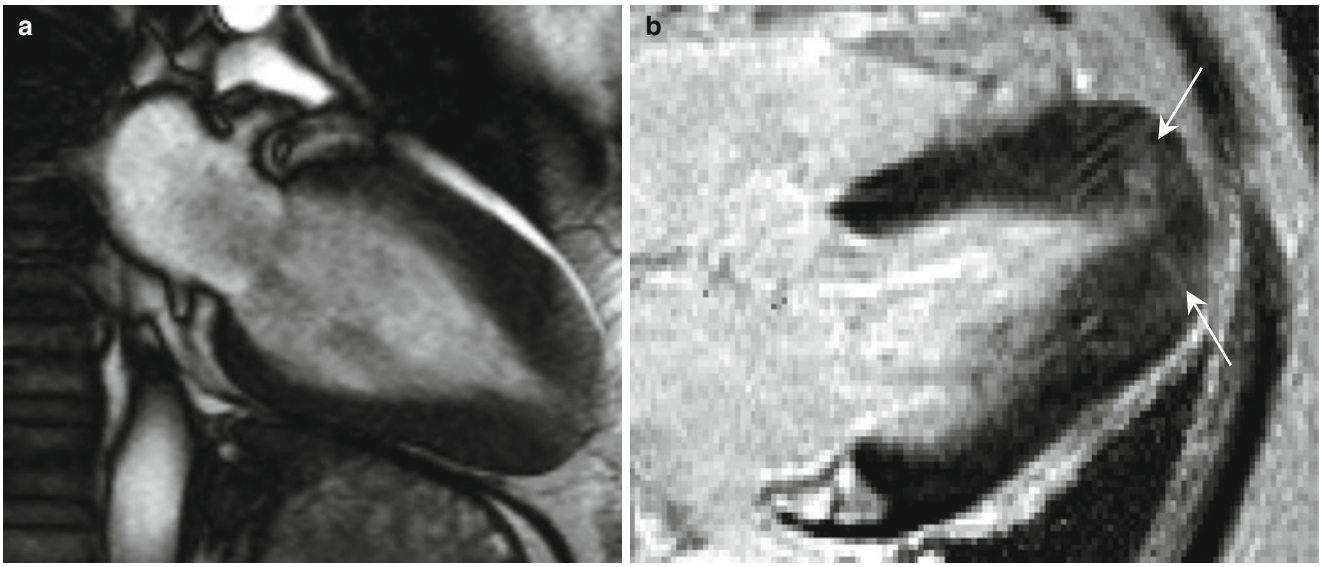

Fig. 14.4 Apical HCM in a 38-year-old man with ECG abnormality including QRS voltages associated with the LV hypertrophy and the giant negative T waves on V5–6. (**a**) Two-chamber SSFP cine MR image shows apical hypertrophy and obliteration of the LV apical cavity at end-diastole with typical "spade-like" configuration. (**b**) Four-chamber delayed MR image shows patchy enhancement (*arrows*) in hypertrophied apical segment

14.4.5 Other Various Types of HCM

14.4.5.1 Mass-Like HCM

- Characterized by focal segmental location of the myocardial disarray and fibrosis.
- Might be differentiated from neoplastic masses.
- MRI with spin-echo imaging, first-pass perfusion, and delayed enhancement technique helps to differentiate between the two entities. Mass-like HCM more precisely parallels the homogeneous signal characteristics and perfusion of adjacent normal myocardium, whereas tumors show heterogeneous signal intensity and enhancement and show perfusion characteristics that differ from those of the remainder of the left ventricle (Fig. 14.7).
- Myocardial tagging with SSFP technique is also useful in differentiating the mass-like HCM from tumor, because of the absence of active contraction in tumor in contrast to the presence of contractility in HCM.

14.4.5.2 Noncontiguous HCM

- Recent reported type as characterized by noncontiguous distribution of segmental areas of LVH present with prevalence of almost 15 % of an HCM cohort [6].
- The morphologic pattern consists of hypertrophied segments separated by regions of non-hypertrophied myocardium, creating abrupt changes in wall thickness in adjacent portions of the wall and a "lumpy" hypertrophic pattern (Fig. 14.8).
- MRI and MDCT can provide an accurate diagnosis with high temporal and spatial resolution than echocardiography.

14.5 Risk Stratification

- SCD is the most devastating and unpredictable complication of HCM, and the overall annual mortality rate ranges from less than 1 % in asymptomatic patients to 6 % in patients with high-risk factors [1].
- Risk stratification is important for ICDs to prevent SCD.
- The risk of SCD increased with the aggregation of these risk factors (Table 14.2).

14.5.1 The Role of Each Imaging Modalities for Risk Factors for SCD

See Table 14.3.

14.5.2 Burned-Out Phase of HCM

- In end-stage of HCM, HCM patients paradoxically evolve into a phase characterized by systolic dysfunction, LV dilatation, and wall thinning, although most patients with HCM have diastolic dysfunction.
- Usually unfavorable outcome from heart failure to heart transplantation.
- Such hypokinesia can occur after an acute myocardial infarction, or it can develop gradually without a clinical infarction.
- Patients with mid-ventricular or apical HCM are at a higher risk of developing segmental or diffuse LV hypokinesia.

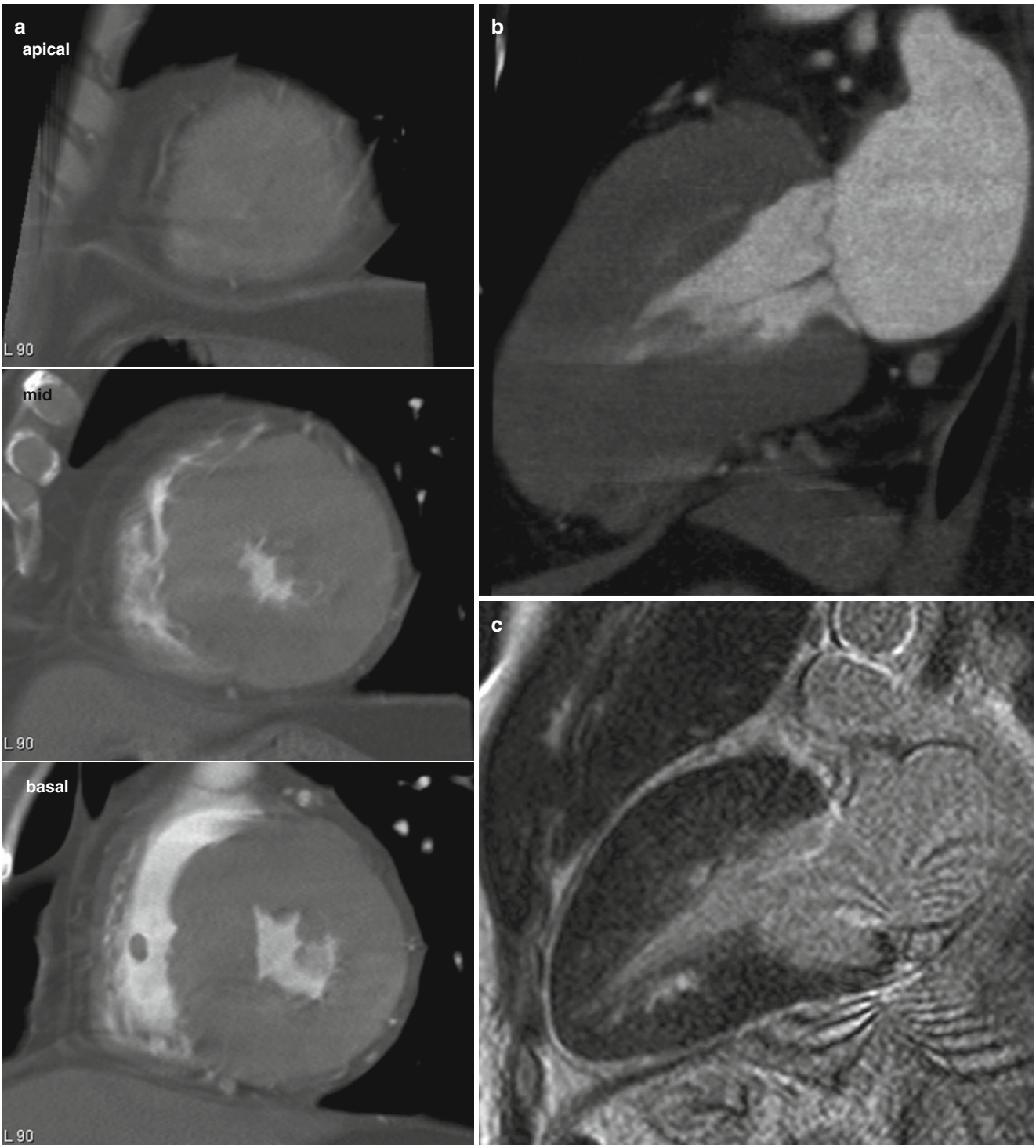

Fig. 14.5 Concentric HCM. MDCT sequential short-axis images (**a**) and two-chamber view (**b**) show concentric LV hypertrophy at the entire LV wall. (**c**) Delayed MR shows multifocal patchy enhancement at hypertrophied entire LV wall

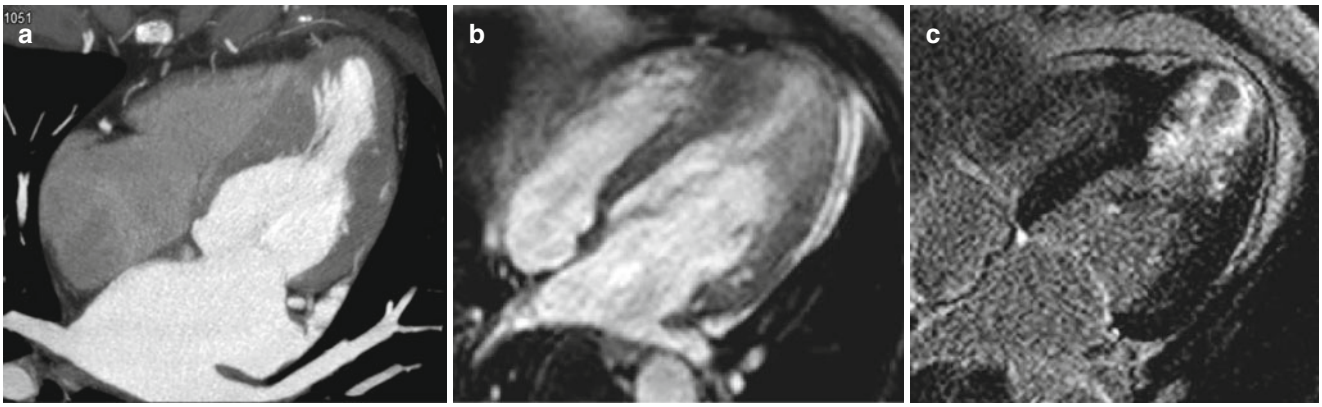

Fig. 14.6 Mid-ventricular HCM. Four-chamber MDCT image (**a**) and MR SSFP cine image (**b**) show the LV hypertrophy predominantly in the middle third of the LV wall, which is assumed to be "dumbbell" configuration. (**c**) Delayed MR image shows subendocardial enhancement at mid- to apical wall

- MRI reveals thin-walled, apical aneurysm showing transmural enhancement which extends into substantial areas of the contiguous ventricular septum and LV free wall, and it can well figure out nonenhnced thrombus in LV cavity. (Fig. 14.9).

14.6 Screening

- Screening of family members of an HCM patient is important because the first-degree relatives of such a patient have a 50 % chance of being a gene carrier (Table 14.4).

14.6.1 Preclinical HCM

- LV crypt, which is defined as the penetration of the compact myocardium, is suggested to be one of the early pathological alterations in HCM with positive genotype and negative phenotype [5].
- Currently, LV crypts are more common than previously thought due to the commonly used cardiac MDCT; it might be caused by locally altered loading conditions or myocardial contractility (Fig. 14.10).
- Besides LV crypt, non-hypertrophied LV myocardium with myocardial fibrosis, mitral leaflet elongation, subclinical diastolic dysfunction, or ECG abnormalities might be needed for screening.

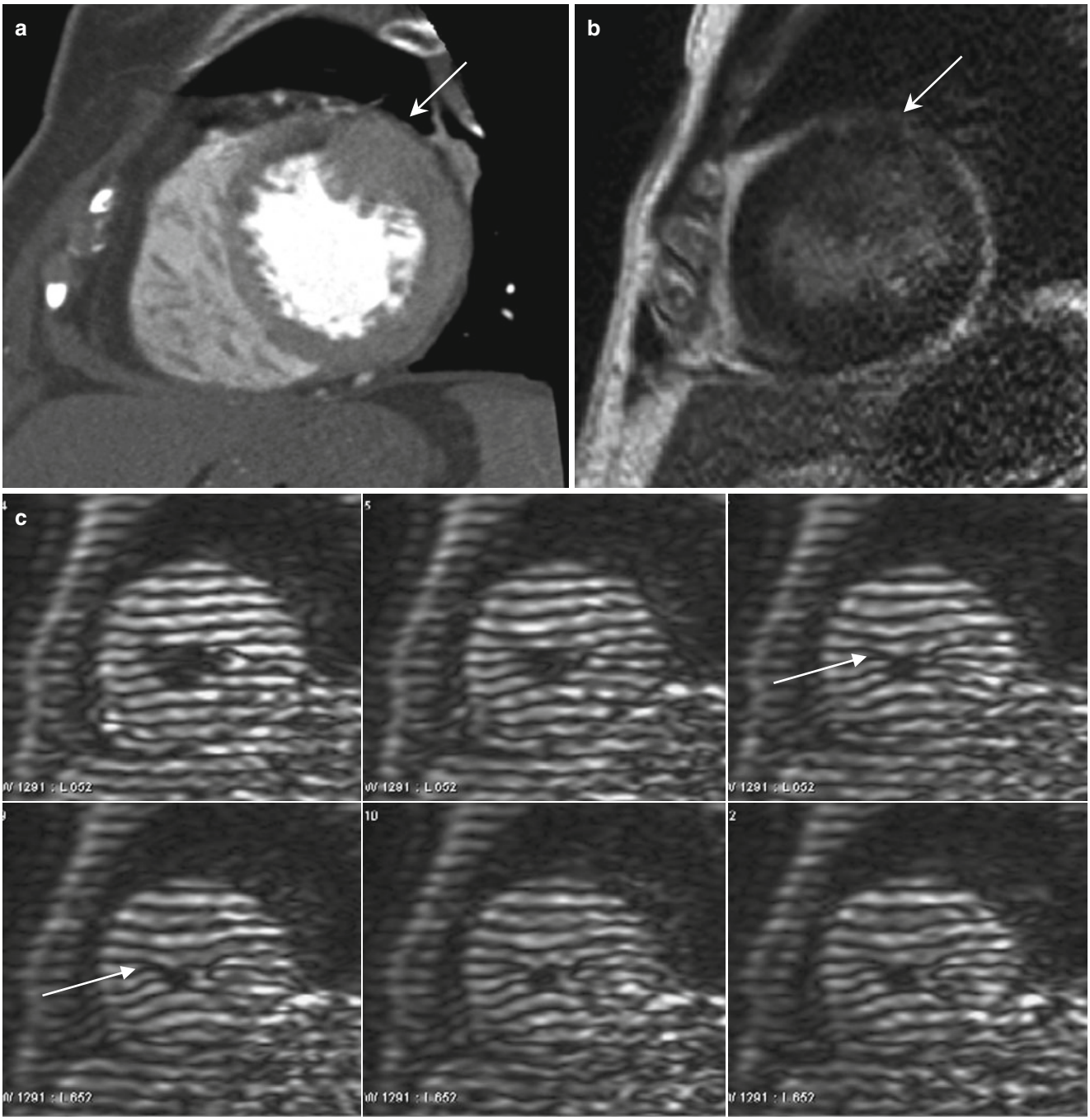

Fig. 14.7 Mass-like HCM. (**a**) Short-axis MDCT image shows mass-like bulging contour at apical anterior wall (*arrow*). (**b**) Short-axis delayed-enhanced MR image shows focal patchy enhancement within mass-like lesion (*arrow*). (**c**) Short-axis image of tagged MRI can diagnose as HCM due to the presence of contractility of that lesion (*arrows*)

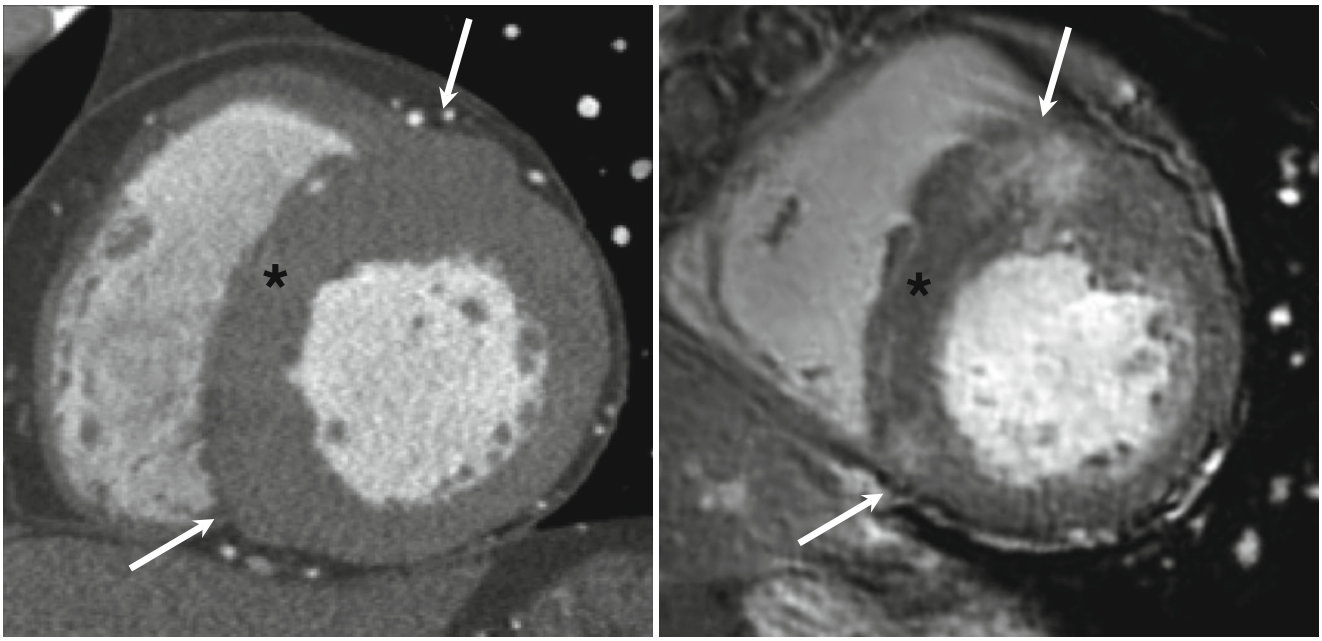

Fig. 14.8 Noncontiguous HCM. (**a**) Short-axis MDCT image shows noncontiguous LV hypertrophy of the anteroseptal wall and inferoseptal wall (*arrows*) separated by septal areas of normal LV wall thickness (*asterisk*). (**b**) Short-axis delayed-enhanced MR image shows multifocal patchy enhancement on hypertrophied myocardium at anteroseptal and inferoseptal wall (*arrows*) with preserving septal wall with normal thickness (*asterisk*)

Table 14.2 Risk factors for SCD

Major risk factors for SCD
1. A personal history for ventricular fibrillation, sustained VT, or SCD events, including appropriate ICD therapy for VT
2. A family history for SCD events, including appropriate ICD therapy for VT
3. Unexplained syncope
4. Documented NSVT defined as 3 or more beats at greater than or equal to 120 bpm on Holter ECG
5. Maximum LV wall thickness greater than or equal to 30 mm
6. Abnormal blood pressure response during exercise
Minor risk factors
1. LVOT obstruction
2. LGE on CMR imaging
3. LV apical aneurysm
4. Genetic mutations

Table 14.3 The role of each imaging modalities for risk factors for SCD

Risk factor	Imaging modality
1. Maximum wall thickness ≥3 cm	Echocardiography, CMR, MDCT
2. End-stage HCM (EF <50 %)	Echocardiography, CMR, MDCT
3. Apical aneurysm	Contrast echocardiography, CMR, MDCT
4. LVOT gradient ≥30 mmHg	Doppler echocardiography
5. Perfusion defects	SPECT, but CMR can be applied
6. Reduced coronary flow reserve	PET, but CMR and MDCT can be applied
7. LGE (presence and extent)	CMR

This table is modified in the report by Nagueh et al. [4]

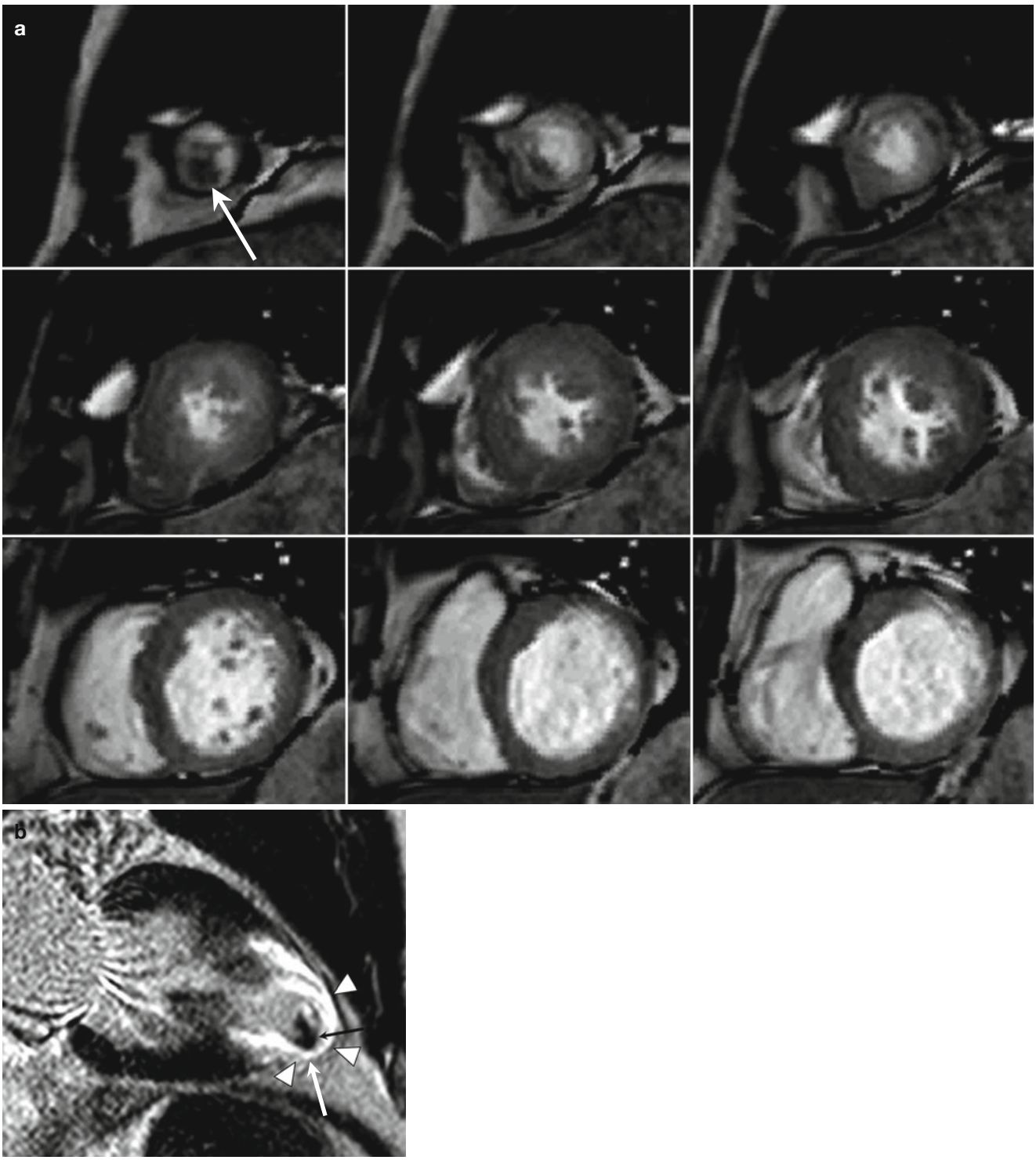

Fig. 14.9 Burned-out phase of mid-ventricular to apical HCM. (**a**) Sequential short-axis images show the mid-ventricular LV hypertrophy with the aneurysmal change at the apex due to the progression of HCM into hypokinetic, burned-out phase. A hypointense focal lesion at the apex is suggestive of thrombus. (**b**) Two-chamber delayed-enhanced MR image clearly notes the enhanced thinned apical LV wall (*arrowheads*) with a mural thrombus (*arrow*). Global systolic function also decreased as ejection fraction = 35 %

Table 14.4 Screening is usually by echocardiography or cardiovascular MR (and 12-lead ECG)

At age <12 years
Indication of screening
Either a malignant family history of premature death from HCM is known or other adverse complications are present
Child is a competitive athlete in an intensive training
Onset of symptoms
Other clinical suspicion of early LVH has been noted
At age 12–21 years
Screening should be performed every 12–18 months
At >21 years
Imaging should be performed either at onset of symptoms or possibly at 5-year intervals (at least though midlife); more frequent intervals are appropriate in families with a malignant clinical course or history of late-onset HCM

This table is referred in the report by Maron and Maron [2]

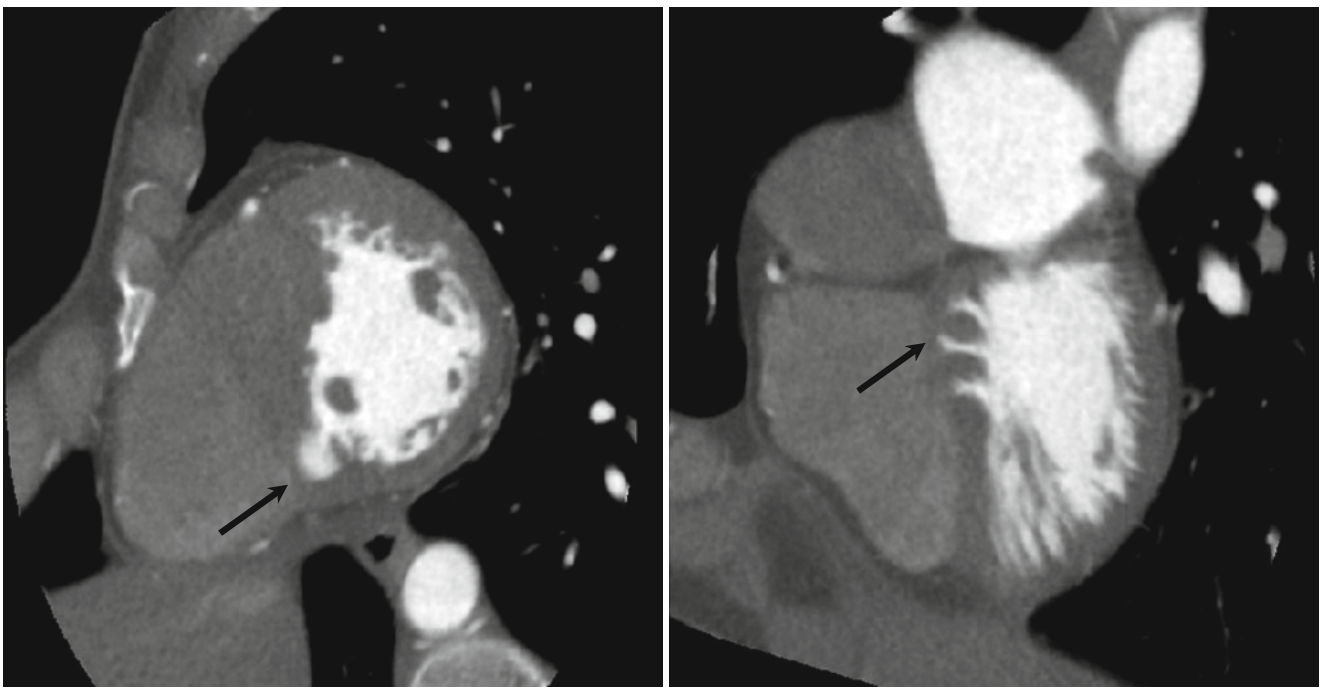

Fig. 14.10 LV crypt. Short-axis (**a**) and four-chamber (**b**) MDCT images show the saclike structure and linear penetrations of the compact myocardium (*arrows*) at the mid-ventricular inferoseptal wall at end-diastole

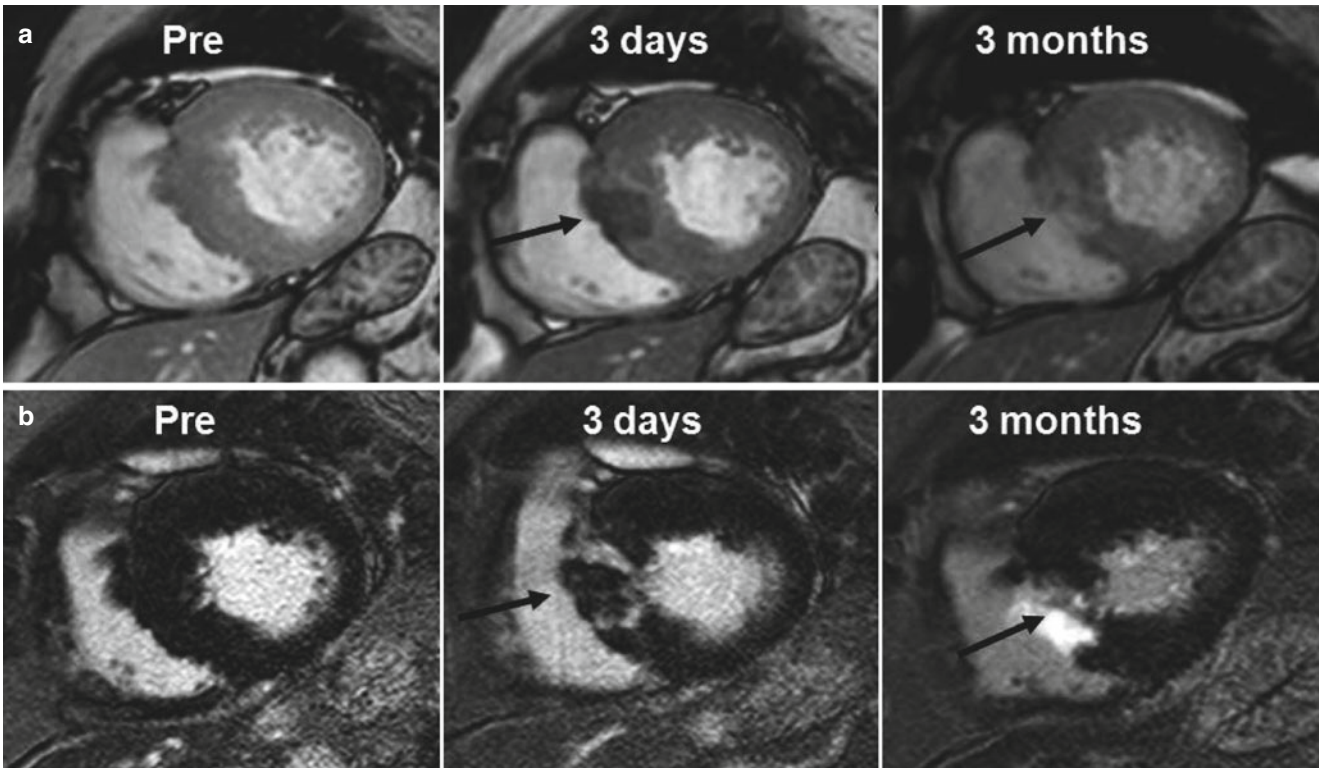

Fig. 14.11 Alcohol septal ablation in patient with asymmetric septal HCM and LVOT obstruction. (**a**) Sequential short-axis SSFP cine MR images show the progressed wall thinning (*arrows*) due to the infarction after ethanol ablation at the basal septum. (**b**) Sequential short-axis DE-MR images present the infracted myocardium at the corresponding areas (*arrows*)

Table 14.5 Differential diagnosis from hypertrophic cardiomyopathy

Diffuse LVH	
Differential diagnosis	Differential point
Compensatory hypertrophy	
Athlete's heart	A ratio of diastolic wall thickness to LV end-diastolic volume corrected to body surface area of less than 0.15 mm/m^2/ml
	Lack of delayed enhancement
Hypertension	More symmetrical LVH less than 15 mm in diameter
Valvular aortic stenosis	Usually subnormal EF rather than hyperdynamic
	Rarely enhancement
Infiltrative disease	
Cardiac amyloidosis	Commonly all chamber involve (especially, pathognomonic when interatrial septum and right atrial free wall by more than 6 mm)
	In LGE, global subendocardial or transmural enhancement
Cardiac sarcoidosis	In LGE, nodular and patchy enhancement often involves the septum (more particularly, the basal portion) and LV wall, whereas papillary and RV infiltration are rarely noted
Eosinophilic endomyocardial fibrosis	In LGE, subendocardial enhancement with thinned apex
	Sometimes associated with mural thrombus in apex
Metabolic storage disease	
Fabry disease	X-linked autosomal recessive metabolic storage disorder caused by a lack of lysosomal α-galactosidase A
	In LGE, usually enhanced at mid-wall in the basal inferolateral segment

(continued)

Table 14.5 (continued)

Diffuse LVH	
Differential diagnosis	Differential point
Glycogen storage disease	X-linked dominant metabolic disorder caused by a primary deficiency in lysosome-associated membrane protein 2
	Nonspecific enhancement pattern
	Associated other abnormality (Wolff-Parkinson-White syndrome, skeletal myopathy, or cognitive disorder)
Mitochondrial myopathy	Mitochondrial oxidative phosphorylation defects
	Nonspecific variable finding from hypertrophy, dilation, or non-compaction
	Associated other anomaly (brain, skeletal muscle, liver or kidney, etc.)
Dynamic LVOT obstruction	
Elderly women with hypertension	After acute MI with apical dysfunction and hyperdynamic basal function
Sigmoid septum	Massive posterior mitral annulus calcification
Hyperdynamic EF	Anomalous papillary muscle
After mitral valve or aortic valve repair	

This table is modified in the report by Nagueh et al. [4] and Hansen et al. [8]

14.7 Treatment

- When medical therapy (beta-adrenergic blockers, calcium channel blockers, disopyramide) has filed or not tolerated, surgical reduction of hypertrophied myocardium (especially at LVOT area) or induced ischemia through alcohol injection into the septal perforator branch of the left anterior descending artery can reduce the contractility to diminish the magnitude of LVOT obstruction.
- Patients with a dynamic obstruction (peak instantaneous gradient ≥50 mmHg at rest or provocation) or septal thickness of >1.6 cm should be considered for septal reduction therapy.
- Imaging such as TEE, MDCT, or CMR can be helpful to guide for preoperative planning and evaluate the postprocedural response or complication [9].

14.7.1 Surgical Myomectomy

- Before myomectomy, we should check as follows: (1) maximum thickness of the septum, (2) distance of maximum thickness from the aortic annulus, (3) location of the endocardial fibrous plaque (friction or impact lesion), and (4) the apical extent of the septal bulge.
- Associated mitral valve abnormalities can be checked for the guide of the necessary valve repair or replacement.

14.7.2 Alcohol Septal Ablation

- To detect the targeted perforator branch is very important, the use of contrast-injected echocardiography is helpful to delineate the vascular distribution of the individual perforator branches.
- Contrast-enhanced CMR can accurately quantify the amount of tissue necrosis after septal ablation as well as provide important information regarding the relationship between the location of scarring and LVOT morphology (Fig. 14.11).

14.8 Differential Diagnosis

- HCM should be differentiated from other causes of increased thickness of LV wall.
- CMR can play an important role in differentiating other causes of myocardial hypertrophy from HCM due to its unique ability to characterize different enhancement patterns in diseased myocardium with DE-MRI (Table 14.5) [8].

References

1. Maron BJ, McKenna WJ, Danielson GK, et al. American College of Cardiology/European Society of Cardiology clinical expert consensus document on hypertrophic cardiomyopathy. A report of the American College of Cardiology Foundation Task Force on Clinical Expert Consensus Documents and the European Society of Cardiology Committee for Practice Guidelines. J Am Coll Cardiol. 2003;42:1687–713.
2. Maron BJ, Maron MS. Hypertrophic cardiomyopathy. Lancet. 2013;381:242–55.
3. Bos JM, Towbin JA, Ackerman MJ. Diagnostic, prognostic, and therapeutic implications of genetic testing for hypertrophic cardiomyopathy. J Am Coll Cardiol. 2009;54:201–11.
4. Nagueh SF, Mahmarian JJ. Noninvasive cardiac imaging in patients with hypertrophic cardiomyopathy. J Am Coll Cardiol. 2006;48:2410–22.
5. Chun EJ, Choi SI, Jin KN, et al. Hypertrophic cardiomyopathy: assessment with MR imaging and multidetector CT. Radiographics. 2010;30:1309–28.
6. Maron MS, Maron BJ, Harrigan C, et al. Hypertrophic cardiomyopathy phenotype revisited after 50 years with cardiovascular magnetic resonance. J Am Coll Cardiol. 2009;54:220–8.
7. Hansen MW, Merchant N. MRI of hypertrophic cardiomyopathy: part I, MRI appearances. AJR Am J Roentgenol. 2007;189:1335–43.
8. Hansen MW, Merchant N. MRI of hypertrophic cardiomyopathy: part 2, differential diagnosis, risk stratification, and posttreatment MRI appearances. AJR Am J Roentgenol. 2007;189:1344–52.
9. O'Mahony C, Tome-Esteban M, Lambiase PD, et al. A validation study of the 2003 American College of Cardiology/European Society of Cardiology and 2011 American College of Cardiology Foundation/American Heart Association risk stratification and treatment algorithms for sudden cardiac death in patients with hypertrophic cardiomyopathy. Heart. 2013;99:534–41.

Restrictive Cardiomyopathy

15

Young Jin Kim and Byoung Wook Choi

Contents

Abstract

Restrictive cardiomyopathy is a myocardial disorder characterized by impaired ventricular relaxation leading to severe diastolic dysfunction. In this chapter, an overview of restrictive cardiomyopathy and role of cardiac MRI will be discussed.

15.1 Overview

15.1.1 Definition

- Uncommon cardiomyopathy with distinct morphologic and hemodynamic characteristics that separate it from the more common dilated and hypertrophic cardiomyopathies.
- A condition characterized by normal ventricular cavity size with normal wall thickness and relative preservation of systolic function but rigid ventricular wall resulting in severe diastolic dysfunction [1, 2].

15.1.2 Clinical Features

- Symptoms and signs of both pulmonary and systemic congestions
- Dyspnea, peripheral edema, palpitation, fatigue, weakness, and exercise intolerance
- Severe elevation of central venous pressure → hepatosplenomegaly, ascites, and anasarca

15.1.3 Hemodynamics

- Increased myocardial stiffness → incompliant ventricle → raised left atrial (LA) pressure and atrial dilatation.
- Characteristic features of restrictive LV filling: short isovolumetric relaxation time, ventricular filling

Electronic supplementary material Supplementary material is available in the online version of this chapter at 10.1007/978-3-642-36397-9_15.

Y.J. Kim • B.W. Choi (✉)
Department of Radiology, Research Institute of Radiological Science, Severance Hospital, Yonsei University College of Medicine, Seoul, Republic of Korea
e-mail: dryj@yuhs.ac; bchoi@yuhs.ac

T.-H. Lim (ed.), *Practical Textbook of Cardiac CT and MRI*,
DOI 10.1007/978-3-642-36397-9_15, © Springer-Verlag Berlin Heidelberg 2015

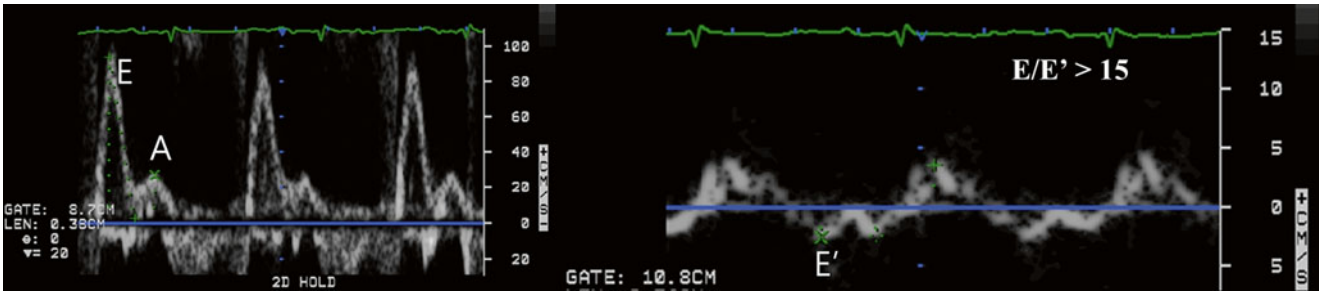

Fig. 15.1 Typical Doppler pattern in restrictive physiology. Restrictive physiology is characterized by mitral flow velocities that show increased E velocity, decreased A velocity (<<E), and shortened DT (<160 ms) and IVRT (<70 ms). Typically, the E/A ratio is more than 2.0. Mitral annulus E' is reduced (<7 cm/s and usually ≤5 cm/s), and E/E' is usually more than 15. *DT* deceleration time, *IVRT* isovolumetric relaxation time

Learning Points of Cardiac Amyloidosis

1. Interstitial expansion because of amyloid deposition alters the dynamics of gadolinium enhancement. One important technical consideration is the choice of the proper inversion time in late-enhancement sequences.
2. Global subendocardial enhancement is a typical imaging finding.

predominantly in early diastole with short deceleration time, small or absent late diastolic filling component.

- Characteristic patterns of pulmonary venous flow: late diastolic flow reversal during atrial systole of a longer duration than the corresponding transmitral flow.
- "Restrictive physiology" can be seen in hypertrophic cardiomyopathy and hypertensive heart disease (Fig. 15.1).

15.1.4 Causes (Table 15.1)

Table 15.1 Causes of restrictive cardiomyopathy [2]

Idiopathic
Amyloidosis
Sarcoidosis
Hemochromatosis
Endomyocardial fibrosis (hypereosinophilic syndrome, drugs, idiopathic, etc.)
Anderson-Fabry disease
Glycogen storage disease
Carcinoid heart disease
Diabetic cardiomyopathy
Scleroderma
Radiation
Drugs (anthracyclines)
Neoplasms

15.2 Imaging Modalities and Findings

15.2.1 Idiopathic Restrictive Cardiomyopathy

Overview

- Uncommon disorder with restrictive physiology in the absence of any identifiable cause
- Slowly progressing disease when compared with other infiltrative restrictive cardiomyopathies (Fig.15.2) [3]

15.2.2 Amyloidosis

Overview

- Amyloidosis is a disease of extracellular deposition of amyloid (amyloid insoluble proteins that is formed from the breakdown of normal or abnormal proteins) and deposits of amyloid in the heart that cause cardiac amyloidosis.
- Two main types of amyloidosis affecting the heart [4]:
  - AL amyloidosis (from light chains): a disease of the bone marrow
    - Treatment strategy is to stop the production of the abnormal light chains by the plasma cells.
  - Transthyretin-related (TTR) amyloidosis (from transthyretin produced by the liver) [5]

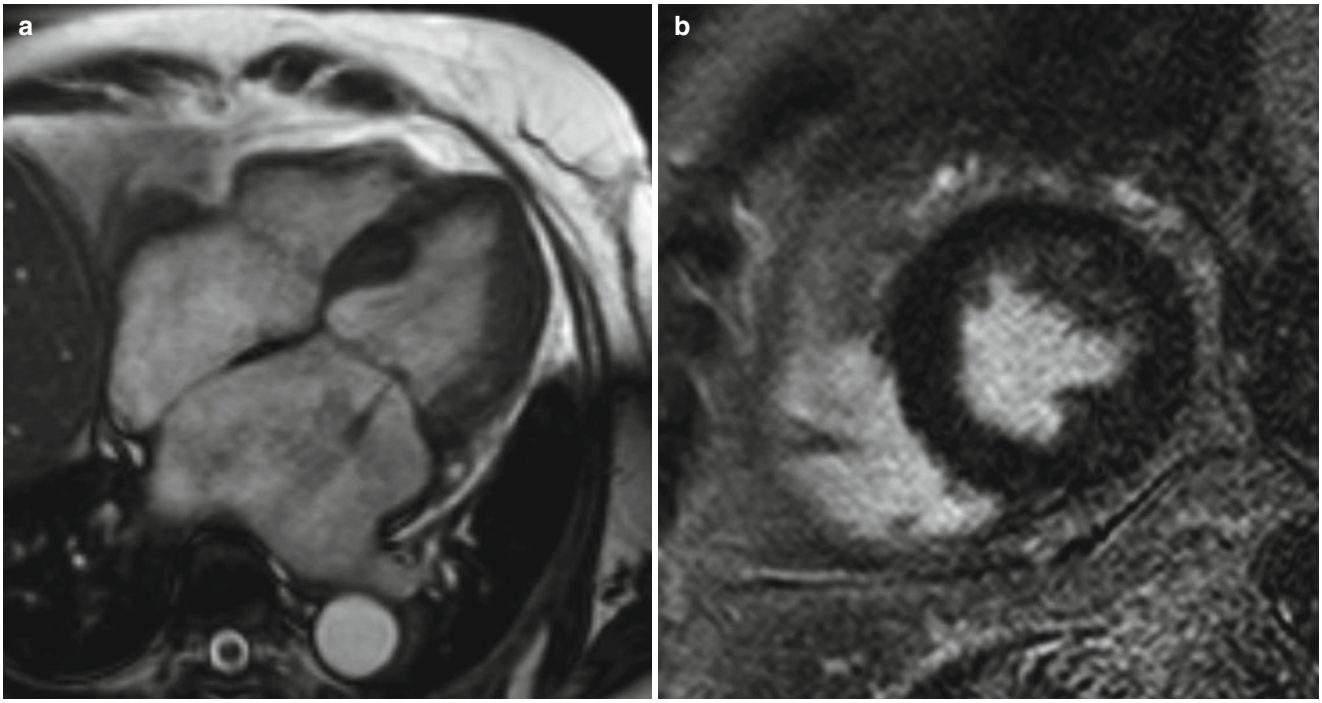

Fig. 15.2 MRI of a patient diagnosed with idiopathic restrictive cardiomyopathy. (**a**) Four-chamber cine MRI shows normal-sized left ventricle with enlarged left atrium and mild mitral regurgitation. (**b**) Delayed enhancement MRI shows no remarkable abnormal delayed myocardial enhancement

  - Hereditary TTR amyloidosis (ATTR; familial amyloidosis): result of inherited defect in the TTR protein; liver transplantation is the current treatment of choice
  - Senile systemic amyloidosis (SSA; nonhereditary TTR amyloidosis); result from the breakdown of the normal TTR molecule; no current existing specific therapy
- Characteristic imaging findings
  - Thickening of the ventricular and atrial walls as well as the interatrial septum
  - Speckled appearance of the myocardium due to amyloid deposition on echocardiography
  - Global subendocardial enhancement (but may be transmural) on DE-MRI (Fig. 15.3) [6]

15.2.3 Sarcoidosis

Overview

- Sarcoidosis is a multisystemic noncaseating granulomatous disease of unknown etiology.
- Pulmonary involvement (90 %), uncommon cardiac involvement (20–27 % in autopsy but clinical manifestations in 5 %).
- Cardiac involvement indicates poor prognosis: heart failure, conduction abnormalities (mainly atrioventricular block), sudden cardiac death → early diagnosis is important.
- Endomyocardial biopsy is the only definite test but relatively insensitive due to the focal nature of myocardial involvement by sarcoidosis.
- Role of cardiac MR in sarcoidosis:
  - Sensitive detection of myocardial involvement: cardiac MR can show three histological stages (edema, noncaseating granulomatous infiltration, and patchy myocardial fibrosis) on T2-weighted and delayed enhancement MRI [7].
  - Characteristic findings: preferential involvement of basal and subepicardial layer on delayed enhancement MRI (Fig. 15.4).
  - Myocardial damage detected by delayed enhancement MRI is helpful in guiding endomyocardial biopsy as well as prognostication [8].

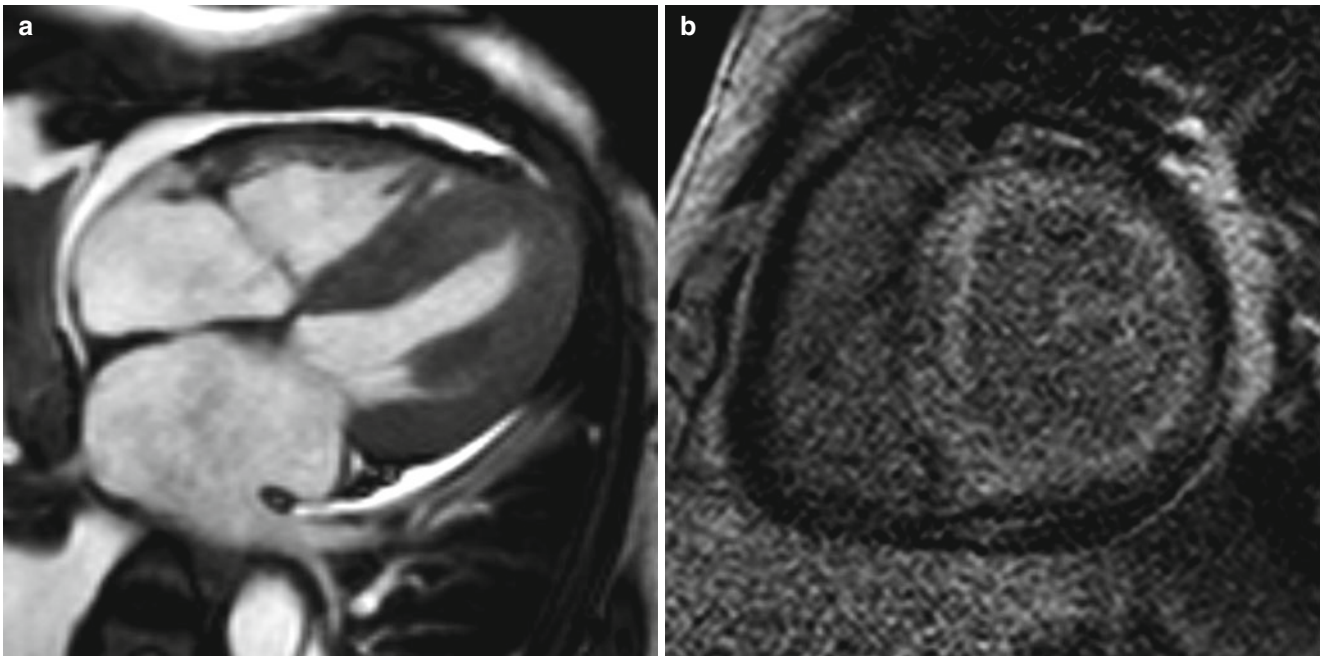

Fig. 15.3 MRI of a patient with multiple myeloma and cardiac amyloidosis. (**a**) Four-chamber cine MRI shows mild concentric LV hypertrophy with enlarged left atrium and pleural and pericardial effusion (http://extras.springer.com/2015/978-3-642-36396-2). (**b**) Delayed enhancement MRI demonstrates typical amyloid pattern of delayed enhancement in the LV, i.e., global subendocardial enhancement

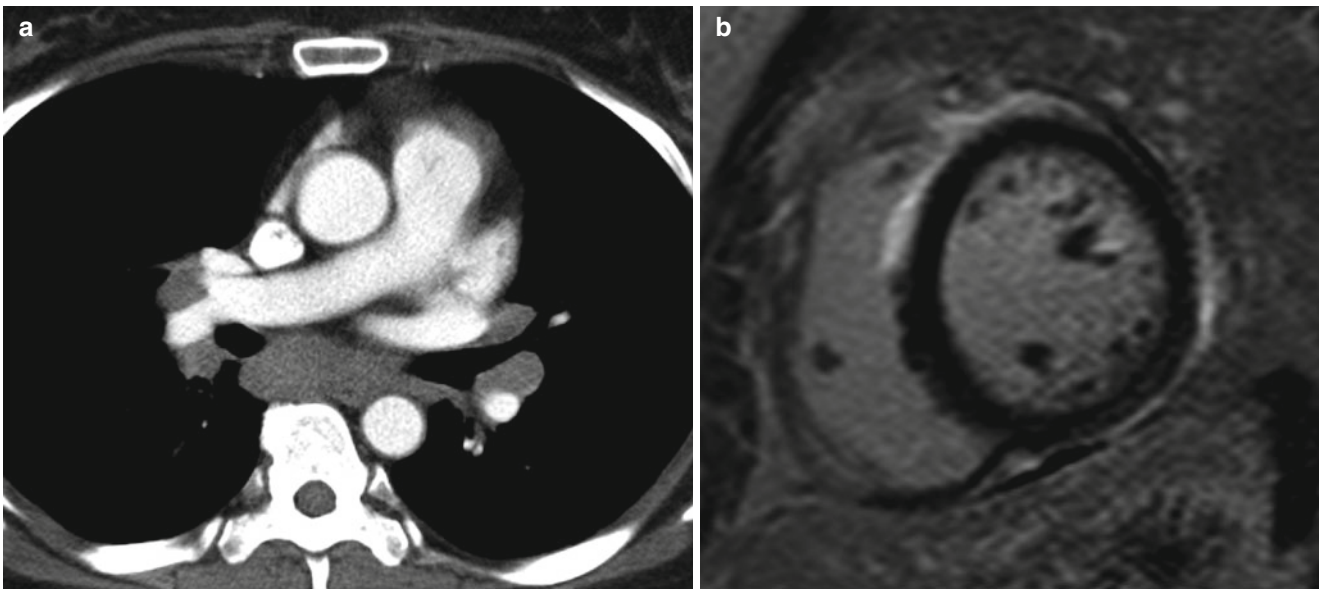

Fig. 15.4 Chest CT and cardiac MRI of a patient with sarcoidosis. (**a**) Chest CT shows multiple enlarged lymph nodes in the hila and mediastinum. (**b**) Delayed enhancement MRI shows focal delayed hyperenhancement in the epicardial side of the anterior wall of the LV and RV side of the interventricular septum

15.2.4 Hemochromatosis (Iron-Overload Cardiomyopathy)

Overview

- Iron deposition in the myocardium in patients with primary and secondary hemochromatosis.
- Cardiac involvement is uncommon (common sites of iron deposition – liver, spleen, and endocrine organs).
- Detection and quantification of cardiac involvement using cardiac MR:
  - Decrease in T2* relaxation time: typically less than 20 ms, considered severe if <10 ms [9, 10]
- Cardiac MR can reduce the morbidity and mortality in hemochromatosis by early detection of myocardial iron overload, direct timely institution of chelation therapy, and treatment monitoring (Fig. 15.5).

15.2.5 Hypereosinophilic Syndrome and Endomyocardial Fibrosis

Overview

- Endomyocardial fibrosis (EMF) is characterized by extensive fibrosis of the subendocardial layer of the myocardium involving the apices and extending to the inflow tracts.
- The cause of EMF is largely unknown but commonly cited etiologic links in EMF are eosinophilia (hypereosinophilic syndrome), infections (toxoplasmosis, rheumatic fever, malaria, helminthic parasites, etc.), and environmental exposure (cerium in the soil in endemic areas).
- Endomyocardial fibrosis forms the substrate for thrombus formation that may obliterate the entire ventricular apex.
- Delayed enhancement MRI is useful in the diagnosis and prognosis of EMF through quantification of the typical pattern of fibrous tissue deposition (Fig. 15.6) [11].

15.3 Differential Diagnosis

- Constrictive pericarditis from the loss of pericardial elasticity leads to impairment of ventricular filling in mid and late diastole that produces hemodynamic changes similar to those in restrictive cardiomyopathy:
  - Elevated B-type natriuretic peptide (BNP) level, minimal respiratory variation in ventricular filling velocity on Doppler echocardiography, and decreased early diastolic tissue velocity on tissue Doppler imaging favor restrictive cardiomyopathy.
  - Normal BNP level, large respiratory variation in ventricular filling velocity, preserved early diastolic tissue velocity, and increased thickness or calcification of the pericardium suggest constrictive pericarditis.

15.4 Summary

Restrictive cardiomyopathy is a specific group of myocardial disorders characterized by impaired ventricular relaxation leading to severe diastolic dysfunction. Cardiac MRI provides anatomical, morphological, and functional information along with information regarding disease mechanisms, treatment guide, and prognostication.

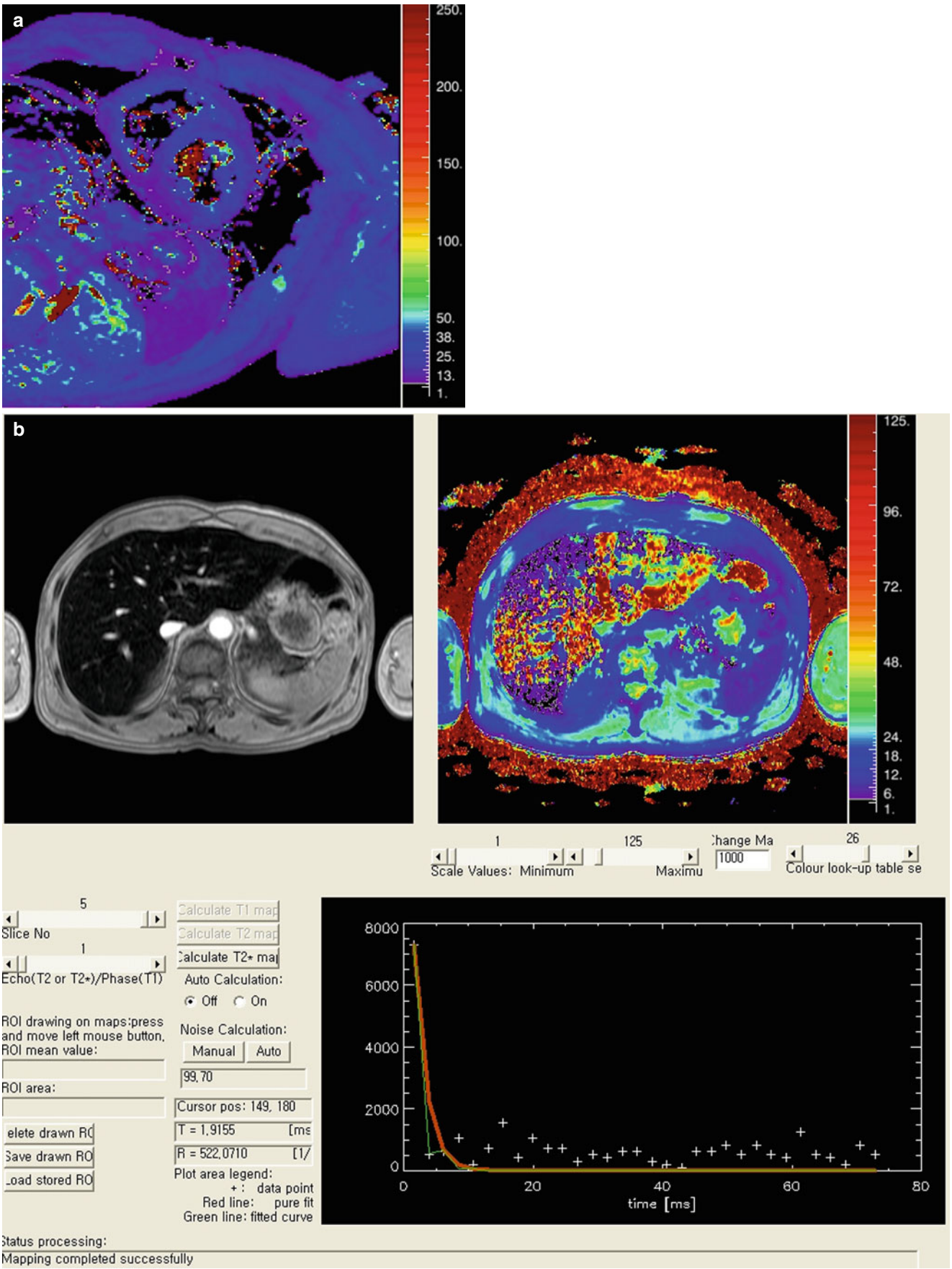

Fig. 15.5 T2* mapping MRI from a patient with aplastic anemia and hemochromatosis. (**a**) T2* maps of the heart (**b**). T2* map of the liver. The T2* value of the heart is 14 ms (suggestive of myocardial iron overload) and that of the liver is 1.2–1.8 ms

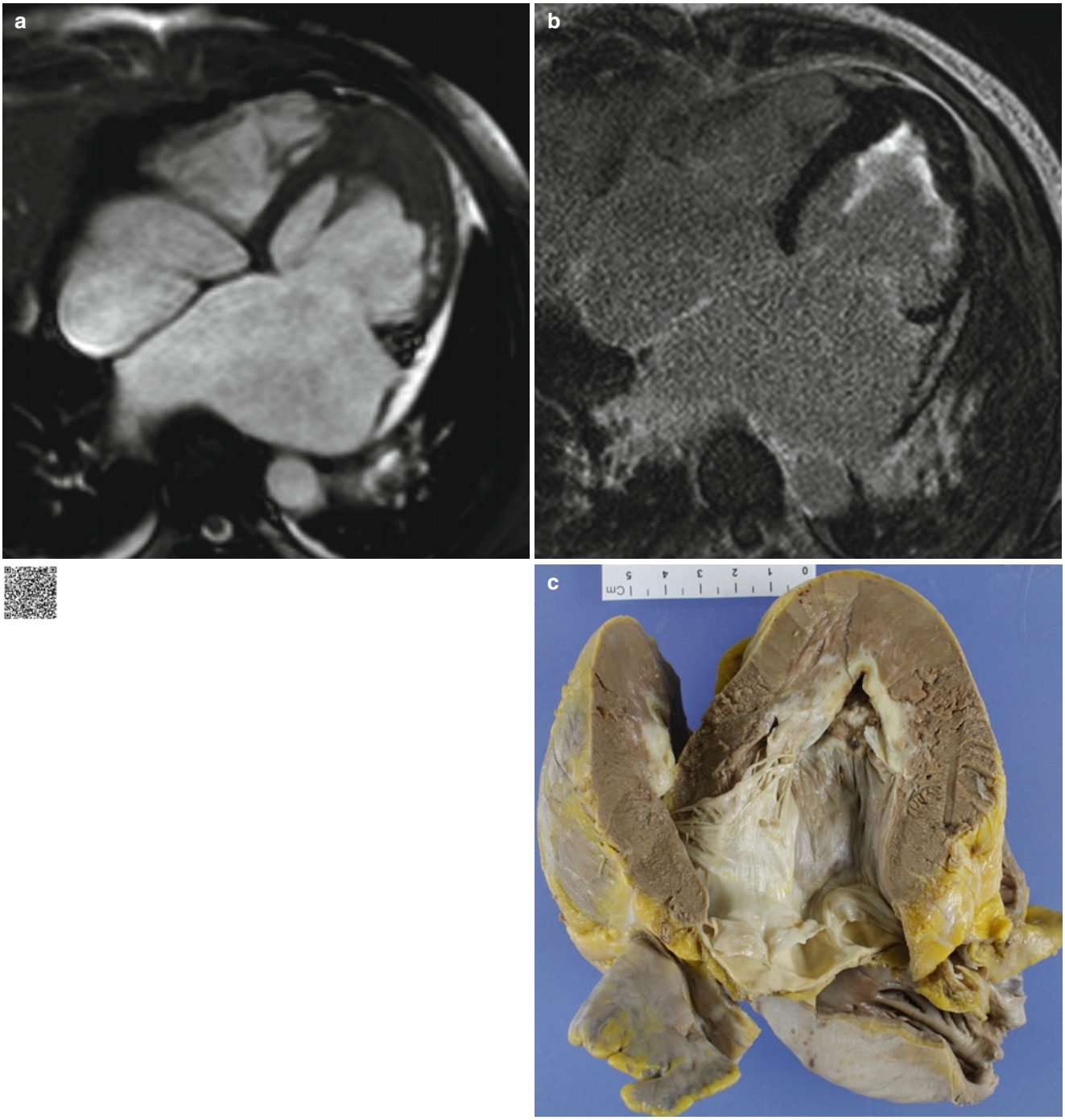

Fig. 15.6 MRI and autopsy specimen from a patient with endomyocardial fibrosis. (**a**) Four-chamber cine MRI shows blunted left ventricular apex and small ventricular chamber size (http://extras.springer.com/2015/978-3-642-36396-2). (**b**) Delayed enhancement MRI shows dense delayed enhancement of the endomyocardial portion of the left ventricular apex. (**c**) The patient underwent cardiac transplantation. The photograph of explanted heart shows thickened white sclerotic area corresponding to the area with delayed enhancement on MRI

References

1. Elliott P, Andersson B, Arbustini E. Classification of the cardiomyopathies: a position statement from the European Society of Cardiology Working Group on Myocardial and Pericardial Diseases. Eur Heart J. 2008;29:270–6.
2. Kushwaha SS, Fallon JT, Fuster V. Restrictive cardiomyopathy. N Engl J Med. 1997;336:267–76.
3. Ammash NM, Seward JB, Bailey KR, et al. Clinical profile and outcome of idiopathic restrictive cardiomyopathy. Circulation. 2000;101:2490–6.
4. Quarta CC, Kruger JL, Falk RH. Cardiac amyloidosis. Circulation. 2012;126:e178–82.
5. Ruberg FL, Berk JL. Transthyretin (TTR) cardiac amyloidosis. Circulation. 2012;126:1286–300.
6. Vogelsberg H, Mahrholdt H, Deluigi CC, et al. Cardiovascular magnetic resonance in clinically suspected cardiac amyloidosis: noninvasive imaging compared to endomyocardial biopsy. J Am Coll Cardiol. 2008;51:1022–30.
7. Patel MR, Cawley PJ, Heitner JF, et al. Detection of myocardial damage in patients with sarcoidosis. Circulation. 2009;120:1969–77.
8. Iannuzzi MC, Fontana JR. Sarcoidosis: clinical presentation, immunopathogenesis, and therapeutics. JAMA. 2011;305:391–9.
9. Kondur AK, Li T, Vaitkevicius P, et al. Quantification of myocardial iron overload by cardiovascular magnetic resonance imaging T2* and review of the literature. Clin Cardiol. 2009;32:e55–9.
10. Guo H, Au WY, Cheung JS, et al. Myocardial T2 quantitation in patients with iron overload at 3 Tesla. J Magn Reson Imaging. 2009;30:394–400.
11. Salemi VM, Rochitte CE, Shiozaki AA, et al. Late gadolinium enhancement magnetic resonance imaging in the diagnosis and prognosis of endomyocardial fibrosis patients. Circ Cardiovasc Imaging. 2011;4:304–11.

Acute Myocarditis and Other Cardiomyopathies

16

Yon Mi Sung and Yeon Hyeon Choe

Contents

Abstract

Heart muscle diseases or cardiomyopathies include a heterogeneous group of cardiac diseases. Imaging provides unique information on morphologic and functional properties. MR findings of acute myocarditis reflect histopathologic changes of disease. Arrhythmogenic right ventricular dysplasia/cardiomyopathy, left ventricular noncompaction cardiomyopathy, and stress cardiomyopathy show characteristic imaging findings. Myocardial involvement of systemic vasculitis can be detected by CT and MR imaging.

16.1 Overview

- Heart muscle diseases or cardiomyopathies include a heterogeneous group of cardiac diseases.
- Imaging is an essential tool in assessment of myocardial functional properties and tissue characteristics.
- This chapter describes myocarditis and cardiomyopathies.

16.2 Imaging Modalities and Findings

16.2.1 Acute and Chronic Myocarditis

- Myocarditis is defined as an inflammatory infiltrate of the myocardium with necrosis or degeneration of myocytes.
  - The hallmarks of acute and chronic myocarditis:
    - Accumulation of inflammatory cells; swelling, necrosis, and/or apoptosis of cardiomyocytes; increase in extracellular space and water content; myocardial remodeling with fibrotic tissue replacement
  - Acute myocarditis has a mainly viral origin, and spontaneous recovery within a few weeks to months is common.
  - Progression of acute myocarditis to chronic myocarditis or dilated cardiomyopathy occurs in about 21 % of cases and is caused by direct cytotoxic effects of viruses or by chronic immune processes.

Electronic supplementary material Supplementary material is available in the online version of this chapter at 10.1007/978-3-642-36397-9_16.

Y.M. Sung
Department of Radiology, Gachon University Gil Hospital, Incheon, Republic of Korea
e-mail: yonmi.sung@gmail.com

Y.H. Choe (✉)
Department of Radiology, Samsung Medical Center, Sungkyunkwan University School of Medicine, Seoul, Republic of Korea
e-mail: yhchoe@skku.edu

T.-H. Lim (ed.), *Practical Textbook of Cardiac CT and MRI*,
DOI 10.1007/978-3-642-36397-9_16, © Springer-Verlag Berlin Heidelberg 2015

- Etiopathogenesis
  - Complex as a great variety of infectious agents can induce cardiac inflammation
  - Noninfectious causes of inflammatory heart disease:
    - Many systemic and autoimmune diseases such as sarcoidosis, giant cell myocarditis, and systemic lupus erythematosus
    - Drugs and toxins
- Autopsy findings in young adults with sudden cardiac death suggest myocarditis in 12–22 %.
- Characteristic imaging findings [1–5]:
  - T2-weighted spin-echo images; myocardial edema caused by lymphocyte infiltrate
  - SSFP cine CMR:
    - Global hypokinesia or akinesia
    - Excellent for assessing recovery of function
    - Pericardial effusion in 32–57 %
  - T1-weighted fast spin-echo images with early gadolinium enhancement (EGE):
    - EGE reflecting hyperemia and capillary leak during the first 2 weeks
  - Late gadolinium enhancement (LGE)/delayed enhancement images:
    - Reflects irreversible myocardial injury (i.e., necrosis and fibrosis)
    - Usually subepicardial enhancement
    - Focal or transmural and global enhancement when disseminated
    - Patchy diffuse or nodular LGE caused by necrosis that does not correspond to a vascular territory
- Suspected chronic myocarditis at cardiac MR [6]:
  - Quantitative CMR of signal EGE and of myocardial edema is helpful for identifying myocardial inflammation, whereas LGE is less helpful.
  - The CMR parameter with the highest specificity and accuracy for the detection of immunohistologically identified inflammation:
    - Global relative enhancement (gRE) of myocardium compared to skeletal muscle, more than 4.0 is diagnostic myocarditis.
    - gRE-based and edema ratio-based CMR techniques have good sensitivity, specificity, and accuracy in the detection of inflammatory processes of the myocardium (Fig. 16.1).

16.2.2 Arrhythmogenic Right Ventricular Dysplasia/Cardiomyopathy (ARVD/C)

- Disorder of the heart muscle characterized pathologically by replacement of the right ventricular myocardium with fatty or fibrous fatty tissue.
- Structurally more vulnerable to mechanical stress such as the inferior, apical, and infundibular part of the thin-walled right ventricle (the so-called triangle of dysplasia), and the inferolateral wall of the left ventricle is prone to involvement.
- Characteristic findings at helical computed tomography [7]:
  - Dilatation of the right ventricle

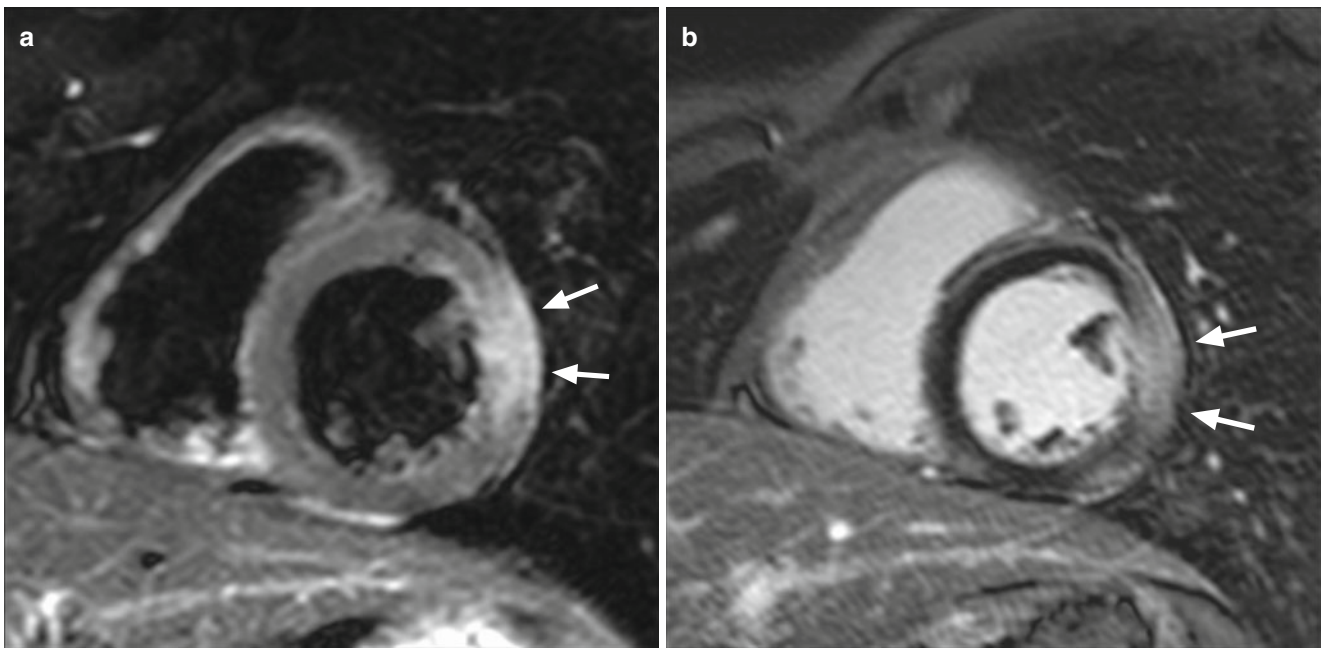

Fig. 16.1 MRI of a patient with acute myocarditis. (**a**) Short-axis T2-weighted image shows myocardial edema in the lateral wall of the left ventricle. (**b**) Short-axis late gadolinium enhancement image reveals transmural enhancement along the lateral wall of the left ventricle

  - Fatty tissue in conspicuous trabeculae of the right ventricle, especially in the anterior wall, apex, and inferior (diaphragmatic) wall
  - A scalloped appearance (bulging) of the right ventricular wall
- Although the diagnosis of fibrofatty replacement is made by endomyocardial biopsy, cardiac MR is emerging as a more definitive diagnostic tool:
  - The use of MRI in the diagnosis of ARVD is well established, but reliance on fat signal intensity in the MRI diagnosis of ARVD has met only variable success.
- Characteristic imaging findings at cardiac MR [4, 8–10]:
  - Accurate diagnosis of ARVD requires recognition of RV dilatation, abnormalities in RV wall motion, and scalloped or bulging appearance of the RV free wall as well as familiarity with findings related to myocardial fat (thin RV free wall; myocardial fat in the RV trabeculae, moderator band, interventricular septum, and epicardial LV free wall).
  - Lipomatous hypertrophy/hyperplasia of the RV without global or regional functional abnormalities appears to be a distinct MRI-defined disorder that should be differentiated from ARVD (Table 16.1) (Figs. 16.2 and 16.3).

16.2.3 Left Ventricular Noncompaction Cardiomyopathy

- Congenital abnormality characterized by a compact thin epicardial layer and thickened trabeculated spongiform-like endocardial layer.
- The apical and mid-ventricular part of the inferior and lateral left ventricular wall are most commonly affected.

Table 16.1 Key differentiating points between physiologic and pathologic myocardial fat [11]

Type of myocardial fat	Location in the heart	Intramyocardial location	Myocardial thickness	Ventricular size
Physiologic	Anterolateral RV free wall, RVOT, sometimes in RV trabeculae and LV apex	Full thickness, probably not in subendocardium	Normal or thick	Normal
ARVC	RVOT, RV free wall, RV trabeculae, moderator band, ventricular septum (RV side), LV free wall	Subepicardium	Thin	Enlarged RV
Healed MI	Territory of coronary artery, usually in LV	Mostly subendocardium	Normal or thin	Normal or enlarged LV
Lipomatous hyperplasia	RV free wall	Subepicardium	Thick	Normal

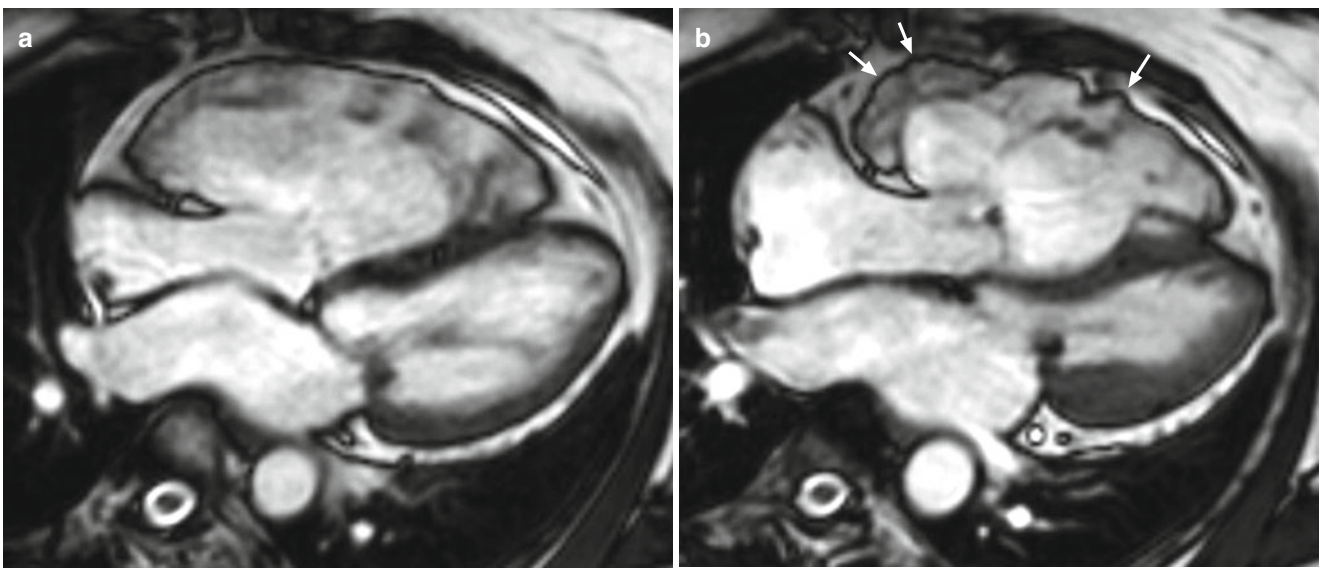

Fig. 16.2 MRI of a patient with arrhythmogenic right ventricular dysplasia/cardiomyopathy (http://extras.springer.com/2015/978-3-642-36396-2). Four-chamber cine images at end-diastole (**a**) and end-systole (**b**) demonstrate important right ventricular dilatation. Several regions (*arrows*) show severely diminished contractility. (**c**) Short-axis late gadolinium enhancement image shows enhancement (*arrows*) along the right ventricle

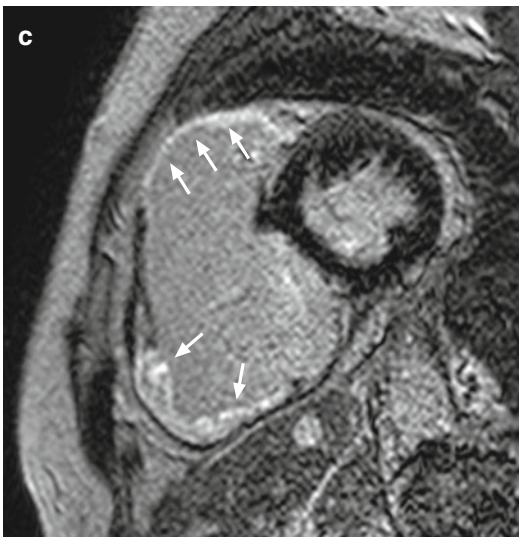

Fig. 16.2 (continued)

- Characteristic imaging findings [12–14]:
  - The ratio of noncompacted to compacted myocardium is more than 2.3 on end-diastole.
  - The presence of late gadolinium enhancement is related to clinical severity and left ventricular systolic dysfunction.
  - Distinguishing crypts in hypertrophic cardiomyopathy from noncompaction cardiomyopathy [15].
    - Crypts in hypertrophic cardiomyopathy penetrate compact myocardium, whereas in noncompaction cardiomyopathy, they mainly are located in the mid and basal inferoseptal segments of the left ventricle and are not associated with a reduced left ventricular ejection fraction.
    - In noncompaction cardiomyopathy, a broad noncompacted layer aligns with a compact layer of myocardium; noncompaction cardiomyopathy mainly occurs in the apical and lateral segments (Fig. 16.4).

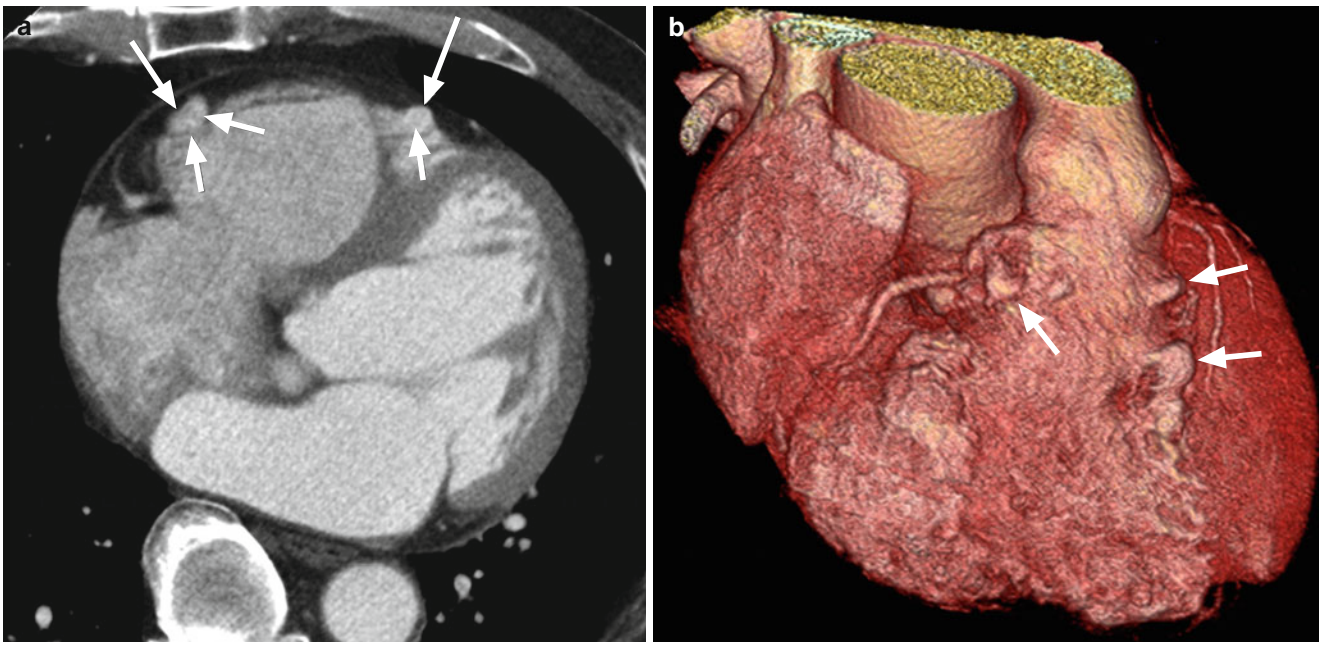

Fig. 16.3 CT of a patient with arrhythmogenic right ventricular dysplasia/cardiomyopathy. (**a**) Axial image and (**b**) volume-rendering image show focal aneurysms of the right ventricle

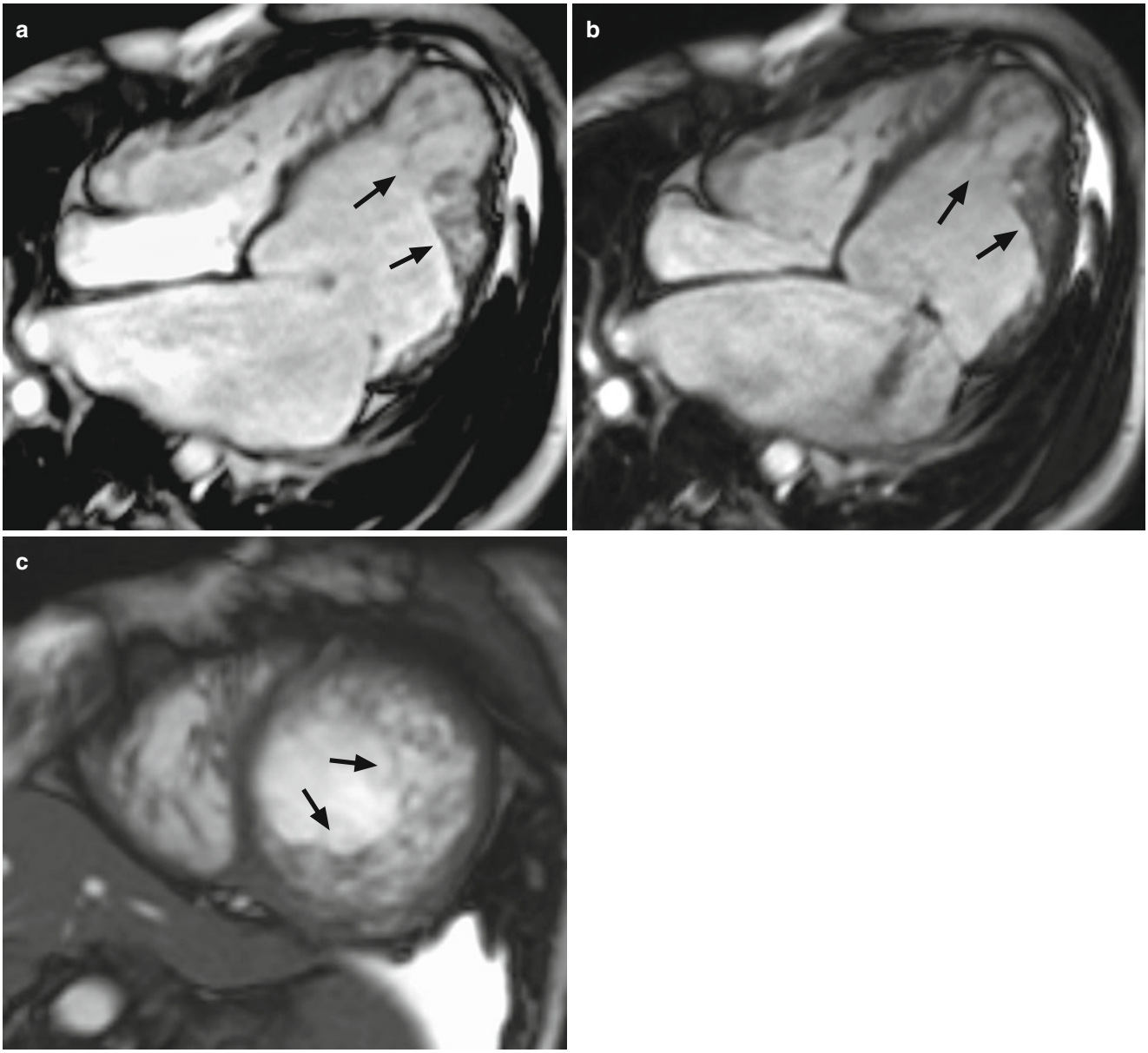

Fig. 16.4 MRI of a patient with left ventricular noncompaction cardiomyopathy (http://extras.springer.com/2015/978-3-642-36396-2). (**a**) Horizontal long-axis cine image at end-diastole. (**b**) Horizontal long-axis cine image at end-systole. (**c**) Short-axis cine image reveals very prominent trabecular network (*arrows in all images*) along the left ventricular lateral wall and apex

16.2.4 Stress Cardiomyopathy

- Stress cardiomyopathy or Takotsubo cardiomyopathy is defined as a reversible left ventricular dysfunction with acute myocardial infarction-like ST-segment elevation without coronary artery lesions and with minimal myocardial enzymatic release.
- Characteristic imaging findings:
  - Cine MRI:
    - Typical presentation is apical akinesia of the left ventricle causing apical ballooning.
    - Hypokinesis or akinesis in the mid and apical segments of the left ventricular wall that typically spares the basal segments in the absence of obstructive coronary lesions.
    - Reversed or inverted variant is recognized involving the basal and mid-ventricular segments with preserved contractility of the apical segments [16].
  - T2 STIR sequence:
    - Ventricular edema that appears as high signal intensity with a diffuse or transmural distribution.
    - The location of the edema is not related to a vascular territory of the coronary arteries, and edema is distributed in both the apical and mid planes of the left ventricle.
    - The area of edema shows dysfunction in the ventricular contraction observed with cine MRI sequences.
  - Contrast-enhanced sequence:
    - No perfusion defects and late enhancement are other clues that differentiate Takotsubo cardiomyopathy from other diseases such as acute myocardial infarction and acute myocarditis.
- Acute mitral regurgitation is a potentially serious complication [17, 18] (Fig. 16.5).

16.2.5 Myocardial Involvement of Systemic Vasculitis

Systemic vasculitis can directly or indirectly cause a wide variety of cardiac involvement.

16.2.5.1 Churg-Strauss Syndrome

- Churg-Strauss syndrome is a rare form of systemic vasculitis characterized by necrotizing small-sized vessel vasculitis, extravascular granulomas, and eosinophilia.
- Cardiac involvement is common and a leading cause of mortality.
- The presence of late gadolinium enhancement correlates with eosinophilic infiltrates.
- Most subendocardial late enhancements were located in the apical and mid-cavity left ventricular segments [4, 19, 20] (Fig. 16.6)

16.2.5.2 Behçet's Disease

- Behçet's disease is a relapsing inflammatory disease with recurrent aphthous stomatitis, genital ulcerations, and uveitis.
- Cardiac involvement is found in only 1–5 % of patients (Fig. 16.7).

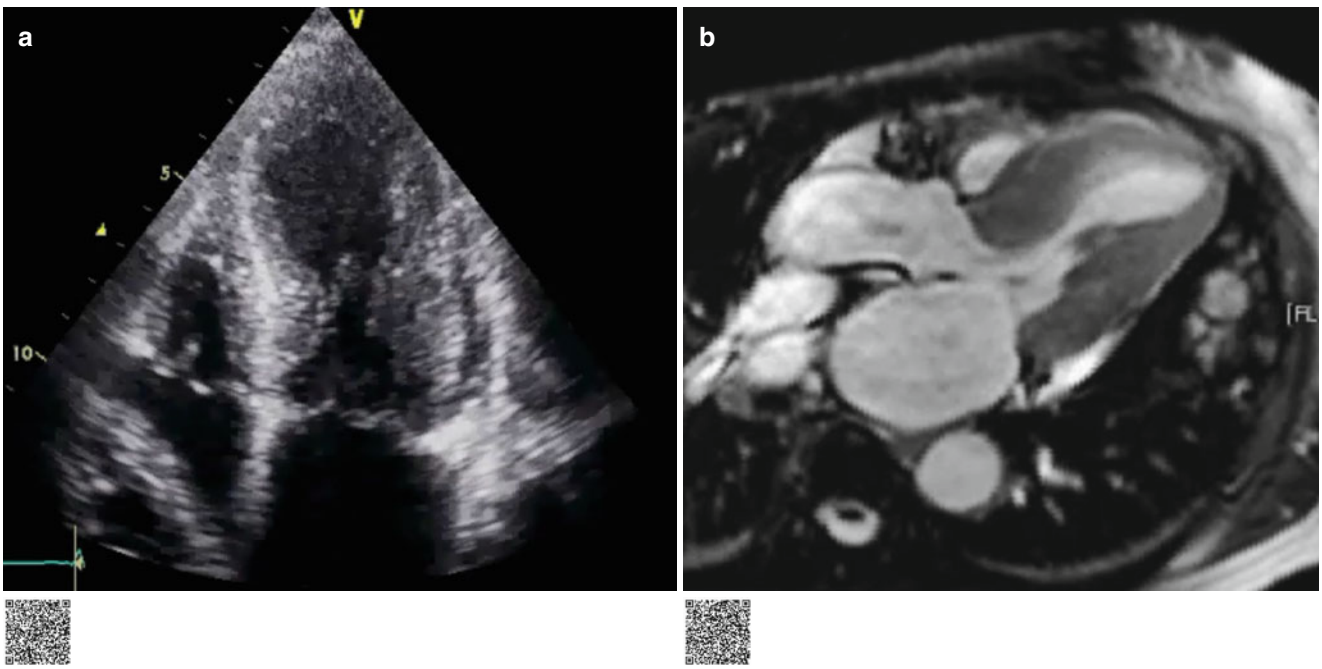

Fig. 16.5 Echocardiography and MRI of a patient with stress cardiomyopathy. Horizontal long-axis cine images (**a**) (http://extras.springer.com/2015/978-3-642-36396-2) on echocardiography and (**b**) (http://extras.springer.com/2015/978-3-642-36396-2) cine MR image show severe hypokinesia or akinesia of the same region and hyperkinesia at the basal level. (**c**, **d**) Increased signal intensity in the entire apical and lower mid-ventricular wall on short-axis T2-weighted image. (**e**, **f**) No evidence of enhancement on late gadolinium enhancement image

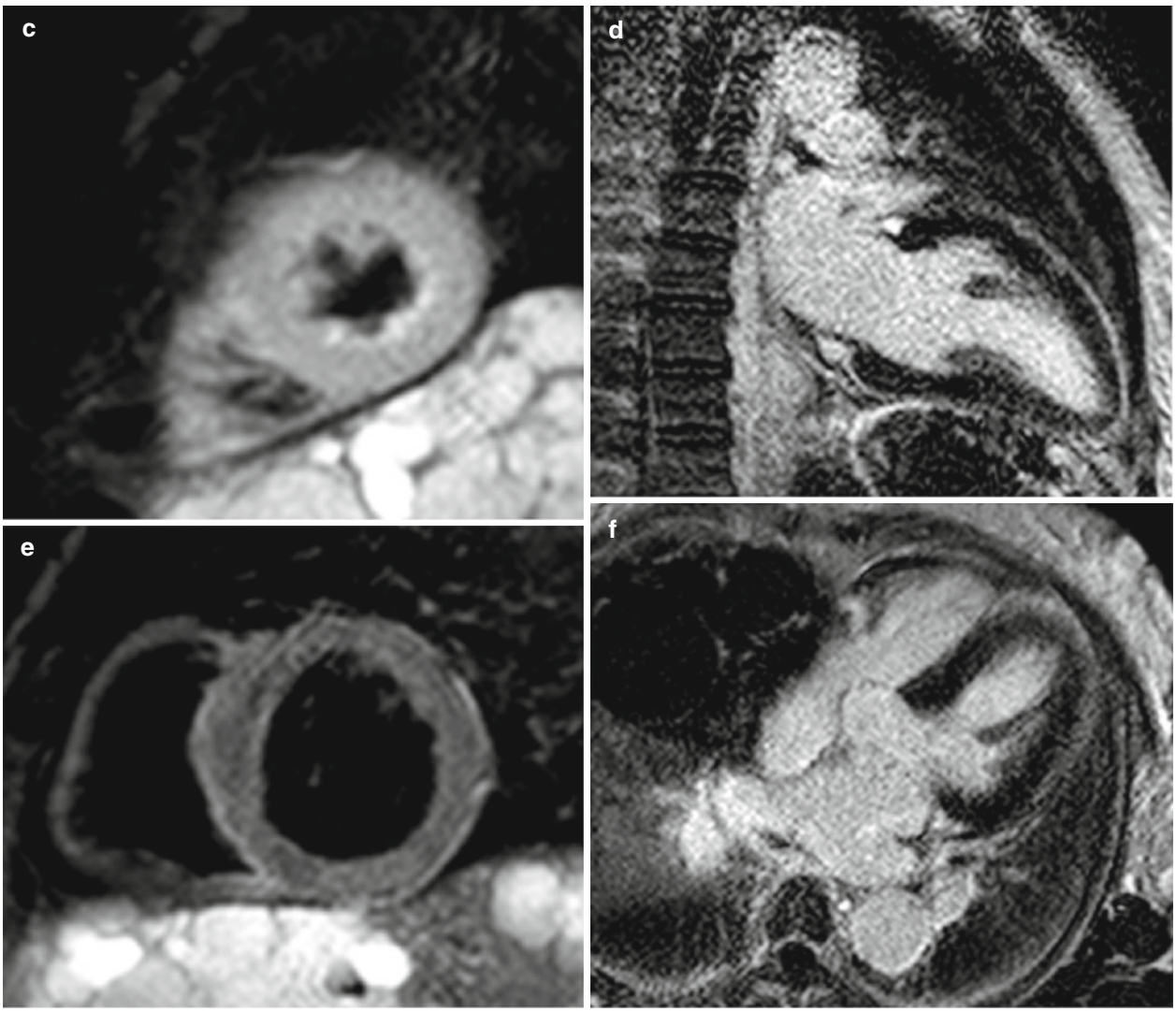

Fig. 16.5 (continued)

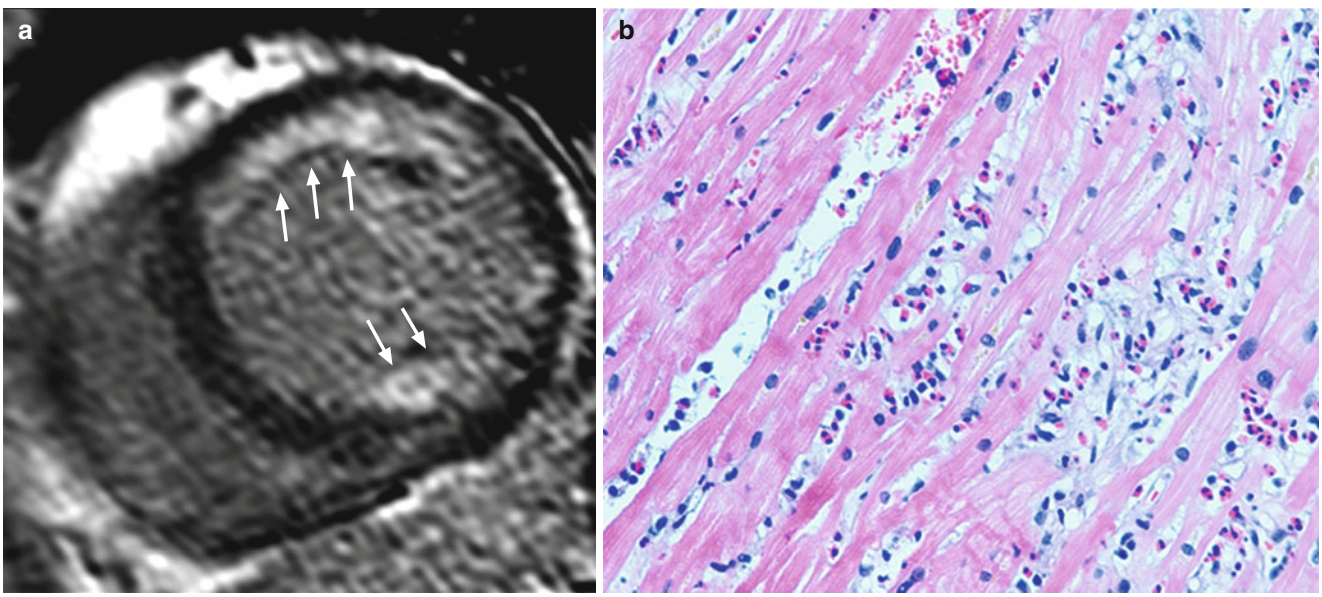

Fig. 16.6 Cardiac involvement in a patient with Churg-Strauss syndrome. (**a**) Short-axis late gadolinium enhancement image shows extensive subendocardial enhancement (*arrows*) in the anterior and inferior walls of the left ventricle. (**b**) Endomyocardial biopsy reveals active myocardial inflammation with eosinophils

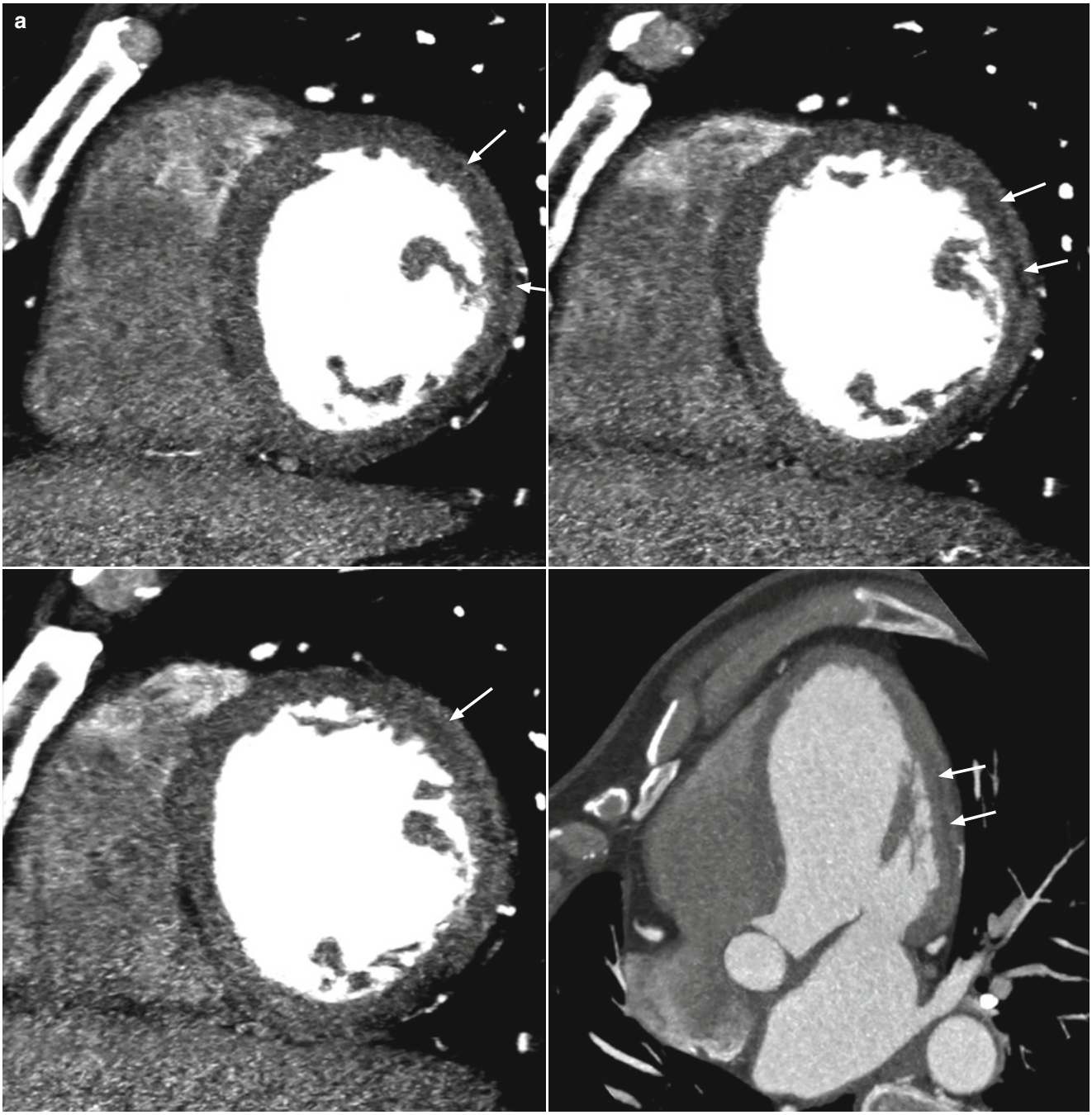

Fig. 16.7 Cardiac involvement in a patient with Behçet's disease. (**a**) CT and (**b**) late gadolinium enhancement MR image show areas of fibrosis and fat infiltration (*arrows*) in the mid-layer of the left ventricle

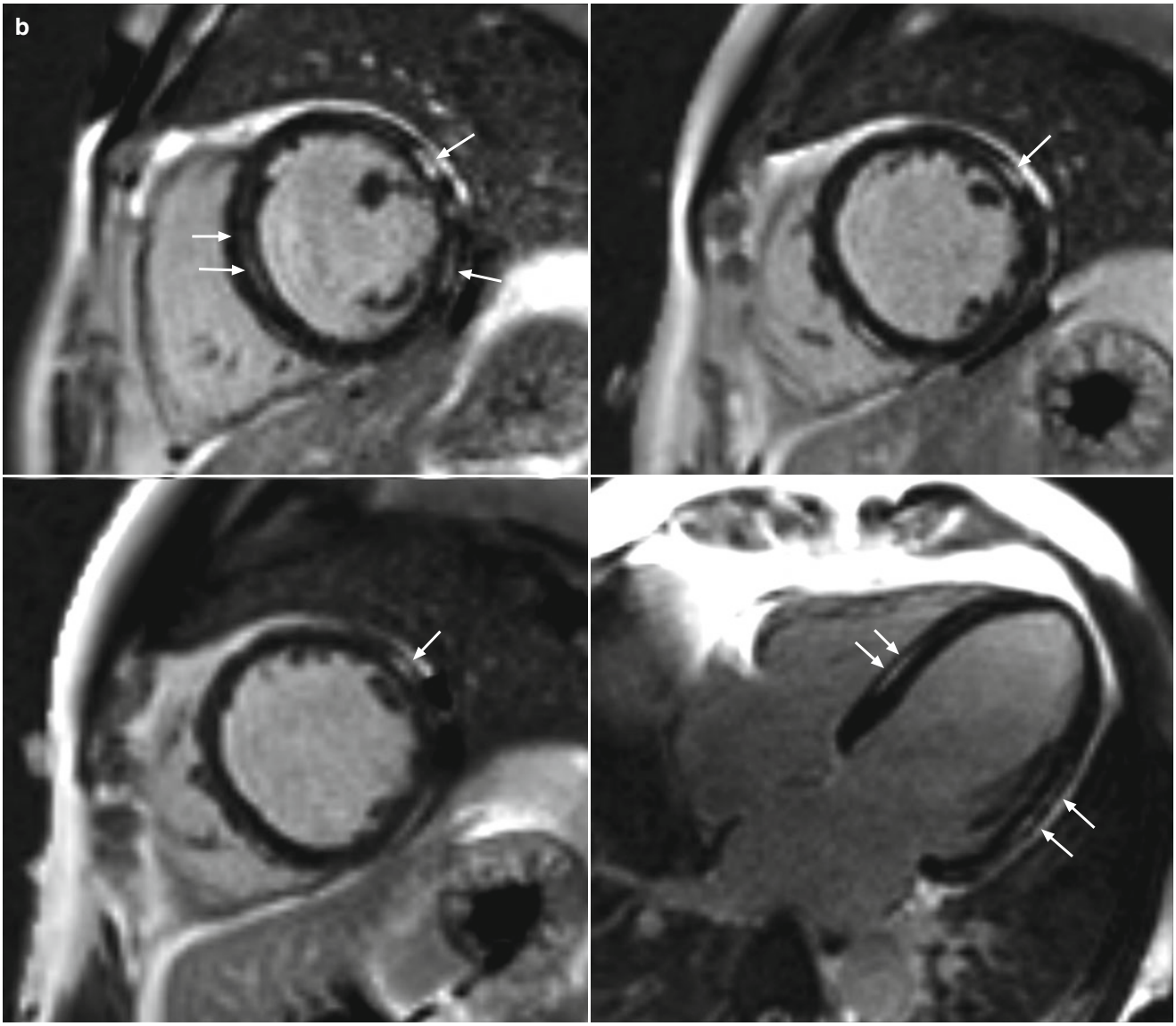

Fig. 16.7 (continued)

16.3 Summary

Imaging provides both morphological and functional information to assess acute myocarditis and various cardiomyopathies.

References

1. Friedrich MG, Sechtem U, Schulz-Menger J, Holmvang G, Alakija P, Cooper LT, White JA, Abdel-Aty H, Gutberlet M, Prasad S, et al. Cardiovascular magnetic resonance in myocarditis: A JACC White Paper. J Am Coll Cardiol. 2009;53(17):1475–87.
2. Childs H, Friedrich MG. Cardiovascular magnetic resonance imaging in myocarditis. Prog Cardiovasc Dis. 2011;54(3):266–75.
3. Yilmaz A, Ferreira V, Klingel K, Kandolf R, Neubauer S, Sechtem U. Role of cardiovascular magnetic resonance imaging (CMR) in the diagnosis of acute and chronic myocarditis. Heart Fail Rev. 2013;18(6):747–60.
4. Ordovas KG, Higgins CB. Delayed contrast enhancement on MR images of myocardium: past, present, future. Radiology. 2011;261(2): 358–74.
5. Friedrich MG. Tissue characterization of acute myocardial infarction and myocarditis by cardiac magnetic resonance. JACC Cardiovasc Imaging. 2008;1(5):652–62.
6. Gutberlet M, Spors B, Thoma T, Bertram H, Denecke T, Felix R, Noutsias M, Schultheiss H-P, Kuhl U. Suspected chronic myocarditis at cardiac MR: diagnostic accuracy and association with immunohistologically detected inflammation and viral persistence 1. Radiology. 2008;246(2):401–9.
7. Kimura F, Sakai F, Sakomura Y, Fujimura M, Ueno E, Matsuda N, Kasanuki H, Mitsuhashi N. Helical CT features of arrhythmogenic right ventricular cardiomyopathy1. Radiographics. 2002;22(5): 1111–24.
8. Tandri H, Macedo R, Calkins H, Marcus F, Cannom D, Scheinman M, Daubert J, Estes 3rd M, Wilber D, Talajic M, et al. Role of magnetic resonance imaging in arrhythmogenic right ventricular dysplasia: insights from the North American arrhythmogenic right ventricular dysplasia (ARVD/C) study. Am Heart J. 2008;155(1): 147–53.
9. Jain A, Tandri H, Calkins H, Bluemke DA. Role of cardiovascular magnetic resonance imaging in arrhythmogenic right ventricular dysplasia. J Cardiovasc Magn Reson. 2008;10:32.
10. Vermes E, Strohm O, Otmani A, Childs H, Duff H, Friedrich MG. Impact of the revision of arrhythmogenic right ventricular cardiomyopathy/dysplasia task force criteria on its prevalence by CMR criteria. JACC Cardiovasc Imaging. 2011;4(3): 282–7.
11. Kimura F, Matsuo Y, Nakajima T, Nishikawa T, Kawamura S, Sannohe S, Hagiwara N, Sakai F. Myocardial fat at cardiac imaging: how can we differentiate pathologic from physiologic fatty infiltration? Radiographics. 2010;30(6):1587–602.
12. Sparrow P, Merchant N, Provost Y, Doyle D, Nguyen E, Paul N. Cardiac MRI and CT features of inheritable and congenital conditions associated with sudden cardiac death. Eur Radiol. 2009;19(2):259–70.
13. Dursun M, Agayev A, Nisli K, Ertugrul T, Onur I, Oflaz H, Yekeler E. MR imaging features of ventricular noncompaction: emphasis on distribution and pattern of fibrosis. Eur J Radiol. 2010;74(1): 147–51.
14. Fazio G, Novo G, D'Angelo L, Visconti C, Sutera L, Grassedonio E, Galia M, Ferrara F, Midiri M, Novo S. Magnetic resonance in isolated noncompaction of the ventricular myocardium. Int J Cardiol. 2010;140(3):367–9.
15. Germans T, Nijveldt R, van Rossum AC. A more detailed view calls for more detailed definition: description of cardiac morphology with high-resolution CT and MRI. Am J Roentgenol. 2008;190(2): W169.
16. Song BG, Chun WJ, Park YH, Kang GH, Oh J, Lee SC, Park SW, Oh JK. The clinical characteristics, laboratory parameters, electrocardiographic, and echocardiographic findings of reverse or inverted takotsubo cardiomyopathy: comparison with mid or apical variant. Clin Cardiol. 2011;34(11):693–9.
17. Izumo M, Nalawadi S, Shiota M, Das J, Dohad S, Kuwahara E, Fukuoka Y, Siegel RJ, Shiota T. Mechanisms of acute mitral regurgitation in patients with takotsubo cardiomyopathy: an echocardiographic study. Circ Cardiovasc Imaging. 2011;4(4):392–8.
18. Haghi D, Rohm S, Suselbeck T, Borggrefe M, Papavassiliu T. Incidence and clinical significance of mitral regurgitation in Takotsubo cardiomyopathy. Clin Res Cardiol. 2010;99(2): 93–8.
19. Marmursztejn J, Vignaux O, Cohen P, Guilpain P, Pagnoux C, Gouya H, Mouthon L, Legmann P, Duboc D, Guillevin L. Impact of cardiac magnetic resonance imaging for assessment of Churg-Strauss syndrome: a cross-sectional study in 20 patients. Clin Exp Rheumatol. 2009;27(1 Suppl 52):S70–6.
20. Knockaert DC. Cardiac involvement in systemic inflammatory diseases. Eur Heart J. 2007;28(15):1797–804.

Part IV

Valvular Heart Disease

Aortic Valvular Heart Disease

17

Sung Min Ko

Contents

Abstract

The aortic valve consists of three cusps, an annulus, and commissures. Aortic stenosis and regurgitation are increasing in prevalence as the population ages. Aortic stenosis is the most common form of valvular heart disease for valve replacement. Bicuspid aortic valve is the most common congenital cardiac malformation and is at increased risk of both valvular and vascular complications. Echocardiography is the standard tool in the evaluation of aortic valve disease. Cardiac computed tomography (CT) and magnetic resonance imaging (MRI) are emerging as powerful imaging tools by providing valve morphology, quantitative evaluation of valvular dysfunction, determination the hemodynamic information of valvular dysfunctions on cardiovascular structures, and anatomic information of the coronary artery and ascending thoracic aorta. The purposes of this chapter are to introduce the role of cardiac CT and MRI in the quantification of the severity of aortic valve dysfunction and to describe the imaging findings of normal anatomy, congenital abnormalities and acquired pathologic condition of the aortic valve, and prosthetic valvular dysfunction.

Electronic supplementary material Supplementary material is available in the online version of this chapter at 10.1007/978-3-642-36397-9_17.

S.M. Ko
Department of Radiology, Konkuk University Hospital, Seoul, Republic of Korea
e-mail: ksm9723@yahoo.co.kr

T.-H. Lim (ed.), *Practical Textbook of Cardiac CT and MRI*,
DOI 10.1007/978-3-642-36397-9_17, © Springer-Verlag Berlin Heidelberg 2015

17.1 Normal Anatomy of the Aortic Valve

- The aortic valve consists of three cusps (right, left, and noncoronary), an annulus, and commissures (Fig. 17.1).
- The morphology of the aortic valve is assessed in parallel and perpendicular planes at the mid-systolic phase and at the mid-diastolic phase.
- Cardiac CT and MRI have the ability to accurately depict morphological and motional abnormalities of the aortic valve.

17.2 Imaging Role of Echocardiography, Cardiac CT, and Cardiac MRI

- Echocardiography is the primary imaging tool used to evaluate the aortic valve disease with high temporal resolution, allowing to characterization of valve anatomy and function.
- Echocardiography is operator dependent and sometimes inadequate for comprehensive evaluation of aortic valve diseases.
- Cardiac computed tomography (CT) and magnetic resonance imaging (MRI) are used for evaluation of aortic valve diseases and determination of the hemodynamic effects of the heart in patients with inconclusive findings at echocardiography.
- Cardiac CT and MRI provide more accurate information of valvular morphology and ascending aorta anatomy than echocardiography in severe calcific aortic stenosis.
- Valvular calcification is detected and quantitatively measured on cardiac CT.
- Cardiac CT with retrospective electrocardiography (ECG)-gating and tube current modulation is used to make cine imaging for aortic valvular cusp mobility and coaptation, providing information about stenotic aortic valve area (AVA) and regurgitant orifice area (ROA).
- Cardiac MRI with balanced steady-state free precession (b-SSFP) cine pulse sequence and phase-contrast (PC) pulse sequence is used for aortic valve morphology, qualitative and quantitative information of valvular dysfunction, and accurate assessment of the left ventricular (LV) function and mass.
- Cardiac MRI with delayed contrast enhancement and T1 mapping allows for the noninvasive detection and quantification of myocardial fibrosis in patients with severe aortic valve disease.

17.3 Aortic Valve Disease

17.3.1 Aortic Stenosis (AS)

- The most common single cardiac valvular lesion.
- The main causes of AS include age-related degenerative calcified AS of an anatomically normal valve or atherosclerotic TAV, congenitally BAV, and rheumatic VHD.
- In the ACC/AHA guidelines, severe AS is defined as (1) a peak aortic velocity greater than 4 m/s, (2) a mean pressure gradient greater than 40 mmHg, or (3) an AVA less than or equal to 1 cm^2 (Table 17.1) [3].

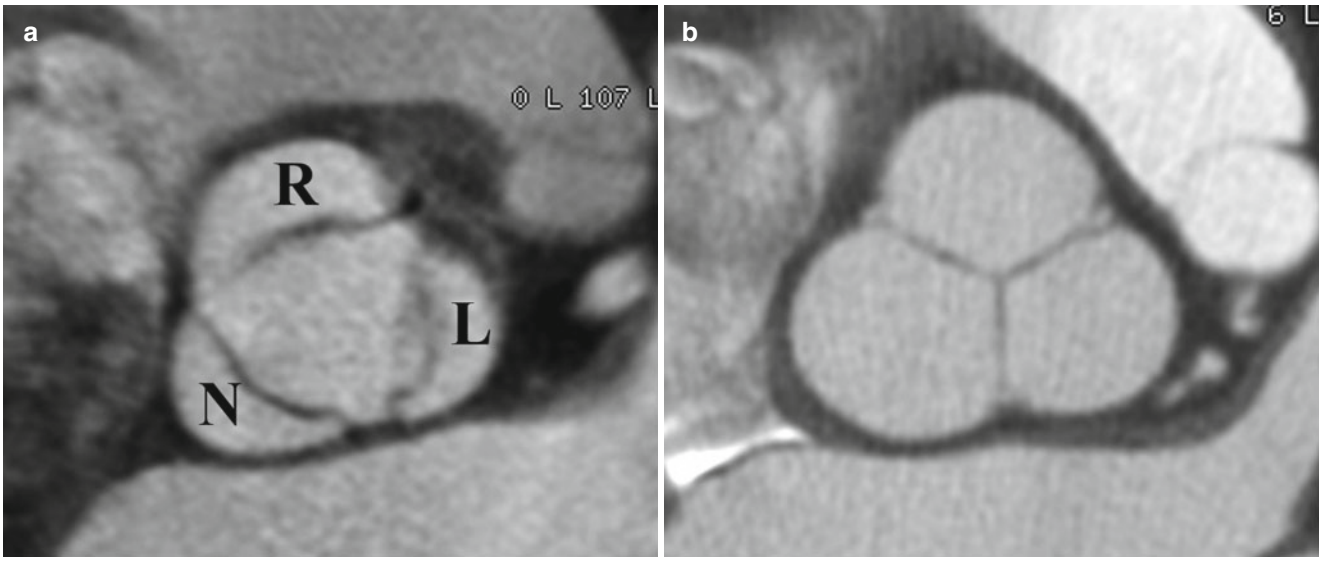

Fig. 17.1 Typical finding of normal aortic valve and aortic root. Oblique axial images of CT (**a**, **b**) show normal-sized opening of aortic valve in mid-systole (**a**) and normal coaptation of the three cusps of aortic valve in mid-diastole (**b**). *R* right coronary sinus, *L* left coronary sinus, *N* noncoronary sinus

Table 17.1 Grade of the severity of AS (echocardiography)

	Mild	Moderate	Severe
Valve area (cm^2)	>1.5	1.0–1.5	<1.0
Mean pressure gradients (mmHg)	<25	25–40	>40
Peak jet velocity (m/s)	<3.0	3.0–4.0	>4.0
Valve area index (cm^2/m^2)			<0.6

Table 17.2 Grade of the severity of AR (echocardiography or catheterization)

	Mild	Moderate	Severe
Color Doppler jet width	Central jet, width <25 % of LVOT	>Mild but no sign of severe AR	Central jet, width >65 % of LVOT
Doppler vena contracta width (cm)	<0.3	0.3–0.6	>0.6
Regurgitant volume (ml/beat)	<30	30–59	≥60
Regurgitant fraction (%)	<30	30–49	≥50
Regurgitant orifice area (cm^2)	<0.10	0.10–0.29	≥0.30

- Classical triad of angina, syncope, and heart failure.
- Treatment: valve replacement, percutaneous balloon valvuloplasty, and transcatheter aortic valve implantation.

17.3.2 Aortic Regurgitation (AR)

- AR can be caused by a wide variety of disease processes affecting the valve cusps or commissures (bicuspid aortic valve, rheumatic heart disease, infective endocarditis, systemic disease), aortic root (hypertension, annuloaortic ectasia, systemic disease, aortic dissection), or both.
- Clinically, chronic AR is insidious and well tolerated for decades, but acute AR may lead to sudden heart failure or cardiogenic shock.
- Severe AR is defined as (1) a vena contracta width >6 mm, (2) proximal regurgitant jet width in comparison to the height of the left ventricular outflow tract (LVOT) ≥65 %, (3) regurgitant volume ≥60 ml/beat, (4) regurgitant fraction (RF) ≥50 %, or (5) effective ROA ≥0.3 cm^2 (Table 17.2) [3].

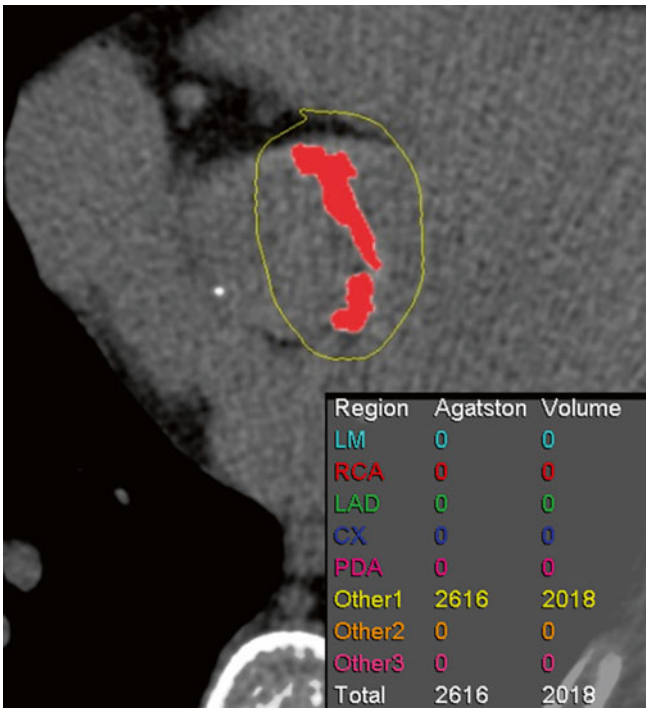

Fig. 17.2 Measurement of valvular calcification. Oblique axial image of pre-contrast CT shows that the amount of aortic valve calcification is expressed as an Agatston score and volume score

17.4 Quantitative Techniques of Comprehensive Assessment of Aortic Valve Diseases Using CT

17.4.1 Measurement of Valvular Calcification

Aortic valve calcium score correlates with AS severity, and not with aortic valve morphology (Fig. 17.2) [4].

17.4.2 Measurement of AVA and ROA Using Cardiac CT

- Phases of maximal opening (mid-systole, approximately 20 % of the R-R interval) and closing (mid-diastole, approximately 60–70 % of the R-R interval) of the aortic valve are determined by reviewing dynamic cine images.
- Cross-sectional planimetric images are used to measure the smallest stenotic AVA (commonly at the tips of the cusps) and ROA parallel to the plane described by the borders of the aortic cusps (both the aortic root long axis and its orthogonal plane).
- The valve plane for planimetry of ROA is reconstructed parallel to the regurgitant orifice in case of eccentric AR.
- A trend toward slight overestimation of anatomic AVA using CT planimetric measurement compared with effective stenotic AVA using echocardiography.

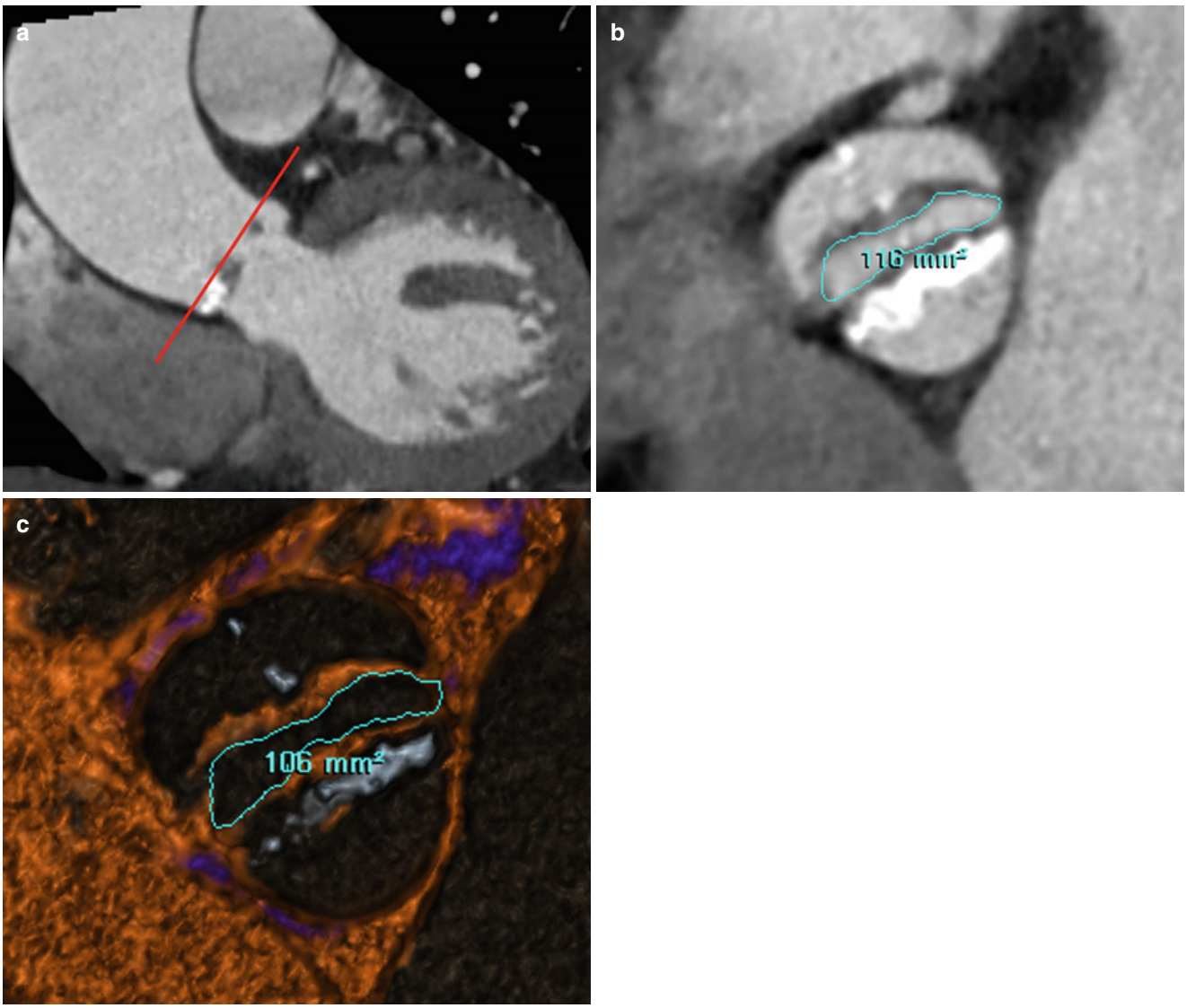

Fig. 17.3 Example of measurement of AVA in patient with BAV stenosis. (**a**, **b**) Oblique coronal (**a**) image of CT demonstrates that measurement of the AVA in the plane described by the borders of the aortic cusps (*red line*). AVAs by planimetry are 1.16 and 1.06 cm^2 on CT oblique axial image (**b**) and CT thick-slab volumetric four-dimensional reconstruction image with blood pool inversion technique (**c**), respectively

- No established cutoff value for grading AR using anatomic ROA even though differentiation among mild, moderate, and severe degrees of AR with cardiac CT is highly accurate when cutoff ROAs (25 and 75 mm^2) are used (Figs. 17.3 and 17.4) [1, 5, 6].

17.4.3 Measurement of Ascending Aorta Dimensions

- The diameters of ascending aorta are measured at 4 levels using oblique coronal reconstruction during mid-diastole: level 1, aortic annulus, defined as the hinge points of the aortic valve cusps; level 2, midpoint of the aortic sinuses of Valsalva; level 3, sinotubular junction; level 4, tubular portion, defined as the level of the right pulmonary artery.
- Patients with severe bicuspid aortic valve (BAV) stenosis have significantly larger ascending aorta diameters than in those with tricuspid aortic valve (TAV) stenosis (Fig. 17.5) [7].

17.4.4 Measurement of LVOT Area and Diameters

- The LVOT area and diameters are measured below the aortic valve and perpendicular to both the aortic root long axis and its orthogonal plane during mid-systole.
- When the true area of LVOT is determined by planimetry and entered into the continuity equation, the difference between flow-derived echocardiographic and anatomic determinations of AVA decreases.

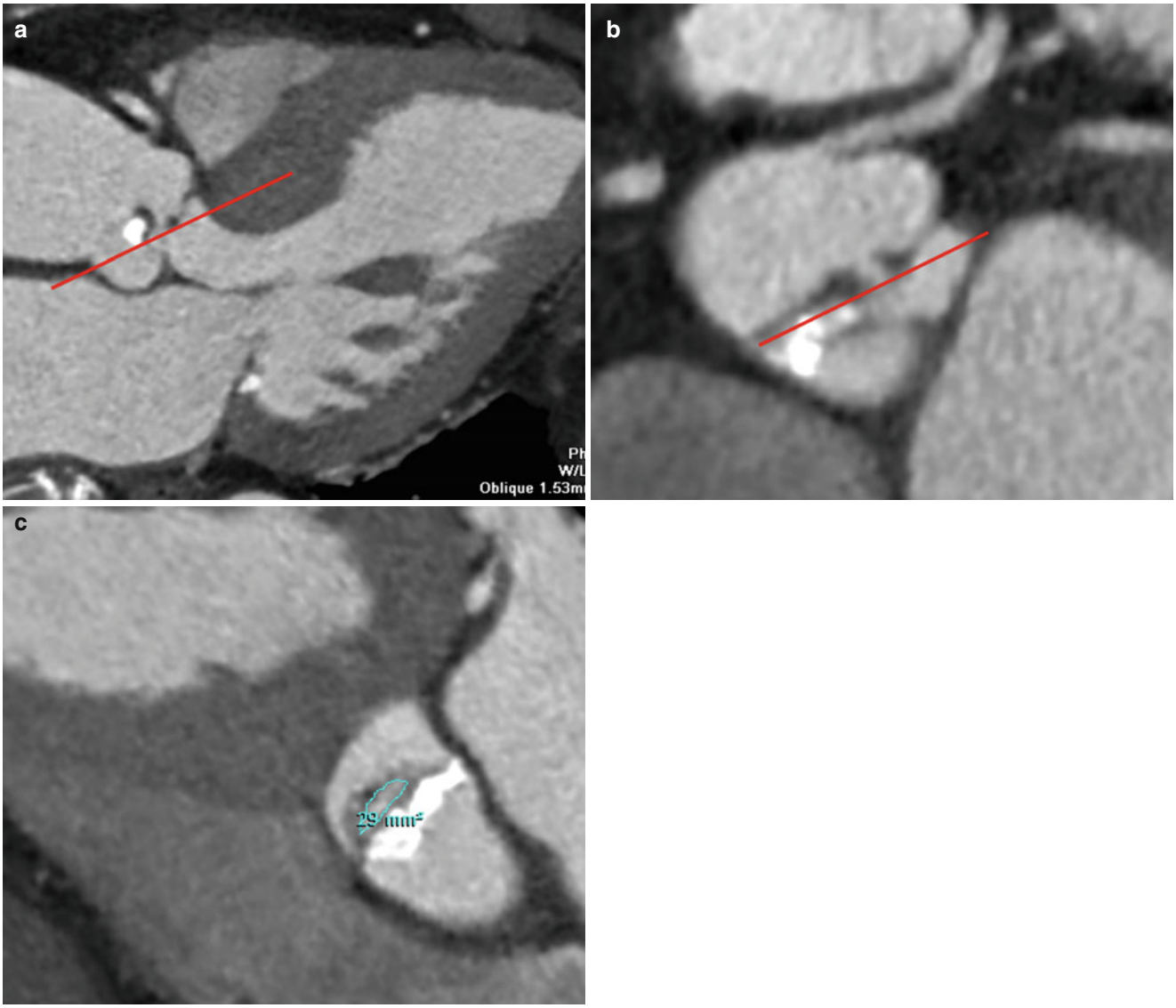

Fig. 17.4 Example of measurement of ROA in patient with eccentric AR. (**a**, **b**) On an oblique sagittal projection of the aortic root (**a**), a transversely orient oblique plane parallel to the regurgitant orifice is placed to produce a modified oblique axial reconstruction of the aortic valve (**b**). A transverse cut-plane parallel to the regurgitant orifice is placed on the modified oblique axial reconstruction of the aortic valve (**b**). (**c**) This transverse cut-plane yields a double oblique axial image of aortic valve for true ROA

- The measurement of LVOT planimetry provides information about septal myectomy at the time of aortic valve replacement for severe AS (Fig. 17.6).

17.4.5 Measurement of LV Volume and Systolic Function

- LV end-diastolic volume (EDV), end-systolic volume (ESV), stroke volume (SV), and ejection fraction (EF) are calculated using short-axis cine images with end-systolic phase and end-diastolic phase and attenuation-based segmentation.
- Cardiac CT measurements of global LV function using attenuation-based technique are highly reproducible and compared more favorable with the cardiac MRI using Simpson's method than echocardiography using modified Simpson's method.

17.5 Quantitative Techniques of Comprehensive Assessment of Aortic Valve Disease Using MRI

17.5.1 Velocity Quantification for the Grade of AS Severity

- PC cardiac MRI is a technique to quantify blood flow and velocity and is based on the accumulated phase of moving protons.

- Measurement of velocity in the blood is assessed at the "through-plane" imaging plane that is positioned perpendicular to the vessel.
- "In-plane" phase-contrast pulse sequences, allowing assessment of velocity along the course of a flow jet, and can assist in planning the "through-plane" slice.

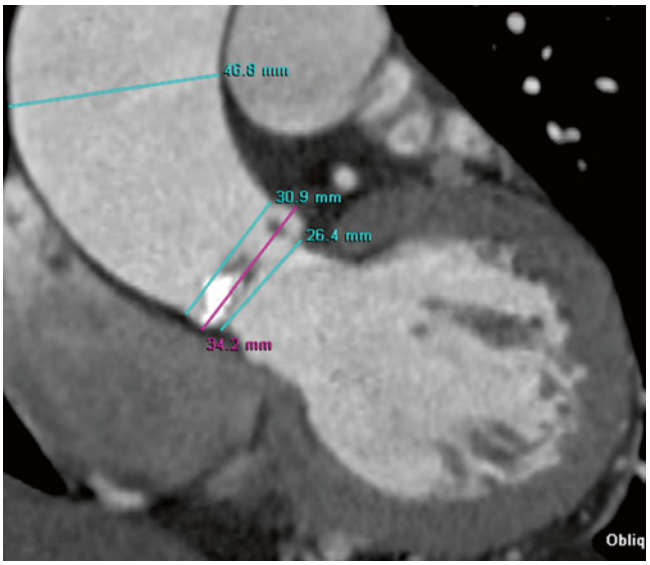

Fig. 17.5 Example of measurement of ascending aorta dimensions. Oblique coronal image of CT shows the measurement of aortic root and tubular portion of the ascending thoracic aorta during mid-diastole in patient with severe BAV stenosis. BAV stenosis is related to aneurysmal dilatation of the tubular portion of the ascending aorta as like this case

- PC cardiac MRI generates a magnitude image reflecting the anatomy of the chosen imaging plane, and phase velocity maps encoding the velocities within each voxel.
- The pressure gradient across the aortic valve is estimated by the modified Bernoulli equation, $\Delta P = 4V^2$, where P is the pressure (mmHg) drop across the stenosis and V is velocity (m/s).
- An important tendency to underestimate the true value in severe AS in flow-based assessment using phase-contrast cardiac MRI because of the lower temporal resolution of cardiac MRI than Doppler echocardiography and intravoxel dephasing of spins related in part to acceleration, turbulence, and partial volume averaging within the vena contracta (Fig. 17.7) [2].

17.5.2 Measurement of LV Volume, Systolic Function, and Mass

- Cardiac MRI with balanced SSFP pulse sequence is considered to be the standard of reference for the assessment of LV volume and myocardial mass. Increased LV mass (pressure overload LV hypertrophy) is a predictor of LV dysfunction.

17.5.3 Measurement of AVA

- AVA either using direct planimetry with balanced SSFP or continuity equation with PC cardiac MRI.

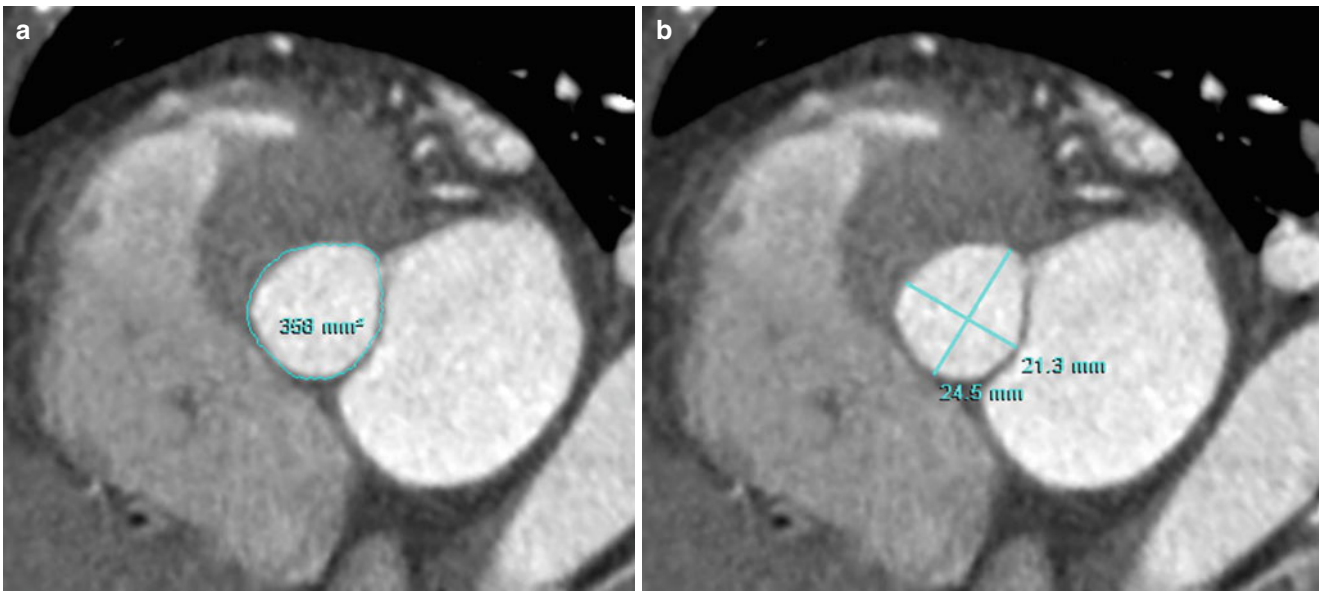

Fig. 17.6 Example of measurement of LVOT area and diameters. (**a**, **b**) Double oblique axial images of CT show the measurement of area (**a**) and diameters (**b**) of the most narrowed LVOT portion during mid-systole

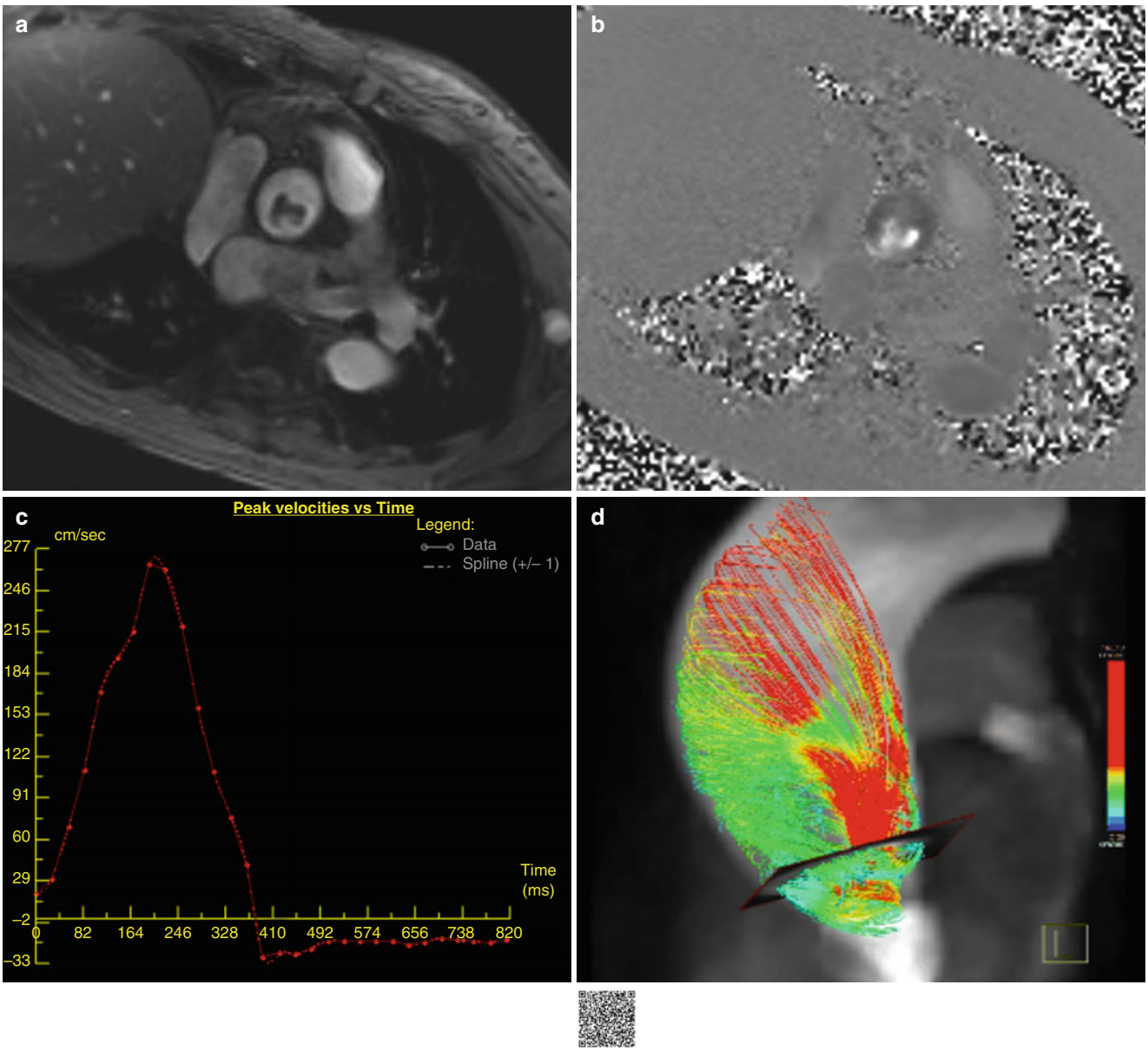

Fig. 17.7 Example of velocity mapping in AS. (**a**, **b**) Quantitative through-plane flow assessment above aortic valve using the PC cardiac MRI. Magnitude image (**a**), phase image (**b**), corresponding PC velocity map (**c**), and 4D flow image (**d**). The peak velocity is 2.7 m/s with an estimated pressure gradient of 29 mmHg according to the modified Bernoulli equation. Abnormal systolic helical flow is seen in the aneurysmal ascending thoracic aorta of patient with severe BAV stenosis on 4D flow image (**d**) (http://extras.springer.com/2015/978-3-642-36396-2)

- Direct planimetry is less optimal in patients with calcific AS because of cusp calcification and turbulent jet flow hampering accurate visualization of the true orifice [2, 8].

17.5.4 Flow Quantification for the Grade of AR

- PC cardiac MRI is performed just proximal to the aortic valve annulus or at the proximal ascending aorta above the sinotubular junction, and total stroke volume and regurgitant volume are measured directly as the antegrade and retrograde transaortic volume flow rates.
- The direct quantification of the regurgitant flow and fraction correlates well with the semiquantitative assessments provided by Doppler echocardiography and angiography.
- The regurgitation fraction limits of cardiac MRI for AR have been estimated by using cardiac MRI as follows: mild <20 %, moderate 20–40 %, and severe >40 % (Fig. 17.8) [2].

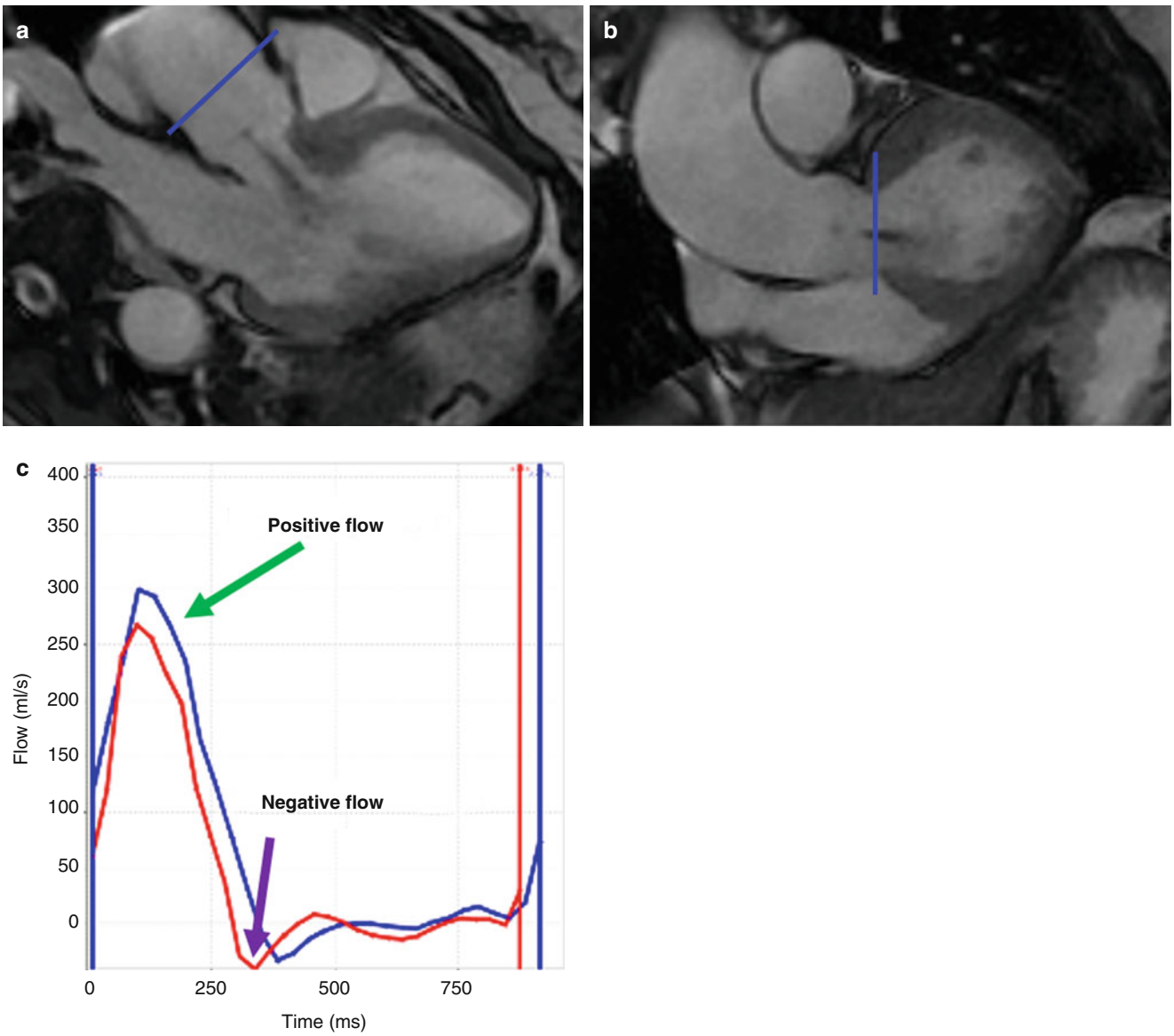

Fig. 17.8 Example of flow mapping in AR. (**a**–**c**) Three-chamber (**a**) and ascending aorta (**b**) b-SSFP cardiac MR images obtained during diastole demonstrate a central regurgitant jet below the aortic valve. (**c**) Graph of aortic flow obtained by PC cardiac MRI shows predominant antegrade flow in systole and retrograde flow in diastole. Quantitative analysis by PC cardiac MRI yield a regurgitant volume of 31.8 ml and fraction of 41 % (**a**) above the aortic valve and a regurgitant volume of 18.4 ml and fraction of 23 % below the aortic valve (**b**)

17.6 Bicuspid Aortic Valve Disease

- The most common congenital cardiovascular malformation with a prevalence of 1–2 % of the population.
- Association with an increased incidence of valvular complications (aortic stenosis, aortic regurgitation, and infective endocarditis) and aortic complications (dilatation of the ascending aorta, aneurysm formation, and dissection).
- The morphological characteristics of the BAV include unequal cusp size (due to fusion of two cusps leading to one larger conjoined cusp), the presence of central raphe or ridge, and smooth cusp margins. Right and left coronary cusp fusion (A-P phenotype) is the most common pattern of BAV and associated with AS and coarctation of the aorta.
- BAV with right coronary and noncoronary cusp fusion (R-N phenotype) is associated with a more significant cuspal pathology, with a particularly more rapid progression of AS and AR in the young patients.
- The typical imaging features of the BAV include a single commissural line in diastole and an elliptical-shaped orifice in systole.
- In patients with a prominent raphe or extensively calcified valve cusps, the BAV may appear as the TAV in diastole.
- AS is the most common complication of BAV with development of superimposed calcific change earlier in life.

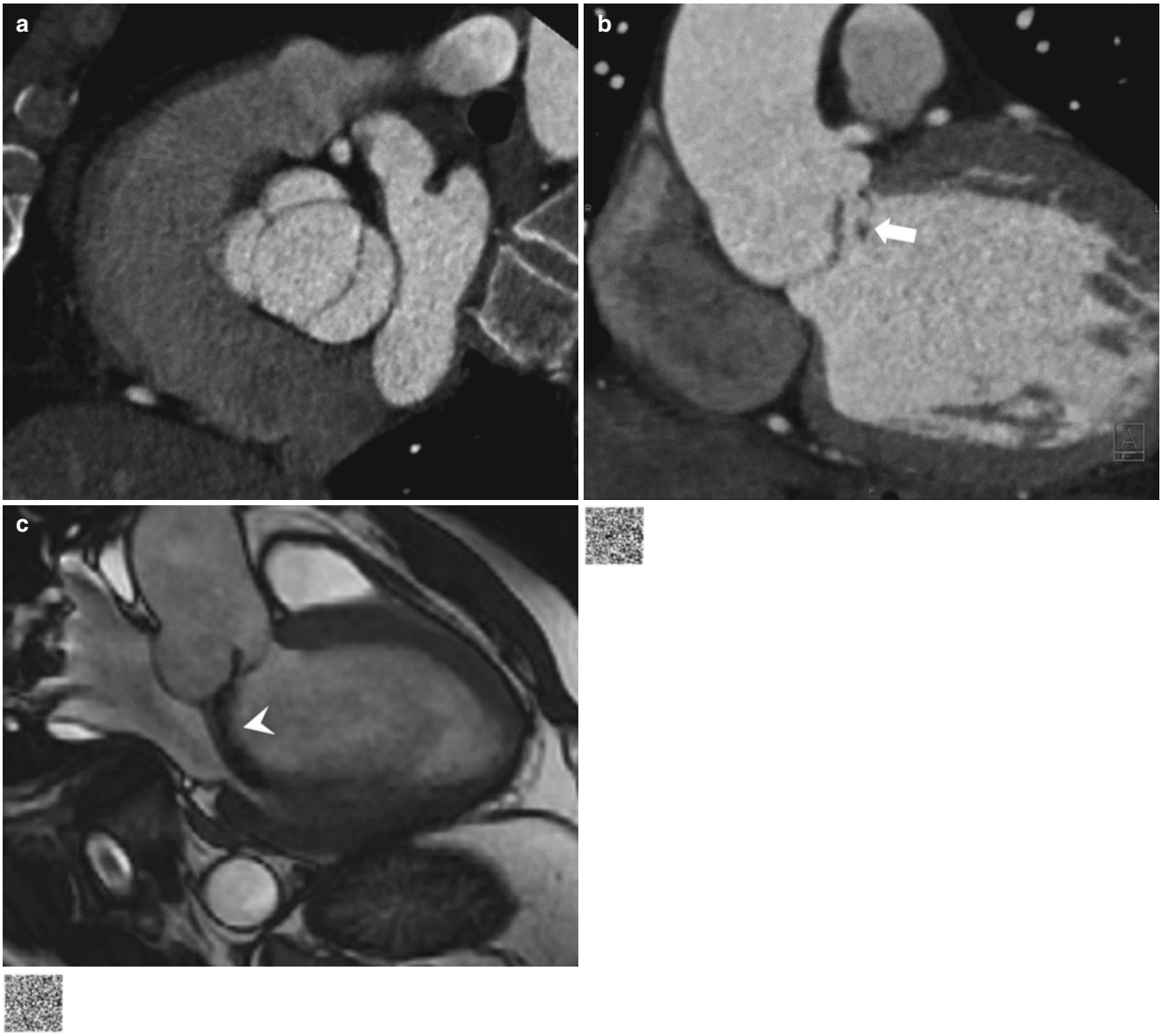

Fig. 17.9 BAV with eccentric AR. (**a**–**c**) Oblique axial images obtained during mid-systole (**a**) and mid-diastole (**b**) (http://extras.springer.com/2015/978-3-642-36396-2) show bicuspid aortic valve with prolapse of valvular leaflet (*arrow*). (**c**) (http://extras.springer.com/2015/978-3-642-36396-2) b-SSFP cardiac MR image obtained during diastole demonstrates an eccentric regurgitant jet (*arrowhead*) below the aortic valve toward mitral valve anterior leaflet

- AR is caused by prolapse of a larger conjoined cusp, fibrotic retraction of the cusps, aneurysmal dilatation of the aortic root, and valve annulus or valvular destruction secondary to infective endocarditis (Fig. 17.9) [9, 10].

17.7 Quadricuspid Aortic Valve Disease (QAV)

- A very rare congenital cardiac anomaly and a well-recognized cause of a significant AR requiring surgical treatment.
- Cardiac CT provides an accurate assessment of morphology of QAV, and associated congenital anomaly and its complications such as AR and cardiac MRI provide functional information of QAV as well as its morphology (Fig. 17.10) [11].

17.8 Sinus of Valsalva Aneurysm with AR

- Rare and either congenital or acquired (infective endocarditis, degenerative, and injury).
- Associated cardiac anomalies: VSD, AR, BAV, and coronary anomalies.
- The right coronary sinus (72 %), noncoronary sinus (22 %), and left coronary sinus (6 %).

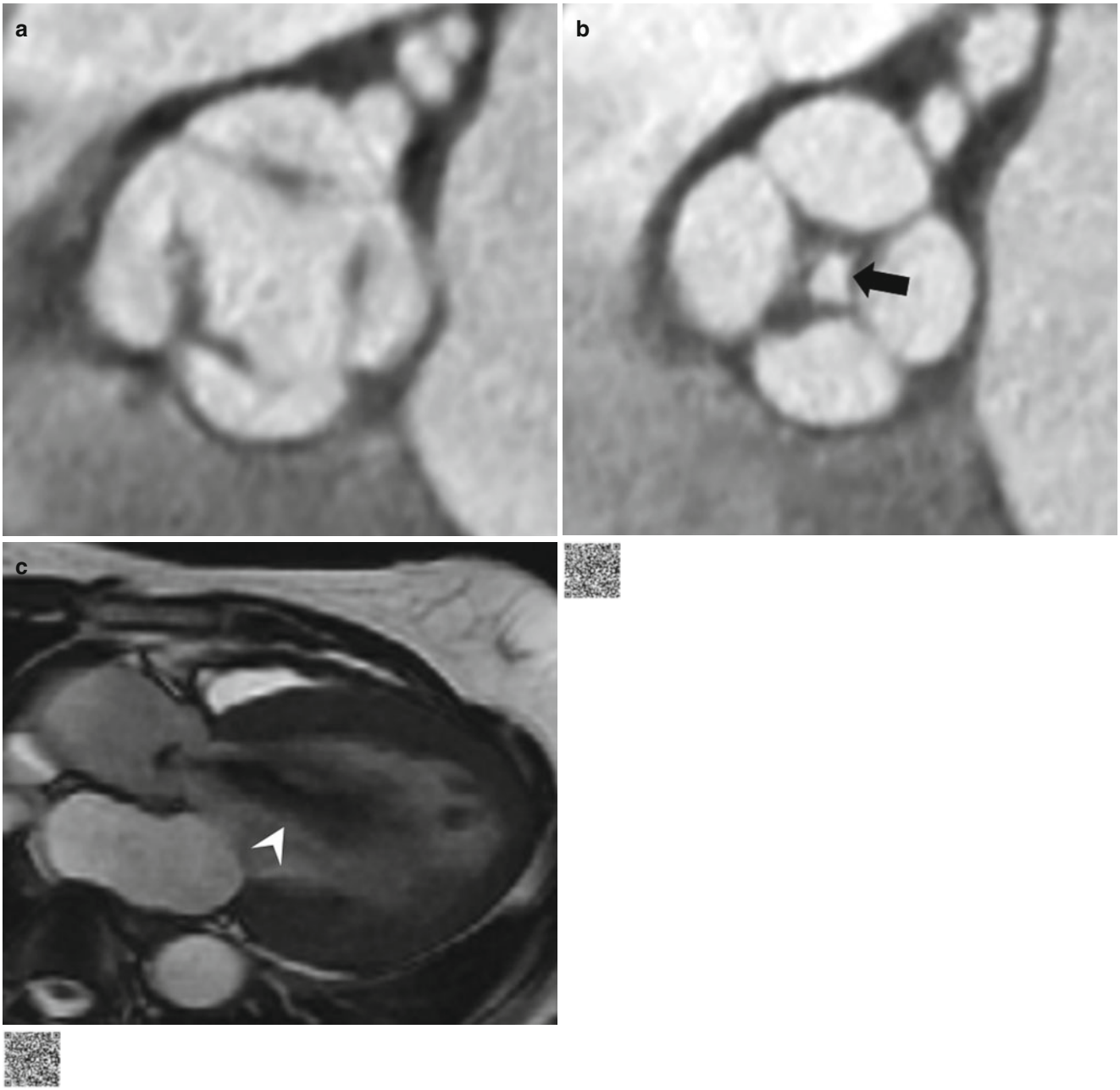

Fig. 17.10 QAV with central AR. (**a**–**c**) Oblique axial images obtained during mid-systole (**a**) and mid-diastole (**b**) (http://extras.springer.com/2015/978-3-642-36396-2) show quadricuspid aortic valve with central coaptation defect (*arrow*). (**c**) (http://extras.springer.com/2015/978-3-642-36396-2) b-SSFP cardiac MR image obtained during diastole demonstrates a central regurgitant jet (*arrowhead*) below the aortic valve

- Nonruptured aneurysms are usually asymptomatic, and symptoms are related to aneurysm rupture or mass effect on adjacent cardiac structures.
- AR is a common (30–50 % of patients) complication of both nonruptured and ruptured aneurysm of the sinus of Valsalva.
- Cardiac CT and MRI provide accurate assessment of the origin and size of Valsalva sinus aneurysms, complications (AR, aortocardiac shunt, right ventricular outflow tract obstruction) and surrounding cardiac structures (Fig. 17.11) [12].

17.9 Degenerative Aortic Stenosis

- Progressive dystrophic calcification and sclerotic thickening of the aortic valve cusps, leading to asymmetrically reduced motion and opening of the valve.
- No commissural fusion.
- Accompanied by calcification of the mitral annulus and coronary arteries.
- Aortic valve calcification is associated with the presence and greater extent of coronary artery plaque burden (calcified and mixed plaque) (Fig. 17.12) [1].

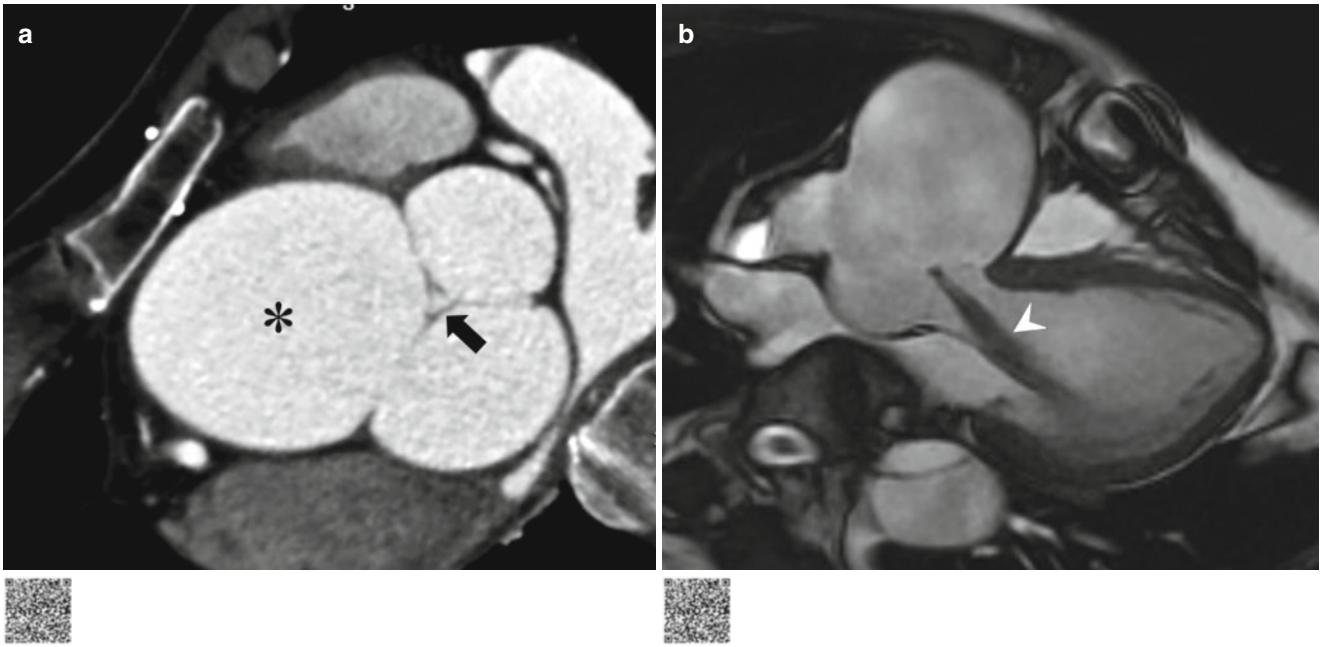

Fig. 17.11 Example of sinus Valsalva aneurysm with AR. (**a**, **b**). Oblique axial image obtained during mid-systole (**a**) (http://extras.springer.com/2015/978-3-642-36396-2) shows a sinus Valsalva aneurysm involving the right coronary sinus (*) and central coaptation defect (*arrow*). (**b**) (http://extras.springer.com/2015/978-3-642-36396-2) b-SSFP cardiac MR image obtained during diastole demonstrates a central regurgitant jet (*arrowhead*) below the aortic valve

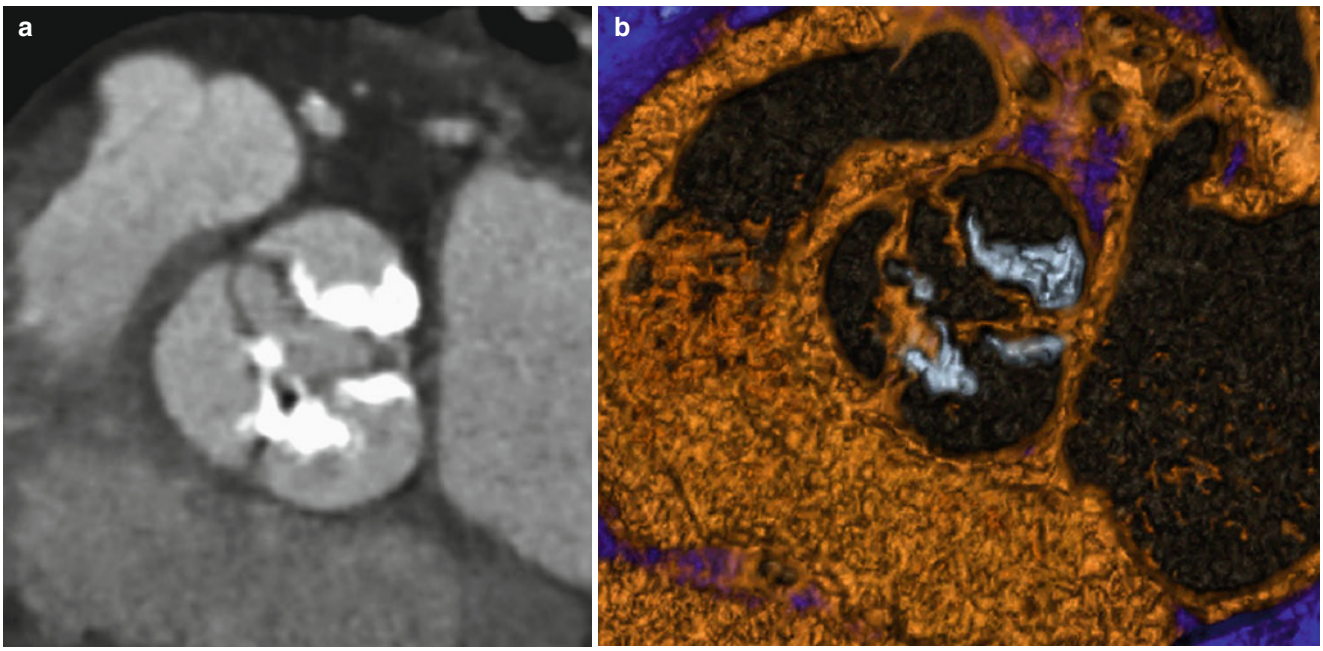

Fig. 17.12 Degenerative AS. (**a**, **b**) Oblique axial image obtained during mid-systole (**a**) and thick-slab volumetric reconstruction (**b**) image show an opening limitation of the aortic valve with dense leaflet calcification (*gray color* in the volumetric reconstruction image)

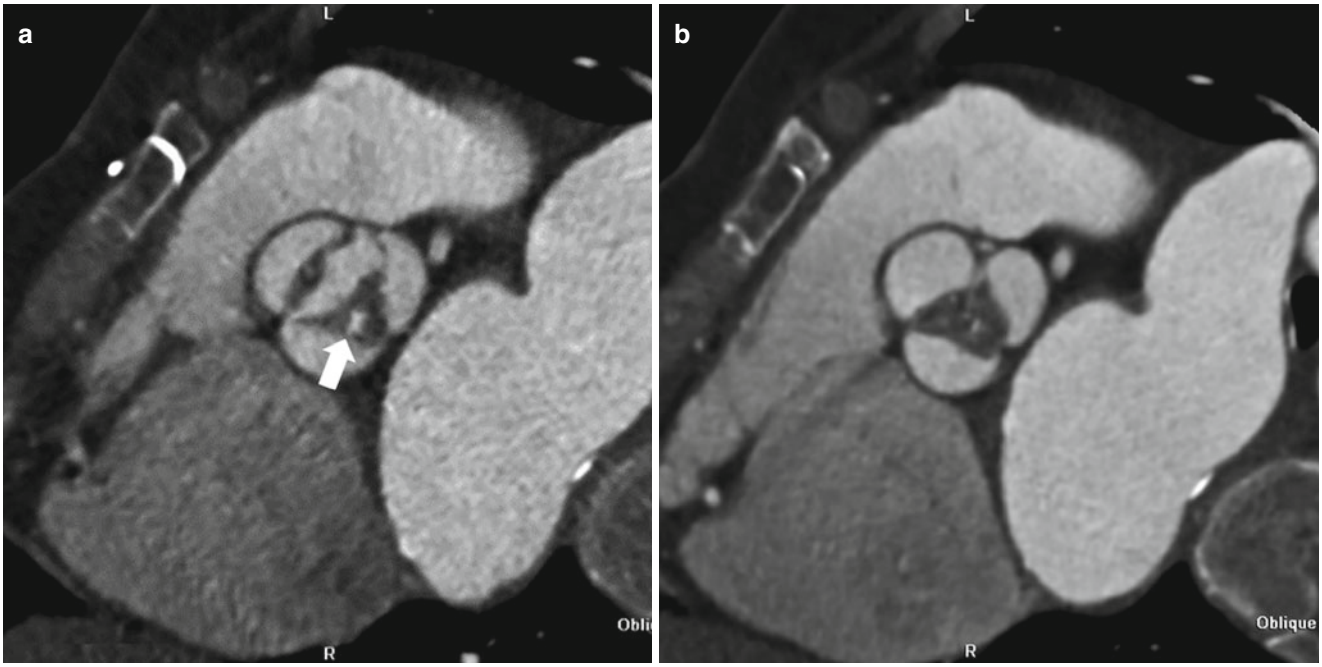

Fig. 17.13 Rheumatic AS. (**a**, **b**) Oblique axial images obtained during mid-systole (**a**) and mid-diastole (**b**) show a commissural fusion (*arrow*) between noncoronary and left coronary cusps. All valvular leaflets were diffusely thickened with minimal calcification

17.10 Rheumatic Aortic Valve Disease

- One or more of the three commissures are often fused, and the cusps may be either focally or diffusely fibrotic with or without commissural fusion or calcification.
- Invariably accompanied with rheumatic mitral valve disease.
- Stenosis, regurgitation, or a combination of the two (Fig. 17.13) [1].

17.11 Annuloaortic Ectasia with Aortic Regurgitation

- Cystic medial necrosis
- Progressive aortic root dilatation and hemodynamically significant severe AR
- Aortic root dissection or rupture
- Marfan syndrome (60–80 %) and idiopathic (30 %)
- Starts with dilatation of the aortic sinuses and progresses into the sinotubular junction and ultimately into the aortic annulus

17.12 Aortic Valve Prolapse and Aortic Regurgitation Associated with Ventricular Septal Defect

- Aortic valve prolapse (AVP), mainly the right coronary cusp prolapse, and aortic regurgitation can occur in a subset of patients with a ventricular septal defect (VSD).
- The most acceptable mechanism of AVP is the Venturi effect.
- AR complicates subarterial VSDs about five times more common than perimembranous VSDs [13].

17.13 Aortic Valve Involvement in Behçet Disease

- A very rare but life-threatening cardiovascular complication and misdiagnosed as infective endocarditis.
- Aortitis involving aortic root and aortic valve, leading to aortic regurgitation which might be associated with valvulitis, aneurysm of the sinus of Valsalva, and prolapse and perforation of the aortic valve.
- The frequency of postoperative complications, such as prosthetic valve dehiscence or periprosthetic leakage, is higher in patients with Behçet disease than in patients with Takayasu's arteritis.
- Cardiac CT is helpful for detecting pseudoaneurysm and vegetation-like mass and postoperative complications (Fig. 17.14) [14].

17.14 Infective Endocarditis

- Aortic valve is involved in about 1/2 of cases.
- Infectious vegetations or nodular excrescences that form on the valve cusps, most commonly on the ventricular surface of the cusps, sometimes lead to embolism.
- Local complications: vegetation, cusp perforation, aneurysm, annular abscess, fistula, chordal rupture, perivalvular abscess, and pseudoaneurysm.

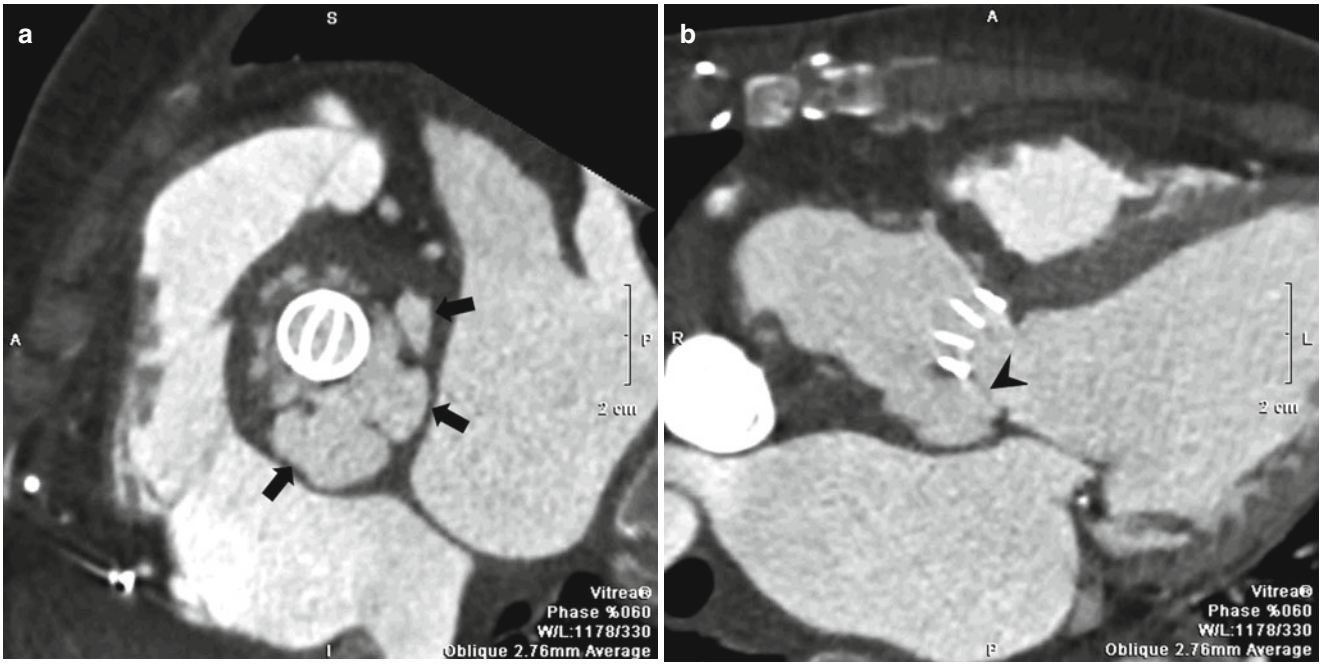

Fig. 17.14 Behçet's disease involving the aortic root with pseudoaneurysm formation. (**a**, **b**) Oblique axial images obtained during mid-systole (**a**) and oblique sagittal image (**b**) show a large and multilobulated pseudoaneurysm formation (*arrows*) around a prosthetic aortic valve in patient with Behçet's disease. There were large paravalvular dehiscence (*arrowhead*) between the prosthetic aortic valve and the aortic annulus

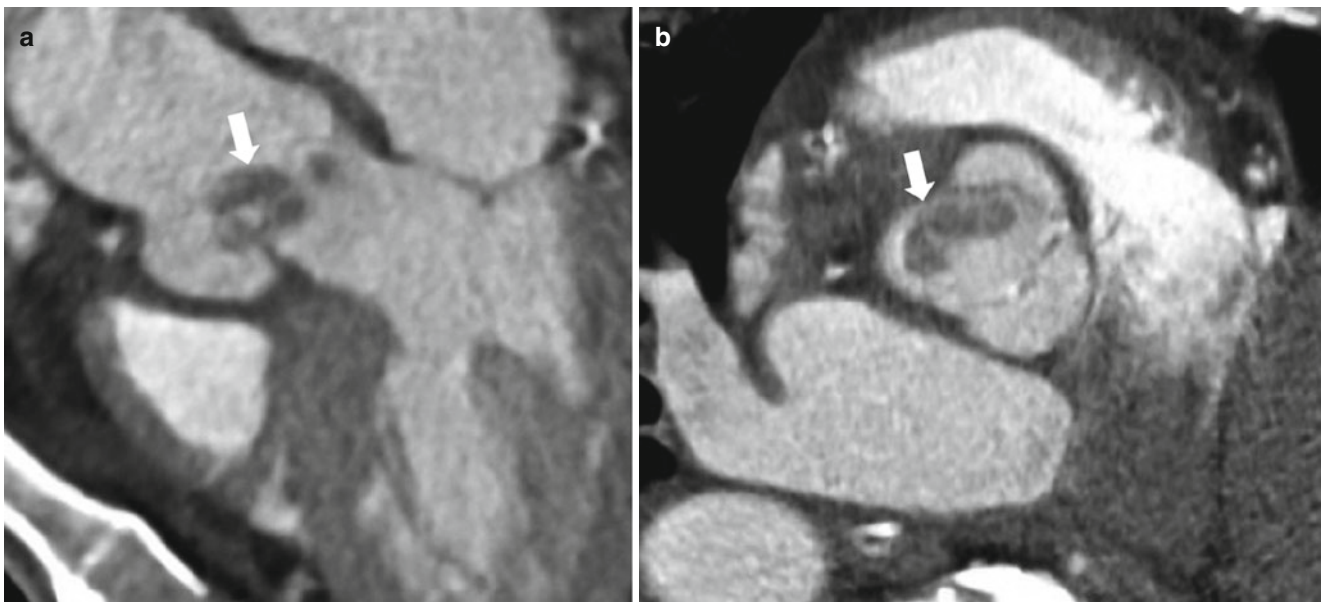

Fig. 17.15 Infective endocarditis involving the aortic valve. (**a**, **b**) Oblique sagittal image (**a**) and oblique axial image (**b**) obtained during mid-systole show a large vegetation (*arrow*) attached left coronary cusp and right coronary cusp in patient with infective endocarditis

- Healed endocarditis: indentation of the cusp free margin, cusp perforation, aneurysm, ruptured chordae tendineae, and healed fistula.
- Cardiac CT: high diagnostic accuracy for vegetation, paravalvular abscess, and pseudoaneurysm compared with transesophageal echocardiography and depiction of other infectious complications such as septic pulmonary emboli and renal infarction (Fig. 17.15) [15].

17.15 Native Aortic Valve Thrombosis

- A rare event associated with aortic valve disease, heart valve replacement, a hypercoagulable state, infective endocarditis, or an autoimmune disease.
- Clinical importance – embolic event and differential diagnosis of aortic valve mass [16]

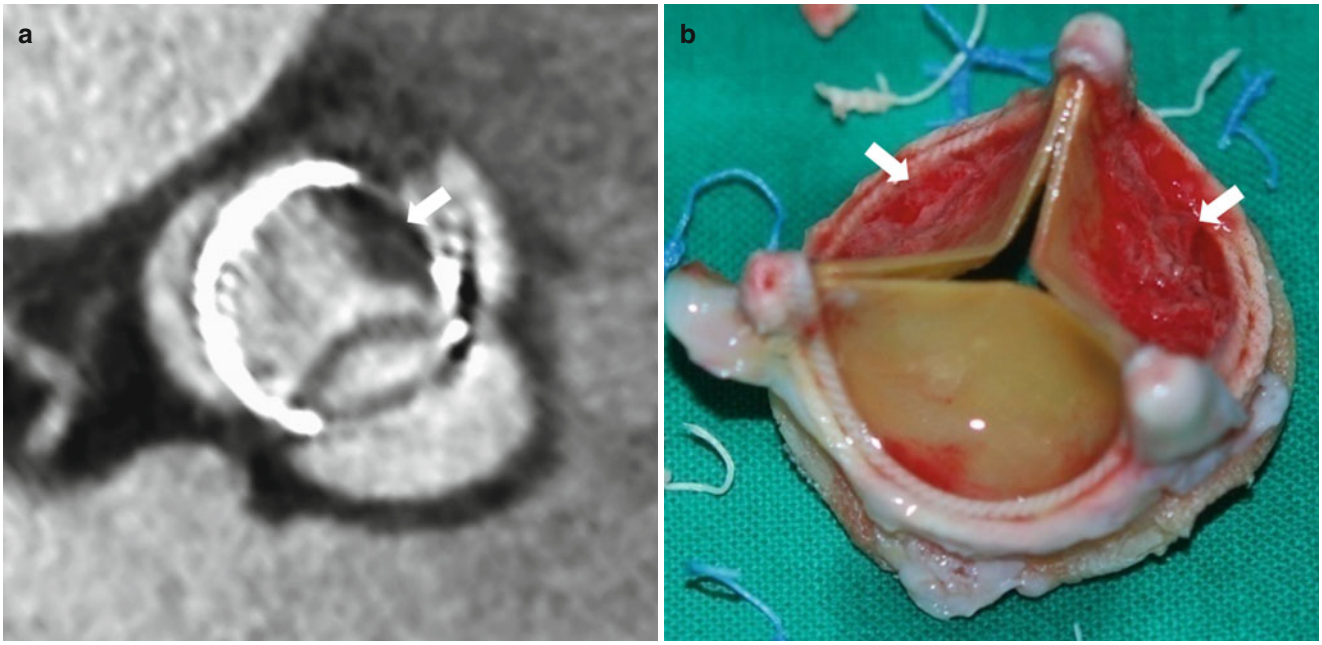

Fig. 17.16 Thrombus formation involving the prosthetic aortic valve. (**a**, **b**) Oblique axial CT image (**a**) obtained during mid-systole shows low-density thrombus formation involving leaflet of biological prosthetic aortic valve (*arrow*). Thrombus formation (*arrows*) was confirmed in the surgical finding (**b**)

17.16 Prosthetic Valve Evaluation

- The St Jude bileaflet tilting disk valve and Carpentier-Edwards bovine pericardial valve are currently the valves most commonly encountered in practice.
- Cardiac CT is well suited for the visualization of the prosthetic valve because of its superior spatial resolution and decreased susceptibility to metallic artifacts.
- Most prosthetic valves are visible on bright-blood cardiac MRI as areas of signal loss.

17.17 Prosthetic Valve Dysfunction

- Prosthetic valve dysfunction can occur as a result of primary structural deterioration or as a secondary phenomenon due to pannus formation, thrombosis, or vegetations.
- Cine cardiac CT can clearly show restricted movement of the prosthetic leaflet caused by thrombus (Fig. 17.16), vegetation, or pannus; complications secondary to infective endocarditis such as perivalvular abscesses, fistulae, or pseudoaneurysms; and prosthetic valvular dehiscence.
- The assessment of mechanical valve prosthesis dysfunction may be limited, and intra- or periprosthetic regurgitation may be easily hidden by the signal loss around the prosthesis [17].

17.18 Cardiac CT Imaging of Transcatheter Aortic Valve Implantation (TAVI)

- Catheter-based implantation of a bioprosthetic aortic valve, usually performed by transfemoral route.
- Cardiac CT evaluates the best access pathway, dimensions of the ascending aorta, aortic root, and aortic annulus, aortic valve structure and calcification, coronary ostial anatomy, and appropriate fluoroscopic projection angles.

17.19 Recent Trend for Severe Aortic Valve Disease Using Cardiac MRI

- Four-dimensional phase-contrast cardiac MRI illustrates multidirectional blood flow velocity data and flow pattern in the thoracic aorta of patients with aortic valve disease, allowing assessment of the hemodynamic effects of aortic valve disease on flow.
- Cardiac MRI with delayed-enhancement technique allows for the noninvasive detection of focal areas of myocardial fibrosis in patients with severe aortic valve disease. Midwall myocardial fibrosis is an independent predictor of survival in severe AS [18].
- Cardiac MRI with T1 mapping provides assessment of diffuse myocardial fibrosis in patients with severe AS.

17.20 Summary

1. Valvular AS is most commonly due to secondary calcification of a congenitally bicuspid aortic valve or degenerative calcific changes of a tricuspid aortic valve.
2. Rheumatic involvement of the aortic valve is characterized by fusion of the commissures between the aortic valve cusps and is invariably accompanied by rheumatic mitral valve disease.
3. Aortic regurgitation results from a wide variety of disease processes affecting the valve cusps or commissures, aortic sinuses, aortic root, or ascending aorta.
4. Bicuspid aortic valve disease is the most common cardiovascular malformation and is associated with increased risk of valvular and vascular complications.
5. Infective endocarditis is a life-threatening disease and occurs on native (congenital or rheumatic aortic valve disease) as well as prosthetic valves.
6. Aortic valve tumors (papillary fibroelastoma, myxoma, fibroma, sarcoma, and hamartoma) are not common and need to be distinguished from vegetation and thrombus.
7. Prosthetic valve dysfunction occurs as a result of primary structural deterioration or as a secondary phenomenon due to pannus, vegetation, thrombus formation, or suture loosening.
8. Cardiac CT and MRI can provide complimentary information about aortic valvular anatomy and hemodynamic function.
9. Cardiac MRI should be considered when echocardiographic evaluation is technically limited and provides accurate information about quantification of aortic regurgitant volume and fraction, myocardial fibrosis, left ventricular function, and ascending aorta dimensions.
10. Cardiac CT is used to evaluate aortic valve calcification, prosthetic valve dysfunction, infective endocarditis, and anatomy of the coronary artery and ascending thoracic aorta.

References

1. Bennett CJ, Maleszewski JJ, Araoz PA. CT and MR imaging of the aortic valve: radiologic-pathologic correlation. Radiographics. 2012;32:1399–420.
2. Cawley PJ, Maki JH, Otto CM. Cardiovascular magnetic resonance imaging for valvular heart disease. technique and validation. Circulation. 2009;119:468–78.
3. Bonow RO, Carabello BA, Chatterjee K, de Leon AC, Faxon DP, Freed MD, et al. Focused update incorporated into the ACC/AHA 2006 guidelines for the management of patients with valvular heart disease: a report of the American College of Cardiology/American Heart Association Task Force on Practice Guidelines (Writing Committee to Revise the 1998 Guidelines for the Management of Patients With Valvular Heart Disease): endorsed by the Society of Cardiovascular Anesthesiologists, Society for Cardiovascular Angiography and Interventions, and Society of Thoracic Surgeons. Circulation. 2008;118:e523–661.
4. Ferda J, Linhartova K, Kreuzberg B. Comparison of the aortic valve calcium content in the bicuspid and tricuspid stenotic aortic valve using non-enhanced 64-detector-row-computed tomography with prospective ECG-triggering. Eur J Radiol. 2008; 68:471–5.
5. Goffinet C, Kersten V, Pouleur AC, le Polain de Waroux JB, Vancraeynest D, Pasquet A, et al. Comprehensive assessment of the severity and mechanism of aortic regurgitation using multidetector CT and MR. Eur Radiol. 2010;20:326–36.
6. Alkadhi H, Desbiolles L, Husmann L, Leschka S, Scheffel H, Vachenauer R, et al. Aortic regurgitation: assessment with 64-section CT. Radiology. 2007;245:111–21.
7. Son JY, Ko SM, Choi JW, et al. Measurement of the ascending aorta diameter in patients with severe bicuspid and tricuspid aortic valve stenosis using dual-source computed tomography coronary angiography. Int J Cardiovasc Imaging. 2011;27 Suppl 1:61–71.
8. Kupfahl C, Honold M, Meinhardt G, Vogelsberg H, Wagner A, Mahrholdt H, et al. Evaluation of aortic stenosis by cardiovascular magnetic resonance imaging: comparison with established routine clinical techniques. Heart. 2004;90:893–901.
9. Alkadhi H, Leschka S, Trindade PT, Feuchtner G, Stolzmann P, Plass A, et al. Cardiac CT for the differentiation of bicuspid and tricuspid valves: comparison with echocardiography and surgery. AJR Am J Roentgenol. 2010;195:900–8.
10. Siu SC, Silversides CK. Bicuspid aortic valve disease. J Am Coll Cardiol. 2010;55:2789–800.
11. Timperley J, Milner R, Marshall AJ, Gilbert TJ. Quadricuspid aortic valves. Clin Cardiol. 2002;25:548–52.
12. Bricker AO, Avutu B, Mohammed TL, et al. Valsalva sinus aneurysms: findings at CT and MR imaging. Radiographics. 2010;30: 99–110.
13. Tweddell JS, Pelech AN, Frommelt PC. Ventricular septal defect and aortic valve regurgitation: pathophysiology and indications for surgery. Semin Thorac Cardiovasc Surg Pediatr Card Surg Annu. 2006;9:147–52.
14. Han JK, Kim HK, Kim YJ, et al. Behcet's diseases as a frequently unrecognized cause of aortic regurgitation: suggestive and misleading echocardiography findings. J Am Soc Echocardiogr. 2009;22: 1269–74.
15. Feuchtner GM, Stolzmann P, Dichtl W, Schertler T, Bonatti J, Scheffel H, et al. Multislice computed tomography in infective endocarditis: comparison with transesophageal echocardiography and intraoperative findings. J Am Coll Cardiol. 2009;53: 436–44.
16. Barandon L, Clerc P, Chauvel C, et al. Native aortic valve thrombosis: a rare cause of acute ischemia of the lower limb. Interact Cardiovasc Thorac Surg. 2004;3:675–7.
17. Tsai IC, Lin YK, Chang Y, Fu YC, Wang CC, Hsieh SR, et al. Correctness of multi-detector-row computed tomography for diagnosing mechanical prosthetic heart valve disorders using operative findings as a gold standard. Eur Radiol. 2009;19:857–67.
18. Weidemann F, Herrmann S, Störk S, Niemann M, Frantz S, Lange V, et al. Impact of myocardial fibrosis in patients with symptomatic severe aortic stenosis. Circulation. 2009;120:577–84.

Non-aortic Valvular Heart Disease

18

Dong Hyun Yang and Tae-Hwan Lim

Contents

Abstract

Cardiac computed tomography (CT) provides detailed anatomic information of cardiac valve and paravalvular structures and has an emerging role in the assessment of cardiac valvular disease. Cardiac magnetic resonance imaging (MRI) provides functional information of cardiac chambers, particularly in hearts deformed or distorted by disease or previous surgery. Planimetry of the mitral valve area by CT and MRI has been shown to be feasible, but tends to overestimate echocardiography. Cardiac CT is particularly helpful in cases with poor image quality on echocardiography. These cases include mitral valve disease with severe valvular or annular calcification, pulmonary valvular disease, and prosthetic valve dysfunction. Thanks to easy applicability of 3D imaging, cardiac CT provides surgeon's view of mitral valve disease, which may be helpful for surgical planning. However, the risk of radiation exposure and of renal failure due to intravenous contrast agent should be taken into consideration. In this chapter, various cases of non-aortic valvular heart disease will be demonstrated using cardiac CT and MRI, and additional value of these modalities over echocardiography will be highlighted.

18.1 Overview

18.1.1 Imaging Modalities and Role of CT and MRI

- Assessment of the mitral valve orifice area (MVA) using cardiac CT and MRI is feasible. However, echocardiography is still the main method to assess the severity of MS.
- Cardiac CT may have additional role for characterization of native cardiac valves in patients with poor sonic window and in patients with severe valvular or annular calcification [1].

Electronic supplementary material Supplementary material is available in the online version of this chapter at 10.1007/978-3-642-36397-9_18.

D.H. Yang • T.-H. Lim (✉)
Department of Radiology and Research Institute of Radiology, Asan Medical Center, University of Ulsan College of Medicine, Seoul, Republic of Korea
e-mail: donghyun.yang@gmail.com; d890079@naver.com

T.-H. Lim (ed.), *Practical Textbook of Cardiac CT and MRI*,
DOI 10.1007/978-3-642-36397-9_18, © Springer-Verlag Berlin Heidelberg 2015

- Cardiac CT provides surgeon's view using three-dimensional technique including volume rendering and virtual endoscopy, which is helpful for surgical planning.
- Cardiac CT provides detailed anatomic information of paravalvular pathology in patients with infective endocarditis or prosthetic cardiac valve. Paravalvular pathology is sometimes hard to evaluate using echocardiography.
- Using velocity-encoded (VENC) MRI and cine MRI, quantification of regurgitant volume is possible in patients with valvular heart disease, which has clinical implication in patients with tetralogy of Fallot or mitral regurgitation.
- Functional assessment of the cardiac atria as well as ventricles using both cardiac CT and MRI.
- Detection of the intracardiac thrombus including left atrial appendage thrombus.
- Preoperative coronary assessment prior to cardiac surgery in patients with intermediate pretest probability of coronary artery disease (CAD) [1].

18.2 Mitral Valve Disease

18.2.1 Mitral Stenosis (MS)

18.2.1.1 Etiology

- Rheumatic fever: predominant cause of MS
- Other causes: congenital, carcinoid syndrome, connective tissue disorder, and Lutembacher syndrome (rheumatic MS with atrial septal defect)
- Conditions simulated physiology of MS: left atrial tumor (particularly myxoma), ball-valve thrombus in the left atrium, and infective endocarditis with large vegetation

18.2.1.2 Morphology

- Rheumatic fever: thickening of the leaflet edges, fusion of the commissures, chordal shortening and fusion, and valvular calcification (Figs. 18.1 and 18.2).
- The diastolic "doming": curved shape in flexible leaflets owing to restriction of motion at the leaflet tips.
- "Fish mouth" shape: symmetric fusion of the commissures results in a small central oval orifice in diastolic phase on short-axis image.
- Degenerative MS is characterized by prominent annular calcification. In contrast to the thickening of leaflet tip in rheumatic disease, mitral annular calcification may extend onto the base of the mitral leaflets (Fig. 18.3).
- Other causes: double orifice mitral valve (Fig. 18.4) and large left atrial myxoma (Fig. 18.5).

18.2.1.3 Pathophysiology

- Normal mitral valve orifice area (MVA) is 4–6 cm^2.
- When the MVA decreases to below 2.0 cm^2, LV pressure begins to rise and transmitral pressure gradient develops.
- Hemodynamic consequences: elevation of LA pressure → rising pulmonary vascular pressure → RV dilatation and failure.
- LV is protected from above hemodynamic consequences. If LV dysfunction is present, combined pathology such as ischemic heart disease or mitral regurgitation should be considered.
- Classification of mitral stenosis severity [2]

	Mild	Moderate	Severe
Specific findings			
Valve area (cm^2)	>1.5	1.0–1.5	<1.0
Supportive findings			
Mean pressure gradients (mmHg)	<5	5–10	>10
Systolic pulmonary artery pressure (mmHg)	<30	30–50	>50

- Complications: atrial fibrillation (the most common complication), systemic embolism caused by left atrial thrombus formation, and infective endocarditis.

18.2.1.4 Role of CT and MRI

- In small patient group, cardiac CT and MRI can provide reliable and reproducible planimetry of the mitral valve orifice in patients with MS [3–5]. Although cardiac CT-derived MVA is larger than that obtained by echocardiography, CT yields good correlation with echocardiography for the detection of moderate-to-severe mitral stenosis [6].
- However, there is seldom data showing an incremental value of CT and MRI over echocardiography in patients with MS.

18.2.2 Mitral Regurgitation

18.2.2.1 Etiology

- Abnormalities of any mitral valve apparatus (mitral leaflets, chordae tendineae, papillary muscle, and mitral annulus) may result in MR (Fig. 18.6).
- Degenerative MR now being the most common because of reduced incidence of rheumatic fever and increased life span in industrialized countries.
- Acute MR due to papillary muscle rupture should be considered in patients presenting with acute pulmonary edema or shock following acute myocardial infarction.
- Causes of acute and chronic mitral regurgitation (Modified from Ref. [7]).

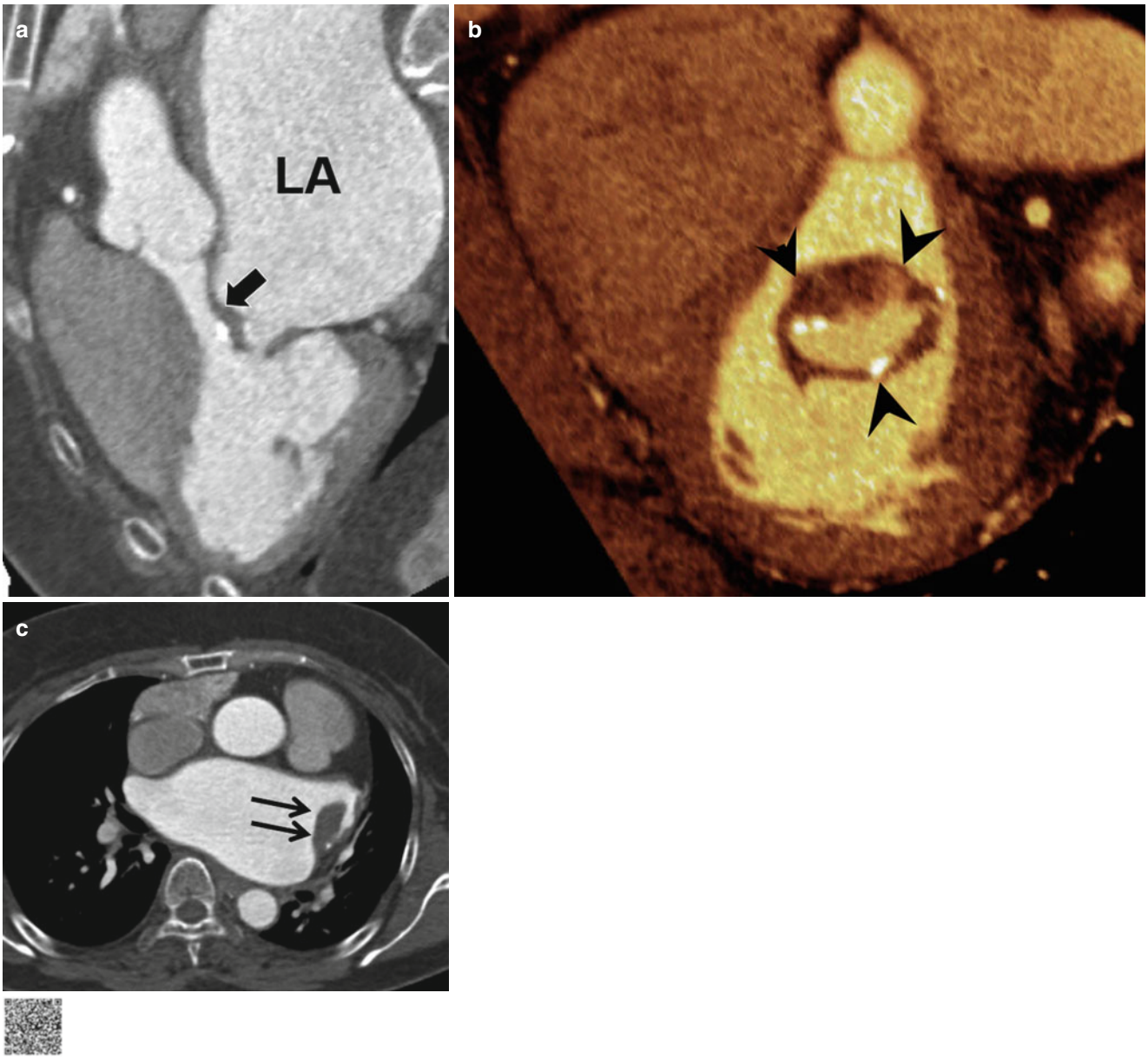

Fig. 18.1 Typical finding of mitral stenosis with left atrial thrombus (http://extras.springer.com/2015/978-3-642-36396-2). (**a**) Three-chamber view of CT shows thickening and doming of the mitral valve (MV) in diastolic phase. Note a "hockey stick" appearance (*arrow*) of the MV anterior leaflet due to motion limitation. The left atrium (*LA*) shows severe dilatation. (**b**) Short-axis view of CT shows typical finding of "fish mouth" appearance (*arrowheads*) resulting from thickening and motion limitation of LV leaflets. (**c**) Axial view of CT shows a large thrombus (*double arrow*) in the left atrium

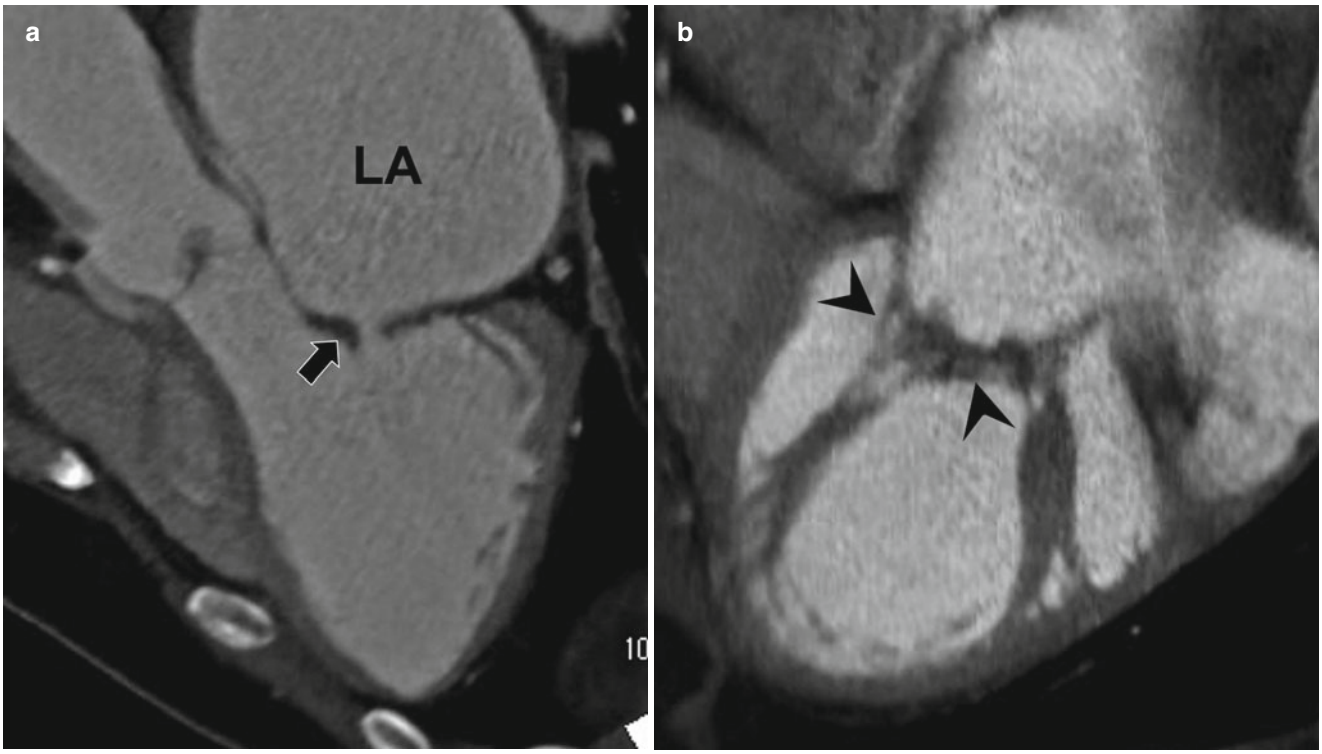

Fig. 18.2 Rheumatic mitral stenosis. (**a**) Three-chamber view of CT shows thickening and doming of the mitral valve (MV). Valvular thickening is more prominent in the posterior leaflet and tip of the anterior leaflet (*arrow*). (**b**) Oblique coronal view of CT shows diffuse thickening and shortening of the chordae tendineae (*arrowheads*), which is a typical appearance of the rheumatic valvular heart disease

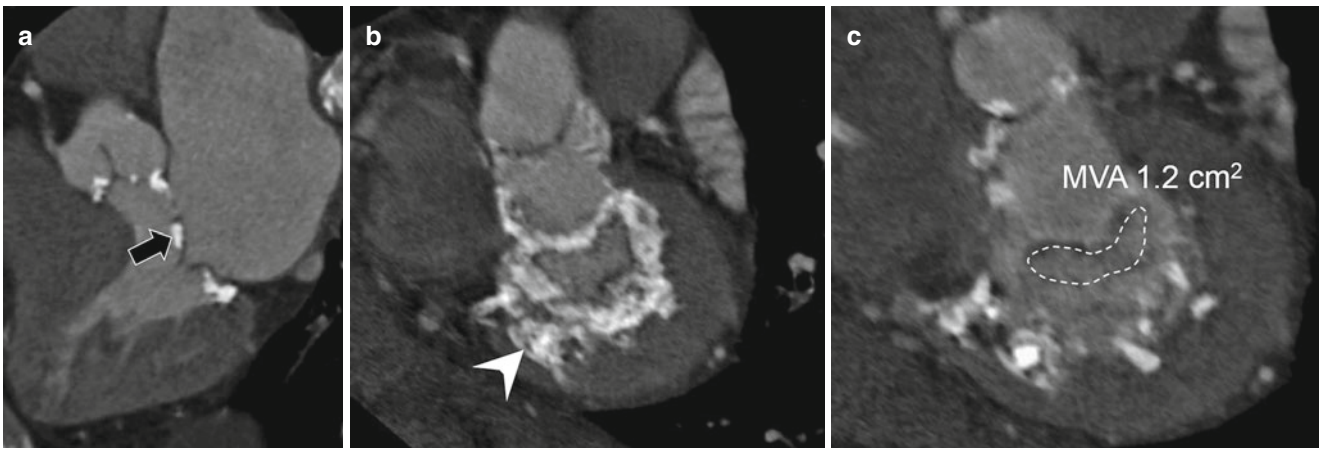

Fig. 18.3 Degenerative mitral stenosis with severe annular calcification. (**a**) Three-chamber view of CT shows mild thickening and small calcification in the anterior leaflet of MV. Note dense calcification along mitral annulus (*arrowhead*). (**b**) Short-axis view of CT shows extensive calcification along mitral annulus. Thick calcification along MV annulus may be problematic when surgeon removes leaflet for valvular replacement surgery. (**c**) Mitral valve area was 1.2 cm^2 on CT. On echocardiography, anatomic planimetry of the mitral valve area is not possible due to severe valvular and annular calcification. Transmitral pressure gradient is elevated (maximum 29 mmHg, mean 18 mmHg), which is suggestive of severe MS

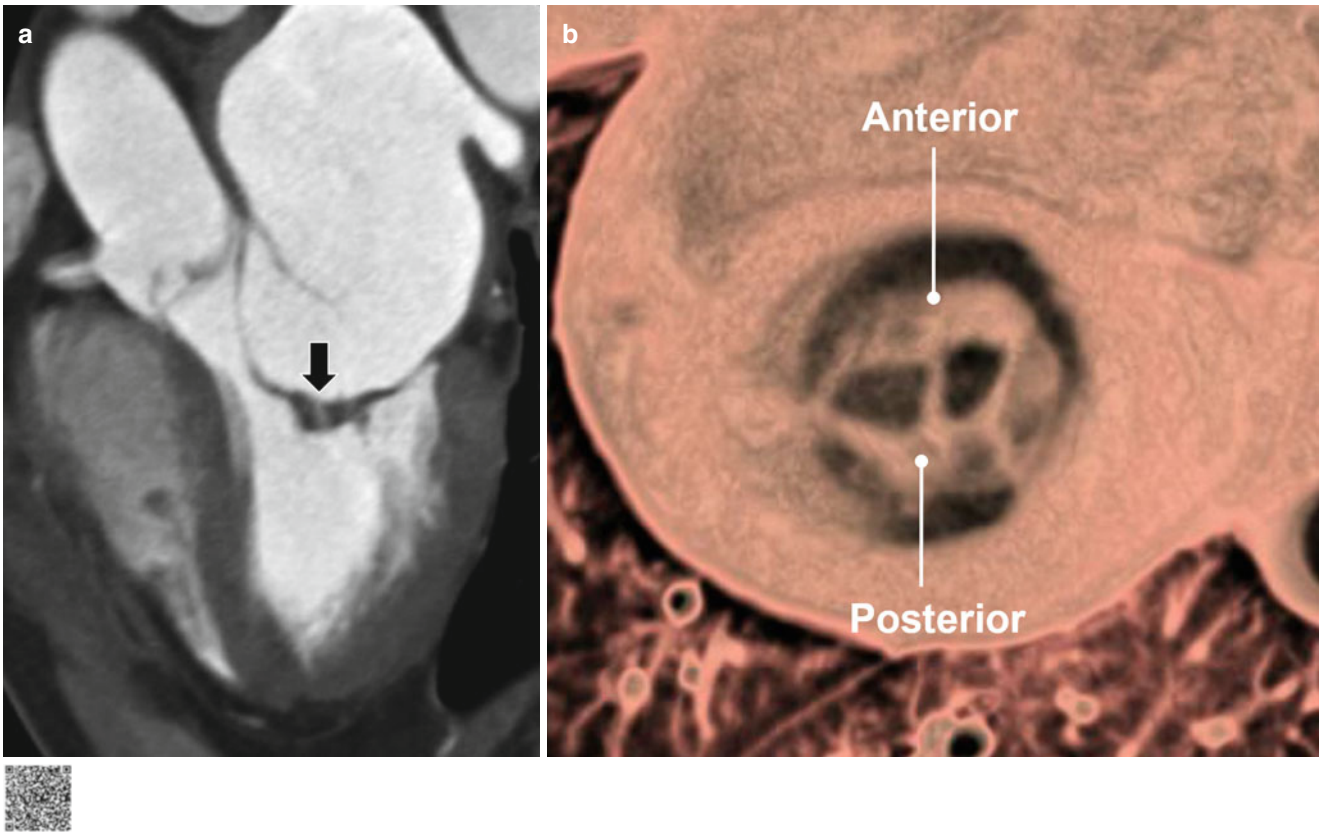

Fig. 18.4 Double orifice of the mitral valve in rheumatic valvular heart disease. (**a**) Three-chamber view of CT shows a bridging formation (*arrow*) between the anterior and posterior leaflet of MV. Leaflet tip of MV is thickened due to involvement of rheumatic valvular heart disease. (**b**) Short-axis view of volume rendering CT image shows double orifice of the mitral valve. Note a linear bridge between the anterior and posterior leaflet (http://extras.springer.com/2015/978-3-642-36396-2)

Acute
Infective endocarditis (annular abscess formation, leaflet perforation, coaptation failure due to leaflet vegetation)
Coronary artery disease (papillary muscle disorder due to LV dysfunction, rarely papillary muscle rupture)
Acute global LV dysfunction
Infiltrative disease (sarcoidosis, amyloidosis)
Trauma (postvalve surgery, postballoon valvotomy, leaflet tear or chordae tendineae rupture due to blunt chest trauma)
Acute rheumatic fever (rupture of chordae tendineae)
Chronic
Inflammatory (rheumatic heart disease (Fig. 18.7), SLE, scleroderma)
Degenerative (myxomatous degeneration of MV leaflets (Fig. 18.8), Marfan syndrome, Ehlers-Danlos syndrome, calcification of MV annulus)
Infective endocarditis (Fig. 18.9)
Structural (ruptured chordae tendineae, rupture or dysfunction of papillary muscle, dilatation of mitral annulus and LV cavity, hypertrophic cardiomyopathy)
Congenital (mitral valve cleft (Fig. 18.10) or fenestrations, parachute mitral valve abnormality)

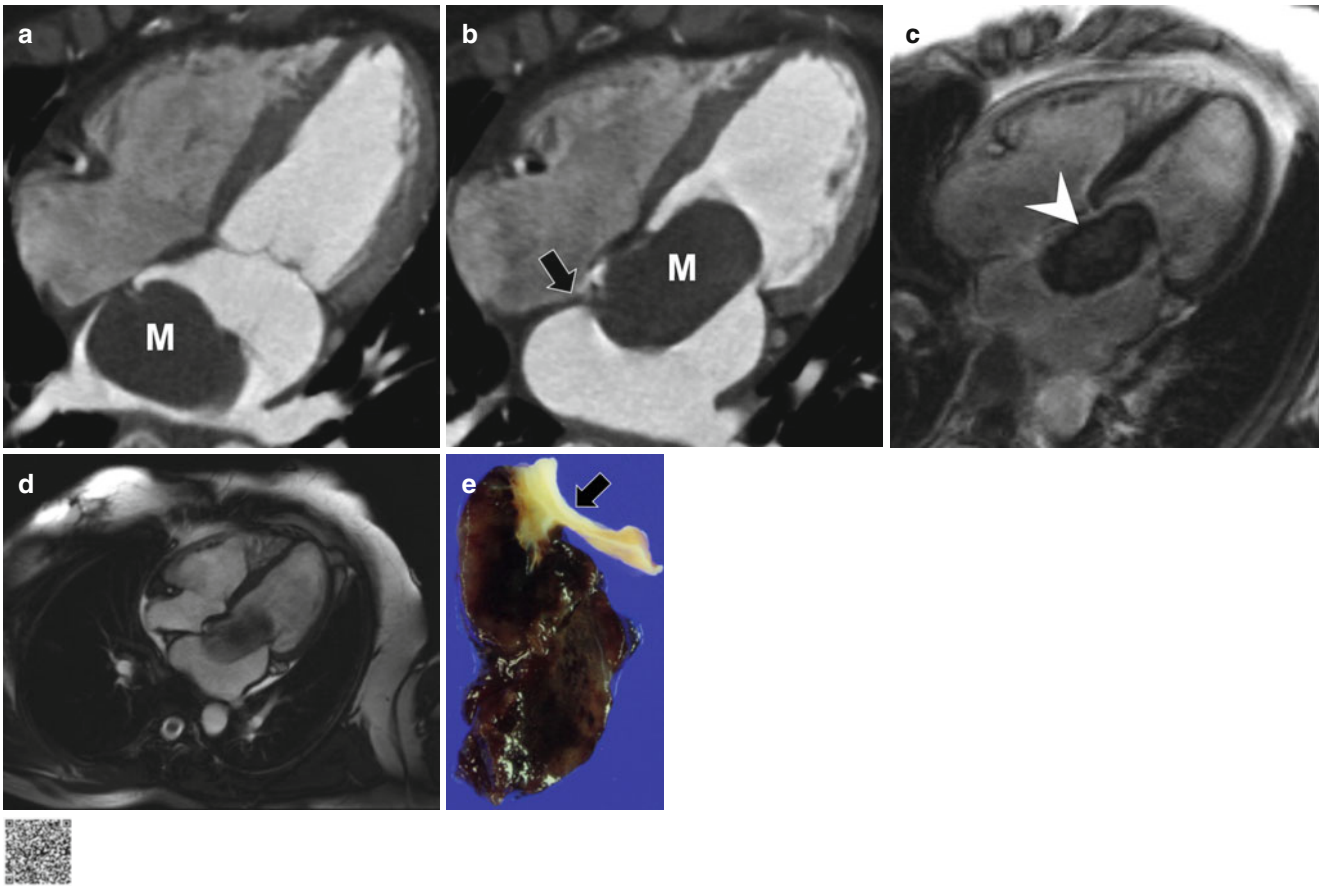

Fig. 18.5 Large myxoma resulting in mitral stenosis. (**a**, **b**) Four-chamber view of CT images (**a**, systolic; **b**, diastolic) shows a large low-density mass (*M*) in the left atrium, attaching interatrial septum (*arrow*). In diastolic phase, inflow tract of the left ventricle is obstructed by the huge mass. (**c**) Four-chamber view of delayed enhancement MR image shows ill-defined contrast enhancement (*arrowhead*) in the central portion of the mass (http://extras.springer.com/2015/978-3-642-36396-2). (**d**) Cine MR image demonstrates dynamic motion of the mass during cardiac phase. (**e**) Gross specimen shows a large solid mass attaching interatrial septum (*arrow*). The mass was confirmed to myxoma on pathologic examination

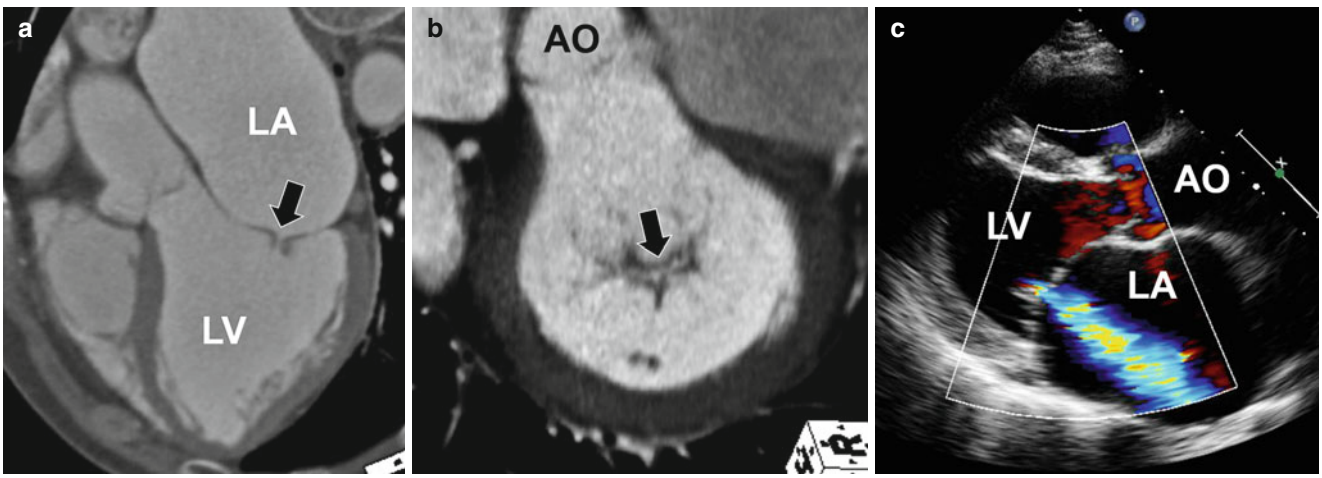

Fig. 18.6 Functional mitral regurgitation due to mitral annular dilatation. (**a**) Three-chamber view of CT image demonstrates central coaptation defect (*arrow*) in the mitral valve due to annular dilatation. The left ventricle (*LV*) is dilated and shows idiopathic systolic dysfunction (not shown). The left atrium (*LA*) is also enlarged. (**b**) Short-axis view of CT image shows a linear shape of the coaptation defect (*arrow*). (**c**) Transthoracic echocardiography shows moderate-to-severe mitral regurgitation without valvular pathology

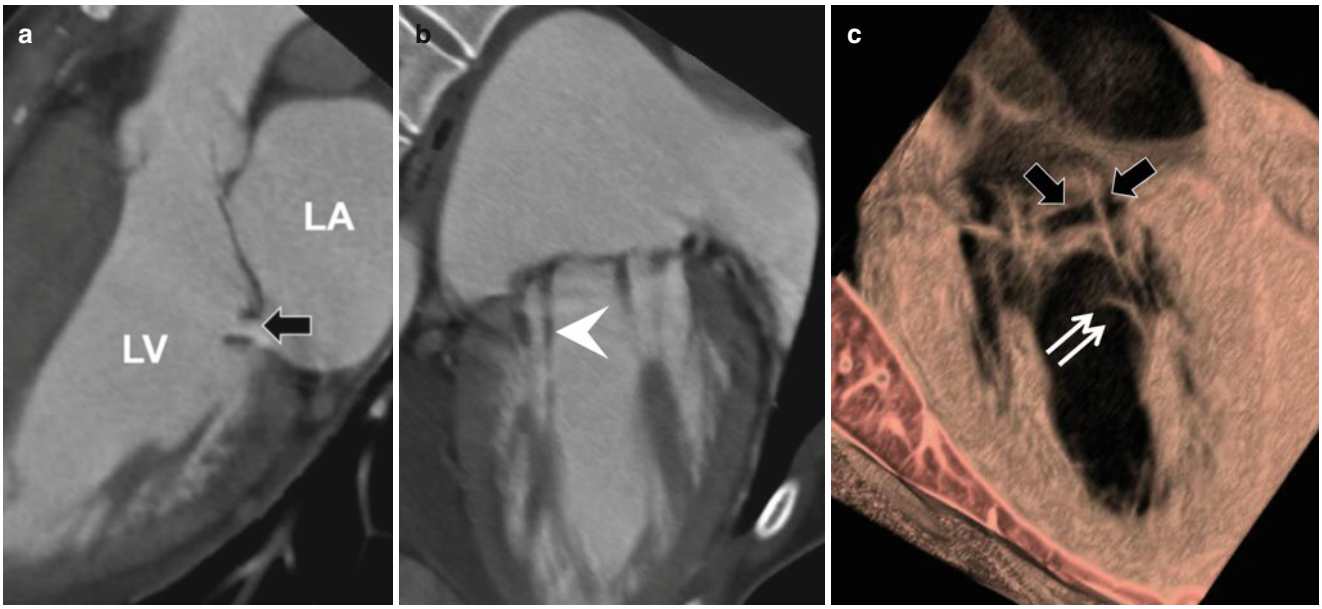

Fig. 18.7 Rheumatic mitral regurgitation due to prolapse of the anterior leaflet. (**a**) Three-chamber view of CT image demonstrates prolapse of the anterior leaflet and resultant coaptation defect (*arrow*). (**b**) Oblique view of CT image shows thickening of chordae tendineae (*arrowhead*) due to involvement of rheumatic valvular disease. (**c**) Volume rendering image depicts shape of the coaptation defect (*arrow*) resulting from the anterior leaflet prolapse. Note a torn chordae tendineae (*double arrows*)

18.2.2.2 Pathophysiology

- Both the LA and LV gradually dilated in response to the reversely ejected portion of the stroke volume.
- When ejection fraction starts to decline, LA and pulmonary capillary pressures start to rise, and symptoms can progress rapidly.
- Echocardiographic criteria for the definition of severe MR (Modified from Ref. [8])

Qualitative indices:
Valve morphology: flail leaflet/ruptured papillary muscle/large coaptation defect
Color flow regurgitant jet: very large central jet or eccentric jet adhering, swirling, and reaching the posterior wall of the left atrium
Semiquantitative indices:
Vena contracta width (mm): ≥7 (for average between apical four- and two-chamber views)
Upstream vein flow: systolic pulmonary vein flow reversal
Inflow: E-wave dominant ≥1.5 m/s in the absence of other causes of elevated left atrial pressure and mitral stenosis
Other: TVI mitral/TVI aortic >1.4
Quantitative indices:
EROA (mm^2): ≥40 (secondary, ≥20)
R vol (ml/beat): ≥60 (secondary, ≥30)
Enlargement of LA and LV

18.2.2.3 Role of CT and MRI

- CT is able to demonstrate and measure a regurgitant orifice area (ROA) in patient with MR [9]. ROA measured on CT was significantly correlated with the results of TEE and ventriculography.
- CT is also able to provide anatomic and geometric information of the mitral valve apparatus in the setting of significant functional MR [10].

18.3 Tricuspid Valve Disease

18.3.1 Tricuspid Valve

- Tricuspid valve stenosis in the least common stenotic valve disease and rheumatic disease is associated in most cases.
- Tricuspid regurgitation (TR) is a commonly diagnosed disease, and mild degree of TR is clinically benign.
- Etiology of TR may be functional (secondary to RV dilatation or tricuspid annulus dilatation without valve pathology) or organic (primary valve pathology) (Fig. 18.11).
- Causes of functional TR include RV infarction, cardiomyopathy, left-sided heart failure, mitral valve disease, left-to-right shunt disease, pulmonary artery or pulmonary valve stenosis, hyperthyroidism, and atrial fibrillation.
- Cause of organic TR includes Ebstein anomaly (Fig. 18.12), infective endocarditis, rheumatic fever, trauma, connective tissue disorder, myxomatous degeneration, and iatrogenic (e.g., pacemaker implantation).

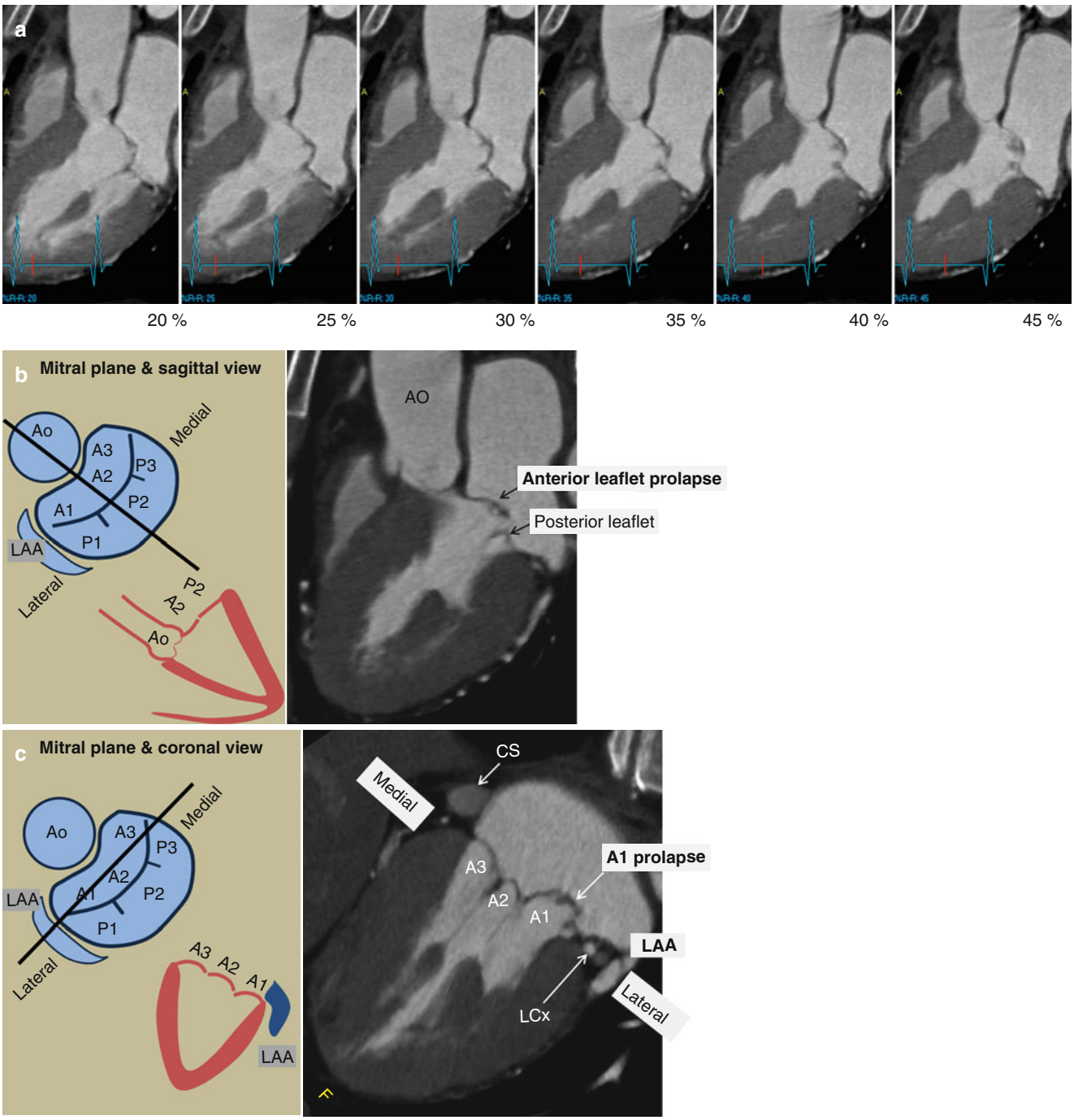

Fig. 18.8 Demonstration of mitral valve prolapse using cardiac CT: 4 steps. (**a**) Step 1: selection of best cardiac phase. In this patient, 25 % of R-R interval was selected for three-dimensional reconstruction. (**b**) Step 2: reconstruction of sagittal reformatted image along mitral annular plane. In this image plane, prolapse of the anterior versus posterior leaflet of the mitral valve was determined. *AO* ascending aorta, *LAA* left atrial auricle. (**c**) Step 3: reconstruction of coronal reformatted image along mitral annular plane. In this image plane, prolapse of medial or middle or lateral scallop was determined. *AO* ascending aorta, *LAA* left atrial auricle, *LCx* left circumflex coronary artery, *CS* coronary sinus. (**d**) Step 4: generation of volume rendering image using thin slab (http://extras.springer.com/2015/978-3-642-36396-2). The location of MV prolapse was confirmed on 3D volume rendering image which is simulating intraoperative finding (*box*)

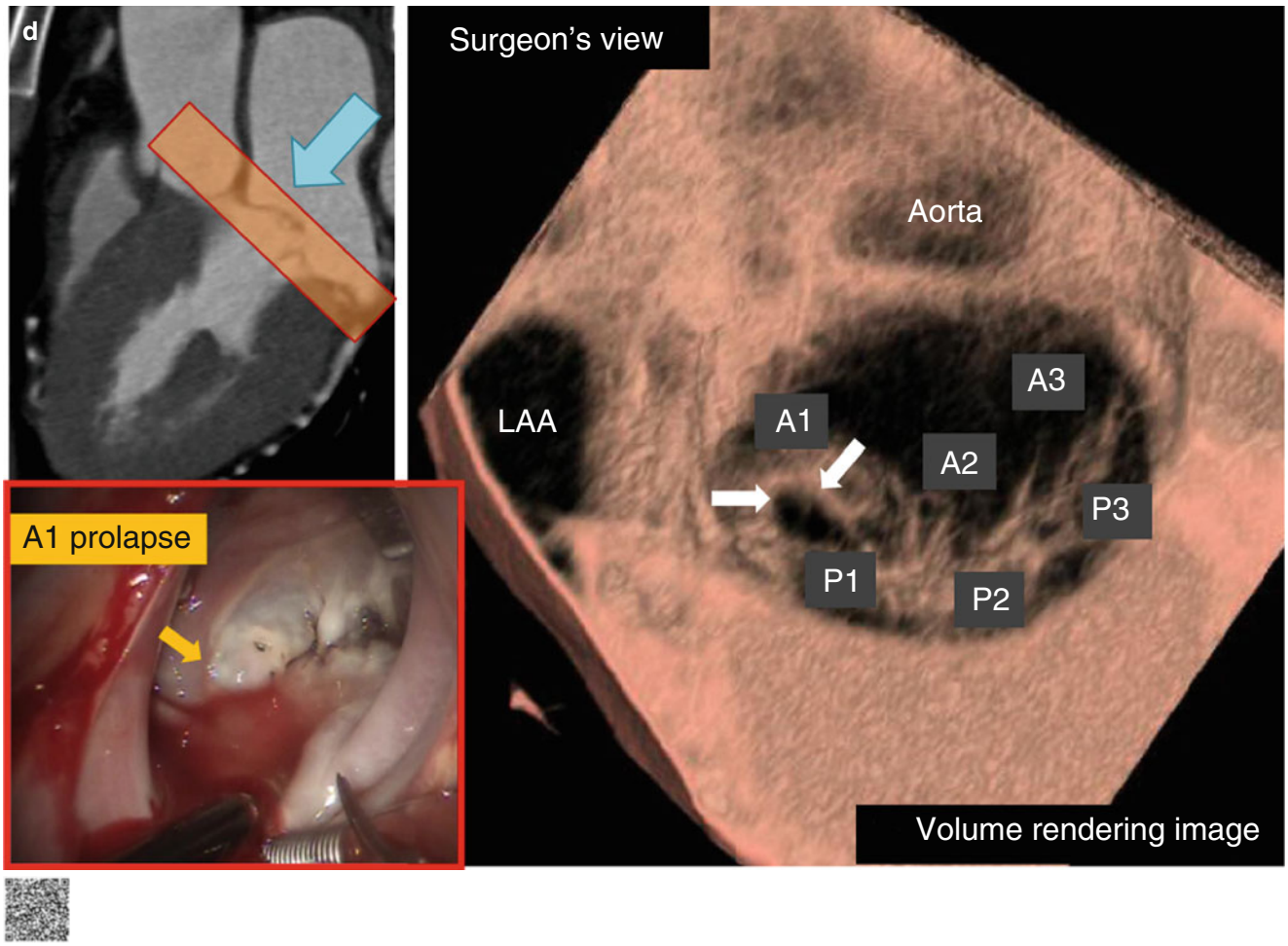

Fig. 18.8 (continued)

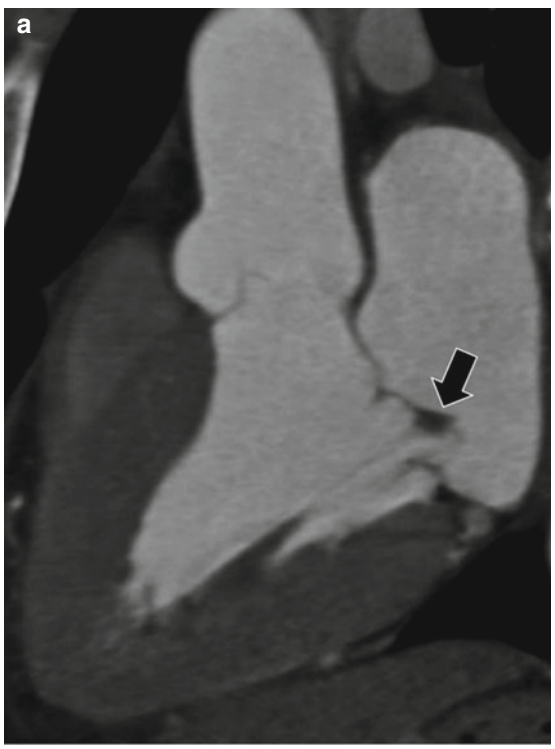

Fig. 18.9 Infective endocarditis involving mitral valve. A 38-year-old man who presents general weakness, myalgia, and fever. (**a**) Three-chamber view of CT shows nodular thickening of the mitral valve anterior leaflet, which is suggestive of vegetation (*arrow*). (**b**) Transesophageal echocardiography shows extensive vegetation (*arrow*) involving both the anterior and posterior leaflets of the mitral valve. (**c**) Thin-slab volume rendering CT image depicts thickening of subvalvular apparatus (*arrowhead*) as well as valvular vegetation in detail. (**d**) Surgeon's view of volume rendering CT image (view from the left atrium) demonstrates the extent of vegetation (*arrow*) involving the mitral view. (**e**) Intraoperative finding using robotic surgery system confirms valvular vegetation involving the anterior leaflet of the mitral valve. Note diffuse thickening of the chordae tendineae (*arrowhead*)

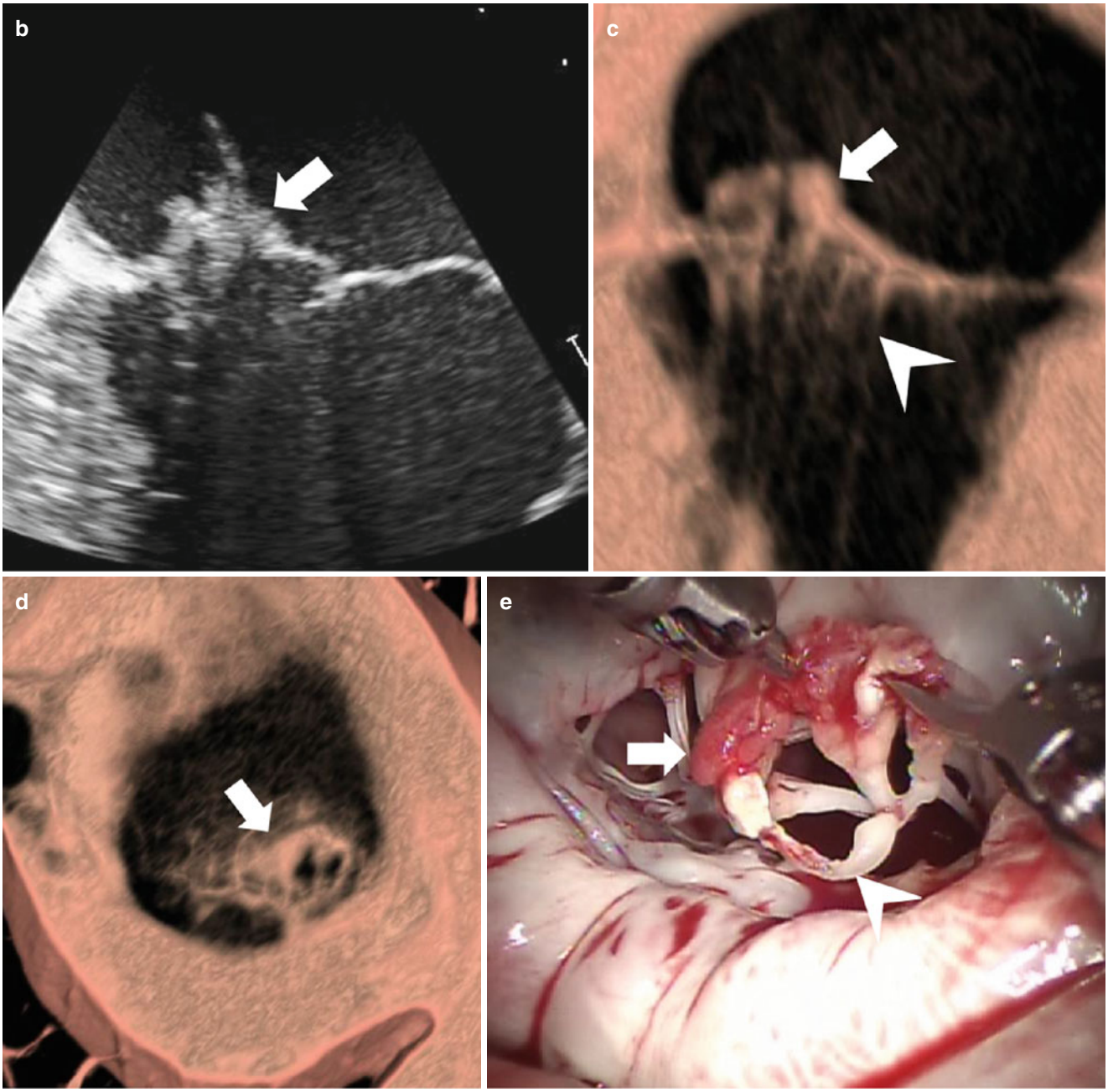

Fig. 18.9 (continued)

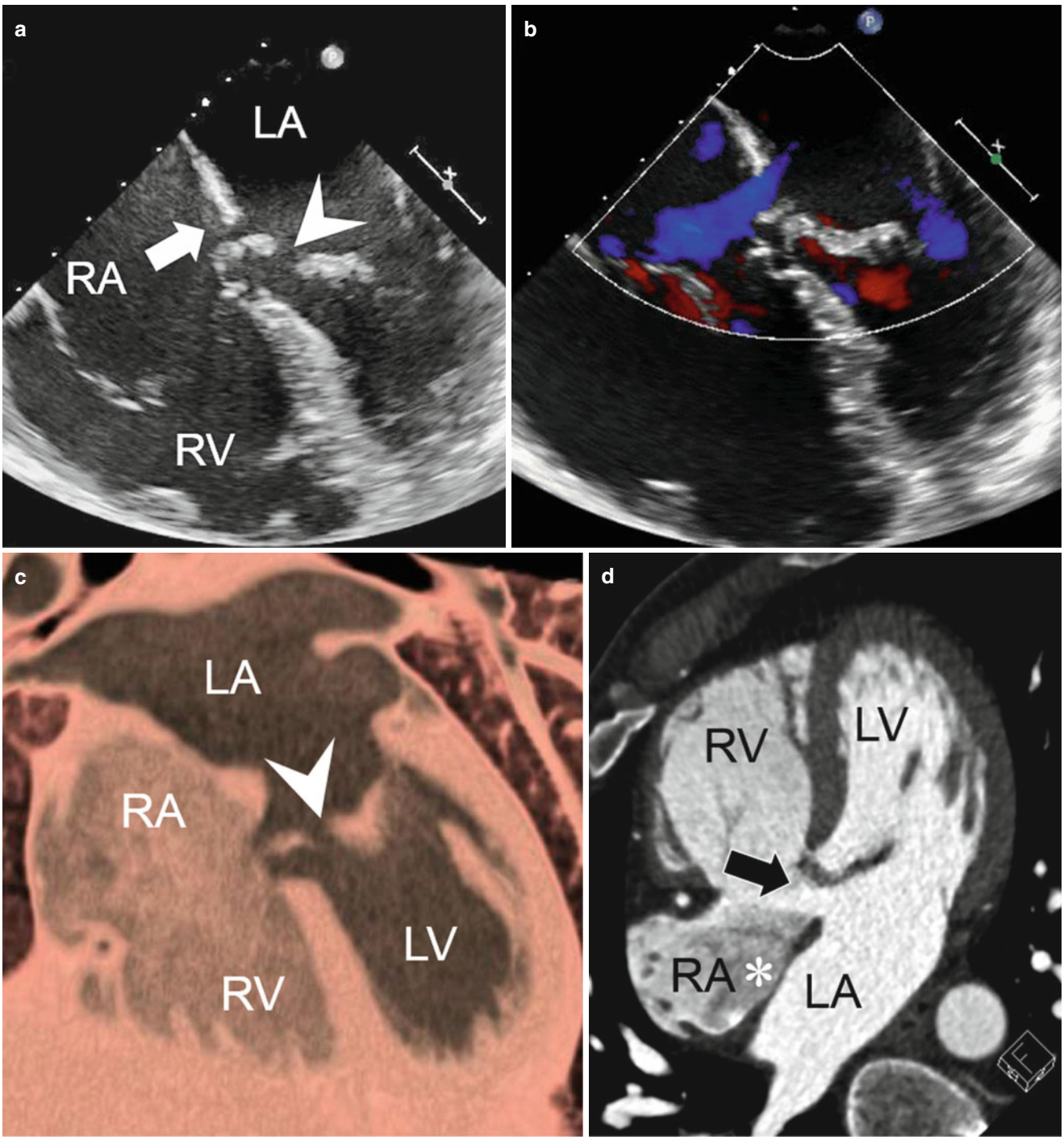

Fig. 18.10 Mitral valve cleft with primum type of atrial septal defect. (**a**, **b**) Transesophageal echocardiography (**b**, color Doppler movie clip) shows an atrial septal defect (ASD) of primum type (*arrow*) and mitral valve cleft (*arrowhead*). (**c**) Oblique axial volume rendering CT image shows mitral valve cleft (*arrowhead*). (**d**) Four-chamber view of CT image demonstrates interatrial septal defect. The location of ASD is inferior than fossa ovalis (*asterisk*). (**e**) Short-axis view of CT image shows a cleft formation (*arrowhead*) in medial scallop of the anterior mitral valve

Fig. 18.10 (continued)

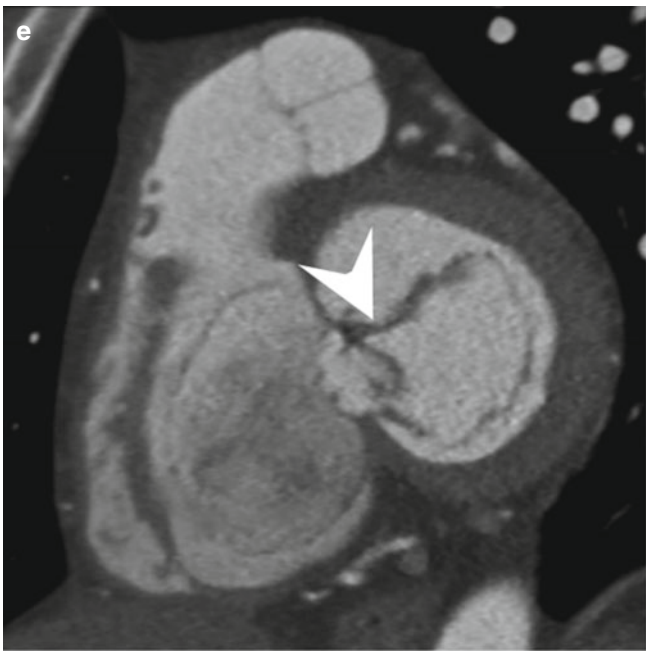

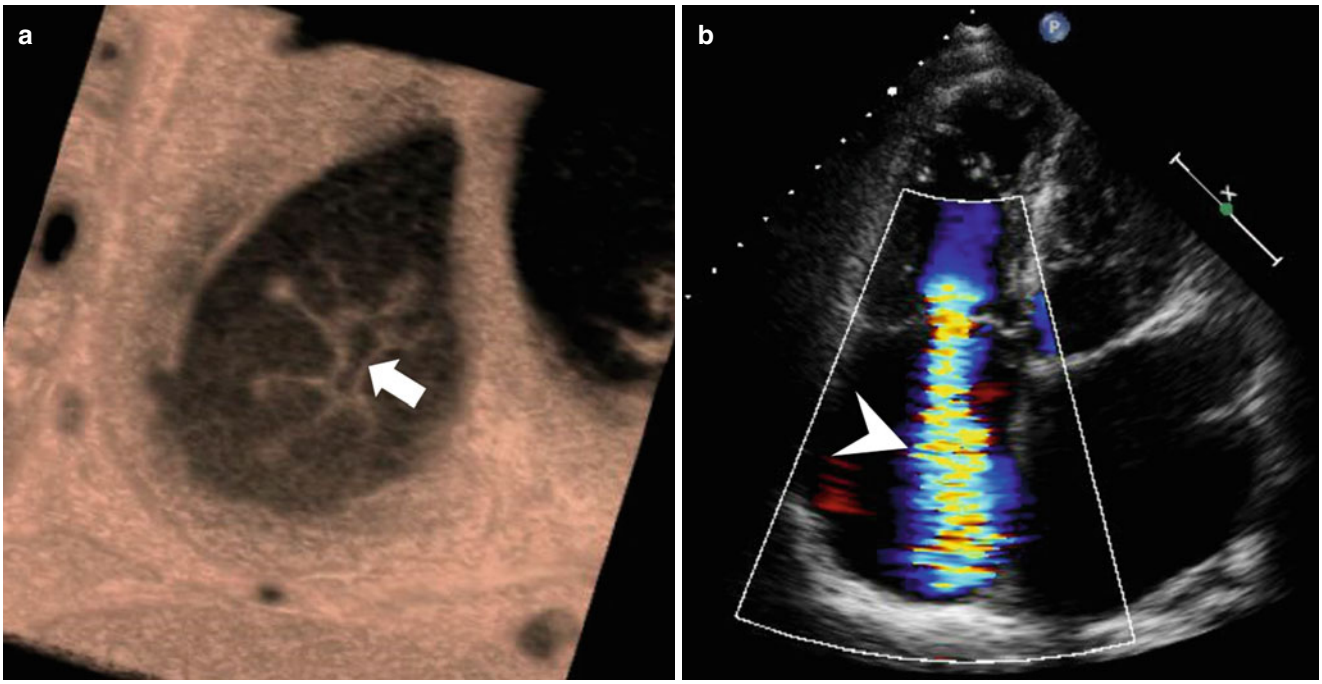

Fig. 18.11 Tricuspid regurgitation with annular dilatation in a patient with mitral stenosis (http://extras.springer.com/2015/978-3-642-36396-2). (**a**) Volume rendering CT image (view from RA) demonstrates coaptation failure (*arrow*) of the tricuspid valve due to annular dilatation. (**b**) Transthoracic echocardiography shows severe tricuspid regurgitation (*arrowhead*). (**c**) Four-chamber view of cine MRI (movie clip) shows severe tricuspid regurgitation

Fig. 18.11 (continued)

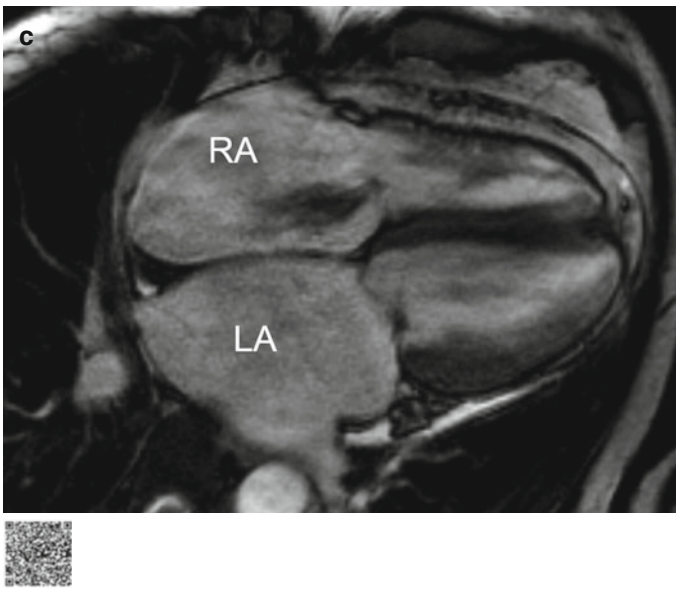

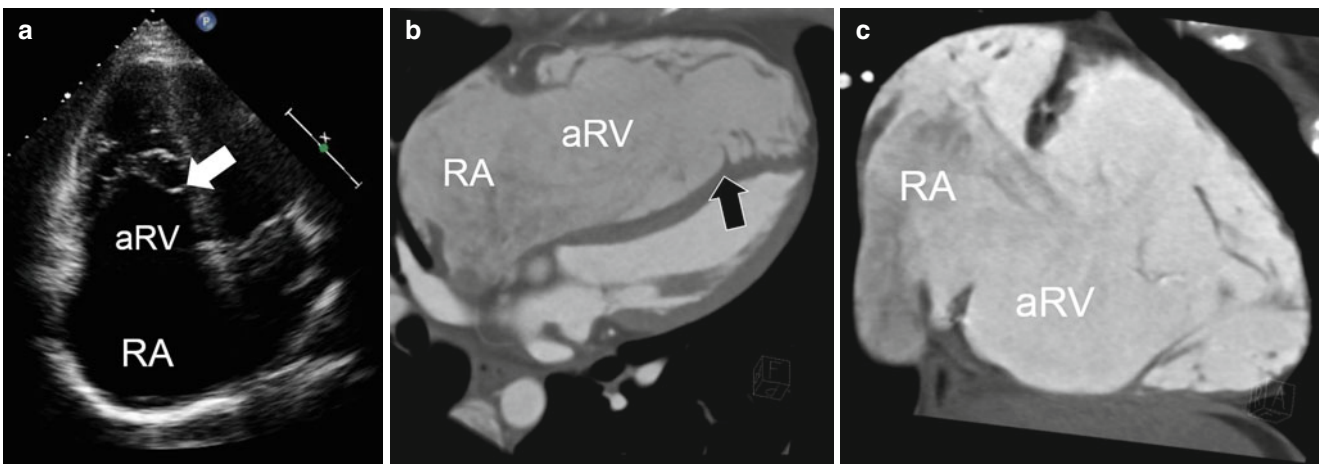

Fig. 18.12 Ebstein anomaly. (**a**) Transthoracic echocardiography shows displacement of septal leaflet to the apical direction (*arrow*). (**b**, **c**) Cardiac CT shows displacement of septal leaflet (*arrow*) and atrialized right ventricle (*aRV*). *RA* right atrium

References

1. Taylor AJ, et al. ACCF/SCCT/ACR/AHA/ASE/ASNC/NASCI/SCAI/SCMR 2010 appropriate use criteria for cardiac computed tomography. A report of the American College of Cardiology Foundation Appropriate Use Criteria Task Force, the Society of Cardiovascular Computed Tomography, the American College of Radiology, the American Heart Association, the American Society of Echocardiography, the American Society of Nuclear Cardiology, the North American Society for Cardiovascular Imaging, the Society for Cardiovascular Angiography and Interventions, and the Society for Cardiovascular Magnetic Resonance. J Am Coll Cardiol. 2010;56(22):1864–94.
2. Zamorano JL, et al. The ESC textbook of cardiovascular imaging. New York/London: Springer; 2010.
3. Messika-Zeitoun D, et al. Assessment of the mitral valve area in patients with mitral stenosis by multislice computed tomography. J Am Coll Cardiol. 2006;48(2):411–3.
4. Djavidani B, et al. Planimetry of mitral valve stenosis by magnetic resonance imaging. J Am Coll Cardiol. 2005;45(12):2048–53.
5. Ucar O, et al. Assessment of planimetric mitral valve area using 16-row multidetector computed tomography in patients with rheumatic mitral stenosis. J Heart Valve Dis. 2011;20(1):13–7.
6. Lembcke A, et al. Assessment of mitral valve stenosis by helical MDCT: comparison with transthoracic doppler echocardiography and cardiac catheterization. AJR Am J Roentgenol. 2011;197(3):614–22.
7. Bonow RO. Braunwald's heart disease: a textbook of cardiovascular medicine. 9th ed. Philadelphia: Saunders; 2012.
8. Joint Task Force on the Management of Valvular Heart Disease of the European Society of Cardiology, et al. Guidelines on the management of valvular heart disease (version 2012). Eur Heart J. 2012;33(19):2451–96.
9. Alkadhi H, et al. Mitral regurgitation: quantification with 16-detector row CT–initial experience. Radiology. 2006;238(2):454–63.
10. Delgado V, et al. Assessment of mitral valve anatomy and geometry with multislice computed tomography. JACC Cardiovasc Imaging. 2009;2(5):556–65.

Part V

Cardiac Tumors and Pericardial Diseases

Cardiac Tumors

19

Joon-Won Kang and Tae-Hwan Lim

Contents

Abstract

The prevalence of cardiac tumors is very low, and the majority of cardiac tumors arise from metastasis. The majority of primary cardiac tumor is benign. Transthoracic echocardiography is widely used for initial evaluation or screening, and advances in cardiac imaging – cardiovascular magnetic resonance (CMR) imaging and computed tomography (CT) – provide additional information about the shape, location, and extent of cardiac tumors. CMR imaging, especially, is more advantageous because of its superior spatial resolution and characterization of tumor tissue and enhancement patterns of the tumor using gadolinium agent. In this chapter, we will describe the clinical aspects of cardiac tumors, recommended imaging strategies used in their acquisition, and present selected images of cardiac masses of various etiologies with a review of the imaging characteristics of each tumor type. We will also describe "tumor-like" lesions that can be mistaken as tumors.

19.1 Overview

19.1.1 Prevalence

- Metastatic cancer – 20–40 times more frequent than primary cardiac tumor.
- Prevalence of primary cardiac tumor – 0.002–0.3 % [1].
  - Benign cardiac tumor consists 75 % of primary cardiac tumor.
    - Myxoma is the most common primary benign cardiac tumor (approximately 50 %).
    - Rhabdomyoma is the most common primary benign cardiac tumor in childhood.
  - Malignant primary cardiac tumor consists 25 % of primary cardiac tumor.
    - Sarcomas are the most malignant primary cardiac tumors (approximately 95 %).
    - Lymphoma consists approximately 5 % of malignant primary cardiac tumors.

Electronic supplementary material Supplementary material is available in the online version of this chapter at 10.1007/978-3-642-36397-9_19.

J.-W. Kang • T.-H. Lim (✉)
Department of Radiology and Research Institute of Radiology, Asan Medical Center, University of Ulsan College of Medicine, Seoul, Republic of Korea
e-mail: joonwkang@naver.com; d890079@naver.com

T.-H. Lim (ed.), *Practical Textbook of Cardiac CT and MRI*,
DOI 10.1007/978-3-642-36397-9_19, © Springer-Verlag Berlin Heidelberg 2015

19.1.2 Clinical Signs and Symptoms [2]

- Generally no symptoms or signs
- Contributing factors
  - Hemodynamic disturbance by location and size of the tumor
  - Embolism
- Signs and symptoms by location of tumor and embolism effect:
  - Left atrium – mitral valve stenosis or regurgitation, systemic embolism through embolism
  - Right atrium – tricuspid valve stenosis or regurgitation, pulmonary hypertension, pulmonary thromboembolism
  - Left ventricle – left heart dysfunction, arrhythmia, conduction disturbance
  - Right ventricle – right heart failure
- Embolism:
  - Most representative clinical symptom
  - Mechanism – fragments of tumor or thrombus at the surface of tumor
  - Most common – cardiac myxoma
  - Right heart tumor – pulmonary embolism; left heart tumor – systemic arterial embolism
  - Patent foramen ovale – systemic arterial embolism from right heart tumor

19.2 Imaging Modalities and Findings

19.2.1 Imaging Modalities

- Chest radiography:
  - Nonspecific, low sensitivity.
  - Findings are based on the morphology change by hemodynamic disturbance.
  - Cardiomegaly by pericardial effusion, mediastinal widening by lymph node metastasis.
- Echocardiography:
  - Detection of small and hypermobile tumor of the cardiac valves
  - Doppler echocardiography – hemodynamic change evaluation, valvular stenosis and/or regurgitation
- CT:
  - Differentiation of tumor from normal heart tissue, evaluation of surrounding tissue invasion
  - Clear visualization of the pericardium, mediastinum, great vessels
  - Multiplanar reformation using volume data
- MRI [1]:
  - Advantages:
    - Best tissue contrast and spatial resolution
    - Generally, no or minimal interobserver variability
    - Extracardiac structure evaluation
    - Function evaluation
  - Disadvantages [1]:
    - In patients with arrhythmia, ECG gating can be difficult.
    - Difficult to demonstrate calcium.
- Angiography:
  - Useful for evaluation of arteriovenous fistula, vessel invasion, and shunt

19.2.2 Recommended Imaging Protocols

- CT – recommended contrast and scan protocol [3].
  - ECG gating.
  - Tube current modulation – usually use retrospective gating. Prospective gating or single heartbeat scan is optional.
    (i) A full R-R interval imaging is required for analysis of dynamic motion or heart function analysis.
    (ii) Prospective gating or ECG pulsing during mid-or end-diastolic phase for anatomy analysis.
- MRI protocols – recommended guidelines [3, 4].
  - Left ventricle structure and function module:
    - Scout image – axial, coronal, and sagittal planes
    - Transaxial steady-state free precession (SSFP) or fast spin echo images through the chest with 8–10 mm slice thickness
    - Scout images for acquisition of short-axis plane
    - SSFP short-axis cine images:
      (i) Range – mitral valve plane to cardiac apex
      (ii) Slice thickness – 6–8 mm; inter-slice gap – 2–4 mm
      (iii) Temporal resolution – ≤45 ms between cardiac phases
      (iv) Parallel imaging use as available
    - SSFP long-axis cine images:
      (i) The 4-chamber long axis
      (ii) Vertical long axis
      (iii) Left ventricular outflow tract (LVOT) long-axis cine images
  - T1-weighted fast spin echo – covers the whole mass and surrounding structures (the number of the slices is varied according to the size of the mass).
  - T2-weighted fast spin echo with fat suppression (T2 images without fat suppression are optional) – covers the whole mass and surrounding structures (the number of the slices is varied according to the size of the mass):
    - Using double inversion recovery is recommended
    - Slice thickness – 6–10 mm
    - Target mid-diastolic phase
  - First pass perfusion module with slices through the mass.
  - Repeat T1-weighted fast spin echo with fat suppression.

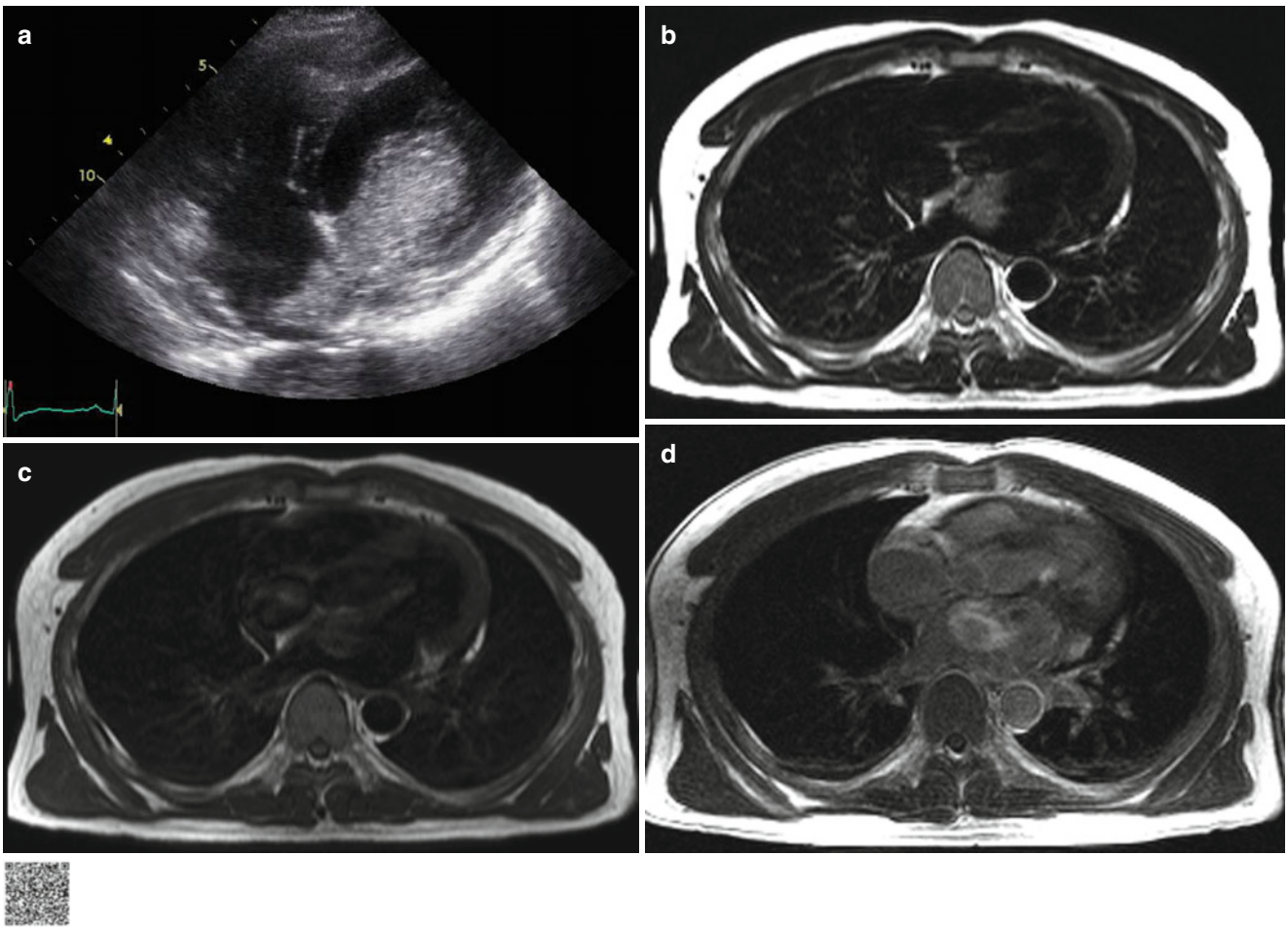

Fig. 19.1 Imaging characteristics of myxoma on CT and CMR. (**a**) Transthoracic echocardiography shows an echogenic mass attached to the interatrial septum. This mass has protruded to the left ventricle at the diastolic phase (http://extras.springer.com/2015/978-3-642-36396-2). (**b**, **c**) T2- and T1WI show the lobulated mass with irregular margin in the left atrium. The mass is hyper-signal intensity in T2-WI and iso-signal intensity in T1WI. (**d**) In the delayed-enhancement image, the mass is hyper-enhanced with a central low signal intensity portion. The mass was confirmed as myxoma through excision (Figs. 19.2 and 19.3)

  - (Option) repeat selected slices of steady-state free precession cine images of post-contrast.
  - Late gadolinium enhancement module; note that TI to null the mass may be different than for myocardium.

19.2.3 Benign Cardiac Tumors

19.2.3.1 Myxoma

- Overview:
  - Most common – 50 % of primary benign tumor [5]
  - Prevalent age – 20–50 years old
  - Usually solitary:
    - Familial myxoma in less than 10 % – autosomal dominant, young age, recurrence after surgery (12–25 %)
    - Carney syndrome – multiple myxomas in the heart and other organ, skin pigmentation, and endocrine tumors
  - Mesenchymal cell origin
  - Differential diagnosis – thrombus, malignant tumor with myxoid degeneration
- Imaging findings:
  - Prevalent location:
    - Typical location – peri-foramen ovale interventricular septum
    - Mitral valve, tricuspid valve
  - Size – 4–8 cm
  - CT:
    - Heterogeneous low attenuation – gelatinous material
    - Calcification
  - MRI:
    - T2 – high signal intensity
    - T1 – iso-signal intensity compared with myocardium
    - Sometimes low signal – due to hemosiderin
    - Heterogeneous post-contrast enhancement
    - No contrast enhancement – thrombus, more likely [6] (Fig. 19.1)

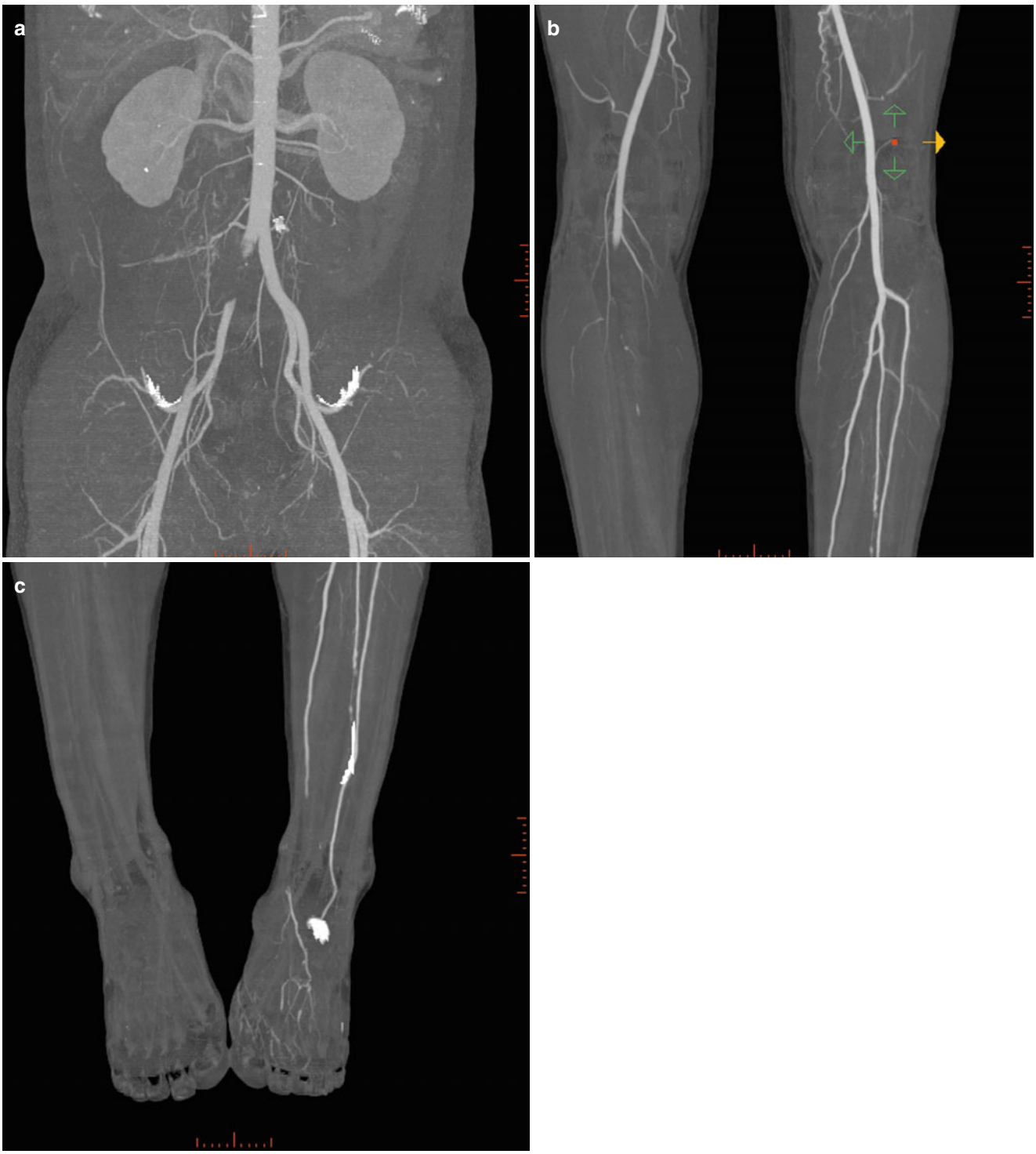

Fig. 19.2 Cardiac myxoma with embolism. (**a**) End-systolic and, (**b**) mid-diastolic phase axial CT images show lobulated mass with irregular margin attached to the interatrial septum. The mass protruded to the left ventricle during the diastolic phase. (**c**) Aortoiliac area, (**d**) bilateral popliteal area, and, (**e**) bilateral ankle area maximum intensity projection CT images show filling defects and abrupt cutoffs at the right common iliac artery and right popliteal artery and decreased arterial flow at the right calf and foot that are caused by embolism due to cardiac myxoma

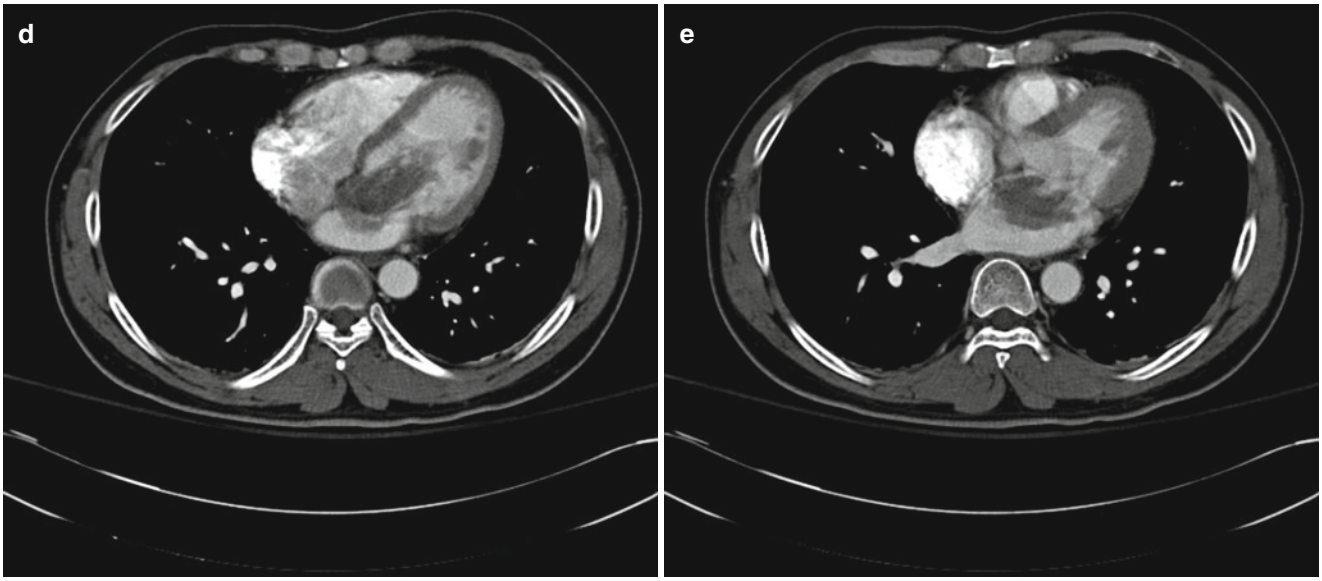

Fig. 19.2 (continued)

19.2.3.2 Papillary Fibroelastoma

- Overview:
  - The second most common benign tumor and the most common valve tumor [7].
  - The mean prevalent age is 60 years old.
  - The prevalence is not different between male and female.
  - Is located in the left heart more often than in the right heart.
    - Most common sites are the aortic valve and mitral valve (tricuspid valve in childhood).
    - Papillary muscle and endocardium around the cardiac valves are the possible location.
    - The tumors are located at the ventricular side of the semilunar valves (aortic valve and pulmonic valve) and at the atrial side of the atrioventricular valves.
  - More likely present as a solitary mass than multiple masses.
  - Has a stalk within 1-cm length.
  - Pathophysiology is considered a reaction to trauma or a kind of hamartoma.
    - The signs and symptoms are usually asymptomatic. However, embolism and valvular dysfunction is caused.
  - Imaging findings [7, 8]:
    - Echocardiography is widely used to detect papillary fibroelastoma due to the mobility and the small size of the mass.
    - When the tumor is small and hypermobile, CT and MRI can miss the lesion.
    - CT – low-attenuated lesion.
    - T2WI – homogeneously low-signal lesion.
    - Calcification is rare (Fig. 19.4).

19.2.3.3 Rhabdomyoma

- Overview:
  - Most common tumor in children.
  - Multiple (90 %) lesions are common. Fifty percent of patients who have cardiac rhabdomyoma have tuberous sclerosis and 60 % of patients under 18 years old who have tuberous sclerosis have cardiac rhabdomyoma.
  - Location – in the myocardium or interventricular septum.
  - It is mostly asymptomatic.
  - Spontaneous regression is possible. But consider surgical treatment if with symptoms such as obstruction or arrhythmia.
- Imaging findings:
  - CT – hypointense lesion compared with normal myocardium in the post-contrast image
  - MR – hyperintense in T2WI and iso-signal in T1WI [7, 8]

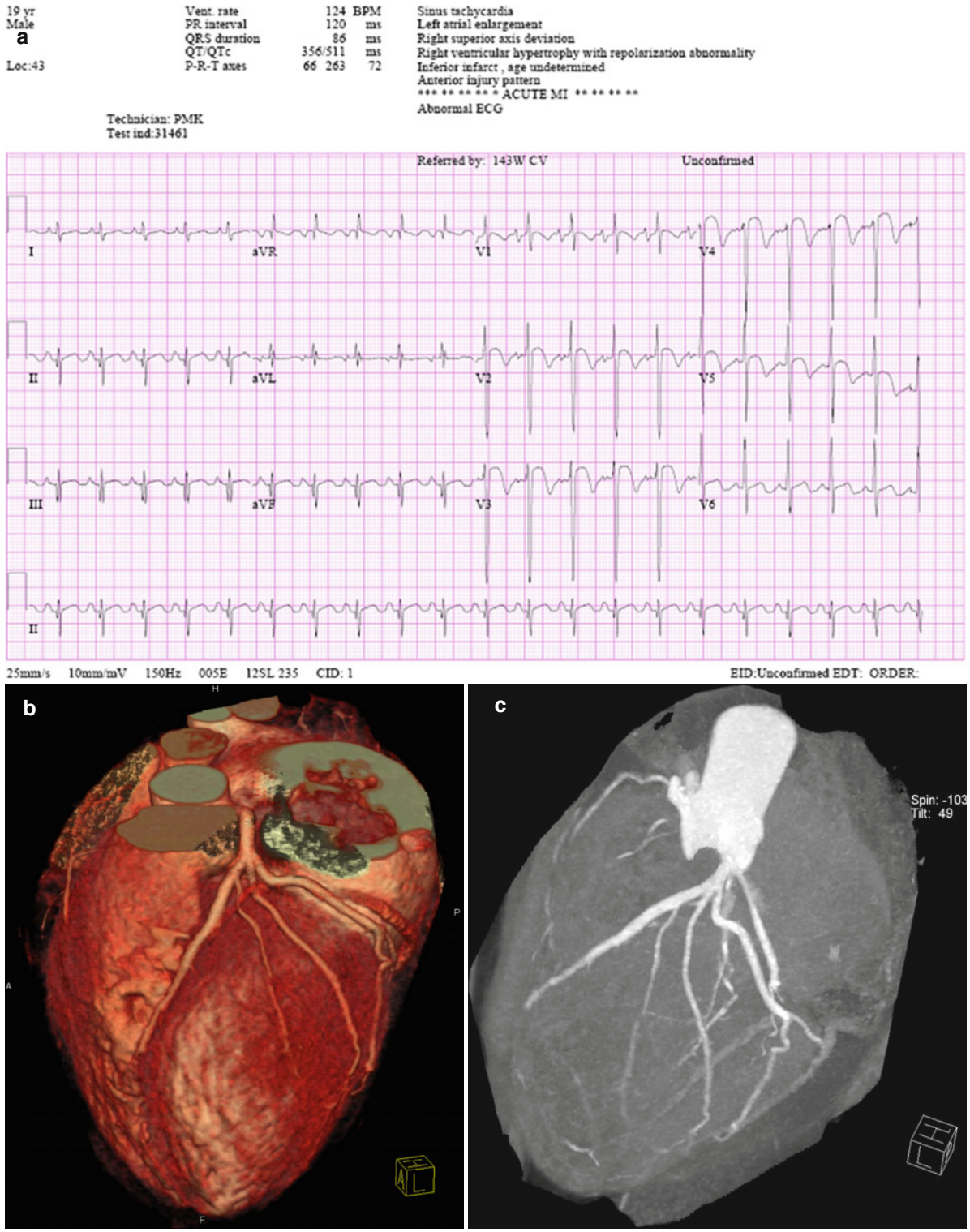

Fig. 19.3 Myocardial ischemia by myxoma. (**a**) Electrocardiogram shows Q wave on lead III and aVF that suggest inferior wall infarct. ST-segment elevation at precordial leads is also seen. (**b**) Volume-rendered image and, (**c**) maximum intensity projection image show abrupt complete occlusion in distal LAD without the evidence of plaque in the coronary arteries. (**d**) Two-chamber view CT image and, (**e**) four-chamber view CT image show a lobulated contoured low-attenuated mass in the left atrium and prolapse of the mass into the left ventricular cavity at diastolic phase. (**f**) End-systolic phase short-axis view and, (**g**) end-diastolic short-axis view of the apical segment of the left ventricle show akinesia of the anterior wall and septal wall of the left ventricle. Also, the attenuation of the anterior wall and septal wall of the left ventricle is decreased, suggesting perfusion defect. (**h**) The gross specimen of the excised mass shows *whitish yellow* myxoid with extensive hemorrhage at the cut surface; a focal whitish solid area is identified as well

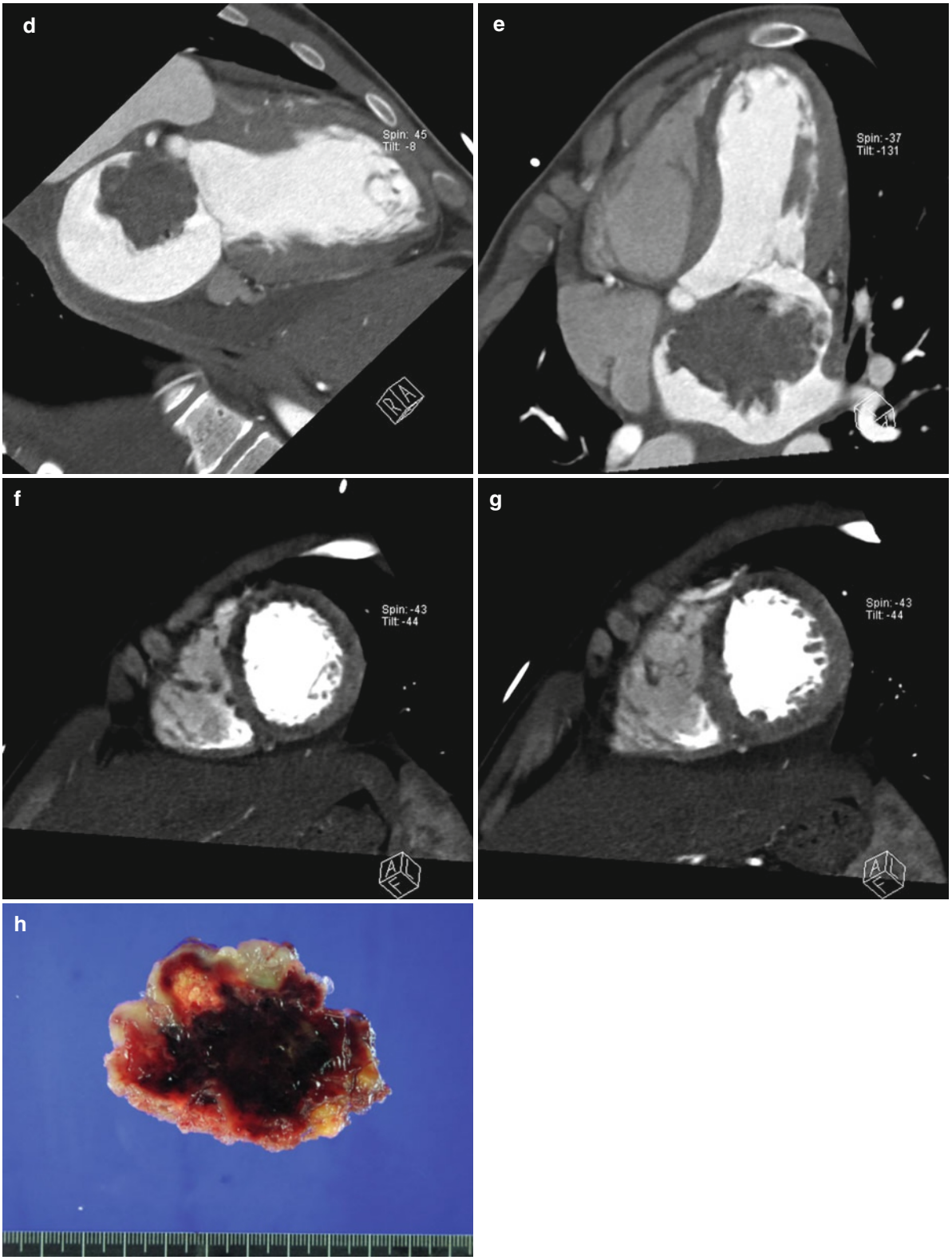

Fig. 19.3 (continued)

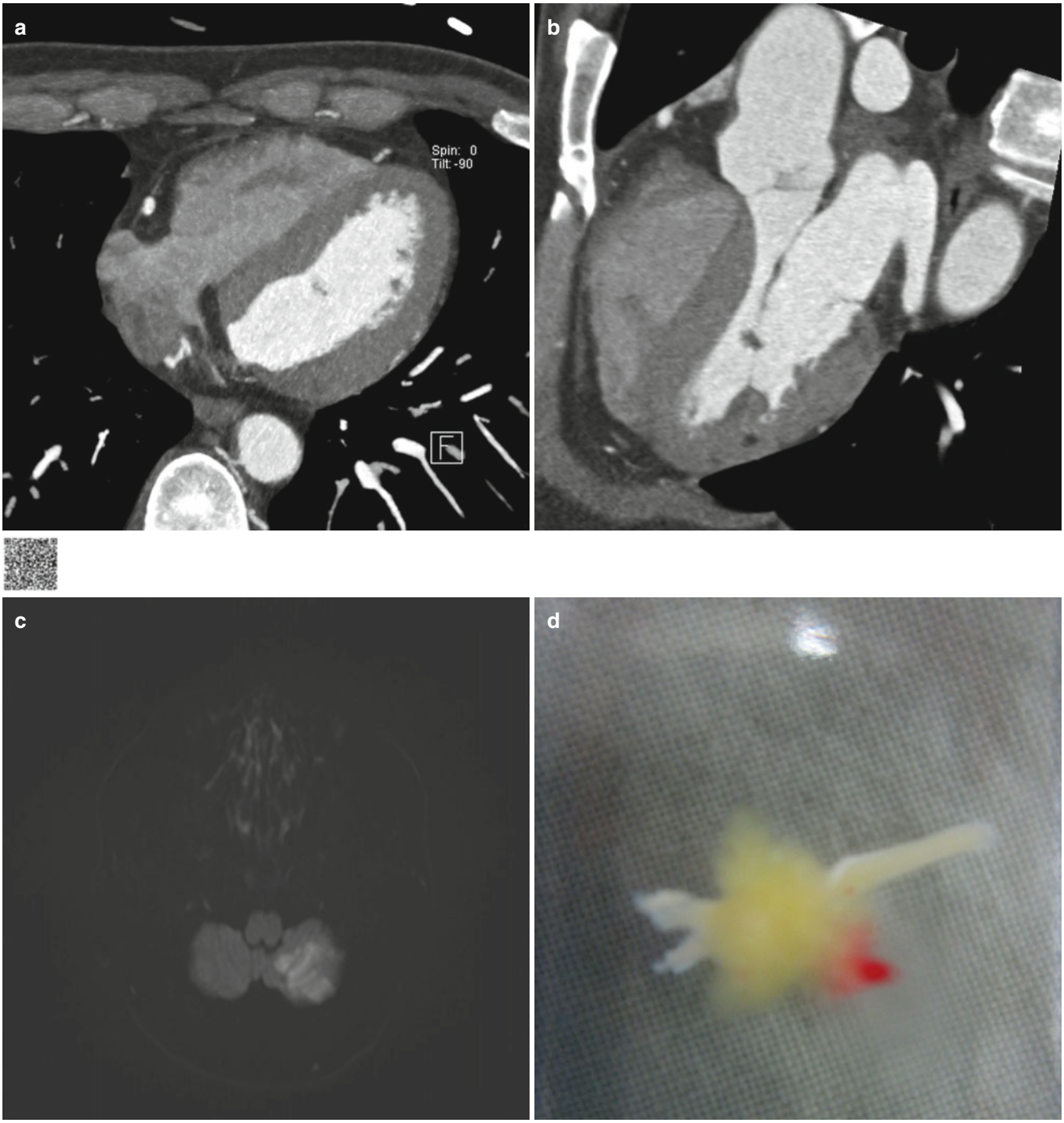

Fig. 19.4 CT findings of papillary fibroelastoma arising at the chordae tendinea. (**a**) Axial and, (**b**) three-chamber view CT images show elongated-shaped mass with multiple spiculations attached to the chordae tendinea of the anterior papillary muscle. The mass is hypermobile through the cardiac cycle (http://extras.springer.com/2015/978-3-642-36396-2). (**c**) In diffusion-weighted MR image of the brain, hypersignal intensity lesion in the left cerebellum is seen that is suggestive of acute infarction. (**d**) The gross specimen of the mass has a flower-like shape with multiple spiculations. (**e**) The microscopic image shows a central core of dense connective tissue and a surrounding layer of endothelial cells, loose connective tissue, and a mesh of elastic fibers

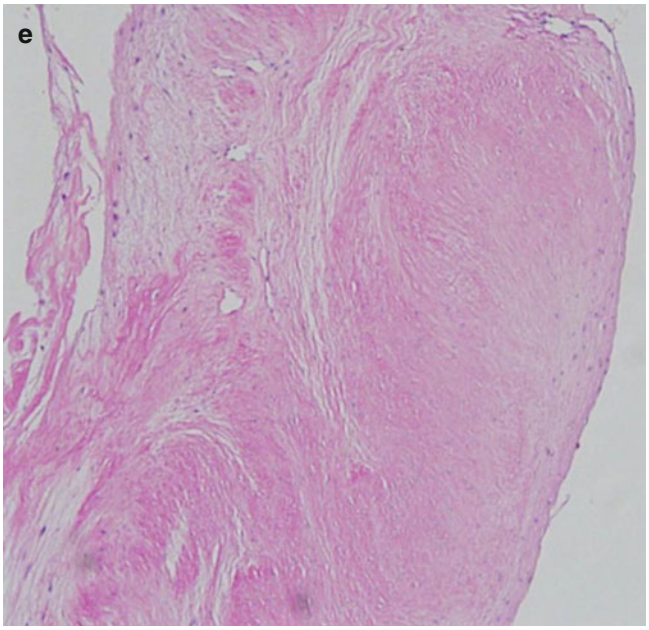

Fig. 19.4 (continued)

19.2.3.4 Fibroma

- Overview:
  - Second most common tumor in children.
  - The prevalence is not different between male and female.
  - Clinical manifestations are conduction disturbance, ventricular arrhythmia, and cardiac failure. However, one-third of patients having cardiac fibroma remain asymptomatic until adulthood.
  - Surgical removal is recommended to avoid sudden death.
  - Cardiac fibroma may be associated with Gorlin syndrome (nevoid basal cell carcinoma syndrome).
- Usually solitary (different from rhabdomyoma), hardly hemorrhagic, and with no cystic change or necrosis (different from rhabdomyosarcoma).
- Prevalent in the anterior wall and interventricular septum of the left ventricle; rare in the inferior wall of the left ventricle or the right ventricle.
- Tumor size ranges from 3 to10 cm.
- Imaging findings:
  - A large, sequestered, and calcified mass in the ventricle
  - CT – low-attenuated lesion due to dense fibrotic lesion, sometimes calcification
  - MRI – hypointense in T2WI and well-enhanced in LGE. Variable signal intensity in T1WI [9, 10] (Fig. 19.5).

19.2.3.5 Hemangioma

- Overview:
  - Consists 5–10 % of primary benign cardiac tumor.
  - The tumor can occur everywhere in the heart and at any age.
  - Clinical manifestation is usually asymptomatic. Mass effect or embolism is possible.
  - Pathology is a sac filled with blood or thrombus lined by endothelial cells.
  - Shape is variable. In the myocardial location, the tumor shows ill-defined, sponge-like shape due to hemorrhage or congestion. In contrast, it shows a well-defined myxoid shape in the epicardial location.
  - It may be a sign of Kasabach-Merrit syndrome (hemangiomatosis, thrombocytopenia, and consumptive coagulopathy).
  - Spontaneous regression is possible; therefore, surgical excision can be deferred when asymptomatic [11].
- Imaging findings:
  - CT – heterogeneous attenuation accompanied with calcification
  - MRI – hyper-signal in T2WI, iso-signal in T1WI, and heterogeneous strong enhancement [7] (Fig. 19.6)

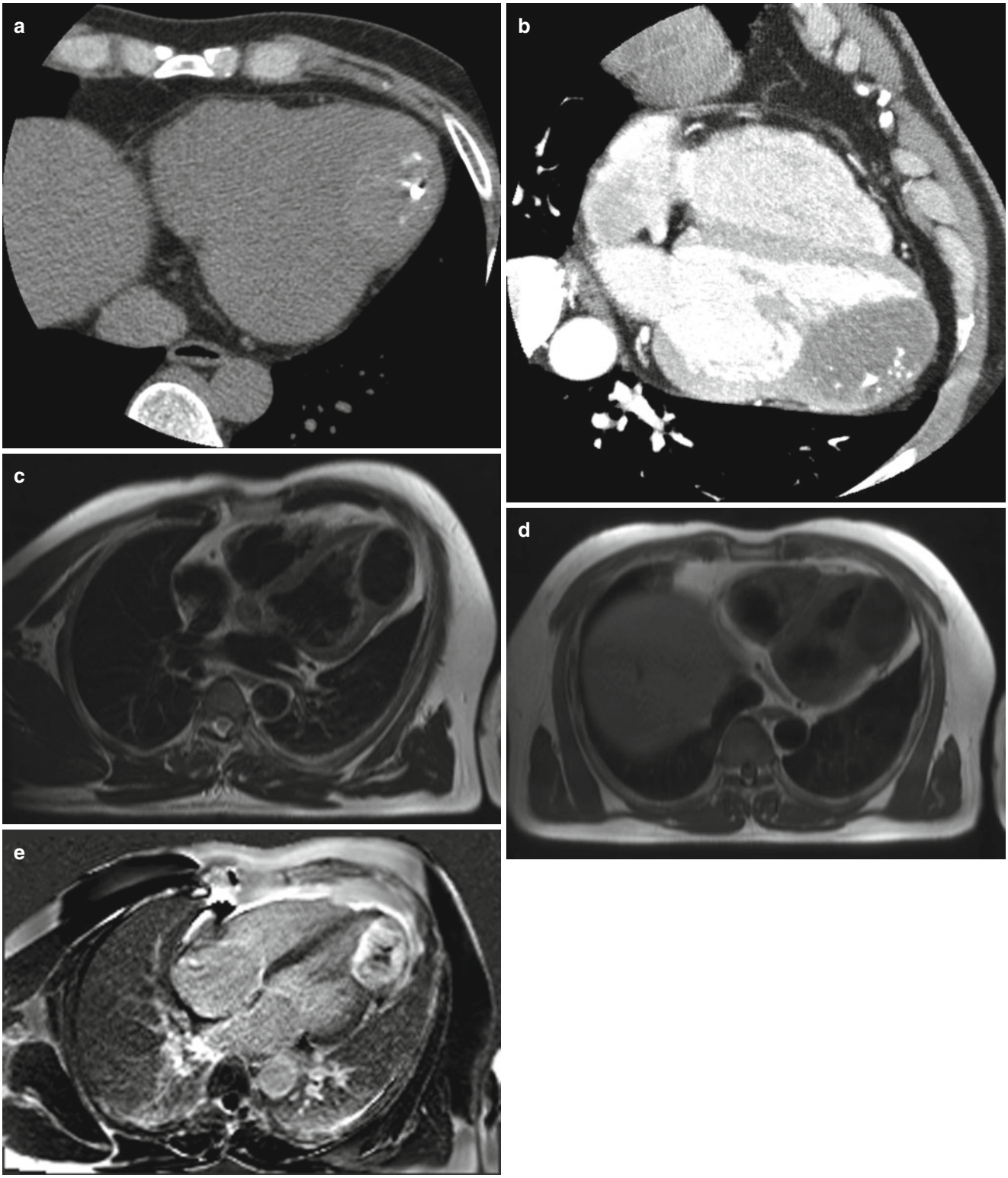

Fig. 19.5 Imaging characteristics of fibroma. (**a**) A non-contrast CT image shows a mass located at the cardiac apex. The mass is slightly high attenuated with central calcification. (**b**) In the contrast-enhanced CT image, the mass is not enhanced. (**c**) In MR T2WI, the mass shows "typical" very low signal intensity. (**d**) In T1WI, the mass shows hypo-signal intensity. (**e**) In delayed-enhancement image, the mass shows a very hyper-enhanced central low signal intensity lesion which is the same area of calcification on the CT image

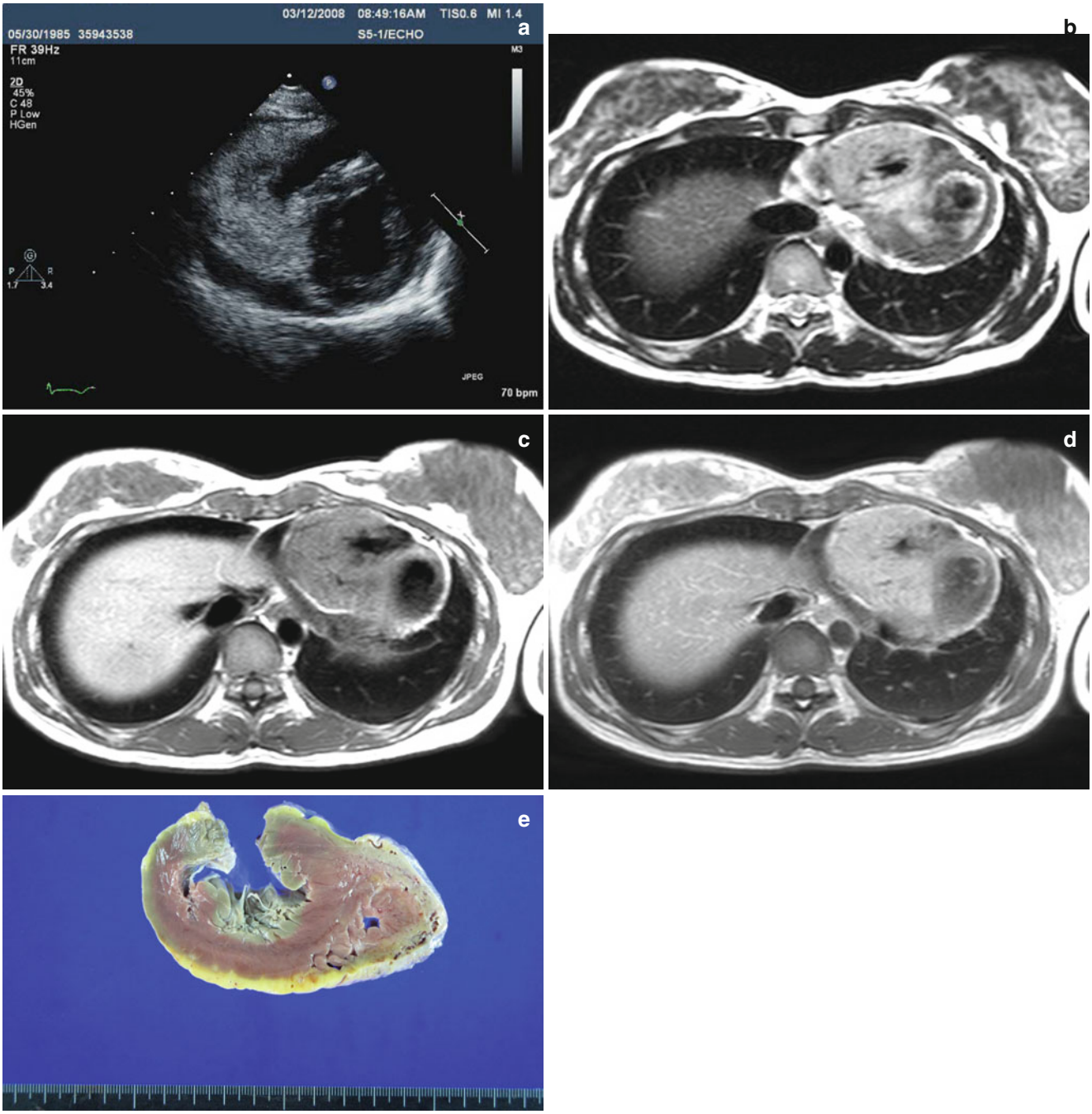

Fig. 19.6 Imaging findings of capillary hemangioma located in the myocardium-F24. (**a**) Short-axis image using transthoracic echocardiography shows highly echogenic, infiltrative mass at the right ventricle (http://extras.springer.com/2015/978-3-642-36396-2). (**b**) T2-weighted MR axial image shows a homogeneously hyper-signal intensity mass at the right ventricle. (**c**) T1-weighted MR axial image shows slightly hyper-signal intensity compared to the left ventricular myocardium. (**d**) Contrast-enhanced T1-weighted MR axial image shows a homogeneous hyper-enhancement of the mass. (**e**) The cut surface of the gross specimen of the right ventricle shows microcystic change and measures up to 1.5 cm in thickness. (**f**) Microscopic pathology of the mass shows diffuse proliferation of the capillaries without mass formation

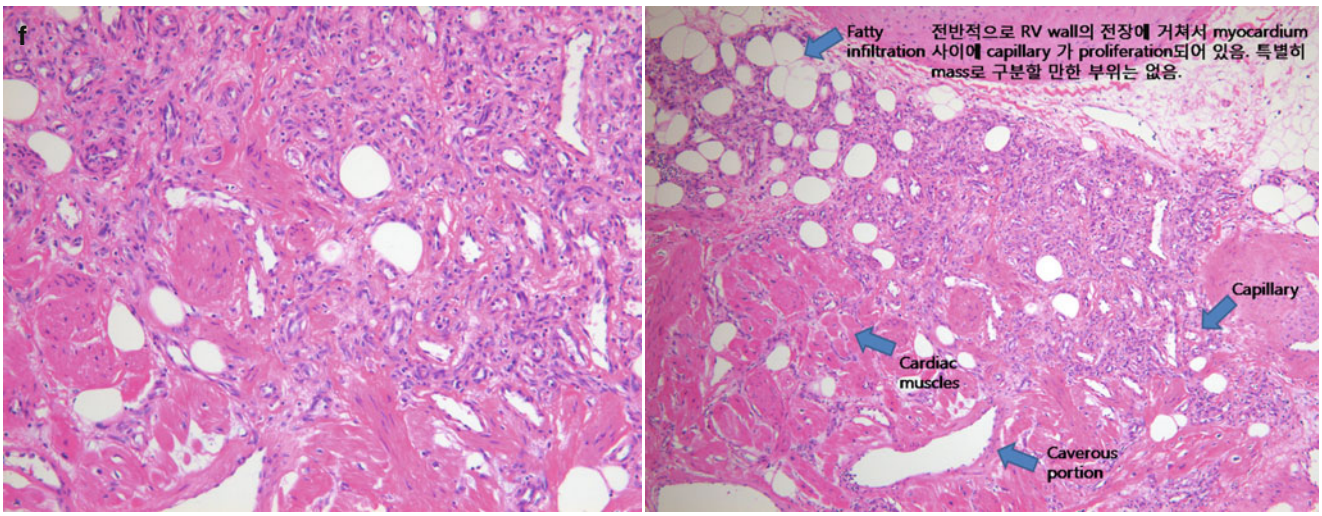

Fig. 19.6 (continued)

Learning Points
A capillary hemangioma has an infiltrative growth that is why it is usually mistaken as a malignant tumor such as lymphoma or sarcoma.

19.2.3.6 Lipoma

- Overview:
  - Mainly found in the adult; however, it is also found in children. The prevalence is not different between male and female.
  - The tumor can occur everywhere in the cavity, myocardium, or epicardium of the heart.
  - Clinical manifestations are variable. Pericardial effusion and cardiac tampon is possible when the tumor has an epicardial origin and growing to the pericardium. Obstructive symptoms are caused by its endocardial location and growth into the cavity. Generally asymptomatic.
  - Tumor size ranges from 1 to15 cm.
- Imaging findings:
  - Echocardiography – variable echogenicity
  - CT – very hypointense, which is same as lipid (below zero in CT number) [12].
  - MRI – hyper-signal in both T2WI and T1WI, which is suppressed using fat suppression pulse. No enhancement is seen in LGE [1] (Fig. 19.7).

19.2.3.7 Paraganglioma

- Overview:
  - Prevalent in the fourth and fifth decade of life.
  - Most prevalent location is the posterior mediastinum. Epicardium of the left atrium or left ventricle and the interatrial septum is also a possible location (along the parasympathetic ganglion).
  - Similar to the symptoms of pheochromocytoma due to secretion of catecholamine.
  - Usually hypervascular and invades the coronaries; therefore, surgical removal is difficult.
  - Necrosis is frequent and calcification is rare.
- Imaging findings:
  - MIBG scan is useful in localizing the tumor.
  - CT – heterogeneously low-attenuated mass.
  - MRI – hyper-signal in T2WI and iso-signal to hypo-signal in T1WI. The mass is hyper-enhanced in LGE without a necrotic portion [13].

19.2.4 Malignant Cardiac Tumors

- Overview:
  - Metastasis is common in malignant cardiac tumors.
  - Among primary malignant cardiac tumors, sarcomas consist 95 % of primary malignant tumor, and lymphoma is the second.
  - The right side of the heart is more commonly involved than the left side.

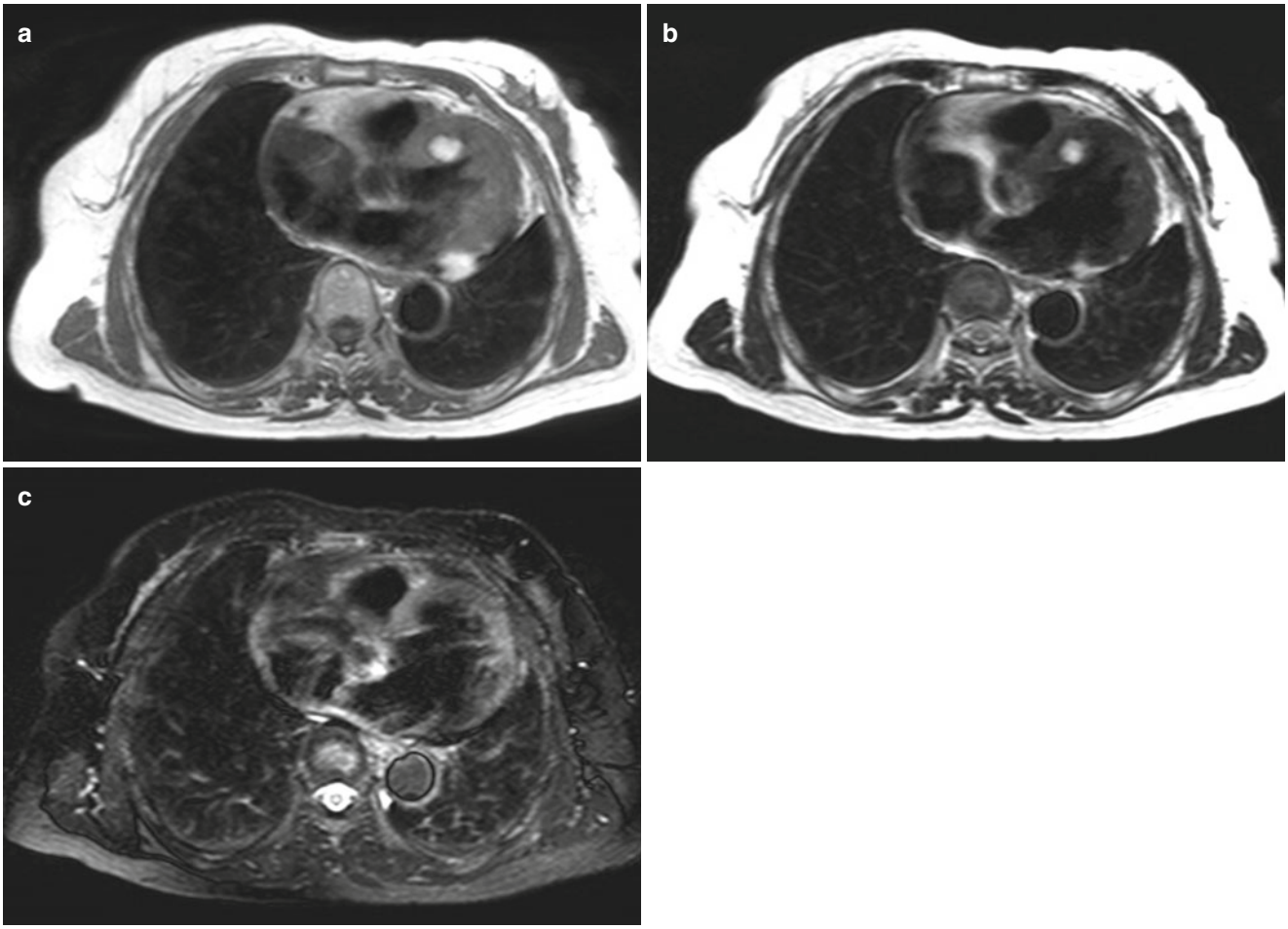

Fig. 19.7 CMR findings of cardiac lipoma. (**a**) T2WI and, (**b**) T1WI show round-shaped hyper-signal intensity mass located in the interventricular septum. (**c**) In the fat-suppressed T2WI, the mass signal is totally suppressed which is consistent with lipoma

  - Hemorrhage, necrosis, invasion, and pericardial effusion are frequently associated.
- Imaging findings:
  - Usually hyper-signal intensity on T2WI
  - Variable degree of hyper-enhancement on LGE

19.2.4.1 Sarcomas

- Angiosarcoma:
  - Overview:
    - Most common malignant cardiac tumor.
    - More prevalent in male than in female; rare in children.
    - Prevalent location is the right atrium; frequently invades the pericardium.
    - Signs and symptoms:
      - Right heart failure and cardiac tamponade
      - Fever, weight loss
      - Frequently accompanied with pericardial effusion; the pericardial effusion may be the only initial finding.
    - No effective treatment
  - Imaging findings:
    - Well-margined mass in the right atrial location
    - Diffuse infiltration in the pericardial location
    - CT – low-attenuated mass, irregular and nodular shape, heterogeneous enhancement
    - MRI:
      - Iso-signal, nodular lesion in both T2WI and T1WI ("cauliflower" appearance) [14]
      - Linear enhancement with diffuse pericardial invasion ("sunray" appearance) (Figs. 19.8 and 19.9)

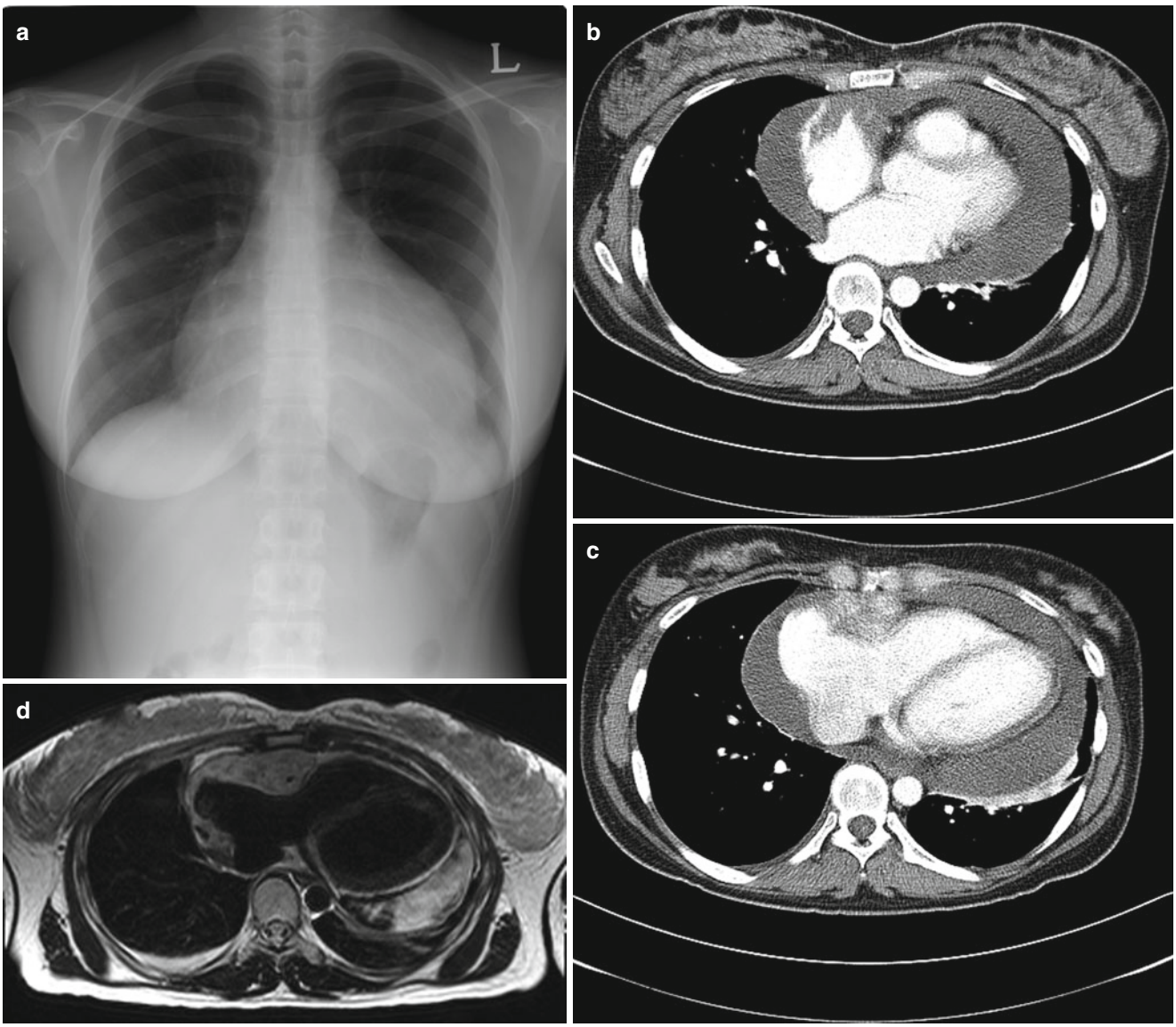

Fig. 19.8 Imaging findings on chest radiography and CMR of angiosarcoma. (**a**) Chest radiography shows cardiomegaly without pleural effusion or increased pulmonary vascularity. (**b**, **c**) CT axial images show lobulated and hyper-enhanced mass around the right atrioventricular groove. The mass invades the RVOT wall. (**d**) In axial T2-weighted MR image, the mass shows hyper-signal intensity compared with the myocardium and infiltrative growth. The right coronary artery is encased by the mass. (**e**) In the axial T1-weighted MR image, the mass shows iso-signal intensity compared with the myocardium. (**f**) In the contrast-enhanced axial T1-weighted MR image, the mass shows heterogeneity and hyper-enhancement. (**g**) Microscopic pathology of the mass shows a large nucleus with dysmorphism and vessel making malignancy or angiosarcoma

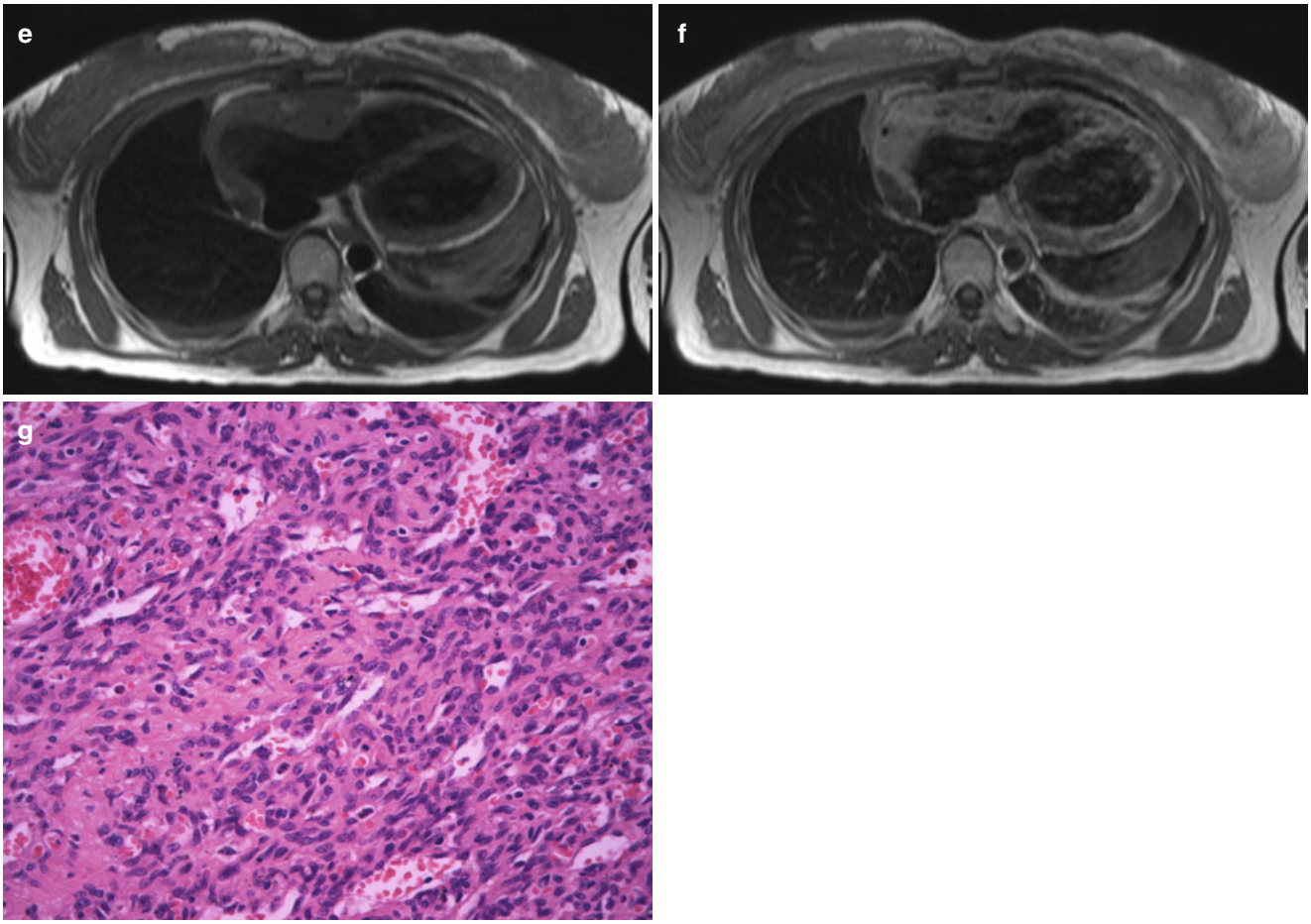

Fig. 19.8 (continued)

Learning Points
The typical MRI signal intensity and enhancement of the angiosarcoma.

- Rhabdomyosarcoma:
  - Overview:
    - Most common primary malignant tumor in childhood
    - Common location – cavity and cardiac valves
    - Multiple masses, nodular growth (cf. angiosarcoma – diffuse growth)
  - Imaging findings:
    - CT – low-attenuated mass with smooth or irregular margin
    - MRI – usually iso-signal compared with the myocardium [15]
    - Differential diagnosis – myxoma
- Fibrosarcoma:
  - Consists 5 % of primary malignant tumor
  - Often invades the left atrium, with valve involvement in more than 50 % of cases – valvular stenosis symptom
  - Imaging findings:
    - CT – low-attenuated mass [16]
    - MRI – heterogeneous iso-signal compared with the myocardium
- Osteosarcoma
  - Overview:
    - Consists 3–9 % of cardiac sarcomas
    - Commonly found in the left atrium and results in heart failure
  - Imaging findings:
    - CT:
      - Low-attenuated mass with dense calcification.
      - Calcification can be mistaken as dystrophic calcification in early period [17].

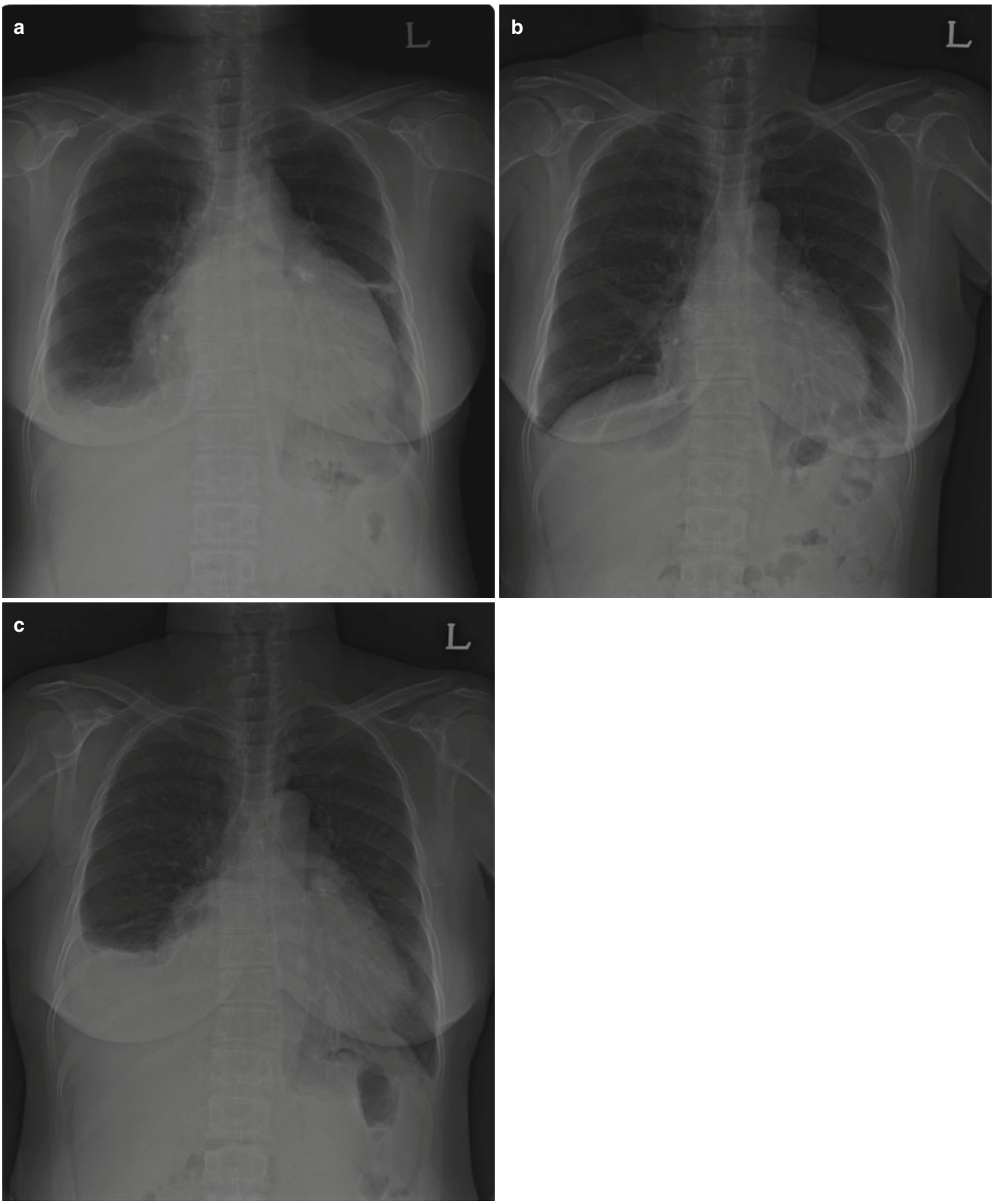

Fig. 19.9 Angiosarcoma initially presented as pericardial effusion. (**a**) On June 2007, severe cardiomegaly with bilateral pleural effusion and linear atelectasis at the left middle lung zone is seen. (**b**) One month later, the size of the heart as well as the amount of bilateral pleural effusion is decreased. (**c**) Another 7 months later, cardiomegaly and bilateral pleural effusion is aggravated. (**d**) Axial image of CT at the same time as A shows marked amount of pericardial effusion and bilateral pleural effusion. However, there is no mass of the heart. (**e**) Axial CT image at the time of C shows diffuse soft tissue mass along the ruptured right atrial wall and right pleural effusion. (**f**) Gross specimen of the mass. (**g**) Microscopic pathology of the mass shows a large nucleus with dysmorphism and vessel making malignancy or angiosarcoma

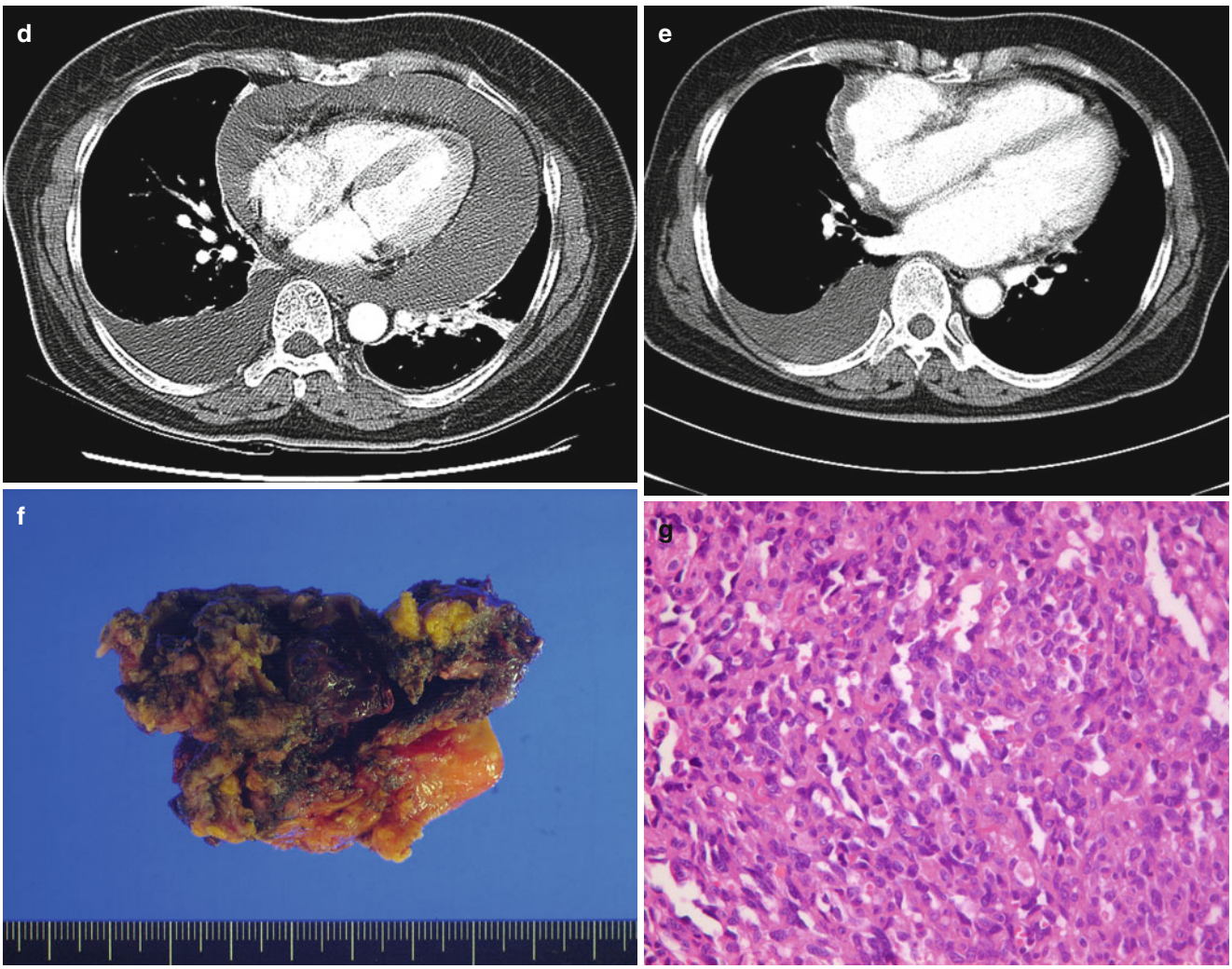

Fig. 19.9 (continued)

- MRI:
  - Heterogenous signal in both T2WI and T1WI.
  - Large base and invasiveness are differential points of myxoma.
- Leiomyosarcoma:
  - Overview:
    - Consists 8–9 % of cardiac sarcomas.
    - Originated from the smooth muscle of the pulmonary vein or pulmonary artery. Endocardial origin is possible.
    - Prevalent location is the left atrium.
  - Imaging findings:
    - CT – lobulated and heterogeneously hypointense mass
    - MRI – hyper-signal in T2WI; iso-signal in T1WI [18]
- Liposarcoma:
  - Imaging findings:
    - No demonstrable fat component
    - Necrosis and/or hemorrhage
- Undifferentiated sarcoma (Fig. 19.10):

19.2.4.2 Lymphoma

- Overview:
  - Extranodal non-Hodgkin's lymphoma, which is exclusively located in the heart or pericardium.
  - Almost all primary lymphomas are B-cell lymphomas.
  - Most often in immunocompromised patients, in whom it is highly aggressive.
  - Early chemotherapy seems to be effective. Although primary cardiac lymphoma is rare, it is mandatory to suspect this entity in the differential diagnosis.

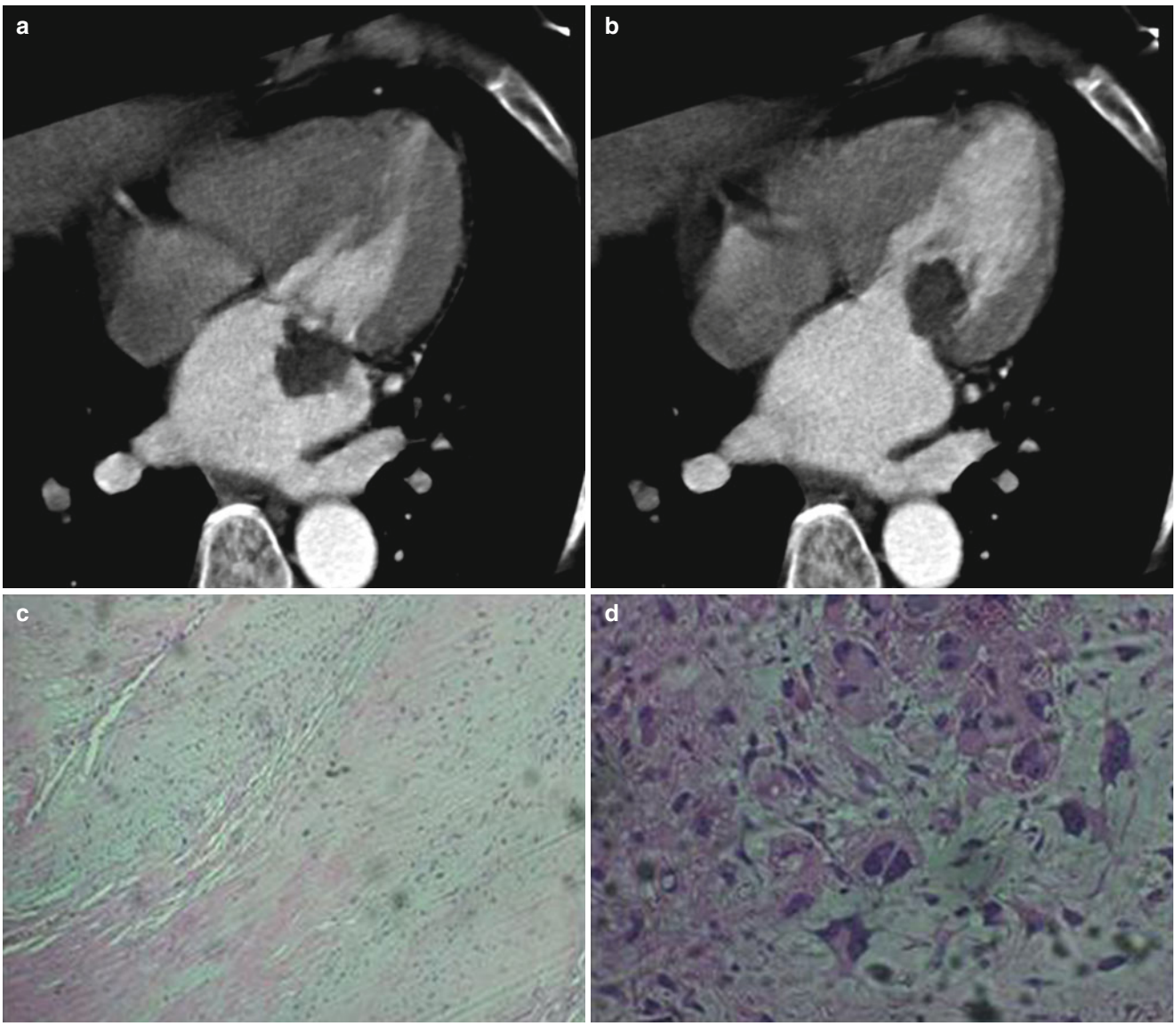

Fig. 19.10 Myxosarcoma. (**a**) End-systolic and, (**b**) mid-diastolic phase axial CT images show lobulated mass attached to the mitral valve annulus. The mass does not show a pedicle. (**c**, **d**) Microscopic image shows that the mass has a bluish or myxoid background (**c**) with atypical cells (**d**) that is consistent with myxosarcoma

- Imaging findings:
  - Location – most often on the right side of the heart, especially in the right atrium, also found in other chambers.
  - Large pericardial effusion is frequently associated – may be the only sign of the lymphoma.
  - Variable morphology from circumscribed polypoid to ill-defined infiltrative lesions.
  - CT – low-attenuated or isodense compared with the myocardium, with and heterogeneous enhancement. [19]
  - MRI – hyper-signal in T2WI, hypo-signal in T1WI, variable enhancement [20] (Fig. 19.11).

Fig. 19.11 CT and CMR findings of cardiac lymphoma. (**a**) Axial and, (**b**) short-axis CT image show diffuse proliferation of soft tissue mass that infiltrates to the left ventricular muscle. The left circumflex artery is also encircled but does not show compression by the mass. Pericardial thickening and effusion are also seen. (**c**) Short-axis view of T2WI and, (**d**) short-axis view T1WI show slightly hyper-signal intensity infiltrative mass with pericardial effusion. (**e**) In the delayed-enhancement image, the mass shows heterogeneous enhancement. The biopsy confirmed diffuse large B-cell lymphoma (Fig. 19.12)

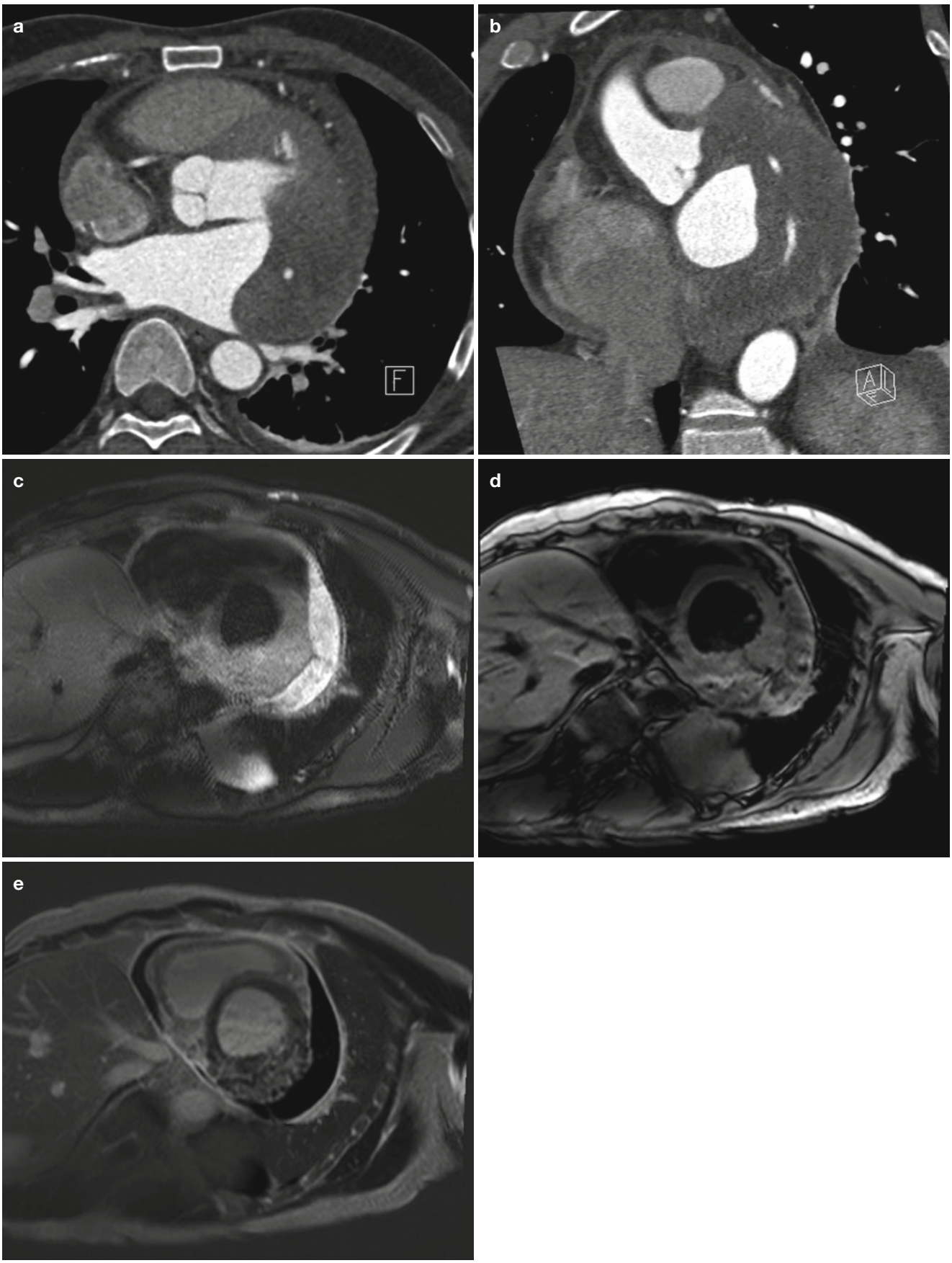
a
b
c
d
e

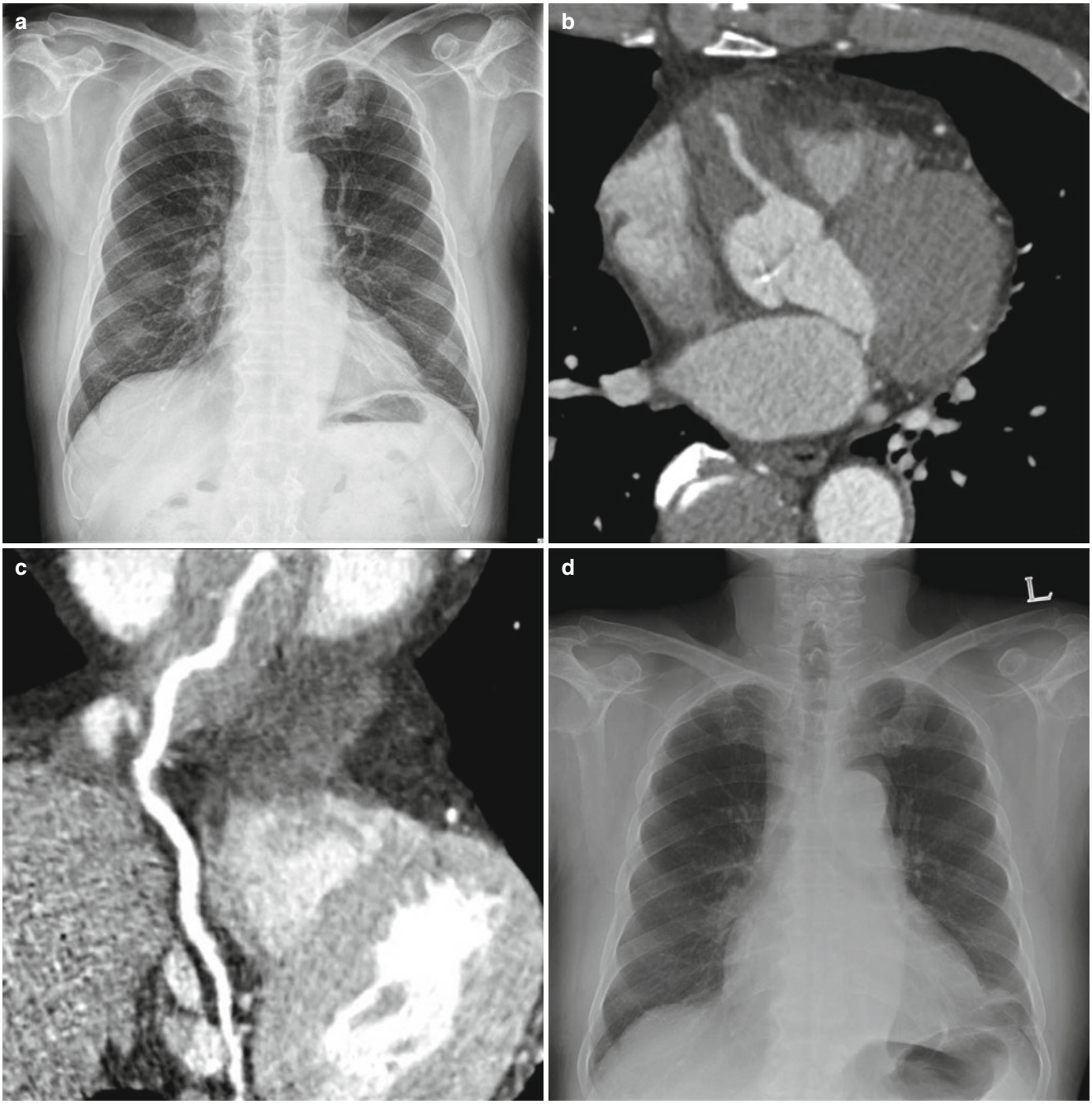

Fig. 19.12 CT and CMR findings of cardiac lymphoma in a time period. (**a**) Chest radiograph acquired 1 month ago shows hypertensive heart configuration, but no cardiomegaly or increased pulmonary vascularity were seen. (**b**, **c**) CT coronary angiographies acquired 1 month ago show homogeneously enhancing soft tissue lesion surrounding the right coronary artery. But the right coronary artery was widely patent and there was no infiltration by the mass on the axial multiplanar reformatted (MPR) image (**b**) and the curved planar reformatted image (**c**). (**d**) Chest radiograph shows moderate cardiomegaly and left pleural effusion. (**e**) CT coronary angiography also shows a markedly growing mass, compressing the right atrium and extending to the interatrial and interventricular septum on the axial MPR image. However, the patency of the right coronary artery remains good. The biopsy confirmed diffuse large B-cell lymphoma

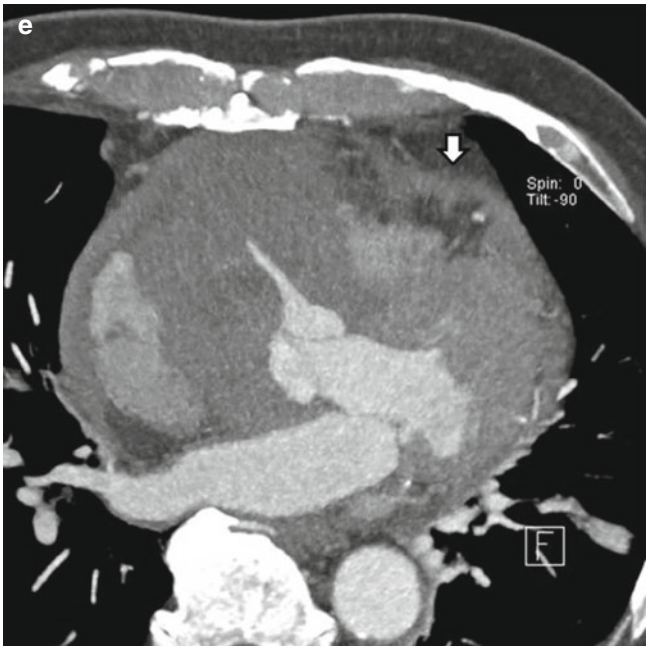

Fig. 19.12 (continued)

19.2.4.3 Metastasis

- The most common primary origins are lung cancer and breast cancer. Others are melanoma, lymphoma, and leukemia. [1].
- Pathway – usually by lymphatic metastasis. Hematogenous metastasis and direct invasion is possible.
- Clinical manifestations:
  - Effusion can be the only sign. Therefore, when pericardial effusion of unknown cause is found, malignancy has to be considered in the differential diagnosis.
  - When cardiac valve is affected, symptoms of vauvular heart disease can be manifested in earlier phase.

19.3 Differential Diagnosis

Prominent AV groove (see Normal Anatomy)
Eustachian, Thebesian valve (see Normal Anatomy)
Artifact
Lipomatous hypertrophy (Fig. 19.13) [21]:
Chiari network (Fig. 19.14)
Inflammatory pseudotumor (Fig. 19.15), giant cell myocarditis
Infective endocarditis (see Disease of the Aortic Valve)
Thrombus (also see Chronic Myocardial Infarction) [22, 23]

- Clinical aspect:
  - Most common intracardiac mass.
  - Location – most frequently the left ventricle and left atrium.
    - Left ventricle – after myocardial infarction, dilated cardiomyopathy
    - Left atrium – atrial fibrillation
    - Other factors that cause stasis of blood in the cavity
  - Embolism is the main concern of thrombus.
- Imaging techniques and findings:
  - MRI has advantages on detecting a thrombus.
    - Gradient echo imaging using T2* shows a low signal intensity thrombus.
    - LGE with "long TI" – null the signal of thrombus [22].
    - Post-enhancement image – tumor is usually enhanced, but thrombus is not (Fig. 19.16).

19.4 Summary

Differential diagnosis of cardiac tumors and "tumor-like" lesions according to their location (modified using [1])

Location	Probable diagnosis
Right atrium	Metastasis
	Angiosarcoma
	Thrombus
	Chiari network
	Eustachian and Thebesian valve
Left atrium	Myxoma
	Thrombus
	Septal lipoma
	Lipomatous hypertrophy
	Paraganglioma
Right ventricle	Thrombus
	Rhabdomyoma
	Angiosarcoma
Left ventricle	Thrombus
	Papillary muscles
	Rhabdomyoma
	Metastasis
	Fibroma
Cardiac valves	Degenerated valve leaflet
	Infective endocarditis
	Thrombus
	Papillary fibroelastoma

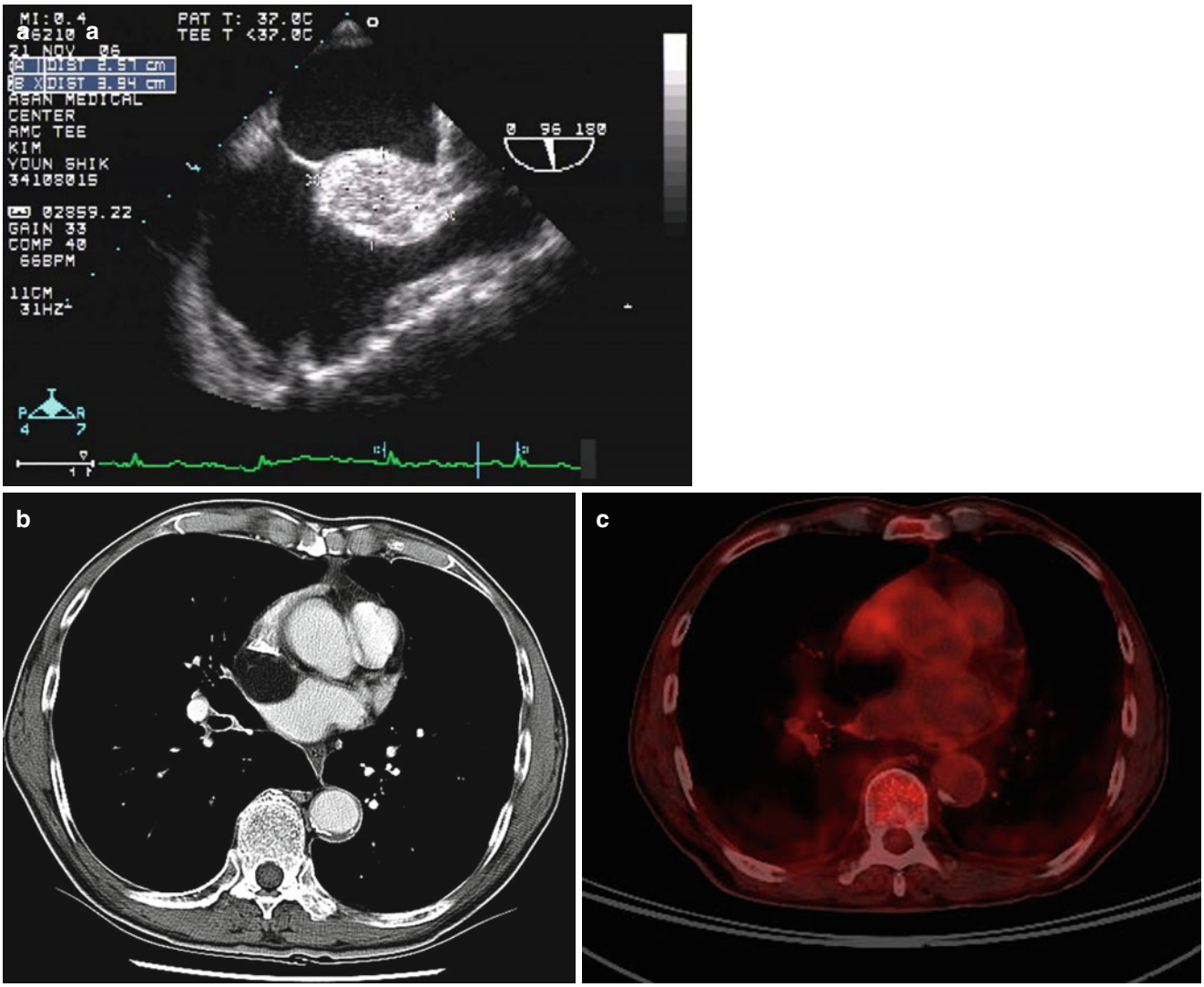

Fig. 19.13 Lipomatous hypertrophy at the interatrial septum. (**a**) Transesophageal echocardiography shows highly echogenic and ovoid mass located in the interatrial septum. (**b**) Axial CT image shows a low-attenuated ovoid-shaped mass. The CT number of the mass was −100 HU that is highly suggestive of lipid. The mass is extended to the epicardial fat. (**c**) PET-CT image shows no FDG uptake of the mass

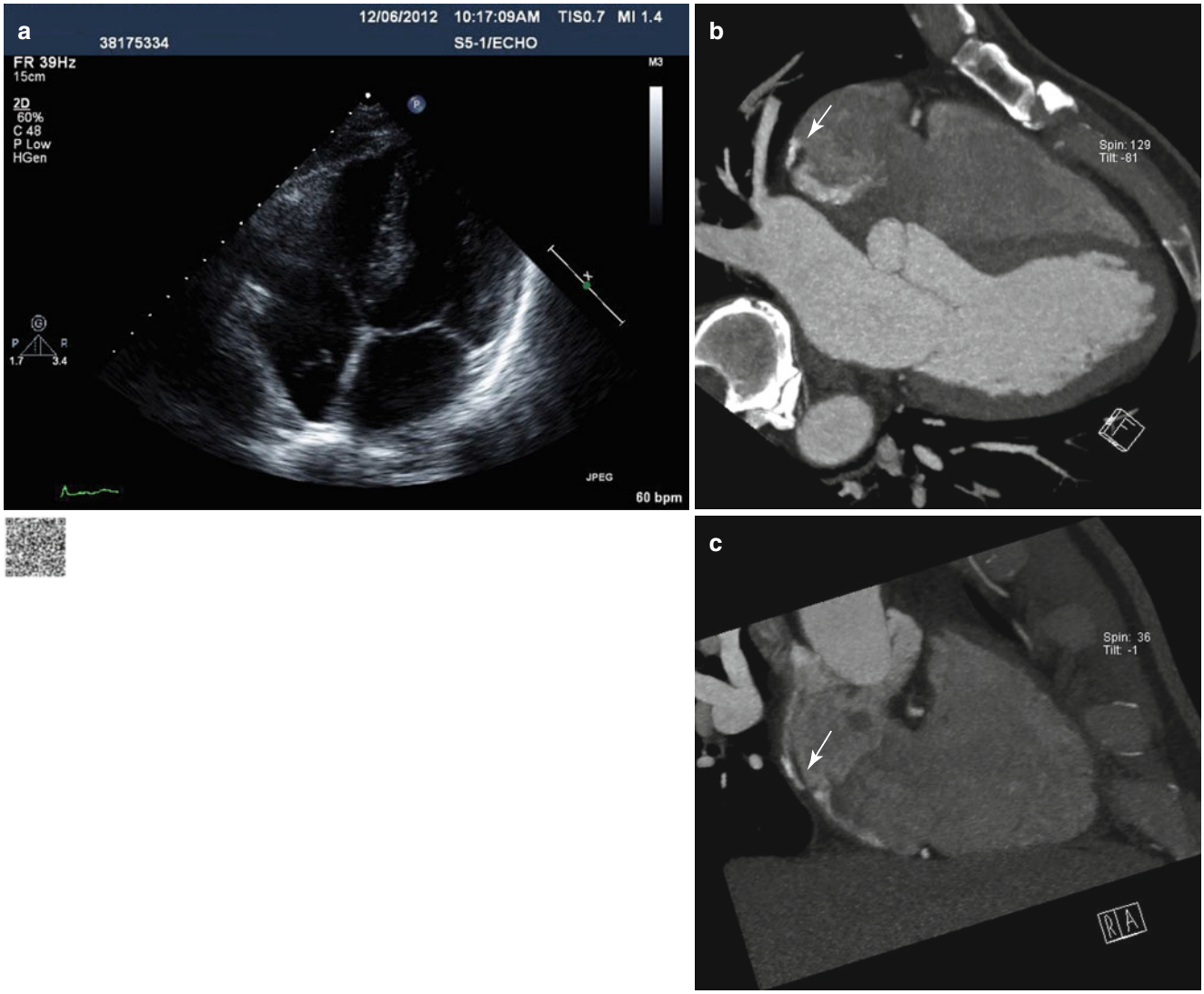

Fig. 19.14 Chiari network. (**a**) Four-chamber view image using transthoracic echocardiography shows the echogenic curvilinear structure attached to the right atrium. This structure shows hypermobility during the cardiac cycle in the cine image (http://extras.springer.com/2015/978-3-642-36396-2). Myxoma, thrombus, or other cardiac tumors were considered as differential diagnosis. (**b**) Four-chamber view and, (**c**) two-chamber view of CT show a low-attenuated curvilinear structure that is attached to the right atrial wall (*arrow*)

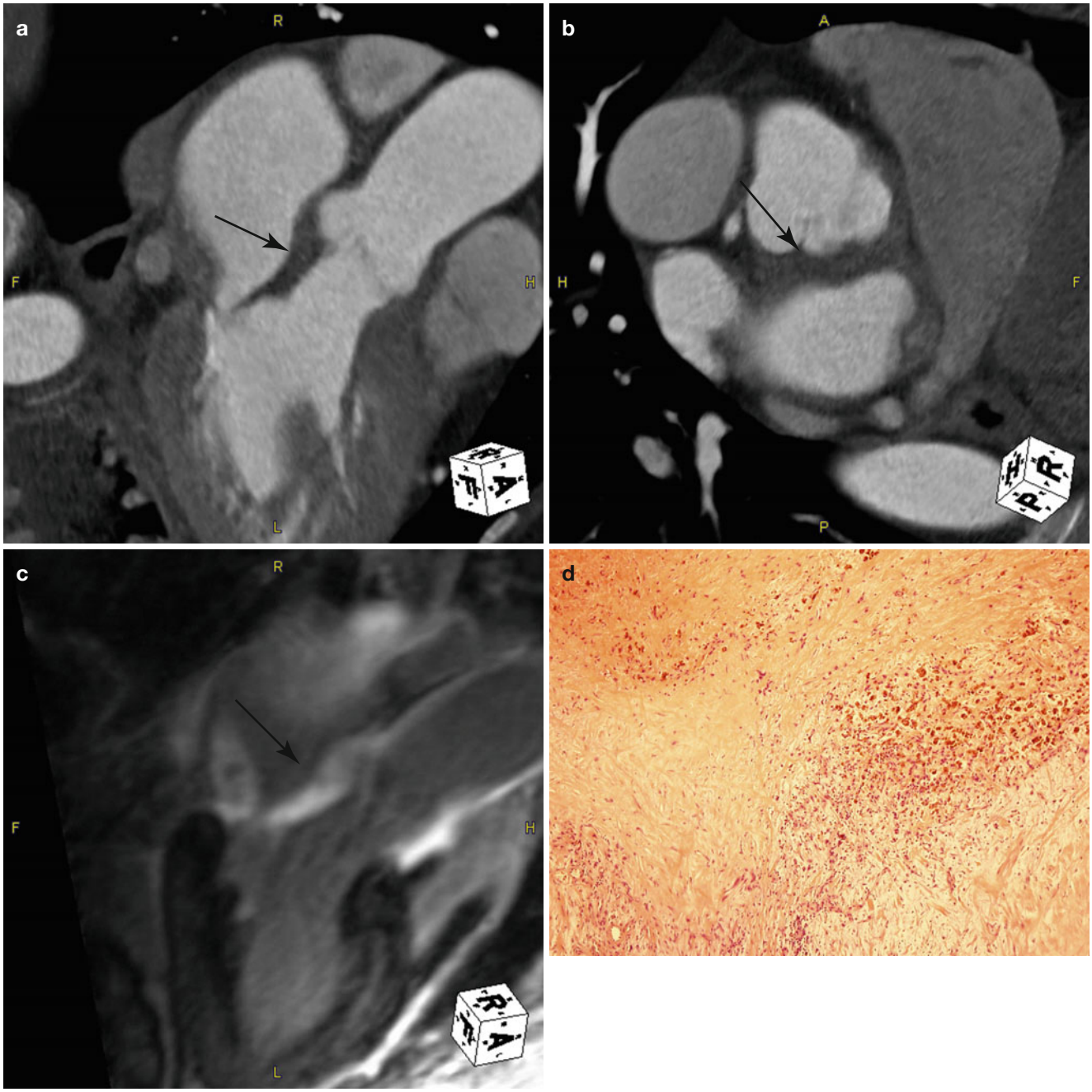

Fig. 19.15 Inflammatory pseudotumor. (**a**) Three-chamber view and, (**b**) short-axis view CT images show diffuse proliferation of soft tissue along the left atrial wall, mitral-aortic interventricular fibrosa, and aortic root. (**c**) Delayed-enhancement MR image shows diffuse hyperenhancement of the lesion [*arrow* in (**a**), (**b**), and (**c**)]. (**d**) Microscopic image shows proliferation of spindle cells, fibroblasts, and chronic inflammatory cells replacing the normal myocardium

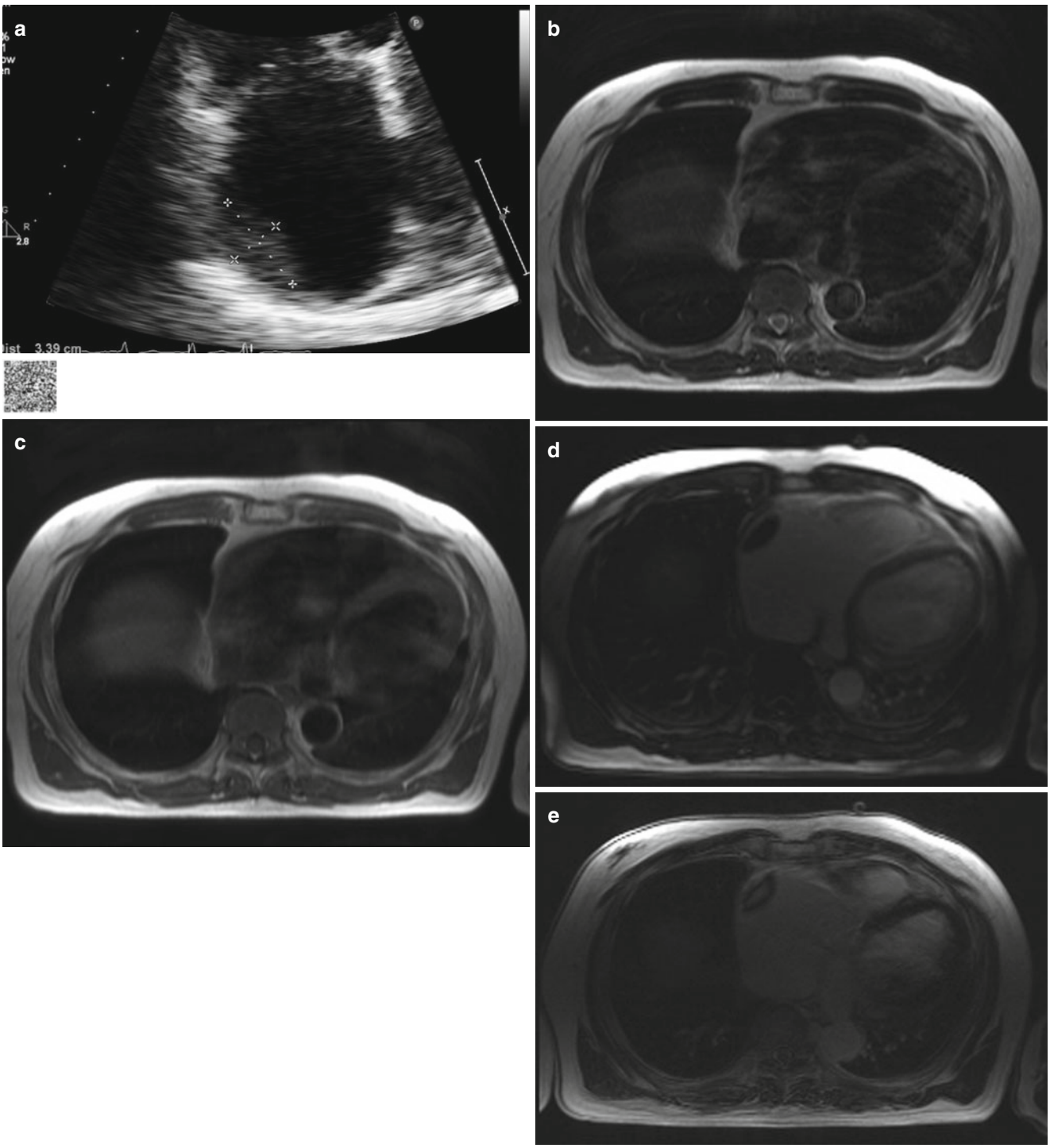

Fig. 19.16 Cardiac thrombus in the right atrium in a patient having hepatic cholangiocarcinoma. (**a**) Transthoracic echocardiography shows an ovoid, echogenic mass in the right atrium. This mass is not mobile at cine image (http://extras.springer.com/2015/978-3-642-36396-2). (**b**) T2WI and, (**c**) T1WI show that this lesion has an iso-signal intensity compared to the normal myocardium. (**d**) Gradient echo image with long inversion time (TI=600 ms) shows dark signal intensity of the mass. (**e**) Delayed-enhancement image shows that this lesion has a dark signal rim. After anti-coagulation therapy, this lesion disappeared

References

1. Sparrow PJ, Kurian JB, Jones TR, Sivananthan MU. MR imaging of cardiac tumors. Radiographics. 2005;25:1255–76.
2. Choi BW. Cardiovascular tumors. In: Park JH, editor. Cardiovascular imaging. Seoul: Ilchokak; 2008. p. 312–32.
3. Buckley O, Madan R, Kwong R, Rybicki FJ, Hunsaker A. Cardiac masses, part 1: imaging strategies and technical considerations. AJR Am J Roentgenol. 2011;197:W837–41.
4. Kramer CM, Barkhausen J, Flamm SD, Kim RJ, Nagel E. Standardized cardiovascular magnetic resonance imaging (CMR) protocols, society for cardiovascular magnetic resonance: board of trustees task force on standardized protocols. J Cardiovasc Magn Reson. 2008;10:35.
5. Reynen K. Cardiac myxomas. N Engl J Med. 1995;333:1610–7.
6. Grebenc ML, Rosado-de-Christenson ML, Green CE, Burke AP, Galvin JR. Cardiac myxoma: imaging features in 83 patients. Radiographics. 2002;22:673–89.
7. Grebenc ML, de Christenson Rosado ML, Burke AP, Green CE, Galvin JR. Primary cardiac and pericardial neoplasms: radiologic-pathologic correlation. Radiographics. 2000;20:1073–103; quiz 1110–71, 1112.
8. Alkadhi H, Leschka S, Hurlimann D, Jenni R, Genoni M, Wildermuth S. Fibroelastoma of the aortic valve. Evaluation with echocardiography and 64-slice CT. Herz. 2005;30:438.
9. Fujita N, Caputo GR, Higgins CB. Diagnosis and characterization of intracardiac masses by magnetic resonance imaging. Am J Card Imaging. 1994;8:69–80.
10. Yan AT, Coffey DM, Li Y, et al. Images in cardiovascular medicine. Myocardial fibroma in gorlin syndrome by cardiac magnetic resonance imaging. Circulation. 2006;114:e376–9.
11. Lo LJ, Nucho RC, Allen JW, Rohde RL, Lau FY. Left atrial cardiac hemangioma associated with shortness of breath and palpitations. Ann Thorac Surg. 2002;73:979–81.
12. Kamiya H, Ohno M, Iwata H, et al. Cardiac lipoma in the interventricular septum: evaluation by computed tomography and magnetic resonance imaging. Am Heart J. 1990;119:1215–7.
13. Fisher MR, Higgins CB, Andereck W. MR imaging of an intrapericardial pheochromocytoma. J Comput Assist Tomogr. 1985;9:1103–5.
14. Kim EE, Wallace S, Abello R, et al. Malignant cardiac fibrous histiocytomas and angiosarcomas: MR features. J Comput Assist Tomogr. 1989;13:627–32.
15. Siripornpitak S, Higgins CB. MRI of primary malignant cardiovascular tumors. J Comput Assist Tomogr. 1997;21:462–6.
16. Shih WJ, McCullough S, Smith M. Diagnostic imagings for primary cardiac fibrosarcoma. Int J Cardiol. 1993;39:157–61.
17. Chaloupka JC, Fishman EK, Siegelman SS. Use of CT in the evaluation of primary cardiac tumors. Cardiovasc Intervent Radiol. 1986;9:132–5.
18. Durand E, Vanel D, Mousseaux E, Meingan P, Fornes P, Bittoun J. A recurrent left atrium leiomyosarcoma. Eur Radiol. 1998;8:97–9.
19. Dorsay TA, Ho VB, Rovira MJ, Armstrong MA, Brissette MD. Primary cardiac lymphoma: CT and MR findings. J Comput Assist Tomogr. 1993;17:978–81.
20. Tada H, Asazuma K, Ohya E, et al. Images in cardiovascular medicine. Primary cardiac B-cell lymphoma. Circulation. 1998;97:220–1.
21. Heyer CM, Kagel T, Lemburg SP, Bauer TT, Nicolas V. Lipomatous hypertrophy of the interatrial septum: a prospective study of incidence, imaging findings, and clinical symptoms. Chest. 2003;124:2068–73.
22. Weinsaft JW, Kim HW, Shah DJ, et al. Detection of left ventricular thrombus by delayed-enhancement cardiovascular magnetic resonance prevalence and markers in patients with systolic dysfunction. J Am Coll Cardiol. 2008;52:148–57.
23. Hong YJ, Hur J, Kim YJ, et al. The usefulness of delayed contrast-enhanced cardiovascular magnetic resonance imaging in differentiating cardiac tumors from thrombi in stroke patients. Int J Cardiovasc Imaging. 2011;27 Suppl 1:89–95.

Pericardial Disease

20

Hwan Seok Yong and Heon Lee

Contents

Abstract

The pericardium consists of two layers of fibrous sac – an inner visceral and outer parietal layer – which enclose the pericardial cavity. Pericardial disease is an important cause of morbidity and mortality in patients with cardiovascular disease and can present clinically as inflammatory diseases of the pericardium with a spectrum ranging from acute pericarditis to chronic constrictive pericarditis, pericardial effusion, and cardiac tamponade. Other important entities that involve the pericardium include benign and malignant pericardial masses, pericardial cysts, and diverticula, as well as congenital absence of the pericardium. The accurate and precise diagnosis of pericardial disease is important to proper management of the patients but still remains a clinical challenge. While transthoracic echocardiography is considered the first-line test for identifying some pericardial diseases, with ongoing advances in technology, cardiac CT and MRI are more widely available and provide novel and complementary information in the aspect of anatomical and functional features of diseased pericardium to aid in determining the etiology. In this chapter, a brief clinical overview and associated various imaging findings of pericardial diseases will be reviewed with a special emphasis on CT findings.

20.1 Normal Anatomy and Physiology

- The pericardium covers not only cardiac chambers but also the proximal ascending aorta and pulmonary trunk.
- The pericardium consists of two layers of fibrous sac – an inner visceral and outer parietal layer – which enclose the pericardial cavity.
- The inner visceral layer (epicardium) intimately adheres to the surface of the heart.
- The outer parietal layer (pericardium) consists of outer fibrocartilaginous fibrosa and inner mesothelium-lined serosa.
- The normal pericardial thickness is less than 2 mm.

H.S. Yong
Department of Radiology, Korea University Guro Hospital, Korea University College of Medicine, Seoul, Republic of Korea
e-mail: yongtoki@korea.ac.kr

H. Lee (✉)
Department of Radiology, Soonchunhyang University Hospital, Bucheon, Republic of Korea
e-mail: acarad@naver.com

T.-H. Lim (ed.), *Practical Textbook of Cardiac CT and MRI*,
DOI 10.1007/978-3-642-36397-9_20, © Springer-Verlag Berlin Heidelberg 2015

- The function of the pericardium: lubrication and mechanical barrier of the heart.
- Relatively easily yielding to small amounts of distention.
- Resists further acute stretching (e.g., acute bleeding) and thus is prone to cardiac tamponade.

20.2 Imaging Findings of Pericardial Disease

20.2.1 Congenital Absence of the Pericardium

- Rare anomaly with reported prevalence of approximately 0.002–0.004 % in surgical and pathologic series.
- The defects are usually asymptomatic and classified as partial and complete. But most defects are partial and occur on the left side.
- Complete defects are of little clinical significance, but rarely, herniation of cardiac chambers through a partial defect of the pericardium can be fatal, presumably because of marked ischemia from compression of the coronary artery.
- Potential associated congenital abnormalities: atrial septal defect, patent ductus arteriosus, mitral valve stenosis, or tetralogy of Fallot.
- Although the pericardium is usually identified on cardiac CT and CMR, visualization at the most common site of defects, the lateral, posterior, and inferior left ventricular wall, can be limited because of a paucity of fat.
- Left-sided complete or sometimes partial absence of the pericardium allows interposition of lung tissue between the aorta and the main segment of the pulmonary artery, between the diaphragm and the base of the heart, and, occasionally, bulging of the left atrial appendage through the defect.
- Leftward cardiac displacement and excessive levorotation usually accompanies complete left pericardial absence and have been proposed as pathognomonic of complete type of defect. Nevertheless, cardiac displacement also can occur in left partial pericardial defects or can be absent in young children with complete pericardial defects (Fig. 20.1).

20.2.2 Pericardial Effusion/Hemorrhage /Cardiac Tamponade

- Originated from the obstruction of venous or lymphatic drainage.
- Common causes of pericardial effusion include heart failure, renal insufficiency, infection (bacterial, viral, or tuberculosis), neoplasm (carcinoma of lung or breast or lymphoma), and injury (from trauma or myocardial infarction).
- Echocardiography:
  - Considered the first-line test of pericardial effusion because of its high sensitivity, specificity, low cost, and lack of ionizing radiation.
  - Loculated effusion in an anterior location is difficult to detect.

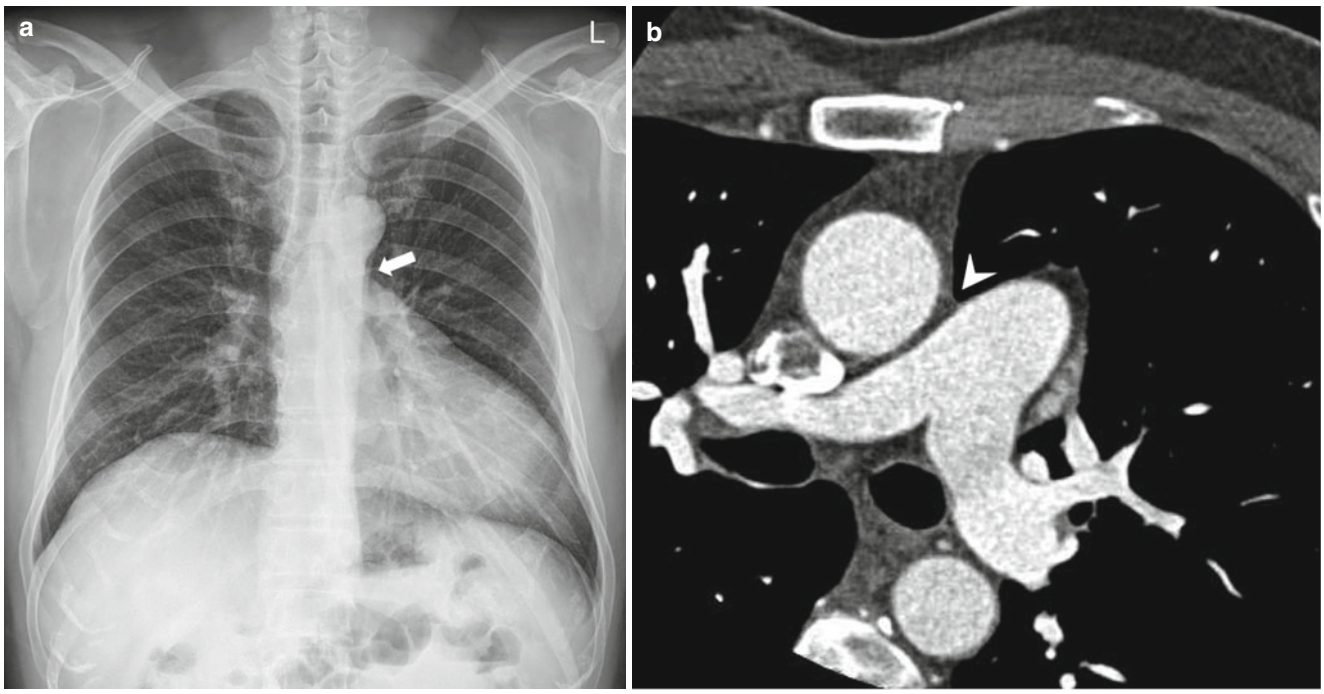

Fig. 20.1 Chest radiographs and CT of a patient with partial pericardial defect. (**a**) Chest PA view. The heart is displaced into the left chest; the right border of the heart is projected over that of the spine. There is abnormal deep notching (*arrow*) at the aortopulmonary window. (**b**) ECG-gated cardiac CT shows interposed lung tissue (*arrowhead*) between the ascending aorta and the pulmonary trunk

- Characterization of pericardial effusion composition by CT:
  - A fluid with attenuation similar to that of water is likely to be a simple effusion.
  - Pericardial effusion with attenuation greater than that of water suggests malignancy, hemopericardium, purulent exudate, or effusion associated with hypothyroidism.
  - Pericardial fluid with lower attenuation suggests the possibility of chylopericardium.
- Cardiac tamponade:
  - A life-threatening condition due to external cardiac compression that resulted from accumulation of pericardial fluid, pus, blood, gas, or tissue within the pericardial cavity.
  - Predisposing factors: trauma, inflammation, scarring, or neoplastic involvement of the pericardial space.
  - Imaging findings:
    - Enlargement of the superior vena cava with a diameter similar to or greater than that of the adjacent thoracic aorta
    - Enlargement of the IVC with a diameter greater than twice that of the adjacent abdominal aorta
    - Periportal lymphedema:
    - Reflux of contrast material within the IVC or the azygos vein
    - Enlargement of hepatic and renal veins (Figs. 20.2, 20.3, and 20.4)

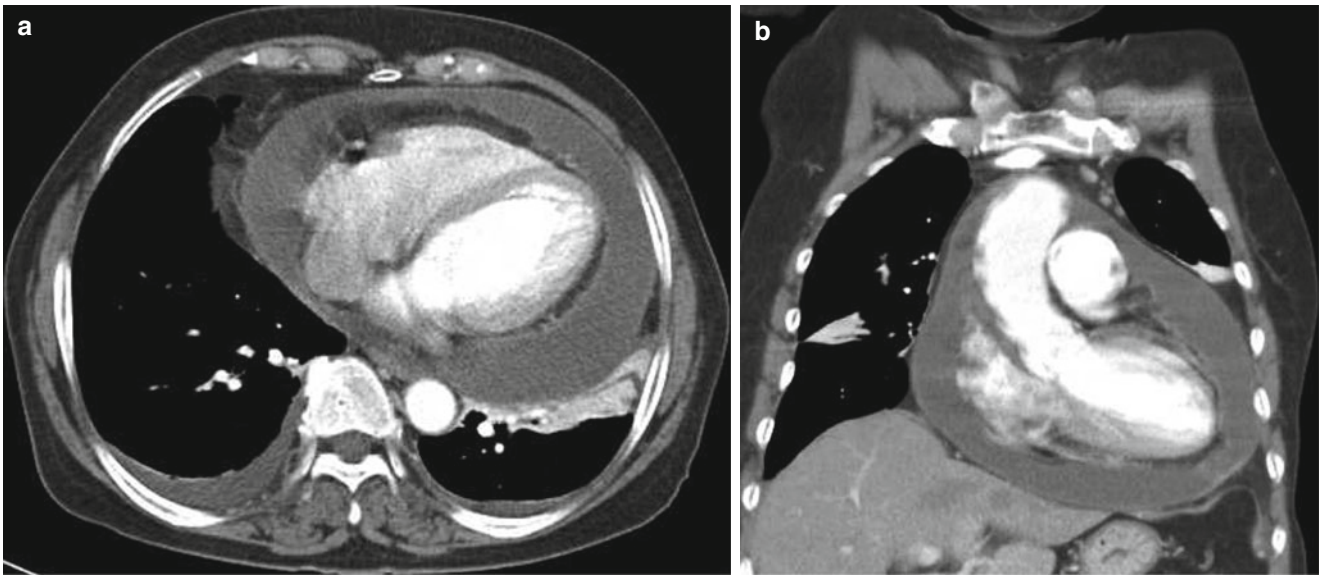

Fig. 20.2 Pericardial effusion. Axial (**a**) and coronal (**b**) CT images show large amount of pericardial effusion with a diffusely thickened pericardium. The attenuation of the pericardial effusion is grossly similar to that of pleural effusion

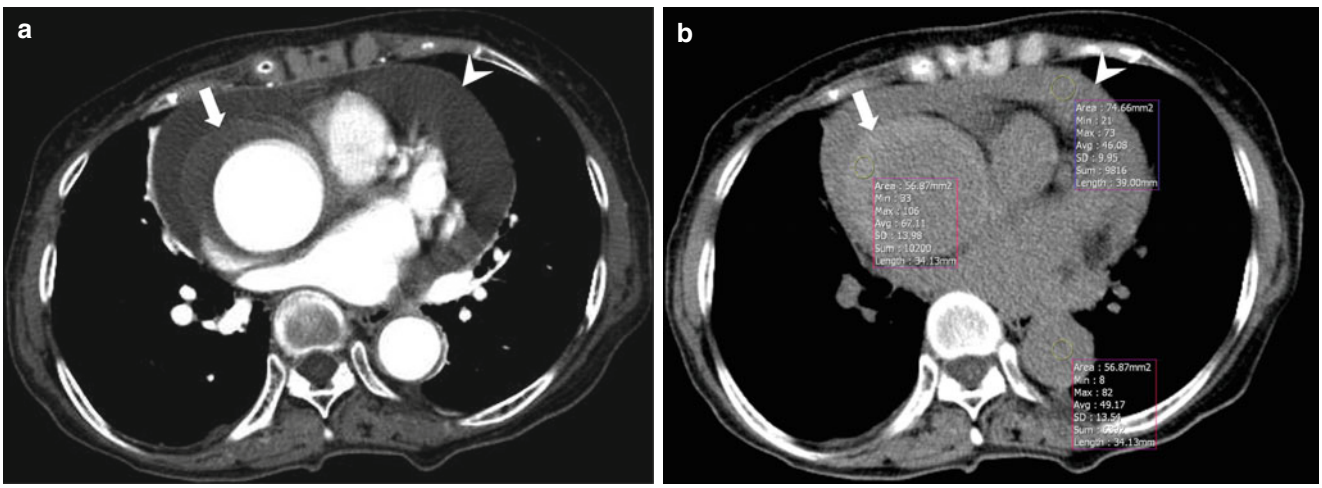

Fig. 20.3 Pericardial hemorrhage. (**a**) ECG-gated cardiac CT shows type A intramural hematoma (*arrow*) and small amount of pericardial effusion. (**b**) Precontrast CT shows high attenuating pericardial effusion suggesting hemorrhage (*arrowhead*). Note the high attenuation of the pericardial effusion (46 HU) which is similar to that of the lumen of the descending aorta (49 HU) and intramural hematoma (67 HU)

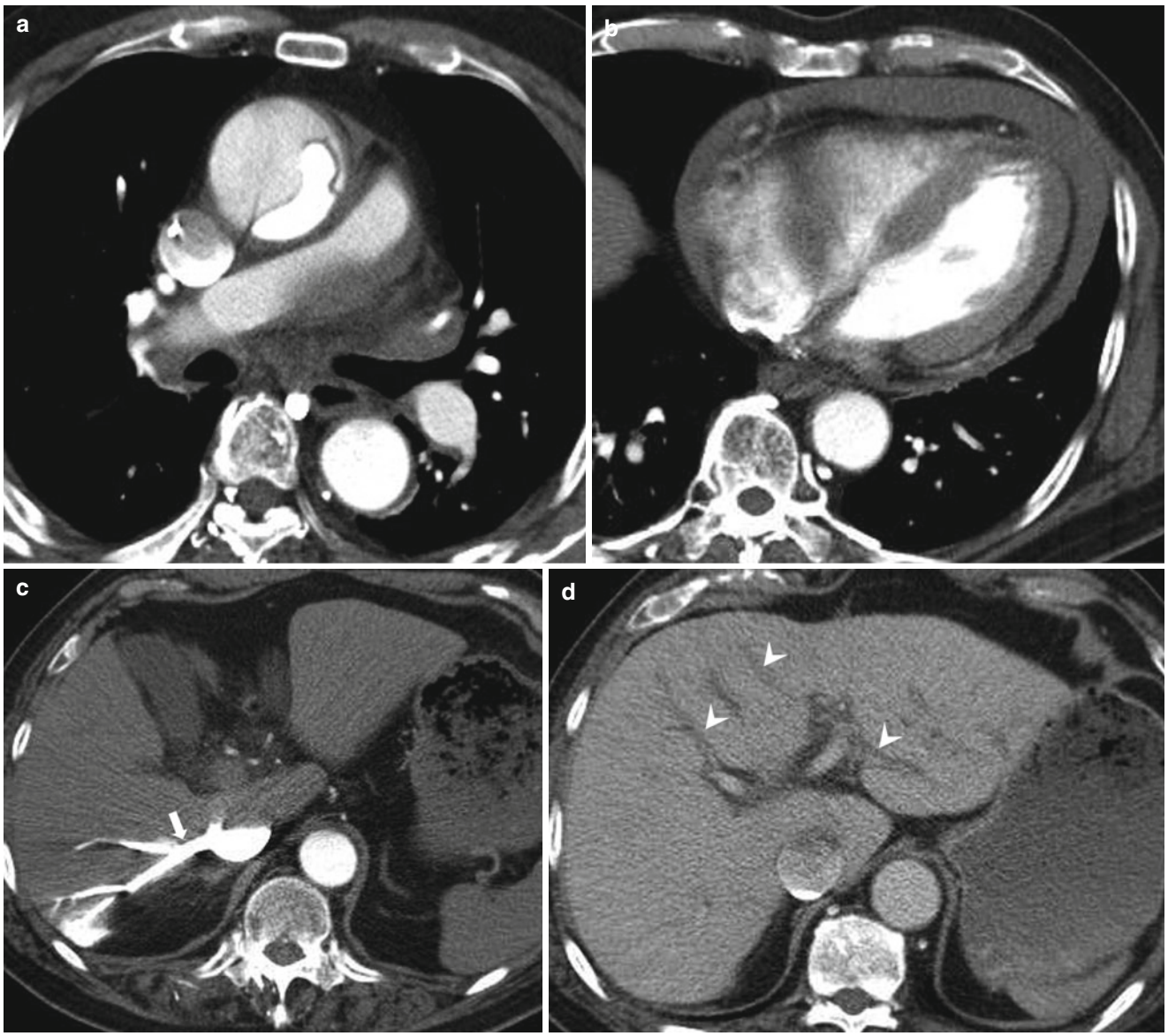

Fig. 20.4 Cardiac tamponade. (**a**) Cardiac CT angiography shows acute type A aortic dissection. (**b**) Axial CT image at the midportion of the left ventricle shows moderate amount of pericardial effusion and flattening of the anterior free wall of right ventricle. Arterial- (**c**) and delayed (**d**)-phase CT images at the liver level show contrast reflux (*arrow*) into the enlarged inferior vena cava and hepatic vein and periportal edema (*arrowheads*) which may be caused by increased right atrial pressure

20.2.3 Pericarditis

20.2.3.1 Acute Pericarditis

- Acute inflammation of the pericardium with or without associated pericardial effusion.
- Can occur as an isolated problem or as a manifestation of systemic disease.
- Echocardiography:
  - Often recommended because it provides a rapid and accurate assessment of the pericardium and underlying cardiac function.
  - The presence of effusion helps to confirm the diagnosis.
  - Can diagnose or exclude the cardiac tamponade physiology when effusion is identified.
- CT imaging:
  - Pericardial thickening is suggestive of acute pericarditis.
  - Pericardial irregularity may develop as the duration of inflammation increases.
  - In the case of pericardial effusion, initial characterization of fluid by attenuation.

  - Measurement: simple serous effusion usually has the same attenuation as water (0–25 HU).
  - Attenuation higher than 25 HU suggests a nonserous composition such as those seen in malignancy, hemopericardium, purulent exudates, or effusion associated with hypothyroidism (Fig. 20.5).

20.2.3.2 Constrictive Pericarditis

- End stage of an inflammatory process involving the pericardium that usually takes years to develop.
- Results in thickening, dense fibrosis, calcifications, and adhesion of the parietal and visceral pericardium.
- The most frequent causes are cardiac surgery and radiation therapy.
- Others include infection (viral or tuberculosis), connective tissue disease, uremia, neoplasm, or idiopathic condition.
- Symptoms and signs: heart failure such as dyspnea, orthopnea, fatigability, hepatomegaly, and ascites.
- Constrictive pericarditis vs. restrictive cardiomyopathy:
  - Characterized by similar clinical manifestation and similar findings at cardiac catheterization and echocardiography.
  - In both conditions, ventricular diastolic filling is restricted, leading to diastolic heart failure. In constrictive pericarditis, diastolic filling is restricted by an inelastic pericardium after an initial expansion of the myocardium. Restrictive cardiomyopathy, however, is defined by a non-dilated ventricle with a stiff myocardium that causes a major decrease in compliance of the heart muscle itself.
- Patients with constrictive pericarditis might benefit from pericardial stripping, whereas those with restrictive disease would not.
- CT and MR diagnosis:
  - Aided by excellent depiction of the pericardium.
  - Able to demonstrate even minute amounts of calcification, a finding highly suggestive of constrictive pericarditis.
  - Can detect irregular calcification anywhere over the heart, but it may be primarily found in regions where pericardial fat is abundant, i.e., the atrioventricular groove.
  - Other findings include a pericardial thickness of over 4 mm (diffuse or localized), narrowing and tubular deformation of the RV, normal or small ventricular size, and straightening or angulation of the interventricular septum.
  - Additional secondary findings include signs of impaired diastolic filling of the RV, reduced RV volume, narrow tubular configuration of RV, dilatation of RA, IVC, hepatic veins in addition to hepatomegaly, ascites, and pleural effusions (Fig. 20.6).

20.2.3.3 Effusive Constrictive Pericarditis

- Unique clinical condition consisting of both pericardial effusion/cardiac tamponade and chronic features of constrictive pericarditis.
- Identified as having effusive constrictive pericarditis when constrictive hemodynamics still persist after adequate removal of the effusion.

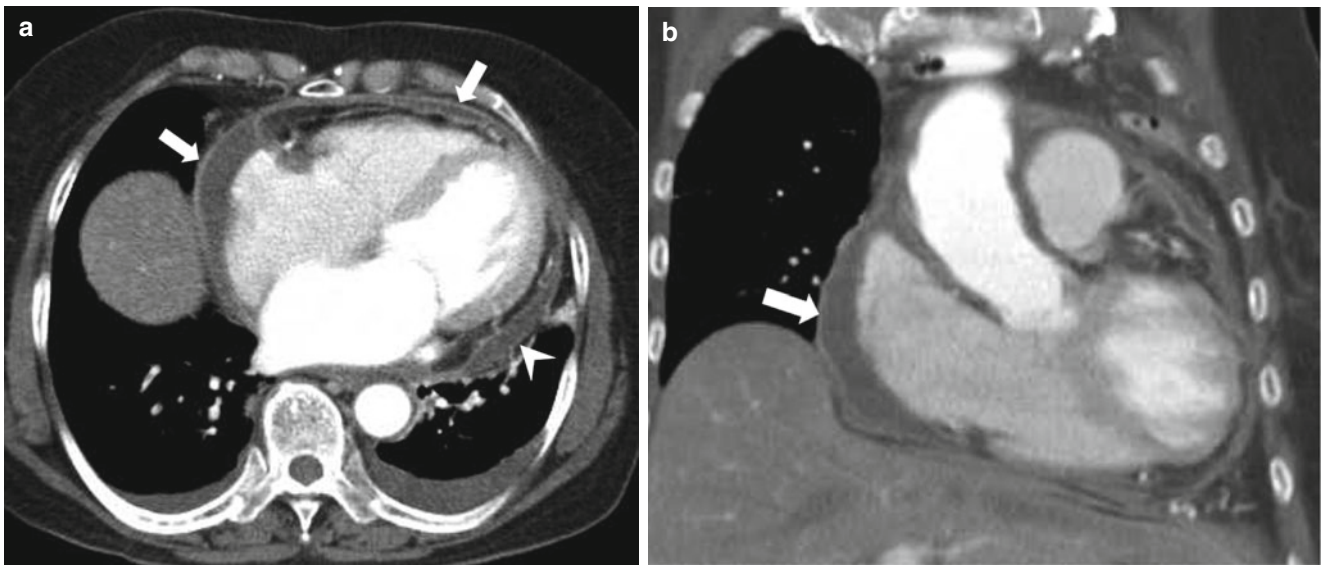

Fig. 20.5 Infectious (tuberculosis) pericarditis. Axial (**a**) and coronal (**b**) chest CT images show thickened and enhanced pericardium (*arrows*), separation of epicardium and pericardium, moderate amount of pericardial effusion, and minimal loculation (*arrowhead*) of effusion around the ventricles

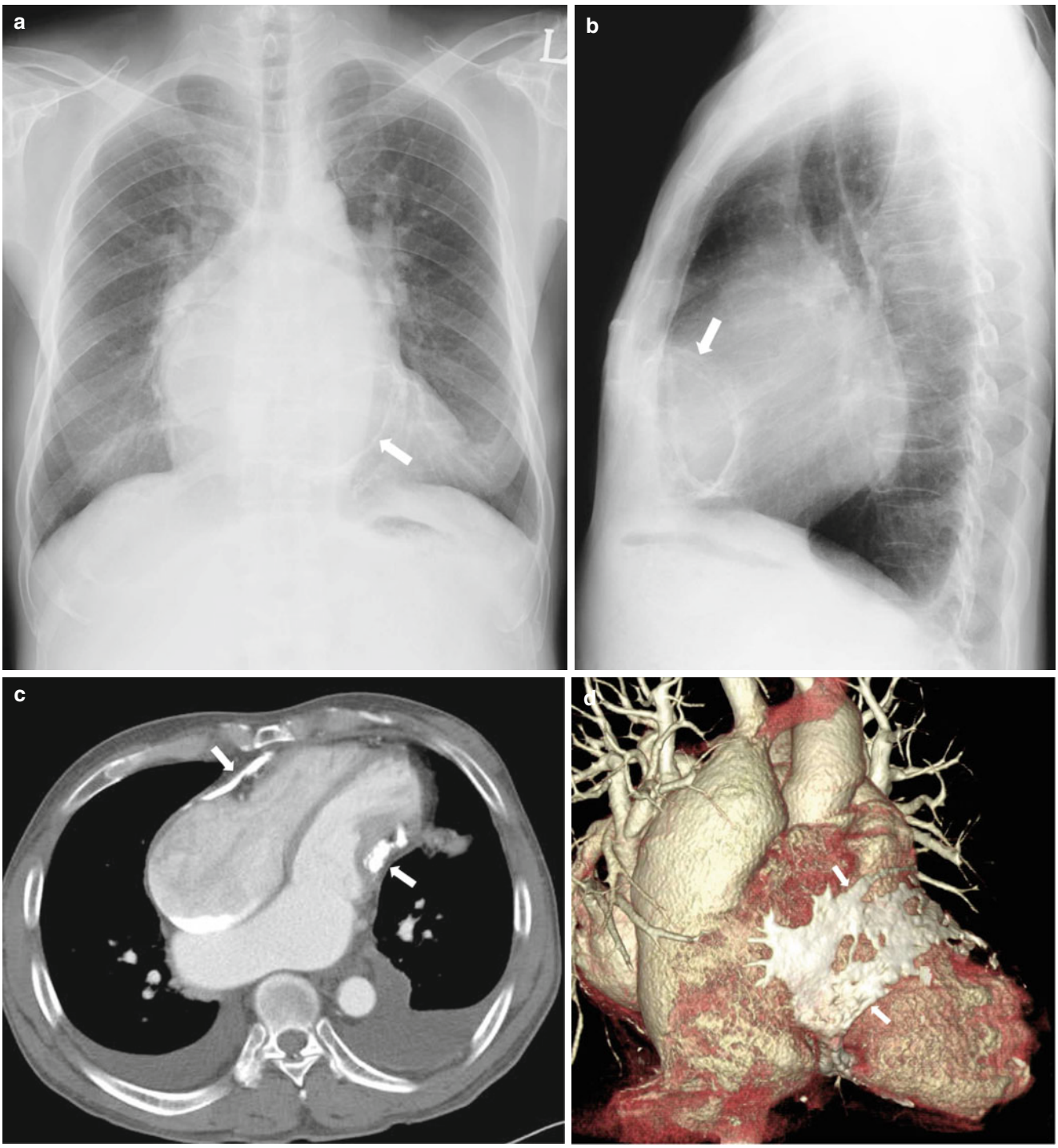

Fig. 20.6 Constrictive pericarditis. (**a**, **b**) Chest PA and lateral views show a ring of calcification (*arrows*) at ventricle. Carinal widening and double contour of right cardiac border suggesting left atrial enlargement are also noted. (**c**) Axial CT image shows extensive ring-like calcification (*arrows*) that encircles through the right atrioventricular groove and midportion of the left ventricle. Both atria are enlarged. (**d**) Volume-rendered images show three-dimensional configuration of pericardial calcification (*arrows*)

- Pericardiocentesis may relieve the symptoms of cardiac tamponade but may then develop symptoms of constrictive pericarditis.
- Combination of noninvasive imaging by echocardiography, cardiac MR, and cardiac CT can demonstrate pericardial effusion, a thickened pericardium, and hemodynamic evidence of constrictive physiology.
- This entity can be considered as an intermediate transition from acute pericarditis/cardiac tamponade to constrictive pericarditis (Fig. 20.7).

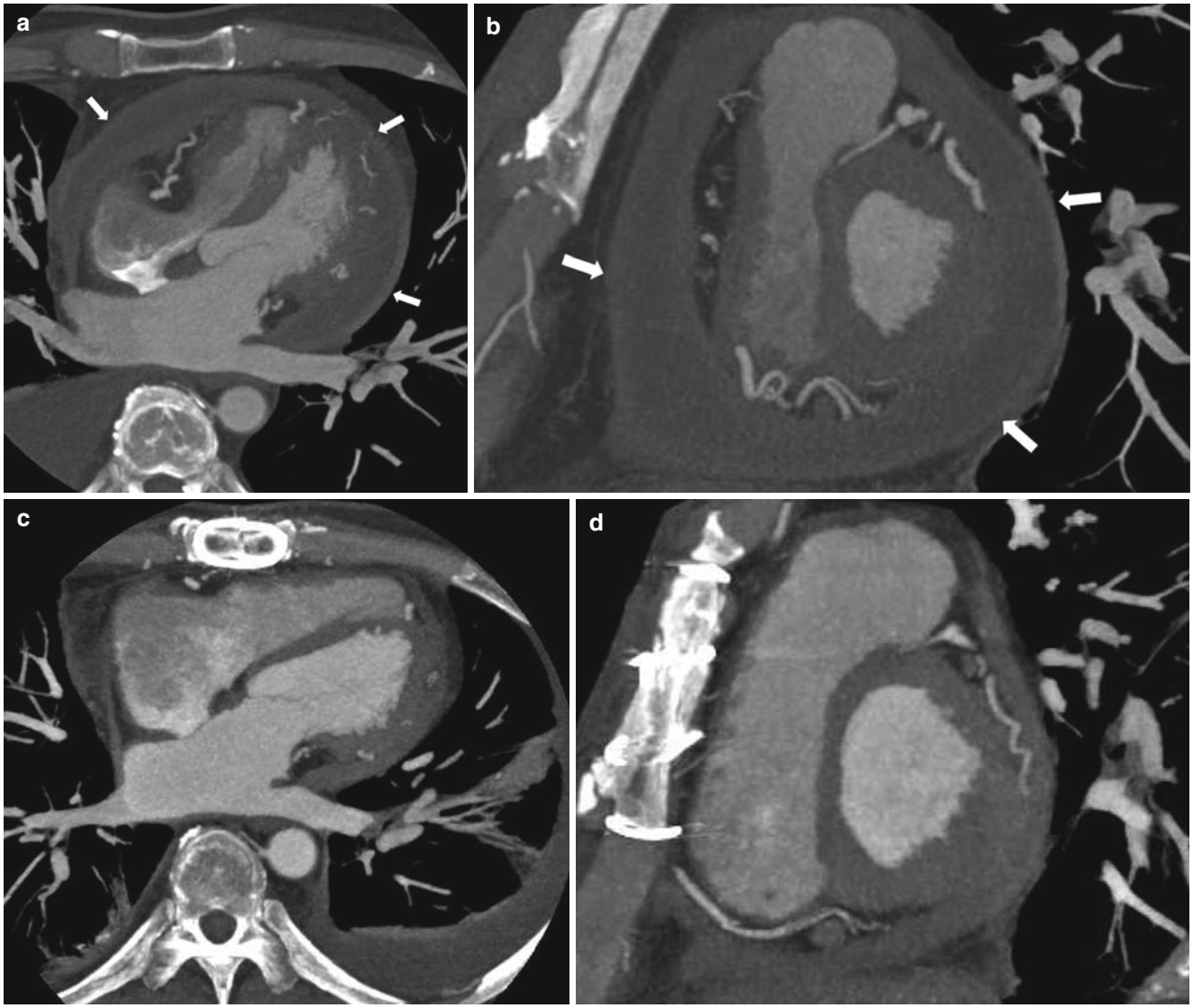

Fig. 20.7 Effusive constrictive pericarditis. Axial (**a**) and short-axis (**b**) images of initial cardiac CT show pericardial effusion, thickened and enhanced pericardium (*arrows*), narrowed both ventricular shape, and inverted interventricular septum. After pericardiectomy pericardial fluid was decreased remarkably on both axial (**c**) and short-axis (**d**) image. However, ventricular narrowing and interventricular septal inversion are still present

20.2.4 Pericardial Masses

20.2.4.1 Pericardial Cyst

- Anomalous fluid-containing mass of the parietal pericardium
- Congenital defect of coelomic development or sequelae of pericarditis
- Imaging findings:
  - Frequently located at the cardiophrenic angle: right 70 %, left 10–40 %
  - Well-marginated rounded homogenous mass
  - Water density/signal intensity: no internal enhancement
  - Imperceptible non-enhancing wall without calcification
  - Unilocular in 80–90 %
- Differential diagnosis:
  - Loculated pleural or pericardial effusion: septation or enhancing wall.
  - Bronchogenic/esophageal duplication cyst: same imaging characteristic as pericardial cyst except frequent location.
  - Thymic cyst: usually separated from the pericardium.
  - Hydatid cyst: daughter membranes form internal trabeculations.
  - Pancreatic pseudocyst: usually extend through esophageal hiatus.

20.2.4.2 Pericardial Tumors

- Primary pericardial tumors are rare and include lipomas, teratomas, fibromas, sarcomas, and mesotheliomas.
- Mostly direct invasion of extracardiac mass or less frequently lympho-hematogenous spread.
- Manifest as pericardial effusions, pericardial thickening, or enhancing nodules or masses (Figs. 20.8 and 20.9).

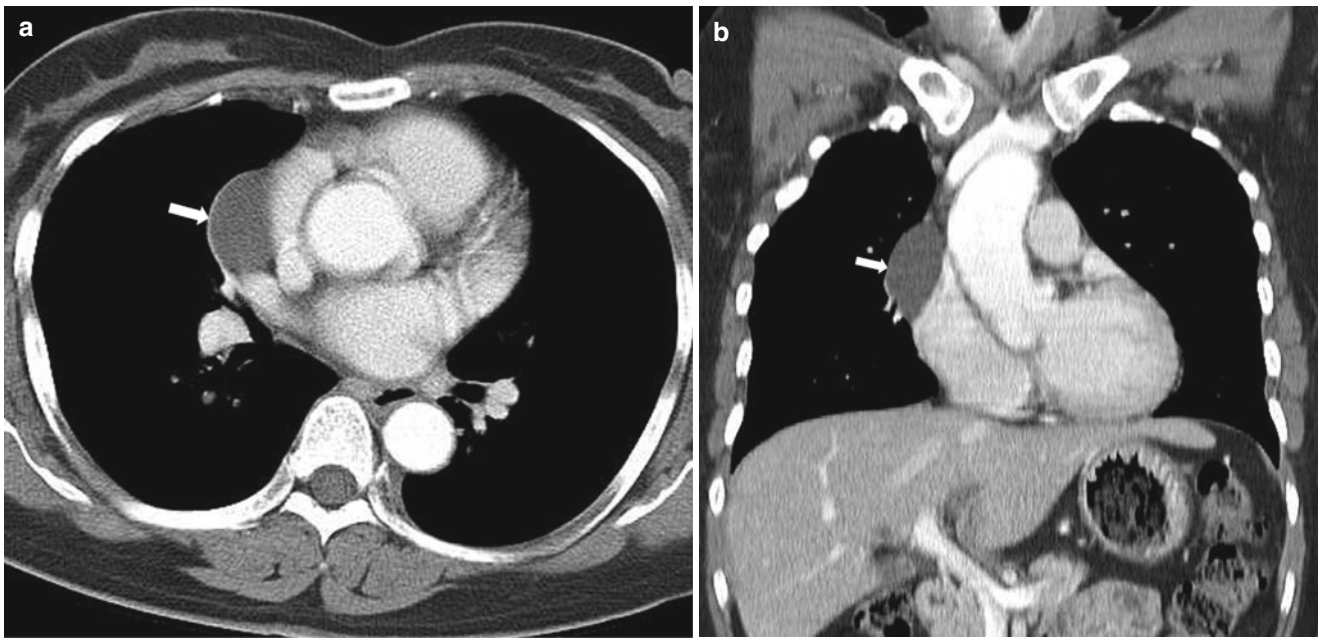

Fig. 20.8 Pericardial cyst. (**a**, **b**) Axial and coronal images of chest CT show lenticular cystic mass (*arrow*) without perceptible thickened wall at right upper cardiac border

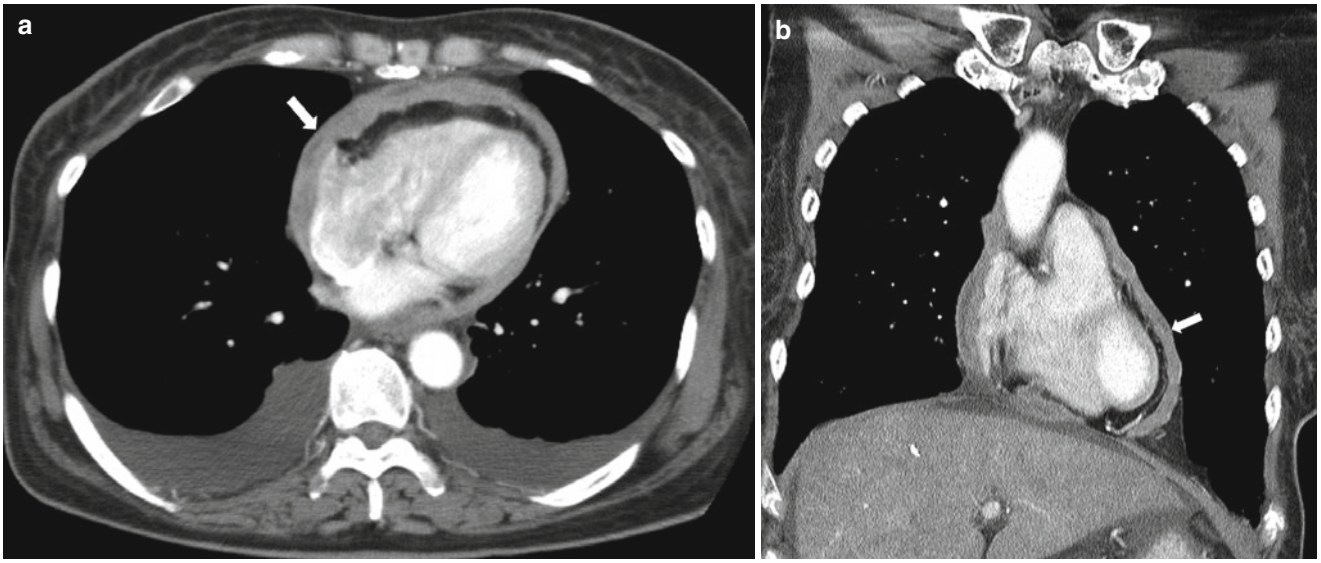

Fig. 20.9 Pericardial mesothelioma. (**a**, **b**) Axial and coronal images of chest CT show diffuse nodular enhancing pericardial thickening (*arrows*) and small amount of bilateral pleural effusion

Suggested Reading

1. Alter P, Figiel JH, Rupp TP, Bachmann GF, Maisch B, Rominger MB. MR, CT, and PET imaging in pericardial disease. Heart Fail Rev. 2013;18:289–306.
2. Rajiah P. Cardiac MRI: part 2, pericardial diseases. AJR Am J Roentgenol. 2011;197(4):W621–34.
3. Restrepo CS, Lemos DF, Lemos JA, et al. Imaging findings in cardiac tamponade with emphasis on CT. Radiographics. 2007;27(6):1595–610.
4. Verhaert D, Gabriel RS, Johnston D, Lytle BW, Desai MY, Klein AL. The role of multimodality imaging in the management of pericardial disease. Circ Cardiovasc Imaging. 2010;3(3):333–43.
5. Wang ZJ, Reddy GP, Gotway MB, Yeh BM, Hetts SW, Higgins CB. CT and MR imaging of pericardial disease. Radiographics. 2003;23 Spec No:S167–80.
6. Yared K, Baggish AL, Picard MH, Hoffmann U, Hung J. Multimodality imaging of pericardial diseases. JACC Cardiovasc Imaging. 2010;3(6):650–60.

Part VI

Technical Overviews

CT Technical Overviews

21

Doo Kyoung Kang

Contents

D.K. Kang
Department of Radiology, Ajou University School of Medicine, Suwon, Republic of Korea
e-mail: kdklsm@ajou.ac.kr

Abstract

This chapter provides information on how to perform cardiac CT. According to workflow of practical CT examination, this chapter described considerations regarding patient preparation, CT acquisition, contrast enhancement, reconstruction parameters, and image display techniques. Because physicians have to select optimal methods for successful CT examination every moment from patient preparation to image reformation, this chapter is described in a step-by-step approach. The technique is covered mainly with the latest models such as 64-slice CT, dual-source CT, and wide detector array CT scanners. Progress in CT technology has continuously contributed to improve temporal and spatial resolution. Nevertheless, efforts are still being made to increase image quality. This chapter also reviews how each factor influences spatial and temporal resolution and image noise. Another focus is patient radiation exposure and strategies for dose reduction. A variety of strategies have been currently

T.-H. Lim (ed.), *Practical Textbook of Cardiac CT and MRI*,
DOI 10.1007/978-3-642-36397-9_21, © Springer-Verlag Berlin Heidelberg 2015

undertaken to reduce the radiation dose. This chapter finally discusses the technical developments and strategies to reduce radiation dose.

21.1 Patient Preparation

21.1.1 Instructions for Patients

- Check allergies to contrast agent, renal insufficiency (eGFR < 60mL/min/m^2), pregnancy, severe heart failure, and contraindications of β-blocker and NTG.
- Adequate oral hydration with drinking clear fluids up to 1 h before the examination.
- Avoid solids for 4 h before the CT examination and caffeine for 12 h before CT examination.
- Taking all usual cardiovascular medications including blood pressure control medicine.
- Discontinuing metformin for at least 48 h before and after contrast injection is mandatory.
- Stop Viagra® (sildenafil) and Levitra® (vardenafil) for 24 h and Cialis® (tadalafil) for 48 h if patient has a plan to administrate NTG [1].

21.1.2 Intravenous Access, Patient Positioning, and ECG Lead Attachment

- Intravenous (IV) access in antecubital vein using 18-G catheter or larger [2].
- The supine, feet-first position in the scanner gantry with lifting both arms above the shoulders.
- ECG leads placement outside scan range (Fig. 21.1).
- Patient education such as breathing instruction and practice.

21.1.3 Heart Rate Control

- To lower the heart rate and to make the regular rhythm during cardiac CT, β-blockers are the first-line treatment agent (Fig. 21.2).
- Metoprolol and then atenolol are the most commonly used cardioselective β-blockers.
- Effect of β-blockers [3]
  - Reduce the heart rate
  - Helpful in patients with irregular heart rates, such as premature atrial or ventricular contractions, supraventricular tachycardias, and atrial fibrillation
  - Prevent the heart rate variation following contrast injection and nitroglycerine administration
  - Diminish the diagnostic value of left ventricular function analysis due to negative inotropic effect
- Contraindication of β-blocker
  - Allergy to β-blocker
  - Sinus bradycardia (HR <60 bpm)
  - Hypotension (systolic blood pressure <100 mmHg)
  - Decompensated cardiac failure
  - Current asthma or severe COPD dependent on β2-agonist inhaler

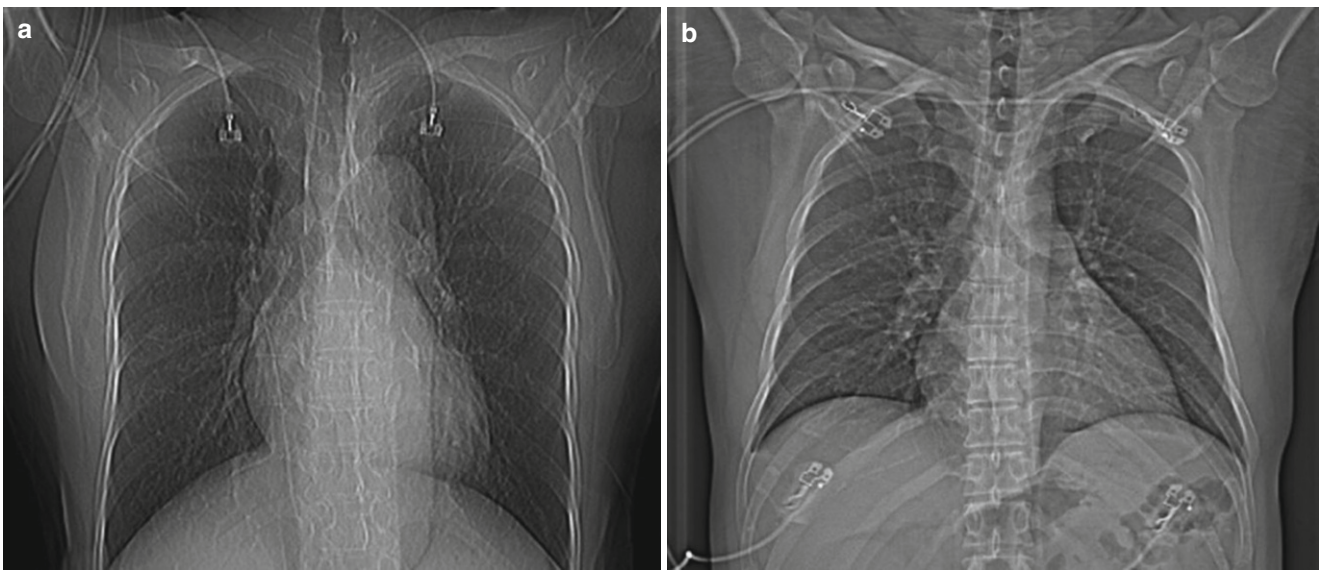

Fig. 21.1 ECG leads attachment. The number and preferred location of leads depend on the scanner type and design. ECG leads should be attached outside scan range to avoid artifact from the ECG electrodes and cables. (**a**) With Brilliance CT (Philips), two upper ECG leads are placed between the 2nd and 4th intercostal spaces on the midclavicular line, and 3rd lower lead is placed on the left mid-abdomen, approximately 10 cm from the umbilicus (not shown). (**b**) With Somatom definition flash (Siemens), the number of ECG leads is four. Two upper leads are placed on the midclavicular line, directly below the clavicle. Two lower leads are placed on the midclavicular line, 6th or 7th intercostal space

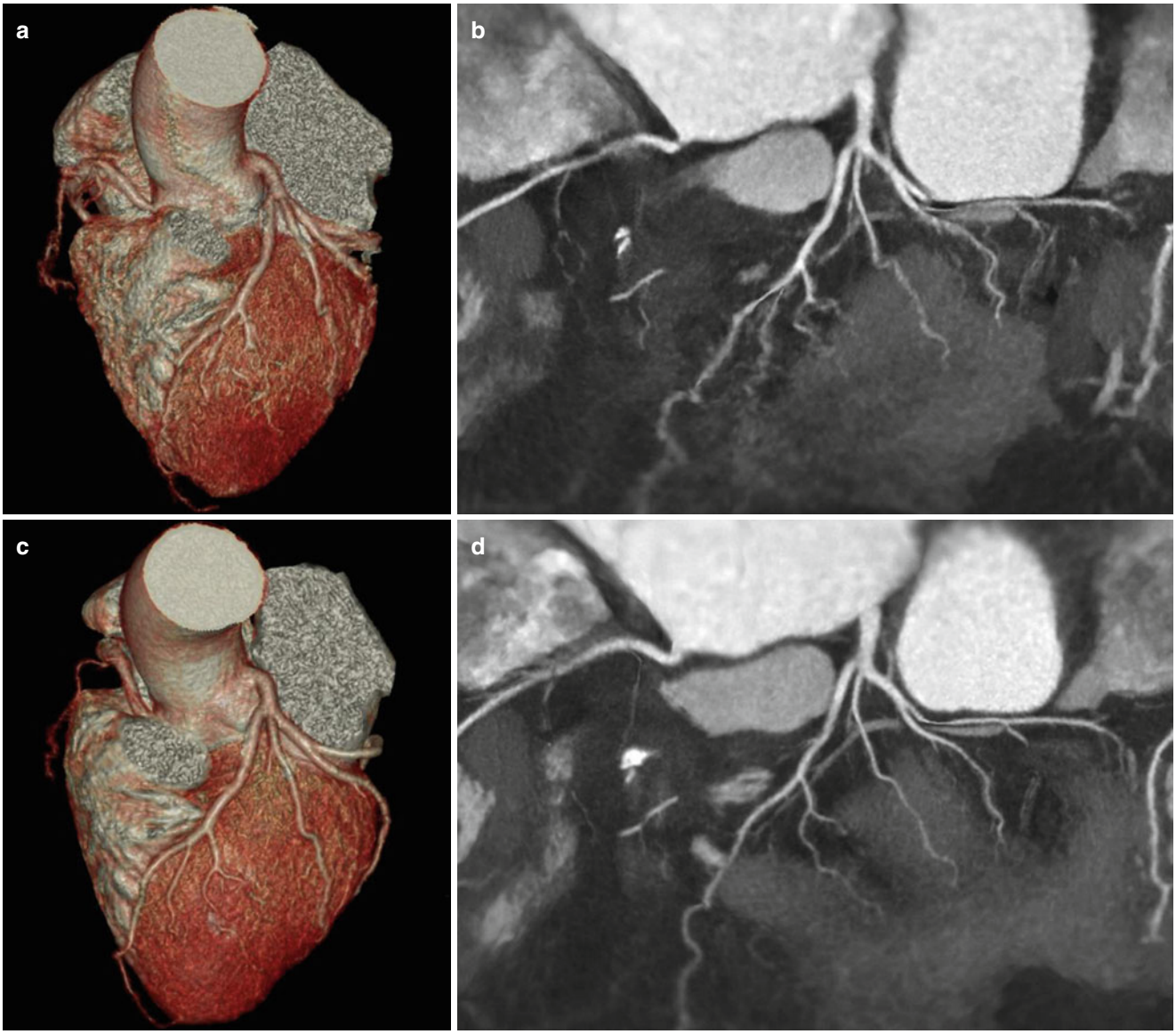

Fig. 21.2 Heart rate control. (**a**, **b**) The VRT and two-dimensional (2-D) map view in a patient with 90 bpm heart rate shows blurring at proximal RCA and all branches of LAD and LCX. (**c**, **d**) The VRT and 2-D map view after β-blocker administration in the same patient show decreased motion blurring and allow clear delineation of branches. *VRT* volume rendered technique, *RCA* right coronary artery, *LAD* left anterior descending, *LCX* left circumflex

  - Active bronchospasm
  - Second- or third-degree atrioventricular block
- Administration of β-blocker
  - Oral administration: 50–100 mg of metoprolol administered orally 1 h prior to CT scanning. → After 1 h, if the heart rate is not in the desired range, additional intravenous β-blocker administration should be considered.
  - IV β-blocker administration: Initially, 2.5 mg dose of metoprolol IV over 1 min → a second dose of 2.5 mg of metoprolol, if the heart rate remains more than 65 bpm after 5 min. → Up to two additional doses of 5 mg each of metoprolol can be given IV, each over 1 min, with a 5 min interval between doses, if the heart rate continues to remain elevated [3].
- Calcium channel blockers are an alternative medication. However, the effectiveness of calcium channel blockers for heart rate reduction is considerably less than that of β-blockers.
- Ivabradine is a pure heart rate-lowering agent, but does not depress myocardial contractility.

21.1.4 Nitroglycerin (NTG)

- Nitroglycerin is a potent vasodilator, which dilates both normal and abnormal coronary arteries by relaxing the vascular smooth muscle.
- The use of nitroglycerin actually improved diagnostic accuracy of coronary CTA for the evaluation of coronary

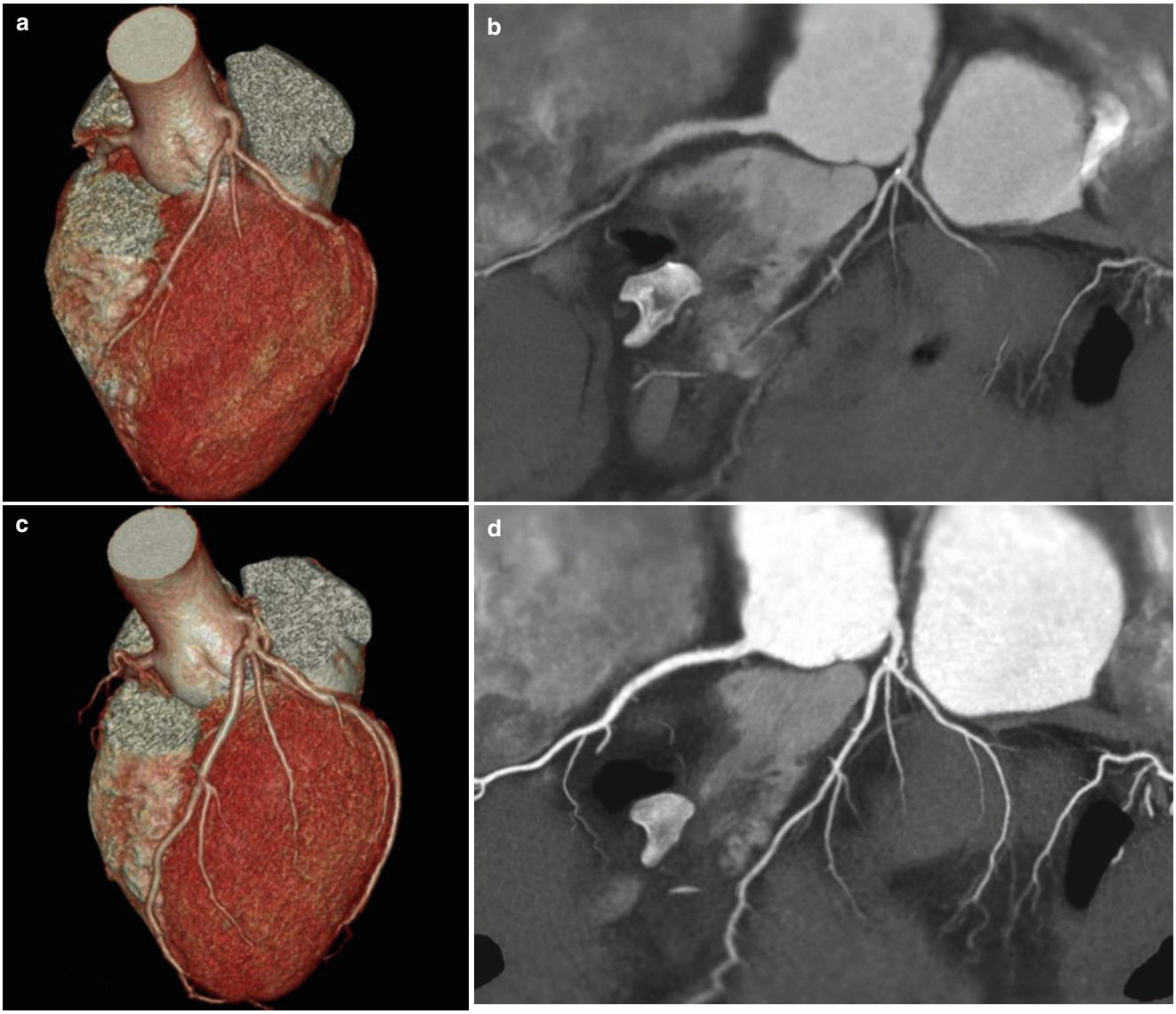

Fig. 21.3 Effect of nitroglycerin (NTG). (**a**, **b**) A 54-year-old female underwent an initial coronary CTA without NTG administration. The VRT and 2-D map view could not fully reveal the branches of the coronary arteries. (**c**, **d**) The same patient underwent a second coronary CTA with NTG administration. Coronary arteries are dilated sufficiently, and the VRT and 2-D map view show normal coronary arteries with excellent visualization of the branches

artery disease in proximal segment and allows more septal branches to be visualized as well (Fig. 21.3) [4].

- Contraindication of NTG
  - Hypersensitivity to NTG
  - Systolic hypotension (<100 mmHg)
  - Severe anemia
  - Severe aortic stenosis
  - Obstructive hypertrophic cardiomyopathy
  - Constrictive pericarditis
  - Acute RV infarction
  - Increased intracranial pressure
  - Glaucoma
- Use of phosphodiesterase type 5 (PDE5) inhibitors such as Viagra® (sildenafil) or Levitra® (vardenafil) in the last 24 h or Cialis® (tadalafil) in the last 48 h
- Administration of NTG [5]
  - Single tablet of nitroglycerin (0.4–0.6 mg) sublingually 1–2 min before CT scanning
  - Two puffs (400–800 mcg) of sublingual spray 5 min before initiation of CT scanning

21.2 Acquisition Parameters

21.2.1 Tube Voltage

- Tube voltage value of 120 kVp is routinely used for most patients, while lower tube voltage of 80–100 kVp is a viable method to reduce radiation doses in pediatric patients and slim young adult with low body mass index (BMI) <25 kg/m^2.

Table 21.1 Optimal tube voltage and tube current tailored for BMI

BMI (kg/m^2)	Tube voltage (kVp)	Tube current (mA)
<22.5	100	450
22.5–24.9	100	500
25–27.4	120	550
27.5–29.9	120	600
30–40	120	650
>40	120	700

Body mass index-adapted scanning protocol (LightSpeed VCT Scanner GE Healthcare) by Tatsugami et al. [6]

- Lower tube voltage settings increase image noise, resulting in degradation of the coronary images. Therefore, tube voltage setting should be determined by considering balance of image quality and radiation dose.
- According to the SCCT guideline [7], tube potential of 100 kV could be considered for patients weighing ≤90 kg or with a BMI ≤30 kg/m^2; a tube potential of 120 kV is usually indicated for patients weighing >90 kg and with a BMI >30 kg/m^2.

21.2.2 Tube Current

- Tube current (mA) may be manually selected or protocolized based on the patient's BMI and chest circumference (Table 21.1) and generally ranges between 300 and 800 mA.
  - mAs = mA × rotation time
  - Eff mAs = mAs/pitch factor
- Higher tube current improves image quality and is useful in heavily calcified coronary artery, intracoronary stent, and obese patients.

21.2.3 Gantry Rotation Time (Speed)

- Time required for the x-ray tube/detector system to rotate 360° around the patient.
- For cardiac CT examination, the fastest gantry rotation time is typically selected.
  - Faster gantry rotation means faster acquisition of the data and subsequently improved temporal resolution.
  - The gantry rotation times of the most recent scanners range from 270 to 350 ms [8].

21.2.4 Collimation

- Detector collimation [9]
  - Describes how the individual detector elements are used to channel data.
  - Depends on the number and width of detector element.
  - Determines the minimum section thickness (voxel length)
  - The minimum channel widths of recent MDCT range from 0.5 to 0.625 mm.
- Beam collimation (total x-ray beam width)
  - Refers to the beam width along the longitudinal axis and can be calculated by multiplying the number of active channels by the channel width during the image acquisition.
  - A detector with 64 channels and a 0.625 mm channel width requires a 40 mm beam width.

21.2.5 Table Increment (Feed) and Pitch

- Pitch is defined as the longitudinal (z-axis) table increment during one gantry rotation (360°) to total x-ray beam width [9].
- In retrospective ECG-gated CT, typical pitch factors for cardiac MDCT range from 0.2 to 0.4.
- If selected pitch is too high for a given heart rate, there will be gaps in the data, resulting in volume gap (or 3D gap) artifact between image stack with missing cardiac anatomy (Fig. 21.4).
- Automatic determination of pitch (automatic pitch adaptation or adaptive pitch technique) is available with dual-source CT scanners, which automatically adjust the pitch value to the patient's heart rate.

21.2.6 Field of View (FOV) and Scan Range

- The field of view (FOV) [10]
  - Represents the size of the image that is going to be reconstructed.
  - FOV of 200–250 mm or less is suitable for cardiac CT.
- Scan range
  - For coronary CTA: from the carina to the bottom of the heart (approximately 10–12 cm long)
  - In patients who underwent bypass grafts: extended upper range to the middle of the clavicle (18–25 cm)

21.3 Acquisition Modes (Scan Techniques)

21.3.1 Prospective ECG Triggering (Step-and-Shoot or Sequential Mode)

- Image acquisition technique [11]
  - The x-ray tube is turned on only during a certain previously defined phase of the R–R interval, but no radiation is delivered during the remainder of the R–R interval (Fig. 21.5).

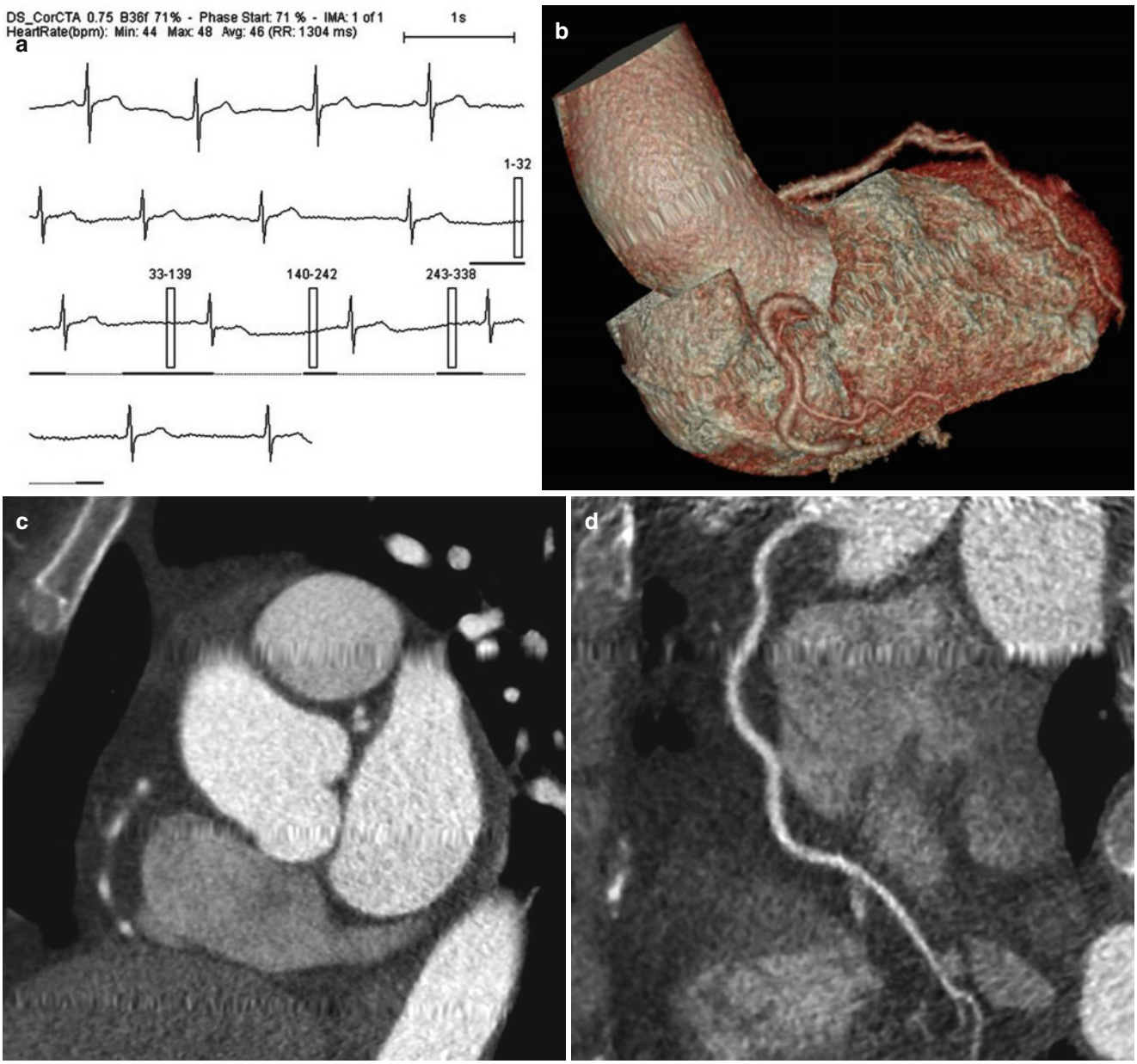

Fig. 21.4 Volume gap due to too high pitch. (**a**) ECG information in a patient with bradycardia (average heart rate of 46 bpm) and heart rate variation represents retrospective ECG-gated technique with ECG-based tube modulation. (**b–d**) VRT, short-axis, and curved MPR images in the patient show missing cardiac anatomies that could not be covered by the scanning

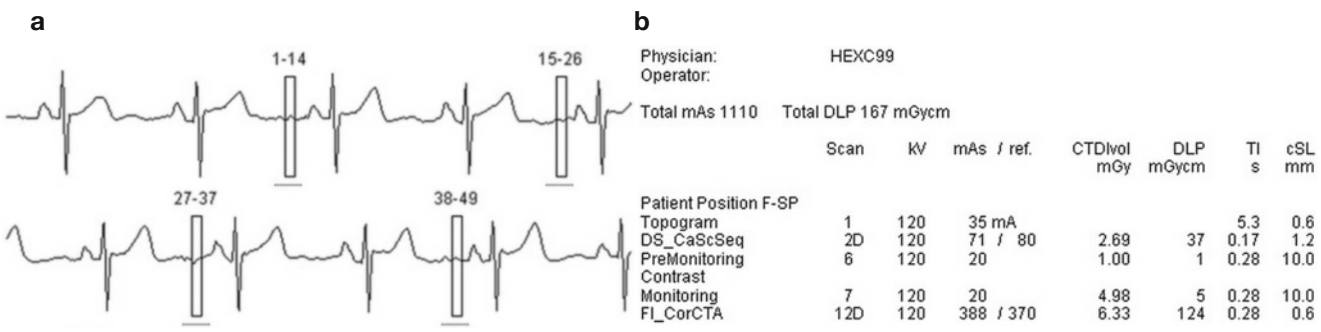

Fig. 21.5 Prospective ECG-triggered technique. (**a**) In a patient with 63 bpm of heart rate, prospective ECG-triggering technique is optimal choice. ECG information represents that the radiation exposure has allowed at only 70 % of R–R interval. (**b**) The total effective radiation dose of the CT examination including calcium scoring study is 2.34 mSv

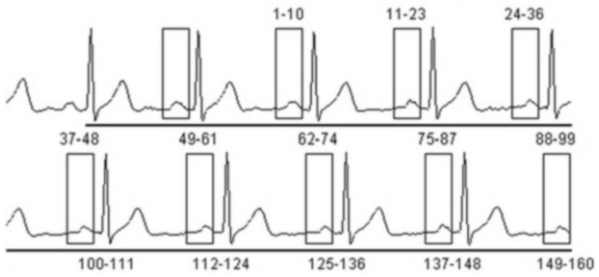

b

Time: Feb 01, 2011, 08:58:26
Total DLP: 1182.8 mGy*cm

Dose

#	Description	Scan Mode	mAs	kV	CTDIvol [mGy]	DLP [mGy*cm]	Phantom Type[cm]
1		Survey	2	120	0.17	6.8	BODY 32 CM
2		Axial	N/A	120	3.84	57.6	BODY 32 CM
3	locator	Stationary	N/A	120	2.50	2.5	BODY 32 CM
4	tracker	Stationary	N/A	120	7.50	7.5	BODY 32 CM
5		Helical	848	120	49.86	1108.4	BODY 32 CM

Fig. 21.6 Retrospective ECG-gating technique. (**a**) In a patient with 71 bpm of heart rate, retrospective ECG-gated technique acquires images through the entire cardiac cycle. Image reconstruction has been performed in 65 % of R–R interval retrospectively. (**b**) The total effective radiation dose of the CT examination including calcium scoring study is 16.5 mSv, which is higher than that of prospective ECG-triggered technique

  - Seventy percent of the R–R interval is optimal phase in patients with a low and stable heart rate.
  - This technique is mainly used for quantification of coronary calcium, but recently it is increasingly used for coronary CTA examinations.
- Advantage and limitation of prospective ECG triggering
  - Relatively lower radiation dose of 3–5 mSv.
  - Image quality is dependent on the heart rate and heart rate variation.
  - Maximum heart rate threshold for prospective ECG triggering is between 60 and 65 bmp of single-source CT and <75 bpm for dual-source CT, respectively.
  - Functional information about cardiac valve motion or wall motion is not available.
- Recent improvement of prospective ECG-triggering technique.
  - Longer *z*-axis coverage available with 256- or 320-slice scanners ranging from 12.8 to 16 cm in one gantry rotation permits full cardiac coverage in one gantry rotation with prospective ECG triggering.
  - With adaptive scan delay (multiphase adaptive prospectively gated axial CT), scan will be triggered on the basis of multiple previous R–R intervals, which is more likely to result in an optimally timed acquisition.
  - The lengthening (padding) of the x-ray tube on time allows a reconstruction in another phase, if motion artifact is problematic in one phase.

21.3.2 Retrospective ECG Gating

- Image acquisition technique [11]
  - Images are acquired throughout the entire cardiac cycle during simultaneous ECG recording (Fig. 21.6).
  - Image reconstruction is performed in specific periods of the cardiac cycle retrospectively referencing to the ECG signal.
  - A low pitch (0.2–0.4) is needed to avoid gaps in anatomic coverage.
- Advantage and limitation of retrospective ECG-gating technique
  - Less dependent on heart rate and allows ECG editing retrospectively
  - Evaluates cardiac function, such as potential regional function and wall motion abnormalities
  - Higher radiation exposure of between 12 and 20 mSv
- ECG-based tube current modulation (ECG-pulsing) technique
  - A lower tube current during the systolic phase, because the majority of useful information is acquired in diastole phase
  - Low heart rate <65 bpm → pulsing window of 65–75 % of R–R interval (Fig. 21.7)
  - Higher heart rate >65 bpm → pulsing widow of 30–70 % of R–R interval to cover both systolic and diastolic phase

21.3.3 Volume CT Technique Using 256- or 320-Slice Wide Detector

- Recent technical development of the large detector arrays is able to acquire images of the whole heart in a single heart beat [12].
  - 256-slice MDCT: detector configuration of 256×0.5 mm, 12.8 cm *z*-axis coverage per rotation, and rotation time of 270 ms.
  - 320-slice MDCT: detector configuration of 320×0.5 mm, 16 cm *z*-axis coverage per rotation, and rotation time of 350 ms.
- No table movement during data acquisition is able to eliminate the stair-step artifacts.
- The lack of slice overlap leads to low radiation exposure.

21.3.4 Dual-Source CT (DSCT)

- As a technology for improving temporal resolution, a dual-source CT system has been recently introduced employed two x-ray sources and two corresponding detectors offset by 90–95°.

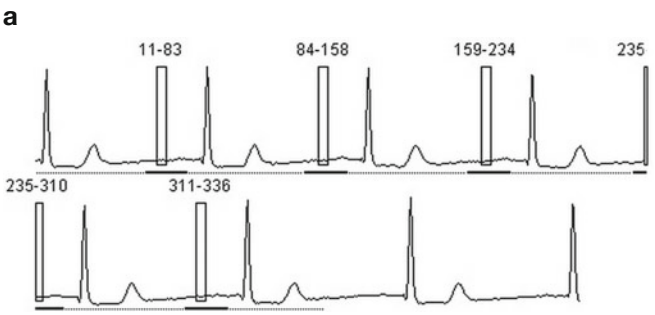

b

Physician:
Operator:

Total mAs 4209 Total DLP 722 mGycm

	Scan	kV	mAs / ref.	CTDIvol* mGy	DLP mGycm	TI s	cSL mm
Patient Position F-SP							
Topogram	1	120	36 mA	0.14 L	5	3.6	0.6
DS_CaScSeq	2D	120	72 / 80	2.74 L	38	0.17	1.2
PreMonitoring Contrast	6	120	20	1.01 L	1	0.28	10.0
Monitoring	7	120	20	10.11 L	10	0.28	10.0
DS_CorCTA	17D	120	146 / 300	43.36 L	668	0.28	0.6

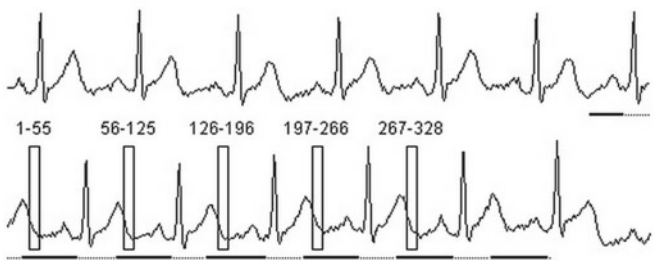

d

Physician: 104878A
Operator:

Total mAs 4195 Total DLP 463 mGycm

	Scan	kV	mAs / ref.	CTDIvol* mGy	DLP mGycm	TI s	cSL mm
Patient Position F-SP							
Topogram	1	120	36 mA	0.14 L	7	4.7	0.6
DS_CaScSeq	2D	120	93 / 80	3.53 L	49	0.17	1.2
PreMonitoring Contrast	6	120	20	1.01 L	1	0.28	10.0
Monitoring	7	120	20	4.04 L	4	0.28	10.0
DS_CorCTA	11D	100	250 / 300	26.15 L	402	0.28	0.6

Fig. 21.7 Retrospective ECG-gated technique with ECG-based tube current modulation. (**a**, **b**) In retrospective, ECG-gated CT with 120 kVp and tube current modulation. Pulsing window ranges from 65 to 75 %. The total effective radiation dose is 10.1 mSv from conversion factor of 0.014 and total DLP of 722 mGycm. (**c**, **d**) With retrospective ECG-gated CT with 100 kVp and tube current modulation in a patient with a rapid heart rate of 90 bpm, pulsing window is extended from 30 to 90 % including end-systolic phase. Although pulsing window is wider, the total effective radiation dose is lower as 6.48 mSv because of lower kVp

- Rotation time of 280–330 ms → temporal resolution of 75–83 ms.
- Less vulnerable to high heart rates.
- Prospective ECG-triggered helical scan (flash mode or high-pitch technique) (Fig. 21.8).
  - A gapless z-sampling with a high pitch up to 3.4 enables complete coverage (120 mm) of the heart in a single heart beat within 300 ms duration.
  - Radiation dose can be reduced to 1 mSv and below.
  - Requires heart rates of less than 60–65 bpm.

21.3.5 Selection of Optimal CT Scan Protocol

- Prospective ECG-triggered techniques should be used in patients who have stable sinus rhythm and low heart rates.
- Retrospective ECG-gated techniques may be used in patients who do not qualify for prospective ECG-triggered scanning because of irregular heart rhythm or high heart rates or both.
- If the cardiac anatomy or coronary artery disease is the main concern, prospective ECG-triggering technique is recommended.
- If cardiac functional information is the main concern, retrospective ECG-gating technique is recommended with additional dose-saving technique.
- If a large detector array of 256- or 320-slice is available, prospective ECG triggering is preferred.

21.4 Contrast Medium Injection

21.4.1 Optimum Level of Coronary Artery Enhancement

- Greater intracoronary attenuation leads to higher diagnostic accuracy in the detection of coronary artery stenosis with MDCT.
  - Higher attenuation >500 HU → significant underestimation of stenosis in smaller vessels.
  - Lower attenuation <200 HU → poor coronary three-dimensional image.
- The optimal vascular attenuation for stenosis detection in coronary CTA ranges from 250 to 350 HU.

21.4.2 Factors Affecting Coronary Artery Enhancement

- Patient's body size and cardiac output
  - Sophisticated method using lean body weight, body surface area, or BMI [13].
  - The scan delay has to be individualized according to each patient's cardiac output [14].
- Concentration of contrast medium
  - Contrast media with higher iodine concentration lead to higher attenuation in the coronary arteries.
  - The use of high iodine concentrations (e.g., 350, 370, or 400 mgI/mL) is recommended.

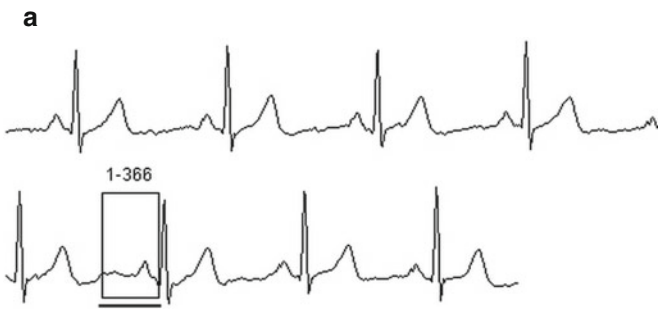

b

Physician: 100271
Operator:

Total mAs 941 Total DLP 145 mGycm

	Scan	kV	mAs / ref.	CTDIvol mGy	DLP mGycm	TI s	cSL mm
Patient Position F-SP							
Topogram	1	120	35 mA			3.6	0.6
DS_CaScSeq	2D	120	56 / 80	2.18	30	0.17	1.2
PreMonitoring	6	120	20	1.00	1	0.28	10.0
Contrast							
Monitoring	7	120	20	4.98	5	0.28	10.0
FI_CorCTA	12D	120	323 / 370	5.27	109	0.28	0.6

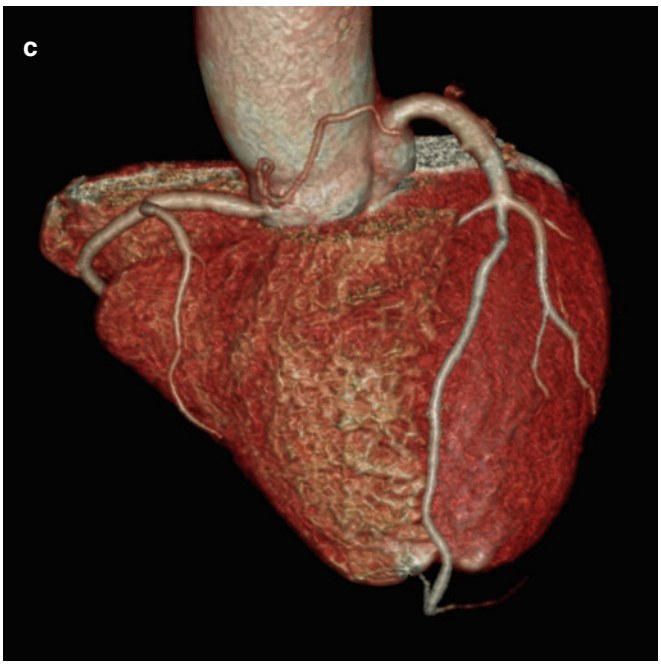

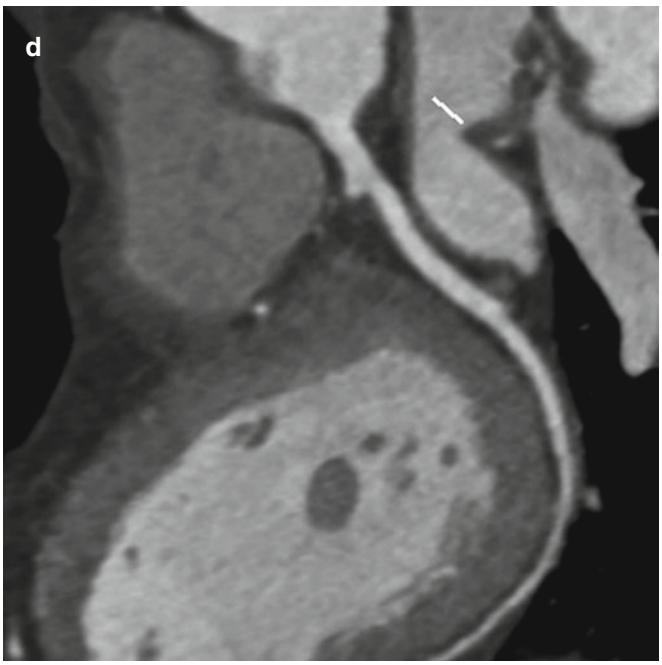

Fig. 21.8 High pitch technique (Flash-mode, Siemens). (**a**) In a patient with 58 bpm of heart rate. CT images are acquired in only one heart beat. (**b**) The total effective radiation dose of the CT examination including calcium scoring study is 1.86 mSv. (**c**, **d**) VRT and curved MPR images show good image quality from the one heart beat CT scan

- Contrast volume
  - As the speed of CT data acquisition increases, smaller amount of contrast media is required. Therefore, injection protocols must be adjusted to reduce unnecessary contrast agent (Table 21.2).
- With 64-slice scanners, the required contrast volume is as low as 50–70 ml.
- Injection rate
  - If the contrast volume and concentration are kept constant, increased injection rate resulted in higher peak enhancement and shorter time to peak [14].
  - Injection rates of up to 4–6 mL/s via an antecubital vein are commonly used for coronary CTA.

Table 21.2 Coronary CT angiography protocol adapted body mass index

BMI (kg/m^2)	Dose of contrast material (mL)	Flow rate (mL/s)
<17.5	50	4.0
17.5–22.4	55	4.0
22.5–24.9	65	4.0
25–27.4	80	4.5
27.5–29.9	80	5.0
30–34.9	85	5.0
35–40	95	5.0
>40	105	5.0

Body mass index (BMI)-adapted contrast material protocol with prospective ECG triggering suggested by Husmann et al. [13]

21.4.3 Saline Chasing Technique and Injection Protocol

- Uniphasic (monophasic) injection protocol
  - Uniphasic injection protocol uses contrast only.
  - Streak and beam-hardening artifacts (Fig. 21.9).
- Biphasic injection protocols
  - Pure (or undiluted) contrast media + saline bolus of 15–20 mL.
  - An injection rate of 4–5 mL/s as a saline chaser is optimal.

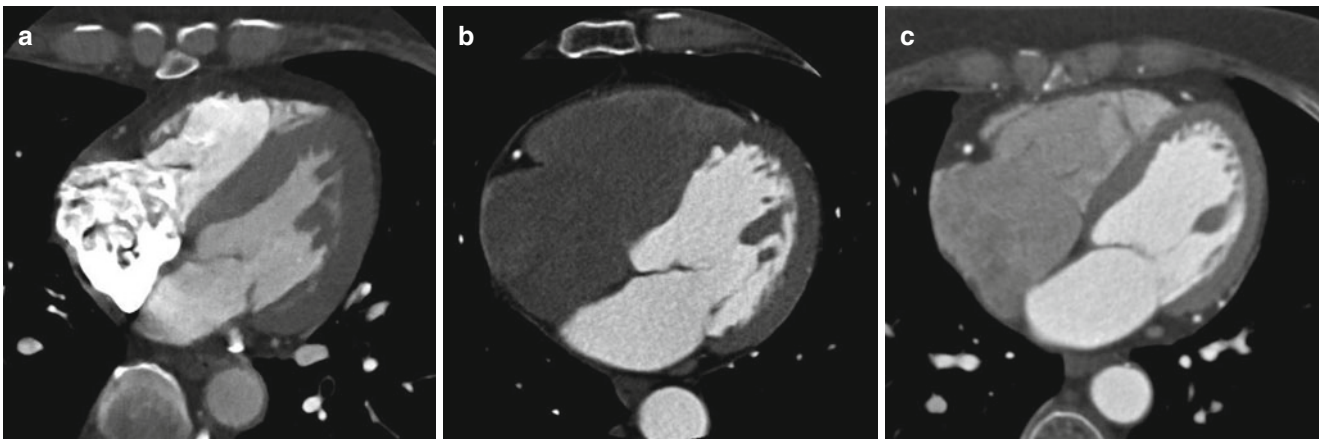

Fig. 21.9 Contrast injection protocols. (**a**) In uniphasic protocol, transaxial CT image shows a streak beam hardening artifact caused by non-diluted dense contrast media in the right atrium. (**b**) In biphasic protocol, shows excellent enhancement of left heart but weakness in the evaluation of the right heart due to complete washout of contrast medium. (**c**) In triphasic protocol groups, the right atrium and right ventricle were all enhanced uniformity, and the right ventricular septal endocardial contours are clearly delineated

  - Reduce a streak and beam-hardening artifacts by clearing of contrast media in the superior vena cava and right heart.
  - Decrease attenuation in right ventricle → limited visualization of the ventricular septum (Fig. 21.9) or pathologic abnormalities, such as thromboembolism or tumors.
  - Biphasic concentration protocol: Initial undiluted contrast bolus + diluted contrast bolus → Improves right ventricular enhancement and reduces streak artifacts
- Triphasic injection protocols
  - Initial pure contrast media bolus + 30 %: 70 % contrast-saline mixture + pure saline flush
  - The second bolus of contrast-saline mixture permits flushes out the high-density contrast media previously injected and also decreases streak artifacts in the superior vena cava (Fig. 21.9).

21.4.4 Contrast Timing Methods

- The determination of the arrival time (or transit time) of the contrast media is crucial for consistent enhancement of coronary arteries and usually done using either test-bolus injection or automated bolus-tracking methods.
- The test-bolus (timing-bolus) method [14]
  - Based on test-bolus IV injection of 10–20 ml of contrast media, followed by a 30–50 ml saline flush during the acquisition of a series of dynamic low-dose (e.g., 120 kVp, 20 mAs) monitoring scans at the level of the vessel of interest such as thoracic aorta in coronary CTA (Fig. 21.10)
  - Scan start delay: time to peak + additional 3–4 s delay
  - Advantage: the opportunity to practice breath-holding, to experience contrast agent infusion before the diagnostic scan, and to test IV access patency and heart rate control.
  - Disadvantages: 15–20 ml of extra contrast media and longer scan time
- Automated bolus-tracking (bolus-triggering) technique
  - Based on real-time monitoring of the main bolus during injection.
  - With the acquisition of a series of dynamic low-dose (e.g., 120 kVp, 20 mAs), the attenuation at the level of the vessel of interest is monitored until the desired attenuation (or trigger threshold) is attained (Fig. 21.10).
  - After a certain trigger threshold (100–200 HU) is exceeded, diagnostic scanning is started manually or automatically.
  - Delay time: 4–8 s after the trigger threshold.
  - Advantages: more simple, convenient, and faster with less contrast volume.

21.5 Image Reconstruction Methods

21.5.1 Slice Thickness and Reconstruction Interval (Increment)

- Slice thickness
  - The thinnest slice thickness offers the highest spatial resolution.
  - Slice thickness usually is chosen to be between 0.5 and 1.0 mm [15].
  - Slice thickness is set to slightly wider than the collimated section width to avoid artifacts, for example, 0.6 mm collimation with 0.75 mm slice thickness.

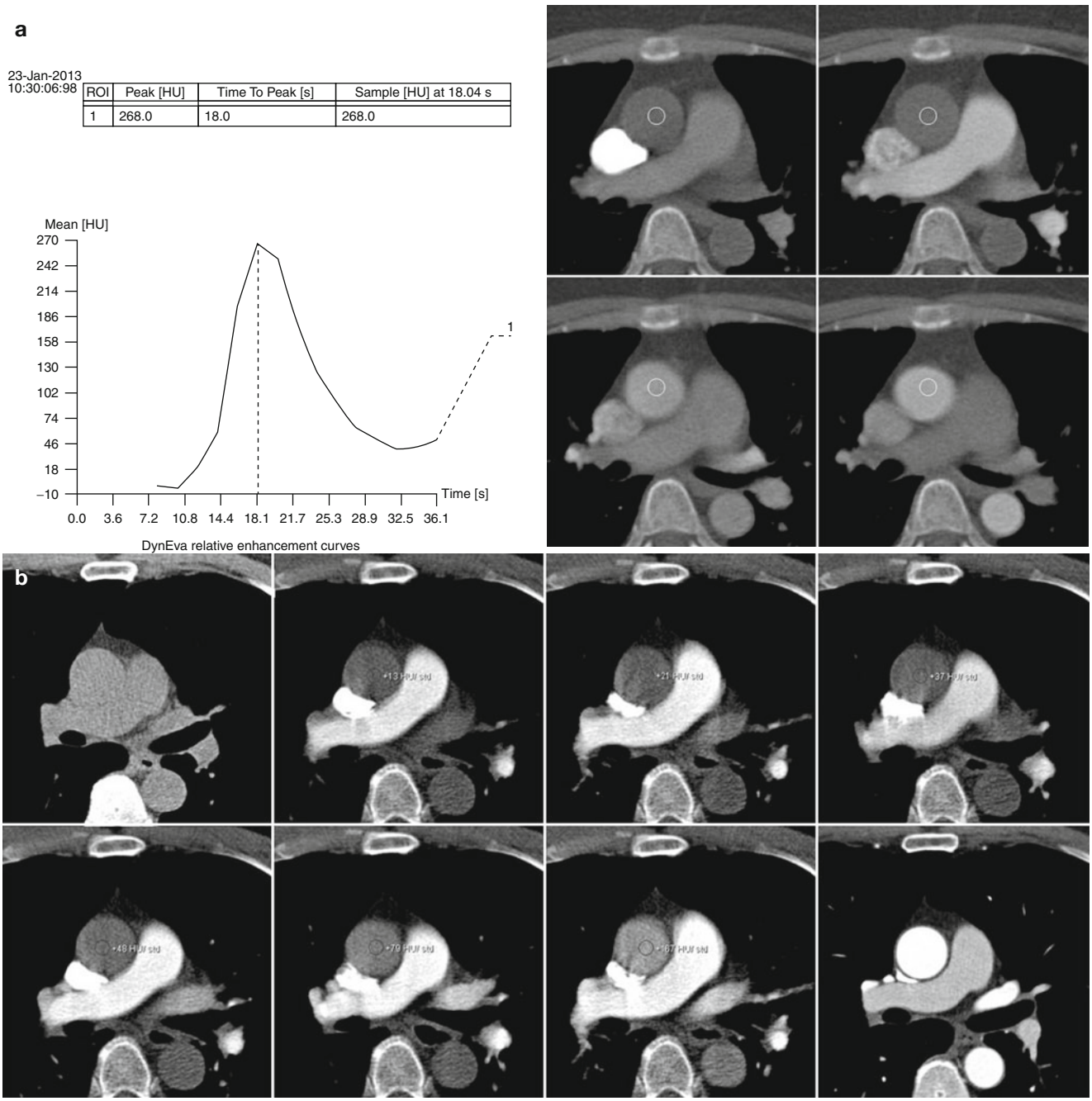

Fig. 21.10 Contrast timing methods. (**a**) Test-bolus method is based on test-bolus IV contrast injection during monitoring scans at the vessel of interest. In this patient, contrast enhancement curve reveals 18 s of time to peak contrast enhancement at the ascending thoracic aorta. Optimal scan delay is time to peak plus additional 3–4 s. (**b**) Bolus-tracking method based on real-time monitoring of the main contrast bolus at the vessel of interest. In this patient, the trigger threshold is 100 HU at ascending thoracic aorta. Optimal scan delay is 4–8 s after reaching to the trigger threshold

- Reconstruction interval (increment)
  - The nominal distance between the centers of consecutively reconstructed slices.
  - Defines the degree of overlap between reconstructed axial images.
  - For cardiac CT, 40–60 % overlap is desirable (e.g., 0.75 mm slice thickness with 0.4 mm increment) [15].

21.5.2 Reconstruction Algorithm (Kernel)

- Convolution filter used to convert the raw data from the spiral scan raw data into interpretable images.
- Different kinds of kernels are provided by manufactures.
  - B20f for smooth, B30f for medium smooth, B40f for medium, and B60f for sharp reconstruction kernels are provided by Siemens.

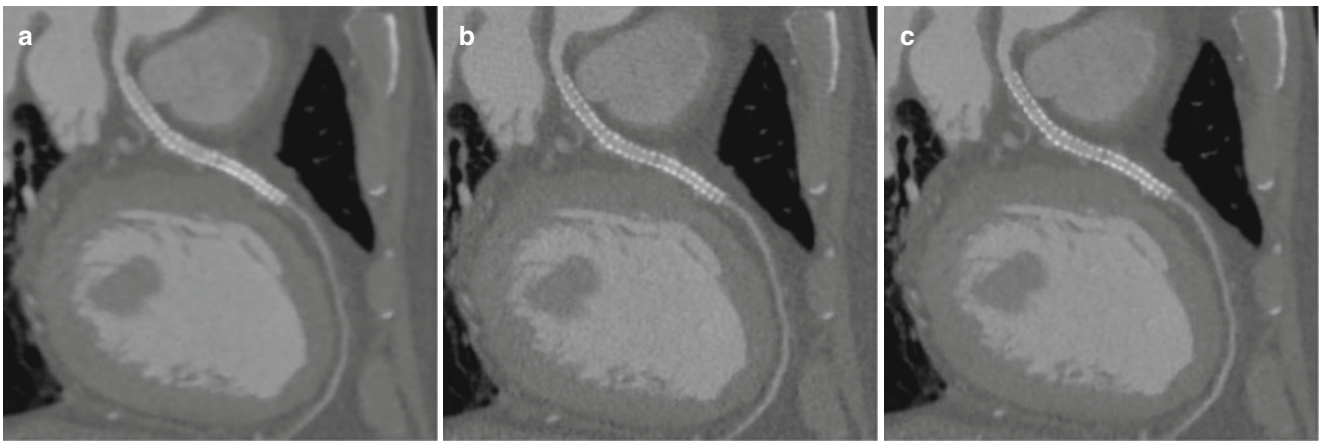

Fig. 21.11 Reconstruction algorithm (Kernel). Transaxial CT images obtained with different contrast injection protocols in the same patient. (**a**) Curved MPR image using soft kernel (B26f) shows blooming artifacts at stent strut due to partial volume averaging effect. (**b**) Curved MPR image using sharp kernel (B46f) shows sharp delineation of strut with homogenous in-stent lumen contrast. (**c**) Curved MPR image using sharp kernel (B46f) and iterative reconstruction (SAFIRE, Siemens) shows sharp delineation of strut with decreased image noise

  - Cardiac sharp (CC), cardiac detailed stent (CD), Y-sharp (YA), Y-detail (YB), Xres smooth (XCA), Xres standard (XCB), Xres sharp (XCC), and Xres detailed stent (XCD) reconstruction algorithms are provided by Philips.
- Medium kernels are typically used for coronary CTA.
- Softer kernels to reduce the image noise.
- Sharp kernel for patients with heavy calcification or stent (Fig. 21.11).

21.5.3 Choosing the Optimal Reconstruction Window

- The time delay can be either relative or absolute and either forward or reverse.
- Relative delay method: certain time delay from the prior wave is determined as a percentage (e.g., 50, 60, 70 %) of the R–R interval.
  - Preview technique: detailed coronary motion analysis by 1 % or 10 ms interval reconstruction at mid-RCA level (Fig. 21.12).
  - Non-preview technique: empirically chooses mid-diastole (60–75 % R–R) for slower regular heart rates <60 bpm or end-systole (30–35 % R–R) for fast heart rate >80 bpm (Fig. 21.12).
- Absolute delay method: a fixed time delay (e.g., 400 or −400 ms, respectively) after the R wave or before the next R wave.
  - Best quality imaging can be obtained with reconstruction intervals of −350 and −400 ms.
- Each of the coronary arteries is most susceptible to motion artifacts in different phases of the cardiac cycle. Therefore, individual coronary arteries are optimally visualized in different phases of the cardiac cycle.
  - Appropriate reconstruction windows: 40 % of R–R interval for RCA, 60–70 % for LAD, and 50–60 % for LCX.
- Automatic selection of best phases for cardiac image reconstruction (Fig. 21.12).
  - PhaseXact (by Toshiba) or BestPhase (by Siemens) based on a 4D motion map → The phases of minimum motion in systole and diastole are automatically detected.

21.5.4 Single-Segment Reconstruction (Partial Scan or Half-Scan Reconstruction)

- A single cardiac cycle is used to create one cross-sectional image.
- The minimum amount of data for reconstruction of one cross-sectional image requires projection data of at least 180° in any axial plane.
- Optimal for patients with a low heart rate less than 65 beats per minute.

21.5.5 Multisegment Reconstruction

- For patients with a high heart rate, data from more than one cardiac cycle can be used to reconstruct the image.
- Depending on the CT manufacturer, a 2–4 segment reconstruction is possible.
- Sensitive to heart rate variation
- Associated with higher radiation exposure due to low pitch

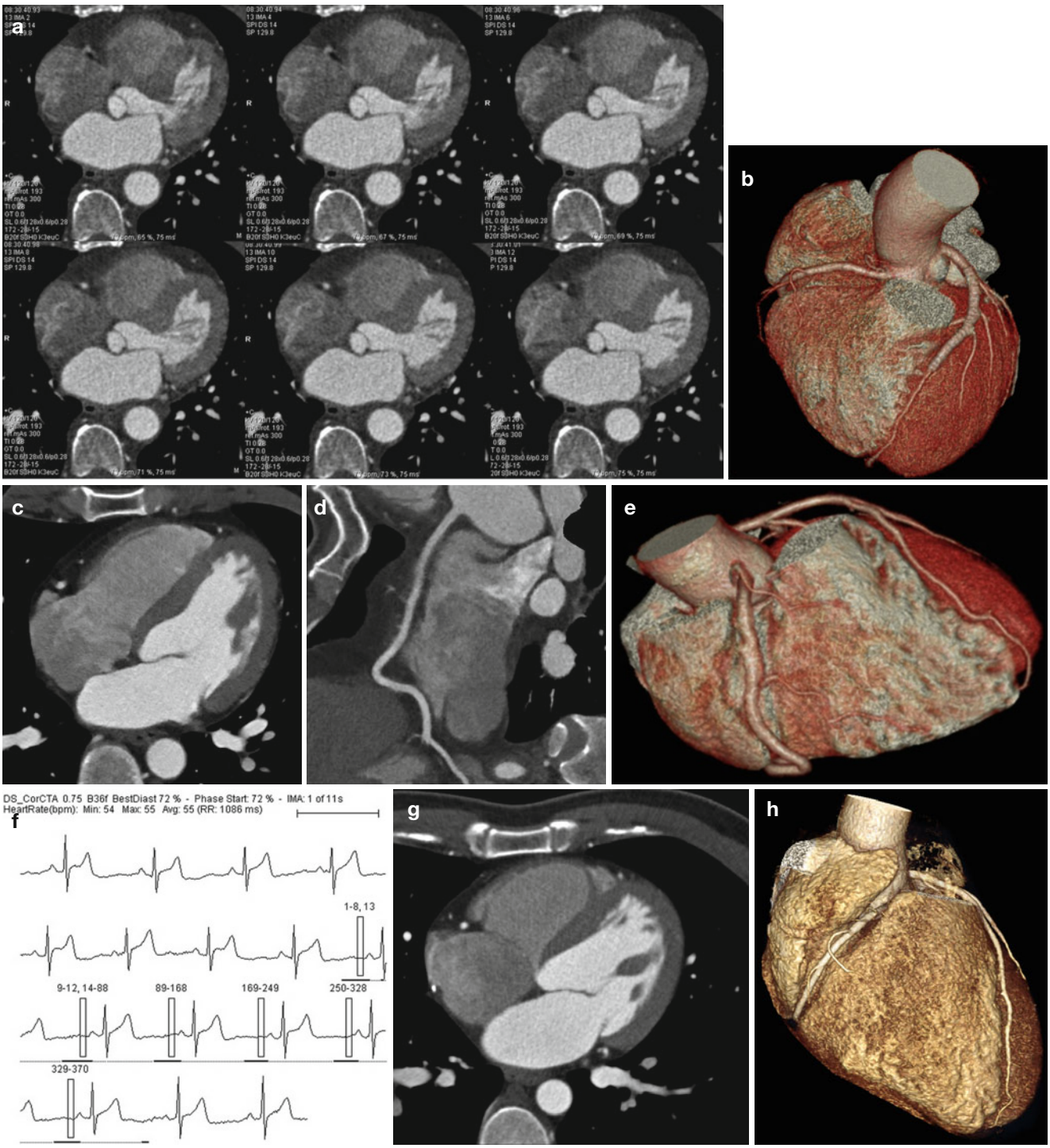

Fig. 21.12 Choosing the optimal reconstruction window. (**a**, **b**) Using preview function, the user can manually select an optimal reconstruction phase with the least motion. (**c**–**e**) Reconstruction phase at 65 % of R–R interval can be empirically selected in patients with heart rate <60 bpm. However, curved MPR and VRT images show a blurring at mid-segment of RCA. (**f**–**h**) Advanced software (BestPhase, Siemens) can automatically select a motion free reconstruction phase. In this patient, 72 % of R–R interval is the best diastolic phase with the least motion. Transaxial and VRT images show sharp delineation of RCA

21.5.6 Iterative Reconstruction

- The greatest potential for significant improvements in spatial resolution for cardiac CT [16]
- Leads to an effective suppression of image noise in predominantly obese patients (Fig. 21.13)
- Reduces blooming artifacts from calcifications in patients with heavily calcified coronary arteries

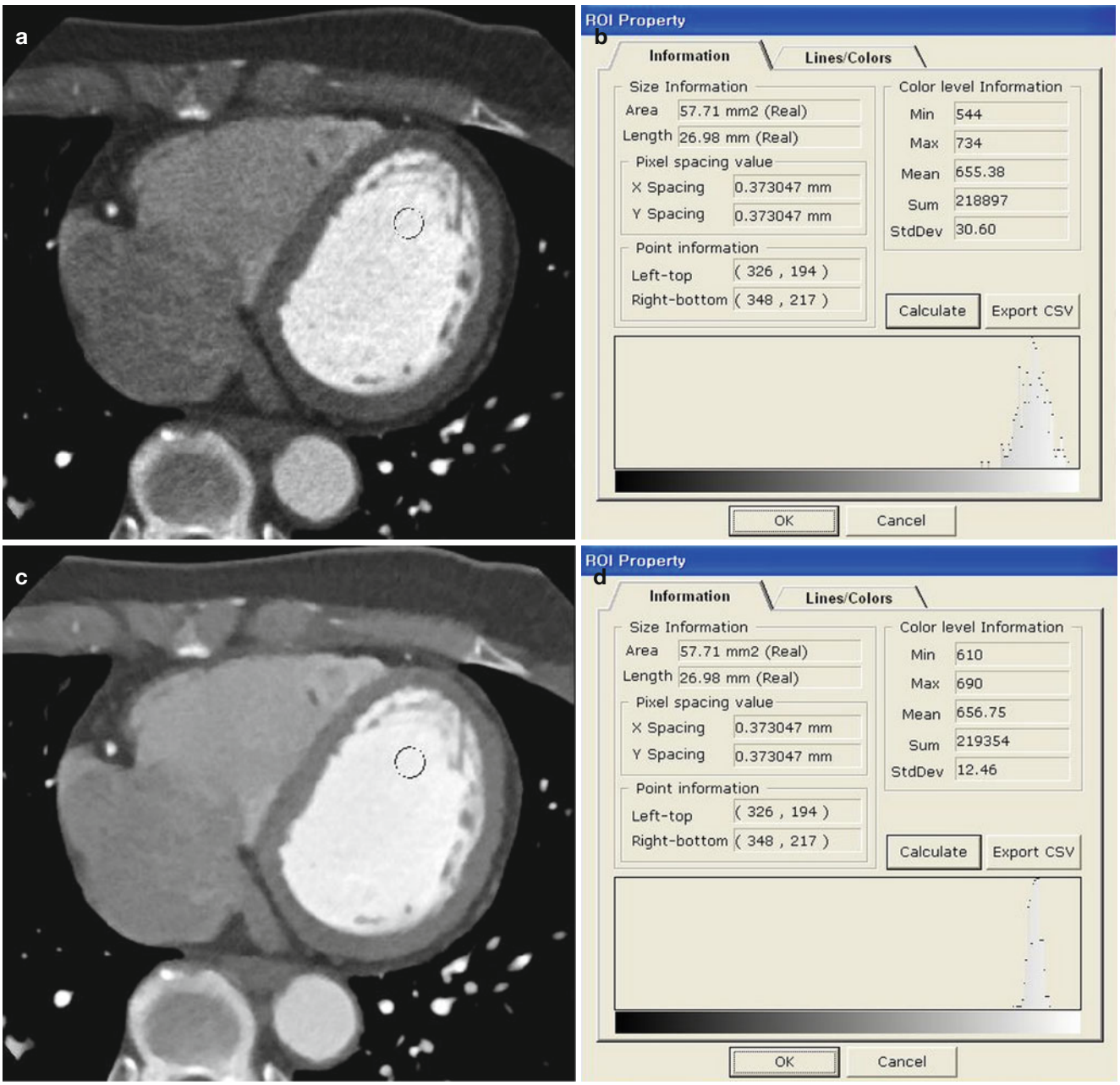

Fig. 21.13 Iterative reconstruction technique. (**a**, **b**) Image reconstructed by filtered back projection technique shows image noise with 30.60 HU of standard deviation. (**c**, **d**) Iterative reconstruction by iDose4 (Philips) in the same patient shows decreased image noise with 12.46 HU of standard deviation

21.6 Image Processing Techniques

- Further processing and evaluation of native axial images is performed on an independent workstation.
- A combination of various viewing methods has been used in most studies.

21.6.1 Axial Review (Scrolling)

- The initial step to check the image quality in terms of contrast enhancement and motion artifacts
- Confirms the optimal phase selected to display each of the coronary arteries [17]
- Offers axial review for the presence and extent of calcified and noncalcified plaque → determine the best post-processing tools.

21.6.2 Multi-planar Reformation (MPR) and Average Intensity Projection (AIP)

- The main planes for the evaluation of the coronary arteries

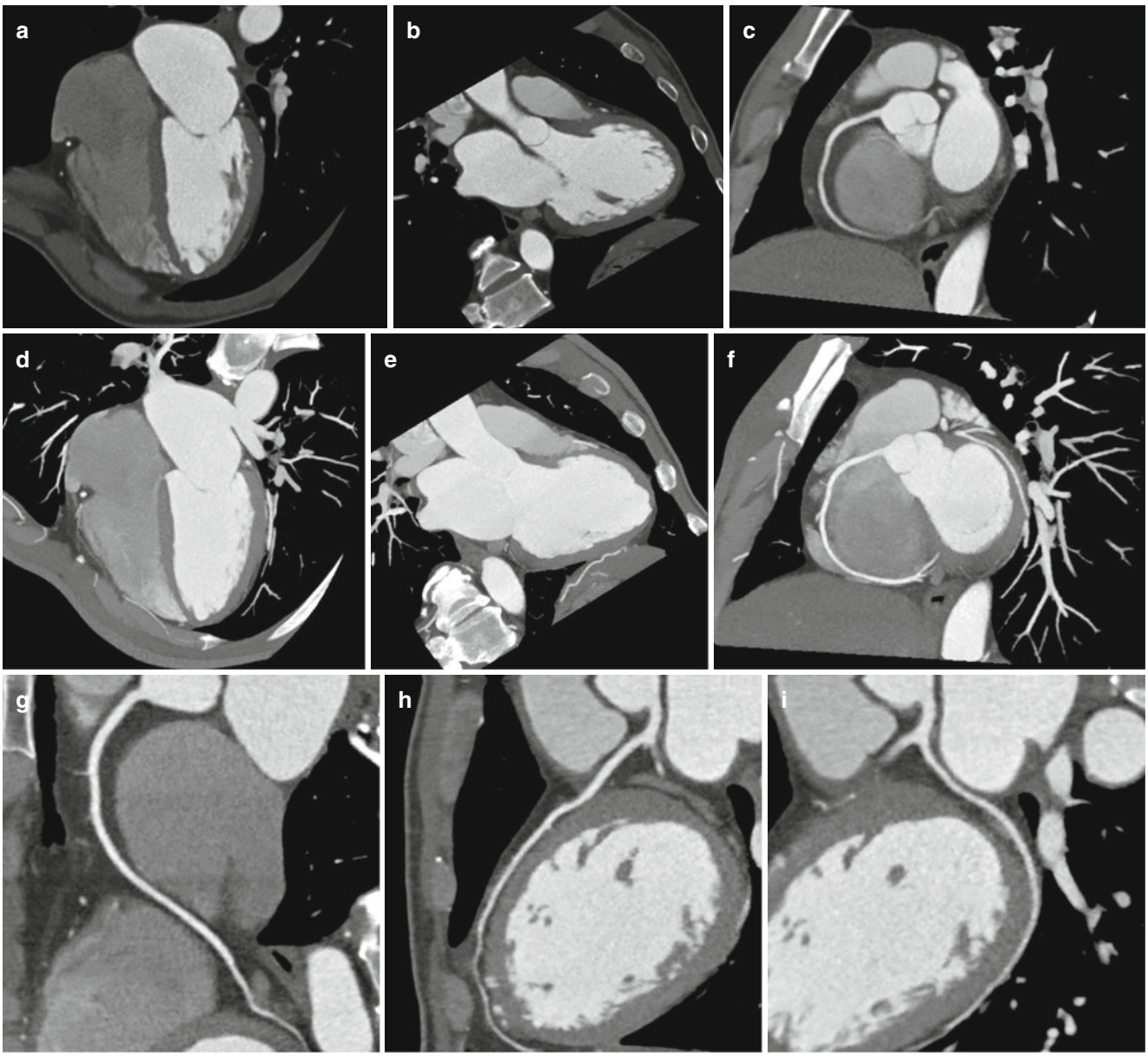

Fig. 21.14 Various image processing techniques. (**a**–**c**) Four-chamber, long-axis, and short-axis views are acquired using average intensity projection (AIP) technique with 3 mm slice thickness, which is one type of multi-planar reformation (MPR). (**d**–**f**) With thin-slab maximum intensity projection (MIP), technique with 8 mm slice thickness, four-chamber, long-axis, and short-axis views show longer segment of coronary arteries and allow better displaying small vessels compared with MPR technique. (**g**–**i**) Curved MPR technique can create an entire length of coronary artery on a single image. RCA, LAD and LCX, respectively, are well visualized without significant stenosis

  - The plane parallel to the atrioventricular groove.
  - The plane parallel to the interventricular groove.
- Suitable to understand relationship between lesion and surrounding structure.
- Limitations [17]
  - Less useful to display the entire length of an artery
  - Allows a potential error of stenosis grading due to partial volume averaging
- Average intensity projection (AIP) shows the average of each component attenuation value encountered by thickening MPRs (Fig. 21.14).

21.6.3 Curved Multi-planar Reformation (Curved MPR)

- Can be created to include an entire structure on a single image (Fig. 21.14).
- Used to identify and quantify the degree of stenosis without potential error by partial volume averaging.
- Allows displaying the cross-sectional profile of a vessel along its length.
- The main potential pitfall of cMPR is an inaccurate centerline determination.

  - Because of the small caliber of the coronary arteries (2–5 mm), off-axis centerline placement may result in misinterpretation of stenosis [17].
  - In the presence of heavy arterial calcification, cMPR has a difficulty discriminating lumen contrast and calcification to define the vessel center.
- Two-dimensional (2-D) map view (Extended Brilliance Workspace, Philips) is a rendering derived from the three-dimensional coronary tree view created by curved MPR images. 2-D map view provides a very quick orientation with respect to the vessels present and their course.

21.6.4 Maximum Intensity Projection (MIP)

- Displaying only the highest attenuation value in a given slice (Fig. 21.14)
- Useful for coronary artery imaging, especially better for displaying small-caliber segments [18].
- Limitations
  - Coronary artery calcification can lead to overestimation of stenosis, even in the presence of small amounts of calcium.
  - Noncalcified plaque without significant luminal narrowing will be overlooked because of its low attenuation value [17].
  - Limited perception of 3D relationships between structures by a lack of depth information.

21.6.5 Minimum Intensity Projection (MinIP)

- MinIP technique is designed to display only the lowest attenuation value in a given slice.
- Useful for assessment of infarcted myocardium.

21.6.6 Three-Dimensional Volume Rendering Technique (VRT)

- Quickly provides an initial overview including spatial relationships [17]
- Accurately defines complex anatomy of the heart and coronary arteries (Fig. 21.15)
  - Particularly useful in patients with coronary artery bypass grafts
- Operator-dependent, poor quantitative measurement (Fig. 21.15)

21.6.7 Dynamic Cine View

- Requires the reconstruction of multiple phases
- Useful for evaluation of the cardiac valves and regional ventricular function, so allows accurate quantitative assessment of ventricular volumes and function, ejection fraction, and regional wall motion and wall-thickening abnormalities [18]

21.7 Image Quality and Artifacts

- The ideal parameters are to enable high temporal resolution with fast gantry rotation, high spatial resolution with thin collimation, and low radiation dose.
  - Faster scanning → improves temporal resolution, but decreases spatial resolution.
  - Imaging protocols for optimizing spatial resolution → reducing the speed of image acquisition → allows more motion artifacts.
  - Scanning for a longer time and narrowing collimation → increase the radiation dose and decrease image contrast resolution.
- When making decisions about imaging protocols, one must consider when to favor temporal resolution over spatial resolution and vice versa.

21.7.1 Temporal Resolution

- Temporal resolution is the time needed to acquire enough data for reconstruction of one cross-sectional CT image.
  - One-half the gantry rotation time for single-source CT scanners
  - One-fourth the gantry rotation time for dual-source CT scanners
- The parameters which affect temporal resolution
  - Gantry rotation speed
  - Pitch
  - Number of detectors
  - The ability to acquire image data in a segmented fashion
- High temporal resolution is critical to minimize or eliminate motion artifact associated with the beating heart (Fig. 21.16).
- With recent technical advances such as decreased gantry rotation times and a dual-source scanner, temporal resolution has significantly improved up to 75 ms (Table 21.3).

21.7.2 Spatial Resolution

- Spatial resolution is defined as the ability to discern two objects as separate from one another.
- Axial (in-plane or *x*–*y* axis) resolution

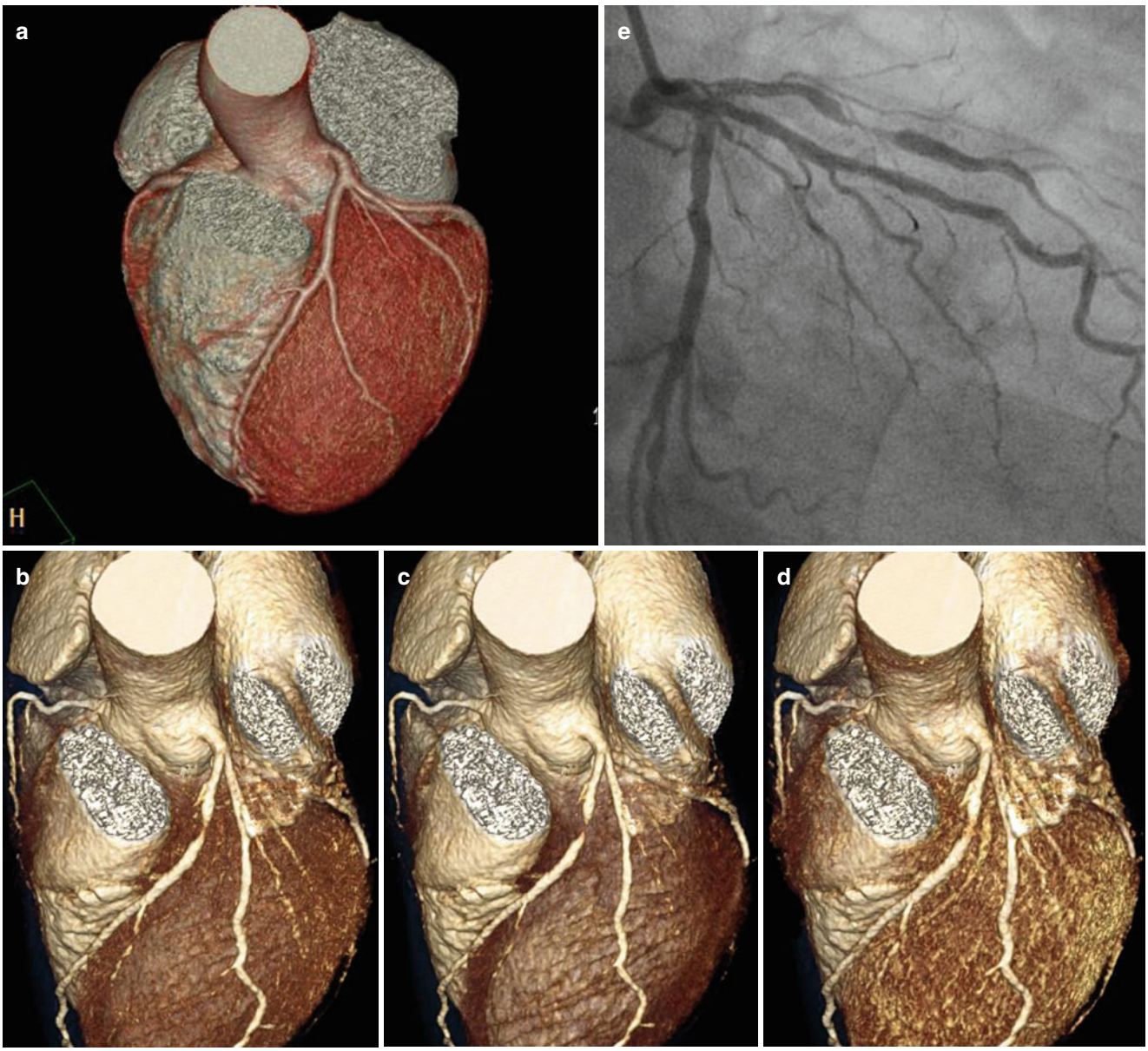

Fig. 21.15 Volume rendered technique (VRT). (**a**) VRT provides a quick initial overview and allows three-dimensional visualization of coronary arteries. However, VRT is user dependent. (**b**) VRT shows a significant stenosis at mid-segment of LAD. (**c**, **d**) According to the different window width and level setting, the lesion looks like obstruction or nonsignificant stenosis. (**e**) Coronary angiography confirmed a tight stenosis at LAD, but not obstruction

  - Dependent on the scan field of view (FOV) and image reconstruction matrix.
  - Conventional 512×512 matrix: the transverse pixel size for a 25-cm FOV is 0.49 mm (250 mm/512).
- Longitudinal (out-of-plain or cross-plane or through-plane or *z*-axis) resolution
  - Depends on x-ray focus size, detector element size, detector collimation, slice thickness, reconstruction increment, filtering (kernel), and FOV.
  - Thicker slices and softer reconstruction kernel reduce spatial resolution.
  - In recent MDCT scanners, longitudinal resolution provides 0.5–0.625 mm widths, so isotropic spatial resolution of $0.5 \times 0.5 \times 0.5$ mm^2 can be achieved [8].
- *Z*-axis flying x-ray focal spot technique and double *z*-sampling
  - Deflection of the focal spot along the *z*-axis acquired with twice the number of measured values in the *z*-direction.
  - With this technique, the longitudinal resolution for 0.6 mm collimated detector widths can be improved to 0.33 mm.

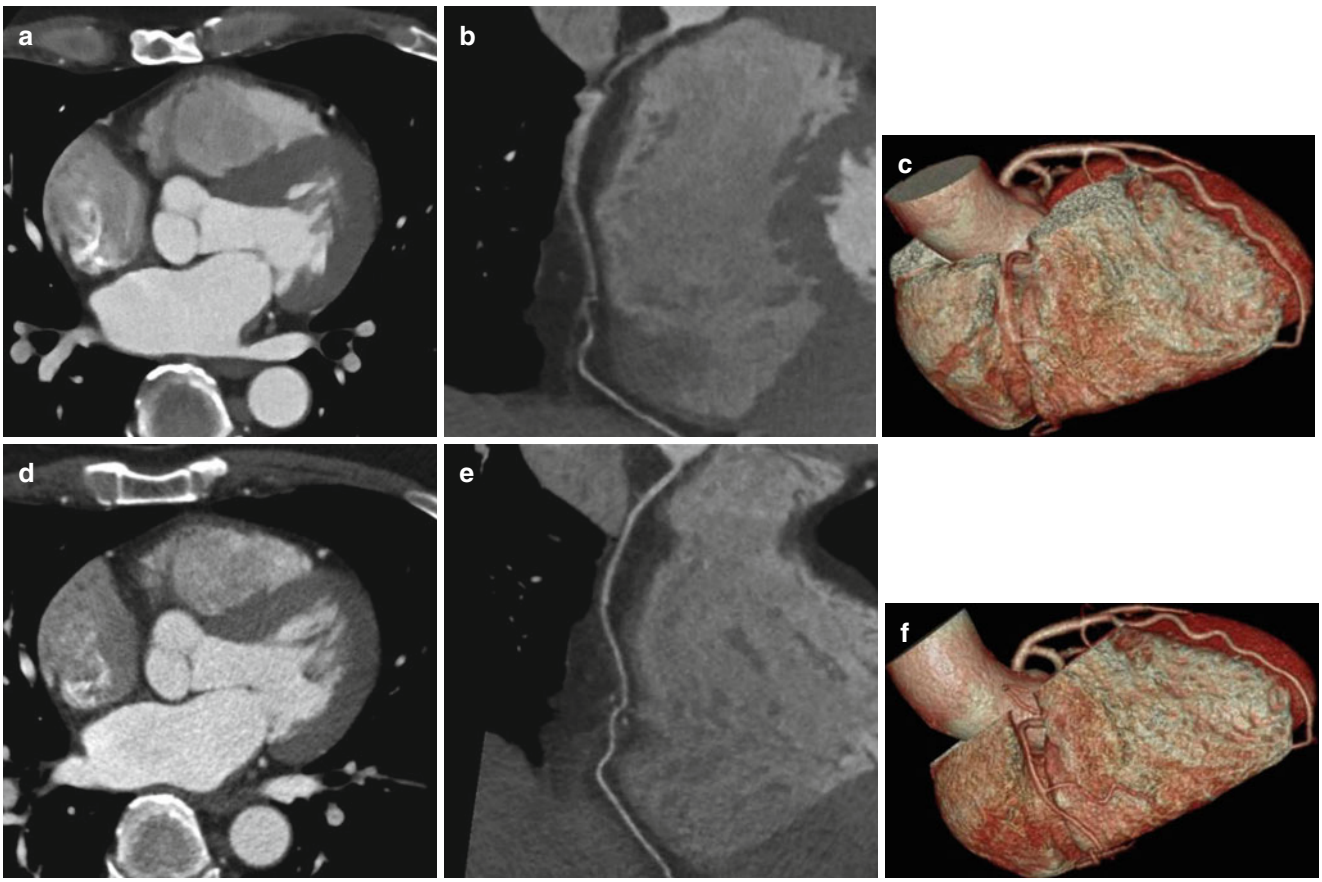

Fig. 21.16 Temporal resolution. (**a**–**c**) In a patient with 63 bpm, transaxial, curved MPR and VRT images using 64-slice CT scanner with 400 ms gantry rotation time show blurring at entire segments of right coronary artery. (**d**–**f**) Transaxial, curved MPR and VRT images in the same patient 2 years after first CT examination using dual-source CT with 280 ms gantry rotation time provide a clear demarcation of right coronary artery, even in subequal heart rate (62 bpm)

Table 21.3 Specifications of the most recent CT scanner

Vendors	Toshiba	GE	Siemens	Philips
Scanner model	Aquilion One	750HD	Somatom definition Flash	Brilliance iCT
Source (x-ray tube)	Single	Single	Dual	Single
Rotation time	350 ms	350 ms	280 ms	270 ms
Temporal resolution				
Half-scan reconstruction	175 ms	175 ms	75 ms	135 ms
Multisegment reconstruction	35 ms			34 ms
Number of detector rows	320	64	64×2	128
Slice number	640 with double-slice technology	128 using 2 energies	128 with flying focal	256 with smart focal
Thickness of detectors (collimation)	0.5 mm	0.625 mm	0.6 mm	0.625 mm
Coverage	320×0.5 mm=160 mm	64×0.625 mm=40 mm	64×0.6 mm=38.4 mm	128×0.625 mm=80 mm
Prospective ECG triggering	1-beat volume scan	SnapShot Pulse	Adaptive Cardio Sequence Flash Spiral	Step-and-Shoot Cardiac
Dose modulation	SUREExposure 3D	Auto mA	CARE Dose 4D	DoseRight ACS
Iterative reconstruction	AIDR	ASiR	SAFIRE	iDose4

AIDR adaptive iterative dose reduction, *ASiR* adaptive statistical iterative reconstruction, *SAFIRE* sinogram affirmed Iterative reconstruction

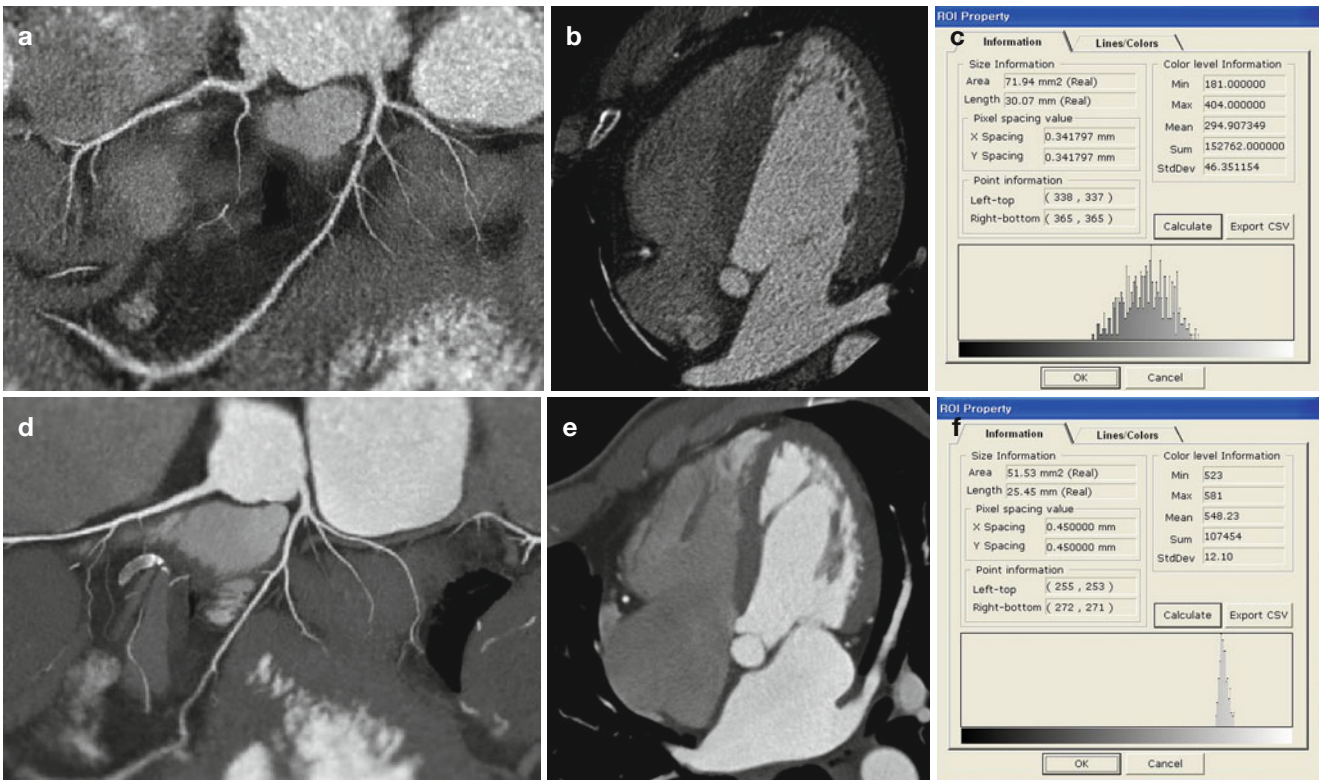

Fig. 21.17 Image noise. (**a**–**c**) 2-D map and four-chamber views reveal poor image quality due to obesity (BMI = 39 kg/m^2). Image noise is 45.4 HU of standard deviation. (**d**–**f**) 2-D map and four-chamber views reveal good image quality in a slim patient (BMI = 22 kg/m^2). Image noise is 21.4 HU of standard deviation

21.7.3 Contrast Resolution (Low-Contrast Resolution) and Noise

- Defined as the degree of contrast to differentiate between tissues with varying attenuation characteristics and is the most important factor to decide image quality.
  - Affected by radiation intensity (tube voltage and tube current), slice thickness, reconstruction algorithms, and image noise
  - Thicker section thickness and smooth kernel → increase contrast resolution, but decrease spatial resolution
  - Long scan duration and increased tube current → increased contrast resolution, but increase radiation dose
- Noise (or quantum noise) in the CT images is the variability of the attenuation value between two neighboring voxels compared to the average attenuation measured in that area.
  - Expressed by standard deviation of CT number (Hounsfield units, HU) of pixel (Fig. 21.17).
  - Affected by patient's body habitus (e.g., obesity), tube current, slice collimation width, pitch, and reconstruction algorithms
  - Decreased by raising the tube current → causes increased radiation exposure
- Consider a balance between sufficient image quality and low radiation dose.

21.7.4 Artifacts

- Various artifacts can degrade image quality at coronary CT angiography.
- Artifacts were categorized according to causes or manifestations, which include motion-related artifact, beam-hardening artifact, partial volume averaging effect, and structure-related artifact.

21.7.4.1 Cardiac Motion Artifact

- Blurring artifacts (Fig. 21.18) ← the motion velocity of the coronary segment of interest exceeds the temporal resolution of the CT technique [16].
- Stair-step artifacts occur due to misregistration of slice registration at multiple planes in patients with heart rate variations or arrhythmia (Fig. 21.19).
- Remedy
  - Rapid heart rate (>70–75 bpm): the use of β-blockers, choosing appropriate reconstruction window for each coronary artery, and multisegment reconstruction are the solutions.

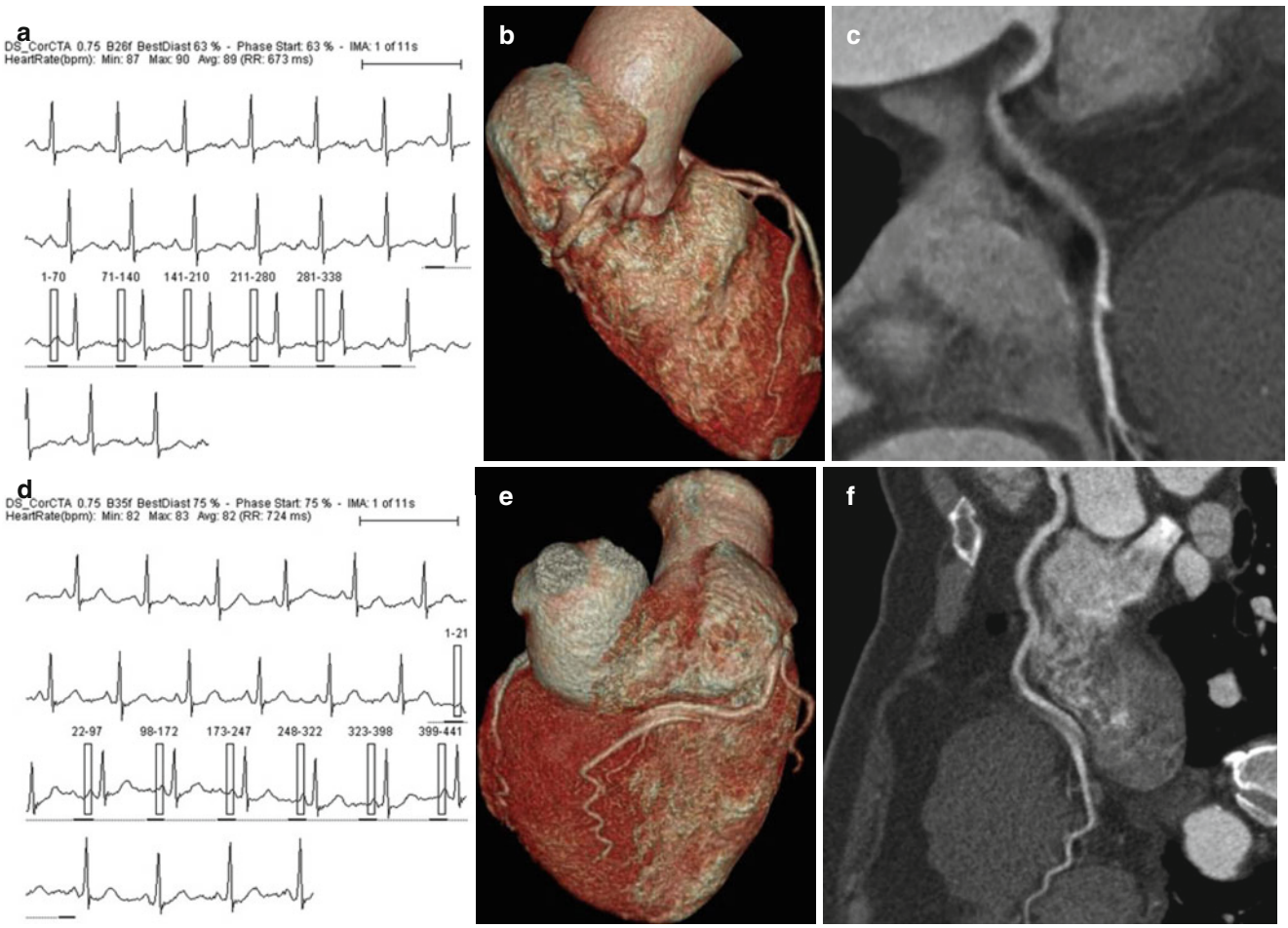

Fig. 21.18 Artifacts due to rapid heart rate. (**a**–**c**) ECG information represents a retrospective ECG-gated technique with tube current modulation in patient with rapid heart rate (89 bpm). VRT and curved MPR images show poor demarcation and blurring at mid-segment of right coronary artery. (**d**–**f**) ECG information represents a retrospective ECG-gated technique with tube current modulation in patient with rapid heart rate (82 bpm). VRT and curved MPR images show double coronary artery appearance of distal RCA

– Arrhythmia: using the ECG editing to eliminate an inappropriate segment or adding a reconstructed data set of desired segment is helpful.

21.7.4.2 Respiratory Motion Artifact

- Patient's breathing during scanning arouses image blurring, image gaps, image overlap (double coronary artery), and also stair-step artifacts.
- Shown as across the scan field (Fig. 21.20).
- Cannot be corrected with image data reconstruction methods.
- Remedy
  - Redundant breathing instruction
  - Oxygen supplementation
  - Use higher detector row scanners or increased anatomic coverage

21.7.4.3 Streak Artifact due to Beam Hardening

- With high-density objects (e.g., surgical clips, pacemaker wires, markers, stents and coronary, contrast bolus in the SVC or right heart), lower energy photons are absorbed and the beam intensity is increased (beam hardening). → Streak artifact (Fig. 21.21).
- Remedy
  - The use of nonmetallic surgical material is helpful in evaluation of bypass grafts.
  - The use of saline chaser after contrast injection.

21.7.4.4 Blooming Artifact due to Partial Volume Averaging Effect

- Blooming artifacts occur due to high-density objects, such as coronary artery calcium and small stents (<3 mm), and can arouse pseudostenosis or non-assessable segments in coronary CTA. The artifact may oversize calcified plaques on the CT image and resulted in subsequent overestimation of luminal narrowing (Fig. 21.22).
- Remedy
  - Use thin section width and high spatial resolution algorithms.

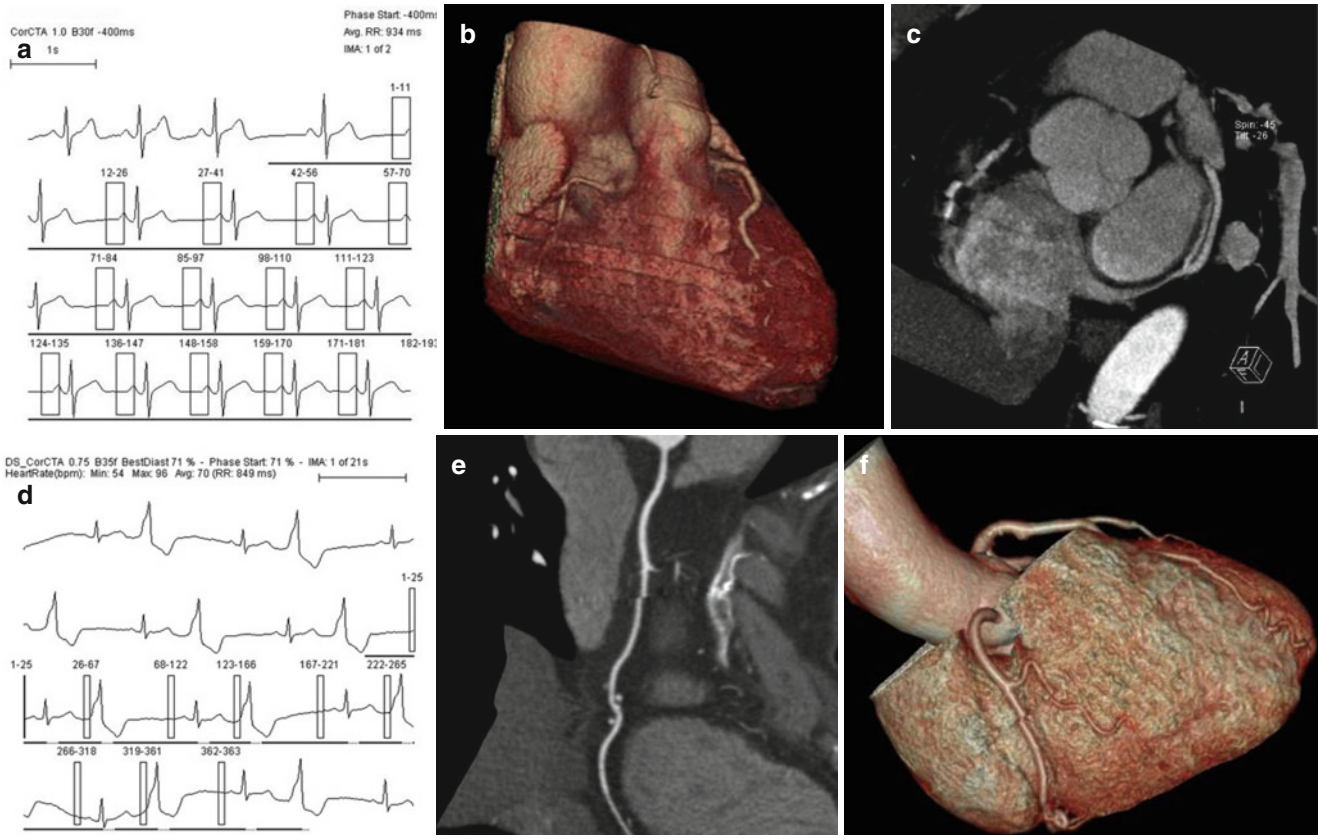

Fig. 21.19 Stair-step artifact. (**a**–**c**) ECG information represents a retrospective ECG-gated technique without tube current modulation in patient with heart rate variation. VRT and curved MPR images show multiple linear offsets across the midportion of the heart that resembles a stepladder. (**d**–**f**) ECG information represents a retrospective ECG-gated technique with wide range of ECG pulsing in patient with ectopic beat. Curved MPR and VRT show stair-step artifact across the midportion of the heart

  - Use iterative reconstruction techniques or dual-energy CT with special edge-enhancing image filters.

21.7.4.5 Structure-Related Artifact

- Overlapping contrast filled normal anatomic structures (e.g., left atrial appendage, cardiac vein) may obscure coronary arteries.
- Venous structures crossing coronary arteries can cause a loss of attenuation within the vessel of interest → may mimic soft plaque.
- Remedy
  - Reviews of various reconstruction phases can reduce this effect.

21.8 Radiation Dose of Cardiac CT

- Radiation exposure varies with types of CT scanner and scan protocols for cardiac examinations.
- With retrospective ECG-gating technique, the radiation dose of 64-slice CT ranges from 8 to 25 mSv, which is clearly a higher than average 7–10 mSv in conventional coronary angiography.
- Following the ALARA (as low as reasonably achievable) principle, all parameters should be considered to reduce radiation exposure to minimum while preserving image quality and to balance the expected benefits and the radiation risk.

21.8.1 Radiation Dose Terminology

- Radiation exposure is the amount of ions produced in air by x-ray beam and is expressed in coulombs per kilogram (C/kg).
- Absorbed radiation dose is the amount of energy that is actually absorbed at a specific point in space (Table 21.4).
- The dose length product (DLP, mGy · cm) represents the integrated radiation dose over all slices from an entire CT examination and is calculated by multiplying $CTDI_{vol}$ by the scan length in centimeters ($DLP = CTDI_{vol} \times$ scan length) [9].
- The effective dose (E, mSv) reflects the risk of potential biological injury of radiation. A good estimation of effective dose (E) can be obtained from multiplying the DLP by a conversion coefficient (k), which is specific to the body region that has been scanned.

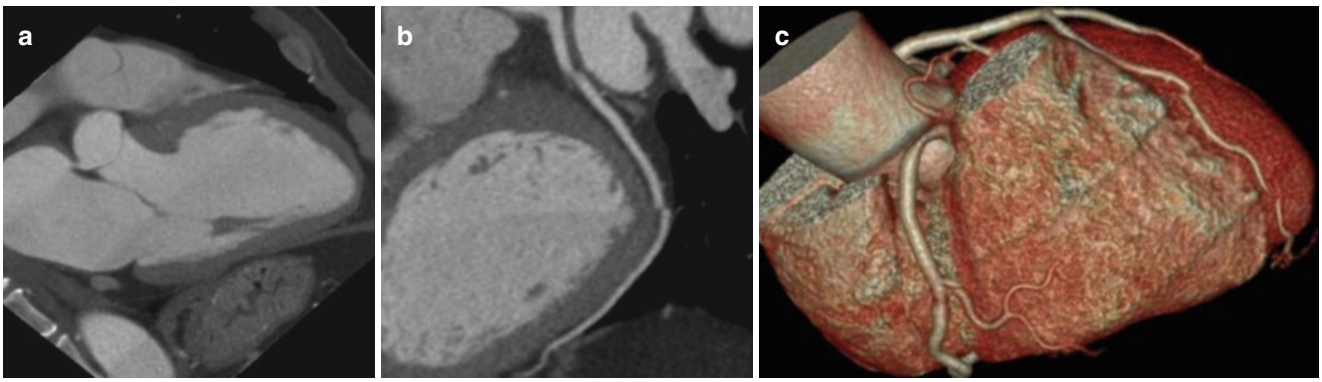

Fig. 21.20 Respiratory motion artifact. Long-axis view (**a**), curved MPR (**b**), and VRT (**c**) images show stair-step artifacts across the entire scan field including chest wall

- The published chest conversion factors applied to the DLP by other groups have varied between 0.014 and 0.017 mSv/(mGy·cm) based on the International Commission on Radiation Protection (ICRP) [19].
- An established conversion factor of 0.014 mSv/(mGy·cm) as has been proposed by the European Working Group for Guidelines on Quality Criteria in CT and endorsed by the American Association of Physicists in Medicine.

21.8.2 Factors Influencing Radiation Dose

- Tube voltage and tube current: Reducing kVp or mA decreases radiation dose but increases image noise.
- Scan time: Long scan time increases radiation dose.
- Table pitch: If the table pitch is increased, the radiation dose is lower, because the anatomy is exposed to the radiation beam for a shorter amount of time.
- Gantry rotation time: If the gantry rotation time is reduced, the radiation dose is decreased.
- Detector configuration: With wide detector arrays, increased *z*-coverage per rotation requires fewer rotations of the gantry to be performed to image the heart; therefore, scan time is decreased and radiation dose is reduced.

21.8.3 Radiation Exposure Reduction

21.8.3.1 Minimization of Scan Coverage

- The smallest possible FOV and scan range that encompasses the entire anatomy of the heart should be selected to acquire maximum spatial resolution and to reduce radiation dose [7].
- Topography image and prior coronary calcium scoring examination can be used as a guidance of scan range.

21.8.3.2 Reduction of Tube Voltage

- Effective means to reduce radiation dose.
  - 100 kVp for the patient's BMI <25 kg/m^2
  - 80 kVp for children and slim young adults with BMI <20 kg/m^2
- CARE kV (Siemens Healthcare, Forchheim, Germany): automatically recommends the optimal kV setting for each individual patient for each specific exam.

21.8.3.3 Anatomy-Based Tube-Current Modulation

- To determine the optimal nominal tube current necessary to achieve the desired noise based on patient attenuation in the scout image [8]
- Automatic exposure control (AEC)
  - In the x–y plane (angular modulation)
  - Along the scanning direction (*z*-axis modulation)
  - Both (combined modulation)
- Recent report involving a different AEC systems (AutomA 3D for General Electric, ACS+Z-DOM for Philips, CARE Dose 4D for Siemens, and SUREExposure 3D for Toshiba) → dose saving of 35–60 % [20].

21.8.3.4 ECG-Based Tube-Current Modulation (ECG Pulsing)

- The tube current is at a maximum only during the cardiac phase of interest and is reduced substantially outside this phase. → Radiation dose can be reduced by 30–50 %.
- The minimum tube current outside pulsing window can be selected by the user (Fig. 21.23).
  - The usual ECG-pulsing dose is 20–40 % of full radiation dose for outside range.
  - MinDose (Siemens Healthcare, Forchheim, Germany) technique applies full dose on selected range of R–R interval and 4 % of mAs for remained range. → similar dose level to prospective ECG-triggering technique.
- User adjustment of the maximum tube-current duration before scanning: the phase of full tube current is limited

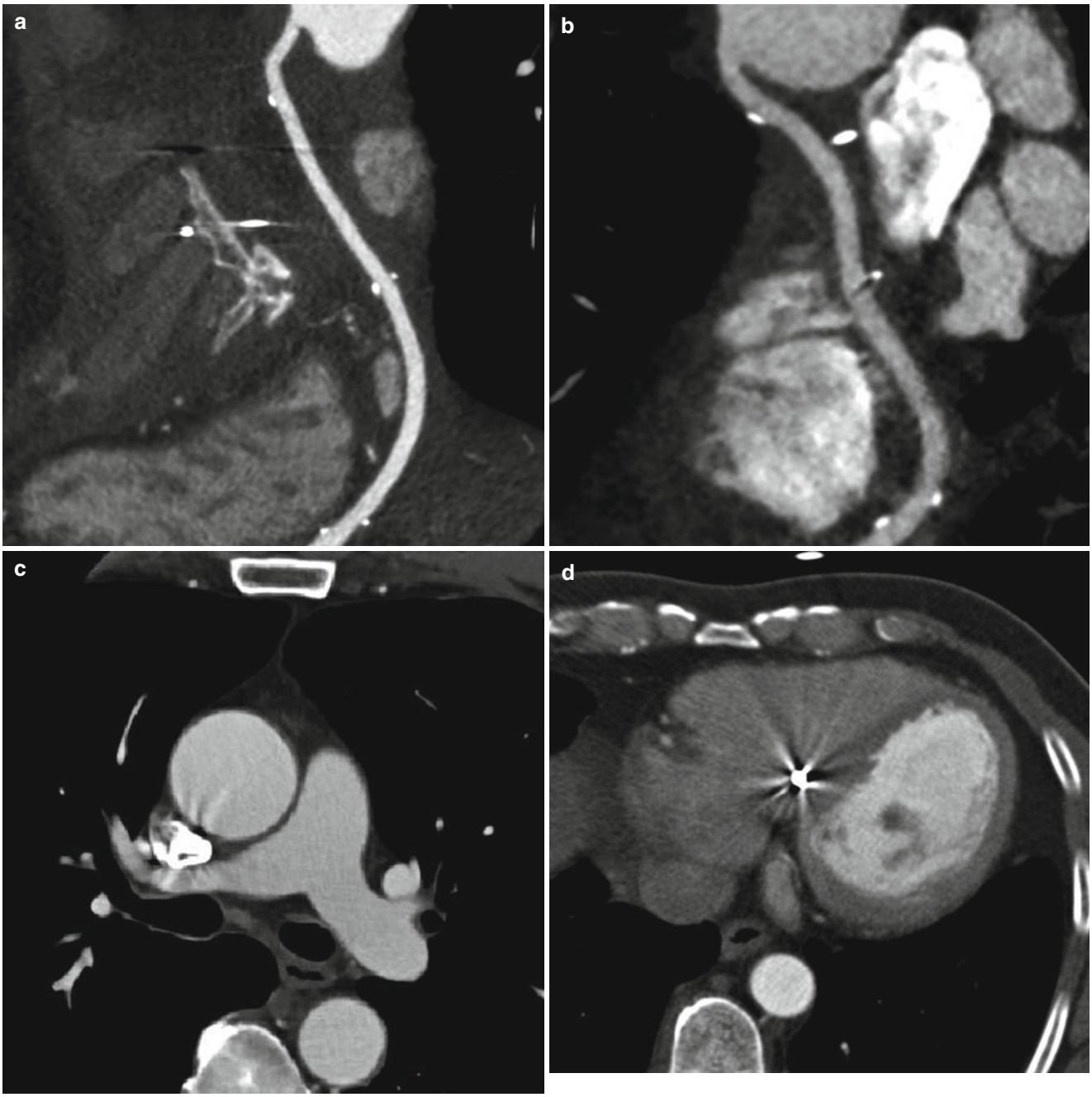

Fig. 21.21 Beam hardening artifact. (**a**) Beam hardening artifact due to surgical wire in patients with coronary artery bypass graft. (**b**) Beam hardening artifact due to surgical clips in patients with coronary artery bypass graft. (**c**) Streak artifact due to contrast media in right atrium. (**d**) Streak artifact due to electric wire in patients with cardiac pacemaker

to 70 % of R–R interval for low and regular heart rate and expanded to a wider between 35 and 70 % of R–R interval for higher heart rate.

- Temporary or permanent suspension of tube-current modulation, if beat-to-beat variation exceeds a threshold value during data acquisition in patients with severe arrhythmia.

21.8.3.5 Prospective ECG Triggering (Step-and-Shoot/Sequence Mode)

- The x-ray tube current is switched on only during the desired cardiac phase, significantly limiting x-ray exposure (Fig. 21.23).
- Accurate images of the coronary arteries can be obtained at doses as low as 1–3 mSv.

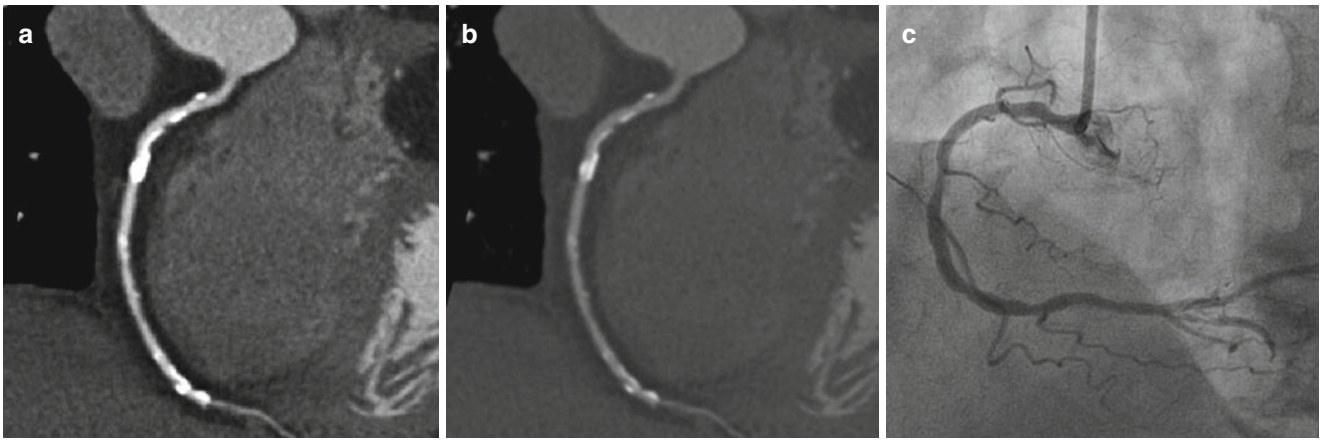

Fig. 21.22 Blooming artifacts. (**a**) In patient with heavy calcifications in right coronary arteries, curved MPR image with usual window setting shows an obliteration of luminal contour at mid-RCA due to blooming artifact. (**b**) Curved MPR image with bone window setting also shows a significant narrowing at the segment. (**c**) However, coronary angiography shows a mild stenosis at the same segments

Table 21.4 Parameters of radiation dose

Parameter	Mean	Calculation (unit)
CTDI100	Dose profile measured with a CT ion chamber, 100 mm long	(mGy)
Weighted CTDI ($CTDI_w$)	Dose corrected for the inhomogenous attenuation	2/3 peripheral $CTDI_{100}$ + 1/3 center $CTDI_{100}$ (mGy)
Volume CTDI ($CTDI_{vol}$)	Slice dose in a scan	$CTDI_w$/pitch (mGy)
Dose-length product (DLP)	Overall dose per scan	$CTDI_{vol}$/scan length (mGy · cm)
Effective dose (E)	Biologic effect of radiation dose received	DLP × k (mSv)

k (conversion coefficient) is 0.014 for chest region

21.8.3.6 High Pitch (Flash Spiral) Technique

- Combining high pitch value (3.2–3.4) and large detector coverage of 38.4 mm. → The entire heart can be scanned within a single heart beat.
- The mean estimated radiation dose has been reported as 0.9 ± 0.1 mV in 100 kVp scans and 1.9 ± 0.2 mSv in 120 kVp scans.
- Require a stable and low heart rate less than 60 bpm.

21.8.3.7 Pre-patient Z-Collimation

- Dynamic z-collimation for retrospective ECG-gated CT: Opposing collimator blades automatically open at the start of helical data acquisition and close at the end of acquisition to block radiation not contributing to image formation.
- Adaptive z-collimation for prospective ECG triggered CT: Reduces x-ray exposure by restricting the divergent x-ray beam along the z-axis and preventing x-rays outside the planned scan length from reaching the patient.

21.8.3.8 Iterative Reconstruction Algorithms

- Adaptive iterative dose reduction (AIDR, Toshiba), Veo (GE), sinogram-affirmed iterative reconstruction (SAFIRE, Siemens), and iDose^4 (Philips)
- Computationally more elaborate but makes more effective use of the acquired x-ray information
- Produce equivalent image quality at lower radiation doses without a loss in spatial resolution compared with "filtered back projections" → permits coronary CTA with very low radiation exposure

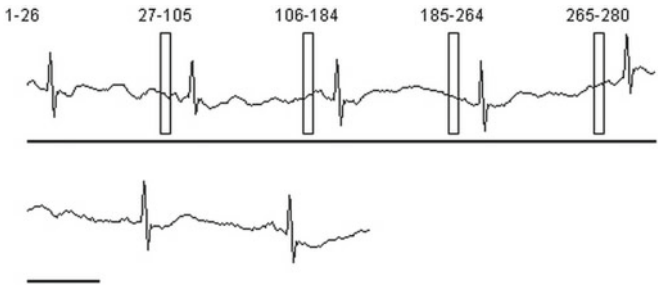

b

Physician: 104878A
Operator:

Total mAs 5789 Total DLP 1013 mGycm

	Scan	kV	mAs / ref.	CTDIvol* mGy	DLP mGycm	TI s	cSL mm
Patient Position F-SP							
Topogram	1	120	35 mA	0.14 L	3	2.5	0.6
DS_CaScSeq	2D	120	76 / 80	2.88 L	40	0.17	1.2
PreMonitoring Contrast	6	120	20	1.01 L	1	0.28	10.0
Monitoring	7	120	20	6.07 L	6	0.28	10.0
DS_CorCTA	13D	120	300	67.25 L	963	0.28	0.6

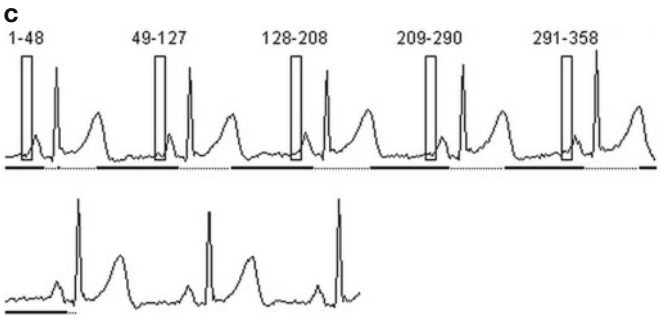

d

Physician: INDM99
Operator:

Total mAs 4927 Total DLP 880 mGycm

	Scan	kV	mAs / ref.	CTDIvol* mGy	DLP mGycm	TI s	cSL mm
Patient Position F-SP							
Topogram	1	120	35 mA	0.14 L	4	2.9	0.6
DS_CaScSeq	2D	120	45 / 82	1.71 L	24	0.17	1.2
PreMonitoring Contrast	6	120	20	1.03 L	1	0.28	10.0
Monitoring	7	120	20	3.08 L	3	0.28	10.0
DS_CorCTA	10D	120	300	51.89 L	848	0.28	0.6

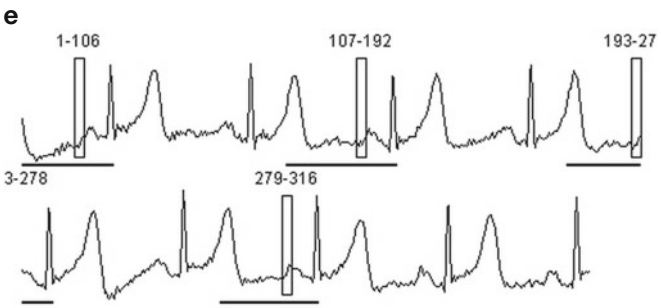

f

Physician: 103247A
Operator:

Total mAs 3852 Total DLP 779 mGycm

	Scan	kV	mAs / ref.	CTDIvol* mGy	DLP mGycm	TI s	cSL mm
Patient Position F-SP							
Topogram	1	120	35 mA	0.14 L	4	2.7	0.6
DS_CaScSeq	2D	120	93 / 84	3.49 L	48	0.17	1.2
PreMonitoring Contrast	6	120	20	1.01 L	1	0.28	10.0
Monitoring	7	120	20	5.05 L	5	0.28	10.0
DS_CorAdSeq	12D	120	300	52.21 L	721	0.86	0.6
Last scan no.	15						

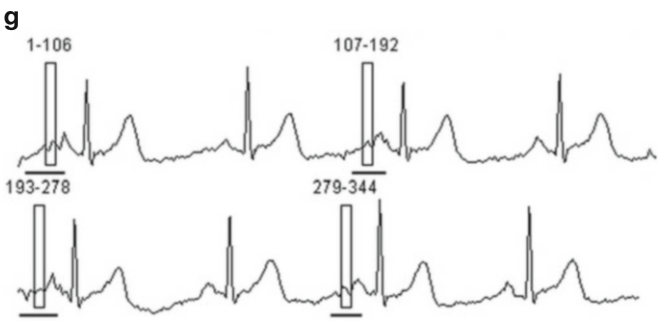

h

Physician: 106396A
Operator:

Total mAs 1773 Total DLP 320 mGycm

	Scan	kV	mAs / ref.	CTDIvol* mGy	DLP mGycm	TI s	cSL mm
Patient Position F-SP							
Topogram	1	120	35 mA	0.14 L	5	3.4	0.6
DS_CaScSeq	2D	120	76 / 84	2.85 L	39	0.17	1.2
PreMonitoring Contrast	6	120	20	1.01 L	1	0.28	10.0
Monitoring	7	120	20	9.10 L	9	0.28	10.0
DS_CorAdSeq	16D	120	300	19.26 L	266	0.34	0.6
Last scan no.	19						

Fig. 21.23 Scan techniques to reduce radiation dose. (**a**, **b**) Retrospective ECG gating; full exposure of the entire R–R interval allows maintenance of image quality during the entire cardiac cycle at the expense of a high radiation dose (14.2 mSv). (**c**, **d**) Retrospective ECG gating with ECG-based tube-current modulation; full tube current is maintained only during a prescribed phase window of the R–R interval (e.g., 30–90 %), with reduction of the tube current (mAs) to 25 % or less during the remainder of the cardiac cycle. The total effective radiation dose is 12.3 mSv. (**e**, **f**) Prospective ECG triggered; exposure is maintained only during a predefined phase window of the R–R interval (e.g., 30–90 %). The total effective radiation dose is 10.9 mSv. (**g**, **h**) Prospective ECG gating with a narrow phase window; exposure is maintained only during a very short window of the R–R interval (e.g., 75 %). The total effective radiation dose is 4.5 mSv

References

1. Taylor CM, Blum A, Abbara S. Patient preparation and scanning techniques. Radiol Clin North Am. 2010;48:675–86.
2. Schoepf UJ, Zwerner PL, Savino G, Herzog C, Kerl JM, Costello P. Coronary CT angiography. Radiology. 2007;244:48–63.
3. Pannu HK, Alvarez Jr W, Fishman EK. Beta-blockers for cardiac CT: a primer for the radiologist. AJR Am J Roentgenol. 2006;186:S341–5.
4. Chun EJ, Lee W, Choi YH, Koo BK, Choi SI, Jae HJ, Kim HC, So YH, Chung JW, Park JH. Effects of nitroglycerin on the diagnostic accuracy of electrocardiogram-gated coronary computed tomography angiography. J Comput Assist Tomogr. 2008;32:86–92.
5. Moscariello A, Takx RA, Schoepf UJ, Renker M, Zwerner PL, O'Brien TX, Allmendinger T, Vogt S, Schmidt B, Savino G, Fink C, Bonomo L, Henzler T. Coronary CT angiography: image quality, diagnostic accuracy, and potential for radiation dose reduction using a novel iterative image reconstruction technique comparison with traditional filtered back projection. Eur Radiol. 2011;21:2130–8.
6. Tatsugami F, Husmann L, Herzog BA, Burkhard N, Valenta I, Gaemperli O, Kaufmann PA. Evaluation of a body mass index-adapted protocol for low-dose 64-MDCT coronary angiography with prospective ECG triggering. AJR Am J Roentgenol. 2009; 192:635–8.
7. Halliburton SS, Abbara S, Chen MY, Gentry R, Mahesh M, Raff GL, Shaw LJ, Hausleiter J, Society of Cardiovascular Computed Tomography. SCCT guidelines on radiation dose and dose-optimization strategies in cardiovascular CT. J Cardiovasc Comput Tomogr. 2011;5:198–224.
8. Halliburton SS. Recent technologic advances in multi-detector row cardiac CT. Cardiol Clin. 2009;27:655–64.
9. Cody DD, Mahesh M. AAPM/RSNA physics tutorial for residents: technologic advances in multidetector CT with a focus on cardiac imaging. Radiographics. 2007;27:1829–37.
10. Abbara S, Arbab-Zadeh A, Callister TQ, Desai MY, Mamuya W, Thomson L, Weigold WG. SCCT guidelines for performance of coronary computed tomographic angiography: a report of the Society of Cardiovascular Computed Tomography Guidelines Committee. J Cardiovasc Comput Tomogr. 2009;3:190–204.
11. Halliburton S, Arbab-Zadeh A, Dey D, Einstein AJ, Gentry R, George RT, Gerber T, Mahesh M, Weigold WG. State-of-the-art in CT hardware and scan modes for cardiovascular CT. J Cardiovasc Comput Tomogr. 2012;6:154–63.
12. Achenbach S, Kondo T. Technical advances in cardiac CT. Cardiol Clin. 2012;30:1–8.
13. Husmann L, Herzog BA, Burkhard N, Valenta I, Burger IA, Gaemperli O, Kaufmann PA. Low-dose coronary CT angiography with prospective ECG triggering: validation of a contrast material protocol adapted to body mass index. AJR Am J Roentgenol. 2009;193:802–6.
14. Weininger M, Barraza JM, Kemper CA, Kalafut JF, Costello P, Schoepf UJ. Cardiothoracic CT angiography: current contrast medium delivery strategies. AJR Am J Roentgenol. 2011;196:W260–72.
15. Achenbach S, Boehmer K, Pflederer T, Ropers D, Seltmann M, Lell M, Anders K, Kuettner A, Uder M, Daniel WG, Marwan M. Influence of slice thickness and reconstruction kernel on the computed tomographic attenuation of coronary atherosclerotic plaque. J Cardiovasc Comput Tomogr. 2010;4:110–5.
16. Choi HS, et al. Pitfalls, artifacts, and remedies in multi- detector row CT coronary angiography. Radiographics. 2004;24:787–800.
17. Johnson PT, Fishman EK. Postprocessing techniques for cardiac computed tomographic angiography. Radiol Clin North Am. 2010;48:687–700.
18. Dalrymple NC, Prasad SR, Freckleton MW, Chintapalli KN. Informatics in radiology (infoRAD): introduction to the language of three-dimensional imaging with multidetector CT. Radiographics. 2005;25:1409–28.
19. Gosling O, Loader R, Venables P, Rowles N, Morgan-Hughes G, Roobottom C. Cardiac CT: are we underestimating the dose? A radiation dose study utilizing the 2007 ICRP tissue weighting factors and a cardiac specific scan volume. Clin Radiol. 2010;65:1013–7.
20. Soderberg M, Gunnarsson M. Automatic exposure control in computed tomography–an evaluation of systems from different manufacturers. Acta Radiol. 2010;51:625–34.

MR Technical Overviews

22

Eui-Young Choi and TaeHoon Kim

Contents

Abstract

Cardiac magnetic resonance imaging (CMR) technique has been steadily improved. However, establishment of comprehensive protocol and selection of optimal imaging sequence in each clinical situation are still challenging. There are lots of technical tips regarding improving signal-to-noise ratio, contrast-to-noise ratio, reducing artifacts, selection of optimal sequence in individual case, consideration of patient's hemodynamic status, and improving patients' comforts. This chapter provides brief guidance for extensive clinical application of CMR by providing protocols and imaging sequences in each clinical scenario.

22.1 Cardiac MRI

Cardiac magnetic resonance imaging (CMR) technique has been steadily improved. However, establishment of comprehensive protocol and selection of optimal imaging sequence in each clinical situation are still challenging. There are lots of technical tips regarding improving signal-to-noise ratio, contrast-to-noise ratio, reducing artifacts, selection of optimal sequence in individual case, consideration of patient's hemodynamic status, and improving patients' comforts. This chapter provides brief guidance for extensive clinical

E.-Y. Choi
Division of Cardiology, Heart Center, Gangnam Severance Hospital, Yonsei University College of Medicine, Seoul, Republic of Korea
e-mail: CHOI0928@yuhs.ac

T. Kim (✉)
Department of Radiology, Gangnam Severance Hospital, Yonsei University College of Medicine, Seoul, Republic of Korea
e-mail: thkim1@yuhs.ac

T.-H. Lim (ed.), *Practical Textbook of Cardiac CT and MRI*,
DOI 10.1007/978-3-642-36397-9_22,

Objects/devices	Safety
Prosthetic heart valve or annuloplasty ring	Not considered contraindication
Implanted cardiac pacemaker	Generally not safe (except MR-compatible new ICDs)
Cardiac closure and occluder devices	MR safe
Implanted cardioverter-defibrillator (ICD)	Generally not safe (except MR-compatible new ICDs)
Loop recorder (event monitor)	MR conditional
Inferior vena cava filters	MR safe (most), MR conditional (few)
Hemodynamic support devices (LVAD, IABP, and so on)	Contraindication to MR
Aortic stent graft	MR safe except "Zenith AAA endovascular graft"
Sternal suture wire after surgery	MR safe
Coronary stents and peripheral stents	MR safe (most), MR conditional (a few stents)

LVAD left ventricular assist device, *IABP* intra-aortic balloon pump, *AAA* abdominal aortic aneurysm

application of CMR by providing protocols and imaging sequences in each clinical scenario.

22.1.1 Clinical Indications

Ischemic heart disease: myocardial perfusion, global and regional wall motion, myocardial viability, and coronary anatomy evaluation

Cardiomyopathy: myocardial tissue characterization, global myocardial function, and chamber geometry

Valvular heart disease: chamber geometry, myocardial tissue characterization, severity of valvular stenosis, or regurgitation

Cardiac mass: tissue characterization and perfusion

Pericardial disease: pericardial thickening, presence of constriction, relationship with adjacent organs, and presence of myocardial involvement

Congenital heart disease: pulmonary circulation and right ventricular geometry

Cardiac involvement of systemic disease: myocardial tissue characterization and relationship with adjacent organs

22.1.2 Safety in Cardiac MRI

MRI uses strong magnetic fields and radio frequency pulses which produce ferromagnetic force or potential risk of tissue heating. Therefore, there are different types of contraindications for MRI examination. Some devices can cause severe artifacts which interrupt image interpretation. Although the majority of devices introduced recently are either nonferromagnetic or weakly ferromagnetic, we always caution that we should check for metallic objects or devices before the MR examination. We also consider the patients' conditions including the renal function in case of using contrast medium.

- Claustrophobia
- Impaired renal function when using gadolinium-based contrast.
  Increased risk of nephrogenic systemic fibrosis.
- Relative contraindication is 30 mL/min/1.73 m^2 < glomerular filtration rate.
  (GFR) < 60 mL/min/1.73 m^2
- Absolute contraindication is GFR <30 mL/min/1.73 m^2.
  Serum creatinine level >3 mg/dL or on dialysis.
- Implanted prosthesis or devices [1].

22.1.3 Cardiac Gating

The most effective form of cardiac gating is ECG gating which requires a high-amplitude QRS complex. In case of inadequate QRS complex, we can use the peripheral pulse from fingertip pulse monitors. An arrhythmia may lead to inappropriate triggering and image blurring or artifacts. An arrhythmia rejection technique is useful but prolongs the acquisition time.

- A prospective ECG gating (Fig. 22.1a)
  Provides better temporal resolution images, but results in longer acquisition time
  Is not sampled at the end of the cardiac cycle
  Can be effective in evaluating cardiac anatomy or tumor
- A retrospective ECG gating (Fig. 22.1b)
  Can cause image blurring due to combining data from different cardiac cycles
  Obtains imaging data from the whole cardiac cycle
  Is less sensitive to arrhythmias
  Is excellent in cine imaging for assessing regional and global wall motion

22.1.4 Respiratory Fixing

When the images are blurred and signal-to-noise ratio (SNR) is too weak due to the respiratory motion, increasing the

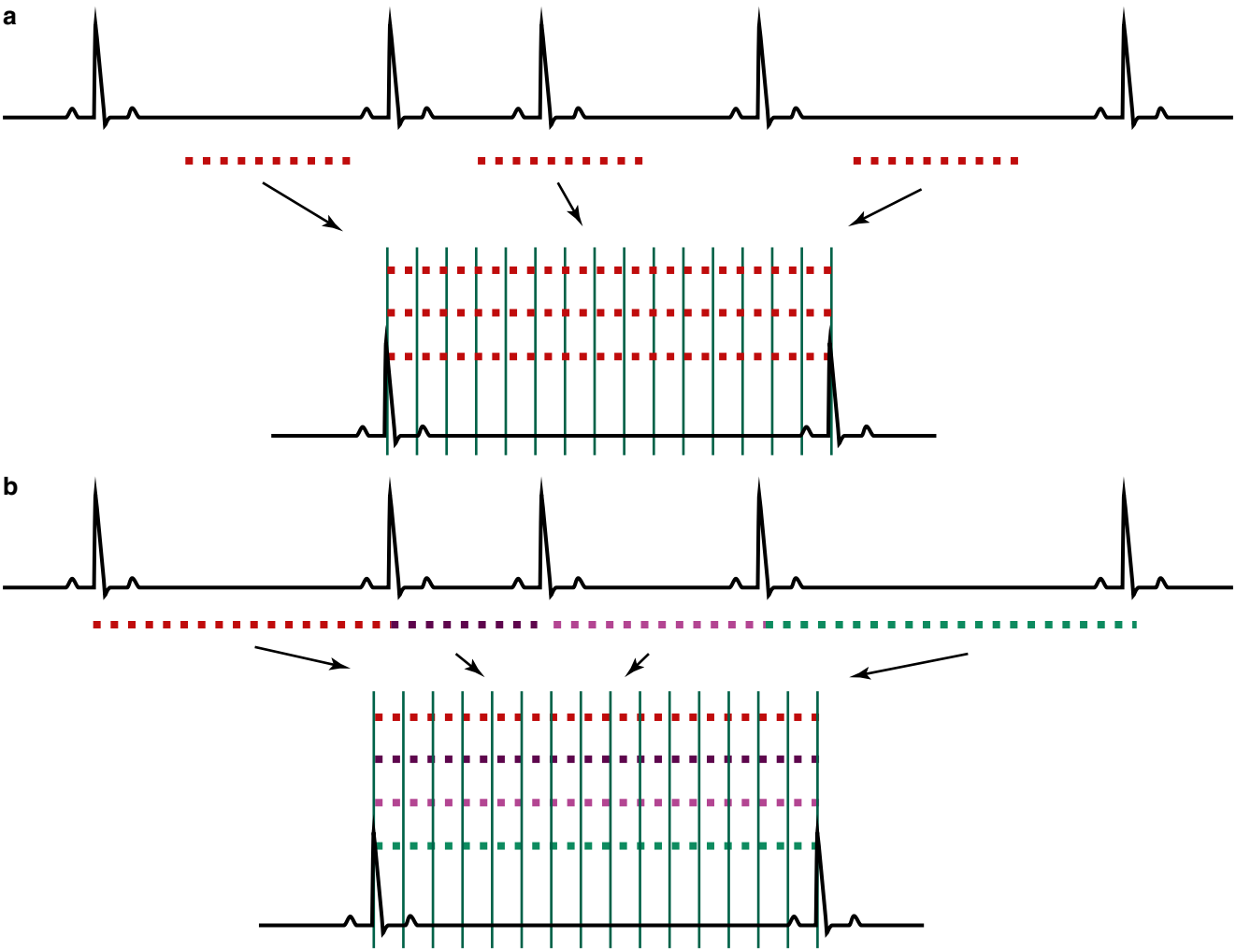

Fig. 22.1 Methods of ECG gating. (**a**) Prospective ECG gating: we obtain signal data after the determined time from the R wave on ECG. Acquisition time is fixed regardless of the R-R interval. If there is a premature heartbeat, scanning ignores the irregular beat which causes image blurring. (**b**) Retrospective ECG gating: we obtain signal data throughout the entire R-R interval which will be filled with the allotted k-spaces. Acquisition time is variable according to the heart rate

number of image acquisitions helps to improve SNR and reduce respiratory motion artifacts [2]. There are different kinds of respiratory fixing methods used in the clinical settings.

- Breath-holding by the patient
  Is the most commonly used during image acquisition
    In standard MR sequences
  May be limited in acquisition time
  Is less available in the elderly or severely ill patients
- Respiratory gating (Fig. 22.2)
  Monitors the patients' diaphragmatic motion
  Obtains the images during the end-expiratory phase
    With a specified gating window which is acceptable if < 5 mm
  May be effective in patient with little cooperation
  Can lead to overall extension of scan time
- Free breathing mode

22.1.5 Contrast Enhancement

The bolus injection of contrast medium is helpful to increase the signal of the blood or the targeted tissue. 3D MRA study is useful in the evaluation of blood vessels. The early phase of enhancement in the targeted tissue is related to the vascularity of the tissue and also reflects the fractional blood volume of the tissue and the extravascular microcirculation of the contrast medium. The inflammation of the targeted tissue or the higher vascularity of the tumors may represent prominent early enhancement. Differential distribution of contrast medium in early dynamic phases is helpful to differentiate between the normal myocardium and the pathologic myocardium in ischemic conditions.

The late phase of enhancement in the targeted tissue can be used to evaluate the abnormal stasis of the contrast

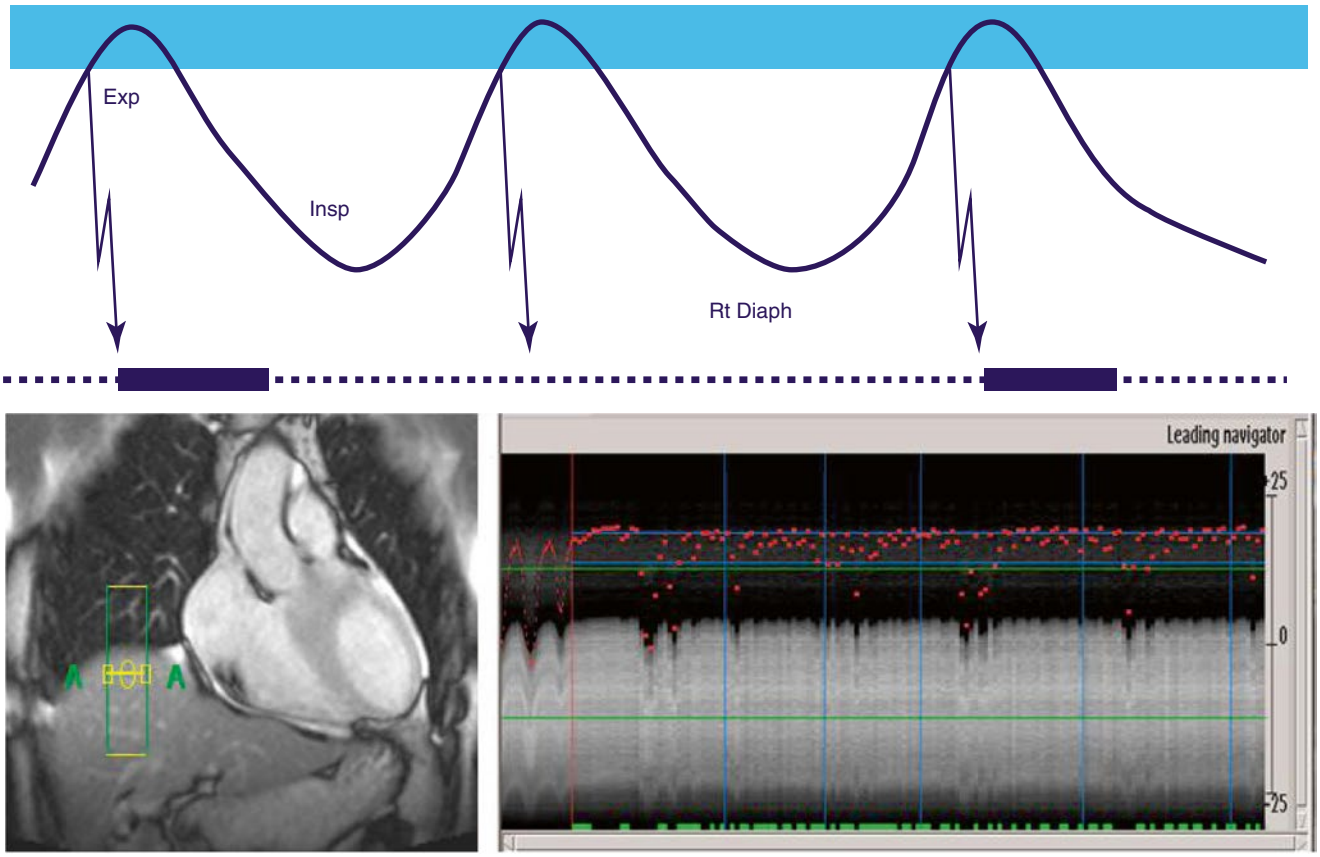

Fig. 22.2 Respiratory gating with navigator echo on the right diaphragm. Scanning is performed when the signal from the right diaphragm is positioned within the acquisition window. Image is good when a gating window is below 5 mm. *Exp* expiration phase, *Insp* inspiration phase, and *Rt Diaph* right diaphragm

medium which is useful to evaluate the areas of fibrosis. Stasis of contrast medium in the myocardium is made more prominent on the images by using the inversion recovery pulse which suppresses the normal myocardial signal.

- Injection of contrast media
  - Is favorable of bolus injection (with 4–5 mL/s for 2–4 s)
  - Follows by injection of a bolus of normal saline
    - To flush the remaining contrast agent out of the injection routes
- Contrast media enhancement
  - Increases SNR for MR angiography
  - Enables to obtain sequential images of different structures
    - Such as artery or vein
  - Improves CNR for tissue characterization
  - Can be useful in obtaining multiple data sets of the targeted images
    - For the dynamic perfusion study
    - Can be utilized in the evaluation of the tumor or inflammation
      - Using the early contrast pooling images
    - Is helpful in the evaluation of the infarct myocardium
      - Using the delayed contrast pooling images

22.1.6 Basic Views of the Heart (Fig. 22.3)

The heart is positioned in the thoracic cage with a little oblique direction to the standard view of the thorax. Therefore, cardiac MR images are generally obtained along the long and short axes of the heart rather than those of the thorax. The long axis of the heart is the line from the cardiac base to the apex, and the short axis is the line perpendicular to the long axis of the heart. Although we can obtain all cardiac views through the freely positioned acquisition windows in any orientation, we usually obtain the dedicated views similar to echocardiography

to allow assessment of cardiac chamber morphology or function and to communicate effectively among the clinicians.

- Two-chamber view
  Can be obtained when the imaging plane passes through the center line of the mitral valve to the cardiac apex
- Short-axis view
  Can be obtained perpendicular to the long axis of the heart from two-chamber or four-chamber views
- Four-chamber view
  Can be obtained when the imaging plane passes through the center of the left ventricle through the inferior septum of the short-axis view of the heart
- Three-chamber view
  Can be obtained when the imaging plane passes through the center of the left ventricle and the aortic valve from the basal short-axis view of the heart
- RVOT view with pulmonary bifurcation
  Can be obtained when the imaging plane passes through the center of the right ventricle and the pulmonic valve from the basal short-axis view of the heart

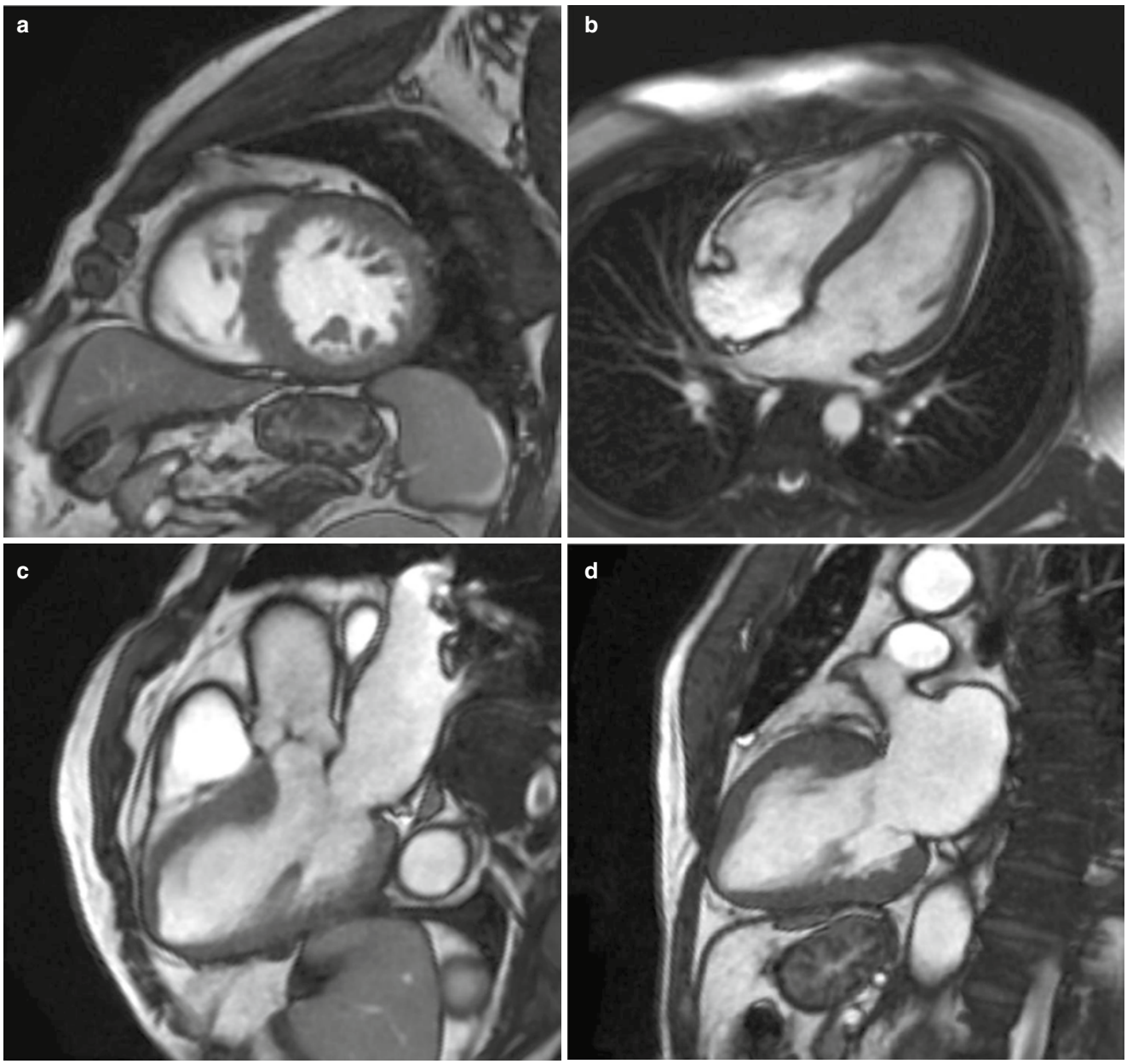

Fig. 22.3 Basic views of the heart. (**a**) Short-axis view, (**b**) four-chamber view, (**c**) three-chamber view, (**d**) two-chamber view, (**e**) RV outflow tract view, (**f**) aortic valve view, and (**g**) aortic arch (candy-cane) view

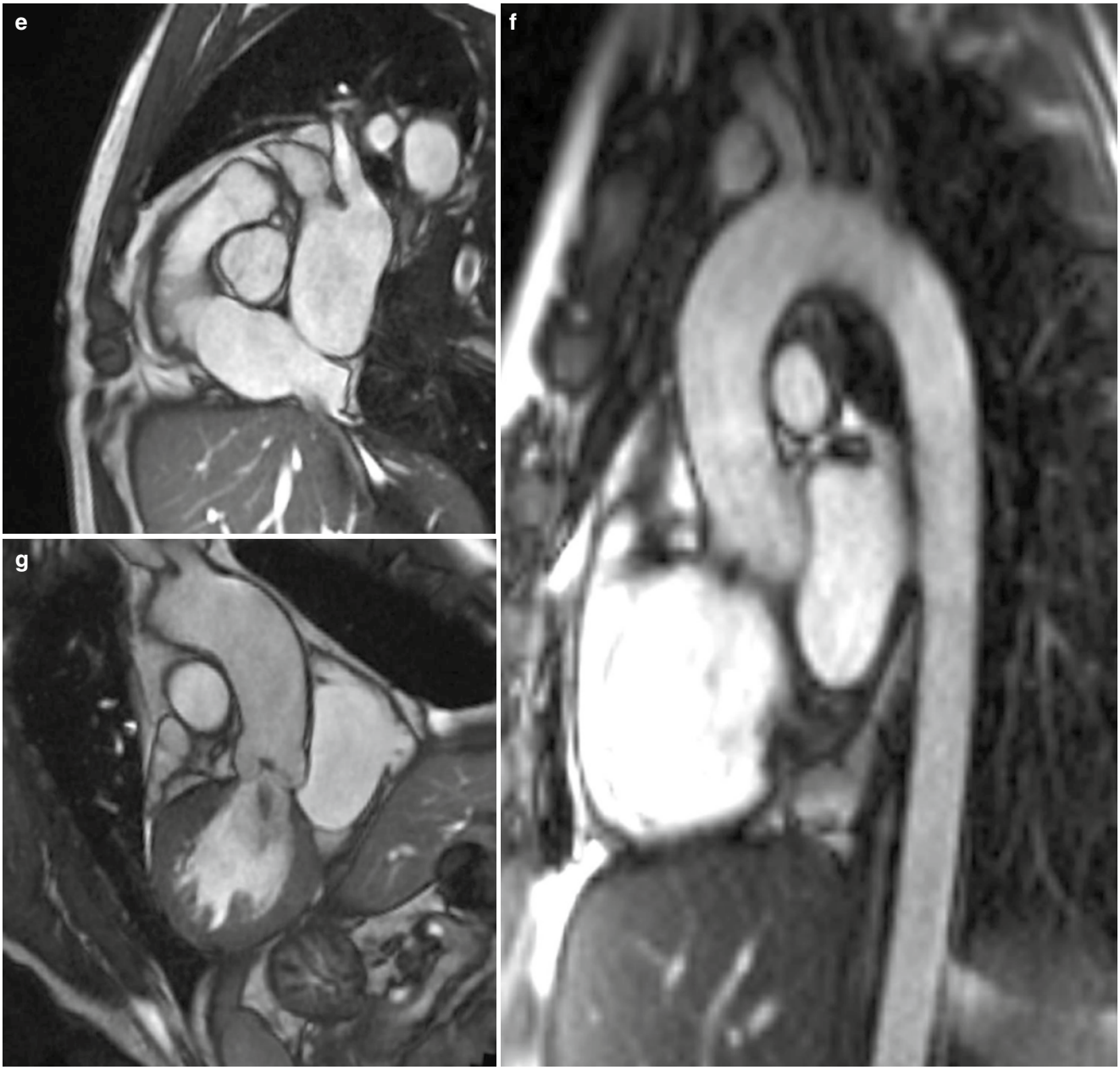

Fig. 22.3 (continued)

- Aorta arch (candy-cane) view
  Can be obtained when the imaging plane passes through the center of the ascending and descending aorta from the axial view of the thorax

22.1.7 Preparation Pulse

MR signal intensity in many situations is too weak to provide an appropriate information from the targeted images. The preparation pulse plays a role to create a preexisting magnetization prior to the application of RF pulses destined for data readout. It was usually applied before the spin echo or gradient echo pulse sequences were performed. Major roles are enhancing tissue contrast and suppressing signal intensity from the targeted tissues. Preparation pulse may prolong the acquisition time.

- Inversion pulse (Fig. 22.4)

Is more effective for T1 weighting in the targeted tissue
Can generate a variety of image contrasts between tissues

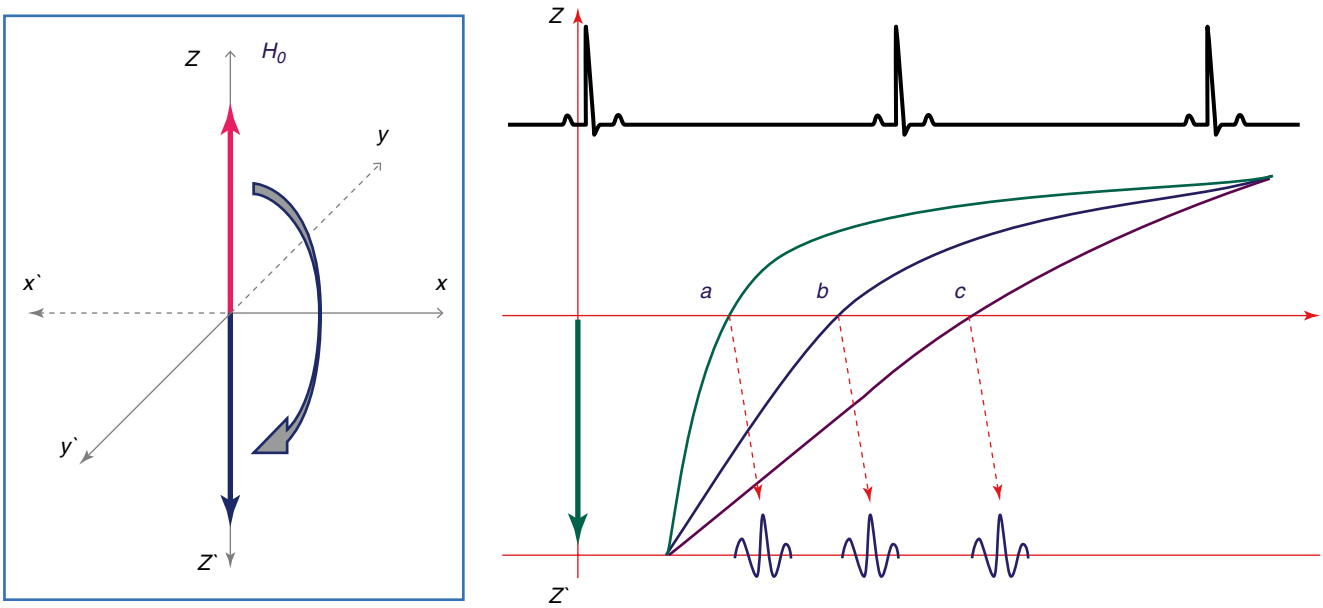

Fig. 22.4 The role of inversion pulse. Inversion pulse uses 180° pulse to reverse longitudinal magnetization. Inversion pulse according to the inversion time can suppress the targeted tissues such as fat, water, myocardium, or blood

Can be used before spin echo or gradient echo
Uses 180° pulse to reverse longitudinal magnetization
Can be used in suppressing the targeted tissues as follows:

1. Double inversion pulses for black blood technique
2. Triple inversion pulses for myocardial edema
   With fat saturation technique
3. Single inversion pulse for myocardium suppression
   Used in viability imaging studies

- T2 preparation pulse
  Is more effective for T2 weighting in the targeted tissue
  Is commonly used in T2 mapping for edema detection
  Uses 90° RF pulse followed by a series of 180° RF pulse, then a −90° RF tip-up
  Can be used in strengthening T2 weighting in the targeted tissues as follows:
  1. T2 mapping for edema detection [3]
  2. Myocardial signal (short T2) suppression
     For coronary artery imaging [4]
  3. Black blood late Gd-enhancement study
     For myocardial infarct imaging [5]

22.2 T1- and T2-Weighted Imaging

MR signal intensities usually depend on the repetition time (TR) and the echo time (TE). The repetition time is the time between consecutive excitations, and the echo time is the time between the excitation and the detection of the signal which are applied for the spin echo or gradient echo. We need to select an appropriate TR or TE to characterize the tissue components.

22.2.1 T1-Weighted Image

The contrast depends on the various T1 time constants of the different tissue types.
Used to visualize anatomy and differentiate fat from the surrounding tissues.
TE is short and TR is usually equal to one R-R interval for spin echo sequence.
Shows higher signal from fat tissue and lower signal from water.
Is very useful for comparison of pre- and post-contrast images.

22.2.2 T2-Weighted Image

TE directly determines how much the transverse signal decays.
Is used to visualize fluid due to edema (inflammation).
TE is longer; overall SNR decreases as TE is increased due to de-phasing.
TR is usually equal to 2 R-R intervals.
Shows a shorter T2 value in fat tissue than in water.
Has variable signal in flowing blood or hematomas.
Can be useful in fat suppression with a short tau inversion recovery
(STIR) technique for edema imaging (Fig. 22.5)

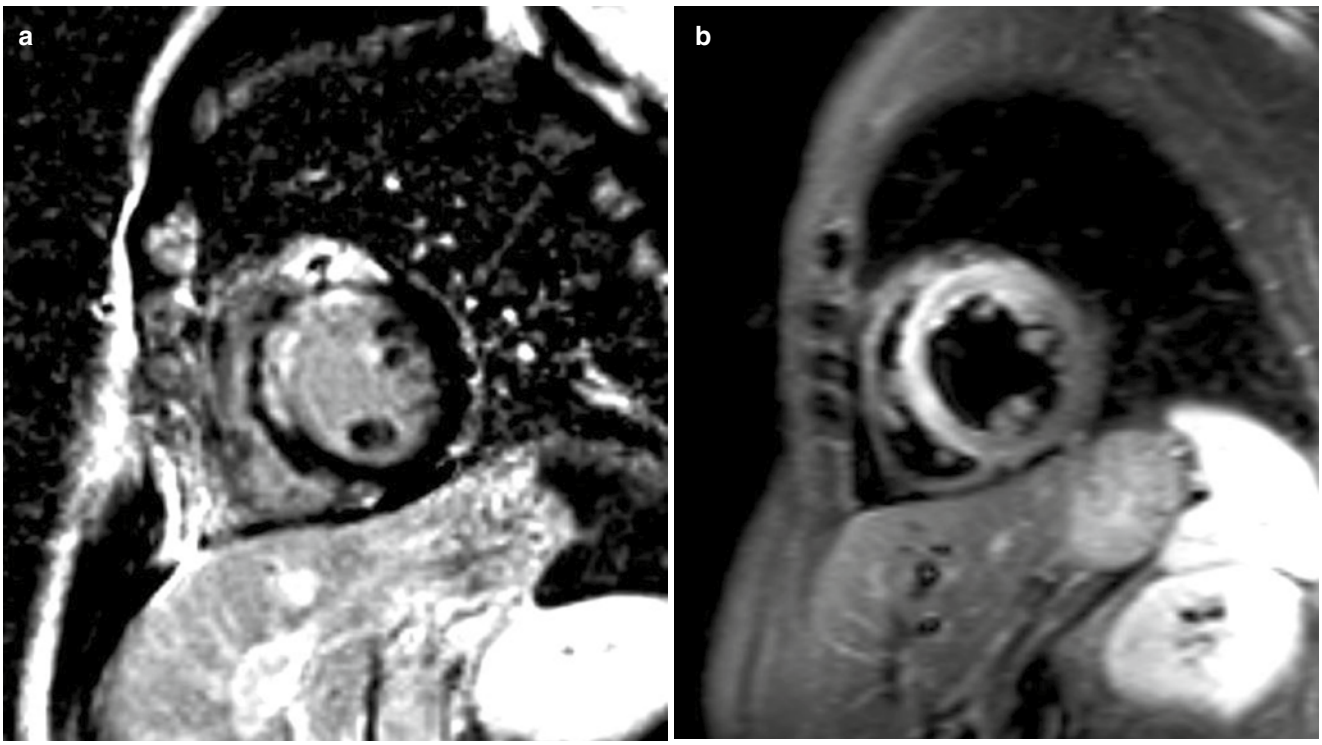

Fig. 22.5 Myocardial infarction and short tau inversion recovery (STIR) image. (**a**) Gd-enhanced image shows strong enhancement in the anterior free wall and ventricular septum of the LV wall from myocardial infarction. (**b**) STIR image shows high signal intensity in the same area of the LV wall due to myocardial edema

22.2.3 T2* Weighted Image

Consists of transverse magnetization (T2 effect) and local magnetic inhomogeneity
Is more sensitive of regional magnetic field inhomogeneities.
Uses gradient echo sequence because no 180° RF pulse is used.
T2* is always shorter than T2.
Shows signal loss in images of old hemorrhage or hemochromatosis

22.3 Bright Blood and Black Blood Imaging

The blood signal can be affected by the different motion effects on the MR signal. MR techniques using the motion effects are time-of-flight (TOF) and phase contrast imaging. The TOF effect is especially useful in imaging the vessels which can show the bright or dark signal according to application of the prepared saturation pulses. Bright blood can be caused by the replacement of the unsaturated blood from the upstream slices which produces a stronger signal as compared to the stationary heart wall, which does not get replaced the new magnetization (flow-related enhancement). Black blood can be produced by the replacement of the suppressed blood from applying the two 180° pulses. The first one is nonselective pulse to null completely all of the things within the RF coil. The next is a selective pulse to restore the targeted tissues within the imaging slice. The selective 180° pulse is followed by either spin echo or gradient echo.

22.3.1 Bright Blood Technique (Fig. 22.6a)

Is related to time-of-flight (TOF) effect
Produces high signal intensity from the full magnetized blood from upstream
  Which replaces the saturated blood in the targeted slices
Is characterized as flow-related enhancement
Is available in gradient (spin echo imaging with slow flow)

22.3.2 Black Blood Technique (Fig. 22.6b)

Can be achieved by application of double inversion pulses which include:
1. A nonselective inversion pulse which is applied to the whole volume

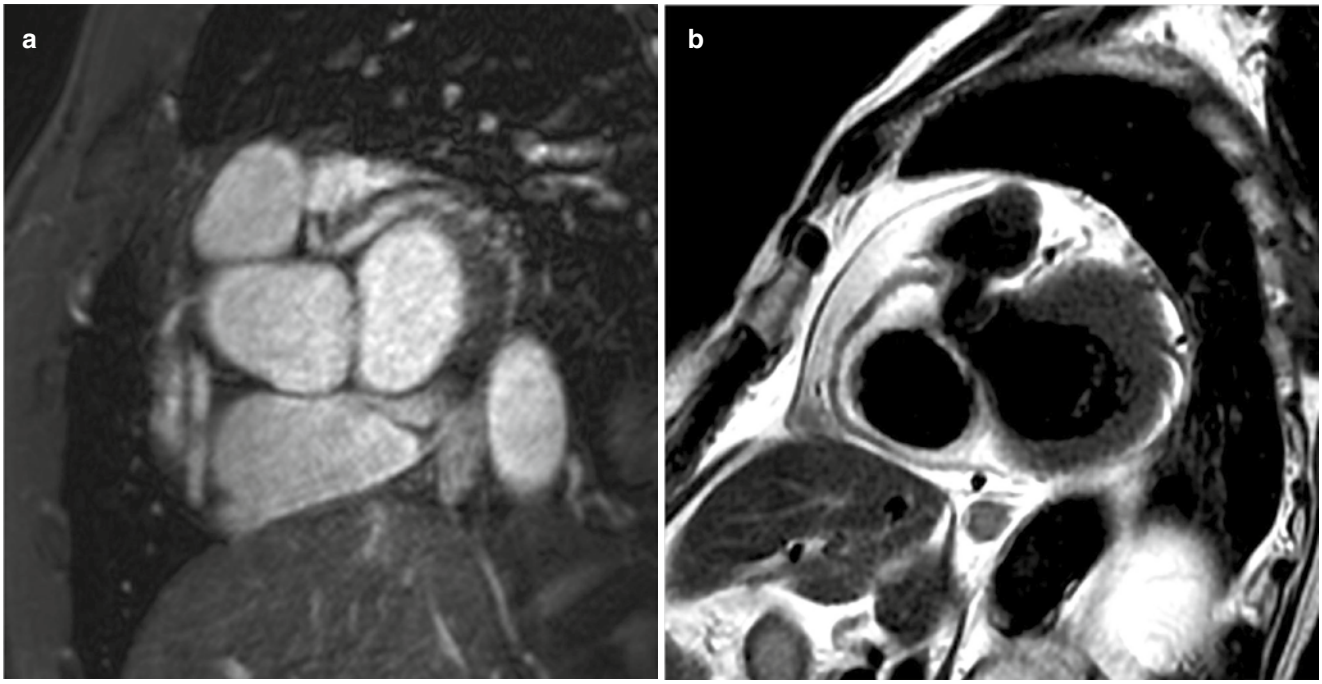

Fig. 22.6 (**a**) Bright blood technique, right coronary artery is visualized bright. (**b**) Black blood technique, right coronary artery is visualized black

2. A selective inversion pulse which restores the targeted tissue magnetization

Obtain signal void in the blood-filled structures replaced by the suppressed blood
From the nonselective inversion pulse

22.4 Cine Imaging

Cine imaging is high-quality movies taken from the different phases of the cardiac cycle. It is usually performed with gradient echo imaging. Therefore, flow-related enhancement depends on the orientation of the image plane; the flow perpendicular to the image plane can lead a bright signal of the moving blood within the vessels or cardiac chambers. The repeated excitation pulses can reduce the signal from the stationary myocardial tissues which can be affected by the flip angle. The echo time is generally kept as short as possible to reduce the acquisition time. The steady-state free precession (SSFP) has become more popular for cine imaging which uses usually retrospective gating due to faster and more stable in imaging.

22.4.1 Steady-State Free Precession (SSFP) (Fig. 22.7)

Is known as TrueFisp, FIESTA, or balanced FFE
Replaces earlier version of FLASH (spoiled gradient echo) due to high CNR and SNR
Has good CNR and temporal resolution
Is weak in the associated heating (SAR) caused by the rapidly repeated excitation pulses
Which is more strong at higher magnetic fields

22.4.2 Ventricular Function Evaluation (Fig. 22.8)

Usually uses a retrospective gaiting
Uses a parallel imaging technique to reduce the acquisition time
With shorter TR of below 40–50 ms and more k-space lines
With high spatial resolution of below 1.5 mm/pixel
Fully covers the LV cavity with short-axis slices

22.4.3 Myocardial Tagging Imaging [6]

Is a variant of cine imaging
Combines cine imaging with magnetization tagging such as spatial modulation of magnetization (SPAMM) (Fig. 22.9)
Is useful in quantifying regional myocardial wall motion abnormality
Can be used in calculating myocardial strain by local deformation of the myocardium

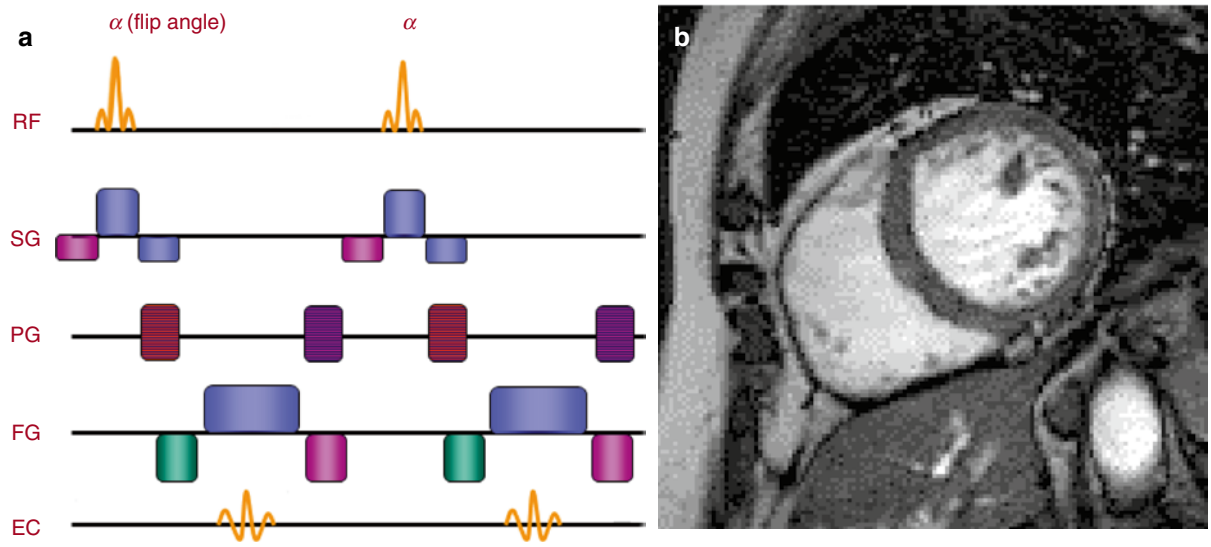

Fig. 22.7 Steady-state free precession (SSFP) sequence. (**a**) Diagram shows balanced echoes along the slice selection and frequency encoding directions. (**b**) Short-axis view of the left ventricle from a TrueFisp sequence

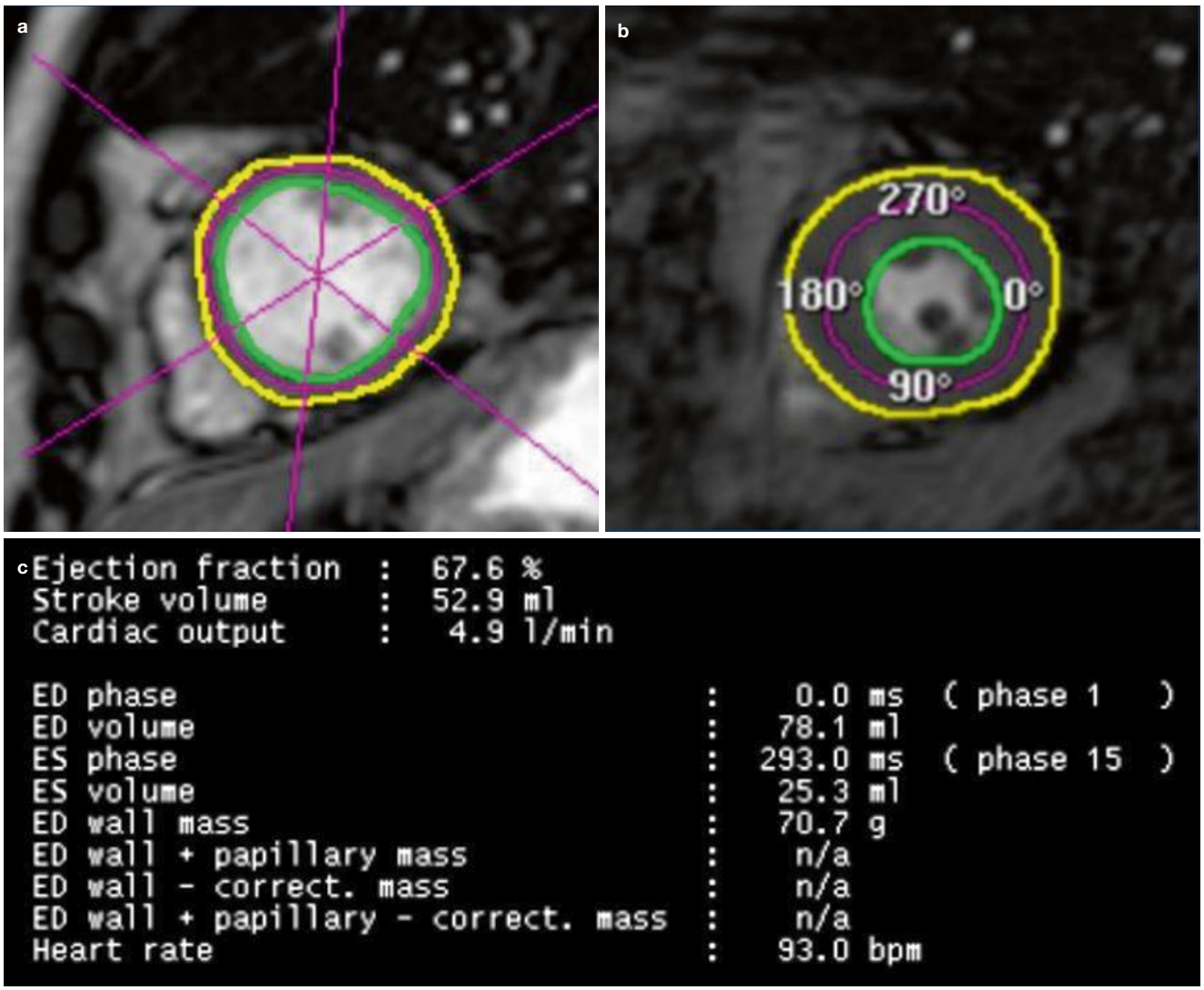

Fig. 22.8 Evaluation of left ventricular function using TrueFisp images. (**a**, **b**) Short-axis images at systole and diastole. (**c**) Data from the continuous short-axis images of the LV using the modified Simpson's method

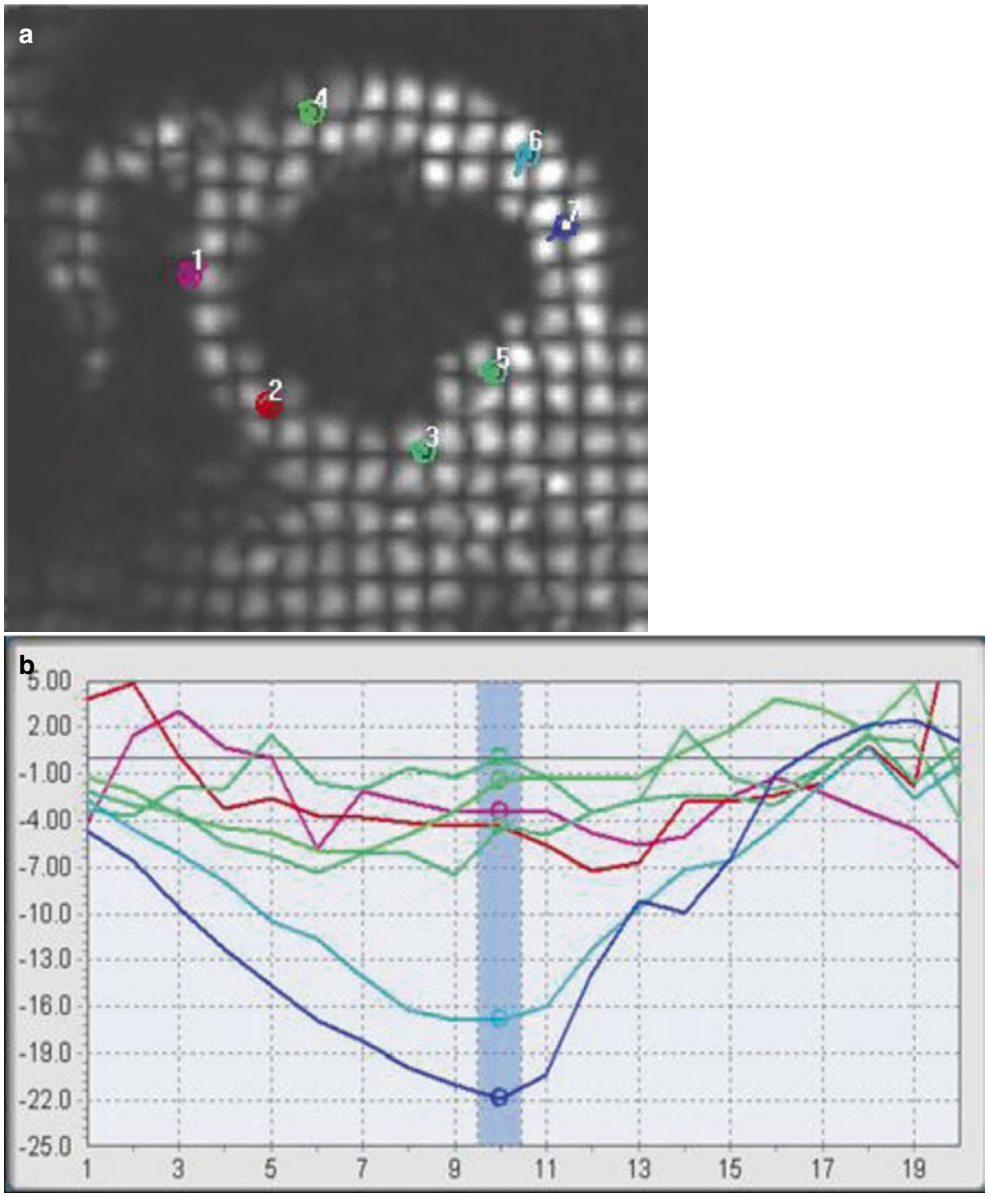

Fig. 22.9 Spatial modulation of magnetization (SPAMM) tagging. (**a**) Tagged MR image. (**b**) Graph shows hypokinesia in septum and inferior wall of the LV. The lateral wall contracted well

22.5 Phase Contrast Imaging (Velocity-Encoded GE Imaging, VENC Imaging)

Phase contrast imaging is also another variant of cine imaging and uses the motion-induced phase shifts. Therefore, we can evaluate the velocity of moving blood as well as flow volume through the imaging plane. To minimize the measurement errors, the imaging plane is optimally selected to be perpendicular to the axis of the targeted vessel lumen. Ideal measurements of the velocity depend on the optimization of the value of the velocity-encoding value (VENC) which should be adjusted to the corresponding velocity. If the VENC is too small or too large, the results show the aliasing of the flow velocity or poor sensitivity due to the low SNR and contrast between velocity changes.

22.5.1 Basic Consideration

It is a variant of cine imaging which is useful in velocity evaluation.

Usually uses the motion-induced phase shifts.

- Which is induced by the bipolar gradient pulses (Fig. 22.10).
- Showing the stationary tissue as a gray color and moving tissue through.
- The plane as a white or black colors depending on the flow direction.
- The more white or black the tissue is, the faster it is moving.

Need to design the perpendicular imaging plane to the flow axis.

- To reduce velocity blurring occurring at $>15°$ of angulation.

Requires proper temporal resolution of above 25 frames/s.

- If with lower TR, underestimates peak velocity.

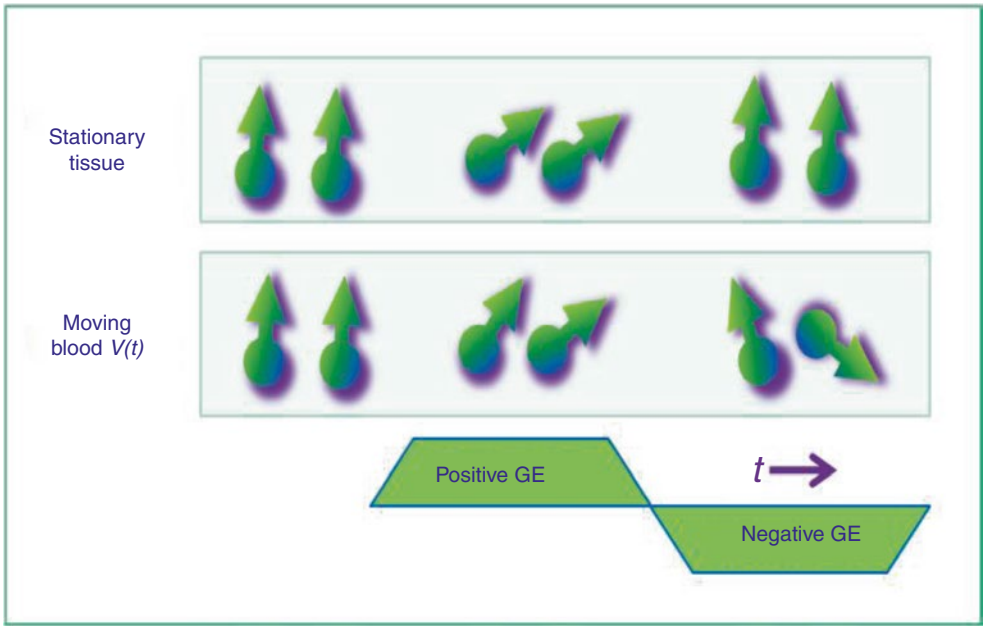

Fig. 22.10 Phase contrast sequence. Stationary tissue recovers completely into the same phase, but blood flow changes in its phase by the bipolar gradient echo

Handles the velocity-encoding values determined by degree of phase shifts
200–250 cm/s in aorta
100–150 cm/s in arterial and valve flow
<100 cm/s in pulmonary venous flow
<50 cm/s in systemic venous flow

22.5.2 Clinical Application

Measures the velocity or volume through the aorta and pulmonary artery
Measures the flow at the LV and RT outflow tracts
Evaluates mitral valve inflow and diastolic dysfunction of the LV wall (Fig. 22.11)
Evaluates tricuspid valve and pulmonic vein inflow

22.6 Myocardial Perfusion Imaging

Early perfusion imaging is related to the tissue vascularity and the delivery capacity of the contrast medium to the myocardial tissue by the blood flow. The change of T1 relaxation time in the myocardial tissue is generated by the arrival of Gd agent in myocardial extracellular space. To cover the entire LV with good CNR, we can usually use the spoiled gradient echo, balanced SSFP, and GRE-EPI. The suitable T1-weighting effects result from a saturation-recuperation pulse using a 90° pulse which highlights the signal of contrast medium arrived in gradient echo single-shot techniques. The imaging time lasts less than 1 min, and the patients should maintain their breath-holding as long as possible.

22.6.1 First-Pass Perfusion Imaging (Fig. 22.12)

Is useful in evaluating myocardial tissue perfusion of contrast medium (wash-in effect)
Uses single-shot gradient echo sequence with a 90° saturation-recuperation pulse
Which suppresses the myocardial tissue and highlights contrast signal
Lasts less than 1 min of imaging period
Acquires all imaging slices at each heartbeat
Uses stress-inducing agent such as adenosine
With 140 ug/kg/min for 6 min

22.7 Gadolinium-Enhancement Imaging

This imaging technique focuses on a relative excess of contrast medium in the pathologic myocardium as compared to the normal myocardium. The basic sequences are used with T1-weighted ultrafast GE or SSFP. The study is usually performed for about 10–15 min after injection of the contrast medium. The normal myocardium is suppressed by the 180° inversion pulse which is optimized by a TI-scouting technique to determine the proper inversion time. However, determination of the proper inversion time is very difficult to adjust depending on the patients' conditions. Phase-sensitive

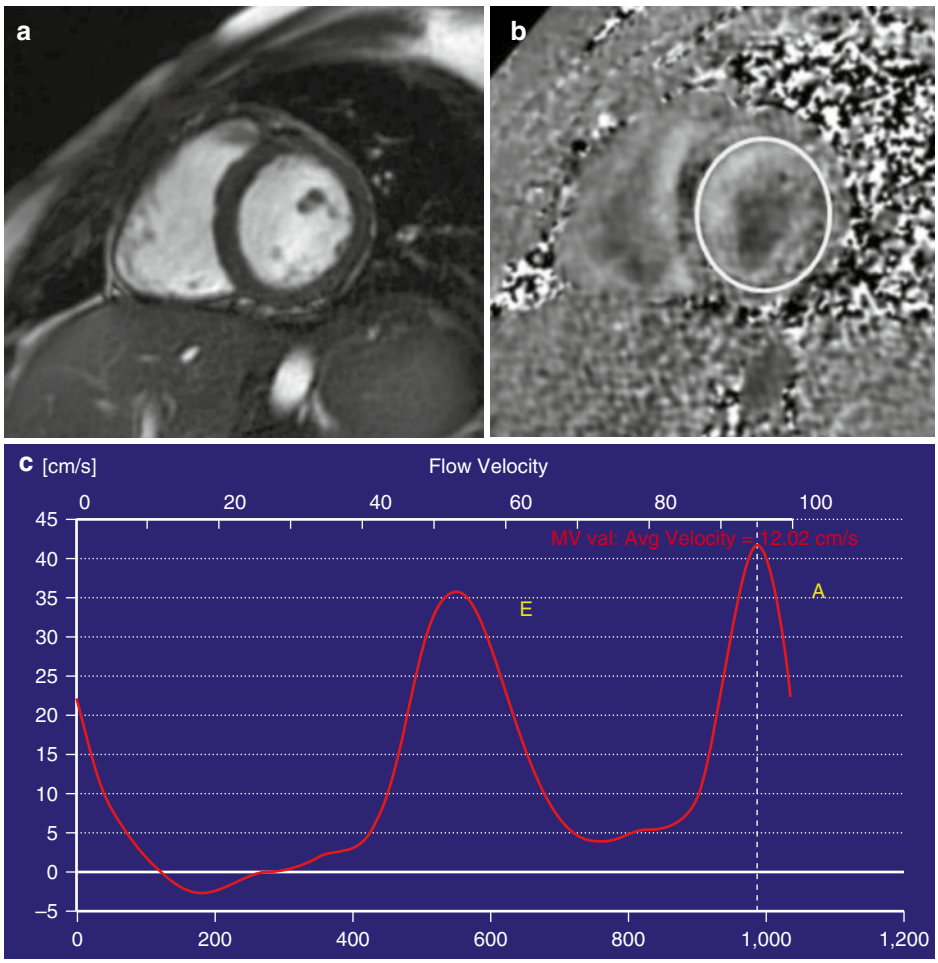

Fig. 22.11 Mitral valve VENC images with diastolic dysfunction. (**a**) Magnitude cine MR image. (**b**) Phase cine MR image. (**c**) Graph shows small E and tall A curve due to diastolic dysfunction of the LV

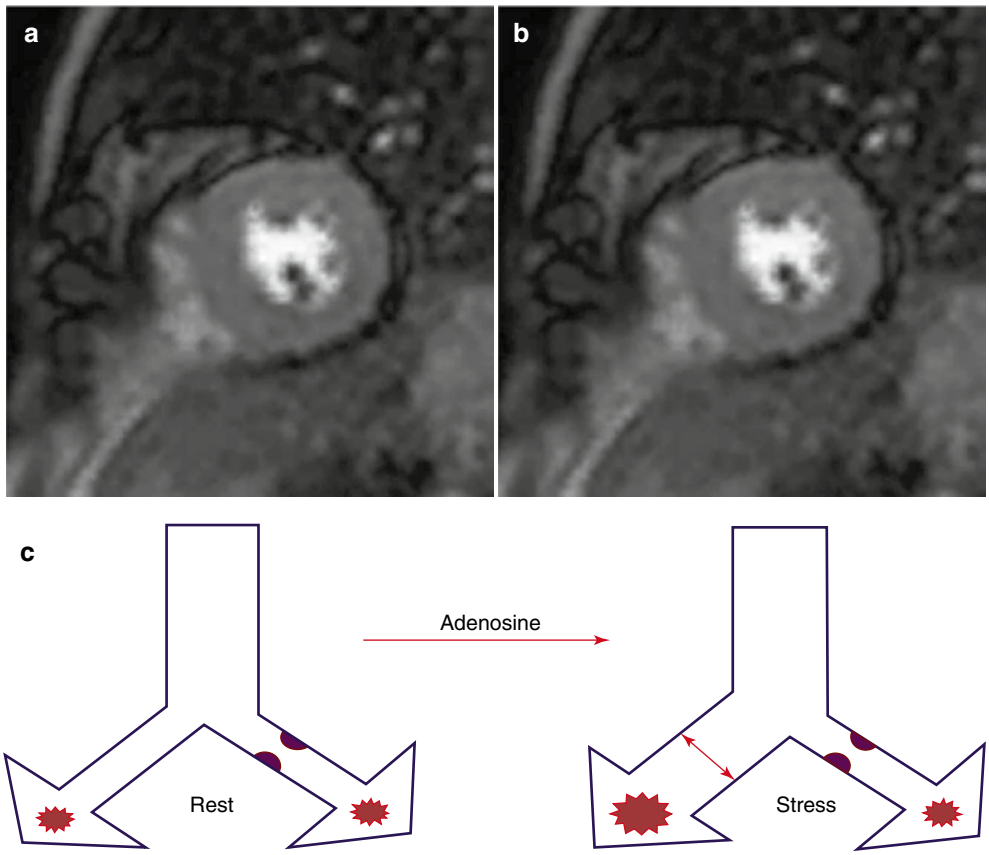

Fig. 22.12 First-pass perfusion imaging. (**a**, **b**) Stress perfusion image shows perfusion defect in the inferior lateral wall of the LV, which area is homogenously enhanced on the rest perfusion image. (**c**) Diagram shows relatively hypoperfusion at the lesion site under the stress condition (*right*)

inversion recovery (PSIR) technique is very useful and more challenging as it is independent of the inversion time.

22.7.1 Gadolinium-Enhancement Imaging

Evaluates contrast stasis in the myocardium (wash-out effect)
Uses T1-weighted ultrafast gradient echo sequence
  With a spoiled GE with preparation of inversion recovery (IR) pulse
  Which suppresses myocardial signal tested by the TI-scout imaging
Is performed for about 10–15 min after injection of contrast medium
- Early phase of Gd-enhancement imaging
  Is useful in myocardial ischemia or subacute MI
  Can evaluate an inflammatory or infectious myocarditis (Fig. 22.13)
  Is useful in evaluating high vascularity in cardiac tumor
- Late phase of Gd-enhancement imaging
  Is useful in evaluating fibrous component in chronic MI (Fig. 22.14)

22.7.2 Phase-Sensitive Inversion Recovery (PSIR) Imaging

Is less sensitive to inversion time
Obtains two image sets of the main data and reference data during two heartbeats
Subtracts the phase of the reference data from the main data
  Shows the infarct tissue to be bright (Fig. 22.15)
Shows normal myocardium to be always dark regardless of the inversion time

22.7.3 Black Blood PSIR (Fig. 22.16)

Uses the T2 preparation pulse (magnetization transfer contrast) prior to inversion pulse

Provides black blood PSIR image
Enhances CNR among infarction, blood, and normal myocardium

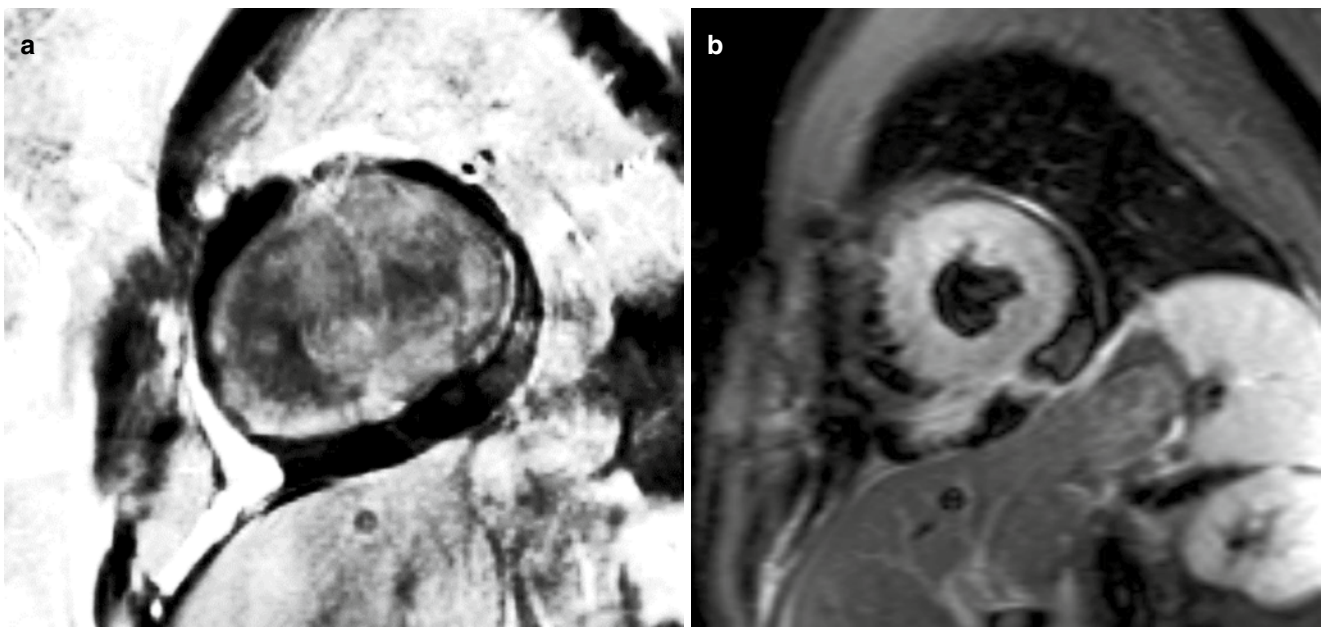

Fig. 22.13 MR images in acute myocarditis. (**a**) Post-contrast MR image shows strong enhancement of the LV wall on the early phase of Gd enhancement. (**b**) STIR image shows high signal intensity in the entire myocardium due to diffuse myocardial edema

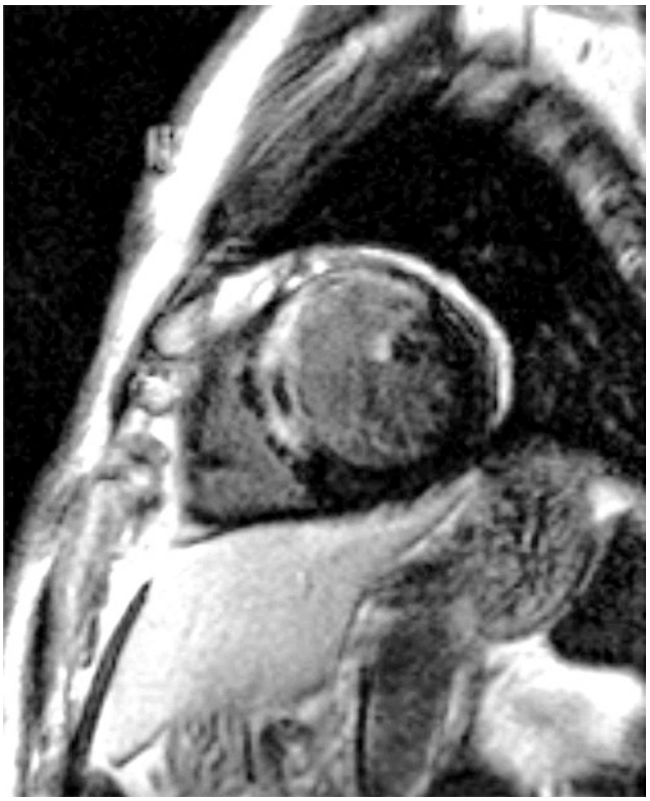

Fig. 22.14 Late Gd-enhancement image shows strong enhancement in the anterior free wall and ventricular septum of the LV from myocardial infarction. Dark band within the myocardial infarction represents microvascular obstruction (MVO) area

22.8 MR Coronary Imaging

Coronary MR angiography is a promising technique because the patients do not need to have a risk of radiation exposure or injection of iodinated contrast medium. The patient with severe calcified plaques can be evaluated by a coronary MR angiography which easily shows the vessel lumen despite of heavy calcification. The breath-hold 2D method has been popularly used since last decade, but these days 3D gradient echo coronary MR angiography sequences were developed with either a breath-hold method or a respiratory-gated free breathing mode. Breath-hold method has an advantage of time efficiency, but it has the expenses of the limited spatial resolution and 3D volume coverage [7]. 3D free breathing mode can cover the whole heart within 10–15 min [8]. Free breathing 3D coronary MR angiography can be performed with a navigator-gated SSFP without the contrast agent at the 1.5 T scanner or a spoiled GE with the injection of contrast medium at 3 T.

22.8.1 MR Protocols for Coronary MR Angiography

Was used with a spin echo sequence under the black blood technique

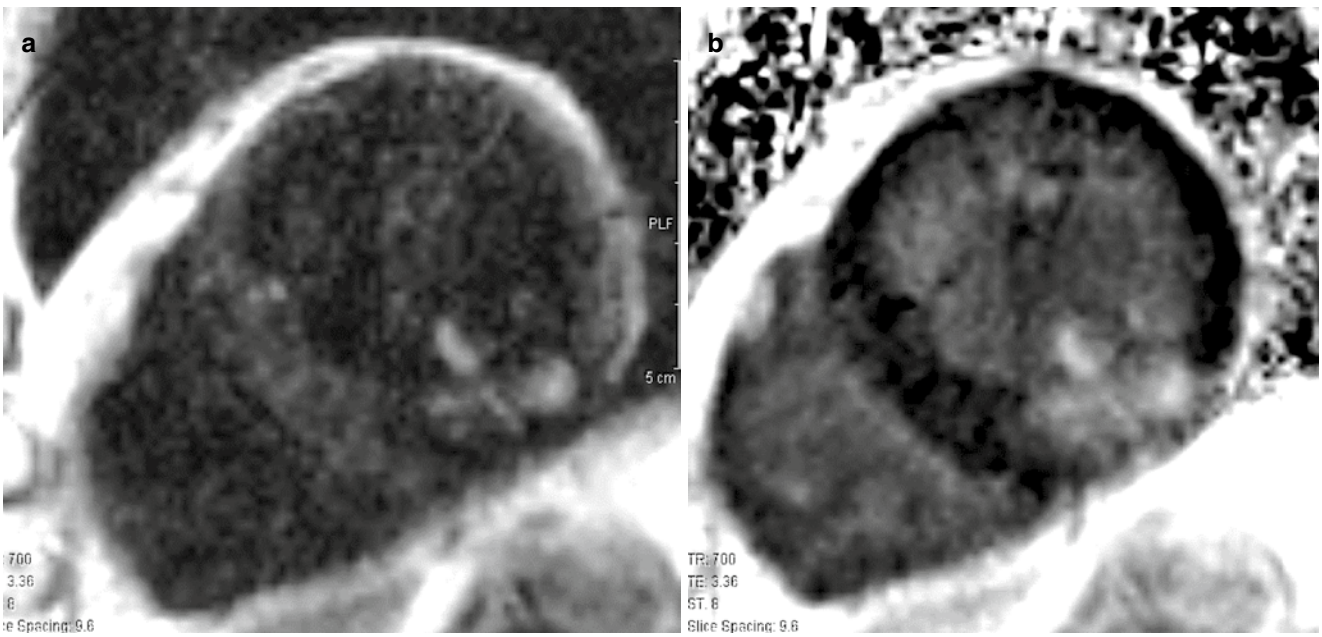

Fig. 22.15 Late Gd-enhancement images with a PSIR protocol. (**a**) Gd-enhanced image shows poor CNR between myocardial infarction and normal myocardium due to improper value of inversion time. (**b**) Phase-sensitive image reconstruction (PSIR) image shows better CNR in the same area without a validation of inversion time

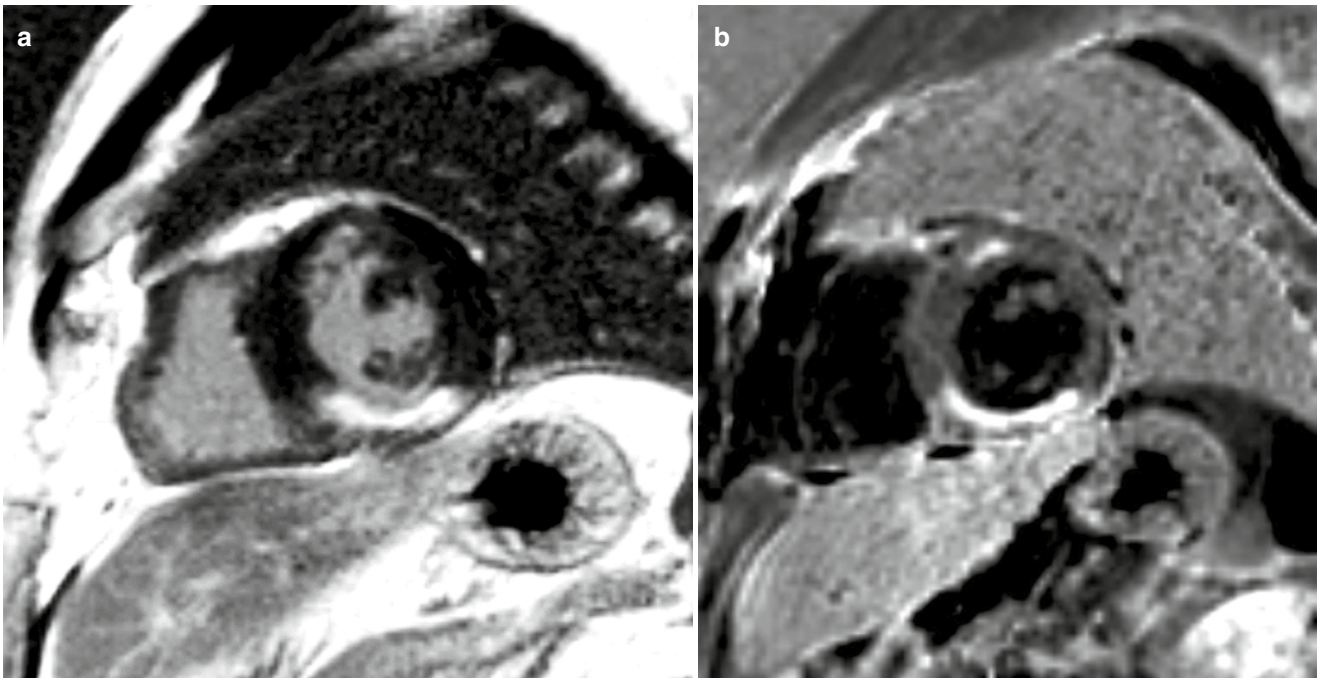

Fig. 22.16 Myocardial infarction and black blood PSIR image (FIDDLE image; works in progress by the Siemens). (**a**) LGE image shows strong enhancement in the inferior wall of the LV. (**b**) FIDDLE image shows good enhancement in the same area of the LV. Ventricular cavity looks dark due to signal loss by the T2 preparation pulse on the FIDDLE imaging protocol

Is now commonly used with a gradient echo sequence which includes:
- An SSFP sequence without the injection of contrast medium at 1.5 T scanner (Fig. 22.17)
- A 3D-TFE sequence with the injection of contrast medium at 3 T scanner (Fig. 22.18)

22.8.2 Clinical Applications

Evaluates coronary stenosis or coronary bypass graft
Analyze the coronary plaques and the arterial walls

22.9 Myocardial Mapping Imaging

Mapping technique is available for tissue characterization which is clinically important in guiding patient treatment. Studies have been done in quantifying fibrosis or water content in the myocardium under various circumstances. The myocardium preserves homeostasis for water, protein, and mineral components. Mapping technique may be useful in detecting myocardial water (edema) on the T1 or T2 maps or in detecting fibrosis or protein deposits on the post-contrast T1 map.

We can basically obtain the T1 or T2 values through a curve fitting process using the T1- or T2-prepared pulses. T1 mapping uses the inversion pulses as the T1-prepared pulse, and T2 mapping uses the 90 and 180° pulses as the T2-prepared pulse. Each value can be expressed in millisecond which reflects the relaxation time of the myocardial tissues. These processes rarely depend on the influences of the acquisition environments or the variations in MR signal intensity.

22.9.1 T1 Mapping

Is generated from the different inversion recovery images with varying inversion time (TI)
- Which can provide high spatial resolution within a single breath-holding

Uses the inversion pulses as the T1-prepared pulses
Obtains the T1 maps through a curve fitting process [9] after robust motion correction
Is less sensitive to motion artifacts
Is useful in evaluating diffuse fibrosis, edema, myocarditis, etc. (Fig. 22.19)
Depends on heart rate and acquisition time after injection of the contrast agent

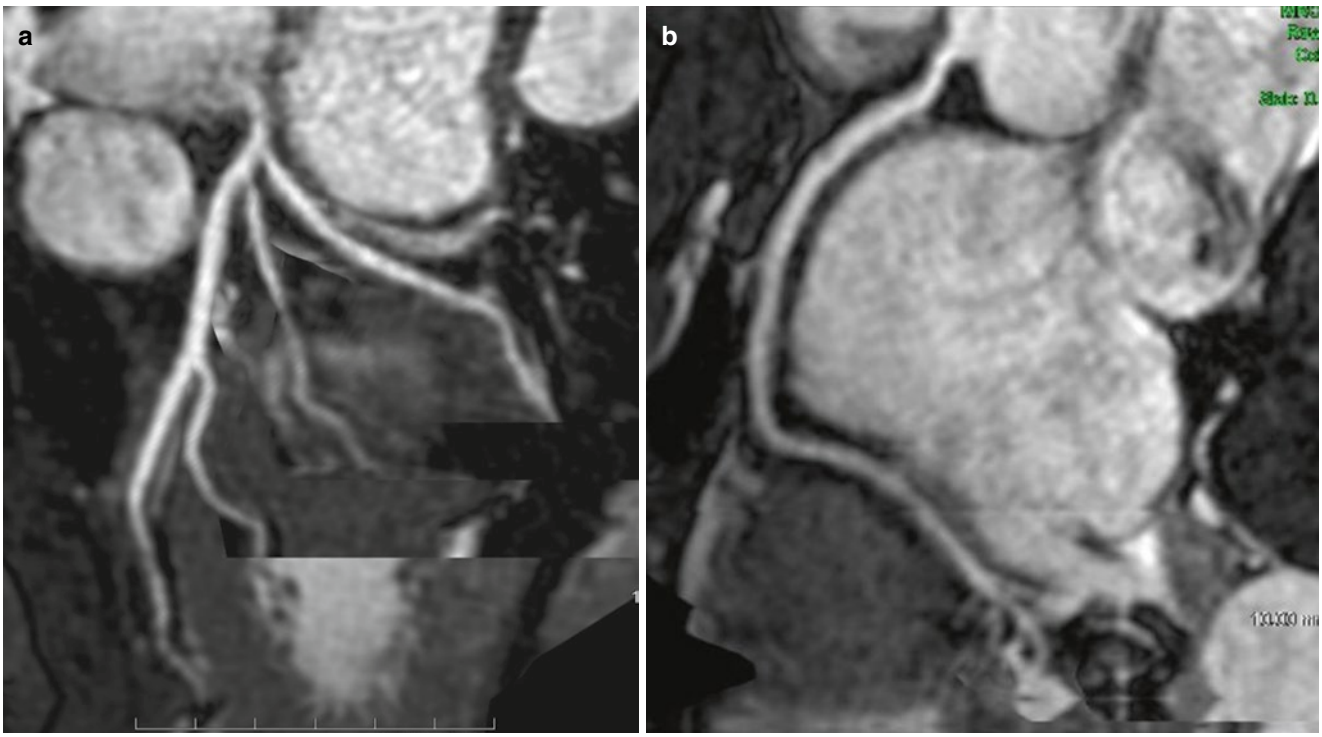

Fig. 22.17 MR coronary angiography at 1.5 T. (**a**, **b**) Curved MPR images of the coronary arteries without contrast enhancement using a balanced FFE sequence

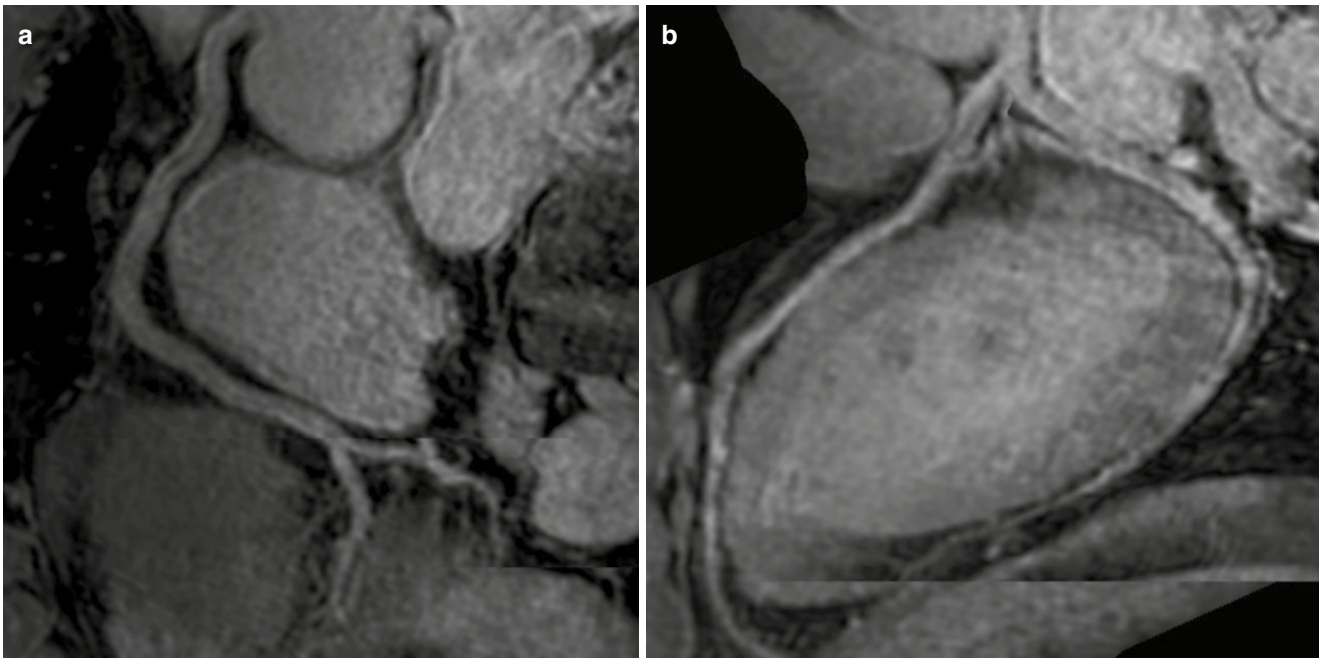

Fig. 22.18 MR coronary angiography at 3 T. (**a**, **b**) Curved MPR images of the coronary arteries with contrast enhancement using a 3D-TFE sequence

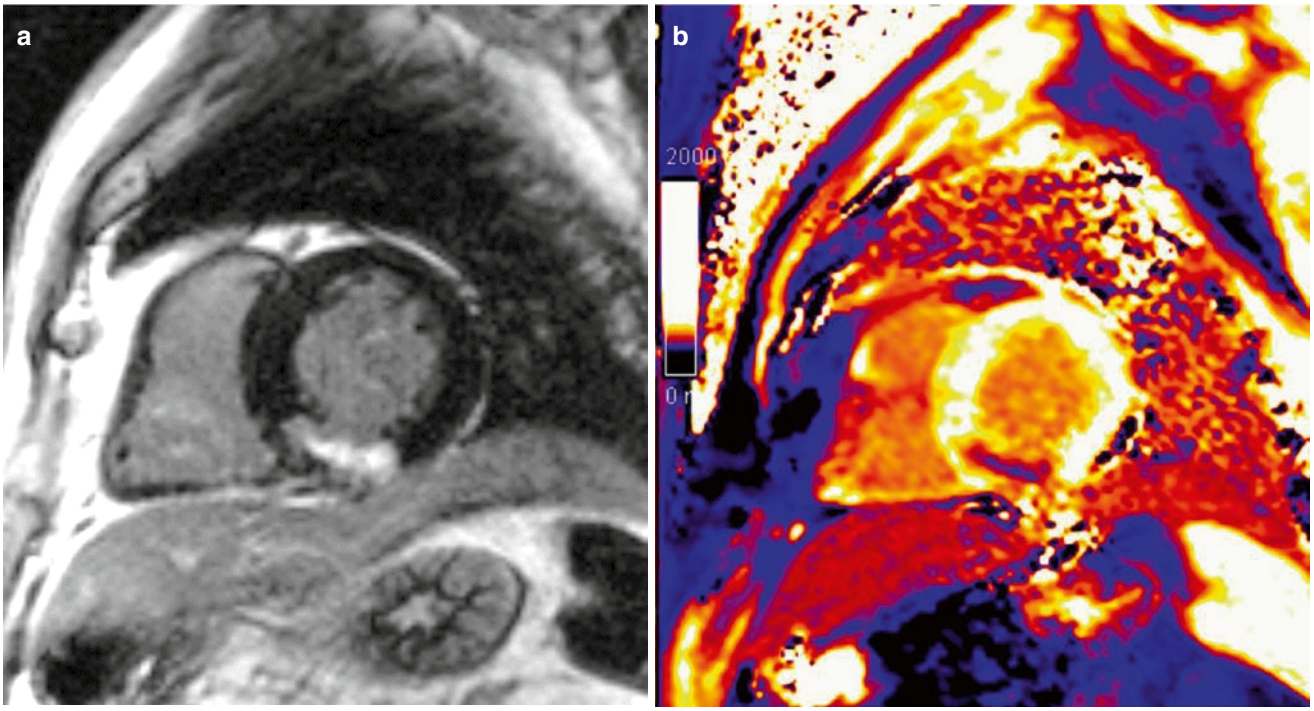

Fig. 22.19 Myocardial infarction and T1 mapping image. (**a**) Late Gd-enhanced image shows strong enhancement in the inferior wall of the LV. (**b**) Color T1 map shows markedly shortening of T1 value due to contrast stasis in the infarct myocardium

22.9.2 Extracellular Volume Mapping

Is related to the volume of extracellular matrix or myocardial fibrosis
May increase according to the orthogonal age
Can be obtained from the following equation [10]:

$$\mathrm{ECV}_{(\mathrm{m})} = \frac{(1/\mathrm{T1})_{\mathrm{myo.post}} - (1/\mathrm{T1})_{\mathrm{myo.pre}}}{(1/\mathrm{T1})_{\mathrm{blood.post}} - (1/\mathrm{T1})_{\mathrm{blood.pre}}} \times (1 - \mathrm{hematocrit})$$

where myo = myocardium, pre = pre-contrast enhancement, and post = post-contrast enhancement.

22.9.3 T2 Mapping [11]

Uses a single-shot balanced SSFP readout
Uses 90° and 180° pulses as the T2-prepared pulse
Produces the T2 maps through a curve fitting algorithm after motion correction
Is related to the volume of intracellular or extracellular water contents
Is less sensitive to motion artifact
Is useful in detection of myocardial edema (Fig. 22.20)

22.9.4 T2* Mapping [12]

Is very sensitive to the paramagnetic effects
Is useful in detecting hemorrhage or iron deposition
Is more strong in days after hemorrhage
Shows a dark signal due to paramagnetic effects from hemorrhage

22.9.5 Clinical Application of Mapping Techniques

T2 mapping images for edema detection
T1 mapping images for myocardial fibrosis or infarction

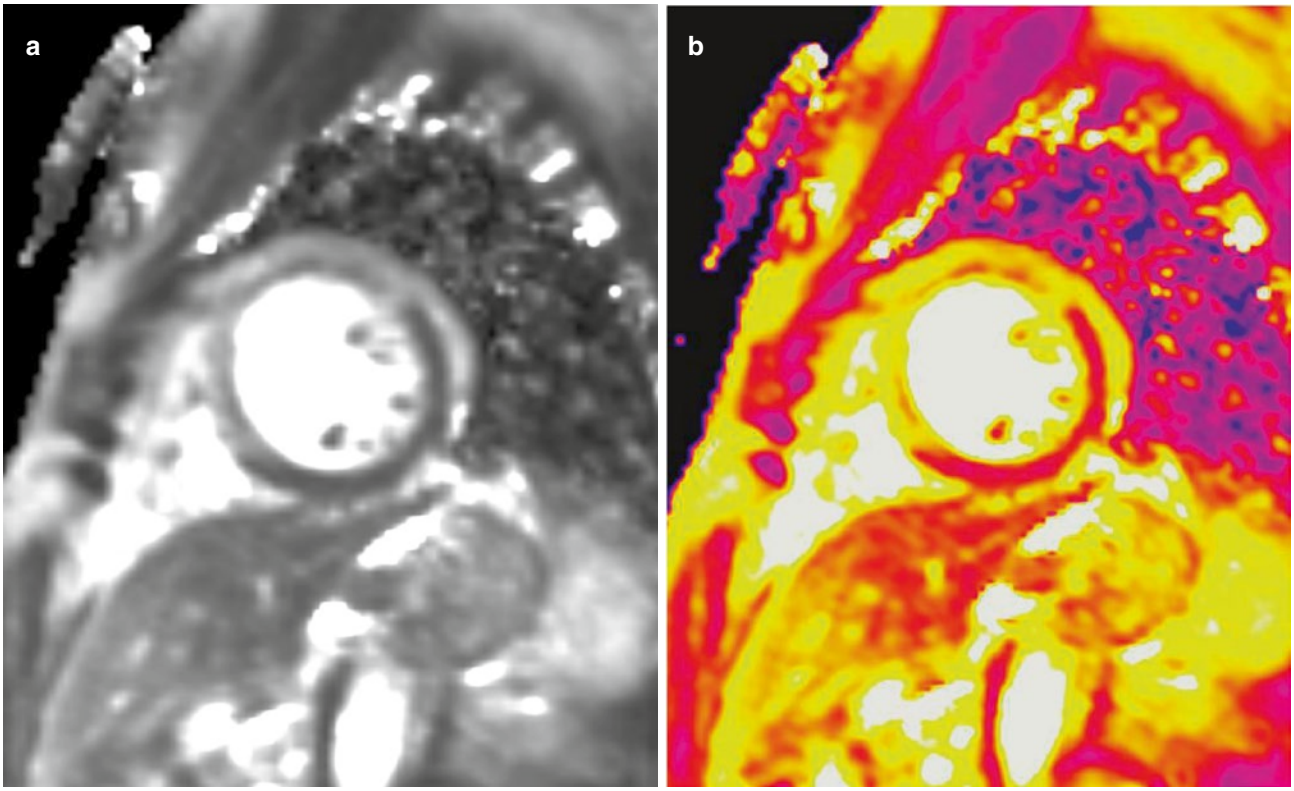

Fig. 22.20 Myocardial edema and T2 mapping image. (**a**) T2W image shows high signal intensity in the anterior wall and LV septum due to myocardial edema. (**b**) Color T2 map shows prolongation of T2 value in the same area of the LV

References

1. Levine GN, Gomes AS, Arai AE, Bluemke DA, Flamm SD, Kanal E, et al. Safety of magnetic resonance imaging in patients with cardiovascular devices: an American Heart Association scientific statement from the Committee on Diagnostic and Interventional Cardiac Catheterization, Council on Clinical Cardiology, and the Council on Cardiovascular Radiology and Intervention: endorsed by the American College of Cardiology Foundation, the North American Society for Cardiac Imaging, and the Society for Cardiovascular Magnetic Resonance. Circulation. 2007;116: 2878–91.
2. Haacke EM, Patrick JL. Reducing motion artifacts in two-dimensional Fourier transform imaging. Magn Reson Imaging. 1986;4:359–76.
3. Verhaert D, Thavendiranathan P, Giri S, Mihai G, Rajagopalan S, Simonetti OP, et al. Direct T2 quantification of myocardial edema in acute ischemic injury. JACC Cardiovasc Imaging. 2011;4: 269–78.
4. Botnar RM, Stuber M, Danias PG, Kissinger KV, Manning WJ. Improved coronary artery definition with T2-weighted, free-breathing, three-dimensional coronary MRA. Circulation. 1999;99: 3139–48.
5. Liu CY, Wieben O, Brittain JH, Reeder SB. Improved delayed enhanced myocardial imaging with T2-Prep inversion recovery magnetization preparation. J Magn Reson Imaging. 2008;28: 1280–6.
6. Ibrahim e SH. Myocardial tagging by cardiovascular magnetic resonance: evolution of techniques–pulse sequences, analysis algorithms, and applications. J Cardiovasc Magn Reson. 2011;13:36.
7. Foo TK, Ho VB, Saranathan M, Cheng LQ, Sakuma H, Kraitchman DL, et al. Feasibility of integrating high-spatial-resolution 3D breath-hold coronary MR angiography with myocardial perfusion and viability examinations. Radiology. 2005;235: 1025–30.
8. Sakuma H, Ichikawa Y, Suzawa N, Hirano T, Makino K, Koyama N, et al. Assessment of coronary arteries with total study time of less than 30 minutes by using whole-heart coronary MR angiography. Radiology. 2005;237:316–21.
9. Messroghli DR, Radjenovic A, Kozerke S, Higgins DM, Sivananthan MU, Ridgway JP. Modified Look-Locker inversion recovery (MOLLI) for high-resolution T1 mapping of the heart. Magn Reson Med. 2004;52:141–6.
10. Kellman P, Wilson JR, Xue H, Bandettini WP, Shanbhag SM, Druey KM, et al. Extracellular volume fraction mapping in the myocardium, part 2: initial clinical experience. J Cardiovasc Magn Reson. 2012;14:64.
11. Giri S, Chung YC, Merchant A, Mihai G, Rajagopalan S, Raman SV, et al. T2 quantification for improved detection of myocardial edema. J Cardiovasc Magn Reson. 2009;11:56.
12. O'Regan DP, Ahmed R, Karunanithy N, Neuwirth C, Tan Y, Durighel G, et al. Reperfusion hemorrhage following acute myocardial infarction: assessment with T2* mapping and effect on measuring the area at risk. Radiology. 2009;250:916–22.